



UNIVERSITAT DE
BARCELONA

Development of an advanced 3D culture system for human cardiac tissue engineering

Maria Valls Margarit

ADVERTIMENT. La consulta d'aquesta tesi queda condicionada a l'acceptació de les següents condicions d'ús: La difusió d'aquesta tesi per mitjà del servei TDX (www.tdx.cat) i a través del Dipòsit Digital de la UB (diposit.ub.edu) ha estat autoritzada pels titulars dels drets de propietat intel·lectual únicament per a usos privats emmarcats en activitats d'investigació i docència. No s'autoritza la seva reproducció amb finalitats de lucre ni la seva difusió i posada a disposició des d'un lloc aliè al servei TDX ni al Dipòsit Digital de la UB. No s'autoritza la presentació del seu contingut en una finestra o marc aliè a TDX o al Dipòsit Digital de la UB (framing). Aquesta reserva de drets afecta tant al resum de presentació de la tesi com als seus continguts. En la utilització o cita de parts de la tesi és obligat indicar el nom de la persona autora.

ADVERTENCIA. La consulta de esta tesis queda condicionada a la aceptación de las siguientes condiciones de uso: La difusión de esta tesis por medio del servicio TDR (www.tdx.cat) y a través del Repositorio Digital de la UB (diposit.ub.edu) ha sido autorizada por los titulares de los derechos de propiedad intelectual únicamente para usos privados enmarcados en actividades de investigación y docencia. No se autoriza su reproducción con finalidades de lucro ni su difusión y puesta a disposición desde un sitio ajeno al servicio TDR o al Repositorio Digital de la UB. No se autoriza la presentación de su contenido en una ventana o marco ajeno a TDR o al Repositorio Digital de la UB (framing). Esta reserva de derechos afecta tanto al resumen de presentación de la tesis como a sus contenidos. En la utilización o cita de partes de la tesis es obligado indicar el nombre de la persona autora.

WARNING. On having consulted this thesis you're accepting the following use conditions: Spreading this thesis by the TDX (www.tdx.cat) service and by the UB Digital Repository (diposit.ub.edu) has been authorized by the titular of the intellectual property rights only for private uses placed in investigation and teaching activities. Reproduction with lucrative aims is not authorized nor its spreading and availability from a site foreign to the TDX service or to the UB Digital Repository. Introducing its content in a window or frame foreign to the TDX service or to the UB Digital Repository is not authorized (framing). Those rights affect to the presentation summary of the thesis as well as to its contents. In the using or citation of parts of the thesis it's obliged to indicate the name of the author.



UNIVERSITAT DE
BARCELONA



Tesi doctoral

Development of an advanced 3D culture system for human cardiac tissue engineering

Memòria presentada per

Maria Valls Margarit

Per optar al grau de **doctora en Biomedicina**

Departament d'Electrònica

Universitat de Barcelona

Programa de Doctorat en Biomedicina

Institut de Bioenginyeria de Catalunya

Dra. Elena Martínez Fraiz **Dr. Ángel Raya Chamorro** **Dr. Josep Samitier Martí**
Directora Director Tutor

Barcelona, 2017

*Savoir s'étonner à propos est le premier pas fait
sur la route de la découverte.*

Louis Pasteur
Chimiste et physicien
Pionnier de la microbiologie

*Ser capaç de sorprendre's és el primer pas en
el camí del descobriment.*

Louis Pasteur
Químic i físic
Pioner de la microbiologia

TABLE OF CONTENTS

I. ABSTRACT.....	1
II. ABBREVIATIONS.....	5
1. INTRODUCTION.....	11
1.1. The human heart.....	13
1.1.1. Anatomy, physiology and histology	13
1.1.2. Cardiomyocyte development and maturation	21
1.1.2.1. Morphology, orientation and proliferation	21
1.1.2.2. Structural properties	22
1.1.2.3. Myofibrillar protein isoforms switch.....	23
1.1.2.4. Functional properties.....	24
1.1.2.5. Pharmacological response	26
1.1.3. Cardiovascular diseases and heart failure	30
1.1.4. Alternative therapeutic strategies	32
1.1.4.1. Cell therapy	32
1.1.4.2. In vitro models for drug discovery and toxicity testing	37
1.1.4.3. Disease modelling	40
1.2. Cardiac tissue engineering.....	43
1.2.1. Cardiac cells.....	45
1.2.2. Biomaterials	46
1.2.2.1. General considerations	47
1.2.2.2. Natural biomaterials	49
1.2.2.3. Synthetic biomaterials	50
1.2.3. Regulatory signals.....	51
1.2.3.1. Three-dimensional (3D) cultures	52
1.2.3.2. Biochemical cues	53
1.2.3.3. Cell patterning and alignment.....	54
1.2.3.4. Mechanical stimulation.....	55
1.2.3.5. Electrical stimulation.....	58
1.2.4. Bioreactors	62
1.2.4.1. Mass transport.....	63
1.2.4.2. Multimodal stimulation platforms	64
1.2.5. Electrophysiological evaluation of cardiac constructs	68
2. HYPOTHESIS AND OBJECTIVES	71
3. MATERIALS AND METHODS.....	75
3.1. Cell culture.....	77
3.1.1. Human foreskin fibroblasts (HFF) culture.....	77

3.1.2. Isolation and primary culture of neonatal rat heart cells	77
3.1.3. Human induced pluripotent stem cells (hiPSC) culture	79
3.1.4. Generation of hiPSC cardiac-specific reporter lines	80
3.1.5. Cardiac differentiation protocol of hiPSC.....	81
3.2. Structural and mechanical properties of the scaffold.....	83
3.2.1. Morphology and porosity	83
3.2.2. Stiffness	84
3.3. Cell seeding in 3D scaffolds.....	84
3.3.1. Static seeding.....	84
3.3.2. Perfusion seeding	84
3.4. Development of a perfusion bioreactor.....	86
3.4.1. Single chamber perfusion bioreactor.....	86
3.4.2. Parallelized perfusion bioreactor	88
3.5. Design and fabrication of a perfusion chamber including electrical stimulation	89
3.5.1. Electric field modelling.....	89
3.5.2. Design guidelines and fabrication of the custom-made perfusion chamber with electrical stimulation	91
3.5.2.1. <i>First prototype: poly(methyl methacrylate) (PMMA) and polydimethylsiloxane (PDMS)</i>	91
3.5.2.2. <i>Second prototype: acrylonitrile butadiene styrene (ABS)</i>	91
3.5.2.3. <i>Third prototype: polypropylene (PP)</i>	93
3.5.3. Electrical stimulation regime for cardiac constructs culture	95
3.6. Flow cytometry analysis	96
3.7. Functional activity of cardiac tissue constructs.....	97
3.7.1. Setup for contractile activity recording.....	97
3.7.2. Measurement of functional parameters	97
3.7.3. Drug response analysis.....	99
3.8. Histological analysis	100
3.8.1. Hematoxylin and eosin staining.....	100
3.8.2. Immunofluorescence staining protocol	101
3.8.2.1. <i>Standard 2D cell cultures</i>	101
3.8.2.2. <i>Cardiac tissue constructs (in toto)</i>	103
3.9. Transmission electron microscopy analysis	104
3.10. Gene expression analysis by quantitative real-time polymerase chain reaction (qRT-PCR)	105

3.11. Recording and processing of bioelectrical signals generated by cardiac tissue constructs	106
4. RESULTS	109
4.1. Matrigel™ as 3D scaffold for cardiac tissue engineering.....	111
4.1.1. Structural analysis of Matrigel™	112
4.1.2. Mechanical properties of Matrigel™	114
4.1.3. Shear stress within Matrigel™ scaffold under perfusion	114
4.2. Development of an efficient method for cell seeding into Matrigel™ scaffolds	117
4.2.1. Static seeding using Matrigel® as cell delivery vehicle	118
4.2.2. Cell seeding using a perfusion loop system	119
4.3. Design and fabrication of a parallelized perfusion bioreactor system	123
4.3.1. Flow distribution in the parallelized perfusion bioreactor	123
4.3.2. Preliminary cellular tests	125
4.3.2.1. Generation of rat cardiac tissue constructs	125
4.3.2.2. Generation of human cardiac tissue constructs.....	129
4.4. Design and fabrication of a custom-made perfusion chamber with electrical stimulation	135
4.4.1. First prototype: poly(methyl methacrylate) (PMMA) and polydimethylsiloxane (PDMS)	136
4.4.2. Second prototype: 3D printing of acrylonitrile butadiene styrene (ABS).....	145
4.4.3. Third prototype: precision machining of polypropylene (PP)	148
4.5. Generation of rat cardiac tissue constructs through perfusion and electrical stimulation	155
4.5.1. Electrical stimulation improves the contractility of cardiac tissue constructs ..	156
4.5.2. Time in culture and electrical stimulation potentiate the structural maturation of rat cardiac tissue constructs.....	159
4.6. Generation of human cardiac tissue constructs through perfusion and electrical stimulation	166
4.6.1. Cardiac differentiation potential of human induced pluripotent stem cells (hiPSC).....	166
4.6.2. Functional maturation of tissue-like human cardiac constructs is enhanced through electrical stimulation.....	168
4.6.3. Perfusion together with electrical stimulation promote the structural maturation of tissue-like human cardiac constructs.....	172
4.6.4. Human cardiac tissue constructs display an increased expression of cardiac specific genes	176

4.7. Electrically stimulated human cardiac tissue constructs elicit ECG-like signals and predict drug-induced cardiotoxicity	177
4.7.1. Bioelectrical signal generated by human cardiac tissue constructs resembles a surface electrocardiogram	178
4.7.2. Electrically stimulated human cardiac tissue constructs can predict drug-induced cardiotoxicity	181
5. DISCUSSION	187
6. CONCLUSIONS	203
7. REFERENCES	207
8. RESUM EN CATALÀ.....	235
9. APPENDICES	241
9.1. Prototype drawings	243
9.2. Journal articles related to the thesis	249
9.3. Other journal articles	283

I. ABSTRACT

Ischemic heart disease is a major cause of human death worldwide owing to the heart minimal ability to repair following injury. Other than heart transplantation, there are currently no effective or long-lasting therapies for end-stage heart failure. Therefore, it is crucial to develop not only alternative therapies that potentiate heart regeneration or repair, but also new tools to study human cardiac physiology and pathophysiology *in vitro*. In this context, cardiac tissue engineering arises a promising strategy, as it is aimed at generating cardiac tissue analogues that would act as *in vitro* models of human cardiac tissue or as surrogates for heart repair. Thus, having 3D human cardiac tissue constructs resembling human myocardium could revolutionize drug discovery and toxicity testing, cardiac disease modelling and regenerative medicine.

A strategy to obtain reliable cardiac tissue constructs is to mimic the native cardiac environment. The classical approach is based on seeding cardiomyocytes in biocompatible 3D scaffolds, and then culturing the construct in a biomimetic signaling system, usually a bioreactor. Although major advances have been made, the generation of thick and mature tissue constructs from human induced pluripotent stem cells-derived cardiomyocytes (hiPSC-CM) is still a challenge. Therefore, the hypothesis of our study is that the combination of hiPSC-CM with 3D scaffolds and appropriate regulatory signals may lead to the generation of mature human cardiac tissue constructs resembling human myocardium, both functionally and structurally. To address this, we have characterized a collagen-based 3D scaffold and established an efficient method for cell seeding into the scaffold. We have also developed a parallelized perfusion bioreactor system, which ensures an effective mass transport between cells and culture medium and allows culturing multiple replicas of tissue constructs. In addition, we have designed and fabricated a perfusion chamber including electrodes to electrically stimulate cells during culture, as well as to monitor tissue function. With this advanced 3D culture system, we have been able to generate thick 3D human cardiac constructs with tissue-like functionality. Our results indicate that perfusion of culture medium combined with electrical stimulation and collagen-based scaffold improve the structural and functional maturation of hiPSC-CM. In general terms, electrical stimulation has improved the structural organization, alignment and coupling of cardiomyocytes in our cardiac tissue constructs. Moreover, electrical stimulation has promoted the formation of synchronous contractile constructs at the macroscale with improved electrophysiological functions. Through the development of a new electrophysiological recording system, we report for the first time to our knowledge a technique that provides information about the electrical activity of intact cardiac tissue constructs in real time. Specifically, the combination of action potentials generated by hiPSC-CM composing cardiac constructs produces ECG-like signals, which could be monitored online. Finally, we have demonstrated the ability of stimulated human cardiac tissue constructs to detect drug-induced cardiotoxicity, as typical features of arrhythmias (e.g. prolongation of RR intervals and regular blockades) could be observed upon treatment with sotalol.

Taken together, results indicate that macroscopic human cardiac tissue constructs with tissue-like functionality can be obtained through the use of our advanced 3D culture system. We have studied the effects of electrical stimulation on cardiomyocytes at multiple levels: molecular (presence, distribution and expression of cardiac proteins), ultrastructural (sarcomere width and presence of specialized cellular junctions), cellular (morphology and alignment), and functional (amplitude, directionality and strain of contractions, and electrophysiological recordings). Findings validate our *in vitro* approach as a valuable system to obtain 3D cardiac patches with an improved maturity and functionality. Importantly, the online monitoring system developed in this study can provide essential electrophysiological information of intact cardiac tissue constructs, which opens up myriad possibilities in the field of cardiovascular research.

II. ABBREVIATIONS

2D: two dimensional
3D: three dimensional
AAS: α -sarcomeric actinin
ABS: acrylonitrile butadiene styrene
ADSC: adipose-derived stromal cells
AH: adult heart
AP: action potential
ASA: α -sarcomeric actin
bFGF: basic fibroblast growth factor
BMC: Bone marrow-derived mononuclear cells
BR: beating rate
Bra: Brachyury
BSA: bovine serum albumin
CBFHH: calcium and bicarbonate-free Hank's balanced salt solution with HEPES
cHES: conditioned HES medium
CHO: Chinese hamster ovary cells
CiPA: Comprehensive *in vitro* Proarrhythmia Assay
CM: Cardiomyocytes
CSC: Cardiac stem cells
cTNC: cardiac troponin C
cTNI: cardiac troponin I
cTNT: cardiac troponin T
CVDs: Cardiovascular diseases
Cx43: connexin 43
DAPI: 4',6-diamidino-2-phenylindole
DCM: dilated cardiomyopathy
DMA: Dynamic Mechanical Analysis
DMEM: Dulbecco's Modified Eagle Medium
ECG: surface electrocardiogram
ECM: extracellular matrix
EFPs: extracellular field potentials
EPC: endothelial progenitor cells
ES: electrically stimulated
ESC: embryonic stem cells
ET: excitation threshold

EtO: ethylene oxide
FAC: fractional area change
FBS: fetal bovine serum
FH: fetal heart
FiPS: fibroblasts-derived iPS cells
FPD: field potential duration
GFP: green fluorescence protein
HCM: hypertrophic cardiomyopathy
HEK293: human embryonic kidney 293 cells
HEPES: N-2-hydroxyethylpiperazine-N-2-ethane sulfonic acid
hERG: human ether-a-go-go-related gene
hESC: human embryonic stem cells
hESC-CM: human embryonic stem-cell derived cardiomyocytes
HFF: human foreskin fibroblasts
hiPSC: human induced pluripotent stem cells
hiPSC-CM: human induced pluripotent stem cell-derived cardiomyocytes
hPSC: human pluripotent stem cells
hPSC-CM: human pluripotent stem cell-derived cardiomyocytes
HSC: hematopoietic stem cells
HyD: hybrid detector
IGF-1: Insulin-like growth factor 1
iPSC: induced pluripotent stem cells
KiPS: keratinocyte-derived iPS cells
LQT: long QT syndrome
MCR: maximum capture rate
MEA: microelectrode arrays
MEF: mouse embryonic fibroblasts
MHC: Myosin heavy chain
MLC: Myosin light chain
MLC2a: atrial isoform of the regulatory myosin light chain
MLC2v: ventricular isoform of the regulatory myosin light chain
MSC: mesenchymal stem cells
NDD: non-descanned detector
Neo^R: neomycin-resistance gene
NKM: non-kardiomyocyte medium

NRV: neonatal rat ventricle
PBS: phosphate buffered saline
PCL: poly ε-caprolactone
PCR: polymerase chain reaction
PDMS: polydimethylsiloxane
PFA: paraformaldehyde
PGA: polyglycolic acid
PGS: poly(glycerol sebacate)
Ph: phalloidin
PIV: Particle Image Velocimetry
PLA: polylactic acid
PLLA: poly-L-lactide
PMMA: poly(methyl methacrylate)
PP: polypropylene
PSC: pluripotent stem cells
PU: polyurethane
PVDF: polyvinylidene fluoride
qRT-PCR: quantitative real-time polymerase chain reaction
rCM: rat cardiomyocytes
Rex-1: reduced expression 1 gene
RT: room temperature
RyR: ryanodine receptors
SD: standard deviation
SEM: scanning electron microscope
SERCA: sarco/endoplasmic reticulum Ca²⁺-ATPase
SHG: Second Harmonic Generation
SR: sarcoplasmic reticulum
ssTnl: slow skeletal troponin I
TBS: tris-buffered saline
TdP: torsades de pointes
TEM: transmission electron microscopy
TPEF: two-photon excited fluorescence
VSO: voltage-sensing optical techniques
VSV: vesicular stomatitis virus
Wnt: Wingless

ABBREVIATIONS

α -MHC: α -heavy chain subunit of cardiac myosin

α -sa: α -sarcomeric actin

α -tub: α -tubulin

β -MHC: β -heavy chain subunit of cardiac myosin

1. INTRODUCTION

1.1. The human heart

1.1.1. Anatomy, physiology and histology

The heart is the first functional organ to develop in the human body: it starts beating only three weeks into gestation. The heart is vital for the growth and survival of the developing embryo, as it has an important role in the distribution of oxygen and nutrients^{1,2}. An adult's heart is about the size of a fist, and it is a muscular organ of unparalleled complexity that continuously pumps blood through the body³. Its main functions are collecting blood from the tissues of the body and pumping it to the lungs, and collecting blood from the lungs and pumping it to all other tissues in the body. Anatomically, the human heart resides in the center of the thoracic cavity, dorsal to the sternum and costal cartilages, and rests on the anterior surface of the diaphragm. It adopts an oblique position in the thorax, with two-thirds to the left of midline. It occupies a space between the pleural cavities called the middle mediastinum. Around the heart there is the pericardium, which is a serous membrane that covers the organ. It is composed of an inner (visceral pericardium) and an outer (parietal pericardium) layers with lubricating fluid in between (**Figure 1.1**)⁴.

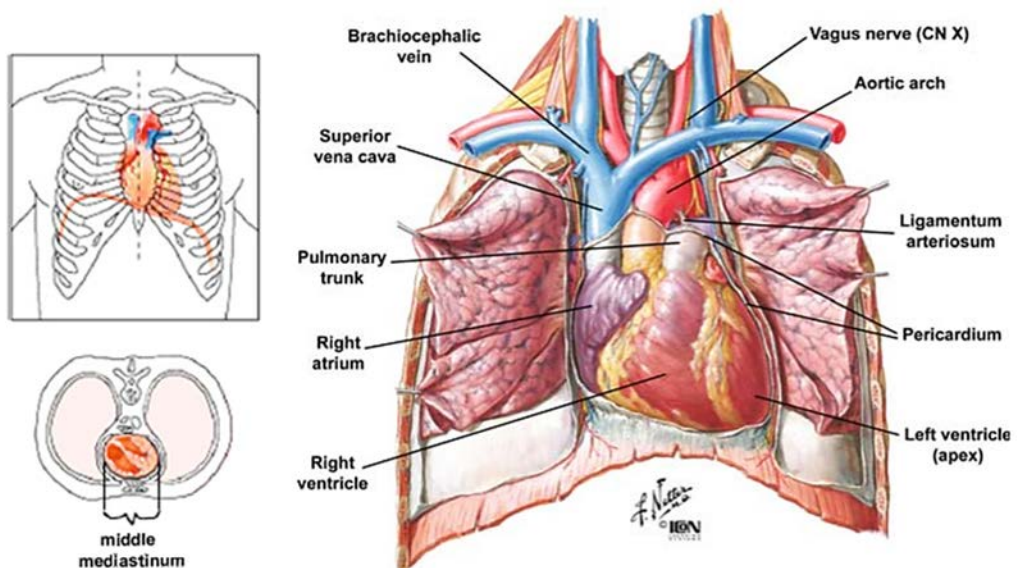


Figure 1.1. Position in the thorax and anterior surface of the heart. The heart lies obliquely in the thorax, dorsal to the sternum and costal cartilages, and rests on the diaphragm. It is located between the two lungs, in a space called middle mediastinum, and is surrounded by the pericardium. The ventral surface of the heart is formed primarily by the right ventricle. The atria are positioned anterior to their respective ventricles. The right lateral border is formed by the right atrium and the left lateral border by the left ventricle. The dorsal surface is formed by the left atrium and ventricle. The great arteries (aorta and pulmonary trunk) arise from the base of the heart, and the most caudal part of the heart is the apex. *Adapted from Weinhaus AJ and Roberts KP⁴.*

The internal anatomy of the heart is composed of four distinct chambers. The two upper chambers (or atria) are responsible for collecting blood; the two lower chambers (ventricles) are responsible for pumping blood and are much stronger. Right atrium and ventricle collect blood from the body and pump it to the lungs, while the left atrium and ventricle collect blood from the lungs and pump it throughout the body (**Figure 1.1**). There is a one-way flow of blood through the heart; this flow is maintained by a set of four valves that prevent the backflow of blood (two atrioventricular valves named tricuspid and bicuspid, and two semilunar valves named pulmonary and aortic)⁴.

Even though the heart is filled with blood, it provides very little nourishment and oxygen to the tissues composing it. The heart walls are too thick to be supplied by diffusion alone, so heart tissues are sustained by a separate vascular supply. Nutrients and oxygen are provided through right and left coronary arteries, which arise from the base of the aorta. Waste products and carbon dioxide are removed through cardiac veins that return deoxygenated blood to the right atrium⁴. A rich vasculature that ensures an efficient blood supply is crucial for the normal function of the heart, as it is an extremely metabolically active organ that cannot tolerate hypoxia for long periods of time⁵.

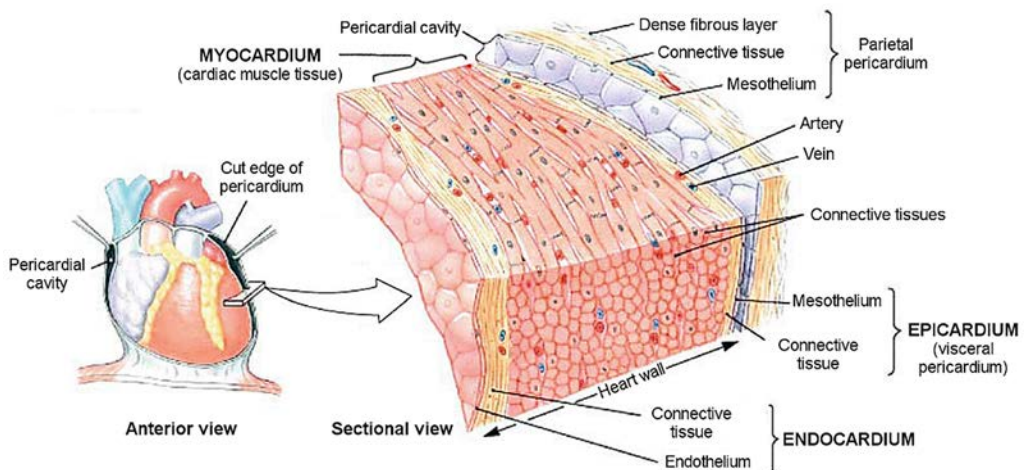


Figure 1.2. Diagram of the internal anatomy of the heart wall. Cross-section cut through the heart wall, where the three constituent layers are shown (endocardium, myocardium and epicardium). The pericardium is also displayed, with its two constituent layers (parietal and visceral pericardium) and the pericardial cavity. *Adapted from Weinhaus AJ and Roberts KP⁴.*

The heart wall consists in three distinct layers: the endocardium (inner layer), the myocardium (middle layer) and the epicardium (external layer, also named visceral pericardium) (**Figure 1.2**). The endocardium is the internal lining of the atrial and ventricular chambers, and is continuous with the endothelium of the incoming veins and outgoing arteries. In fact, the endocardium is a sheet of epithelium called endothelium

that rests on a dense connective tissue layer, consisting of collagen and elastic fibers. Regarding the epicardium, it is composed of a single layer of flat-shaped epithelial cells called mesothelium, which covers the free surface. Mesothelial cells secrete a small amount of serous fluid to lubricate the movement of the epicardium on the parietal pericardium. The epicardium also includes a thin layer of fibroelastic connective tissue that supports the mesothelium, and a broad layer of adipose tissue which serves to connect the fibroelastic layer to the myocardium. Finally, the myocardium constitutes the bulk of the heart tissue, and is composed of cardiac muscle that contracts to carry out heart pumping function⁴.

The myocardium is the cardiac muscle tissue of the heart, a highly differentiated tissue that follows an asymmetrical, helical architecture^{6,7}. The cardiac helix form consists in two loops that start at the pulmonary artery and end in the aorta, leading to circularly and spirally arranged networks of muscle cells that squeeze blood through the heart⁸. Two types of myocardial tissue can be identified: the myocardium composing atria and ventricles (being much thicker in the ventricles, ~1 cm in left ventricle), and the myocardium specialized for initiating and conducting the electrical impulses through the heart, named the conduction system of the heart⁹.

Atrial and ventricular myocardium consists of tightly packed cardiomyocytes (CM), fibroblasts, endothelial cells and smooth muscle cells (**Figure 1.3**). Cardiomyocytes are striated and contractile muscle cells that comprise only 30 to 40% of the total cells in the heart, but occupy approximately 75% of normal myocardial tissue volume¹⁰. Most of the remaining cells are non-myocytes, mainly fibroblasts, which are found surrounding cardiomyocytes and between the myocardial tissue layers. Fibroblasts represent about 60-70% of human heart composition, and contribute to cardiac development, myocardial structure, cell signaling and electromechanical function of the myocardium^{11,12}. The remaining cell types, such as endothelial and vascular smooth muscle cells, represent comparatively small populations¹³.

Regarding the conduction system of the heart, it has the capacity of spontaneous rhythmicity and is constituted by specialized connecting bundles for a rapid and highly coordinated impulse propagation^{9,14}. At the cellular level, it is composed of specialized cardiomyocytes named pacemaker cells and Purkinje fibers. Pacemaker cells reside in the sinoatrial node located in the right atrium, and spontaneously generate electrical impulses to initiate heart contraction (**Figure 1.3**)¹⁵. Sinoatrial node is considered the natural pacemaker, as pacemaker cells determine the cardiac rhythm¹⁶. Regarding Purkinje fibers, they are responsible for conducting the electrical impulses throughout the heart (**Figure 1.3**)¹⁷.

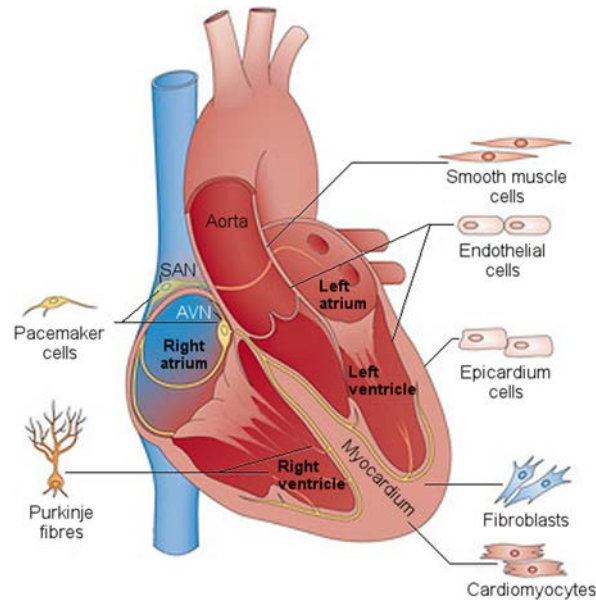


Figure 1.3. Cellular composition of the heart. Cell types of the heart, all of which contribute to structural, biochemical, mechanical and electrical properties of the functional heart. SAN: sinoatrial node; AVN: atrioventricular node. Adapted from Xin *et al.*¹⁵.

Another important component of the heart wall is the cardiac extracellular matrix (ECM), which comprises the non-cellular components of the tissue. The cardiac ECM is a complex meshwork of structural and non-structural proteins and sugars that provide cells with microenvironmental cues, mechanical support and architectural guidance¹⁸. Fibrous proteins (collagens and elastins) have a structural function, whereas matricellular proteins (e.g. tenascin and osteopontin) have non-structural roles. Other glycoproteins (e.g. fibronectin and laminin), as well as proteoglycans have also relevant roles in both functions of the ECM^{19,20}. In the adult myocardium, the most abundant collagen types are I and III, followed by IV, V and VI types, and elastin fibers confer elasticity to the cardiac tissue²¹.

Electrical coupling between cardiomyocytes allow the spreading of depolarizing electrical impulses from the sinoatrial node through the atria. The excitation and subsequent contraction of the atria is reflected by the P-wave on the surface electrocardiogram (ECG) (**Figure 1.4**). The electrical impulse is then conducted from the atria to the atrioventricular node, and from the atrioventricular node to the apex of the heart through a small band of specialized cardiac muscle named bundle of His. Then, Purkinje fibers transmit the electrical impulse from the apex of the heart to the cardiomyocytes of the right and left ventricles. The excitation and subsequent contraction of the ventricles is represented by the QRS complex on the surface ECG (**Figure 1.4**). Finally, the T-wave is indicative of ventricular repolarization (recovery)^{22,23}.

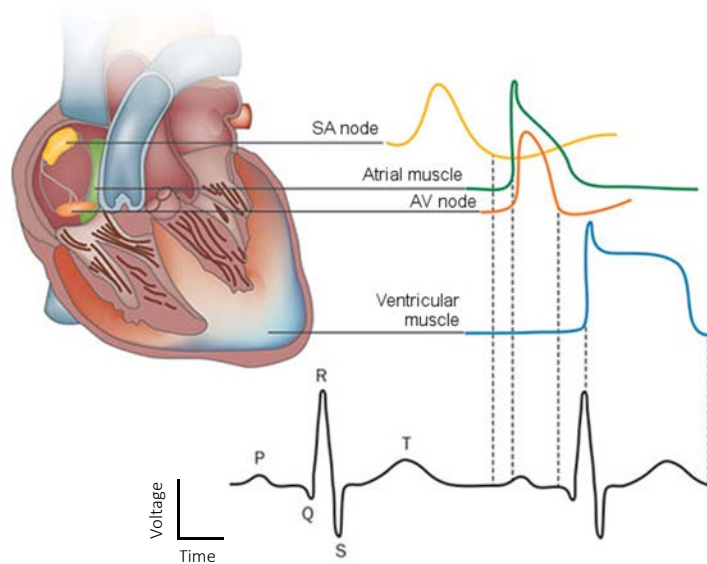


Figure 1.4. Normal electrical activity of the heart recorded by a surface electrocardiogram (ECG). Schematic representation of the cardiac conduction system, and the correlation between the action potentials of cardiomyocytes in distinct regions of the heart and a surface ECG. SA: Sinoatrial; AV: atrioventricular. *Adapted from Giudicessi et al.*²².

In normal physiologic conditions, the dominant pacemaker in the adult heart is the sinoatrial node, which fires at a rate between 60 and 100 beats/min. However, the cardiac rhythm can be modulated by sympathetic and parasympathetic afferent innervation, and by local changes produced by perfusion and/or chemical environment. At resting conditions, modulation by the parasympathetic nervous system slows the sinoatrial node rate to about 75 beats/min, which is the normal resting heart rate¹⁶.

Among all the cell types composing the heart, cardiomyocytes are responsible for the permanent blood flow through coordinated heart contractions. The electrical impulses that drive those coordinated contractions depend on action potentials generated by individual cardiomyocytes, which sequentially open and close multiple ion channels²². Briefly, an action potential is initiated when the membrane potential (dominated by K^+ equilibrium, phase 4 in **Figure 1.5**) is shifted towards a more positive value (from -90 mV to about -60 mV) mainly due to an electrical impulse transmitted by a neighboring cell. At this threshold potential, voltage-gated fast Na^+ channels open and Na^+ rapidly crosses the cellular membrane (phase 0, **Figure 1.5**), as the cytosol is electrically more negative than extracellular fluid and Na^+ concentration is higher in the extracellular fluid¹⁶. This depolarization is followed by a rapid repolarization through transiently activating and inactivating outward K^+ channels (phase 1 in **Figure 1.5**) and a plateau phase (phase 2 in **Figure 1.5**), which is mainly determined by the entry of Ca^{2+} through voltage-gated L-type calcium channels. This entry of Ca^{2+} activates Ca^{2+} -dependent ryanodine receptors (RyR) located in the sarcoplasmic reticulum (SR).

is the internal storage site for Ca^{2+} , and activation of RyR initiates the coordinated release of Ca^{2+} from the SR through a process called calcium-induced calcium release²⁴. Therefore, the intracellular increase of Ca^{2+} is not only mediated by its influx from the extracellular fluid, but also by its release from the sarcoplasmic reticulum. Then, repolarization is initiated by the inactivation of calcium channels and opening of voltage-gated K^+ channels, which increase net outward potassium currents (phase 3 in **Figure 1.5**). Finally, the resting membrane potential is restored to -90 mV by inwardly-rectifying potassium channels (phase 4 in **Figure 1.5**)^{16,25}.

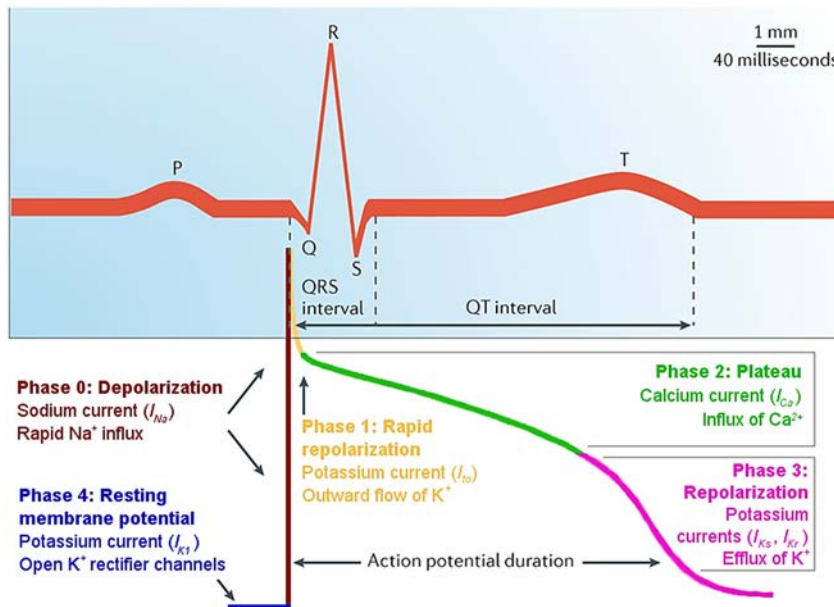


Figure 1.5. Temporal correlation between action potential duration and the QT interval on a surface electrocardiogram (ECG). Numerous inward and outward ionic currents determine the morphology, duration, and phases of the action potential of ventricular cardiomyocytes. The QRS complex is produced by the upstroke (phase 0) of the action potential, and S-T segment corresponds to the plateau (phase 2). The T-wave is indicative of ventricular repolarization (phase 3), and the resting membrane potential corresponds to phase 4. *Adapted from Fermi et al.*²⁵.

Due to its continuous contractile activity, cardiomyocytes are the most metabolically active cells in the human body²⁶, so they have high oxygen and nutrients demand^{27,28,29}. Morphologically, adult cardiomyocytes are highly anisotropic, adopting elongated and rod shapes with an aspect ratio of about 7:1 (length to width; about 120 μm in length and 20-30 μm in diameter) (**Figure 1.6A**)^{30,31,32}. Cardiomyocytes are mainly cylindrical, but can also include short branch-like projections (**Figure 1.6A-B**)³³. Importantly, they are longitudinally aligned in the context of the cardiac tissue, facilitating fast electrical conduction and efficient muscle contraction via intercalated discs^{34,35}. Intercalated discs are a specific type of cell-cell junction found at the bipolar ends of the adult rod-shaped cardiomyocytes, and provide robust mechanical and electrical

coupling between myocytes (**Figure 1.6A and C**)^{36,37}. Intercalated discs allow the formation of oriented cellular networks through three types of intercellular junctions located in them: adherens junctions, which anchor actin filaments through transmembrane linkers (cadherins); desmosomes, which anchor intermediate filaments; and gap junctions, which mediate ion transfer^{38,39}. While adherens junctions and desmosomes are involved in mechanical coupling through transmission of contractile forces, gap junctions maintain the electrical coupling between cardiomyocytes, which then work as a functional syncytium through electrical impulse propagation^{40,36}.

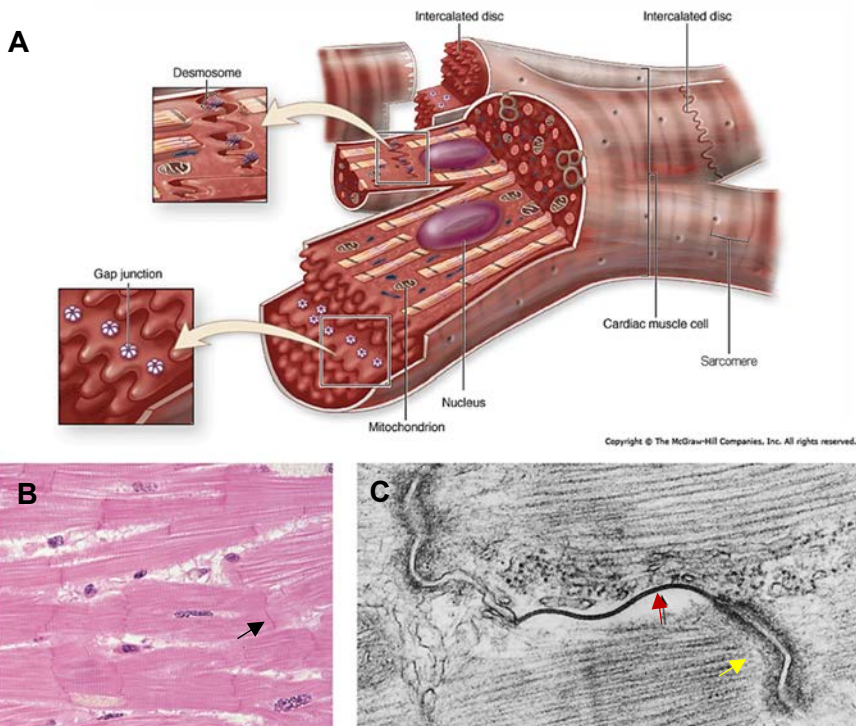


Figure 1.6. Cardiomyocytes forming cardiac muscle fibers. **A**, Diagram of cardiomyocytes connected by intercalated discs comprising desmosomes, gap junctions and adherens junctions. *Adapted from Mescher*³⁵. **B**, Longitudinal cross-section of cardiac muscle, where branch-like projections, intercalated discs (black arrow) and sarcomeres (striations) are displayed. *Adapted from Gartner et al.*³⁹. **C**, Transmission electron micrograph of an intercalated disc, where a gap junction (red arrow) and a desmosome (yellow arrow) are shown. *Adapted from Gartner et al.*³⁹.

The contractile function of cardiomyocytes is mediated by a highly organized contractile apparatus, a cytoskeletal lattice of proteins that appears as striations under the microscope (**Figure 1.6B**). The fundamental unit of the contractile apparatus is the sarcomere, a repeating micrometer-sized element found at regular intervals that dominates the anatomy of cardiac muscle⁴¹. A sarcomere is defined as the arrangement of contractile proteins that resides between two consecutive Z-discs along a muscle fiber (**Figure 1.7**). Z-discs are structures formed by a transverse matrix of α -actinin and

actin proteins. Actin thin filaments are anchored on each face of Z-discs, while myosin thick filaments sit in the center of each sarcomere and extend toward the Z-discs^{33,41}. Muscle contraction occurs when myosin filaments use ATPase-generated force to pull the thin filaments, sliding the two types of filaments across each other to reduce sarcomere length⁴².

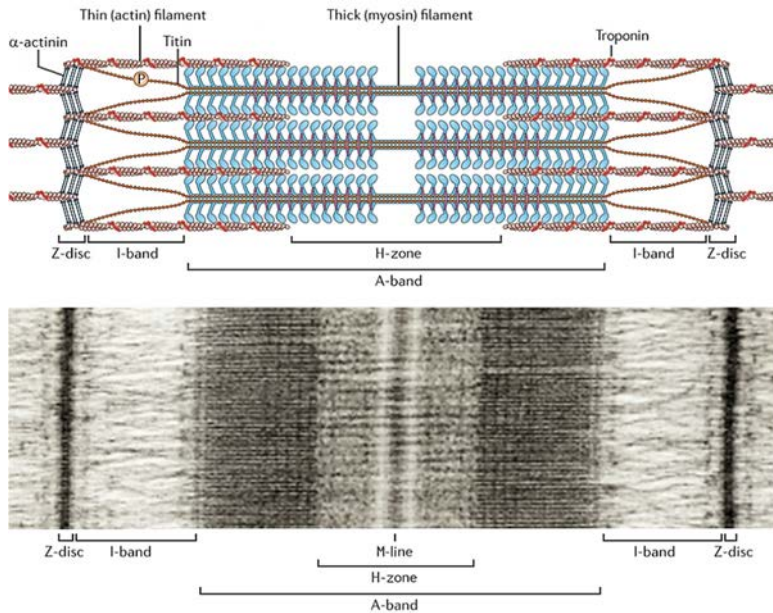


Figure 1.7. Basic structure of the sarcomere. **A**, Diagram of sarcomere structure showing thin actin filaments, thick myosin filaments and other cardiac regulatory proteins. The sarcomere is limited by two Z-discs. *Adapted from Hwang et al.*⁴¹. **B**, Transmission electron micrograph of a sarcomere showing dark and light bands that correspond to actin and myosin filaments distribution. *Adapted from Mescher*³⁵.

Among sarcomeric proteins composing thin filaments, the regulatory tropomyosin-troponin complex is of special importance. Tropomyosin is a double-stranded protein that spans seven actin monomers, and troponin is a globular protein complex constituted by three subunits: troponin C (TNC), a calcium-binding subunit; troponin I (TNI), that inhibits muscle contraction; and troponin T (TNT), which connects the troponin complex to tropomyosin and actin. At resting Ca^{2+} concentrations, the troponin complex maintains tropomyosin in a “blocked” state that avoids the interaction between actin and myosin⁴³. When intracellular Ca^{2+} concentration increases, a conformational change in troponin complex allows tropomyosin to shift into “open” position, thus promoting strong actin-myosin binding, the shortening of the sarcomere and triggering muscle contraction⁴⁴. The process through which an electrical impulse (excitation, membrane depolarization) stimulates the movement of Ca^{2+} to activate muscle contraction is known as cardiac excitation-contraction coupling. Finally, there is a reduction in cytosolic Ca^{2+} through sarcolemmal $\text{Na}^+/\text{Ca}^{2+}$ -exchanger, which

transports Ca^{2+} out of the cell, and sarco/endoplasmic reticulum Ca^{2+} -ATPase (SERCA), which actively pumps Ca^{2+} into the sarcoplasmic reticulum. Consequently, Ca^{2+} is dissociated from TNC, TNI inhibition is reestablished and muscle relaxes⁴⁵. Thus, the sarcomere is in a dynamic equilibrium between relaxation and contraction, with calcium concentrations shifting the balance⁴¹.

1.1.2. Cardiomyocyte development and maturation

From the embryonic heart until the adult organ, cardiomyocytes go through a complex series of structural and physiological changes that ultimately lead to their adult phenotype. Thus, fetal and neonatal cardiomyocytes differ considerably from adult morphology and physiology in several aspects, which are reviewed below. However, there is currently no clear agreement about what constitutes a mature cardiomyocyte, or which specific marker can accurately track the differentiation status of myocytes⁴⁶.

1.1.2.1. Morphology, orientation and proliferation

Adult cardiomyocytes (CM) are typically rod-shaped with an aspect ratio of about 7:1 (length to width) (**Figure 1.6**). *In vivo*, immature cardiomyocytes are also rod shaped, but they are smaller in size and have lower aspect ratios.^{31,32} Interestingly, this distinction becomes more apparent upon dissociation and *in vitro* culture: the high degree of internal organization of adult cardiomyocytes enables them to maintain their rod shape in short-term culture, while immature cardiomyocytes flatten, adopt spherical or polygonal shapes and spread in all directions^{40,47}. In culture, it has been reported that human adult ventricular CMs have surface areas ranging from 10212 to 14418 μm^2 , whereas human fetal cardiomyocytes have surface areas ranging from 1171 to 1261 μm^2 , thus being about ten times smaller^{48,49}. Regarding their alignment and orientation, adult CMs are longitudinally aligned in the context of the *in vivo* cardiac tissue, forming aligned myofibers that promote fast electrical conduction and efficient muscle contraction^{50,51}. Conversely, fetal cardiomyocytes and monolayers of human embryonic stem-cell derived cardiomyocytes (hESC-CM) are chaotically organized⁵².

During heart development, the proliferative capacity of cardiomyocytes decreases⁴⁷. The growth of embryonic and fetal heart is mainly achieved through cardiomyocyte proliferation⁵³. However, as postnatal human cardiomyocytes mature, they increase in size from 30- to 40-fold through a process called physiological hypertrophy^{40,54,55}. Two hypertrophic phenotypes have been identified: concentric hypertrophy, consisting in addition of sarcomeres in parallel due to pressure overload (lateral growth); and eccentric hypertrophy, consisting in addition of sarcomere in series due to volume overload (longitudinal growth)⁵⁶. Physiological hypertrophy enables cardiomyocytes to increase their work output, which improves cardiac pump function.

The cease of proliferation and initiation of hypertrophy processes implies that cardiomyocytes withdraw from the cell cycle, indicating a terminal differentiation state^{57,58}. The adult heart is predominantly composed of terminally differentiated cardiomyocytes that do not reenter the cell cycle, although a limited capacity to proliferate has been demonstrated⁵⁹. Besides, a minority of resident stem cells have been identified, which are self-renewing and multipotent cells that support heart regeneration to some extent^{60,58}. Another phenomenon that occurs as cardiomyocytes shift to a non-proliferative state is binucleation. Usually, cardiomyocytes have a single nucleus centrally located, but ~25% of cardiomyocytes become binucleated and are maintained through adulthood^{54,59}. Therefore, the number of nuclei per cell can distinguish adult and fetal cardiomyocytes, as the latter are almost exclusively mononucleated⁵².

1.1.2.2. Structural properties

As previously described, the sarcomere is the fundamental unit of the contractile apparatus of cardiomyocytes, composed of proteins that form thick and thin filaments (**Figure 1.7**). In the human fetal heart, this unit is organized during development, with Z-discs and I-bands forming first and H-, A- and M-bands afterwards⁶¹. Sarcomeric length, width⁶², abundance and alignment all increase with cardiomyocyte maturity. For example, adult cardiomyocytes contain considerably longer sarcomeres than both fetal and human pluripotent stem cell-derived cardiomyocytes (hPSC-CM)⁶³. The average length of sarcomere in relaxed adult cardiomyocytes is of about 2.0-2.2 μm ⁶⁴, while in fetal cardiomyocytes is around 1.8 μm ⁴⁹. The sarcomerogenesis process also occurs in maturing hPSC-CM; however, in most cells only Z-discs are formed, and sarcomeres are 25-30% shorter than in adult cardiomyocytes and 6-11% shorter than in fetal cardiomyocytes (1.6-1.7 μm)^{63,65}.

Myofibrils composing adult cardiomyocytes have near perfect alignment of distinct, abundant and well-developed sarcomeres, with highly aligned and organized Z-disc structures of uniform width⁴⁷. Moreover, they show a high density of sarcomeres that occupy almost the entire area of their cytoplasm, whereas fetal cardiomyocytes display lower densities of poorly organized sarcomeres than their adult counterparts⁶⁶. hPSC-CM display underdeveloped sarcomeric structures with a reduced organization and alignment compared with fetal cardiomyocytes. Besides, they show an uneven distribution of sarcomeres throughout the cell, with Z-discs of variable widths⁶⁷.

Regarding cell-cell junctions, adult cardiomyocytes are interconnected at their longitudinally edge by intercalated discs (**Figure 1.6C**). Among protein structures composing intercalated discs, gap junctions and adherens junctions are of special interest in human cardiomyocyte development. Gap junctions are closely-packed

clusters of transmembrane intercellular channels that enable the rapid propagation of the action potential, and the predominant protein is connexin 43 (encoded by *GJA1* gene)⁶⁸. Regarding adherens junctions, they enable the transmission of contractile force from one cell to another, and one of their major constituents is the protein N-cadherin³⁸. In adult cardiomyocytes, connexin 43 and N-cadherin accumulate at intercalated discs, whereas in fetal cardiomyocytes and hPSC-CM they are distributed around all sides of the membrane, often establishing gap junctions at the lateral borders^{69,70}. The localization of connexin 43 and N-cadherin at intercalated discs has been related to faster conduction velocities⁷¹, thus supporting the notion of an immature phenotype for cardiomyocytes with those proteins randomly distributed throughout the membrane.

1.1.2.3. Myofibrillar protein isoforms switch

Several myofibrillar proteins assembled in the sarcomeres undergo an isoform switch, having an impact on the contractile function of cardiomyocytes. One of those proteins is titin (encoded by the *TNN* gene), which is involved in the maintenance of sarcomere integrity and elasticity⁷². Titin shifts from a long isoform (fetal cardiac titin, FTC) to two adult isoforms: a long and relatively compliant isoform (N2BA) and a shorter and stiffer isoform (N2B)^{73,74}. Functionally, the switch from the compliant FTC isoform to stiffer adult isoforms regulates the passive tension of maturing cardiomyocytes^{75,76}.

In human cardiomyocytes, cardiac muscle myosin is a hexamer composed by two heavy chains and four light chains. Myosin heavy chain (MHC) and myosin light chain (MLC) also undergo a developmentally regulated isoform switching. The slow β -heavy chain subunit of cardiac myosin (β -MHC, encoded by *MYH7* gene) is the mainly isoform expressed at all stages, but there is more atrial (fast) α -heavy chain subunit of cardiac myosin (α -MHC, encoded by *MYH6*) in fetal than in adult hearts^{77,78}. Interestingly, the ratio of β -MHC/ α -MHC in hPSC-CM is different from fetal and adult ventricular cardiomyocytes, and it changes little over time. A possible explanation for this may be that hPSC-CM are often a mixture of atrial and ventricular cardiomyocytes^{63,79}. In rodents, there is also a switch from β -MHC before birth to α -MHC after birth, which correlates with postnatal heart rate increase⁸⁰. Regarding MLC proteins, the two predominant isoforms are the atrial isoform of the regulatory myosin light chain (MLC2a, encoded by *MYL7* gene) and the ventricular isoform of the regulatory myosin light chain (MLC2v, encoded by *MYL2* gene). In fetal human hearts, the isoform MLC2a is expressed in all chambers, whereas in adult hearts it is restricted to the atria. As human cardiomyocytes mature, MLC2a expression gradually decreases in human fetal ventricle, finally leading to an almost exclusively expression of MLC2v isoform, which is restricted to the ventricles throughout development and adulthood^{81,82,83}. In hPSC-CM both MLC isoforms are expressed, probably due to the presence of multiple cardiomyocyte subpopulations as previously commented.

Troponin I also presents two isoforms that are sequentially expressed in the developing heart: the slow skeletal troponin I (ssTnI, encoded by *TNNI1* gene) and the cardiac troponin I (cTnI, encoded by *TNNI3*). Fetal cardiomyocytes express ssTnI protein, and shortly after birth this isoform is completely and irreversibly shifted to cTnI, which is the isoform present in adult hearts. From a functional point of view, each isoform has a different Ca^{2+} binding kinetics and cardiac muscle relaxation rates^{84,85}.

1.1.2.4. Functional properties

The generation of action potentials (AP) in adult cardiomyocytes requires the orchestrated activity of several ion channels (**Figure 1.5**). During fetal and postnatal heart development, these channels undergo developmental changes that lead to the acquisition and maintenance of a cardiac phenotype electrophysiologically mature⁴⁰. Specifically, adult and fetal cardiomyocytes differ in the availability of their ion channels, which results in different AP profiles. For example, adult cardiomyocytes exhibit a stable resting membrane potential at -90 mV thanks to the activity of the rectifying K^+ current (I_{K1}) (**Figure 1.5**)⁸⁶. Conversely, immature cardiomyocytes exhibit very low levels of K^+ rectifying channel (its α -subunit Kir2.1 being encoded by *KCNJ2* gene), resulting in less negative resting membrane potentials (about -60 mV) than adult cardiomyocytes^{87,88}. This low or absent I_{K1} current is one of the reasons why immature cardiomyocytes, such as hPSC-CM, exhibit gradual diastolic depolarization and, consequently, show spontaneous contractile activity⁶³. Another ionic channel that is developmentally regulated is the voltage-gated Na^+ channel (its α -subunit Nav1.5 being encoded by *SCN5A* gene), which contributes to the I_{Na} current (**Figure 1.5**). Immature cardiomyocytes such as fetal and hPSC-CM express lower levels of Nav1.5 compared with their adult counterparts, resulting in a 6- to 50-fold slower depolarization velocity than human adult cardiac tissue^{88,89}.

Regarding Ca^{2+} handling and excitation-contraction coupling, it is an extremely efficient process in adult cardiomyocytes, while in fetal cardiomyocytes and hPSC-CM kinetics are slow and amplitudes are small^{90,91}. In adult cardiomyocytes, calcium-induced calcium release from the sarcoplasmic reticulum (SR) contributes to almost 70% of the total Ca^{2+} release, whereas fetal cardiomyocytes have underdeveloped SR with a limited capacity to load Ca^{2+} ^{92,93}. Similar to fetal cardiomyocytes, hPSC-CM have very little SR function and, although SR-mediated Ca^{2+} release has been described, Ca^{2+} intrusion in those cells may be deeply dependent on L-type calcium channels (**Figure 1.8**)^{91,94,95}. Consequently, immature cardiomyocytes display an abnormal diffusion of Ca^{2+} in the cell, causing for example greater Ca^{2+} transient peak amplitudes in the cell periphery than in the center, thus reducing the contractile synchrony, which is necessary for the generation of large contractile forces^{96,47}.

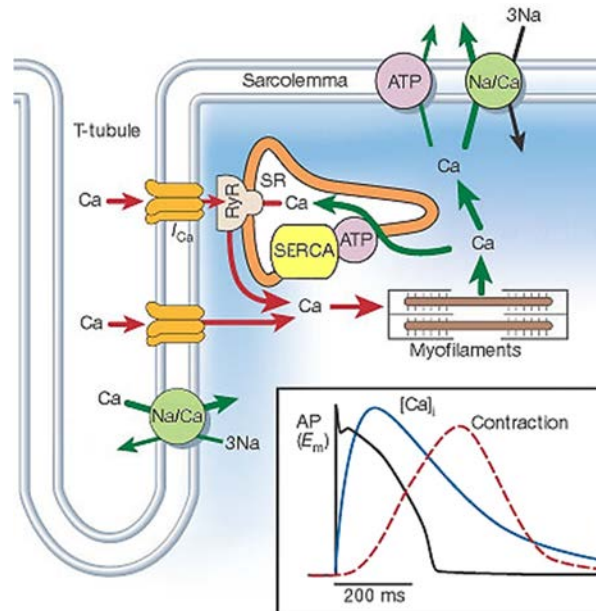


Figure 1.8. Diagram of Ca^{2+} transport in ventricular cardiomyocytes. Inset shows the time course of an action potential, Ca^{2+} transients and contraction measured in a rabbit ventricular myocyte at 37°C . L-type calcium channels are also detailed (orange). RyR: ryanodine receptor; SR: sarcoplasmic reticulum; Na/Ca: $\text{Na}^+/\text{Ca}^{2+}$ - exchanger; SERCA: sarco/endoplasmic reticulum Ca^{2+} -ATPase; ATP: ATPase; AP: action potential. *Adapted from Bers*⁹².

Another component of the Ca^{2+} handling system that is missing in fetal cardiomyocytes and hPSC-CM in comparison with adult cardiomyocytes are transverse tubules (T-tubules) (**Figure 1.8**). T-tubules are invaginations of the membrane where L-type Ca^{2+} channels concentrate, near RyR channels, and they are responsible of fast excitation-contraction coupling and synchronized contraction in adult cardiomyocytes. Therefore, their absence in fetal cardiomyocytes and hPSC-CM, together with the low expression of important proteins related to calcium handling (e.g. calsequestrin and ryanodine receptors), result in a slower excitation-contraction coupling^{97,98}.

An important functional parameter that is also developmentally regulated is the contractile force of cardiomyocytes, as adult myocardium develops more force than fetal myocardium⁴⁷. At tissue level, a peak twitch tension of $44.0 \pm 11.7 \text{ mN/mm}^2$ was reported for strips of adult human myocardium, whereas forces of $0.8\text{-}1.7 \text{ mN/mm}^2$ were reported for strips of newborn ventricular muscle^{99,100}. At cellular level, active forces of $10\text{-}50 \text{ mN/mm}^2$ have been found for adult ventricular cardiomyocytes⁵². When measured under similar substrate conditions, fetal cardiomyocytes generate contractile stresses of $\sim 0.4 \text{ mN/mm}^2$, and hPSC-CM of $0.15\text{-}0.30 \text{ mN/mm}^2$ ⁴⁷. Regarding passive forces (resulting from myofibrillar compliance), adult myocardium typically exhibits a positive force-frequency relationship, that is, an increase of force with increasing beating

frequency. Neonatal myocardium has a flat or slightly negative force-frequency relationship that becomes positive with age, and both fetal cardiomyocytes and hPSC-CM have a negative force-frequency relationship, mainly due to the already mentioned insufficiencies in Ca^{2+} handling^{92,100,101}. Finally, the adult heart presents a positive Frank-Starling relationship, which is an increase of force of contraction after increasing fiber length. This mechanism is associated with an increase in Ca^{2+} sensitivity, appears in human fetal heart after 10-15 weeks of gestation^{102,103} and has been observed in some preparations containing hPSC-CM^{104,105}.

1.1.2.5. Pharmacological response

Taking into account all the above-mentioned differences between immature and mature cardiomyocytes, it is to be expected that they also respond differently to pharmacological stimulations. In fact, it has become apparent that the developmental stage of cardiomyocytes affects their sensitivity and response to many pharmacological agents (summarized in **Table 1.1**)¹⁰⁶. Some of the effects of drugs on cardiomyocyte function are designated inotropic, chronotropic, lusitropic, and dromotropic. An inotropic response refers to a change in cardiomyocyte force of contraction, while a chronotropic response refers to a change in the beating rate. Lusitropic effects involve a change in the rate of cardiomyocyte relaxation, and dromotropic effects involve a change in the conduction velocity, that is, the rate of electrical impulses.

The response to β -adrenergic receptors stimulation is considered a measure of cardiomyocytes maturity. Epinephrine and norepinephrine are natural catecholamines, while isoproterenol is a synthetic catecholamine. Catecholamines are agonists of adrenergic receptors, so they stimulate the sympathetic nervous system and regulate several functions in the organism, such as cardiac muscle contraction. In the adult myocardium, β -adrenergic stimulation induces positive inotropic, chronotropic and lusitropic effects¹⁰⁷. This response requires a mature and functional sarcoplasmic reticulum to occur, as a rapid release of high amounts of Ca^{2+} is needed¹⁰⁸. In immature cardiomyocytes, the positive inotropic response is often less pronounced than in adult hearts¹⁰⁹, and a chronotropic response is usually observed in the absence of an inotropic response¹⁰⁵. For example, one study found that isoproterenol induced a dose-dependent chronotropic effect on the spontaneous beating of human embryonic stem cell-derived cardiomyocytes (hESC-CM), but did not change the developed isometric force. This lack of inotropic response despite an important chronotropic response could be explained by the immaturity of the sarcoplasmic reticulum¹¹⁰. Conversely, other studies found inotropic effects for norepinephrine, epinephrine and isoproterenol in single hPSC-CM using atomic force microscopy or a video-edge detecting system^{111,112}. On the whole, hPSC-CM display smaller responses to β -adrenergic stimulation than adult cardiomyocytes¹¹³, but more studies are needed to clarify this issue.

Another pharmacological agent frequently used to analyze cardiomyocyte maturity is the cholinergic agonist carbachol. Carbachol binds with high affinity to cholinergic receptors, which induce a negative chronotropic, dromotropic and inotropic response in adult human cardiac preparations. In human fetal ventricular cells and hESC-CM, carbachol displays similar negative chronotropic effects than their adult counterparts^{47,114}, but still in hESC-CM dromotropic and inotropic effects are not evidenced.

Drug name	Target	Effect in human adult CM/ myocardium	Effect in human fetal CM/myocardium	Effect in hPSC-CM
Isoproterenol (ISO) Epinephrine (EPI) Norepinephrine (NOR)	β -adrenergic receptor agonist	<ul style="list-style-type: none"> Positive inotropic, chronotropic, lusitropic¹⁰⁷ Right-shifted force-Ca²⁺ relationship (3 μM ISO; RV trabecular intact muscle)¹¹⁵ EC₅₀=11-80 nM (ISO; LV muscle strips)^{47,116} EC₅₀=1.21-2.43 μM (NOR; LV papillary muscle strips)¹¹⁶ 	<ul style="list-style-type: none"> Positive inotropic (NOR, ISO; fetal atria)¹¹⁷ Gestation-dependent \uparrow in inotropic effects (0.1 μM ISO; fetal atria)¹¹⁷ \uparrow Ca²⁺ transient peak and decay (ISO; monolayer)¹¹⁸ Positive chronotropic (EPI, NOR, ISO; fetal heart)¹¹⁹ 	<ul style="list-style-type: none"> Positive chronotropic (ISO; hESC-CM)^{105,114} EC₅₀=12.9 nM (ISO; chronotropic; hESC-CM)¹²⁰
Carbachol	Cholinergic agonist	<ul style="list-style-type: none"> Negative inotropic, chronotropic, dromotropic^{47,121} EC₅₀=140 nM (inotropic; LV papillary muscle strips)¹²² 	<ul style="list-style-type: none"> Negative inotropic (0.1-10 μM; 12-20 week hearts)¹²³ Negative chronotropic (100 μM; 16-17 week CM)¹¹⁴ Gestation-dependent \downarrow in repolarization time¹²³ 	<ul style="list-style-type: none"> Negative chronotropic (hESC-CM)¹¹⁴
Verapamil	K _v 11.1 (hERG) & Ca _v 1.2 channel antagonist	<ul style="list-style-type: none"> Negative inotropic, chronotropic, dromotropic⁴⁷ IC₅₀=143 nM (K_v11.1; transfected cell line)¹²⁴ IC₅₀=0.24-4.3 μM (Ca_v1.2; transfected cell line)^{47,125} IC₅₀=0.32-1.21 μM (inotropic; LV papillary muscle strips)¹²⁶ IC₅₀=89-170 nM (inotropic; RA trabecular muscle strips)¹²⁷ 	<ul style="list-style-type: none"> Blocked AP propagation (5 μM; 16-17 week ventricular CM)¹¹⁴ 	<ul style="list-style-type: none"> Blocked AP propagation (5 μM; hESC-CM)¹¹⁴ Negative inotropic, positive chronotropic, \downarrowFPD (0.01-0.3 μM; hiPSC-CM monolayer)¹²⁴ Negative chronotropic, \downarrowFPD (1-5 μM; hiPSC-CM clusters)¹²⁸ IC₅₀=62-80 nM (hiPSC-CM monolayer)¹²⁹ IC₅₀=73-120 nM (hESC-CM monolayer)¹²⁹
Nifedipine	L-type Ca ²⁺ channel antagonist	<ul style="list-style-type: none"> Negative inotropic¹²⁶ IC₅₀=16-24 nM (Ca_v1.2; transfected cell line)¹²⁵ IC₅₀=50-200 nM (inotropic; ventricular muscle)^{47,126} IC₅₀=76-166 nM (inotropic; RA trabecular muscle strips)¹²⁷ 	<ul style="list-style-type: none"> Negative inotropic (10-20 μM; 7-9 week beating clusters)¹³⁰ Blocked L-type Ca²⁺ current (10 μM; 20 week CM)¹³¹ 	<ul style="list-style-type: none"> Negative inotropic, positive chronotropic, \downarrowFPD (0.003-1 μM; hiPSC-CM monolayer)¹²⁴ \downarrowAPD (1 μM; hESC and hiPSC-CM)¹³² Blocked AP propagation (10 μM; hESC and hiPSC-CM)¹³² IC₅₀=39 nM (hiPSC-CM)¹³³ IC₅₀=2-4 nM (hiPSC-CM monolayer)¹²⁹ IC₅₀=5-7 nM (hESC-CM monolayer)¹²⁹
Nisoldipine	Ca _v 1.2 channel antagonist	<ul style="list-style-type: none"> Negative inotropic (ventricular muscle)¹³⁴ IC₅₀=67-81 nM (Ca_v1.2; transfected cell line)¹³⁵ IC₅₀=200-400 nM (inotropic; ventricle)¹³⁴ 	<ul style="list-style-type: none"> Blocked L-type Ca²⁺ current (1-2 μM; 13-24 week CM)¹³⁶ 	<ul style="list-style-type: none"> Inhibition of AP propagation and contraction (1 μM; hESC-CM)⁵⁰

INTRODUCTION

Tetrodotoxin (TTX)	Nav1.5 channel antagonist	<ul style="list-style-type: none"> Negative chronotropic¹³⁷ ↑APD, ↓V_{max} (2 μM; papillary muscle)¹³⁸ IC₅₀ ≥ 1 μM¹³⁹ 	<ul style="list-style-type: none"> Insensitive to TTX (10 μM; 10 week ventricular CM)¹⁴⁰ Cessation of contraction (0.63 μM; 13-15 week LA)¹⁴¹ 	<ul style="list-style-type: none"> Blocked AP propagation in a subset of cells (100 μM; hiPSC-CM)¹³² Blocked AP propagation in most cells (10 μM; hESC-CM)¹³²
Caffeine	Ryanodine receptor agonist	<ul style="list-style-type: none"> Positive inotropic, chronotropic¹⁴² Left-shifted force-Ca²⁺ relationship (10 mM; RV trabecular intact muscle)¹¹⁵ 	<ul style="list-style-type: none"> ↑Ca²⁺ transient amplitude in subset of cells (10 mM; 65%; 16-18 week LV CM)¹⁴³ 	<ul style="list-style-type: none"> ↑Ca²⁺ transient amplitude (10-40 mM; hiPSC-CM)⁹⁴ ↑Ca²⁺ transient amplitude in subset of cells (10 mM; 35-40%; hESC-CM)¹⁴³
E-4031	Kv11.1 (hERG) channel antagonist	<ul style="list-style-type: none"> ↑APD¹⁴⁴ ↓I_K current amplitude (5 μM; RV CM)¹⁴⁴ IC₅₀=7–32 nM (Kv11.1; transfected cell line)^{47,124} 	<ul style="list-style-type: none"> Gestation-dependent effect on APD (1 μM; 5 week CM, no effect on APD; 7.5-9.5 week CM, ↑APD)¹⁴⁵ Irregular AP pattern (1 μM; week 5-9.5 CM)¹⁴⁵ ↓AP amplitude and ↑inter AP interval (1 μM; weeks 5-7 fetal CM)¹⁴⁵ 	<ul style="list-style-type: none"> ↑APD, EADs and ↑short-term variability in APD (1 μM; hESC-CM)¹⁴⁶ ↑APD and EADs (12 nM; hiPSC-CM clusters)¹⁴⁷
Terfenadine	K ⁺ , Na ⁺ and Ca ²⁺ cardiac ion channel antagonist	<ul style="list-style-type: none"> ↓I_K current, ↑current decay rate and ↓current amplitude (3 μM; Kv1.5; transfected cell line, whole cell)¹⁴⁸ IC₅₀=367 nM (Kv1.5; cell patch, transfected cell line)¹⁴⁸ IC₅₀=26 nM (Kv11.1; atrial CM)¹⁴⁹ Blocked I_{Kr} and I_{to} currents (atrial CM and Kv1.5; transfected cell line)¹⁵⁰ Frequency-dependent inhibition of L-type Ca²⁺ current¹⁵¹ ↑I_{NCX} current frequency (1 μM; atrial CM)¹⁵¹ IC₅₀=1.7-8.1 μM (Na_v1.5; atrial CM)¹⁴⁹ 		<ul style="list-style-type: none"> ↑APD (30 nM; hiPSC-CM)¹³³ ↑FPD (100 nM; hiPSC-CM monolayer)¹²⁴ ↓AP amplitude (1 μM; hiPSC-CM monolayer)¹²⁴ Negative chronotropic (0.01–0.3 μM; hiPSC-CM monolayer)¹⁵² Time- and dose-dependent irregular AP pattern (0.3 μM; hiPSC-CM monolayer)¹⁵² Blocked AP propagation (≥1 μM; hiPSC-CM monolayer)¹⁵²
Thapsigargin	SERCA antagonist	<ul style="list-style-type: none"> Negative inotropic¹⁵³ Negative inotropic at high frequency, resulting in flattened FFR (1 μM; LV CM)¹⁵⁴ 		<ul style="list-style-type: none"> ↓Ca²⁺ transient amplitude (1-20 μM; hiPSC-CM)⁹⁴ ↓Ca²⁺ transient amplitude a subset of cells (0.5 μM; 35-40%; hESC-CM)¹⁴³ ↓Max Ca²⁺ decay velocity (0.5 μM; hESC-CM)¹⁴³
Lidocaine	Na ⁺ channel antagonist	<ul style="list-style-type: none"> ↑APD, ↓V_{max} (ventricular muscle)¹⁵⁵ IC₅₀=34–38 μM (Na⁺ current; transfected cell line)¹⁵⁶ 		<ul style="list-style-type: none"> Blocked Na⁺ influx, ↓CV (hiPSC-CM)¹²⁸ Blocked AP propagation (50 μM; hiPSC-CM)¹³² Blocked AP propagation (1 mM; hESC-CM)¹³² ↓V_{max}, ↑APD and MDP depolarization (500 μM; hESC-CM)¹³²

Table 1.1. Comparison of the pharmacological responses of human adult and fetal CM/myocardium and hPSC-CM. CM: cardiomyocytes; hPSC-CM: human pluripotent stem cell-derived cardiomyocytes; hiPSC-CM: human induced pluripotent stem cell-derived cardiomyocytes; hESC-CM: human embryonic stem cell-derived cardiomyocytes; IC₅₀: half maximal inhibitory concentration; LV: left ventricle; RV: right ventricle; RA: right atria; LA: left atria; AP: action potential; APD: action potential duration; FPD: field potential duration; FFR: force-frequency relationship; EAD: early after depolarization; V_{max}: depolarization velocity; MDP: maximum diastolic potential; TTX: Tetrodotoxin. *Adapted from Feric et al.*⁴⁷.

Other drugs whose effect depends on cardiomyocyte maturity level are verapamil, nifedipine, nisoldipine, tetrodotoxin, caffeine, E-4031, terfenadine, thapsigargin, and lidocaine (**Table 1.1**). Verapamil inhibits $K_v11.1$ (human ether-a-go-go-related gene, hERG) and $Ca_v1.2$ channels, and induce negative dromotropic, chronotropic and inotropic effects in adult cardiac tissue⁴⁷. In fetal cardiomyocytes and hESC-CM, verapamil inhibits the propagation of action potentials, but fetal cardiomyocytes are more responsive¹¹⁴. Besides, verapamil induces a positive chronotropic effect in human induced pluripotent stem cell-derived cardiomyocytes (hiPSC-CM), which may be indicative of differences in Ca^{2+} handling^{124,152}.

Regarding nifedipine and nisoldipine, both are L-type Ca^{2+} channel antagonists and induce negative inotropic effects on adult cardiomyocytes^{126,134}. In immature cardiomyocytes such as hPSC-CM, nifedipine displays a dose-dependent decrease in action potential duration, as well as negative inotropic and positive chronotropic responses^{124,152}. Concerning nisoldipine, it inhibits action potential propagation and contraction in hESC-CM⁵⁰.

Drugs considered Na^+ channel antagonist include, among others, tetrodotoxin and lidocaine. Tetrodotoxin induces a negative chronotropic response in adult cardiomyocytes¹³⁷, and in fetal myocardium it either exerts no effect or induces cessation of contraction^{140,141}. In hPSC-CM, tetrodotoxin blocks action potential propagation, but effective concentrations and the number of responding cells vary among cell types¹³². Concerning lidocaine, it was demonstrated to prolong action potential duration and slow depolarization velocity in human ventricular muscle preparations¹⁵⁵. In hiPSC-CM, lidocaine blocked Na^+ influx, action potential propagation, and decreased conduction velocity, but did not affect action potential duration^{128,132}. However, in hESC-CM a decreased conduction velocity and prolonged action potential duration was observed¹³².

To evaluate sarcoplasmic reticulum (SR) functionality, thapsigargin and caffeine are some of the pharmacological agents of choice¹⁴³. Thapsigargin is an inhibitor of the SERCA Ca^{2+} reuptake pump of the SR (**Figure 1.8**). In adult cardiomyocytes, the depletion of Ca^{2+} from the SR induces a strong negative inotropic effect^{153,154}. In immature cardiomyocytes such as hESC-CM and hiPSC-CM, thapsigargin has more modest effects, displaying a decrease in Ca^{2+} transient amplitude at concentrations higher than $0.5 \mu M$ ^{94,143}. Regarding caffeine, it is an agonist of ryanodine receptors, which are the primary Ca^{2+} release channels in the SR (**Figure 1.8**)⁴⁷. In adult myocardium it induces positive chronotropic and inotropic effects¹⁴², while in immature cardiomyocytes the response is quite controverted. Some preparations of hESC-CM are insensitive to caffeine (10 mM)¹⁰⁸, while others respond to increasing caffeine concentrations with an increase in Ca^{2+} transient amplitude⁹⁴. Relative to fetal

cardiomyocytes, some works indicate that the increase in Ca^{2+} transient amplitude induced by 20 mM caffeine is significantly lower in hESC-CM¹⁵⁷, while others suggest that it is the same when treating with 10 mM caffeine, and the difference is the fraction of responsive cells¹⁴³.

E-4031 is an antagonist of the $\text{K}_v11.1$ (hERG) channel, which mediates the repolarizing current in the action potential (I_{Kr} , **Figure 1.5**). Inhibition of I_{Kr} increases the time between depolarization and repolarization, thus affecting action potential duration¹⁵². Although fetal cardiomyocytes and hPSC-CM are responsive to E-4031, the effects and the concentrations to trigger them differ from adult cardiomyocytes^{124,127,133}.

Finally, Terfenadine is an antihistamine that acts as an antagonist of K^+ , Na^+ , and Ca^{2+} cardiac ion channels, and it was withdrawn from the market due to unacceptable risk of arrhythmia⁴⁷. In adult human atrial cardiomyocytes, Terfenadine inhibits $\text{Na}_v1.5$ and L-type Ca^{2+} channels, and blocks the hERG current^{149,151}. In transfected cell lines expressing hERG channel, hERG blockage was also identified⁴⁷. In hPSC-CM, terfenadine treatment prolonged action potential duration, and induced a negative inotropic effect¹³³.

1.1.3. Cardiovascular diseases and heart failure

Cardiovascular diseases (CVDs) are the leading cause of mortality and morbidity worldwide, accounting for approximately 30% of all human mortality¹⁵⁸. CVDs include heart pathologies, brain vascular diseases and blood vessel disorders, and caused 17.5 million deaths in 2012, with ischemic heart disease accounting for 7.4 million deaths. Unfortunately, annual cardiovascular disease mortality is projected to increase from 17.5 million deaths in 2012 to 22.2 million in 2030^{159,160}.

One of the main reasons why diseases affecting the heart have such high mortality and morbidity is the heart tissue's minimal ability to repair following injury¹⁶¹. In the case of ischemic heart disease, partial or total blockage of coronary arteries limits blood supply and prevents the required oxygen and nutrients from reaching the heart tissue¹⁶². The lack of a constant oxygen supply causes death of cardiomyocytes and, consequently, an important loss of viable myocardium in the infarcted zone¹⁶³. A cascade of events are initiated in ischemic conditions, such as inflammation, weakening of the extracellular matrix and scar tissue formation (**Figure 1.9**). The scar is fibrous, non-elastic and non-contractile, and it affects the conductivity of the electric impulse. Therefore, there is an impairment of the heart's pumping function, which is compensated by the release of several neurohormones that increase heart rate, fluid retention and contractility¹⁶⁴. The maintenance of such situation for a long time can lead to progressive left ventricular remodeling, which is a modification of the normal

ventricular architecture in terms of volume, shape and wall thickness^{165,166}. This remodeling process implies ventricular wall thinning and dilation, which finally causes decompensation, ventricular arrhythmia and heart failure¹⁶² (**Figure 1.9**).

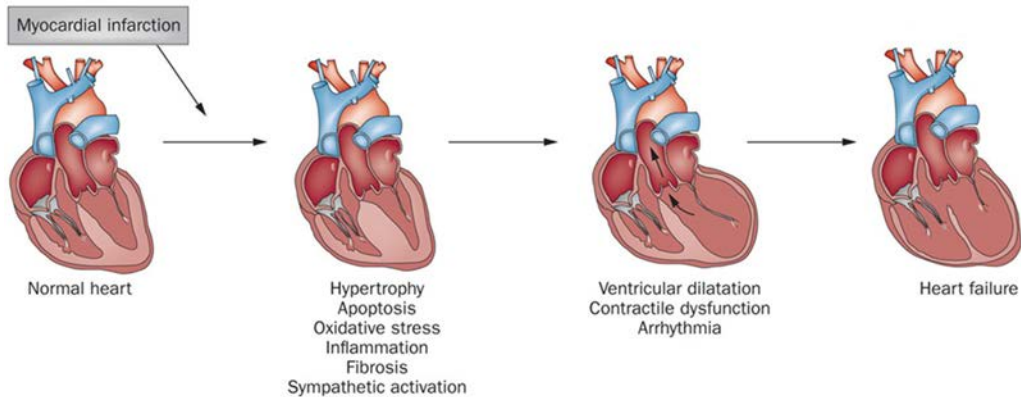


Figure 1.9. Pathologic cardiac remodelling and heart failure after myocardial infarction. The acute loss of myocardium results in the activation of remodelling mechanisms, which finally lead to decompensation, arrhythmia and heart failure. *Adapted from Jiang et al.*¹⁶⁶.

Medical advances in pharmacological, interventional and surgical cardiology have importantly decreased the mortality at the acute stage of myocardial infarction, as well as increased patients' life expectancy. However, current available therapies for end-stage heart failure are either limited or symptomatic, as they are not able to regenerate the diseased heart. Current treatments are based on pharmacological approaches, surgical interventions, left ventricular assist devices and heart transplantation. Drugs that reduce the heart work load (e.g. diuretics) and protect it from toxic humoral factors (e.g. β -blockers, spironolactone) are the current standard conservative treatment¹⁶⁷. Although pharmacological therapies can delay the progression to end-stage disease, they cannot prevent or reverse progression of the failing state¹⁶⁸. Moreover, over 50% of patients with heart disease do not respond to currently available drug therapies, thus evidencing their limitations¹⁶⁹. Regarding interventional therapies such as implantation of pacing devices or surgical procedures, they improve survival of patients¹⁷⁰ but neither avoid disease progression to the end stage nor regenerate the dead myocardium¹⁷¹. Therefore, the only curative treatment available for patients with severe heart failure is heart transplantation. Regrettably, donor unavailability and the side effects of long-term immunosuppression limit the treatment of patients suffering such disorders¹⁶⁸.

In view of this scenario, it is clear that there is an urgent need to develop alternative therapeutic strategies that potentiate heart regeneration or repair. Importantly, it is also crucial to develop new tools to study human cardiac physiology and pathophysiology *in vitro*. Having *in vitro* cardiac tissue analogues that capture the

complex features of the *in vivo* environment could improve the efficiency of the drug discovery process, as they would have better predictive capacity of potential adverse effects (e.g. cardiotoxicity)¹⁷². Besides, cardiac tissue analogues could be used to model cardiac diseases, thus enabling the development of therapies to prevent or cure them¹⁷³.

1.1.4. Alternative therapeutic strategies

1.1.4.1. Cell therapy

As previously mentioned, the regenerative capacity of the heart is very limited. Current therapies to treat heart failure after a myocardial infarction improve symptoms and prolong life of patients, but do not address the fundamental problem of massive loss of cardiomyocytes, vascular cells and interstitial cells¹⁷⁴. To increase the number of cardiomyocytes in the damaged zone and improve cardiac function, cell transplantation was conceived as a potential new therapy more than 15 years ago^{175,176}. However, regenerating heart tissue is a really challenging task: approximately 1 billion cardiomyocytes can be lost after an insult, supporting cells have also to be supplied, and the environmental cues required to guide transplanted cells into multicellular, three-dimensional heart structures might be absent^{177,178}.

Initial experimental studies were based on transplanting fetal, neonatal and adult cardiomyocytes in injured hearts, with encouraging results showing their capability to form stable grafts^{179,180}. However, these cell types are not suitable for large-scale clinical applications, as they have limited capacity for *ex vivo* expansion, limited availability, an allogeneic origin and possess ethical concerns¹⁸¹. Therefore, stem cells emerged as a promising human cell source for regenerative medicine applications. Multiple stem cell populations have been identified in a wide variety of adult tissues, such as skeletal and cardiac muscle, bone marrow, blood or adipose tissue. In addition, human pluripotent stem cells (hPSC) derived either from developing blastocysts (human embryonic stem cells, hESC) or from reprogrammed somatic cells (human induced pluripotent stem cells, hiPSC) also constitute an important source of human cardiomyocytes, as they have demonstrated an unprecedented cardiogenic potential. **Figure 1.10** summarizes cell types and mechanisms that have been proposed for cardiac stem cell therapy¹⁸², which will be explained in more detail below.

- Skeletal myoblasts

One of the first cellular therapies for cardiac regeneration consisted in the injection of autologous skeletal myoblasts into ischemic myocardium¹⁸³. Skeletal myoblasts give rise to skeletal muscle, are resistant to ischemia, can expand *in vitro*

and have an autologous origin, making them good candidates for cardiac tissue repair. However, they cannot differentiate into cardiomyocytes because they possess a strict commitment to the myogenic lineage, so myotubes do not integrate electrically with surviving cardiomyocytes and thus do not beat in synchrony with the surrounding myocardium¹⁸⁴. Nevertheless, preclinical animal studies demonstrated that myoblasts were capable to engraft and improve the cardiac function of the infarcted myocardium, as well as improve regional wall thickening and attenuate ventricular remodeling^{185–187}. Moreover, myoblasts secreted growth factors involved in angiogenesis (e.g. VEGF, angiopoietin) and enzymes involved in matrix remodeling, thus having beneficial effects on cardiac tissue through paracrine signaling¹⁸⁸. However, clinical trials (e.g. myoblast autologous grafting in ischemic cardiomyopathy (MAGIC)) showed that patients treated with autologous myoblast injections had cardiac arrhythmias and no significant improvement in ventricular contractile function¹⁸⁹. Therefore, skeletal myoblasts were not considered the best candidates for cardiac regenerative therapy.

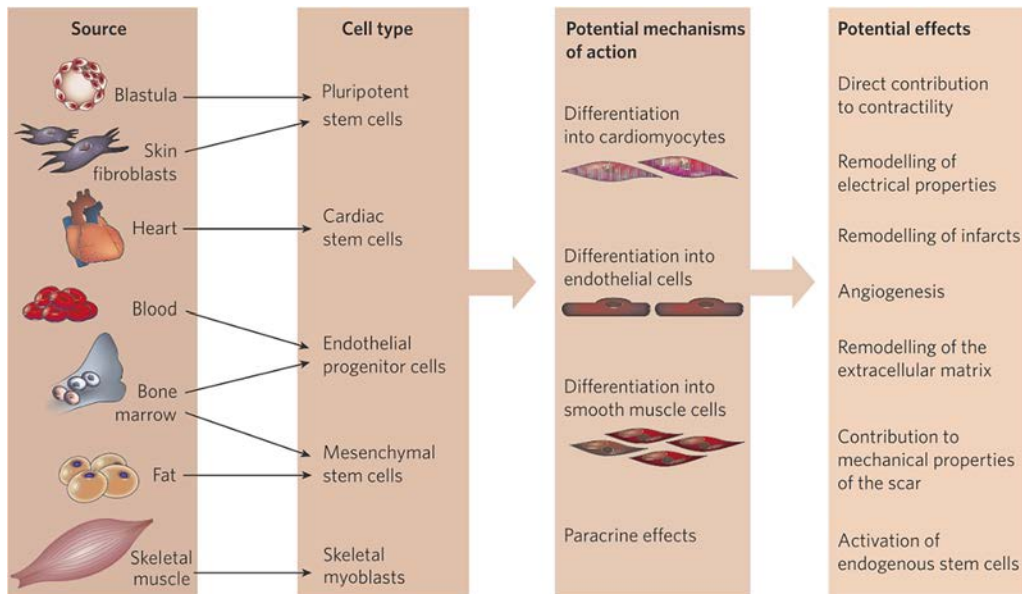


Figure 1.10. Cell types and mechanisms proposed for cardiac stem cell therapy. Stem cells and progenitor cells can be isolated from either autologous or allogeneic sources. Different types of stem cells and progenitor cells have been shown to improve cardiac function through various mechanisms, including the formation of new myocytes, endothelial cells and vascular smooth muscle cells, as well as through paracrine effects. *Adapted from Segers et al.*¹⁸².

- Bone marrow-derived cells (BMC)

Bone marrow-derived mononuclear cells (BMC) have been the most widely studied adult stem cell population, and include a variety of cell populations, being the most relevant hematopoietic stem cells (HSC), mesenchymal stem cells (MSC) and

endothelial progenitor cells (EPC). It has been reported that bone marrow cell transplantation improves tissue vascularization and collagen content, and reduce infarct size in a porcine model, leading to improvements in cardiac function¹⁹⁰. Specifically, MSC have better engraftment than BMC, and present proangiogenic and antifibrotic capacities¹⁹¹. However, the best current evidence indicate that benefits achieved through BMC transplantation is not achieved by differentiation into new cardiomyocytes, but through paracrine mechanisms. It has been shown that cells produce signals that control the response of the native cells native of the myocardium, thereby modulating cardiac repair. This paracrine signaling involves growth factors and cytokines with multiple targets (e.g. angiogenesis, inflammatory response, cardiomyocyte survival), which synergistically contribute to improved tissue protection and function^{54,192}. Some of the most recent and ongoing clinical trials using bone marrow-derived cells are summarized in **Table 1.2**.

- Adipose-derived stromal cells (ADSC)

Adipose tissue is a source of mesenchymal stem cells, specifically the stromal fraction of adipose tissue, and it has been studied for the purpose of cardiac repair. A rich mixture of progenitor cells, including cardiovascular progenitors, can be easily extracted by liposuction¹⁹³. It has been demonstrated that the stromal fraction can be cultured *in vitro*, and derives towards a homogeneous population with mesenchymal phenotype termed adipose-derived stromal cells (ADSC). Preclinical studies have shown that ADSC not only induce a benefit over cardiac function, but they can also improve tissue metabolism, vascularization and reduce infarct size through paracrine action. In fact, paracrine signaling has been postulated as their main mechanism of action because their rate of cardiac differentiation is negligible^{191,194,195}. Some of the most recent clinical trials using ADSC are summarized in **Table 1.2**.

- Cardiac stem cells (CSC)

Cardiac stem cells (CSC) are localized in small clusters at the interstitium of the heart, and play an important role in the slow but continuous renewal of heart cells (including myocytes)¹⁹⁶. CSC can be isolated, grown and differentiated *in vitro* towards cardiac and vascular cells¹⁹⁰. Moreover, they improve cardiac function after implantation in a murine model of acute myocardial infarction. However, the present description of this cell population is still confusing, since they have been characterized by different markers. They were first described by Dr. Anversa and colleagues, and were phenotypically characterized by the expression of the cKit marker in mice^{60,197}. Surprisingly, another cell population defined by the opposite phenotype, Sca-1⁺ cKit⁻, was also identified and its cardiac differentiation potential when transplanted into the ischemic heart was also demonstrated¹⁹⁸. Other populations like Islet-1⁺ cells¹⁹⁹ and the *in vitro* derived cardiospheres²⁰⁰ have also been described. However, despite the

positive effects exerted by the cited populations *in vivo*, a limited self-renewal and proliferative potential has been described, as well as an inefficient differentiation towards cardiomyocytes and limited availability²⁰¹. Therefore, it is essential to better characterize this cell population in order to isolate them and control their progenitor properties in a reproducible and consistent manner^{184,190}. Some of the most recent and ongoing clinical trials using CSC are summarized in **Table 1.2**.

The regenerative capacity of all the above mentioned adult stem cells is quite limited. In the best cases they contribute to vascular tissue, not to robust myocardial regeneration, and they are increasingly considered non-necessarily contracting reservoirs that release a wide variety of biomolecules. This paracrine signaling from the transplanted cells involve multiple targets (e.g. stimulation of angiogenesis, attenuation of fibrosis, inflammation and apoptosis, and recruitment of tissue-resident stem/progenitor cells) that helps to preserve cardiac function and structure through an improved tissue protection^{192,202}. At present, clinical studies (**Table 1.2**) are being performed to evaluate the safety and feasibility of the mentioned strategies. However, to efficiently restore cardiac tissue, pluripotent stem cells (embryonic stem cells (ESC) and induced pluripotent stem cells (iPSC)) may possess the greatest capacity.

- Pluripotent stem cells (PSC)

Pluripotent stem cells (PSC) are a promising cell source for regenerative medicine applications, as both ESC and iPSC can be propagated indefinitely while still retaining their pluripotency, and show the greatest cardiac differentiation potential^{203,204}. Different protocols have been developed to efficiently generate cardiomyocytes from human PSCs²⁰⁵, followed by purification procedures such as the use of cell surface markers or glucose-free culture conditions optimized for cardiomyocytes survival^{206,207}. Moreover, PSC can differentiate into other relevant cell types for cardiac repairing, including cardiac progenitors, endothelial cells and smooth muscle cells²⁰². These advantages of PSCs are especially important in cardiac regeneration, as large number of multiple cell types may be needed to form functional cardiac tissue²⁰⁸. Numerous experimental studies have shown that, in animal models of myocardial infarction, ESC-derived cardiomyocytes could successfully remuscularize the failing heart²⁰⁹, induce electro-mechanical coupling between the grafted cells and those of the host²¹⁰, and almost consistently improve cardiac function^{211,212}. Similarly, human iPSC-derived cardiomyocytes were retained within the infarcted heart of a rat, with induction of heart positive remodeling after the ischemic damage²¹³. In addition, co-administration of human iPSC with MSC considerably increased human iPSC retention in the myocardium of a pig model of myocardial infarction, with iPSC-derived endothelial cells found integrated into the cardiac vasculature²¹⁴. Despite positive effects of iPSC on the cardiac function of animal models, clinical trials have not yet been initiated, while the first clinical trial using ESC (ESCORT, **Table 1.2**) started recently²¹⁵.

Trial, Design phase and Title	Cell type	Estimated n° patients	Delivery method	Initiation / Status
Phase I/II; Prospective Randomized Study of Mesenchymal Stem Cell Therapy in Patients Undergoing Cardiac Surgery (PROMETHEUS) ²¹⁶	Autologous hMSCs	45	Intramyocardial	2007 / Completed
Phase I/II; The Transendocardial Autologous Cells (hMSC or hBMC) in Ischemic Heart Failure Trial (TAC-HFT) ²¹⁷	Autologous hMSC or hBMC	67	Intramyocardial (transendocardial)	2008 / Completed
Phase I/II; The Percutaneous Stem Cell Injection Delivery Effects on Neomyogenesis in Dilated Cardiomyopathy (POSEIDON-DCM) ²¹⁸	Autologous hMSCs Allogenic hMSCs	36	Intramyocardial (transendocardial)	2011 / Ongoing
Phase I/II; Autologous Mesenchymal Stromal Cell Therapy in Heart Failure ²¹⁹	Mesenchymal stromal cells	60	Intramyocardial	2008 / Completed
Phase II; A Phase II Dose-Escalation Study to Assess the Feasibility and Safety of Transendocardial Delivery of Three Different Doses of Allogenic Mesenchymal Precursor Cells (MPCs) in Subjects With Heart Failure (REVASCOR) (Ref. NCT00721045)	Mesenchymal precursor cells	60	Intramyocardial (transendocardial)	2008 / Completed
Phase II; Safety and Efficacy Study of Intramyocardial Stem Cell Therapy in Patients With Dilated Cardiomyopathy (NOGA-DCM) ²²⁰	Autologous hBMCs (CD34 ⁺ cells)	60	Intramyocardial	2011 / Completed
Phase I; Cardiac Stem cell Infusion in Patients With Ischemic Cardiomyopathy (SCIPIO) ²²¹	c-kit ⁺ cardiac progenitor cells	33	Intracoronary	2009 / Completed
Phase I/II; Allogeneic Heart Stem Cells to Achieve Myocardial Regeneration (ALLSTAR) (Ref. NCT01458405)	Cardiosphere-derived cells	274	Intracoronary	2012 / Ongoing
Phase III; Safety and Efficacy of Autologous Cardiopoietic Cells for Treatment of Ischemic Heart Failure (CHART-1) (Ref. NCT01768702)	Bone marrow mesenchymal cardiopoietic cells	240	Intramyocardial	2012 / Ongoing
Phase II; An Efficacy, Safety and Tolerability Study of Ixmyelocel-T Administered Via Transendocardial Catheter-based Injections to Subjects With Heart Failure Due to Ischemic Dilated Cardiomyopathy (ixCELL DCM) ²²²	Bone marrow cells (CD90 ⁺ hMSCs, CD14 ⁺ monocytes and alternatively activated macrophages)	108	Intramyocardial (transendocardial)	2012 / Ongoing
Phase I; Cardiosphere-derived autologous stem cells to reverse ventricular dysfunction (CADUCEUS) ²²³	Cardiosphere-derived stem cells	31	Intracoronary	2009 / Completed
Phase I; Transplantation of Human Embryonic Stem Cell-derived CD15 ⁺ Isl-1 ⁺ Progenitors in Severe Heart Failure (ESCORT) ²¹⁵	Embryonic stem cell-derived CD15 ⁺ Isl-1 ⁺ progenitors	6	Epicardial delivery of a fibrin patch	2013 / Recruiting participants
Phase I; Bone Marrow Transfer to Enhance ST-Elevation Infarct Regeneration (BOOST-1) ²²⁴	Autologous bone marrow cells	60	Intracoronary	2002 / Completed
Phase III; Reinfusion of Enriched Progenitor Cells And Infarct Remodeling in Acute Myocardial Infarction (REPAIR-AMI) ²²⁵	Enriched autologous bone marrow cells	204	Intracoronary	2004 / Completed
Phase II; Mesenchymal Stromal Cell Therapy in Patients With Chronic Myocardial Ischemia (MyStromalCell Trial) (Ref. NCT01449032)	Adipose-derived mesenchymal stem cells	60	-	2010 / Completed
Phase I; A Randomized Clinical Trial of Adipose-derived stem & Regenerative Cells In the Treatment of Patients With Non revascularizable ischemic Myocardium (The Precise Trial) ²²⁶	Adipose-derived stem cells	27	Transendocardial injection	2007 / Completed

Table 1.2. Recent clinical trials of stem cell therapy. hBMC: human bone marrow cell; hMSC: human mesenchymal stem cell. *Adapted from Sanganalmath et al.²²⁷ and Faiella et al.¹⁹³.*

Despite the positive results obtained, PSC-derived cardiomyocytes are, in general, a mixture of nodal-like, atrial-like and ventricular-like cells²²⁸. Moreover, they display a relatively immature phenotype, being more similar to fetal rather than adult cardiomyocytes. Among other properties, they show disorganized sarcomeres, small forces of contraction and small action potentials compared with their adult counterparts⁵². This immaturity limits their use in cardiac tissue repair, as some features such as spontaneous activity and slow conduction may cause lethal arrhythmias after transplantation in the heart²¹⁰. Therefore, maturing human PSC-derived cardiomyocytes to a more adult state would significantly increase their value in stem cell therapy.

Another important issue that has limited stem cell therapy is cell engraftment and survival in the host tissue. More than 70% of the transplanted cells are lost within the first 48 h in most studies. The development of pro-survival cocktails has improved the survival of human PSC-derived cardiomyocytes as islands in rat hearts after myocardial infarction, ameliorating cardiac function²⁰³. However, achieving large areas of adult-like cardiomyocytes fully integrated in the cardiac tissue remains a challenge, as the lack of matrix anchorage together with a hypoxic, pro-inflammatory and/or fibrotic environment hampers cell survival¹⁹⁰.

In this context, tissue engineering techniques can improve cardiomyocyte maturation, engraftment and survival in the host tissue, thus helping to overcome the mentioned limitations. Therefore, to boost the therapeutic effects of stem cell therapy, the field of cardiac tissue engineering has become a really promising strategy, which will be explained in “1.2. Cardiac tissue engineering” section.

1.1.4.2. In vitro models for drug discovery and toxicity testing

Drug discovery and development is a costly and inefficient process, and suffers from a high failure rate (~90%)²²⁹. The average time between drug discovery and commercialization is 10-15 years, with median costs over \$5 billion²³⁰. Current methods to evaluate drug safety and efficacy have poor predictive power of some adverse side-effects, such as cardiotoxicity, neurotoxicity and hepatotoxicity²³¹. Specifically, cardiotoxicity remains a major cause of drug failure during preclinical and clinical development, with high rates of already approved medicines being withdrawn from the market (**Figure 1.11**)^{232,233}. Furthermore, cardiotoxicity is an adverse side effect exhibited not only by drugs to treat cardiovascular diseases, but also other diseases such as diabetes, inflammation and cancer. Therefore, the development of improved *in vitro* models for predictive cardiotoxicity and target validation is absolutely needed^{234,235}.

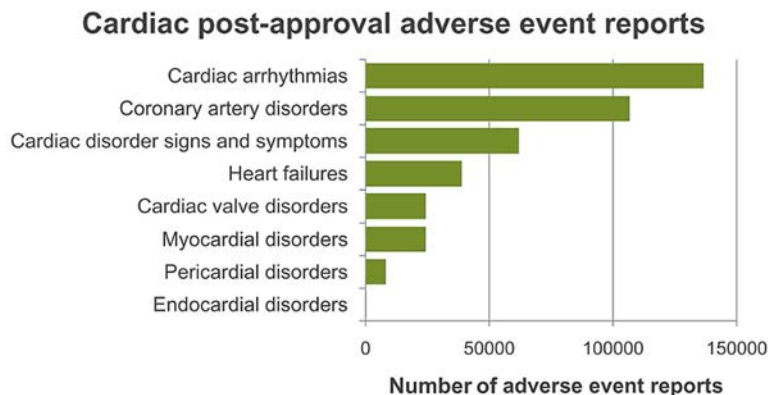


Figure 1.11. Cumulative number of post-approval cardiac adverse events reports since 1969. Within each category, adverse event reports are ranked by decreasing order of incidence. Data should be taken with caution, as the linkages with drugs are not always demonstrated. Note the large number of adverse event reports related to arrhythmias. *Adapted from Laverty et al.*²³³.

In conventional preclinical studies, safety and toxicology testing of new drugs involve cell monolayer models and animal models. Cell monolayer models typically consist on heterologous expression systems of human cardiac ion channels in non-cardiac cell lines cultured in two-dimensional (2D) conditions. Most of the cardiotoxicity and arrhythmia safety tests are performed in Chinese hamster ovary (CHO) and human embryonic kidney 293 (HEK293) cells overexpressing individual human ion channels, most commonly the human ether-a-go-go-related gene (hERG) channel. Drug screening data from human cell sources is also obtained from primary heart cells and tissues, as well as tumor-derived immortalized mammalian cardiac cell lines. However, these human-specific models are limited by genetic instability, the absence of important cardiac cell characteristics, short survival *in vitro* or by the fact that ectopic expression of cardiac ion channels not always recapitulates function in human cardiomyocytes^{236,237}. Moreover, Petri dish cultures lack three-dimensional (3D) cell-cell and cell-matrix interactions, spatial and temporal gradients of biochemical and physical signals, and systemic regulation that otherwise are present in *in vivo* models²³⁸. Therefore, Petri dish models are not always predictable of whole tissue and organ behavior, making really difficult the extrapolation of results to preclinical studies in animals and clinical trials in humans.

Regarding preclinical drug screening in animal models, they are the current standard and allow to study drug effects within whole organisms, thus becoming invaluable for studies of toxicity testing²³⁸. The availability of mouse models with targeted gene modifications (*knock-out* and *knock-in*) has allowed studying the function of numerous genes during development. Moreover, it has allowed the generation of rodent strains with compromised immune systems, permitting the analysis of human cells function *in vivo* without immune rejection^{239,240}. Nevertheless, animal models have

several limitations when used in disease modeling and toxicological studies, as they fail to fully recapitulate human physiology and pathophysiology. There are important interspecies differences between animal models and humans in ion channels, biological pathways and pharmacokinetic properties, which ultimately hamper a reliable prediction of human cardiotoxicity²⁴¹. For example, mice are the most widely used animal model, and show profound differences with respect to human beating rate (500-724 bpm compared to 60-90 bpm in humans) and electrophysiological properties (QT interval is four times shorter in mice than in human, among other differences in electrocardiogram duration, repolarization currents and ion channel expression levels)²⁴². These differences limit the use of current research models, as their poor predictive power leads to drugs that pass animal studies but fail in human trials, adding expenses and risks to the drug discovery and development process. Another limitation of *in vivo* models is that they offer scarce control over the cell microenvironment in cell transplantation studies, and monitoring the outcome is more challenging than in controlled *in vitro* systems²³⁸.

Since 1997, cardiotoxicity-related drug withdrawals have dramatically increased from 5.1 % to 33%, constituting one of the leading causes of drug attrition²⁴³. As examples, Terfenadine was withdrawn in 1998 for inducing cardiac arrhythmias, Grepafloxacin in 1999 for prolonging the QT interval, and Rofecoxib in 2004 for the risk of myocardial infarction¹⁷². An important focus remains on avoiding the drug-induced and life-threatening ventricular arrhythmia torsades de pointes (TdP) (**Figure 1.12**). TdP is associated with a delayed repolarization, a surrogate marker of proarrhythmia observed as a prolongation of the QT interval on the surface electrocardiogram (ECG). Blockade of the hERG current (a repolarizing potassium current carried by the hERG channel and also known as K_v11.1 current) is recognized as a predominant mechanism for drug-induced delayed repolarization²⁴⁴. Current drug safety paradigm assesses ventricular arrhythmias by measuring *in vitro* hERG channel blockade in the above mentioned cell lines and *in vivo*/clinical QT interval prolongation. This approach has contributed to prevent new drugs with unanticipated potential for proarrhythmia from entering the market, thus removing TdP risk for new chemical entities. However, lack of specificity of such studies may also have stopped the development of potentially valuable therapeutics, as false positives have been encountered (e.g. Verapamil, Phenobarbital, Tolterodine and Ranolazine)²⁴⁵. Besides, this method does not address any other ion channels involved in cardiomyocyte electrophysiology, and fails to capture drug-induced cardiotoxicity²⁴⁶. Therefore, given that hERG blockage alone is not highly specific for predicting either delayed repolarization or clinical proarrhythmia, there is a need for more comprehensive, efficient and multi-parametric approaches that unravel the mechanisms responsible for these complex toxicities. One possible approach is the Comprehensive *in vitro* Proarrhythmia Assay (CiPA)²⁴⁴, which proposes to define proarrhythmic risk based on *in silico* reconstructions of human ventricular electrical activity. These reconstructions would integrate drug effects on multiple human cardiac

currents, and results would be confirmed with *in vitro* electrophysiological responses from human stem cell-derived cardiomyocytes.

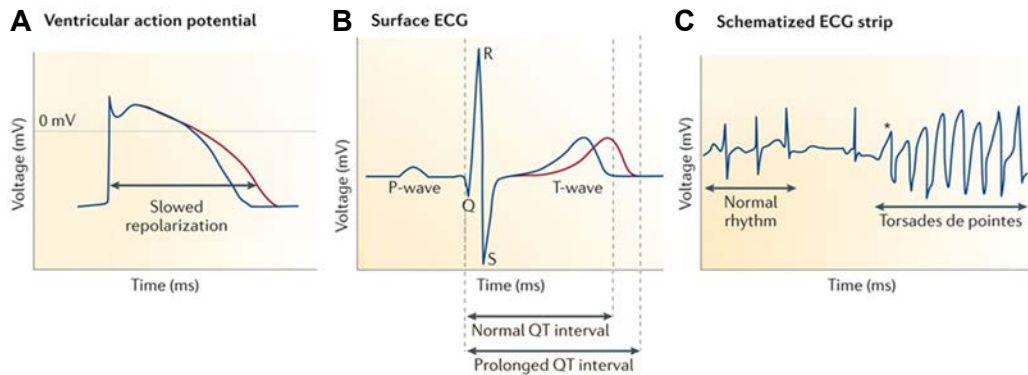


Figure 1.12. Link between delayed repolarization and torsades de pointes (TdP) proarrhythmia. **A**, The slowed ventricular repolarization on a cellular level results from a drug-induced decrease in net outward current. **B**, Although the relationship between ventricular repolarization and TdP is complex, on a cellular level, delayed ventricular repolarization leads to prolongation of QT interval on a surface electrocardiogram (ECG). **C**, Prominent QT prolongation may further dysregulate repolarization, giving rise to a premature ventricular beat before the end of the T wave (indicated with *) to initiate TdP. Adapted from Gintant *et al.*²⁴⁴.

In view of this scenario, the development of human *in vitro* models of cardiac tissue that are predictive of human drug response and cardiac toxicity would be a major advancement. They would allow understanding, studying, and developing new drugs and strategies for treating cardiac diseases. Moreover, they would reduce the risk at which individuals enrolled in clinical trials are exposed, as well as the overall cost of drug development²⁴⁶. To this end, using human stem cells and their differentiated progeny, would be highly beneficial for drug development. As discussed in the previous section, human pluripotent stem cells (hESC and hiPSC) emerge as an ideal cell source to generate human cardiac tissue models, due to their unlimited self-renewal capacity and pluripotent differentiation ability, naturally including cardiac differentiation. Moreover, if combined with new technologies and environments capturing critical aspects of the *in vivo* milieu, human hESC and hiPSC cell derivatives could acquire a more mature phenotype. Therefore, they could lead to the generation of 3D cardiac tissue models able to provide relevant information about human physiology^{66,241}.

1.1.4.3. Disease modelling

Another approach that can improve the treatment of cardiac diseases is understanding their pathophysiology through the generation of disease-specific models. Human induced pluripotent stem cells (hiPSC) emerge as a unique method for obtaining

patient-specific cardiomyocytes to model genetic and other cardiac diseases²⁴⁷. Unlike other cells, hiPSC reflect a person's unique genotype because they are derived from its own somatic cells (e.g. peripheral blood mononuclear cells or skin fibroblasts). Therefore, using hiPSC from multiple patients could allow the study of large and diverse genetic disease pools, as well as overcoming many of the current limitations of drug discovery and advance towards personalized medicine²³⁸.

Currently, there is an important increase in the number of publications about modelling cardiovascular diseases *in vitro* using hiPSC-derived cardiomyocytes (hiPSC-CM)²⁴⁸. One of the first studies reporting the generation of hiPSC-CM from patients with a hereditary cardiac disease was published in 2010. The authors studied patients with LEOPARD syndrome, which is a rare disorder comprising multiple congenital anomalies in the skin, face and heart. A major disease phenotype in patients with LEOPARD syndrome is hypertrophic cardiomyopathy, and hiPSC-CM obtained from those patients displayed an increased surface area and a higher degree of sarcomeric organization compared with cardiomyocytes derived from healthy individuals²⁴⁹. From then on, both electric and structural inherited cardiac diseases have been studied in hiPSC-CM that exhibit key characteristics of the disease²⁵⁰. For example, channelopathies such as congenital long QT syndrome (LQT) have also been modelled using hiPSC-CM. LQT is a familial arrhythmogenic syndrome characterized by delayed repolarization, a prolonged QT interval in the surface electrocardiogram, torsades de pointes (TdP) ventricular tachycardia and sudden cardiac death²⁵¹. Long-QT syndrome type 1 (LQT1), a repolarization disorder due to mutations in *KCNQ1* gene, was the first to be modelled. Patient-derived cells recapitulated the electrophysiological characteristics of the disorder, and maintained the genotype of the disease²⁵². Similarly, Itzhaki *et al.* developed a disease-specific hiPSC line from a patient suffering Long-QT syndrome type 2 (LQT2), a repolarization disorder due to mutations in the *hERG* gene (also known as *KCNH2*). Cardiomyocytes derived from diseased hiPSC showed a significant prolongation of the action potential duration when compared to healthy controls, and were used to evaluate antiarrhythmic properties of some therapeutic agents²⁵¹. Other inherited cardiac arrhythmia syndromes, such as long-QT syndrome type 3 (LQT3), Brugada syndrome, long-QT syndrome type 8 (LQT8)/Timothy syndrome and catecholaminergic polymorphic ventricular tachycardia have also been modelled using hiPSC-CM, with patient-derived cells recapitulating important characteristics of each disease^{253–255}.

Some hiPSC-derived cellular models have been developed for cardiac diseases involving disorders on structural genes, such as dilated cardiomyopathy (DCM) and hypertrophic cardiomyopathy (HCM). DCM is a cardiomyopathy characterized by systolic dysfunction, ventricular dilation and progressive heart failure. Sun *et al.* generated hiPSC-CM from DCM patients carrying a point mutation in cardiac troponin

T gene (*TNNT2*), and cardiomyocytes exhibited altered regulation of Ca^{2+} , decreased contractility and abnormal distribution of sarcomeric α -actinin compared to healthy individuals²⁵⁶. HCM, in turn, is a disease characterized by abnormal thickening of the left ventricular myocardium, and it is linked to progressive heart failure, arrhythmia and sudden cardiac death. hiPSC-CM from HCM patients carrying a mutation in the gene encoding β -myosin heavy chain (*MYH7*) were successfully obtained, and key features of the disease such as abnormal calcium handling, increased myofibril content and cellular hypertrophy could be observed²⁵⁷.

Although disease-specific hiPSC-CM have contributed to significant progress in the development of human normal and pathologic conditions, the full potential of this technology has not been uncovered. First, and as previously commented, the immaturity of cardiomyocytes derived from both hESC and hiPSC hinders their predictive capacity of adult outcomes. Second, hiPSC-CM cultured in standard Petri dishes are not able to model disease phenotypes present at the tissue level, such as interstitial fibrosis, myocyte disarray or other vascular and structural disorders^{250,257}. Therefore, it would be an important advance to develop methods for recreating the three-dimensional architecture of vascular and myocardial tissue, as representative physiological models would lead to more realistic assays (**Figure 1.13**).

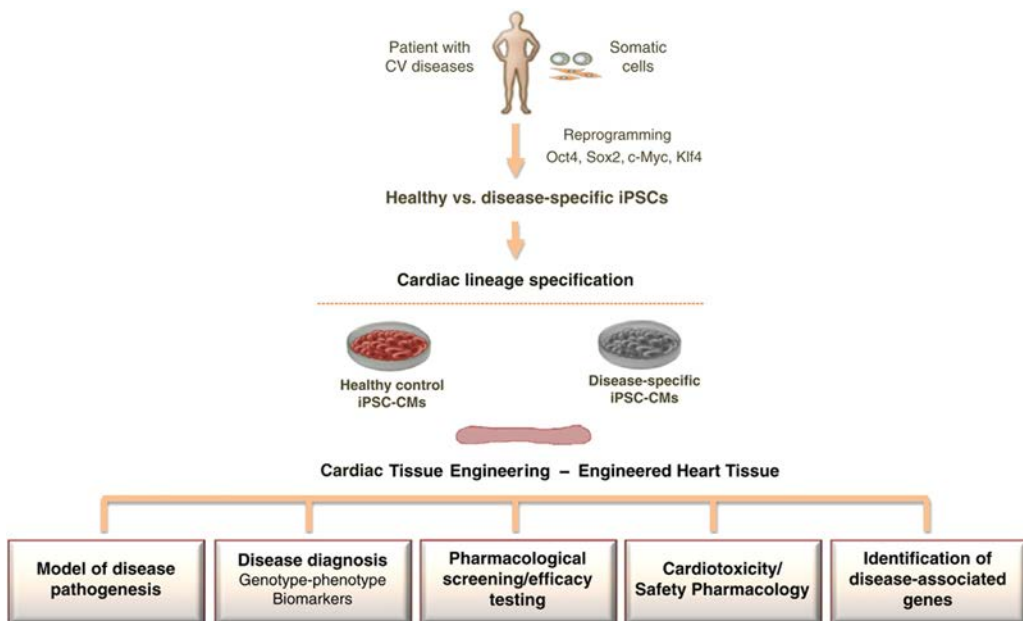


Figure 1.13. hiPSC-CM for patient-specific heart tissue models. Cardiac tissue engineering can help establishing normal and disease-specific cardiac tissue models through the development of engineered heart tissues. *Adapted from Tzatzalos et al.*¹⁷².

1.2. Cardiac tissue engineering

To put cardiac tissue engineering into perspective, it is important to consider the limitations and further requirements of the alternative therapeutic strategies discussed before. Concerning stem cell therapy, the low degree of cell retention, engraftment and survival in the host tissue are among the most important limitations. In the case of human *in vitro* models of cardiac tissue for drug discovery, toxicity testing and disease modelling, the immaturity of cardiomyocytes derived from hPSC remains a critical issue, as well as the lack of tissue level information from standard 2D cultures. In this context, the innovative field of cardiac tissue engineering arises as a promising strategy to work out the mentioned difficulties and advance towards the treatment of cardiac diseases. By combining cardiac cells with biocompatible scaffolds, the site accuracy of cell delivery as well as cell survival could be definitely improved, as cells would be provided with a mechanical support element. Moreover, mimicking native cardiac environment through the use of advanced signaling systems would provide cells with important regulatory signals that are absent in standard 2D cultures. Therefore, the immature phenotype of hPSC-CM could be evolved towards a more adult-like phenotype.

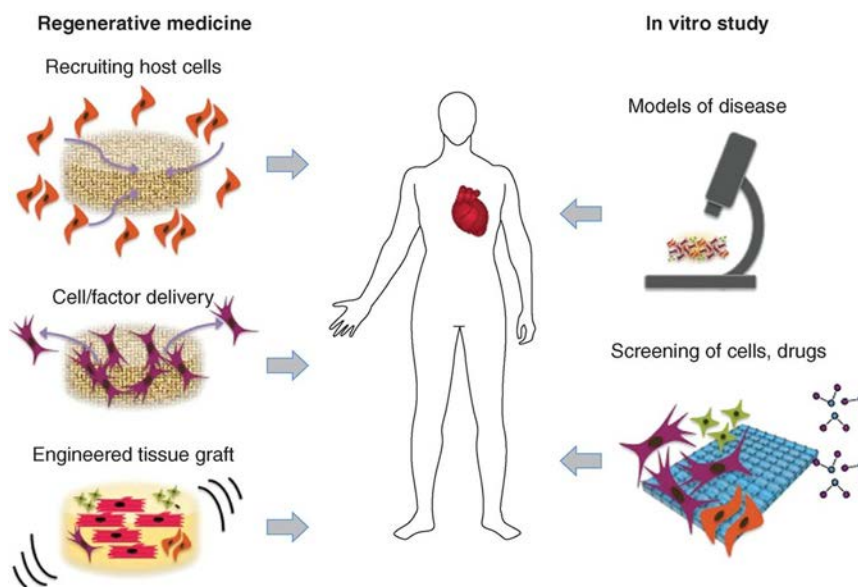


Figure 1.14. Cardiac tissue engineering. Cardiac tissue engineering aims at generating mature and functional 3D myocardial tissue constructs for regenerative medicine purposes, disease modelling and drug discovery and toxicity testing. Alternatively, host cells can be recruited to the repair the injured site by implanted biomaterials, with or without cells. *Image taken from Vunjak-Novakovic et al.*⁶⁶.

Tissue engineering was officially established at a conference in Lake Tahoe, California, in 1988, and was originally defined as “the application of principles and methods of engineering and life sciences toward fundamental understanding of

structure-function relationships in normal and pathological mammalian tissues and the development of biological substitutes to restore, maintain, or improve tissue function". From then on, tissue engineering and regenerative medicine advanced rapidly: the stream of publications grew from about 12 in 1991, to more than 36000 by the end of 2010³. In the context of cardiac tissue engineering, its initial goal was the generation of cardiac tissue analogues to repair or replace the damaged myocardium (**Figure 1.14**). Nowadays, it is still a central goal for the scientific community, but it has to overcome major hurdles before clinical implementation. However, a range of more immediate *in vitro* applications for those cardiac tissue analogues are becoming increasingly important, such as safety pharmacology assays and disease modelling (**Figure 1.14**). This would mean translating the laboratory research to treatment for patients, with engineered heart tissues acting as a tool rather than as a medicine⁶⁶.

Basic design approaches for tissue engineering may include cell structures only, cells combined with biomaterials, or biomaterials only²⁵⁸. However, to generate reliable 3D cardiac tissue constructs that resemble myocardial tissue, three elements are often seen as essential: (1) a large number of cardiac cells to reach physiological densities; (2) scaffolds made of biocompatible materials that replicate the native 3D environment; and (3) biomimetic signaling systems, which may include signaling molecules and other mechanical and electrical regulatory signals (**Figure 1.15**)¹⁸¹. These elements constitute the classical approach to cardiac tissue engineering, and they will be individually discussed in the following sections.

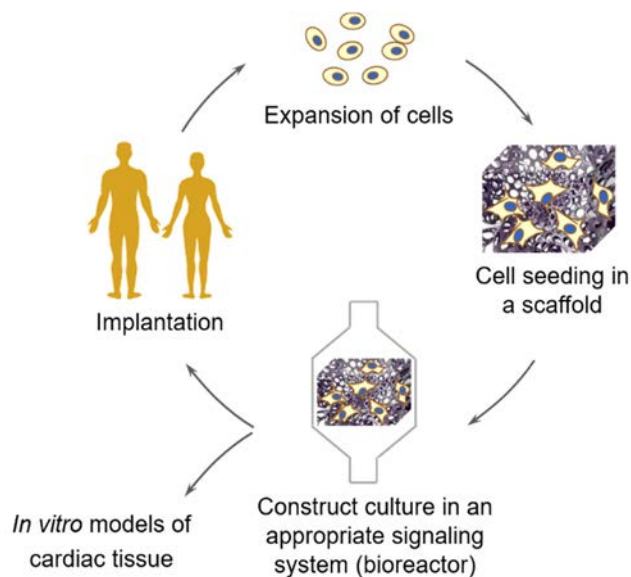


Figure 1.15. Classical approach to human cardiac tissue engineering. It is based on obtaining and expanding human cardiac cells, seeding them in biocompatible 3D scaffolds, and culture the cardiac tissue construct in a biomimetic signaling system, usually a bioreactor. Adapted from Wollert *et al.*¹⁸¹.

1.2.1. Cardiac cells

The first challenge of engineering a tissue or an organ is finding appropriate cell sources in large quantities. To date, the vast majority of the work in developing 3D cardiac tissue analogues has been performed using rat²⁵⁹, mouse^{260,261} and chick²⁶² cardiomyocytes. However, due to recent progress in the field of human stem cells, cardiac tissue engineering has begun to move away from animal-based cardiac tissue constructs, translating the acquired knowledge into the production of human cardiac tissue constructs.

As previously discussed, human pluripotent stem cells (hESC and hiPSC) are conceived as the ideal cell source to efficiently restore human cardiac tissue and generate human cardiac tissue models. Human embryonic stem cells (hESC) are derived from the inner cell mass of an early-stage fertilized embryo²⁶³. They have unlimited cell-division capacity, so they can be expanded in culture to obtain large cell quantities. When cultured with the appropriate extracellular signals, hESC differentiate along particular lineages to form functional cells with properties similar to those observed *in vivo*. Similarly, human induced pluripotent stem cells (hiPSC) share many of the properties of hESC, particularly unlimited proliferation and multilineage differentiation potential. However, they are derived from adult and mature differentiated cells through the forced expression of particular pluripotency genes^{264–266}. Therefore, hiPSC circumvent the ethical and legal issues associated with hESC, and can generate cardiomyocytes that are genetically equivalent to the cells of a given patient^{229,248}. For these reasons, hiPSC represent an excellent source of cardiomyocytes for cardiac tissue engineering approaches, even though some hurdles will have to be overcome before clinical application (e.g. stable patient-specific lines generation, regulatory agencies approval and low-level immunogenicity suppression)^{267–269}.

Most of the existing differentiation protocols for hPSC use 2D culture systems^{203,270,271}. Although 2D differentiation yields the desired cell lineages and allows direct characterization of the cells during differentiation processes, they do not take into account the importance of the entire context of cell microenvironment. 2D systems might promote unnatural interactions with relevant external factors (e.g. multiple cell types, extracellular matrix, cytokines, and physical factors), which can change or affect cellular responses²⁷². The idea of designing biomimetic models both in 2D and 3D is to unlock the full potential of stem cells by reproducing some aspects of the *in vivo* physiological context, as the cues presented to cells are principal determinants of their phenotype. This would allow directing pluripotent cells to differentiate towards the desired cell type in the right place and at the right time to assemble functional tissue structures²⁷³. Some studies have indicated that cues such as electrical stimulation or substrate patterning enhance hESC differentiation into the cardiac lineage^{274,275}, so improving hPSC differentiation could be achieved by mimicking native cardiac environment. However,

most studies focused on obtaining 3D cardiac tissue constructs use hPSC that have been predifferentiated into cardiomyocytes, and then hPSC-CM are assembled in 3D structures to improve their maturity level.

To develop human cardiac tissue analogues, not only cardiomyocytes have to be taken into account. As previously commented, the human heart is composed of about 60-70% of human cardiac fibroblasts, 30% of cardiomyocytes and 10% of other cells such as endothelial and vascular smooth muscle cells. Human cardiac fibroblasts are known to secrete growth factors and extracellular matrix proteins such as collagen type I and III, as well as to support the structure and electromechanical function of the myocardium^{11,276}. This supporting effect has also been demonstrated when generating cardiac tissue constructs, as co-cultures of cardiomyocytes and non-cardiomyocytes enhance the formation and maturation of functional human cardiac patches^{277,104}. Specifically, human cardiac tissue constructs developed maximal contractile forces when hPSC-CM:non-cardiomyocyte composition was of 1:1²⁷⁸, in agreement with previous results obtained in rodent and human constructs^{279,280}. Interestingly, when human cardiac tissue constructs were generated from purified hPSC-CM populations, cardiomyocytes did not condense and displayed round morphologies (**Figure 1.16**). Conversely, when purified cardiomyocytes were mixed with human foreskin fibroblasts (HFF), cardiomyocytes were elongated, displayed an enhanced expression of maturity-related genes, and cardiac constructs had an improved contractile function²⁷⁸ (**Figure 1.16**). Therefore, co-culturing hPSC-CM with non-cardiomyocytes is essential to generate human cardiac constructs with improved functional and structural properties.

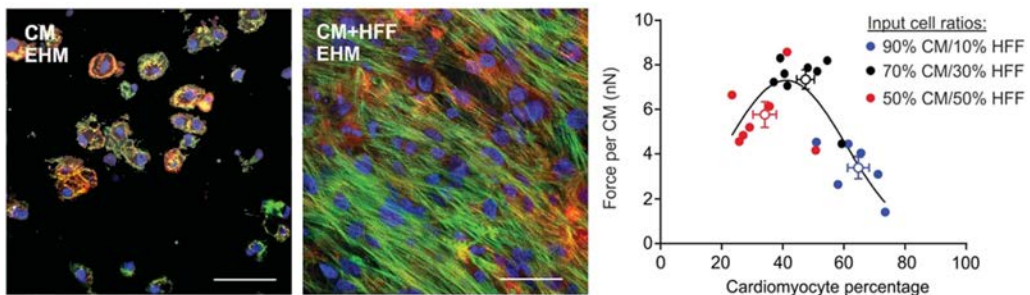


Figure 1.16. Defining cell populations in engineered human myocardium. Actinin (green, CM), f-actin (red, CM and HFF) and nuclei (blue, CM and HFF) of EHM. The optimal CM:HFF input ratio was determined by measuring force per CM in 2 week old constructs. Empty circles show mean \pm standard error of the mean. CM: cardiomyocytes; HFF: human foreskin fibroblasts; EHM: engineered human myocardium. Scale bars: 50 μ m. *Adapted from Tiburcy et al.*²⁷⁸.

1.2.2. Biomaterials

Natively, the extracellular matrix (ECM) surrounding cardiac cells provides microenvironmental cues, mechanical support and architectural guidance that instruct

their growth and function¹⁸. Therefore, to generate reliable 3D cardiac tissue constructs, it is essential the use biomaterials that recapitulate important characteristics of the native cardiac ECM, such as its anisotropic fibrillar structure, mechanical properties and biomimetic molecular composition (**Figure 1.17**). Biomaterials act as scaffolds or templates upon which cardiac cells could attach, organize and mature, or as delivery vehicles for cell transplantation¹⁸. They can be used either in solid or in gel states, and can be processed in a wide variety of shapes and sizes. Solid polymers are usually prepared as sheets, knitted meshes or 3D porous scaffolds, while gels are hydrogels used as substrates to generate cardiac tissue constructs or injectable gels to improve cell delivery¹⁶⁷. Focusing on scaffolds for the generation of cardiac tissue constructs, they can be fabricated using naturally-derived materials (e.g. collagen, Matrigel® and chitosan^{281–283}), synthetic materials (e.g. poly(glycerol sebacate), poly(glycolic acid) and polycaprolactone^{284–286}), a combination of both²⁸⁷, or native heart matrix (obtained after decellularization^{288,289}).

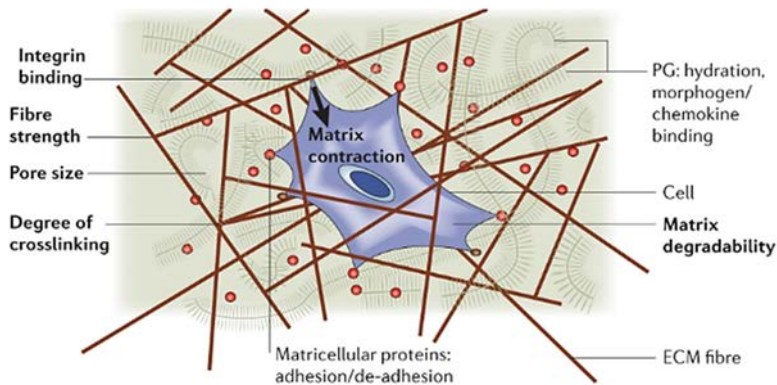


Figure 1.17. The importance of the 3D environment to engineer cell function. The composition, architecture and degree of crosslinking dictate the mechanical properties of the extracellular matrix (ECM) and control multiple cellular processes such as adhesion, survival, migration and differentiation. PG: proteoglycans. *Adapted from Griffith et al.*¹⁷³.

1.2.2.1. General considerations

When conceiving a cardiac tissue engineering approach, it is important to consider the objective of the final application. Thus, the design criteria will be different if the biomaterial is a vehicle for cell delivery or a scaffold to generate tissue patches. However, there are some common properties that have to be addressed, such as biocompatibility, biodegradability, and mechanical support. Injectability has to be considered in the case of hydrogels, and clinically relevant thicknesses are required for cardiac patches²⁹⁰.

For cardiac tissue engineering applications, the biocompatibility of a material refers to its ability to support cardiac cell attachment, proliferation, survival and differentiation both *in vitro* and *in vivo*. For *in vivo* studies and clinical applications, it should also avoid adverse immune responses and promote the contractile function of the myocardium¹⁶⁷. Regarding biodegradability, it refers to the inherent lifespan of a material and the mechanism through which it breaks down when implanted. In cardiac tissue engineering, a material is considered biodegradable if the degradation occurs through disintegration, a hydrolytic mechanism or an enzymatic activity present in the *in vivo* milieu. It is essential that the degradation products are biocompatible as well, and that the biodegradation rate is appropriate for tissue regeneration (it should remain long enough to have the desired effect, but no longer than necessary)^{168,290}.

Mechanical properties of the biomaterials are critical in cardiac tissue engineering. Matching the mechanical properties of the myocardium becomes especially important in *in vivo* studies, as it has to withstand the mechanical forces exerted by the heart (contraction and dilation) without interfering the normal function of the surrounding tissue. It is important to note that during heart development there is a process of myocardium stiffening, partly due to collagen accumulation during embryonic development that lasts until several weeks after birth. This results in a 3-fold increase of elastic modulus (passive stiffness) from embryonic to neonatal stages in mice²⁹¹, and 2-fold increase in rats²⁹². The Young's modulus of the adult human myocardium ranges from 10-20 kPa (end of diastole) to 200-500 kPa (end of systole), and the rat myocardium ranges from 0.1 to 140 kPa^{290,293}. Therefore, a material designed to thicken the ventricle wall and avoid ventricular remodeling should have a stiffness in the high end of the range, whereas a material to be injected or to act as temporary matrix could have low-end stiffness. Concerning biomaterials for *in vitro* applications, they can have very low stiffness as long as cardiac cells seeded into it (hydrogels or scaffolds) can remodel it into a final product that is mechanically similar to the native myocardium²⁹⁰. However, scaffold stiffness affects the maturation, organization and functional behavior of cells, so it has to be taken into account to obtain reliable cardiac tissue constructs^{294,295}. Some works showed that soft bulk materials (~2 kPa) helped obtaining cardiac tissue constructs with greater contraction amplitudes and enhanced matrix deposition than stiffer ones²⁹⁶. Conversely, literature shows conflicting reports because many works suggest that artificial substrates with bulk stiffness of about 10-50 kPa enhance cardiomyocyte maturation⁴⁰, so it is an issue under debate.

In the case of hydrogels, another property to take into account is injectability, as it determines their capability to be administered into the heart in a safe manner. The hydrogel should be capable to pass through a fine-gauge needle, and its polymerization time should be in the range of minutes to tens of minutes to ensure its successful delivery and engraftment⁵. In the case of cardiac patches, the biomaterial should

support the cultivation of tissue constructs with clinically relevant thicknesses. Full-thickness cardiac grafts should be around 10 mm thick, whereas tissue patches can be thinner²⁹⁰. In any case, the limits of oxygen diffusion in a tissue construct with a high density of metabolically active cells restricts tissue thickness at about 100 μm ²⁹⁷. Therefore, a vascular network or a channel array for culture medium perfusion must be incorporated to the design to allow appropriate mass transfer within the tissue.

1.2.2.2. Natural biomaterials

Natural biomaterials are made of proteins or carbohydrates from plants and animals, containing extracellular matrix (ECM) components²⁹⁸. Thus, they have a molecular composition excellent for cell attachment, survival, and differentiation, and are degraded *in vitro* and *in vivo* within days or weeks by cellular enzymes into non-toxic degradation products. Moreover, cells can turn over those materials and replace them with their own ECM components²⁹⁹. However, natural biomaterials have weak mechanical properties, as they present limited accessibility to structural modification and elastic moduli in the range of tens of Pa to tens of kPa^{167,300}. Besides, they present variable physicochemical properties because they come from different protein sources, so there is batch-to-batch and source-to-source variability. Although they do not cause dramatic immunological responses when implanted, they may retain surface antigens that elicit an immune response. However, it is not a major hindrance since there are sources of ECM-derived biomaterials that have been approved for human use^{167,301}.

Several components of the ECM (proteins, glycosaminoglycans, glycoproteins and small molecules) can be isolated and prepared to be used as scaffolds. The most common are collagen^{278,297,302–304}, alginate^{305–307}, chitosan^{283,308–310}, Matrigel^{®7,262,282,311}, fibrin^{312–315}, and gelatin^{12,275,306,316}. Collagen is the most abundant naturally-derived material for scaffolds, and it provides considerable mechanical strength in its natural polymeric state. Moreover, a lack of adverse immune responses to xenogeneic collagen implantation has been reported, mainly because its aminoacid sequence and surface epitopes are highly conserved between species. In fact, trademarks including bovine and porcine type I collagen are already in use in injectable form or as solid scaffolds in numerous clinical applications³⁰⁰. As collagen is one of the main constituents of the cardiac ECM²⁰, it has been extensively used in cardiac tissue engineering. Good results have been obtained with collagen-based 3D matrices, as mature, contractile and force-generating cardiac tissue constructs have been produced for both *in vitro* and *in vivo* applications^{280,297,317–319}.

Finally, the native ECM itself can be used as a scaffold after decellularization of the whole heart or sections of it^{62,288,289,320}. The main advantage of this approach is that it faithfully recapitulates the *in vivo* macroscopic and microscopic architecture of the

heart, as well as its extracellular composition. The decellularization process does not damage vascular channels, and re-seeded cardiac cells attach and display contractile activity within the matrix. However, in the case of heart tissue sections, the directionality of the sectioning is important because different cut planes result in different scaffold architectures and pore sizes¹⁸. Moreover, it should be taken into account that the decellularized matrix from adult hearts does not contain developmental cues that may be important for instructing stem cell differentiation and/or cardiomyocyte maturation. Finally, it is still necessary to define standardized decellularization protocols and recellularization methodologies, as well as establish common guidelines for the assessment of the functionality of the organ.

1.2.2.3. Synthetic biomaterials

Contrary to natural biomaterials, synthetic biomaterials are synthesized by finely controlled processes, thus tuning their mechanical properties, topography, structure, biocompatibility and biodegradability. Therefore, they can be produced in a predictable and reproducible manner, thus ensuring their off-the-shelf availability²⁴¹. However, synthetic biomaterials often do not support cell adhesion and survival, and need to be functionalized with appropriate bioactive molecules. Moreover, they may present some hurdles when implanted *in vivo*, such as eliciting inflammatory reactions, being eroded, not being compliant enough, not being able to integrate within the host tissue, or generating degradation products that are not fully removed from the body^{167,290}.

Multiple synthetic polymers have been used to generate 3D scaffolds for cardiac tissue engineering applications. Among the most frequently used, there is polyurethane (PU), poly ε-caprolactone (PCL), polylactic acid (PLA), polyglycolic acid (PGA), poly(glycerol sebacate) (PGS), and their copolymers²⁴¹. For example, electrospun PU scaffolds seeded with primary cultures of neonatal rat cardiac cells displayed aspects of mature phenotype when fibers were aligned³²¹. Similarly, by combining tissue-like PGS scaffolds with neonatal rat heart cells and appropriate molecular and electrical signals, contractile cardiac tissue constructs with maturity-related characteristics could be obtained³²². In other studies, PCL nanofibrous scaffolds potentiated the adhesion and electrical communication between different layers of neonatal rat cardiomyocytes³²³, and electrospun poly-L-lactide (PLLA) scaffolds supported the growth and proliferation of rat myocytes better than PLLA scaffolds blended with other polymers²⁸⁵. However, it is important to note that on exposure to long term cyclic strain, polyester based polymers such as PLA, PCL, PGA and its copolymers were found to undergo plastic deformation and failure¹⁶⁷.

Up to date, there is no single material that can provide all the properties required for cardiac tissue engineering. Therefore, in an attempt to combine the advantages of

natural and synthetic biomaterials, composite scaffolds containing both components have also been generated, obtaining optimal results^{277,324,325}. Nevertheless, the majority of current investigations use natural-based biomaterials for cardiac tissue engineering, as they have demonstrated to support cardiac cells attachment, survival and maturation both *in vitro* and *in vivo*.

1.2.3. Regulatory signals

Heart development and maturation is regulated by the interplay between multiple biochemical and biophysical stimuli occurring in a 3D context. Human cardiomyocytes *in vivo* need years to reach an adult form in terms of size, shape, molecular composition, metabolism, and physiological function³²⁶. Therefore, to generate functional human cardiac tissue constructs *in vitro*, biochemical, mechanical and electrical stimuli are being incorporated in cell culture platforms through biomimetic bioreactor settings or microphysiological systems. The tissue constructs developed need to demonstrate characteristic features of the heart muscle, such as anisotropic cell alignment (for proper signal propagation), excitation-contraction coupling, synchronous contractions at physiological rates, responsiveness to electrical pacing stimuli and effective exchange of nutrients and metabolites between the cells and their environment³²⁷.

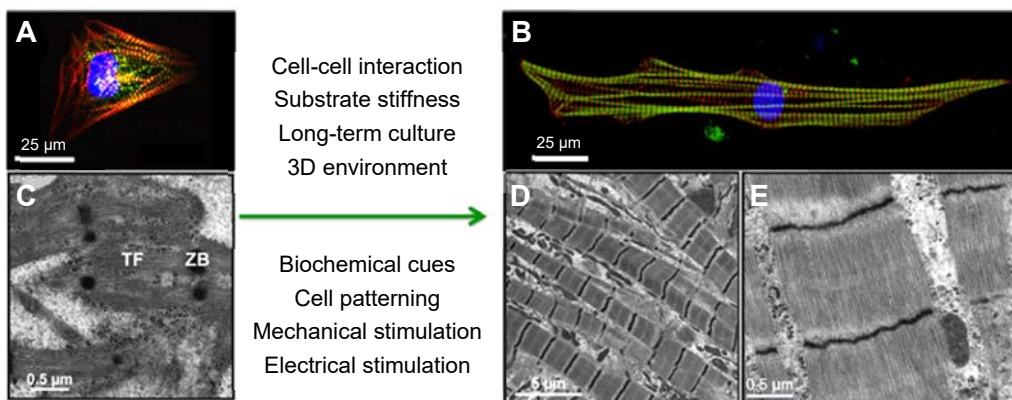


Figure 1.18. Summary of current approaches for cardiomyocyte maturation. Representative immature (A) and intermediate (B) hPSC-CM. Cells were stained for α -actinin (green), filamentous actin (red) and nuclei (blue). Transmission electron micrographs of the sarcomeric organization of immature (C) and intermediate (D, E) hPSC-CM. Elongated cardiomyocytes with longer and more organized sarcomeres were achieved with regulatory signals. Adapted from Yang *et al.*⁴⁰.

A variety of physiological parameters have demonstrated to affect structural and functional maturation of hPSC-CM (Figure 1.18). The most relevant include interaction with other cell types³²⁸, substrate stiffness²⁹⁶, long-term culture⁶³, 3D environment³²⁹, biochemical factors³³⁰, cell patterning and alignment³³¹, mechanical stimulation and

loading^{278,332}, and electrical stimulation^{319,333}. The effects on cardiomyocytes maturation of co-cultures with non-myocytes and substrate stiffness have been discussed in the previous sections. Regarding the effects of long-term culture, hPSC-CM withdrew from the cell-cycle and showed ultrastructural maturation in 35 days⁶⁵, acquiring an unprecedented level of structural maturity after 6 months of culture⁶³. Increased conduction velocities were observed after 2 months of culture³³⁴, but no improvements in contraction force were reported after 2-3 months³³⁵. 3D environments, biochemical cues, cell patterning and electromechanical stimulation will be discussed in detail below.

1.2.3.1. Three-dimensional (3D) cultures

The notion that a 3D environment would be favorable for cardiomyocytes maturation came from the observation that cardiomyocytes tend to form 3D structures over time in culture, as well as and during hPSC-CM differentiation. It has been reported that growth in 3D structures affects cardiomyocyte phenotype, and that it better mimics the real myocardium than 2D plastic dishes⁵². Primary cardiomyocytes dedifferentiate in culture, but in 3D environments this phenomenon is attenuated. For example, the loss of their sarcomeric organization and contractile force is lower than in 2D cultures³³⁶.

The most common approach to generate cardiac tissue constructs is to cast molds that will determine their 3D structure. For this strategy, hydrogels containing cardiac cells are widely used. Hydrogels are placed in casting molds or between two anchor points to provide them with mechanical loading or stretching^{278,280,332,336,337}. Other strategies to construct 3D environments are the use of porous scaffolds^{281,297,318}, decellularized heart tissue^{288,289}, stacked cardiac cell sheets³³⁸, modular assembly of multiple layers³²⁵ and 3D bioprinting³³⁹.

Most information about the effects of 3D growth on cardiomyocytes maturity has been obtained from chicken embryos and rodents^{262,336}. To give one example, culture of neonatal rat ventricular myocytes in 3D for 12 days induced immature cardiomyocytes to almost terminally differentiate and mature in a remarkably organotypic manner³⁴⁰. However, 3D cultures are often combined with other stimuli that promote cardiomyocyte maturation (e.g. electric or mechanical stimulation), and result in 3D cultures not always really comparable with 2D cultures. Despite this, results are unambiguous when directly compared with 2D monolayers: hPSC-CM in 3D tissue constructs display a downregulation of fetal genes (e.g. *MYH6* and *MYL7*), upregulation of important ionic channels (e.g. *KCNJ2*, *SERCA2A* and *CASQ2*), lower proliferation rates, larger surface areas and longer sarcomeres than in monolayers. Moreover, they have more negative resting membrane potentials, higher action potential upstroke velocities, faster conduction velocities and less automaticity than 2D controls, indicating an increased maturity^{277,319}.

1.2.3.2. Biochemical cues

Several cytokines, growth factors and small molecules promote the maturation of cardiomyocytes, including hPSC-CM and rodent cardiomyocytes. Coating cell culture substrates with extracellular matrix proteins act as messenger molecules, as integrin receptor activation induces the maturation of hPSC-CM through modulation of gene expression and contractile function³⁴¹. Physiological maturation of cardiomyocytes can also be induced by adrenergic receptor agonists, even though they are traditionally used to model pathological hypertrophy. When treated with norepinephrine, fetal and neonatal murine cardiomyocytes hypertrophie and increase significantly their protein synthesis³⁴². In hESC-CM, administration of phenylephrine results in a 1.8-fold increase in cell area, 3.8-fold increase in cell number with organized sarcomeres, and 2-fold increase in cell volume³⁴³.

Another essential factor for normal cardiac development is thyroid hormone³⁴⁴, as it regulates isoform switching of some myocardial proteins such as MHC and titin in the perinatal period³⁴⁵. In murine ESC-CM, treatment with triiodothyronine increases expression levels of some maturity-related genes, (*MYL2*, *MYH7*, *SERCA*, *KCNJ2* and *RYR2*), reduces resting membrane potential and improves Ca^{2+} handling³⁴⁶. In hiPSC-CM, the addition of triiodothyronine increases human cardiomyocyte size, sarcomere length and elongation. Moreover, it increases their force of contraction, expression levels of *SERCA* and *MYH7* genes and improves Ca^{2+} handling^{79,347}.

Insulin-like growth factor 1 (IGF-1) regulates cardiomyocyte proliferation, differentiation and postnatal growth, as well as the maturation of the heart⁴⁰. In neonatal rat ventricular myocytes, the addition of IGF-1 upregulates MLC2v and troponin I expression, increases protein synthesis, increases cell size in 2-fold and influences the maturation of cardiomyocyte metabolism^{348,349}. In cardiac tissue constructs, IGF-1 improves their viability, differentiation, contractile amplitude and excitability³⁵⁰. Although IGF-1 is involved in postnatal hypertrophy of the human heart³⁵¹ and is a mitogen for hESC-CM³⁵², it has not been studied in regulating hPSC-CM maturity.

Ascorbic acid stimulates cardiomyocyte differentiation³⁵³, but also induces the maturation of mouse iPSC-CM. It improves their sarcomeric organization, Ca^{2+} handling and response to β -adrenergic and cholinergic stimulations³⁵⁴. In hiPSC-CM, ascorbic acid enhances contraction forces and improves sarcomeric organization, intercalated disc assembly, titin expression, collagen deposition and metabolic activity²⁸⁰.

Neuregulin-1 β is a factor involved in the specification of cardiomyocyte subtypes (e.g. promotes hESC differentiation to ventricular-like cardiomyocytes³⁵⁵), and it also plays a role in promoting cardiomyocyte maturation. In mouse iPSC-CM, neuregulin-1 β

upregulates maturity-related genes such as *Myh6*, *Ryr2* and *Serca2a*, increases action potential upstroke velocities and reduces resting membrane potential³⁵⁶.

Another strategy to identify modulators of cardiomyocyte maturation is the analysis of microRNA profiles of hESC, hESC-CM, fetal and adult human cardiomyocytes. For example, it allowed the identification of miR-1 as a potential regulator of cardiomyocyte maturation, as its overexpression in hESC-CM decreased action potential duration and hyperpolarized resting membrane potential³⁵⁷. Similarly, miR208 has been identified as a potential promoter of cardiomyocyte maturation, as it is involved in thyroid hormone responsiveness and myosin isoform switch^{358,359}.

1.2.3.3. Cell patterning and alignment

Cardiomyocytes in their native environment are exposed to topographical cues that maintain them aligned, elongated and rod shaped. Therefore, many techniques have been developed to induce alignment and elongation of cardiomyocytes through the substrate topography, both at the nano and the microscale^{360,361}. It has been demonstrated that cardiomyocyte maturation can be improved by forcing them to adopt an anisotropic morphology. For example, an increase of conduction velocity in the longitudinal direction has been reported, mainly due to the formation of appropriate intercalated discs, and both cell and sarcomere alignment are potentiated^{40,362}.

Micropatterning has been used as a way to control the architecture of the extracellular environment in 2D. Neonatal rat and mouse cardiomyocytes seeded onto patterned stripes formed aligned myofibers with improved sarcomere organization, formation of cell-cell junctions at their longitudinal edges, contractile strength and protein expression profiles^{362–365}. Similarly, an anisotropically nanofabricated substrate induced the alignment of neonatal rat cardiomyocytes, which displayed properties more similar to the native heart than non-aligned cultures (e.g. faster conduction velocities and increased connexin 43 expression levels)³⁶⁶. By combining surface topography and substrate stiffness, it was possible to demonstrate that morphology and orientation of cardiomyocytes were mainly influenced by topography, whereas contractile function was regulated by both cues³⁶⁷. In 3D, cell alignment can be obtained with electrospun nanofiber-based scaffolds that successfully mimic the structure and orientation of native cardiac ECM, helping cardiomyocytes to adopt an anisotropic structure.

Concerning hiPSC-CM, they also display a disorganized and circular morphology when cultured in 2D²⁴⁶. One strategy to potentiate their elongation and anisotropic morphology is to culture hiPSC-CM on micropatterned films, obtaining strips of aligned cardiomyocytes that contract in the direction of alignment³⁶⁸. Topographical cues have also been used to induce hESC-CM alignment^{275,369}. Aligned cardiomyocytes have been

used to study physiological action potential propagation, as well as responses to pharmacological agents such as E-4031 and isoproterenol³⁷⁰. If aligned uniformly by controlling the direction of passive tension, hESC-CM displayed improved maturation, excitation-contraction coupling and sarcomere structure than monolayer cultures²⁷⁷.

1.2.3.4. Mechanical stimulation

The generation of contractile force is a key component in cardiac development and cardiac function, as the myocardium is always exposed to hemodynamic load. During embryonic heart development, the adaptation to increasing hemodynamic load induce enormous changes in tissue architecture, function and growth. In postnatal hearts, load adaptation induces physiological hypertrophy of cardiomyocytes and changes in the myocardial extracellular matrix. Improper hemodynamic loading in both prenatal and postnatal hearts is related to disease conditions such as congenital defects or pathological hypertrophy^{371,372}. Beating is a repetitive loading and unloading of the heart, the cardiomyocyte and the sarcomere. Preload refers to the pressure during the diastolic filling of the ventricles (forces due to myocardium wall distention), and afterload refers to the pressure developed by the ventricles during systole. *In vivo*, the heart adapts to hemodynamic changes such as blood volume and viscosity, peripheral resistance and hydrostatic pressure. Handling those changes depends basically on the myocardium capacity to increase mechanical force when increasing beating frequencies (positive force-frequency relationship, Bowditch phenomenon) and when increasing myofiber length (positive force-preload relationship, Frank-Starling mechanism)³⁷³. As cardiomyocytes are continuously subjected to cyclic mechanical strain *in vivo*, is not surprising that even adult cardiomyocytes dedifferentiate when cultured in 2D without mechanical loading. Thus, the inclusion of mechanical stimulation to the cell culture platforms has become an attractive hypothesis to improve the maturation level of cardiomyocytes *in vitro*.

In 2D culture systems, mechanical forces have been applied to cardiomyocytes through mainly two strategies: using materials with varying mechanical properties, or mechanically stretching the substrate on which cells are grown, either in a static fashion (applying an initial stretch after cell seeding that is maintained over time), in a step-wise fashion (substrate is stretched in incremental steps that are held for extended periods of time) or under cyclic stretch (substrate is stretched and relaxed at regular intervals)³⁷¹. In the first approach, stiffness is the mechanical property more extensively studied. As previously commented, results show that polyacrylamide substrates stiffer than healthy cardiac tissue (~50 kPa) hinder cardiomyocyte maturation, while mimicking mechanical properties of the heart can enhance some aspects of it^{374,375}. In the second approach, early investigations demonstrated that cardiomyocytes cultured under static or step-wise stretching displayed an improved myofibrillar architecture and turnover, gene

expression, activity of stretch-activated ion channels and development of organized focal adhesions than non-stimulated ones³⁷¹. Regarding cyclic stretch, many studies have demonstrated that it affects the intracellular organization of cardiomyocytes, induces physiological hypertrophy, modifies gene and protein expression and promotes focal adhesion formation^{371,376}. Indeed, commercially available systems such as Flexcell® System have been developed, enabling the evaluation not only of the role of dynamic stretching on cardiomyocyte phenotype, but also its combination with small molecules or growth factors³⁷⁷.

In 3D cardiac tissue constructs, mechanical loading can be applied through three main mechanisms, by the suspension of the tissue construct between (a) fixed holders (static tension, promoting isometric contractions), (b) motorized holders (cyclic stretching, resembling isotonic contractions) or (c) resilient mounts (promoting auxotonic contractions)³⁷² (**Figure 1.19A**). Theoretically, these regimes of mechanical stimulation can be applied along one axis (uniaxial), two axis (biaxial) or all tissue axes (multiaxial)³⁷⁸ (**Figure 1.19B**). The simplest way to load cardiac tissue constructs is the uniaxial regime using two fixed posts, as it is easy to implement, can be performed for extended periods of time without tissue rupture and the holder distance can be modified to alter the preload²⁶². Regarding cyclic stretching, it is experimentally more demanding, as the cycle length has to be adapted to the endogenous beating frequency of the tissue, so tissue rupture after 10 days of culture has been reported³⁷². Finally, auxotonic contractions seem to resemble considerably the physiologic contraction cycle, but it is difficult to adapt to the continuously developing contractile properties.

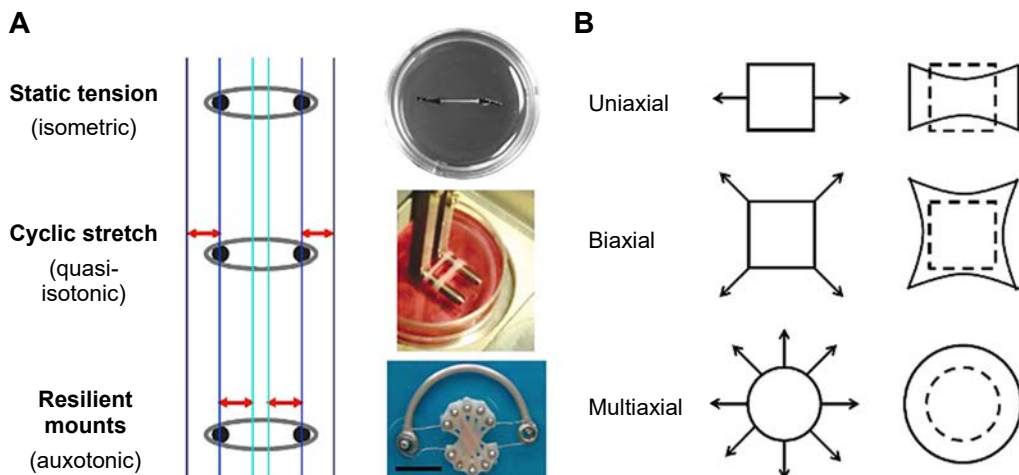


Figure 1.19. Mechanical loading in cardiac tissue engineering. **A**, Loading protocols of cardiac tissue constructs (gray circle in the scheme) and examples. Blue line: slack length at diastole; Dark blue line: extension from slack length; Cyan line: length at peak systole. Red arrows indicate the displacement of the tissue. *Adapted from Zimmermann WH*³⁷². **B**, Examples of stretch regimens to be applied to cardiac tissue constructs. *Adapted from Rangarajan et al.*³⁷⁸.

In addition to the traditional methods of mechanical stimulation, compressive mechanical strain³⁰⁵ and fluid shear stress via continuous or cyclical perfusion³⁷⁹ can also be used. Despite having a potential important role in regulating cardiomyocyte phenotype, further studies using these alternative methods are needed, especially in assessing hPSC-CM maturation.

Several investigations have incorporated mechanical loading to *in vitro* cultures to improve cardiomyocytes maturation, being initially established by the pioneering work of Eschenhagen, Zimmermann and colleagues³³⁶. Neonatal rat ventricular cells were mixed with collagen type I/Matrigel® hydrogels, casted in circular molds and subjected to cyclic stretch. Cardiac cells hypertrophied and showed interconnected, longitudinally oriented cardiac muscle bundles with a well-developed T-tubular system. Moreover, cardiac tissue constructs contracted with a high ratio of twitch-to-resting tension, and showed a strong β -adrenergic inotropic response, low and stable resting membrane potential and fast upstroke kinetics. A similar system was then applied to human cardiac tissue constructs using hPSC-CM^{50,278,380}. On the one hand, when applying uniaxial cyclic stretch, human cardiac tissue constructs displayed densely packed and aligned muscle bundles with organized sarcomeres. Besides, they beat spontaneously, generated Frank-Starling curves and showed positive inotropic response after extracellular Ca^{2+} and isoproterenol treatments³⁸⁰. On the other hand, when suspending the tissue constructs between two flexible posts, hESC-CM displayed well-developed sarcomeres with an increased alignment compared to age-matched embryoid bodies. Functionally, human cardiac tissue constructs showed excitation-contraction coupling, but isolated cardiomyocytes showed highly variable action potential duration and firing patterns. Tissue constructs recapitulated some findings in conventional toxicity tests, such as positive chronotropic and inotropic responses to extracellular Ca^{2+} and isoproterenol treatments, negative chronotropic response to carbachol, and decreases in relaxation velocity and irregular beating after treatments with proarrhythmic compounds (e.g. E-4031, quinidine, and cisapride)⁵⁰.

Other groups have also incorporated mechanical loading to human cardiac tissue constructs. In general, static stretch (including fixed and flexible posts) promoted uniform cardiomyocyte distribution^{104,280}, increased alignment of cells, collagen myofibrils and Z-discs^{104,105,329}, increased cardiomyocyte size and number¹⁰⁴, well-developed and organized sarcomeres^{104,105,280,329}, and increased expression of maturity-related genes^{105,329}. At the functional level, static stretch demonstrated excitation-contraction coupling^{104,105}, action potential duration restitution and recapitulation of some adult cardiac tissue responses when treated with various pharmacological compounds^{105,329}. However, action potential duration and firing patterns were highly variable, and maximal contractile stress was an order of magnitude lower than the maximal reported for human cardiac tissue constructs⁴⁷. Relative to static

stretch, cyclic stretch improved morphological properties of human cardiac tissue constructs (e.g. cardiomyocyte size), upregulated genes and proteins associated with adult phenotypes and downregulated immaturity-related ones^{47,104}. Relative to unstretched constructs, cyclic stretch improved hESC-CM distribution, hypertrophy, elongation, sarcomeric organization, connexin 43 distribution, expression of maturity-related genes and Ca²⁺ handling properties³³². Interestingly, step-wise stretch in combination with ascorbic acid and hPSC-derived cardiac bodies was found to be superior to both static and cyclic stretch with respect to the maximum active and passive force generated, cardiomyocyte alignment and sarcomere length and alignment²⁸⁰. Thavandiran *et al.*³²⁹ also determined that uniaxial mechanical stress generated human cardiac tissue constructs with more aligned collagen fibrils, more elongated hESC-CM and well-developed sarcomeric organization than biaxial stimulation. Finally, *in vivo* applications of stretched human cardiac tissue constructs showed that statically-stretched ones did not evoke adverse immune responses, retained sarcomeric organization and cell alignment and were vascularized by host vessels¹⁰⁴. Regarding cyclically-stretched constructs, they also retained cell organization, could electrically couple with the host myocardium, and could prevent wall thinning in a rat ischemia/reperfusion model³³². Currently, mechanical stimulation is mainly incorporated to human cardiac tissue constructs through configurations including two flexible posts, but any of the mentioned regimes has been completely dismissed.

1.2.3.5. Electrical stimulation

During embryo development, endogenous electric fields influence the emergence of spatial patterns and aid tissue morphogenesis³⁸¹. In the case of the heart, excitation-contraction coupling is critical for heart development and function, and in the adult stage the maintenance of continuous and synchronous contractions is crucial for human life³⁷⁸. These processes are primarily regulated by electrical impulse propagation, which depends on a complex network of interconnected cardiomyocytes. Gap junctions mediate cardiomyocyte communication, and voltage-gated ion channels control internal and external ion levels³⁷¹. The implications of the electrical activity on cardiac physiology and pathophysiology outlined the idea that electrical stimulation could be used to promote the maturation of cardiomyocytes *in vitro*. To date, electrical stimulation has demonstrated to induce the establishment of synchronous contractions within cardiac tissue constructs, as it affects rate, duration and number of action potentials within cardiomyocytes³⁷¹. Accordingly, cardiomyocytes alignment and ultrastructural organization has also been reported to increase when 3D cardiac tissue constructs undergo electrical stimulation²⁸¹.

Multiple types of electrical stimulation regimes and methods to deliver the electrical stimulus have been used in *in vitro* cell culture systems. The most basic

stimulation regime is DC voltage generated by batteries. More complicated stimuli comprise monophasic or biphasic sinusoidal, sawtooth or square-wave signals, injected in pulses, pulse bursts or continuously. These complex signals can be generated by stimulator chips, signal generators or dedicated therapeutic systems. Regarding the methods to deliver the electrical stimulus, they can be based on direct coupling, where the electrode is in direct contact with the cell culture, the tissue construct or the cells, or indirect coupling, which is a non-invasive approach that circumvents some drawbacks of direct coupling (**Figure 1.20**). Three main techniques are used in indirect coupling, which are capacitive, inductive and combined coupling methods (**Figure 1.20**)³⁸².

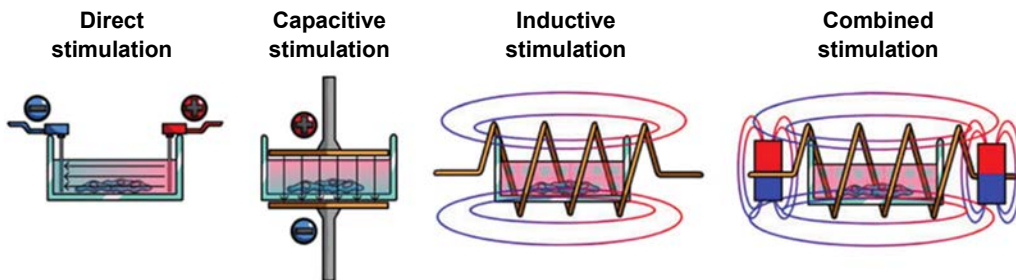


Figure 1.20. Methods of *in vitro* electrical stimulation. Diagrams of the four main techniques for delivering electrical stimulation, which have been used to engineer multiple tissues. *Adapted from Balint et al.*³⁸².

Direct coupling is the simplest way of delivering electrical stimulation to tissue constructs. Most devices include two electrodes placed on opposite sites of the constructs, and electrodes have a straight edge for an even field distribution³⁸³. The field strength is inversely proportional to the distance between electrodes, and electrical impulses are conducted through the culture medium over the engineered tissue construct. Therefore, the conductivity of the cell culture medium is an important factor when predicting the electric field penetration into the tissue. However, there are some toxicity problems related to direct electrical stimulation, such as insufficient biocompatibility of the electrodes³⁸⁴, changes in pH³⁸⁵, reduced levels of molecular oxygen³⁸⁴, and the generation of dangerous nonreversible Faradaic reactions, which are associated with electrode degradation and production of harmful byproducts (e.g. reactive oxygen species in the culture medium)³¹⁸. Additionally, the stimulus can be biased by the formation of a capacitive electrochemical double layer³¹⁸, and the effects of the stimulation depend heavily on whether they are measured near the anode or the cathode³⁸², so these are important issues to take into consideration when using this method. Despite these drawbacks, direct stimulation has been largely used to improve cardiac tissue constructs functionality and orientation. Apart from its simplicity and low cost, direct stimulation may promote the current to pass into cardiomyocytes intracellular conductive pathways instead of staying confined to extracellular space,

thus exerting more important regulator effects than other delivery methods³⁸⁶. Therefore, toxicity-related problems have been virtually solved by using specific materials and stimulation regimes. Electrodes are often carbon rods or platinum wires, but carbon rod electrodes are larger, cheaper, highly resistant to corrosion and highly biocompatible. Moreover, carbon rods have demonstrated the best charge transfer characteristics for cardiac tissue engineering when compared with stainless steel, titanium and titanium nitride electrodes^{387,388}. Finally, optimization of the stimulation duration, voltage and frequency not only avoids toxicity-related issues, but also improves cell response for specific configurations³⁷¹.

Indirect coupling avoids toxicity-related problems of the direct coupling, as electrodes are not in contact with culture medium. However, indirect coupling has been mainly used in bone and cartilage tissues, probably because it decreases the stress responses related to the exposure of non-excitabile tissues to electric field stimulation^{383,389}. From a design point of view, capacitive coupling generates a homogeneous electromagnetic field between two parallel layers of metal or carbon that are separated by a small gap from the culture medium (0.5 - 2 mm)³⁸². However, its use can be limited by the high voltage required to be generated (~100 V)³⁹⁰. Alternatively, inductive coupling can be used, which uses controlled electromagnetic fields generated by coils placed around the cell culture to generate nearly uniform electromagnetic fields. This generates small-magnitude currents and potentials in the proximity of the targeted cells, which has been proven to be favorable in bone tissue³⁸⁵. Finally, combined stimulation methodology combines a static magnetic and an alternating current generated by a transient electromagnetic field, and it has mainly been used in bone cells studies³⁸².

Electrical stimulation of cardiomyocytes has shown to improve their maturation level, as it promotes ultrastructural organization, hypertrophy, alignment, excitability and electrical coupling³⁷⁸. For example, fetal murine cardiomyocytes seeded in 2D were stimulated with monophasic pulses of 10 Hz of frequency, 1 V of amplitude and 5 ms duration for six days. This stimulation increased their alignment, anisotropic morphology, and expression of connexin 43 and potassium channels compared to non-stimulated samples³⁹¹. Similarly, applying an electrical pacing of 1-3 Hz on 2D cultures of neonatal rat cardiomyocytes stabilized their action potential duration and conduction velocity, and enhanced the expression of ion channel and gap junction proteins³⁹².

The pioneering work of Radisic and colleagues demonstrated the positive effect of electrical stimulation on the maturation of 3D cardiac tissue constructs²⁸¹. When applying rectangular pulses of 1 Hz, 5 V/cm and 2 ms to neonatal rat cardiomyocytes seeded in collagen sponges with Matrigel®, cardiomyocytes aligned, electrically coupled, displayed well-developed sarcomeres and upregulated cardiac genes in

comparison with non-stimulated constructs. Interestingly, the positive effects of electrical stimulation strongly depended on the time of its initiation: if applied early (day 1 of culture) electrical stimulation inhibited the accumulation of cardiac proteins and yielded poor contractile behavior, whereas if applied late (day 5 of culture) it was unable to enhance the functional assembly the cells. From then on, multiple investigations have demonstrated the beneficial effects of electrical stimulation on cardiomyocytes maturation. In the case of neonatal rat cardiomyocytes, it was proposed that monophasic square-wave pulses at 3 Hz of frequency, from 2 to 4 V/cm of amplitude and 2 ms of duration were the optimal parameters for their stimulation³⁸⁷. Monophasic pulses avoided the possible undesirable effect of biphasic pulses in inhibiting action potentials³⁹³, 1-2 ms was a sufficiently long pulse to excite cells and minimized potential adverse effects of electrodes in long-duration pulses³¹⁸, and 2-4 V/cm of amplitude was determined based on the functional performance of tissue constructs³⁸⁷.

In the case of hPSC-CM, the beneficial effects of electrical stimulation on their functional and structural maturation has been less explored. In 2D cultures, electrical stimulation (2.5 V/cm, 1 Hz, 5 ms) increases the repolarization current I_{Kr} of hESC-CM and, consequently, they display lower resting membrane potential, increased Ca^{2+} transient amplitude, upstroke and decay rate and higher degree of sarcomeric organization³⁹⁴. Most studies use a physiological pulse rate of 1 Hz, but higher frequencies seem to generate more robust responses^{319,337}. In this regard, Nunes *et al.* demonstrated the use of a platform designated "biowire" to mature hPSC-CM in 3D human cardiac microtissues by applying a high-frequency electrical stimulation regime³¹⁹. By mixing hPSC-CM and supporting cells with a collagen hydrogel and cast the solution around a surgical suture, they generated aligned constructs of about 300 μ m in diameter with frequent and well-developed striations. By applying a frequency ramp-up regimen of electrical stimulation (rectangular, biphasic pulses of 1 ms, 3-4 V/cm, and 1 to 6 Hz), cardiomyocytes displayed physiological hypertrophy, higher conduction velocities, increased ultrastructural organization, and enhanced Ca^{2+} handling properties in comparison with the other groups of study. Similarly to the biowire, hiPSC-CM mixed with a fibrin/Matrigel[®] gel and subjected to high frequency electrical stimulation (biphasic pulses, 2 V/cm, 4 ms and 1.5 - 2 Hz) displayed an improved structural and functional maturation compared with the non-stimulated or stimulated with lower frequencies³³⁷. High frequency group displayed better alignment, anisotropic morphology and sarcomeric organization, and exerted higher forces of contraction than non-stimulated ones. However, they showed a less mature phenotype that rat cardiac tissue constructs cultured under the same conditions. Finally, a recent study by Eng and colleagues confirmed the decisive role of the electrical stimulation regime on hPSC-CM. They demonstrated that 3D aggregates of cardiomyocytes adapted their autonomous beating rate to the frequency at which they were stimulated, calling into question the suitability of high frequency regimens on hPSC-CM

functionality³³³. This effect was mediated by the emergence of a rapidly depolarizing cell population and by the expression of hERG, which was previously shown to determine maximum diastolic potential in stem-cell derived cardiomyocytes³⁹⁵. This rate-adaptive behavior was long lasting and transferable to the surrounding cardiomyocytes, and was accompanied by an enhanced expression of connexin.

In general, the mechanisms underlying increased maturation of hPSC-CM through electrical stimulation remain unclear. It seems that they are mostly indirect, as pacing varies the transmembrane potential of cardiomyocytes and induces their contraction, but they can also be direct, as electrical stimulation has shown to alter gene transcription to a more mature profile⁵². Therefore, further studies are needed to understand the role of electrical stimulation in the context of human cardiac tissue engineering. Similarly, future work in this area should aim at optimizing important electrical stimulation parameters such as amplitude, pulse duration, frequency and timing to achieve more mature and functional human cardiac tissue constructs³⁷¹.

1.2.4. Bioreactors

As described in previous sections, environmental cues are key determinants of cardiomyocyte phenotype and function, and regulate their capacity to form functional tissue units. Therefore, to obtain thick 3D cardiac tissue constructs that resemble myocardial tissue, it is essential not only to mimic the native cardiac environment, but also to ensure an effective mass transport within the construct. To meet all these requirements, it is necessary the use of bioreactors. A bioreactor can be defined as any device that attempts to reproduce physiological conditions to encourage growth and development of cells on biomaterials³⁹⁶. It facilitates oxygen supply to the cultured cells, and exchange of nutrients and metabolites between the cells and the culture medium in a controlled physicochemical microenvironment. Bioreactors can provide a wide variety of physical stimuli, can be adapted to the tissue of interest, and are widely used as model systems to investigate *in vitro* tissue formation and maturation³⁹⁷. Moreover, they can be used to study cell function and tissue development in specific environmental conditions, such as different concentrations of oxygen and biochemical factors, hydrodynamic conditions, and pharmacological agents.

Advanced bioreactor systems should include sensors for real time monitoring and control of culture parameters within the culture chamber (e.g. temperature, pH, oxygen concentration and electromechanical stimulation), recirculation or perfusion systems to guarantee an effective mass transport, and physical stimulation systems to support tissue formation and maturation (**Figure 1.21**). Thus, to successfully produce *in vitro* human tissue models, it is essential to define both cell culture parameters and bioreactor design, which will be defined depending on the tissue to be produced^{396,397}.

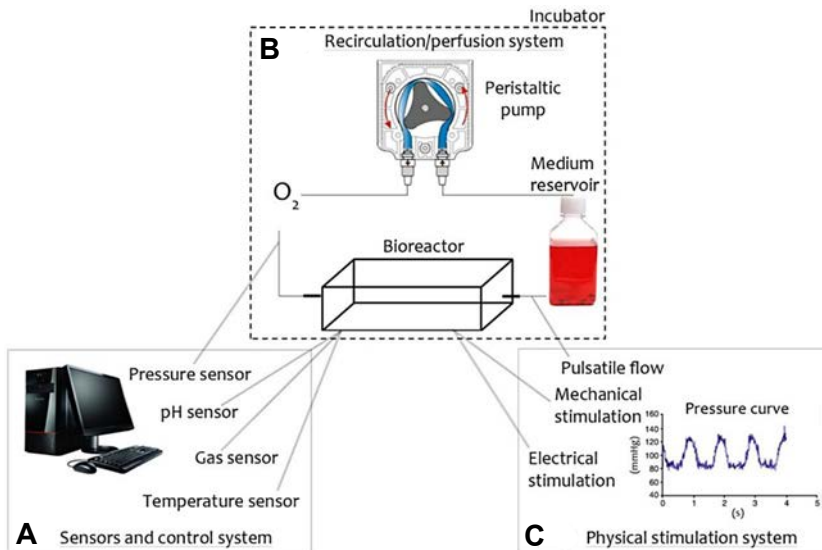


Figure 1.21. Scheme of an advanced bioreactor system. **A**, Sensors and control systems for real time monitoring. **B**, Recirculation or perfusion system to guarantee an effective mass transfer. **C**, Physical stimulation systems. *Image taken from Massai et al.*³⁹⁷.

1.2.4.1. Mass transport

In addition to regulatory signals, advanced bioreactor systems must ensure an effective mass transport. Traditional cell culture systems such as tissue culture plates and flasks are static and rely on diffusional transport mechanisms, which are efficient only within the thin superficial layer in contact with culture medium ($\sim 100\text{-}200\ \mu\text{m}$ ^{297,398}). Therefore, they fail to support 3D tissues: high cell densities deplete nutrients and oxygen over short distances, leading to the formation of a necrotic core in the tissue interior due to low mass transfer rates and high metabolic demand of cells^{18,399}. To increase mass transfer between cells and culture medium, several bioreactors have been developed (**Figure 1.22**).

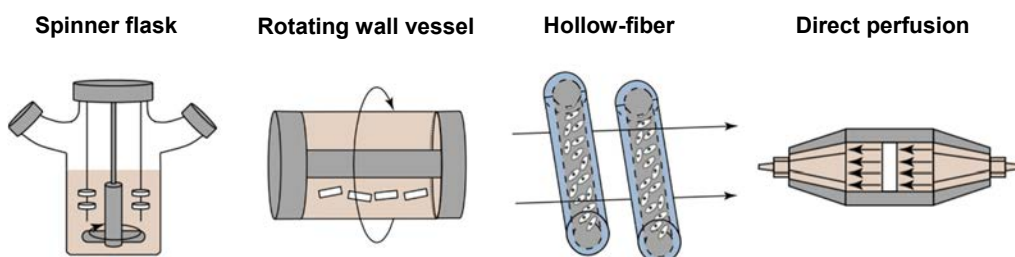


Figure 1.22. Representative bioreactors for tissue engineering applications. Arrows indicate the direction of rotation in spinner flask and rotating wall vessel, while in hollow-fiber and perfusion bioreactors indicate the direction of the medium flow. Cells and tissue constructs are represented in white. *Adapted from Martin et al.*³⁹⁹.

Spinner flasks were among the first bioreactors used to promote the circulation of the medium (**Figure 1.22**). They agitate the external culture medium through the use of stirring elements. Despite increasing overall cell viability compared to static cultures, they generate hydrodynamic and turbulent shear stresses that affect the viability of shear-sensitive cells such as cardiomyocytes⁴⁰⁰. To provide stirring while limiting the shear stress applied to the cells, rotating wall vessel bioreactors were developed. By controlling the rotation speed, a dynamic flow is created where rotational, gravitational and drag forces are balanced to maintain tissue constructs suspended in culture medium in a state of free fall (“microgravity”). Although improvements in cell viability, hypertrophy and electrical function were reported in cardiac tissue constructs cultured in rotating wall vessels with respect to spinner flasks, mass transfer still depends strongly on the internal diffusion of nutrients^{18,401}. Bioreactors that perfuse medium either through or around semi-permeable hollow fibers have been successfully used to maintain the functionality of highly metabolic cells (e.g. hepatocytes)⁴⁰². However, perfusing culture medium directly through the pores of cell-seeded scaffolds reduces mass transfer limitations both at the construct periphery and within its internal pores. Therefore, direct perfusion bioreactors are the most commonly used in tissue engineering. The culture medium is continuously pumped through a porous scaffold, providing high transfer rates of gases and nutrients inside the porous material, stabilizing pH, and removing toxins in an effective manner. Perfusion bioreactors increase diffusion (net movement of molecules along a concentration gradient) with convection (movement of all molecules due to the bulk motion of a fluid), and the type of flow is laminar instead of turbulent^{18,378}. Perfusion bioreactors have shown to be superior regarding cell seeding efficiency and homogeneity in 3D porous scaffolds^{398,403}, and promote cardiomyocyte viability and long-term maintenance of 3D *in vitro* cultures²⁹⁷. However, it is crucial to take into account the shear stress to which cells are subjected during interstitial perfusion, as it can negatively affect the viability of cardiomyocytes⁴⁰⁴. For *in vivo* applications, the removal of thick tissue constructs from perfusion conditions should be compensated by a vascularization technique, as otherwise their survival would be compromised⁴⁰⁵.

1.2.4.2. Multimodal stimulation platforms

To reproduce cardiac native environment in *in vitro* cell culture platforms, multimodal bioreactors with the ability to simultaneously provide several physical regulatory signals have been proposed (**Figure 1.23**). One of the first designs was capable of delivering electrical and mechanical stimulation to cardiac tissue constructs. By applying an electrical pulse of 10 V at the beginning of each period of cyclic stretch, both size and contractile properties of cardiomyocytes were improved⁴⁰⁶. From then on, some multimodal bioreactors have been designed, which have been basically validated using murine cardiomyocytes. For example, Barash et al.⁴⁰⁷ constructed a bioreactor

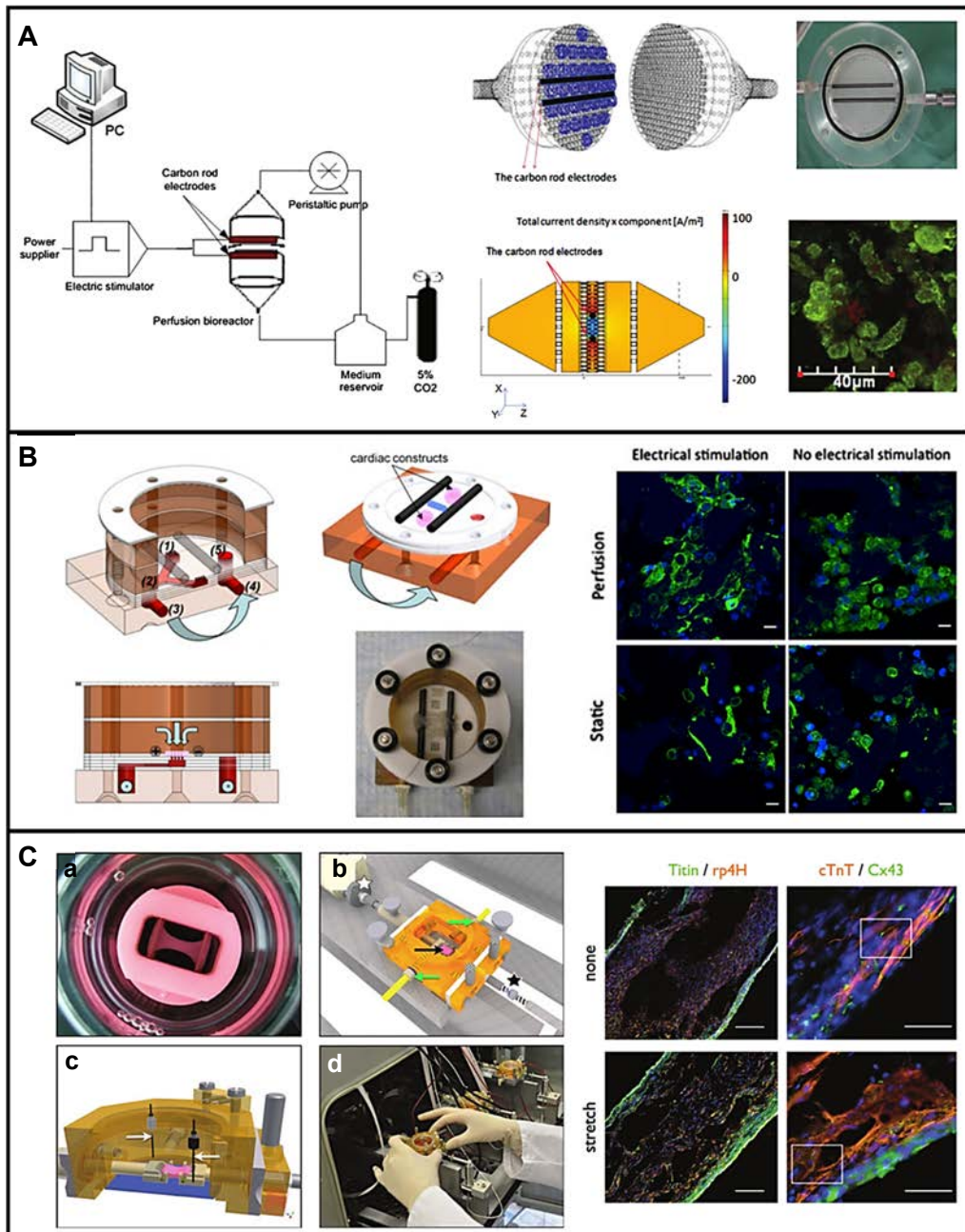


Figure X. Multimodal bioreactors. **A**, Bioreactor setup and electric field model displaying the current density (blue discs: constructs). Immunofluorescence image shows rat cardiomyocytes cultured under perfusion and electrical stimulation. Green: α -sarcomeric actinin; red: nuclei. *Images taken from Barash et al.*⁴⁰⁷ **B**, Perfusion-stimulation bioreactor setup. Blue arrows show medium flow direction. Immunofluorescence images show rat cardiomyocytes (green, troponin I; blue: nuclei). Scale bars: 10 μm . *Images taken from Maidhof et al.*⁴⁰⁸ **C**, Modular bioreactor. Constructs are cast in a mold (**a**), transferred to the bioreactor (**b**, **c**) and placed in an incubator (**d**). White star: linear motor; black star: force sensor; green arrows: perfusion; black arrow: construct; white arrows: fittings for electrodes. rp4H: prolylhydroxylase, cTnT: troponin T; Cx43: connexin 43; blue: nuclei. Scale bars: 200 μm and 50 μm . *Images taken from Kensah et al.*⁴⁰⁹

that delivered electrical stimulation (4 days, bipolar pulses of 5 V, 2 ms and 1 Hz) and perfusion of culture medium (25 ml/min) to cardiac tissue constructs (**Figure 1.23A**). Although rat cardiomyocytes presented higher protein levels of connexin 43 in constructs subjected to both stimuli than in the ones cultured only under perfusion, they did not acquire high anisotropic morphologies with a well-developed sarcomeric organization. Another study also fabricated a bioreactor combining electrical stimulation (monophasic square-wave pulses, 3 V/cm, 2 ms and 3 Hz) and culture medium perfusion (0.018 ml/min), and found that rat cardiac tissue constructs cultured under both stimuli contracted with an amplitude almost 2-fold higher than constructs cultured under perfusion or electrical stimulation separately (**Figure 1.23B**)⁴⁰⁸. Moreover, contractions were more uniform and displayed an orientation towards the construct center in the perfused and electrically stimulated constructs compared to other groups of study, but rat cardiomyocytes did not exhibit well-developed sarcomeric organization. An advanced multimodal bioreactor was designed by Kensah et al.⁴⁰⁹, capable of delivering electrical stimulation, mechanical stimulation, perfusion through the cultivation chamber and real-time monitoring (**Figure 1.23C**). Cyclic stretch induced neonatal rat cardiomyocytes hypertrophy and alignment in the direction of the strain, and systolic forces exerted by the constructs were increased with respect to those cultured in static conditions. Significantly higher forces were observed after β -adrenergic stimulation, but combined mechanical and β -adrenergic stimulation had no synergistic effect. The effect of combining other regulatory signals (e.g. mechanical and electrical stimulation) on tissue constructs functionality and organization was not addressed.

Much less works have been published applying multimodal stimulation bioreactors to human cardiac tissue engineering. In fact, the generation of functional and thick 3D human cardiac tissues with multicellular composition is still a challenge in the field. Most of the advances using hPSC-CM have reported the production of cardiac microtissues and microphysiological systems. The vast majority of the investigations involve the fabrication of microtissues by using natural-based hydrogels, which are cast in band or ring shapes and are fixed at both ends mainly through a two-post configuration^{50,104,278,280,337,410–413} (**Figure 1.24A-B**). Other configurations include casting cell/hydrogel mixture in hexagonal posts²⁷⁷ (**Figure 1.24C**) or around a wire-like template (e.g. a surgical suture or a tubing) to obtain biowires^{319,414} (**Figure 1.24D**). These designs include static stretch and some of them also include other regulatory signals, such as electrical pacing^{319,329,337,412,414}, cyclic stretch^{104,278}, co-culture with non-myocytes^{104,278,280,319}, ascorbic acid supplementation²⁸⁰ or rocking in cardiac medium²⁷⁷. These signals improve the maturation level of cardiomyocytes and demonstrate important applications in predictive toxicology and cardiac disease modelling. Similarly, highly miniaturized microphysiological systems, called “heart-on-chip” technologies, allow for increased throughput and controlled microenvironments for drug screening⁴¹⁵

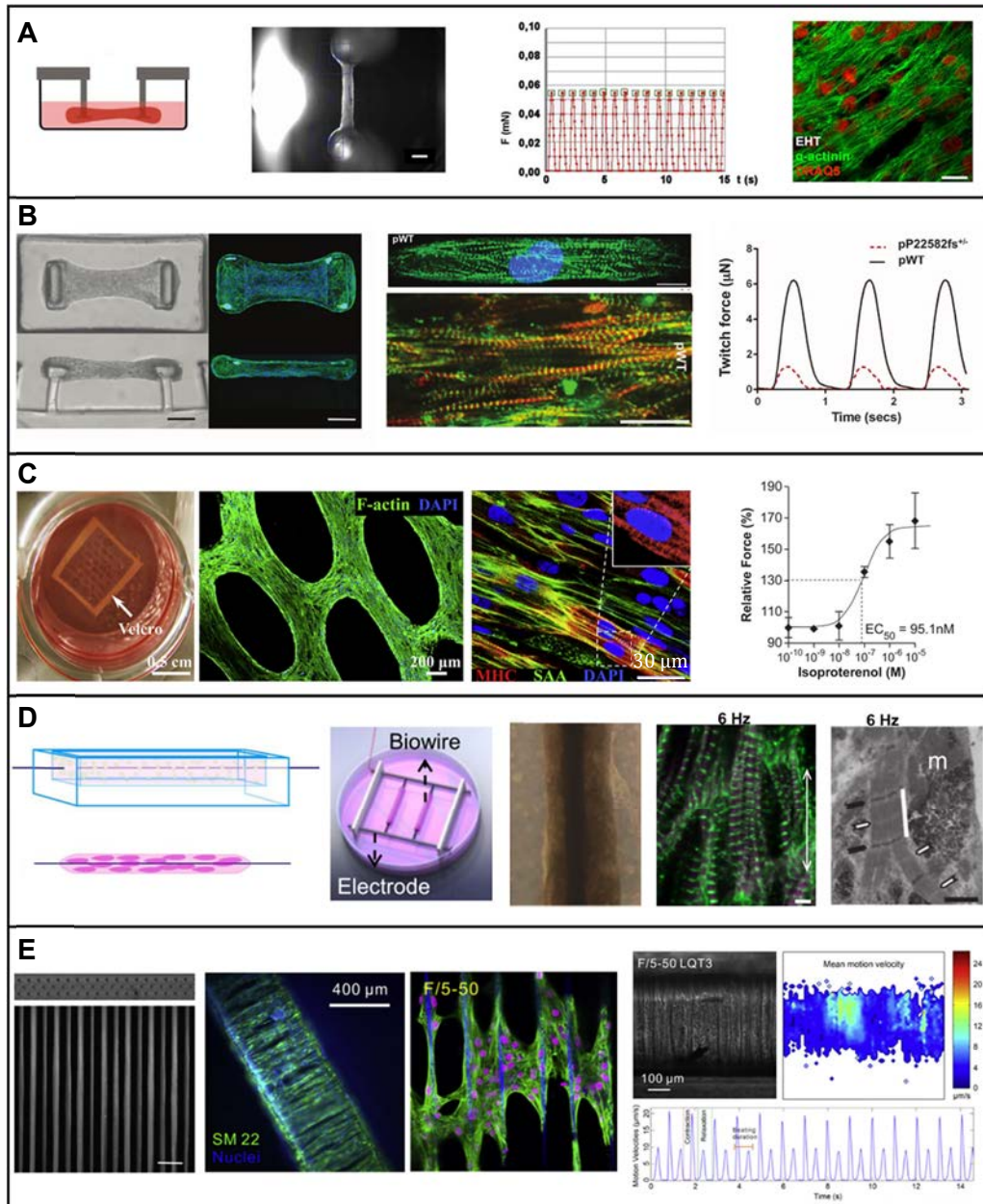


Figure 1.24. Representative 3D human cardiac tissue constructs. **A**, Engineered heart tissues (EHT) from hESC-CM for drug screening. α -actinin: green; nuclei: red. Scale bars: 1 mm and 20 μ m. Images taken from Schaaf *et al.*⁵⁰. **B**, Engineered heart microtissues from hiPSC-CM used to model dilated cardiomyopathy. α -actinin A: green; F-actin: red; nuclei: blue. Scale bars: 50 μ m and 20 μ m. Images taken from Hinson *et al.*⁴¹⁰. **C**, Cardiac tissue patch containing elliptical pores surrounded by densely packed hESC-CM. MHC: myosin heavy chain; SAA: sarcomeric α -actinin. Images taken from Zhang *et al.*²⁷⁷. **D**, Biowires generated from hiPSC-CM and subjected to electrical stimulation. α -actinin: green; actin: red; arrow: suture axis; black arrowheads: Z disc; white arrowheads: H zone; m: mitochondria. Images taken from Nunes *et al.*³¹⁹. **E**, Filamentous matrix seeded with hiPSC-CM from healthy or LQT3 patients. Sarcomeric α -actinin: green; nuclei: purple; scaffold: blue. Images taken from Ma *et al.*⁴¹⁸.

and study of human cardiac diseases⁴¹⁶. For regenerative therapy purposes, hiPSC-engineered cardiovascular cell sheets reported improved cardiac function in rat infarcted hearts^{12,417}. However, these approaches are still far from the initial goal of cardiac tissue engineering, which is the generation of thick 3D human cardiac tissue constructs not only for *in vitro* studies, but also with appropriate dimensions and easy to handle for regenerative medicine purposes. This idea of generating 3D tissue-like human cardiac constructs has only been attempted in a few recent studies where hPSC-CM are seeded in 0.5-1 mm thick scaffolds^{278,418} (**Figure 1.24E**). However, they do not stimulate the generated tissue with combined electromechanical signals neither make use of perfusion bioreactors to maintain the viability of the construct, so their functionality and structure is still far from resembling the adult myocardium.

Overall, multimodal bioreactors hold great promise in providing biomimetic culture environments for the growth and maturation of human cardiac tissue constructs. However, with increased bioreactor complexity, the susceptibility to failure increases, as well as the difficulties in identifying the optimal regime of stimulation. In addition, translational potential of the entire approach may decrease due to regulatory and commercialization issues. All those factors must be considered when designing a viable tissue engineering strategy for use in toxicology screening, drug development, and regenerative therapies³⁷⁸. Despite these issues, advanced 3D culture systems that combine multiple regulatory signals and ensure an effective mass transport may be essential to obtain tissue-like human cardiac construct. As they bring additional complexity with respect to currently available microtissue models, they could lead to the generation of functional and thick 3D human cardiac constructs that resemble the adult myocardium, which is still a challenge in the field.

1.2.5. Electrophysiological evaluation of cardiac constructs

Ion currents and electrical conduction play a pivotal role in the evaluation of the functionality of cardiac tissue constructs. For example, deciphering the electrical function of hiPSC-CM allows the characterization of their maturity level, distinguishing between healthy and diseased cells, and even between ventricular and atrial cells⁴¹⁹. Importantly, electrophysiological markers are among the most useful to evaluate proarrhythmia when hPSC-CM are treated with multiple pharmacological agents²⁴⁴. Therefore, several screening technologies are emerging that permit studying and characterizing hPSC-CM electrophysiological functions.

The electrical function of hPSC-CM can be measured through transmembrane action potentials²³⁷, microelectrode arrays (MEA) recordings⁴²⁰, impedance measurements⁴²¹, and optical signals using calcium³²⁵ or voltage-sensitive dyes⁴²² (**Figure 1.25**)²²⁹.

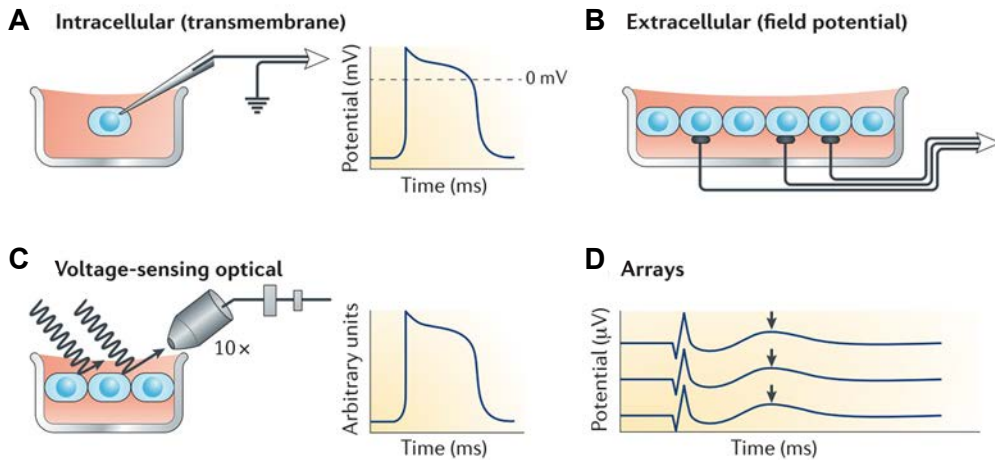


Figure 1.25. Approaches to evaluate cardiomyocyte electrophysiological functions. **A**, Recording of intracellular transmembrane potentials using microelectrodes (e.g. patch clamp). **B**, Microelectrode array (MEA) recordings provide localized extracellular field potentials from electrodes located on the chamber floor. **C**, Voltage-sensitive dyes provide optical signals of transmembrane potentials based on changes in fluorescence. Changes in action potential duration or repolarization can be obtained from multiple myocytes in a reasonable throughput. **D**, Changes in field potential duration (FPD) are reliably measured from the peak of the repolarization wave (arrows), being easily translated to clinical effects. Altered repolarization can also be recorded. *Image taken from Gintant et al.*²⁴⁴.

A widely used approach to evaluate the electrophysiological function of cardiomyocytes is recording transmembrane action potentials through patch clamp technique (**Figure 1.25A**). Patch clamp is a single cell electrophysiology system that is useful to gather information about the role of specific currents and ions of cardiomyocytes. It allows to directly monitor cardiac action potentials, and has demonstrated to be especially useful when evaluating arrhythmogenic effects of pharmacological agents or modelling cardiac diseases⁴¹⁹. Nevertheless, recording of intracellular transmembrane potentials using microelectrodes is slow, technically demanding and difficult to adapt to high throughput systems. Automated patch clamp platforms have permitted to collect large amounts of data, but they are technically difficult and not readily available for widespread use⁴²³. Moreover, individual currents of particular interest in hPSC-CM research (e.g. I_{Kr}) are quite small and difficult to measure with patch clamp techniques. Finally, the applicability of patch clamp techniques to cardiac tissue constructs is not straightforward.

Cardiac action potentials can also be directly monitored using MEA (**Figure 1.25B and D**)^{420,424}. MEA are a valuable tool to gather information about the activity of several cells in a dish, and are effective, stable and minimally invasive^{420,425}. Possibly, they are the easiest approach to obtain electrophysiological data, as they do not require recording from a single cell and have high spatial and temporal resolution⁴²⁶. MEA

record extracellular field potentials (EFPs), which are the charge redistribution in cardiomyocytes surrounding medium as a consequence of action potential firing. Typically, MEA allow the measurement of field potential duration (FPD, action potential duration of a single cell that corresponds to the QT interval on the surface ECG), beating frequency, amplitude of initial depolarization spike, conduction parameters, and incidence of altered repolarization²⁴⁴. FPD has been established as an important parameter for researchers using hPSC-CM to model arrhythmic diseases or as a platform for drug discovery^{425,427,428}. Finally, voltage-sensing optical (VSO) techniques can provide similar measures than MEA, as they can show changes in the duration and time course of repolarization (**Figure 1.25C-D**)²⁴⁴. Calcium flux can be detected in beating cardiomyocytes using plate-based detection systems, such as fast kinetic fluorescence imaging of calcium-sensitive dyes⁴²⁹. They allow quantifying calcium oscillations in synchronously beating cardiomyocyte monolayers, or in hundreds of individual cells per well²²⁹.

In cardiac tissue engineering, once the 3D cardiac tissue constructs have been generated, the *in vitro* assessment of their quality in terms of electrical activity without affecting their performance is limited. To date, action potentials in cardiac tissue constructs are recorded through patch clamp techniques on a representative cell population at the time of seeding²⁷⁷ or on isolated cardiomyocytes after tissue formation^{50,319}. Alternatively, electrophysiological data such as conduction velocity and Ca²⁺ handling properties can be obtained from constructs through VSO techniques³¹⁹. However, it is necessary to develop an electrophysiological recording system that provides information about action potentials from intact engineered heart tissues¹⁷². The field of tissue engineering continues to grow, and it is essential to integrate electrical sensors to complex 3D structures to remotely monitor cellular activities⁴³⁰. Having established methodologies would facilitate the comparison between different designs and hPSC-CM sources, as well as the identification, study and interpretation of optimal culture conditions in comparison with native ventricular cardiomyocytes.

2. HYPOTHESIS AND OBJECTIVES

The discovery of human induced pluripotent stem cells (hiPSC) represents a great promise for cardiovascular research and therapeutic applications. However, despite the ability of hiPSC to differentiate into cardiomyocytes, their use has been limited mainly by their immature, fetal-like phenotype.

It has been described that mimicking native cardiac environment through the use of advanced instructive systems promote animal-derived cardiomyocytes maturation in 3D tissue constructs.

Therefore, the **hypothesis** of our study is that the combination of hiPSC-derived cardiomyocytes with 3D scaffolds and appropriate instructive signals may lead to the generation of mature human cardiac tissue constructs resembling human myocardium, both functionally and structurally. The 3D cardiac constructs obtained in this way could be used as *in vitro* models in cardiovascular research and/or as surrogates for regenerative medicine applications.

Based on these premises, this thesis attempts to fulfill the following **objectives**:

1. To develop an advanced 3D culture system including perfusion of culture medium and electrical stimulation to produce thick 3D cardiac tissue constructs.
2. To generate tissue-like human cardiac constructs from hiPSC-CM and determine the role of electrical stimulation in tissue formation and cardiomyocyte maturation.
3. To develop an electrophysiological recording system to monitor the activity of human cardiac constructs online and study their ability to predict drug-induced cardiotoxicity.

3. MATERIALS AND METHODS

3.1. Cell culture

3.1.1. Human foreskin fibroblasts (HFF) culture

Vials containing $1 \cdot 10^6$ human foreskin fibroblasts (HFF) (ATCC® SCRC-1041™) were thawed by dipping the lower half of the vial into 37°C water bath until a small amount of ice remained inside. Then, the content of the vial was transferred to a 15 ml conical Falcon tube (Thermo Fisher Scientific, Spain) with 10 ml of culture medium warmed at 37°C. Culture medium was composed of DMEM 4.5 g/l glucose (Life Technologies, Thermo Fisher Scientific, Spain) supplemented with 10% fetal bovine serum (FBS) (Gibco®, Thermo Fisher Scientific, Spain), sodium pyruvate 1 mM (Life Technologies, Thermo Fisher Scientific, Spain), 2 mM L-glutamine (Invitrogen, Spain) and penicillin-streptomycin 50 U/ml (Sigma-Aldrich Química, Spain). Cell suspension was pipetted up and down with a 10 ml pipette to disperse cells and centrifuged at 1200 rpm for 5 min. Supernatant was discarded and cell pellet was resuspended in warm culture medium. Cells were counted with a Neubauer Chamber (Thermo Fisher Scientific, Spain) and seeded in cell culture treated flasks (Nunc™, Thermo Fisher Scientific, Spain) at a cell density of $1 \cdot 10^4$ cells/cm². Cells were incubated at 37°C and 5% CO₂ air humidified incubator (Thermo Fisher Scientific, Spain), and culture medium was changed every two days until the culture was approximately 90% confluent. Then, culture medium was removed from the flask, cells were washed once with 10 ml of pre-warmed Phosphate Buffered Saline (PBS) (Thermo Fisher Scientific, Spain) and 2 ml of 0.25% trypsin-EDTA solution (Sigma-Aldrich Química, Spain) at 37°C was added to the flask. After 4 min incubation at 37°C, during which cells detached, 5 ml of culture medium were added to the flask and cells were transferred to a sterile 15 ml conical Falcon tube. Cells were counted with a Neubauer Chamber (Thermo Fisher Scientific, Spain) and the appropriate volume to have the desired cell number was pipetted from the cell suspension and transferred to a new tube. Finally, cells were centrifuged at 1200 rpm for 5 min, supernatant was discarded and cells were resuspended in culture medium to have a cell suspension ready to be seeded either in the 3D scaffold (for further details, see “3.3.2. *Perfusion seeding*” section) or on 0.1% gelatin-coated 12-well plates.

3.1.2. Isolation and primary culture of neonatal rat heart cells

Cardiac cells were obtained from ventricles of 2-3-day-old Sprague-Dawley rats following a protocol approved by Animal Experimentation Ethics Committee of the University of Barcelona (Barcelona, Spain). Twenty to fifty pups were sacrificed by decapitation, upper thorax opened and hearts extracted with tweezers and collected in ice-cold, filtered and freshly prepared Calcium and Bicarbonate-Free Hank's Balanced Salt Solution with HEPES (CBFHH) buffer. CBFHH was composed of 136.8 mM NaCl, 5.4 mM KCl, 0.81 mM MgSO₄(H₂O)₇, 0.44 mM KH₂PO₄, 0.34 mM Na₂HPO₄(H₂O)₂,

5.6 mM Glucose and 20 mM HEPES (N-2-hydroxyethylpiperazine-N-2-ethane sulfonic acid) (Sigma-Aldrich Química, Spain). Hearts were washed in CBFHH and auricles and rests of other tissues (thyme, lungs, etc.) were eliminated. Ventricles were cut into two parts to remove blood as much as possible, and were washed with ice-cold CBFHH buffer. Then, ventricles were cut sharply into small pieces (<1 mm³), collected in a 50 ml Falcon tube and subjected to 20-25 digestion cycles (**Table 3.1**) using ice-cold 2 mg/ml trypsin (BD Difco™, Spain) in CBFHH and ice-cold 4 µg/ml DNase I (Calbiochem, Merck Millipore, Spain) in CBFHH⁴³¹. The first digestate (predigestion), performed incubating the tissue with trypsin solution during 8 min at room temperature in agitation, was discarded. The following digestion cycles were performed alternating trypsin incubations (in agitation at room temperature) with DNase I ones (pipetting up and down 20-25 times using a glass pipette with a large tip width (~3 mm, custom made)), until tissue pieces became whitish and smaller (**Table 3.1**). After each incubation, supernatants containing cell suspensions were collected using a glass pipette with a large tip width into a collection tube with 2.5 ml of ice-cold fetal bovine serum (FBS) (Gibco®, Thermo Fisher Scientific, Spain). Tubes containing cell suspensions were centrifuged at 100 x g for 12 min, supernatant discarded and pellets resuspended in 2 ml of ice-cold non-cardiomyocyte medium (NKM), containing DMEM 1 g/l glucose (Life Technologies, Thermo Fisher Scientific, Spain) supplemented with 10% FBS, 100 µM non-essential amino acids (Life Technologies, Thermo Fisher Scientific, Spain), 2 mM L-glutamine (Life Technologies, Thermo Fisher Scientific, Spain), 50 U/ml penicillin and 50 µg/ml streptomycin (Life Technologies, Thermo Fisher Scientific, Spain). All cell suspensions were collected in one tube and incubated with 10 µg/ml DNase I by gently pipetting 20-25 times. Finally, cells were centrifuged at 100 x g for 12 min, resuspended in ice-cold NKM and filtered through a 250 µm stainless steel test sieve (Filtro Vibración, Spain) to obtain the final cell suspension. Cardiomyocytes were counted using a Neubauer Chamber (Thermo Fisher Scientific, Spain), excluding other cell types by morphology. We acknowledge Dr. Maria López Cavanillas from Reparative Therapy of the Heart group, led by Dr. Manuel Galíñanes at Vall d'Hebron Institut de Recerca (VHIR), for providing the protocol to isolate and culture cardiac cells from neonatal rat ventricles. We also acknowledge the use of facilities and the technical support from the Animal Experimentation Service at Faculty of Pharmacy and Food Sciences, University of Barcelona (UB).

Right after obtaining, cardiac cells were seeded either into Matrigel™ scaffolds (BIOSER NORESTE, MBA, Spain), on top of Matrigel®-coated (Corning, Spain) glass coverslips, being Matrigel® a gelatinous protein mixture secreted by Engelbreth-Holm-Swarm mouse sarcoma cells, or on 0.1% gelatin-coated (Merck Millipore, Spain) 12-well plates. Cells were cultured in cardiomyocyte medium, containing DMEM 4.5 g/l glucose (Life Technologies, Thermo Fisher Scientific, Spain) supplemented with 10% horse serum (Life Technologies, Thermo Fisher Scientific, Spain), 2% Chick Embryo

Extract (EGG Tech, United Kingdom), 100 μ M non-essential amino acids, 2 mM L-glutamine, 50 U/ml penicillin and 50 μ g/ml streptomycin.

	Enzyme	Volume (ml)	Time (min)	Rounds	Comments
Predigestion	Trypsin	8	8	1	Discard supernatant
Collection tube 1 (CT1)	Trypsin	8	4	Up to fill the tube	Collect supernatant
	DNase I	7	Pipetting		Collect supernatant
Collection tube 2 (CT2)	Trypsin	7.5	3	Up to fill the tube	Collect supernatant
	DNase I	6.5	Pipetting		Collect supernatant
Collection tube 3 (CT3)	Trypsin	7	2	Up to fill the tube	Collect supernatant
	DNase I	6	Pipetting		Collect supernatant
Collection tube 4 (CT4)	Trypsin	6.5	1	Up to fill the tube	Collect supernatant
	DNase I	5.5	Pipetting		Collect supernatant
Collection tube 5 (CT5)	Trypsin	6	1	Up to fill the tube	Collect supernatant
	DNase I	5	Pipetting		Collect supernatant
Collection tube 6 (CT6)	Trypsin	6	1	Up to fill the tube	Collect supernatant
	DNase I	5	Pipetting		Collect supernatant
Collection tube 7 (CT7)	Trypsin	6	1	Up to fill the tube	Collect supernatant
	DNase I	5	Pipetting		Collect supernatant

Table 3.1. Digestion cycles of neonatal rat heart ventricles to obtain a primary cell culture. Trypsin incubation is alternated with DNase I incubation for an efficient cell extraction. Adapted from Di Guglielmo, C⁴³¹.

3.1.3. Human induced pluripotent stem cells (hiPSC) culture

Human keratinocyte-derived iPS cells (KiPS3F.7; cell line generated in the Centre of Regenerative Medicine in Barcelona (CMRB) from a healthy donor) were cultured with conditioned HES medium (cHES), which is culture medium conditioned for 24 h with irradiated mouse embryonic fibroblasts (MEF; obtained and irradiated by Control of Stem Cell Potency group, Institute for Bioengineering of Catalonia (IBEC)) and composed of Knockout™ DMEM (Life Technologies, Thermo Fisher Scientific, Spain) supplemented with 20% Knockout Serum Replacement (Life Technologies, Thermo Fisher Scientific, Spain), 100 μ M non-essential amino acids (Life Technologies, Thermo Fisher Scientific, Spain), 2 mM GlutaMax (Life Technologies, Thermo Fisher Scientific, Spain), 50 U/mL penicillin, 50 μ g/mL streptomycin (Life Technologies, Thermo Fisher Scientific, Spain), 50 μ M 2-mercaptoethanol (Life Technologies, Thermo Fisher Scientific, Spain), and 10 ng/mL basic fibroblast growth factor (bFGF; Peprotech, United

Kingdom). *Work performed by Dr. Claudia Di Guglielmo from Control of Stem Cell Potency group at Institute for Bioengineering of Catalonia (IBEC).*

Human fibroblasts-derived iPS cells (FiPS Ctrl1-mR5F-6; cell line registered in the National Stem Cell Bank, Institute of Health Carlos III, Spanish Ministry) were cultured on Matrigel[®]-coated (Corning, Spain) 10 cm dishes with mTeSR[™]1 medium (STEMCELL Technologies, France). Medium was changed every day, excluding the day right after passaging. Cells were split 1:6 – 1:10 by incubation with 0.5 mM EDTA (Invitrogen, Spain) for 2 min at 37°C and cell aggregates were plated on Matrigel[®]-coated dishes and maintained in culture for subsequent passages (*work performed by Dr. Olalla Iglesias from Center of Regenerative Medicine in Barcelona (CMRB)*).

3.1.4. Generation of hiPSC cardiac-specific reporter lines

This part of the work has been performed by Dr. Claudia Di Guglielmo from Control of Stem Cell Potency group at Institute for Bioengineering of Catalonia (IBEC). For further details, readers are encouraged to refer to Dr. Di Guglielmo's PhD thesis⁴³¹.

During *in vitro* differentiation of human induced pluripotent stem cells (hiPSC), many different cell types arise in culture in a non-synchronized way. For this reason, a critical factor in differentiation protocols is to monitor the effectiveness of differentiation during time, as it allows the selection and expansion only of the cell population of interest. For this purpose, we generated a set of transgenic hiPSC lines using the KiPS3F.7 cell line that allowed the monitoring of the differentiation process through expression of green fluorescence protein (GFP) (**Figure 3.1A**). Two different reporter cell lines were generated: one expressing GFP when hiPSC were differentiated to early mesoderm (KiPS3F.7 T/Bra:GFP_Rex1:Neo^R), and another one expressing GFP when hiPSC were differentiated to cardiomyocytes (KiPS3F.7 α MHC:GFP_Rex1:Neo^R) (**Figure 3.1B**). Brachyury (Bra) is a transcription factor encoded by T gene, and is transiently expressed during mesoderm specification. Conversely, the alpha-myosin heavy chain (α -MHC) gene encodes a cardiac muscle-specific protein involved in active force generation. To specifically monitor the cardiac differentiation process at early and late stages, GFP was expressed under the control of Bra or α -MHC promoters. In both vectors, we added the promoter of reduced expression 1 (Rex-1) gene, which is a marker of pluripotency, and neomycin-resistance gene (Neo^R), which allows cell survival in the presence of the antibiotic neomycin. Hereby, Rex1-Neo^R cassette enabled selection of stable hiPSC lines with integrated promoter-reporter constructs that would be expressed in cells differentiating towards the cardiogenic lineage.

T/Bra:GFP_Rex1:Neo^R and α MHC:GFP_Rex1:Neo^R transfer vectors for lentivirus production were acquired from Addgene (plasmid #21222 and #21229, respectively⁴³², USA). For lentivirus production, human embryonic kidney cells

(HEK293T; ATCC® CRL-3216™) were transiently and separately transfected with the mentioned transfer vectors, the second generation packaging construct pCMVR8.74 (Addgene plasmid #22036, USA) and the vesicular stomatitis virus (VSV) envelope-expressing construct pCMV-VSV-G (Addgene plasmid #8454, USA). High-titre VSV-pseudotyped lentivirus stocks were produced, purified and resuspended to a final volume of 50 µl in phosphate buffered saline (PBS). Finally, KiPS3F.7 cells maintained in culture were transferred to an Eppendorf with a final concentration of $1 \cdot 10^6$ cells/ml, infected with 5 µl of viral particles and incubated for 1 h at 37°C. Cells were then plated into a Matrigel®-coated 6-well plate and cultured with 1 ml of cHES medium. After 24 h, medium was replaced and cells were cultured as usual. After 4 days from infection, selection with neomycin (Sigma-Aldrich Química, Spain) was performed during 10 days, diluting it 1:1000 into culture medium to a final concentration of 50 µg/ml. Proper lentiviral integration in the genome of the cells was confirmed by polymerase chain reaction (PCR), using specific primers targeting GFP sequence (**Table 3.5**).

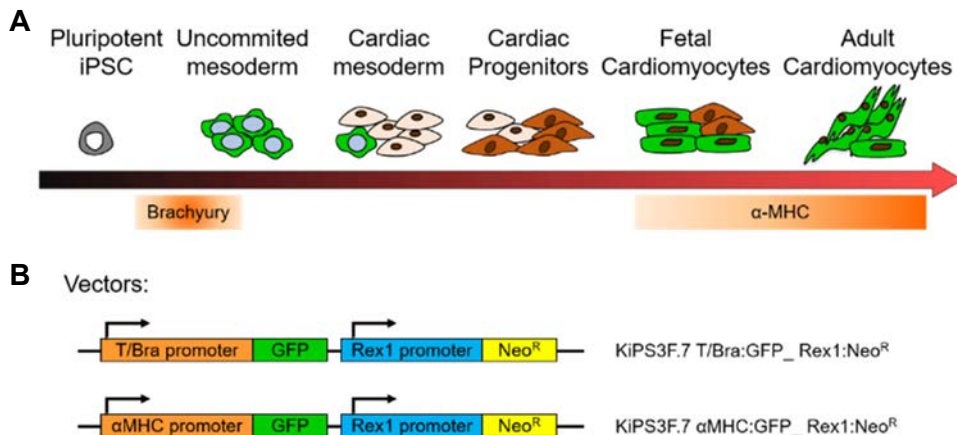


Figure 3.1. Myocardial differentiation of human induced pluripotent stem cells (hiPSC) and reporter cell lines generation. **A**, Diagram of hiPSC differentiation into cardiomyocytes. Our reporter cell lines express green fluorescent protein (GFP) under the control of Brachyury (Bra) and alpha-myosin heavy chain (α -MHC) promoters, represented by green cells in the timeline. **B**, Vectors used to generate hiPSC cardiac-specific reporter lines using KiPS3F.7 cell line. T/Bra: gene T encoding Brachyury; Rex1: reduced expression 1 promoter; Neo^R: neomycin-resistance gene. Adapted from Di Guglielmo, C⁴³¹.

3.1.5. Cardiac differentiation protocol of hiPSC

Human induced pluripotent stem cells (hiPSC) were differentiated into cardiomyocytes in monolayer culture with modulators of canonical Wnt signaling following a previously described protocol⁴³³ with slight modifications (**Figure 3.2**, work performed by Dr. Claudia Di Guglielmo from Control of Stem Cell Potency group at

Institute for Bioengineering of Catalonia (IBEC), and Dr. Olalla Iglesias from Center of Regenerative Medicine in Barcelona (CMRB)). In brief, cells maintained on Matrigel® in mTeSR™1 medium were dissociated into single cells with Accutase (Labclinics, Spain) at 37°C for 8 min and seeded onto Matrigel®-coated 12-well plate at a density of $1.5 \cdot 10^6$ cells per well in mTeSR™1 medium supplemented with 10 μ M ROCK inhibitor (Sigma-Aldrich Química, Spain) (day -4). Cells were cultured in mTeSR1 medium, changed daily during 3 days. When human FiPSC achieved confluence, cells were treated with 10 μ M GSK3 inhibitor (CHIR99021, Stemgent, USA) in RPMI medium (Invitrogen, Spain) supplemented with B27 lacking insulin (Life Technologies, Thermo Fisher Scientific, Spain), 1% GlutaMax (Gibco, Thermo Fisher Scientific, Spain), 0.5% penicillin-streptomycin (Gibco, Thermo Fisher Scientific, Spain), 1% non-essential amino acids (Lonza, Switzerland), and 0.1 mM 2-mercaptoethanol (Gibco, Thermo Fisher Scientific, Spain) (RPMI/B27-insulin medium) for 24 h (day 0 to day 1). After 24 h, the medium was changed to RPMI/B27-insulin and cultured for another 2 days. On day 3 of differentiation, cells were treated with 5 μ M Wnt inhibitor IWP4 (Stemgent, USA) in RPMI/B27-insulin medium and cultured without medium change for 2 days. Cells were maintained in RPMI supplemented with B27 (Life Technologies, Thermo Fisher Scientific, Spain), 1% L-glutamine, 0.5% penicillin-streptomycin, 1% non-essential amino acids, and 0.1 mM 2-mercaptoethanol (RPMI/B27 medium) starting from day 5, with medium change every 2 days. On day 12, contracting cardiomyocytes were obtained. Beating clusters were disaggregated (at day 20 and at day 35) by incubation with 0.25% trypsin-EDTA (Gibco, Thermo Fisher Scientific, Spain) for 5-8 min at 37 °C, both for their characterization and *in vitro* studies.

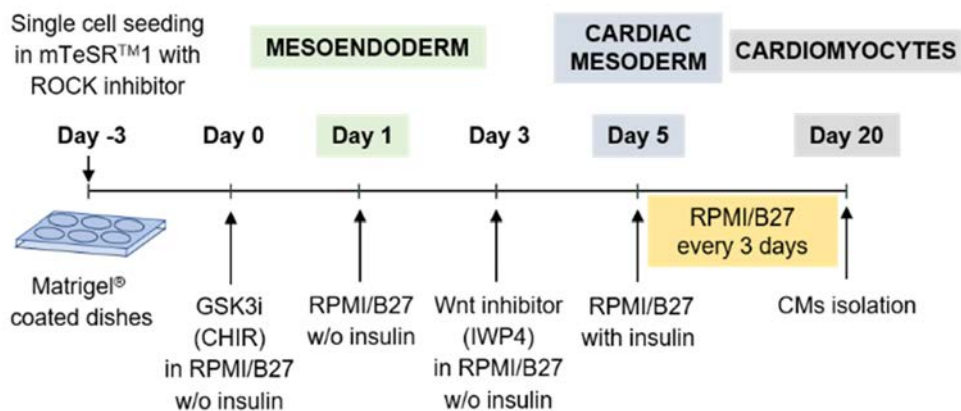


Figure 3.2. Human iPSC (hiPSC) differentiation into cardiomyocytes. Human iPSC were differentiated into cardiomyocytes in a defined growth factor and serum-free system by treatment with modulators of canonical Wnt signalling⁴³³.

3.2. Structural and mechanical properties of the scaffold

3.2.1. Morphology and porosity

A commercially available collagen-based sponge (Matriderm™, BIOSER NORESTE, MBA, Spain) was used as scaffold. According to manufacturer's datasheet, it is a 3D matrix composed of native structurally intact collagen and elastin to support dermal regeneration. The collagen is obtained from bovine dermis and contains the dermal collagen types I, III and V. The elastin is obtained from bovine nuchal ligament by hydrolysis. The absence of chemical cross-linking of the collagen results in a matrix which is especially biocompatible, so we used it as provided by the manufacturer (1 mm thickness and ~94% porosity). To analyze scaffold morphology and mean pore size in dry conditions, a scanning electron microscope (SEM; Nova NanoSEM 230, FEI, The Netherlands) was employed. Low vacuum mode (1 mbar water vapor pressure) and a low vacuum detector were used, so even though the sample was nonconductive, it was imaged without using any special sample preparation or conductive coating. Data was collected over three selected areas of the surface of two different samples, and 2D images were generated. For pore size calculation, Feret's diameter was measured, which is the longest distance between any two points along a selected boundary, in this case scaffold's pores. At least 120 pores per sample were measured using ImageJ free software⁴³⁴ (National Institutes of Health, USA). Finally, measurements were fitted in a single peak following an extreme value distribution. We acknowledge the use of facilities from the Nanotechnology Platform at Institute for Bioengineering of Catalonia (IBEC).

To elucidate scaffold morphology in hydrated conditions, Second Harmonic Generation (SHG) and two-photon excited fluorescence (TPEF) was used. SHG is an optical technique based on nonlinear light-matter interaction. This interaction happens in biological tissues without adding any type of staining, and is very useful to obtain high contrast images in a non-invasive manner^{435,436}. Collagen is a non-centrosymmetric molecule considered a strong source of SHG, and both collagen and elastin are a significant source of extracellular matrix autofluorescence that can be imaged by TPEF, with an emission spectra that overlap significantly⁴³⁷. The SHG-TPEF setup consisted of an inverted confocal microscope (Leica SP5, Leica Microsystems, Spain) equipped with an IR Mai Tai Wide Band (710-990 nm) laser (Spectra-Physics, USA). The exciting laser beam was tuned to 900 nm and the SHG signal was obtained using an external non-descanned detector (NDD) with a 447-453 nm bandpass filter. In another channel, the TPEF signal was collected by tuning the exciting laser beam to 810 nm and using a Leica hybrid detector (HyD) with a 460-600 nm bandpass filter. Images were analyzed using ImageJ free software⁴³⁴ (National Institutes of Health, USA). Finally, 3D distribution of scaffold fibers was analyzed using IMARIS software (Bitplane AG, Switzerland). We acknowledge the use of facilities and the technical support from the Advanced Digital Microscopy unit at Institute for Research in Biomedicine (IRB).

3.2.2. Stiffness

Scaffold stiffness was measured in compression using a Q800 Dynamic Mechanical Analyzer (TA instruments, USA) by applying a ramp strain of -0.5 %/min rate to a maximum strain of -5.0 % and a preload force of 0.01 N. Young Modulus (E) was determined from the slope of the stress-strain curves at room temperature and at 37°C. The difference between group means was assessed using a two-sample t-Test. The software used was Origin 8.5 (OriginLab, Northampton, USA), and differences were considered significant when $p < 0.05$. We acknowledge the use of facilities and technical support from Dr. Eloi Pineda, Group of Characterization of Materials, Barcelona School of Agricultural Engineering, Polytechnic University of Catalonia (UPC).

3.3. Cell seeding in 3D scaffolds

3.3.1. Static seeding

Static seeding in Matriderm™ scaffold was performed as described previously²⁹⁷, using Matrigel® as cell delivery vehicle. Briefly, a primary culture of neonatal rat cardiac cells was resuspended in Matrigel® in a concentration of $1 \cdot 10^6$ cells/5 μ l Matrigel®, and $12 \cdot 10^6$ cells per scaffold were inoculated by putting the pipette tip at multiple locations of scaffold top part. Finally, scaffolds were incubated at 37°C and 5% CO₂ during 30 min to allow for cell attachment and were transferred into the bioreactor.

3.3.2. Perfusion seeding

Matriderm™ scaffold was cut with a biopsy punch (1 cm diameter, Acu-Punch, Acuderm, USA) and rehydrated in phosphate buffered saline (PBS) (Thermo Fisher Scientific, Spain) for 24 h, and then in culture medium for at least 1 h before use. For rat cardiac tissue constructs generation, $3.5 \cdot 10^6$ cardiomyocytes isolated from rat ventricles were resuspended in 1 ml of supplemented DMEM (see “3.1.2. Isolation and primary culture of neonatal rat heart cells” section for further details). For human cardiac tissue constructs generation, $3.5 \cdot 10^6$ human iPSC-derived cardiomyocytes selected at day 20 of differentiation and $0.5 \cdot 10^6$ human foreskin fibroblasts (HFF) were resuspended in 1 ml of RPMI culture medium. Each cell suspension was seeded into the scaffold using an adapted version of a previously described perfusion loop²⁹⁷. The system had the following components (**Figure 3.3**): both endings of a (1) PharMed® BPT 3-Stop pump tubing (0.89 mm inner diameter, Thermo Fisher Scientific, Spain) were connected to two pieces of (2) Tygon tubing (4.8 mm inner diameter x 8 mm outer diameter, Thermo Fisher Scientific, Spain). At their edges, both pieces of tubing were connected to a (3) three-way stopcock (Smith Medicals, Spain), one of its exits attached to another piece of Tygon tubing with a second three-way stopcock. Then, the (4)

perfusion chamber (Swinnex filter holder 13 mm, Merck Millipore, Spain) was attached to one of the three-way stopcock, and circuit closed through a piece of (5) Tygon tubing in U shape. Inside the perfusion chamber was placed the (6) scaffold, squeezed at its edges by two (7) silicone gaskets of 5 mm inner diameter. All connections between the components were performed using male and female polyvinylidene fluoride (PVDF) luer lock connectors (for 4.8 mm and 1.6 mm inner diameter tubes, Value Plastics, USA).

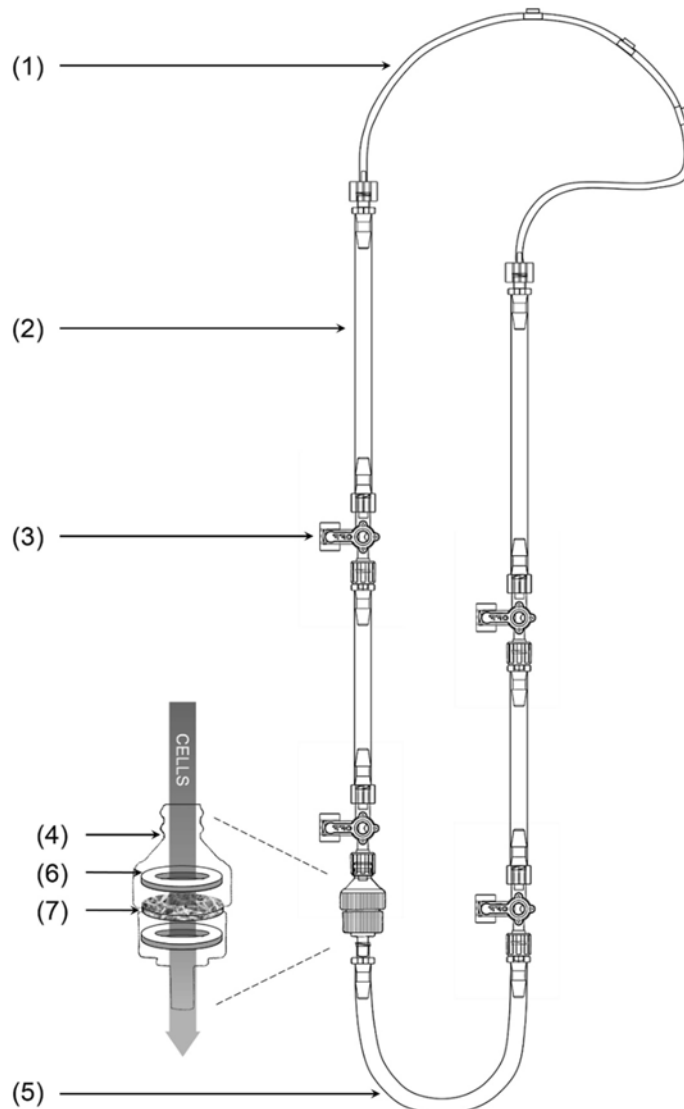


Figure 3.3. Illustration of the perfusion loop used to seed cells inside Matriderm™ scaffold. The loop was composed of a (1) pump tubing, (2) Tygon tubing, (3) three-way stopcocks, a (4) perfusion chamber and (5) U shape Tygon tubing. Inside the perfusion chamber, Matriderm™ scaffold (7) was held in place by two silicone gaskets (6). For cell seeding, cells were suspended in 1 ml of culture medium and one-way perfusion at 1 ml/min was applied (gradient grey arrow). Cells are retained inside the scaffold when passing through it.

For cell seeding inside Matriderm™ scaffold, the cell suspension was loaded inside the loop and a flow rate of 1 ml/min was applied in one direction, forcing the cell suspension to pass through the scaffold. As the scaffold was held in place by two silicone gaskets, only the central part of it was seeded with cells. After seeding, tissue constructs were placed in a 60 mm ultra-low attachment dishes (Corning, Spain) and incubated at 37°C in 5% CO₂ and humidified atmosphere to allow cell attachment. Rat cardiac tissue constructs were incubated for 1.5 h, while human ones were incubated for 3.5 h. Finally, tissue constructs were transferred into the bioreactor chambers.

3.4. Development of a perfusion bioreactor

3.4.1. Single chamber perfusion bioreactor

The single chamber perfusion bioreactor (**Figure 3.4**) was inspired in a previously published bioreactor²⁹⁷. It was composed of a (1) medium reservoir, which was a Nunclon™Δ Surface flask (25 cm² culture area, Thermo Fisher Scientific, Spain) with two holes drilled at its wall. Two plastic Pasteur pipettes exited from the flask, with both edges cut and gas-permeable platinum-cured silicone tubing (1.6 mm inner diameter x 3.2 mm outer diameter, Thermo Fisher Scientific, Spain) passing through them. One silicone tubing was connected to a (2) three-way stopcock (Smith Medicals, Spain), which in turn was assembled to a (3) high fidelity de-bubbling system (Leventon, WerfenLife Company, Spain) to avoid entrapment of bubbles inside the (4) perfusion chamber. Then, the perfusion chamber was connected to another three-way stopcock, which in turn was assembled to a piece of silicone tubing attached to a PharMed® BPT 3-Stop pump tubing (0.89 mm inner diameter, Thermo Fisher Scientific, Spain). Finally, the pump tubing was connected to a (6) gas exchanger, constituted by 3 m of platinum-cured silicone tubing coiled around a holder, and the gas exchanger was attached to the medium reservoir to close the circuit. All connections were performed using male and female polypropylene (PP) luer lock connectors for 1.6 mm inner diameter tubing (Thermo Fisher Scientific, Spain), and perfusion at 0.1 ml/min was applied using a (5) multichannel peristaltic pump (REGLO Digital, 2 channels, Ismatec, Germany).

As a perfusion chamber, a Swinnex filter holder (13 mm, Merck Millipore, Spain) was used, with two silicone gaskets of 5 mm inner diameter in its interior to hold the scaffold in place during culture. Alternatively, the perfusion chamber was substituted by prototypes of the perfusion chamber incorporating electrical stimulation to test their suitability (for further details, see “3.5. *Design and fabrication of a perfusion chamber including electrical stimulation*” section). All components were sterilized by either autoclave (high pressure saturated steam at 121°C) or 70% ethanol with subsequent distilled water rinse to remove any remaining ethanol. The whole system was placed inside an incubator with temperature and CO₂ control (37°C and 5% CO₂).

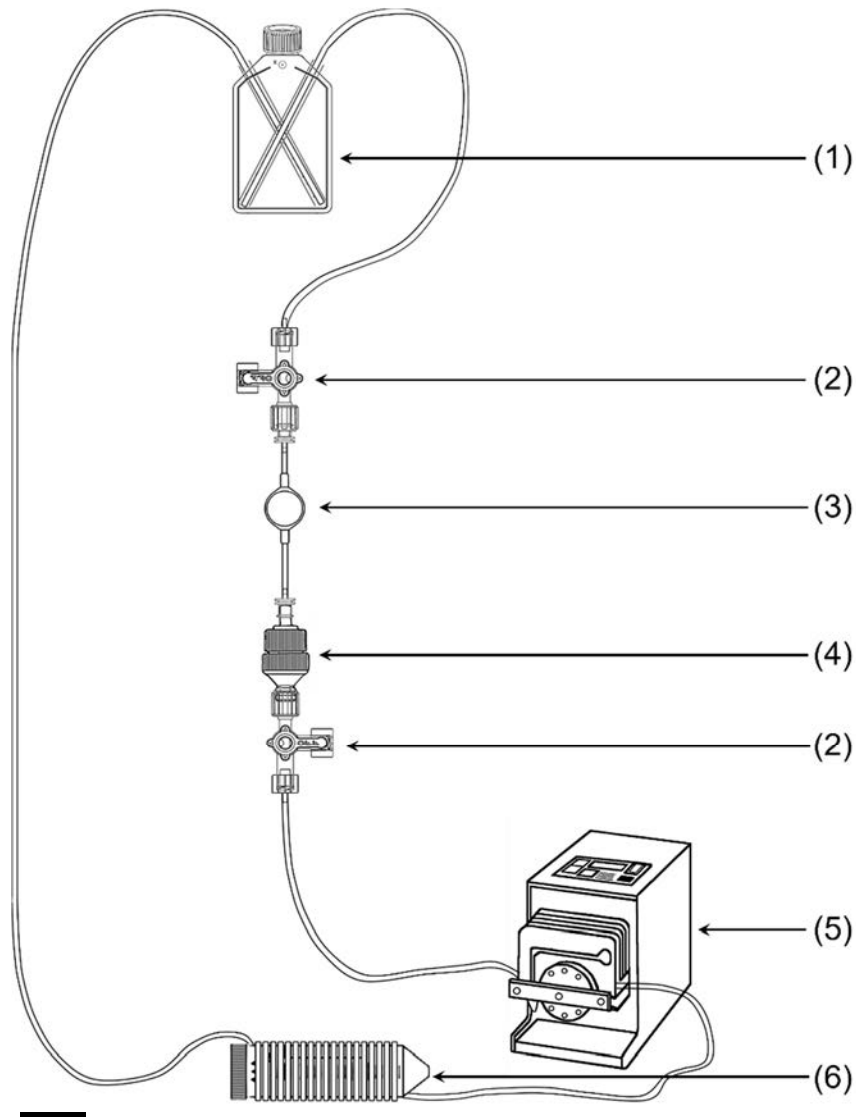


Figure 3.4. Illustration of the single chamber perfusion bioreactor. A. The bioreactor was composed of a (1) medium reservoir, (2) three-way stopcocks, a (3) de-bubbling system, a (4) perfusion chamber, (5) a peristaltic pump and (6) a gas exchanger. Scale bar: 4 cm.

After cell seeding inside the 3D scaffold (see “3.3.2. *Perfusion seeding*” section), tissue constructs were transferred into the bioreactor chambers and were cultured under perfusion at different As 2D controls, $0.5 \cdot 10^6$ cells (isolated from rat ventricles or cardiomyocytes derived from hiPSC together with 10% human foreskin fibroblasts) were seeded in a 12-well plate containing 0.1% gelatin-coated coverslips (Merck Millipore, Spain).

3.4.2. Parallelized perfusion bioreactor

Parallelized perfusion bioreactor (**Figure 3.5**) was composed of a (1) medium reservoir (Sartorius Stedim Spain, Spain) connected through gas-permeable platinum-cured silicone tubing (1.6 mm inner diameter x 3.2 mm outer diameter, Thermo Fisher Scientific, Spain) to a PharMed® BPT 3-Stop pump tubing (0.89 mm inner diameter, Thermo Fisher Scientific, Spain). Another piece of silicone tubing connected the pump tubing to a (2) four port luer manifold (Thermo Fisher Scientific, Spain), where the culture medium was equally distributed in four branches throughout (4) flow restrictors (L25915-250D2 microfluidic channels, Leventon, WerfenLife Company, Spain). A high fidelity (3) de-bubbling system (Leventon, WerfenLife Company, Spain) was installed before (6) perfusion chambers to avoid entrapment of bubbles inside them. The de-bubblers together with the flow restrictors were connected to an (5) in-line luer injection port (Inycom, Spain) that allowed direct drug injections in the chamber without breaking sterility. The injection port was then connected to perfusion chambers, which in turn were assembled with another four port luer manifold. This luer manifold was attached to a (7) gas exchanger, composed of 3 m of gas-permeable platinum-cured silicone tubing coiled around a Teflon® holder or a falcon tubing. Finally, the gas exchanger was connected to the medium reservoir to close the circuit. All connections between the components were performed using male and female polyvinylidene fluoride (PVDF) luer lock connectors (for 1.6 mm inner diameter tubing, Value Plastics, USA).

Two different perfusion chambers were used to either electrically stimulate cardiac tissue constructs or not. The perfusion chamber without electrodes was a Swinnex filter holder (13 mm, Merck Millipore, Spain), while the perfusion chamber that enabled electrical stimulation was designed and fabricated in-house (see “3.5.2.3. *Third prototype: polypropylene*” section for further details). In both chambers the cardiac construct was held in place using two gaskets, and a continuous perfusion of culture medium at 0.4 ml/min was applied by connecting the pump tubing to a (8) multichannel peristaltic pump (REGLO Digital, 2 channels, Ismatec, Germany). For details about the electrical stimulation regime, see “3.5.3. *Electrical stimulation regime for cardiac constructs culture*” section. All the components were sterilized by either autoclave (high pressure saturated steam at 121°C) or 70% ethanol with subsequent distilled water rinse to remove any remaining ethanol. The whole system was placed inside an incubator with temperature and CO₂ control (37°C and 5% CO₂).

As 2D controls, 0.5·10⁶ cells isolated from rat heart ventricles or day 20 differentiated cardiomyocytes together with 10% HFF were seeded in a 12-well plate containing a 0.1% gelatin-coated coverslip (Merck Millipore, Spain).

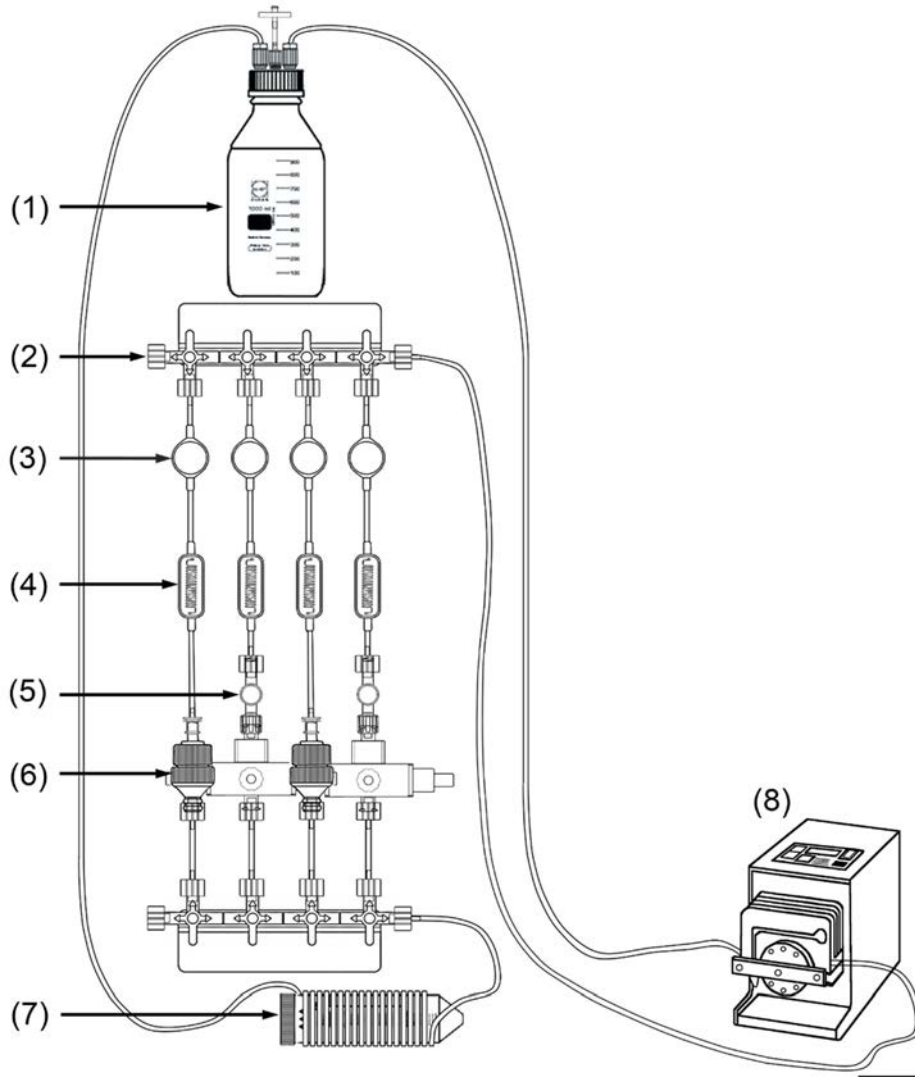


Figure 3.5. Illustration of the parallelized perfusion bioreactor. A, The bioreactor was composed of a (1) medium reservoir, a (2) luer manifold, (3) de-bubbling systems, (4) flow restrictors, (5) in-line luer injection ports, (6) perfusion chambers, a (7) gas exchanger and a (8) peristaltic pump. It supported up to four chambers to culture multiple tissue constructs under the same physicochemical conditions, but at different time points. Scale bar: 4 cm.

3.5. Design and fabrication of a perfusion chamber including electrical stimulation

3.5.1. Electric field modelling

To predict the electric field that stimulates cells in our custom-made perfusion chamber, we used COMSOL Multiphysics software (Burlington, MA, USA). We applied the electric currents module, which considers the conductivity and permittivity of each

material to solve a current conservation problem for a given electric potential. We run the simulation considering steady state electric currents because our interest was to predict the electric field distribution throughout our geometry and its average value in terms of electric potential. Therefore, it was not necessary to take into account transient charging and discharging of the capacitor of the electrode-electrolyte interface, as previous studies also demonstrate^{318,387,407}.

The model employs the electric current analogue of Poisson's equation (obtained from Maxwell's equations) to calculate electric fields throughout our geometry:

$$-\nabla \cdot (\sigma \nabla V - J_e) = Q_j \quad \text{Eq. 3.1}$$

Where σ is culture medium conductivity (S/m), ∇V is gradient of potential (V), J_e is an external current density (A/m²) and Q_j is a local current source. The simulation solves the equation when applying a differential potential on the electrodes and considering the boundaries of all solid parts an insulator (except the electrodes). Current density (J) and electric field (E) values are derived from the electric potential (V), as shown in equations 3.2 and 3.3⁴³⁸.

$$J = \sigma E + J_e \quad \text{Eq. 3.2}$$

$$E = -\nabla V \quad \text{Eq. 3.3}$$

To run the simulation, we defined the exact geometry of our perfusion chamber except for its internal part, where we drew a prism instead of a cylinder to faithfully reproduce the contact surface between electrodes and culture medium. The model solved for a mesh with an average element size of 0.0473 mm² when applying a differential potential of 5 V between the electrodes. The materials selected to run the simulation were the following (**Table 3.2**): graphite for the electrodes³⁸⁸, silicone for both gaskets and culture medium. The conductivity value of the cell culture medium used in the model was 1.44 ± 0.03 S/m, measured with a conductivity meter (Crison, Spain) using DMEM 4.5 g/l glucose (Life Technologies). The scaffold was modelled as part of the culture medium due to its high medium content (~94% porosity according to manufacturer's datasheet). The model allowed us not only to predict electric field and current density values in the custom-made perfusion chamber, but also to define which geometry and electrodes distance was appropriate for a suitable electrical stimulation.

Material	Electrical conductivity (σ)	Relative permittivity (ϵ)
Graphite	$3 \cdot 10^3$ S/m	12
Silicone	$2 \cdot 10^{-12}$ S/m	2.70
Culture medium	1.44 S/m	80

Table 3.2. Electrical conductivity and relative permittivity of the materials used to run the simulation. Culture medium conductivity was measured experimentally.

3.5.2. Design guidelines and fabrication of the custom-made perfusion chamber with electrical stimulation

3.5.2.1. First prototype: poly(methyl methacrylate) (PMMA) and polydimethylsiloxane (PDMS)

The first prototype of the custom-made perfusion chamber with electrical stimulation was fabricated by precision machining of poly(methyl methacrylate) (PMMA) plastic (*work performed in collaboration with Dr. Oscar Castillo-Fernández, Institute of Microelectronics of Barcelona, IMB-CNM (CSIC)*). Two 5 mm thick sheets of PMMA polymer (Goodfellow, United Kingdom) were structured using a numerical control milling machine, with internal chamber dimensions and geometry resembling the ones of Swinnex filter holder (13 mm, Merck Millipore, Spain) (**Figure 3.6A**). To achieve a watertight chamber, both sheets of PMMA were mechanically bound using screws and washers, and polydimethylsiloxane (PDMS) seal was employed as reversible sealing (**Figure 3.6B-C**). PDMS (Sylgard 184 Silicone Elastomer kit, Dow Corning, Germany) prepolymer was prepared by mixing the base polymer with the curing agent in a 10:1 ratio and degassing the mixture under a vacuum for 1 h. Then, prepolymer was either spun using a Spin Coater (Laurell Technologies Corporation, USA) to obtain a thin sheet, or poured over the structured PMMA to obtain a replica. Then, prepolymer was cured for 24 h at room temperature and peeled off from the substrate or the mold, cut to fit PMMA chamber and mechanically bound to PMMA sheets (**Figure 4.19** and **4.24**).

To test for prototype's watertightness and sterility, chambers were connected to a closed-circuit filled with culture medium and perfusion was applied for at least 2 days. Sterilization of machined PMMA sheets was performed by irradiation with UV light for at least 20 min, followed by a rinse with ethanol and Milli-Q water. For PDMS sterilization, replicas were soaked into ethanol and sonicated for 15 min, then washed with Milli-Q water and finally autoclaved (high pressure saturated steam at 121°C).

3.5.2.2. Second prototype: acrylonitrile butadiene styrene (ABS)

The second prototype of the custom-made perfusion chamber was fabricated by 3D printing of acrylonitrile butadiene styrene (ABS) plastic (Bio-model, Spain) (**Figure 3.7**). It was composed of a cap and a base that were threaded together, and an internal gasket to hold the cardiac tissue construct in place. To connect the chamber to the bioreactor circuit, polypropylene luer lock connectors (for 1.6 mm inner diameter tubing, Value Plastics, USA) were glued afterwards using cyanoacrylate. To electrically stimulate cells, two carbon rod electrodes of 3/16" in diameter (Monocomp Instrumentación, Spain) were also glued. Two holes were drilled at one edge of each carbon rod and a solid tinned annealed copper wire (RS Pro, UK) was threaded through

the holes. Insulation of the connection was performed using Araldite® epoxy resin, and waterproofing of carbon rod electrodes was achieved using heat-shrink tubing (Thermo Fisher Scientific, Spain). Finally, a hole was drilled in the center of a polypropylene male luer cap (Value Plastics, USA), and a gold wire of 0.125 mm diameter (Advent Research Materials, England) was introduced through it to have a recording electrode.

To test for prototype's watertightness and sterility, chambers were connected to a closed-circuit filled with culture medium and perfusion was applied for at least 2 days. Sterilization of the 3D printed perfusion chamber was performed either by irradiation with UV light for at least 30 min or ethylene oxide (EtO) sterilization process.

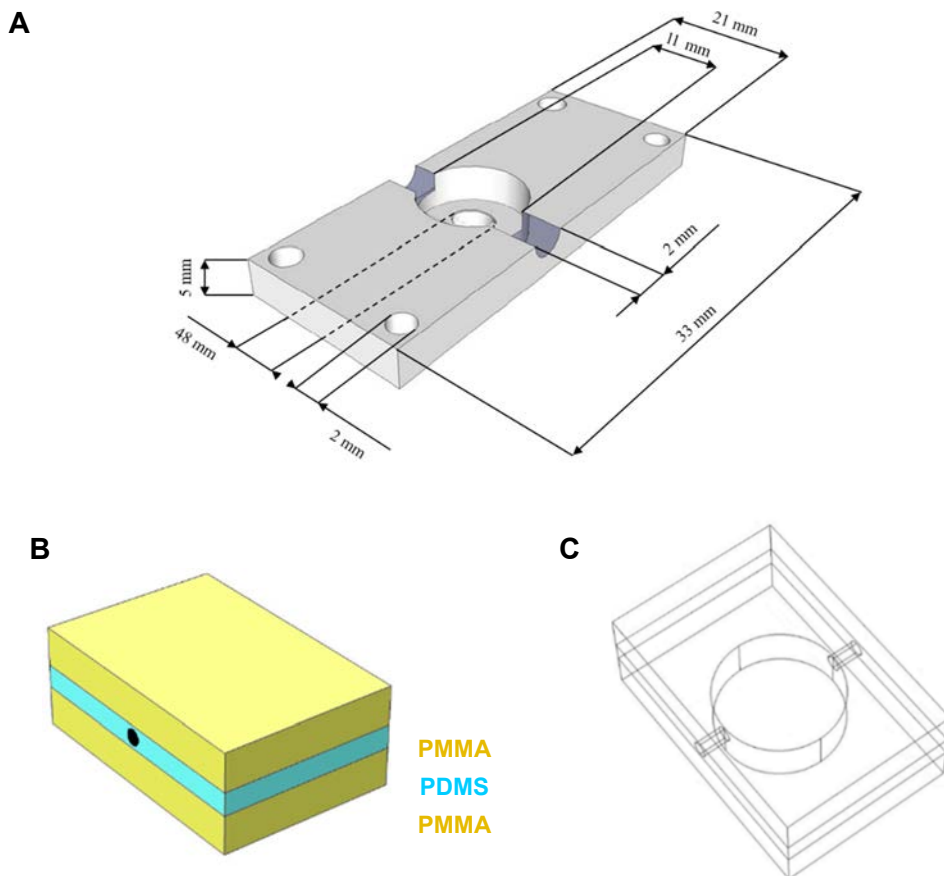


Figure 3.6. Illustrations of the first prototype of the perfusion chamber with electrical stimulation. **A**, Illustration of the machined poly(methyl methacrylate) (PMMA) sheet. The central cylindrical hole (also represented in **C**) was designed to hold the cardiac construct. Lateral cylindrical holes were designed to let the electrodes (black dot in **B** and lateral cylinders in **C**) reach the cardiac construct for electrical stimulation. The holes located in each corner of the PMMA sheet were designed to mechanically bind two PMMA sheets with a polydimethylsiloxane (PDMS) seal (**B**). **B**, Scheme of the assembled perfusion chamber with electrical stimulation. **C**, Interior view of the assembled perfusion chamber with electrical stimulation.

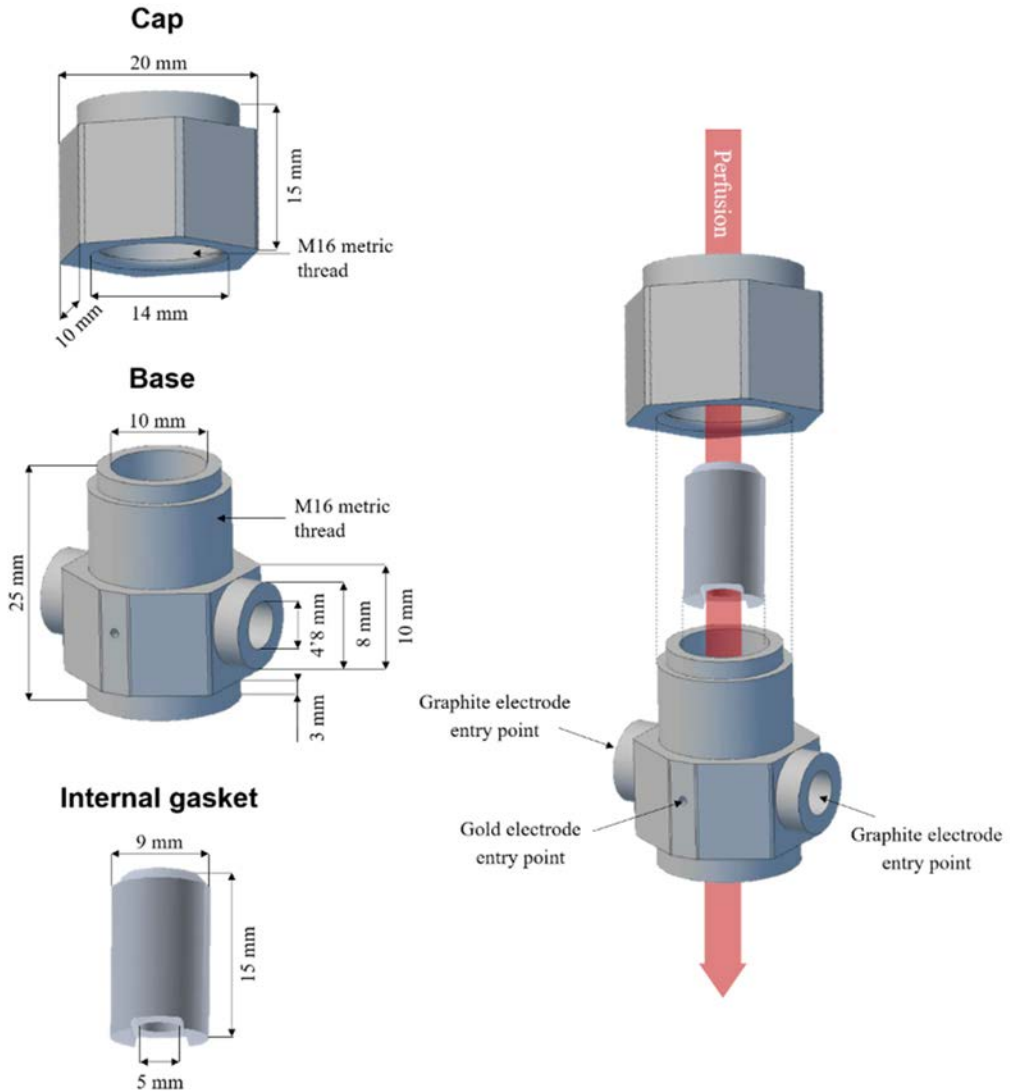


Figure 3.7. Illustration of 3D printed acrylonitrile butadiene styrene (ABS) plastic to obtain the second prototype of the perfusion chamber with electrical stimulation. The prototype is composed of a cap and a base that are threaded together to set up the chamber. To hold the cardiac construct in place, an internal gasket is installed inside the perfusion chamber.

3.5.2.3. Third prototype: polypropylene (PP)

The final version of the custom-made perfusion chamber including electrical stimulation (**Figure 3.8**) was fabricated by precision machining of polypropylene (PP) plastic, followed by gluing of luer connectors using cyanoacrylate (Bio-model, Spain). To achieve a completely watertight chamber, we used silicone gaskets and thread seal tape. The perfusion chamber had an inlet and an outlet to allow medium perfusion, two carbon rod electrodes of 3/16" in diameter (Monocomp Instrumentación, Spain) to

electrically stimulate cells and one gold electrode of 0.5 mm in diameter (Advent Research Materials, England) as a recording electrode. To characterize the system, electric potentials between graphite electrodes and between one graphite electrode and the center of the chamber (gold electrode) were performed. The prototype was connected to a closed-circuit filled with culture medium, a scaffold was installed inside the chamber and electric potential values were measured using a function generator (Agilent Technologies, Spain) and an oscilloscope (Agilent Technologies, Spain).

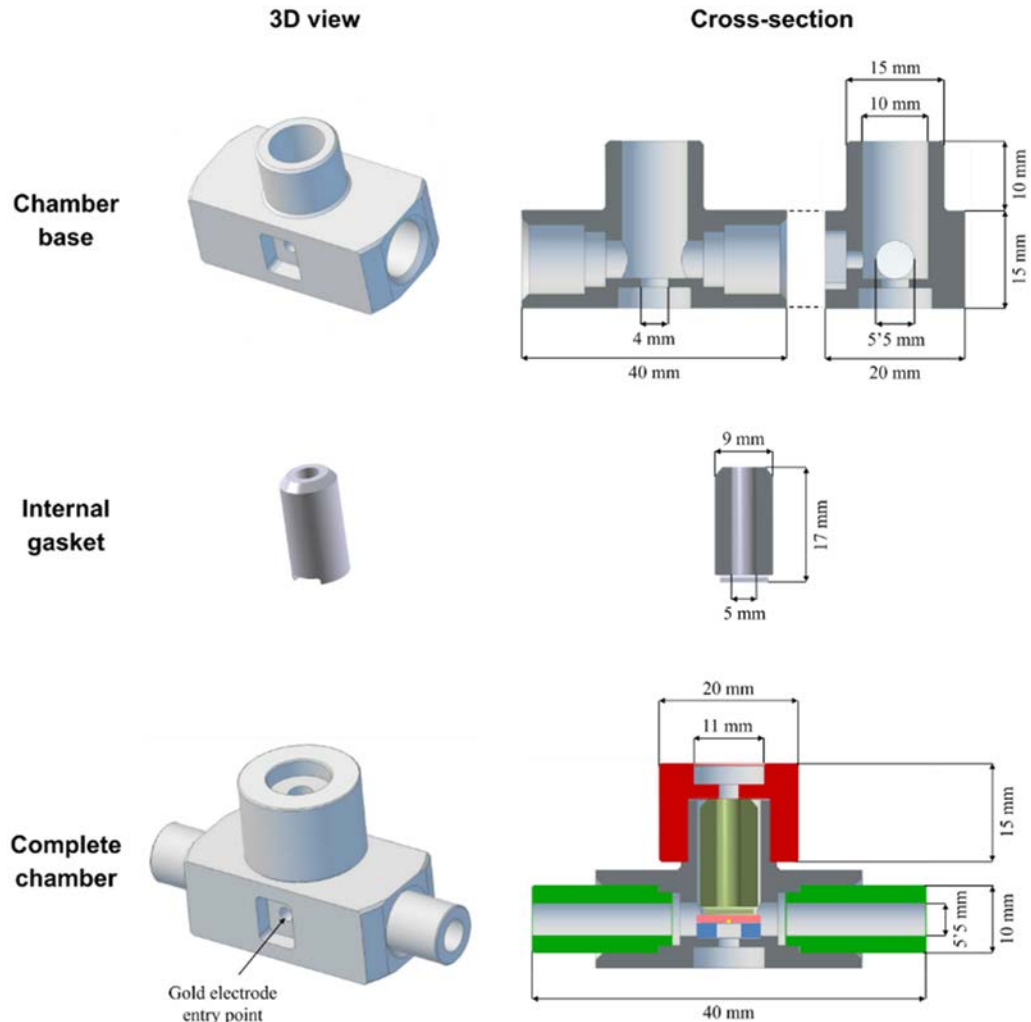


Figure 3.8. Illustration of the perfusion chamber with electrical stimulation obtained by precision machining of polypropylene (PP) plastic. The prototype is composed of a cap (red at the cross-section) and a base that are threaded together to set up the chamber. To hold the cardiac construct (pink at the cross-section), two gaskets (yellow and blue at the cross-section) are installed inside the perfusion chamber. To introduce carbon rod electrodes in a reversible manner, two adapters (green at the cross-section) are screwed to the chamber base, and electrodes are installed inside them. As a recording electrode, a gold electrode (yellow dot at the cross-section) was inserted just below the cardiac construct.

For a suitable fastening of crocodile clips from the function generator (Agilent Technologies, Spain) with 3/16" carbon rod electrodes, two holes were drilled at one edge of each carbon rod electrode. Then, solid tinned annealed copper wire (RS Pro, UK) was threaded through the holes, and insulation of the connection was performed using Araldite® epoxy resin. Waterproofing of carbon rod electrodes was achieved using heat-shrink tubing (Thermo Fisher Scientific, Spain). Inside the perfusion chamber we placed the cardiac tissue construct, squeezed at its edges by two gaskets: one made of PP fabricated by precision machining (in yellow at **Figure 3.8**, complete chamber cross-section), and the other made of polydimethylsiloxane (PDMS) molding (in blue at **Figure 3.8**, complete chamber cross-section). The mold was fabricated by 3D printing of acrylonitrile butadiene styrene (ABS) plastic (*kindly printed by Dr. Raimon Sunyer*), and allowed us to obtain 12 gaskets of 9 mm outer diameter, 5 mm inner diameter and 2 mm depth (**Figure 3.9**).

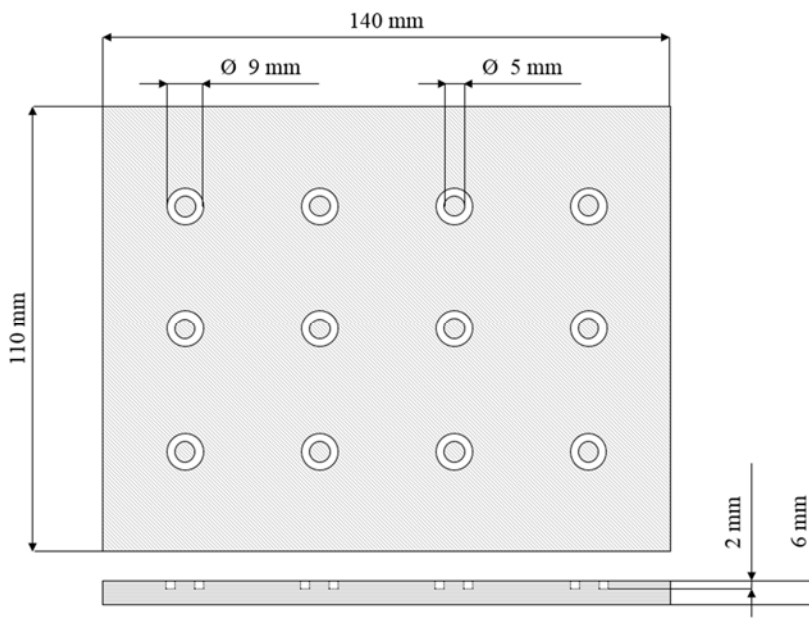


Figure 3.9. Acrylonitrile butadiene styrene (ABS) mould to fabricate polydimethylsiloxane (PDMS) gaskets. Gaskets dimensions are designed to fit inside the perfusion chamber with electrical stimulation and put the cardiac construct in the midpoint of carbon rod electrodes. PDMS gasket is illustrated in blue in Figure 3.9 (complete chamber cross-section).

3.5.3. Electrical stimulation regime for cardiac constructs culture

After cell seeding inside the 3D scaffold, the obtained tissue constructs were transferred into the bioreactor chambers (**Figure 3.10A**) and were cultured under perfusion during 3 days. At day 4 of culture, electric field stimulation regimen was

applied on electrostimulated cardiac tissue constructs, which consisted in trains of monophasic square-wave pulses of 2 ms of duration, 5 V_{pp} of amplitude and 3 Hz of frequency³⁸⁷ (**Figure 3.10B**). Control cardiac constructs were cultured only under perfusion. All cardiac constructs were cultured either for 7 or 14 days before assessing their maturation level, and culture medium was changed every 2 days before applying electrical stimulation or every day when applying electrical stimulation.

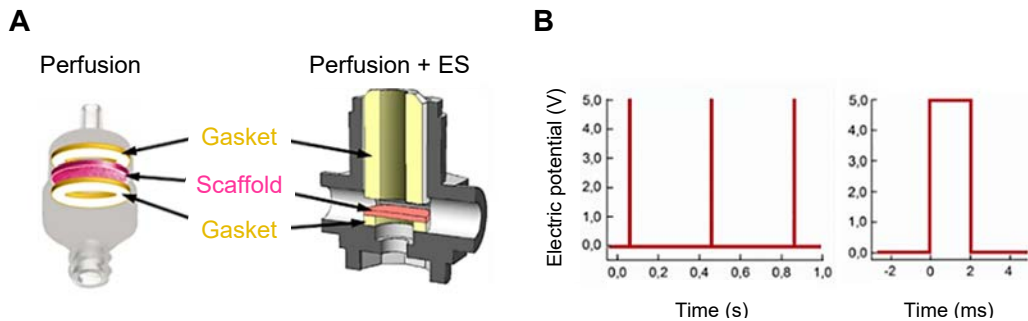


Figure 3.10. Perfusion chambers for cardiac constructs cultivation and stimulation. **A**, Cross-sections of the two different perfusion chambers used to culture cardiac constructs, either without (left) or with (right) electrical stimulation. In both chambers the cardiac construct was held in place using two gaskets. **B**, Electrical stimulation regime applied to electrostimulated cardiac constructs (3 Hz of frequency, 5 V_{pp} of amplitude and 2 ms of duration). ES: electrical stimulation.

3.6. Flow cytometry analysis

Characterization of human induced pluripotent stem cell-derived cardiomyocytes (hiPSC-CM) was performed by flow cytometry analysis. Cells were dissociated on day 19 of differentiation using 0.25% trypsin-EDTA (Gibco®, Thermo Fisher Scientific, Spain) at 37 °C for 5 min and then fixed with 4% paraformaldehyde (Sigma-Aldrich Química, Spain) for 20 min at room temperature. After washing with 1X saponin (Sigma-Aldrich Química, Spain), cells were permeabilized using Cell Permeabilization Kit (Invitrogen, Spain) and blocked with 5% mouse serum (Thermo Fisher Scientific, Spain) during 15 min at room temperature. Then, cells were stained with the antibodies mouse PE-anti myosin heavy chain (MHC) (IgG2b, 1:400 BD Biosciences, Spain) and mouse Alexa Fluor 647 cardiac troponin I (cTnI) (IgG2b, 1:100, BD Biosciences, Spain). Mouse IgG2b PE (1:400 BD Biosciences, Spain) and mouse IgG2b Alexa Fluor 647 (1:100, BD Biosciences, Spain) antibodies were used as isotype controls. After incubation during 15 min at room temperature in the dark and washing twice with 1X saponin, cells were analyzed with FACS MoFlo (Beckman Coulter, Spain) and data acquisition and analysis performed by Kaluza software (Beckman Coulter, Spain). We acknowledge the use of facilities and the technical support from the Flow Cytometry Unit at Centre of Regenerative Medicine in Barcelona (CMRB).

3.7. Functional activity of cardiac tissue constructs

3.7.1. Setup for contractile activity recording

Contractile function of cardiac tissue constructs was assessed in response to electric field stimulation or spontaneous beating as previously described^{281,318}. Briefly, two holes were drilled at one edge of two carbon rod electrodes of 3/16" in diameter (Monocomp Instrumentación, Spain). A gold wire of 0.5 mm in diameter (Advent Research Materials, England) was thread through them to properly fasten crocodile clips from the function generator to the electrodes. Insulation of the connection was performed using heat-shrink tubing (Thermo Fisher Scientific, Spain), and both electrodes were glued using cyanoacrylate at the bottom of a 35 mm MatTek glass bottom dish (MatTek In Vitro Life Science Laboratories, Slovak Republic), 1 cm apart from the edge of each electrode (**Figure 3.11**). The space between the electrodes was filled with Tyrode's salts solution (Sigma-Aldrich Química, Spain). Cardiac constructs were positioned at the center of the MatTek dish and imaged and video recorded using a Stereo Microscope Leica MZ10F (Leica Microsystems, Spain) equipped with a DFC4025C Digital Microscope Camera (Leica Microsystems, Spain). A microscope-stage automatic thermocontrol system for transmitted light bases (Leica MATS Type TL, Leica Microsystems, Spain) was used to maintain Tyrode's solution at 37°C, and electrical pulses were applied using a function generator (Agilent Technologies, Spain).

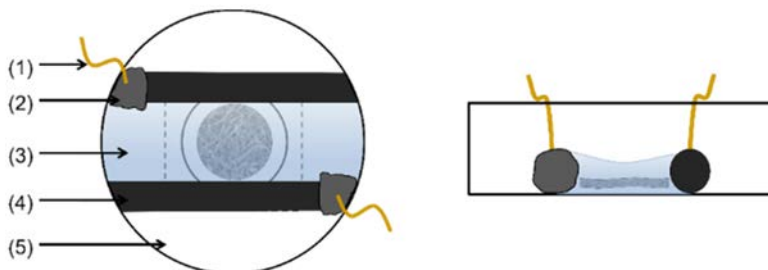


Figure 3.11. Diagram of MatTek petri dish used for functional assessment of cardiac constructs. It is composed of (1) gold wires, (2) heat-shrink tubing, (3) Tyrode's salt solution, (4) carbon rod electrodes separated 1 cm apart and (5) 35 mm MatTek glass bottom dish. Floating in Tyrode's salt solution there is the cardiac construct, and the whole system is fixed in a stereo microscope with temperature control for video recording.

3.7.2. Measurement of functional parameters

The excitation threshold (ET) of cardiac tissue constructs was determined by applying initially square-wave pulses of 2 ms of duration, 2 Hz of frequency and 1 V_{pp} of amplitude and then increasing amplitude of the pulses in 0.1 V increments until the construct started to beat at 2 Hz instead of at its spontaneous frequency²⁸¹. Maximum

capture rate (MCR) was determined by applying initially square-wave pulses of 2 ms of duration, 10 V_{pp} of amplitude and 1 Hz of frequency and then increasing frequency in 0.1 Hz until the construct stopped contracting at the paced frequency or contractions became irregular. To obtain quantitative data of the amplitude of contraction of each cardiac construct, both spontaneous beating and beating when applying pulses at 1 Hz of frequency, 10 V_{pp} of amplitude and 2 ms of duration was recorded for at least 10 s. Then, the fractional area change (FAC) of cardiac constructs was analyzed and calculated using a published custom MATLAB program³¹⁸ (The MathWorks, Natick, USA; *work performed in collaboration with Roberto Paoli, Institute for Bioengineering of Catalonia, (IBEC)*). Briefly, the MATLAB program identifies the area in pixels of the largest object in each frame of the video (which corresponds to that of the construct) and stores it in a spreadsheet. Then, the data is used to calculate the FAC by applying the following formula:

$$FAC (\%) = \frac{(\text{relaxed area} - \text{contracted area})}{(\text{relaxed area})} \cdot 100 \quad \text{Eq. 3.4}$$

To assess the difference between control and electrically stimulated group means, FAC was presented as a fold induction relative to control mean or evaluated using a Student's t-Test. The software used was Origin 8.5 (OriginLab, Northampton, USA), and differences were considered significant when $p < 0.05$.

Particle Image Velocimetry (PIV), an optical method initially used to measure velocity vectors fields in flows⁴³⁹, was employed to measure the velocity fields in beating cardiac tissue constructs (*work performed in collaboration with Dr. Jordi Comelles, Institute for Bioengineering of Catalonia (IBEC)*). Briefly, spontaneous beating of cardiac constructs was video recorded using Stereo Microscope Leica MZ10F (Leica Microsystems, Spain) equipped with a DFC4025C Digital Microscope Camera (Leica Microsystems, Spain). Then, movies were analyzed using the MatPIV software package for MATLAB (The MathWorks, Natick, USA)⁴⁴⁰. The displacement carried out by the cardiac construct between each frame of the video was studied using a 77 μm x 77 μm square interrogation window. Each frame was cross-correlated with the preceding one, obtaining local displacement fields and, thus, the velocity field. Three beating cycles per cardiac construct were analyzed, being a beating cycle from relaxation to contraction state and then going to relaxation again.

The alignment between velocity vector fields and the direction of the electric field (θ), was assessed by the order parameter $\langle \cos 2\theta \rangle$ (**Figure 3.12**). It is a suitable function to represent vector arrangement because if vectors are aligned in the electric field axis (meaning vectors with an angle of 360° or 180°, that is, parallel to electric field axis), its value will be of 1, whereas if vectors are perpendicular to the electric field (meaning vectors with an angle of 90° or 270°), its value will be of -1. Random distribution will be represented by a $\langle \cos 2\theta \rangle$ value close to 0.

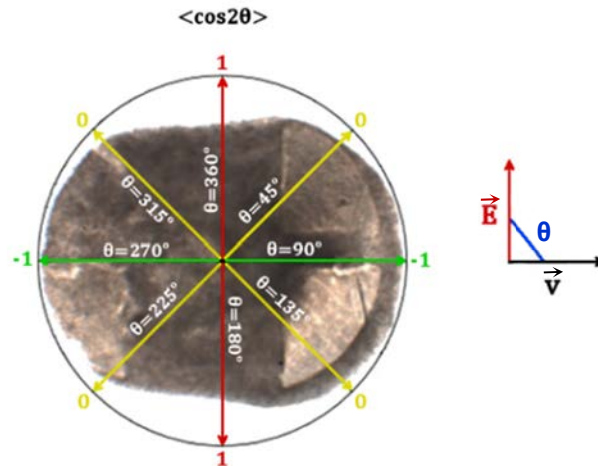


Figure 3.12. Study of the alignment between velocity vector field and electric field direction. The order parameter $\langle \cos 2\theta \rangle$ was used to evaluate the arrangement of vectors obtained after Particle Image Velocimetry (PIV) analysis. If vectors are aligned in the direction of the electric field, $\langle \cos 2\theta \rangle$ will be of 1. If vectors are perpendicular to the direction of the electric field, $\langle \cos 2\theta \rangle$ will be of -1. Random distribution will be represented by a $\langle \cos 2\theta \rangle$ close to 0. E: electric field; v: velocity vector field; θ : angle between velocity vector field and electric field.

To assess the difference between control and electrically stimulated group means, normal distribution of $\langle \cos 2\theta \rangle$ values was tested using the Shapiro-Wilk and Kolmogorov-Smirnov normality tests. Non-parametric analysis was performed using Mann-Whitney U test. The software used was Origin 8.5 (OriginLab, Northampton, USA), and differences were considered significant when $p < 0.05$.

3.7.3. Drug response analysis

To study cardiac tissue constructs response to drug treatments, isoproterenol, carbachol and sotalol were used (Sigma-Aldrich Química, Spain). All chemicals were dissolved in distilled water to make stock solutions, and working solutions were freshly and immediately prepared in culture medium (RPMI medium (Invitrogen, Spain) supplemented with B27 (Life Technologies, Thermo Fisher Scientific, Spain), 1% L-glutamine (Life Technologies, Thermo Fisher Scientific, Spain), 0.5% penicillin-streptomycin (Sigma-Aldrich Química, Spain), 1% non-essential amino acids (Life Technologies, Thermo Fisher Scientific, Spain), and 0.1 mM 2-mercaptoethanol (Life Technologies, Thermo Fisher Scientific, Spain)).

Drug effects on cardiac tissue constructs were evaluated through video-optical recordings using a published MATLAB program³¹⁸ (The MathWorks, Natick, USA; *work performed in collaboration with Roberto Paoli, IBEC*) or electrical signal recording (see “3.11. Recording and processing of bioelectrical signals generated by cardiac tissue constructs” section for further details). In the case of video recordings, the setup

depicted in **Figure 3.11** was used, and drug effects were restricted to affections of constructs contractility. For electrical signal recordings, drugs were injected in the perfusion bioreactor through an injection port (**Figure 3.13**), and effects were assessed in real time by direct measures of electrical activity of constructs.

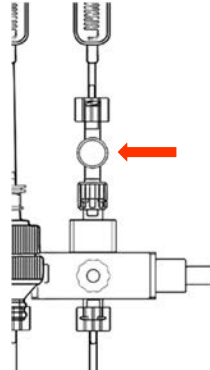


Figure 3.13. In-line luer injection port for drug delivery. To assess the effect of cardioactive drugs on the electrical activity cardiac tissue constructs, drugs were injected in the perfusion bioreactor through an in-line injection port (red arrow). Then, changes in electrical activity of cardiac constructs was assessed in real time using the recording system described in section

To test changes in the β -adrenergic response, cardiac constructs were incubated with 1 μM isoproterenol for 10 min, and immediate electrical signal or video recording was performed. After 5 min of washout with fresh culture medium, cholinergic response was studied by incubating cardiac constructs with 10 μM carbachol for 10 min, with immediate electrical signal or video recording. After 5 min of washout with fresh culture medium, the blockade of the human ether-a-go-go-related gene (hERG) potassium channel was evaluated by incubating cardiac constructs with sotalol for 10 min at either low (1 μM) or high (10 μM) concentrations, followed by immediate electrical signal or video recording. Spontaneous activity of cardiac constructs was recorded as baseline period to study changes in contractile behavior caused by the mentioned drug treatments. The effect of isoproterenol and carbachol treatments on cardiac tissue constructs beating rate was assessed using Mann-Whitney U test, relative to baseline. Differences were considered statistically significant when $p < 0.001$.

3.8. Histological analysis

3.8.1. Hematoxylin and eosin staining

Cardiac constructs were fixed overnight with 4% paraformaldehyde (PFA; Sigma-Aldrich Química, Spain) at 4°C and washed 3 times in 10 M phosphate buffered saline (PBS) with 30% sucrose. Afterwards, scaffolds were cut into halves, embedded in Tissue-Tek® O.C.T. Compound to obtain cross-sections, and frozen at -20°C overnight.

Cardiac constructs were sectioned in 10 µm thick sections using a cryostat (Leica Biosystems, Spain). Then, sections were placed in SuperFrost™ Plus microscope slides (Thermo Fisher Scientific, Spain) and analyzed by hematoxylin and eosin staining.

For hematoxylin and eosin staining, slides were rinsed for 5 min in deionized water and gradually dehydrated using ethanol series. Afterwards, slides were dunked in hematoxylin for 6 min and rinsed in basic water (pH=9) for 10 min. Then, slides were dunked in alcoholic eosin Y for 30 seconds and in absolute ethanol for 1 min. Next, slides were dunked again in absolute ethanol for 5 min and 10 min more, and finally in eucalyptol for 10 min. Images were taken using in an Inverted Laboratory Microscope with LED Illumination (Leica Microsystems, Spain) and Leica Application Suite (LAS) software. Images were analyzed using ImageJ free software⁴³⁴ (National Institutes of Health, USA). We acknowledge the use of facilities and technical support from Unit of Experimental Toxicology and Ecotoxicology (UTOX) at Barcelona Science Park (PCB).

3.8.2. Immunofluorescence staining protocol

3.8.2.1. Standard 2D cell cultures

Neonatal rat cardiac cells and hiPSC-CM seeded on Matrigel® (Corning, Spain) or gelatin-coated (Merck Millipore, Spain) coverslips (Neuvitro, USA) were used as 2D controls. Cells were fixed with 4% paraformaldehyde (PFA; Sigma-Aldrich Química, Spain) for 20 min at room temperature and washed 3 times in 10 M phosphate buffered saline (PBS), 10 min each. Then, coverslips were washed thrice with 1X tris-buffered saline (TBS) for 5 min each and incubated in blocking solution I (1X TBS with 0.5% Triton-X100 (Sigma-Aldrich Química, Spain) and 6% donkey serum (Chemicon®, Merck Millipore, Spain)) for 1 h at room temperature. Primary antibodies (**Table 3.3**) were diluted in blocking solution II (1X TBS with 0.1% Triton-X100 and 6% donkey serum) and coverslips were incubated for 48 h at 4°C. After three washes of 5 min in 1X TBS, coverslips were incubated with secondary antibodies (**Table 3.4**) diluted in blocking solution II for 2 h in the dark at 37°C. Finally, coverslips were washed thrice with 1X TBS for 5 min each and incubated with DAPI 1:10000 (4',6-diamidino-2-phenylindole; Invitrogen, Spain) for 10 min at room temperature. For observation, microscope slides were prepared by placing a drop of home-made fluorescence mounting medium⁴⁴¹ on a glass slide (Corning, Spain) and mounting the coverslip with cells on top. Coverslips were sealed with nail polish and slides stored in dark at 4°C. Images were taken using an inverted confocal microscope (Leica SP5, Leica Microsystems, Spain) or a fixed-stage upright microscope (Eclipse E1000, Nikon Instruments, Netherlands), and analyzed using ImageJ software⁴³⁴ (National Institutes of Health, USA). We acknowledge the use of facilities and technical support from Bioimaging and histology unit at Centre of Regenerative Medicine in Barcelona (CMRB).

Target molecule	Immunoglobulin	Host	Dilution	Source
Actin (α -sarcomeric)	Monoclonal IgM	Mouse	1:400	Sigma-Aldrich, A2172
α -actinin (sarcomeric)	Monoclonal IgG1	Mouse	1:100	Sigma-Aldrich, A7811
α -tubulin	Monoclonal IgG1	Mouse	1:500	Sigma-Aldrich, T6074
Brachyury	Polyclonal IgG	Goat	1:25	R&D Systems, AF2085
Connexin 43	Polyclonal IgG	Rabbit	1:250	Abcam, ab11370
Green fluorescent protein (GFP)	IgY fraction	Chicken	1:500	Aves Labs, GFP-1010
Heavy chain cardiac Myosin	Monoclonal IgG1	Mouse	1:100	Abcam, ab15
Troponin I	Polyclonal IgG	Rabbit	1:25	Santa Cruz, sc-15368
Troponin T	Monoclonal IgG1	Mouse	1:100	Thermo Fisher, MS-295-P

Table 3.3. List of primary antibodies used for immunohistochemistry analysis. They were used to characterize both 2D cell cultures and 3D cardiac tissue constructs.

Target molecule	Chromogen	Host	Dilution	Source
Chicken IgY	DyLight™ 488	Donkey	1:200	Jackson, 703-485-155
Goat IgG	Alexa Fluor® 488	Donkey	1:200	Jackson, 705-545-147
Mouse IgG	Alexa Fluor® 488	Goat	1:200	Jackson, 115-546-071
Mouse IgG	Alexa Fluor® 488	Donkey	1:200	Jackson, 715-545-151
Mouse IgG	Cy™3	Goat	1:200	Jackson, 115-165-071
Mouse IgG	Cy™5	Goat	1:200	Jackson, 115-175-071
Mouse IgM	Cy™2	Goat	1:200	Jackson, 115-225-075
Mouse IgM	Cy™3	Donkey	1:200	Jackson, 715-165-140
Mouse IgM	Cy™3	Goat	1:200	Jackson, 115-165-075
Mouse IgM	DyLight™ 649	Goat	1:200	Jackson, 115-495-075
Mouse IgM	Cy™5	Rabbit	1:200	Jackson, 315-175-049
Rabbit IgG	Alexa Fluor® 488	Donkey	1:200	Jackson, 711-545-152
Rabbit IgG	Cy3	Donkey	1:200	Jackson, 711-165-152
Phalloidin	Texas Red®	-	1:40	Life technologies, T7471

Table 3.4. List of secondary antibodies used for immunohistochemistry analysis. They were used to characterize both 2D cell cultures and 3D cardiac tissue constructs.

3.8.2.2. Cardiac tissue constructs (*in toto*)

Cardiac tissue constructs were fixed overnight with 4% paraformaldehyde (PFA; Sigma-Aldrich Química, Spain) at 4°C, and washed 3 times in 1X phosphate buffered saline (PBS) at 4°C, 30 min each. Then, tissue constructs were included in 4% or 8% agarose (low melt point agarose D1, CONDA, Spain) using cryomolds (Tissue-Tek, The Netherlands), and blocks were obtained by cooling it down for 5 min at 4°C. Blocks were cut in 200 µm thick sections using a vibratome (0.075 mm/s advance rate, 81 Hz vibration and 1 mm amplitude) (Leica VT1000S, Spain), and tissue constructs were accurately positioned to obtain cross-sections oriented in the direction of the electric field (**Figure 3.14**).

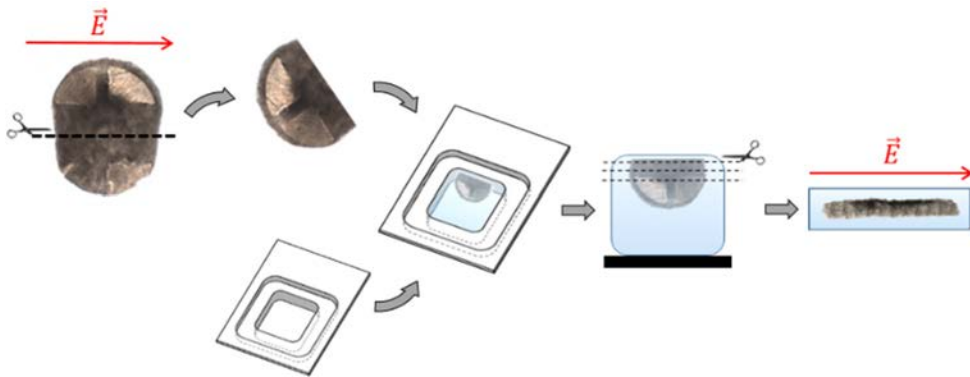


Figure 3.14. Diagram of cardiac constructs inclusion and sectioning for immunohistochemistry analysis. Cardiac constructs were cut in half (for electrostimulated constructs, the cut was performed in the direction of the electric field) and included in agarose using cryomolds. Then, the agarose block was glued to the vibratome stage and sections 200 µm thick were performed, obtaining cross-sections of the constructs (in the case of electrostimulated constructs, oriented in the direction of the electric field).

During the whole immunostaining protocol, tissue sections were in agitation. After three washes of 30 min in 1X tris-buffered saline (TBS), sections were incubated in blocking solution I (1X TBS with 0.5% Triton-X100 (Sigma-Aldrich Química, Spain) and 6% donkey serum (Chemicon®, Merck Millipore, Spain)) for 4 h at room temperature. Then, sections were incubated with primary antibodies (**Table 3.3**) diluted in blocking solution II (1X TBS with 0.1% Triton-X100 and 6% donkey serum) for 2 h at room temperature, followed by 72 h at 4°C and again 2 h at room temperature. After four washes in 1X TBS (30 min each), sections were incubated with secondary antibodies (**Table 3.4**) diluted in blocking solution II for 2 h in the dark at room temperature and overnight at 4°C. When using Texas Red®-X phalloidin (Thermo Fisher Scientific, Spain) a special blocking buffer was employed, composed of 1X TBS with 0.05% saponin (Sigma-Aldrich Química, Spain) and 0.1% bovine serum albumin (BSA; Sigma-Aldrich Química, Spain). Finally, sections were washed thrice with 1X TBS for 30 min each and

incubated with DAPI 1:1000 (4',6-diamidino-2-phenylindole; Invitrogen, Spain) for 1 h at room temperature. Tissue sections were prepared in microscope slides by placing them in glass slides (Corning, Spain) and mounting a coverslip (Menzel-Gläser, Germany) with 300 μ l of home-made fluorescence mounting medium⁴⁴¹ on top. Eventually, coverslips were sealed with nail polish to prevent drying and movement under microscope and slides stored in dark at 4°C until observation. Images were taken using an inverted confocal microscope (Leica SP5, Leica Microsystems, Spain) and analyzed using ImageJ free software⁴³⁴ (National Institutes of Health, USA). We acknowledge the use of facilities and the technical support from the Bioimaging and histology unit at Centre of Regenerative Medicine in Barcelona (CMRB).

3.9. Transmission electron microscopy analysis

Cardiac constructs were fixed with 2.5% glutaraldehyde (Electron Microscopy Sciences, USA) diluted in 0.1 M cacodylate buffer (pH=7.2) for 2 h at 4°C. After 3 washes of 10 min each in cacodylate buffer at room temperature and gently shaking, samples were post-fixed in 1% osmium tetroxide for 2 h at 4°C. Then, cardiac constructs were gradually dehydrated using ethanol series until absolute ethanol and embedded in epoxy resin (Ted Pella, USA) in a specific orientation (**Figure 3.15**). Semi-thin sections (0.25 μ m) were cut with a diamond knife using an ultramicrotome (Leica UC6, Spain), and stained lightly with 1% toluidine blue (Panreac, Spain) to identify high cell density zones. Later, ultra-thin sections (0.08 μ m) were cut with a diamond knife and stained with uranyl acetate (Electron Microscopy Sciences, USA) and lead citrate (Electron Microscopy Sciences, USA). Imaging was performed at JEOL 1011 transmission electronic microscope (JEOL, Japan), and images were analyzed using ImageJ free software⁴³⁴ (National Institutes of Health, USA). We acknowledge the use of facilities and the technical support from the Bioimaging and histology unit at Centre of Regenerative Medicine in Barcelona (CMRB).

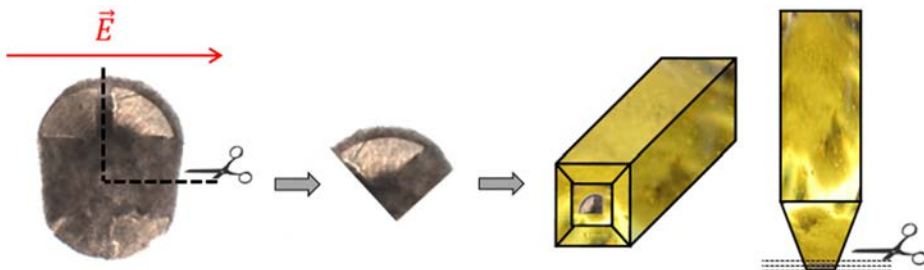


Figure 3.15. Diagram of cardiac tissue constructs embedding and sectioning for transmission electron microscopy analysis. One quarter of cardiac constructs was cut and embedded in epoxy resin. To obtain semithin and ultrathin sections with high number of cells, constructs are oriented to pick up the top part (cardiac constructs top view).

Images were acquired at direct magnifications from 10000 to 25000 only where typical cardiomyocyte structures could be seen (e.g. cell junctions, sarcomeres, etc.). Quantitative analysis involved measuring the average sarcomeric width (defined as Z-disc length, indicated by black square brackets in **Figure 3.16**) in at least 35 fields per sample by systematically scanning equivalent areas. Data was collected from at least 2 independent experiments per group and 2 grids/group.

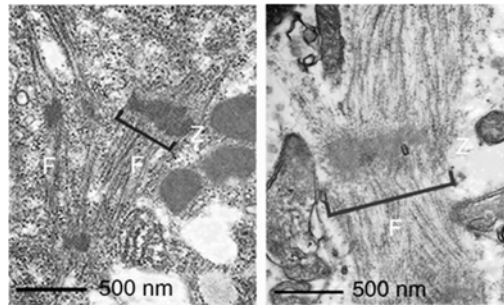


Figure 3.16. Sarcomere width measurement from transmission electron microscopy images. Transmission electron micrographs of sarcomeres showing actin and myosin filaments distribution. Black square brackets indicate the length of the Z-discs, used for the measurement of the sarcomere width. F: myofibrillar bundle; Z: Z-disc. *Adapted from Lu TY⁶².*

To assess the difference between group means, the normal distribution of sarcomere width values was tested using Shapiro-Wilk and Kolmogorov-Smirnov normality tests. Non-parametric analysis was performed using Mann-Whitney U test. The software used was Origin 8.5 (OriginLab, Northampton, USA), and differences were considered significant when $p < 0.05$.

3.10. Gene expression analysis by quantitative real-time polymerase chain reaction (qRT-PCR)

To study gene expression in standard 2D cell cultures, cells were incubated with trypsin (0.25%, Gibco®, Thermo Fisher Scientific, Spain) for 5 min at 37°C, neutralized with DMEM 4.5 g/l glucose (Life Technologies, Thermo Fisher Scientific, Spain) supplemented with 10% fetal bovine serum (FBS) (Gibco®, Thermo Fisher Scientific, Spain) and centrifuged 1000 rpm for 3 min. After washing with 1X phosphate buffered saline (PBS), cells were centrifuged at 2000 rpm for 5 min and lysed using TRIzol® RNA Isolation Reagent (Life Technologies, Thermo Fisher Scientific, Spain).

To study gene expression in 3D cardiac constructs, a quarter of the construct was incubated with 1 ml of trypsin (0.25%, Gibco®, Thermo Fisher Scientific, Spain) for 6-10 min and disaggregated by pipetting. Trypsin was neutralized with DMEM 4.5 g/l glucose (Life Technologies, Thermo Fisher Scientific, Spain) supplemented with 10% FBS

(Gibco®, Thermo Fisher Scientific, Spain) and tubing centrifuged at 1200 rpm for 5 min. After washing with 1X PBS, cells were centrifuged at 1200 rpm for 5 min and lysed using TRIzol® RNA Isolation Reagent (Life Technologies, Thermo Fisher Scientific, Spain).

Total RNA of 2D cell cultures and 3D cardiac constructs was isolated by incubating samples 5 min at room temperature, adding 200 µl of chloroform and vigorous shaking by hand for 15 s. Then, samples were incubated at room temperature for 2-3 min and centrifuged at 12000 g for 15 min at 4°C to obtain a phase separation, with RNA located in the upper aqueous phase. Aqueous phase was transferred to a new tube and RNA precipitated by adding 500 µl of isopropyl alcohol, with 10 min incubation at room temperature and centrifuging 10 min at 12000 g and 4°C. Finally, pellet was air dried, dissolved in 30 µl of RNase-free water and concentration measured at 260 nm and 280 nm with Nanodrop ND-1000 (Thermo Fisher Scientific, Spain).

To retrotranscript RNA to cDNA, 1 µg or 2 µg of RNA was used and transcriptor first strand cDNA synthesis kit (Roche Diagnostics, Spain) employed according to the manufacturer's protocol. The qRT-PCR was carried out using the 7300 Real-Time PCR System (Applied Biosystems, Thermo Fisher Scientific, Spain) and SYBR™ Green master mix (Thermo Fisher Scientific, Spain). Relative fold increase in gene expression was calculated with “ $2(-\Delta\Delta C(T))$ ” method⁴⁴², and human GAPDH expression was used as housekeeping gene. RNA from human fetal and adult hearts (Clontech, Takara Bio, France) were used as positive controls. Specific primers are listed in **Table 3.5**. We acknowledge the technical support from the Centre of Regenerative Medicine in Barcelona (CMRB).

3.11. Recording and processing of bioelectrical signals generated by cardiac tissue constructs

Extracellular field potentials (EFPs), generated by the charge redistribution in cardiomyocytes surrounding medium, were acquired through three electrodes using an advanced transducer amplifier (*work performed in collaboration with Biomedical Signal Processing and Interpretation group at Institute for Bioengineering of Catalonia (IBEC)*). The gold electrode of the perfusion chamber with electrical stimulation acted as internal reference, and electrical activity of cardiac tissue constructs was acquired using both graphite electrodes (**Figure 4.51**). The obtained ECG-like signal is generated by synchronized action potentials of cardiomyocytes. Its shape is similar to regular surface ECG signals for humans, including QRS complex and T wave (**Figure 1.4**).

Species	Gene	Forward primer	Reverse primer
Human	<i>GFP</i>	GAACCGCATCGAGCTGAA	TGCTTGTCGGCCATGATATAG
Human	<i>T/Bra</i>	TGCTTCCCTGAGACCCAGTT	GATCACTTCTTTCCCTTGCATCAAG
Human	<i>MHC</i>	ACAAGAAGGAGGGCATTGAGTGG	GCGTGGCTTCTGGAAATTGTTGGA
Human	<i>MYH6</i>	ATTGCTGAAACCGAGAATGG	CGCTCCTTGAGGTTGAAAAG
Human	<i>MYH7</i>	GCATCATGGACCTGGAGAAT	ATCCTTGCCTTGAGAGCATT
Human	<i>ACTC1</i>	GCTCTGGGCTGGTGAAGG	TTCTGACCCATACCCACCAT
Human	<i>TNNT2</i>	TGCAGGAGAAGTTCAAGCAGCAGA	AGCGAGGAGCAGATCTTTGGTGAA
Human	<i>MLC2V</i>	CAACGTGTTCTCCATGTTCCG	GTCAATGAAGCCATCCCTGT
Human	<i>RYR2</i>	ACAGCACAAGCCATTCTGCAAGA	ATGTAATCCAGCCCACCCAGACAT
Human	<i>SERCA2A</i>	TGAGACGCTCAAGTTTGTGG	TCATGCACAGGGTTGGTAGA
Human	<i>CACNA1C</i>	TTTGGTCCATGGTCAATGAG	GCATTGGCATTGATGTTGG
Human	<i>GJA1</i>	CAATCACTTGGCGTGACTTC	CCTCCAGCAGTTGAGTAGGC
Human	<i>GAPDH</i>	AGGGATCTCGCTCCTGGAA	AGGGATCTCGCTCCTGGAA

Table 3.5. Primers used for quantitative real-time polymerase chain reaction (qRT-PCR) analysis. They were used to study gene expression of both 2D cell cultures and 3D cardiac tissue constructs. *GFP*: green fluorescent protein; *T/Bra*: Brachyury; *MHC*: myosin heavy chain; *MYH6*: α -myosin heavy chain; *MYH7*: β -myosin heavy chain; *ACTC1*: cardiac muscle alpha actin; *TNNT2*: cardiac troponin T; *MLC2V*: myosin light chain 2v; *RYR2*: ryanodine receptor 2; *SERCA2A*: Sarcoplasmic Reticulum Ca^{2+} -ATPase isoform 2a; *CACNA1C*: calcium voltage-gated channel subunit alpha1 C; *GJA1*: connexin 43; *GAPDH*: glyceraldehyde 3-phosphate dehydrogenase.

The biomedical instrumentation for recording the bioelectrical signals was the Biopac MP100 system (Santa Barbara, CA, USA, 16 Bits AD conversion; DAC100C, gain 50, maximum bandwidth DC-5KHz, input impedance 2 M Ω , CMRR = 90 dB min). EFPs recordings were monitored and stored in a computer using the AcqKnowledge software v.4.1, and were analyzed with MATLAB (v.R2014b, Natick, MA, USA). EFPs signals were recorded at a sampling frequency of 12.5 KHz, and were filtered and decimated at a sampling rate of 500 Hz. Bioelectrical signals were bandpass filtered (zero-phase fourth-order Butterworth filter with cut-off frequency of 0.2 and 40 Hz, respectively) to use the main bandwidth of the classical electrocardiographic studies. Previously, the 50 Hz line interference and harmonics were cancelled by a comb-notch filter. To a better identification of different patterns in the ECG-like signals, Ensemble Empirical Mode Decomposition⁴⁴³ (Noise level: 1 dB; Iterations: 200) was used to cancel the multicomponent noise.

Instantaneous heart rate expressed as beats per minute (bpm) was calculated over extracellular field potentials generated in both control and electrically stimulated constructs at baseline and after application of drugs. Relative beating rate (BR) to baseline was calculated to evaluate the behavior of cardioactive drug effects. The

square root of the mean squared differences of successive intervals (RMSSD)⁴⁴⁴, one of the most commonly used measures to evaluate the BR variability in clinical settings, was also calculated.

The differences of the beating rate (BR) at baseline between control and electrically stimulated recordings were assessed using the Mann-Whitney U test. The same test was used to evaluate the effect over the BR after isoproterenol and carbachol treatments (minute 10) relative both to their corresponding baseline (first minute). Differences were considered statistically significant when $p < 0.001$.

4. RESULTS

4.1. **Matriderm™ as 3D scaffold for cardiac tissue engineering**

A prerequisite for obtaining faithful cardiac tissue constructs in cardiac tissue engineering is to mimic the cell native cardiac environment⁴⁴⁵. Therefore, selecting an appropriate scaffold is of paramount relevance, as it should mimic the cardiac extracellular matrix. Cardiac extracellular matrix is mainly constituted of collagen together with other proteins, such as elastin, laminin, and fibronectin^{20,446}. Collagen-based scaffolds are suitable for the generation of contractile cardiac tissue constructs, as they are natural substrates that potentiate cell attachment and survival, and cells can remodel them^{318,282}. For this reason, we chose as 3D scaffold a commercially available collagen-based sponge called Matriderm™ (MedSkin Solution Dr. Suwelack AG, Billerbeck, Germany). It is a highly porous membrane (~94%)^{447,448} of 1 mm thickness, and is composed of 3D coupled collagen (types I, III and V) and elastin. The collagen of the matrix is obtained from the bovine dermis, and the elastin is obtained from the bovine nuchal ligament by hydrolisis. Matriderm™ is currently being used in clinics to support dermal regeneration, restore the skin and modulate scar formation, so it can be cut to the desired size and is easily obtained from a reliable and reproducible source^{448,449}. According to manufacturer's datasheet, the absence of chemical cross-linking of the collagen results in a matrix which is especially biocompatible, and has demonstrated low antigenicity. When implanted, Matriderm™ becomes fully degraded within 4 weeks in animal models and within 6 weeks in humans, and reduces the risk of hematoma that occurs after skin grafting due to its hemostatic properties. In addition, Matriderm™ promotes cell growth, supports production of collagen matrix by fibroblasts, and is rapidly vascularized in human dermal regeneration processes⁴⁴⁹. There are many reports of successful engraftment through a one-step procedure using Matriderm™ and skin grafting *in vitro*⁴⁵⁰, *in vivo*^{451–454} and in clinical trials⁴⁵⁵.

Before its use, Matriderm™ has to be rehydrated in phosphate buffered saline (PBS). The scaffold has to be laid on the surface of the liquid to avoid air bubbles entrapment, and it is ready for use when its appearance changes from “white” to “translucent” and softens (**Figure 4.1**).

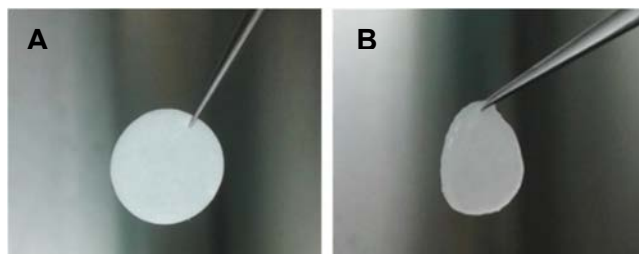


Figure 4.1. Image of Matriderm™ scaffold cut in a 1 cm diameter disk. A, Matriderm™ appearance in dry conditions. B, Matriderm™ appearance after 24 h rehydration in phosphate buffered saline (PBS).

4.1.1. Structural analysis of Matriderm™

To check Matriderm™ surface morphology and architecture and have information about its pore size, a scanning electron microscope (SEM) was used. The analysis demonstrated that Matriderm™ was a compact and uniform matrix, with interconnected pores ranging from 5 μm to 90 μm (**Figure 4.2**). According to literature reports, two types of pores were found in the scaffold: macropores from 50 to 90 μm in diameter combined with numerous micropores from 5 to 50 μm in diameter, being the most frequent pore size 17 μm . Macropores support cell migration, proliferation, angiogenesis and mass transport⁴⁵⁶, and extensive micropores enhance intercellular communication while facilitating mass transport⁴⁵⁷. Therefore, Matriderm™ properties were considered suitable to support cell attachment and survival in 3D, thanks to its composition and ability to allow an appropriate mass transport.

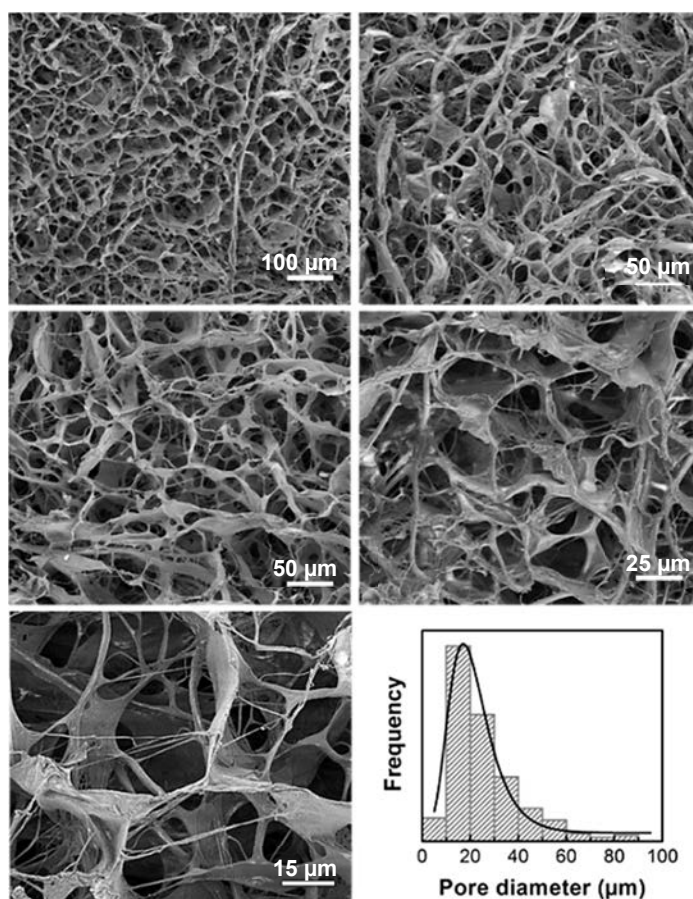


Figure 4.2. Matriderm™ surface morphology and porosity analysis by scanning electron microscopy (SEM). Matriderm™ is a uniform and highly porous scaffold with interconnected macro and micropores ranging from 5 to 90 μm . Values have been fitted in a single peak, and the most frequent pore size is of 17 μm .

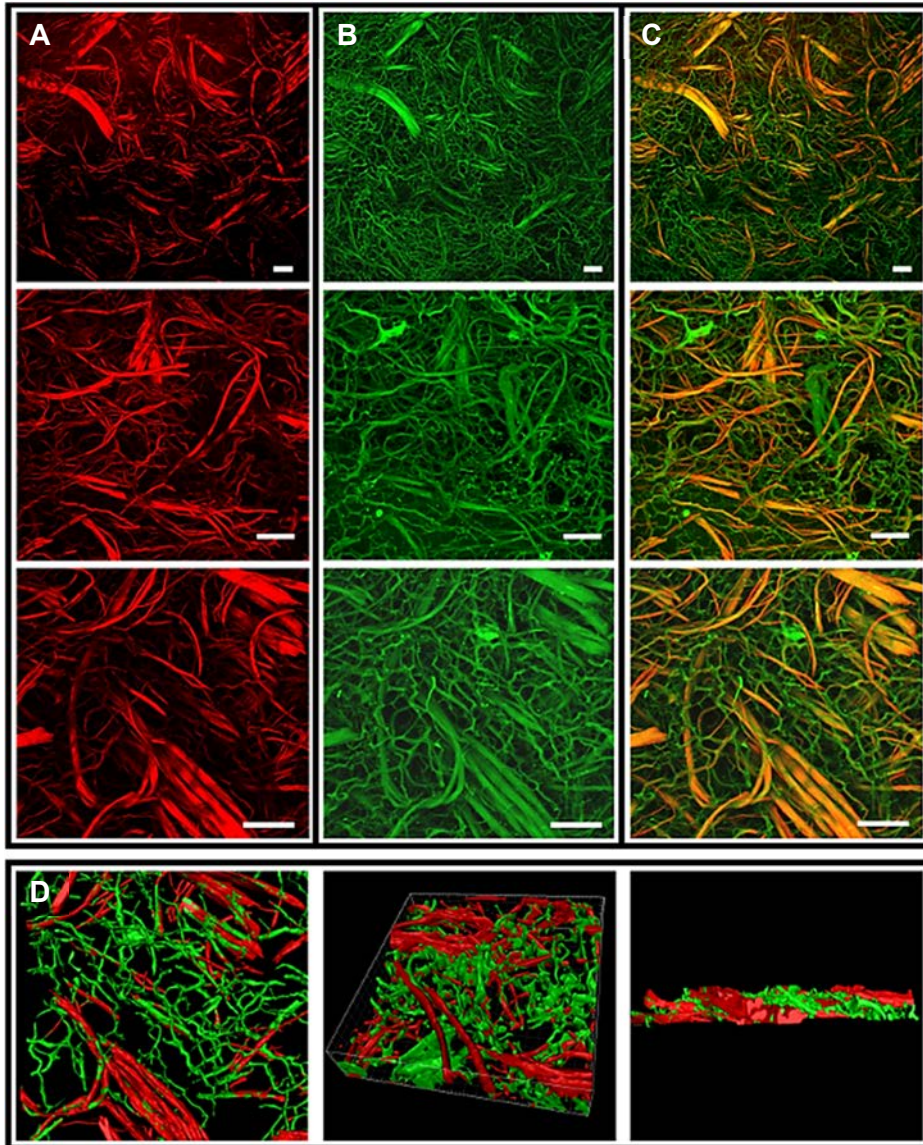


Figure 4.3. Selective imaging of Matriderm™ by Second Harmonic Generation (SHG) and Two-Photon Excited Fluorescence (TPEF). Z projection of Matriderm™ imaged by SHG (A) and TPEF (B) at different magnifications. C, Merged images of A and B at different magnifications. D, 3D reconstruction of highest magnification merged image. Scale bars: 100 μm .

To assess the 3D morphology of the scaffold in hydrated conditions and the distribution of collagen and elastin fibres, we imaged Matriderm™ using Second Harmonic Generation (SHG) and autofluorescence by Two-Photon Excited Fluorescence (TPEF) microscopy techniques (Figure 4.3). As fibrillar collagen is a strong source of SHG, it could be effectively imaged by SHG (Figure 4.3A). Also, both collagen and elastin show a high degree of autofluorescence (Figure 4.3B), so the combination of SHG and autofluorescence signals (Figure 4.3C) allowed us to

distinguish both structural components. Images confirmed that Matrigel™ was a complex matrix with collagen fibres (up to ~35 µm in diameter) that are forming thick bundles (up to ~100 µm in diameter) and thinner elastin fibres (up to ~10 µm in diameter) in a net-like structure, interacting in an intricate manner and randomly distributed. Finally, to have a better idea of scaffold fibres spatial distribution, a 3D reconstruction using IMARIS software (**Figure 4.3D**) was performed.

4.1.2. Mechanical properties of Matrigel™

Scaffold stiffness affects the maturation, organization and functional behaviour of cardiomyocytes^{296,294}. Consequently, to further characterize our collagen-elastin matrix, its bulk stiffness was measured by compression using Dynamic Mechanical Analysis (DMA) (**Figure 4.4A**). Representative stress-strain curves of the mechanical tests at room temperature and 37°C are plotted in **Figure 4.4B**. Low-density elastomeric open-cell foams such as Matrigel™ show a stress-strain curve with three distinct regimes (linear elastic regime, collapse plateau regime and densification regime). For elastic modulus calculation, only the linear elastic regime was taken into account, which is shown in **Figure 4.4B** for each condition. Results showed that hydrated Matrigel™ was a very soft material, and its stiffness was dependent on the temperature at which measurements were performed (**Figure 4.4C**). Values of the elastic modulus measured at room temperature (0.19 ± 0.05 kPa; mean \pm standard deviation) and at 37°C (0.06 ± 0.01 kPa; mean \pm standard deviation) showed statistically significant differences. Those results were in agreement with the elastic modulus obtained for hydrated porous collagen-based scaffolds under uniaxial compression, reported as 0.2 kPa⁴⁵⁸. Having such a soft scaffold encouraged us to use it for cardiac tissue constructs generation, as soft bulk materials (~2 kPa) have shown to help in obtaining constructs with improved contraction amplitudes and enhanced cell matrix deposition than stiffer ones²⁹⁶. However, other literature reports suggest that stiffer artificial substrates (10-50 kPa) enhance cardiomyocytes maturation⁴⁰, so it is an issue under debate.

4.1.3. Shear stress within Matrigel™ scaffold under perfusion

To obtain thick 3D cardiac tissue constructs it is crucial to ensure an effective mass transport between cells and culture medium. Static cultures rely on diffusional transport mechanisms, which are efficient only within a superficial cell layer (~100-200 µm⁴⁵⁹) and fail to support 3D tissues. Therefore, to improve oxygen and nutrients supply to cells cultured in the tissue interior (>200 µm in depth), tissue constructs will be cultured under perfusion of culture medium through the use of a bioreactor.

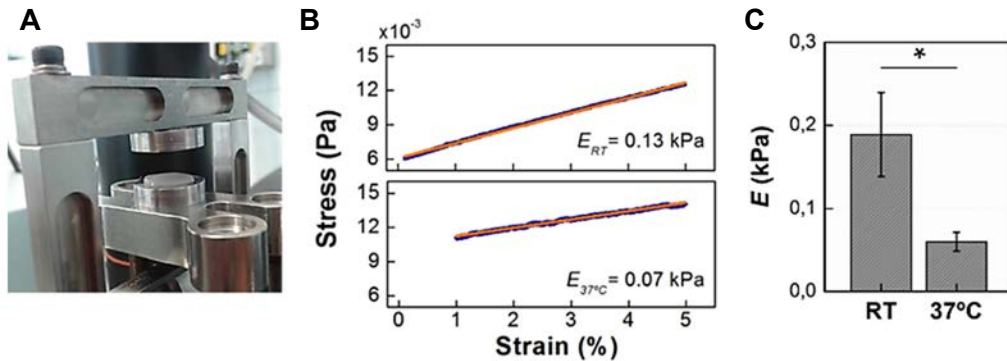


Figure 4.4. Results of compression tests on hydrated Matrigel™ scaffolds. **A**, Experimental setup, with disks of Matrigel™ (10 mm in diameter and 1 mm in thickness) placed in the Dynamic Mechanical Analyser. **B**, Representative stress-strain curves at room temperature (RT) and at 37°C. Blue lines correspond to experimental data, while orange lines correspond to the linear fitting ($R^2= 0.999$ for RT; $R^2= 0.996$ for 37°C). Young's Modulus (E) is determined from the slope (E_{RT} and $E_{37°C}$ respectively). **C**, Mean values of scaffold stiffness in compression at RT and at 37°C ($n=3$). *: Significance level $p<0.05$. Error bars indicate standard deviation (SD).

An important parameter to analyze the convenience of Matrigel™ to culture cardiac constructs in a perfusion bioreactor is the shear stress to which cells will be subjected^{398,460,461}. It has been reported that physiological shear stress values (~ 0.6 dyn/cm²) improve cardiac cell-cell interaction and myofibrillar organization, whereas higher values (over 2.4 dyn/cm²) have deleterious effects on cell survival⁴⁰⁴. Therefore, to get an optimal interstitial flow in our system, we calculated the shear stress to which cells were exposed following a model previously described²⁹⁷. A summary of the calculations is provided in **Table 4.1**.

First, we calculated the minimum flow rate needed in the perfusion chamber for the optimal culture of cardiac tissue constructs. This flow rate was determined by taking into account the overall mass balance of oxygen, that is, the concentration supplied by the culture medium and the consumption carried out by cells:

$$Q(C_{in} - C_{out}) = RN \quad \text{Eq. 4.1}$$

Where Q (ml/min) is the flow rate of culture medium, C_{in} is the inlet oxygen concentration in culture medium ($2.2 \cdot 10^8$ pmol/L at 37°C and 21% oxygen, as in the incubator air)²⁹⁷, C_{out} is the outlet oxygen concentration in culture medium (0 pmol/L, assuming that all oxygen was consumed in a single pass), R is the average oxygen consumption rate (pmol/h/cell, specific of each cell type) and N is the total number of cells ($3.5 \cdot 10^6$ cardiomyocytes). It was previously reported that neonatal rat cardiomyocytes (rCM) had an oxygen consumption rate two to three times lower than human induced pluripotent stem cell-derived cardiomyocytes (hiPSC-CM), being of 0.29 pmol/h/cell and 0.71 pmol/h/cell, respectively²⁹. Consequently, different minimum

flow rates should be applied for each cell type, being of 0.08 ml/min for rCM culture and 0.18 ml/min for hiPSC-CM. For technical issues, we applied a volumetric flow rate of 0.1 ml/min for rCM cardiac tissue constructs culture, and of 0.2 ml/min for hiPSC-CM.

After deciphering the suitable volumetric flow rate for each cell type, we calculated the shear stress experienced by cells when cultured inside Matrigel™ scaffold. Scaffold pores were considered cylindrical and following a tortuous pathway, represented by a length of $2H$ (being H the scaffold thickness)²⁹⁷. The calculation was based on the scaffold volume experiencing the interstitial medium flow, that is, the volume limited by the inner diameter of the silicone gasket (**Figure 3.8**):

$$U = \frac{2HQ}{\varepsilon V} \quad \text{Eq. 4.2}$$

Where U (m/s) is the average fluid velocity through each pore, $2H$ (m) is the length of the tortuous pathway (pores), Q (m³/s) is the volumetric flow rate calculated for each cell type, ε is the void fraction (scaffold porosity, 0.94) and V (m³) is the scaffold volume ($1.96 \cdot 10^{-8}$ m³). For rCM cardiac tissue constructs, the average fluid velocity was calculated as $1.8 \cdot 10^{-4}$ m/s, while for hiPSC-CM it was of $3.6 \cdot 10^{-4}$ m/s. Then, the following equation was used to estimate the shear stress (τ_w)²⁹⁷:

$$\tau_w = \eta \frac{4U}{R_c} \quad \text{Eq. 4.3}$$

Where η (dyn s/cm²) is the viscosity of the fluid ($7.8 \cdot 10^{-3}$ dyn s/cm² for DMEM culture medium)⁴⁶², U (cm/s) is the calculated average fluid velocity and R_c (cm) is the most frequent pore radius ($8.5 \cdot 10^{-4}$ cm). For rCM cardiac tissue constructs, the calculated shear stress was 0.66 dyn/cm², while for hiPSC-CM was 1.32 dyn/cm². When culturing cardiac cells under shear stress values ranging from 0.05 to 1.5 dyn/cm², compact and contractile cardiac tissue constructs with high expression of cardiac proteins could be obtained^{305,350}. Therefore, we considered our shear stresses appropriated for cardiomyocytes culture, and proceeded with Matrigel™ as a promising scaffold to obtain thick cardiac tissue constructs.

Species	Minimum flow rate (Q)	Average fluid velocity (U)	Shear stress (τ_w)
Rat	0.1 ml/min	$1.8 \cdot 10^{-4}$ m/s	0.66 dyn/cm ²
Human	0.2 ml/min	$3.6 \cdot 10^{-4}$ m/s	1.32 dyn/cm ²

Table 4.1. Summary of the calculations used to determine the shear stress within Matrigel™ scaffold under perfusion. Rat and human cardiomyocytes have different oxygen consumption rate, so different minimum flow rates must be applied.

4.2. Development of an efficient method for cell seeding into Matrigel™ scaffolds

Cell seeding into a 3D scaffold is the first step towards the generation of thick cardiac tissue constructs using perfusion bioreactors. It has been demonstrated that initial cell density has great influence on viability, mechanical integrity and functionality of the engineered tissue^{403,463,464}. Ideally, the generated tissue constructs should have a cell density approaching the one found in the myocardium ($\sim 10^8$ cells/cm³), and cells should be uniformly distributed for an enhanced rate of homogeneous tissue development⁴⁵⁹. Therefore, an efficient method of cell seeding is essential for a successful production of mature and functional cardiac tissue constructs *in vitro*.

In this context, we studied two types of cell seeding inside Matrigel™ scaffold: static seeding using Matrigel® as a cell delivery vehicle, or perfusion seeding using a perfusion loop system based on a previously published work²⁹⁷ (for further details, see “3.3. Cell seeding in 3D scaffolds” section). The suitability of each method was evaluated after several days of culture in a perfusion bioreactor (**Figure 4.5**) (for further details, see “3.4.1. Single chamber perfusion bioreactor” section).

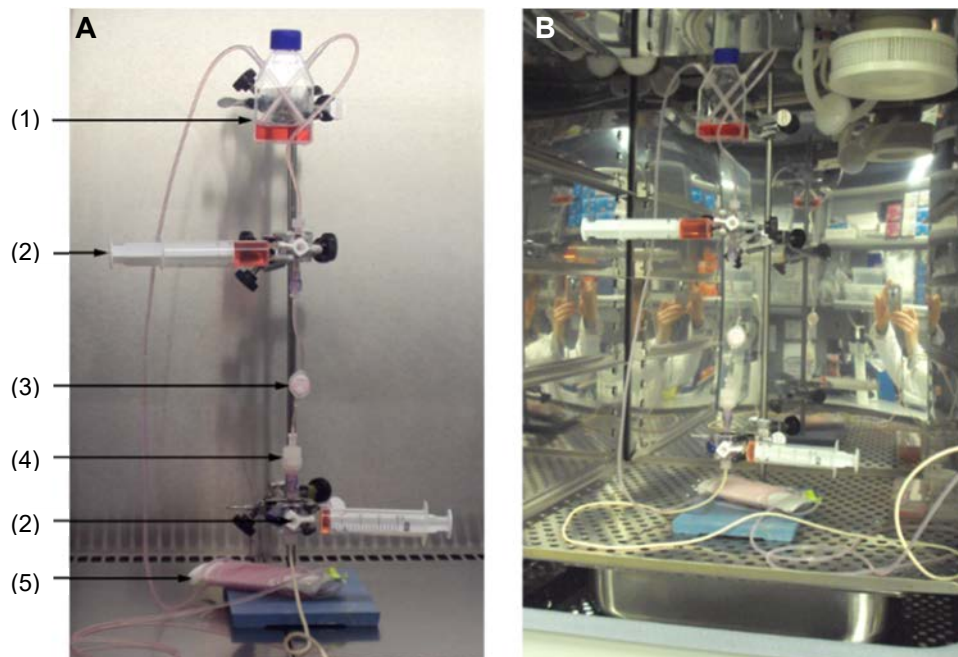


Figure 4.5. Single chamber perfusion bioreactor for cultivation of cardiac tissue constructs. **A**, Image of the bioreactor, composed of (1) medium reservoir, (2) three-way stopcocks with syringes inserted, (3) de-bubble system, (4) perfusion chamber and (5) gas exchanger. **B**, Image of the perfusion bioreactor inside an incubator with CO₂ and temperature control for cardiac tissue constructs culture.

4.2.1. Static seeding using Matrigel® as cell delivery vehicle

The first methodology assayed was a static seeding using Matrigel® as cell delivery vehicle, since thick and compact cardiac tissue constructs could be obtained when using it on top of collagen-based scaffolds²⁹⁷. Thus, we mixed $12 \cdot 10^6$ cells from a primary culture of neonatal rat heart cells with 60 μ l of Matrigel®, and the suspension was seeded on top of a Matriderm™ scaffold. After 30 min incubation to allow for cell attachment, the construct was transferred inside the perfusion bioreactor, and it was cultured under perfusion for 4 days. Finally, the cardiac construct was fixed, sectioned to obtain cross-sections and stained as described in “3.8. *Histological analysis*” section.

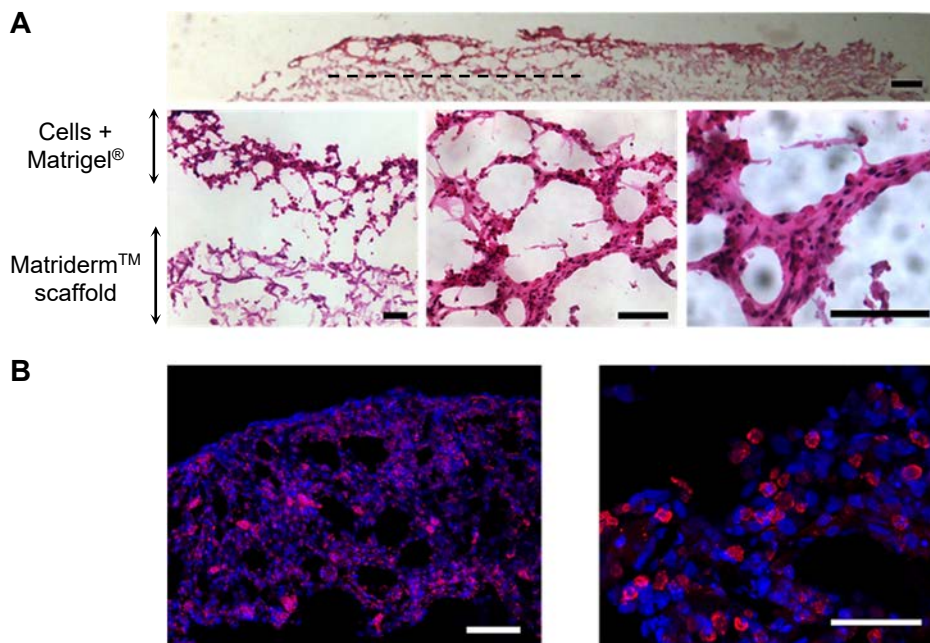


Figure 4.6. Distribution of neonatal rat cardiomyocytes in Matriderm™ scaffold when seeded statically. **A**, Hematoxylin and eosin staining of a construct cultured during 4 days in the perfusion bioreactor. Nuclei are stained blue, whereas cytoplasm and collagen scaffold have varying degrees of pink. Dashed lines indicate the maximum depth at which cells were found. Cross-section scale bar: 500 μ m; high magnification images scale bars: 200 μ m. **B**, Immunostaining of the construct with an antibody against cardiac troponin T (red, specific of cardiomyocytes) and 4',6-diamidino-2-phenylindole (DAPI, blue, cell nuclei staining). Scale bars: 100 μ m (left) and 50 μ m (right).

The hematoxylin and eosin staining of the cross-section of the tissue construct revealed that cells were not able to penetrate more than 400 μ m deep in the scaffold, suggesting that the scaffold pore size was critical for cell colonization (**Figure 4.6A**). Higher magnification images showed that, in fact, cells were attaching inside Matrigel® instead of inside the scaffold. A top layer with high density of cells could be seen, which was detached from Matriderm™ scaffold at some locations (**Figure 4.6A**).

Immunostaining analysis confirmed that cardiomyocytes were distributed only through Matrigel[®], and that although viable, they remained round after 4 days of culture (**Figure 4.6B**). Therefore, static seeding of Matriderm[™] was not suitable for our purposes, as the gelatinous matrix avoided cardiomyocytes attachment and homogeneous distribution along all the scaffold volume. In addition, cardiomyocytes showed a round morphology instead of the elongated shape characteristic of mature myocardium⁴⁰.

4.2.2. Cell seeding using a perfusion loop system

The second seeding methodology that we assayed was focused on overcoming the limitations of the static seeding, which were poor cell attachment and distribution through the scaffold due to bad penetration of Matrigel[®]. Therefore, we assembled a perfusion loop (**Figure 4.7A**) and tried to seed cells by perfusing them throughout the scaffold without using any hydrogel as cell delivery vehicle. The size of Matriderm[™] pores respect to cardiomyocytes size in suspension (17 μm and 10 μm ⁴⁶⁵, respectively) and the fact that pores were interconnected following a tortuous pathway, suggested that cells could be retained inside the scaffold when passing through it.

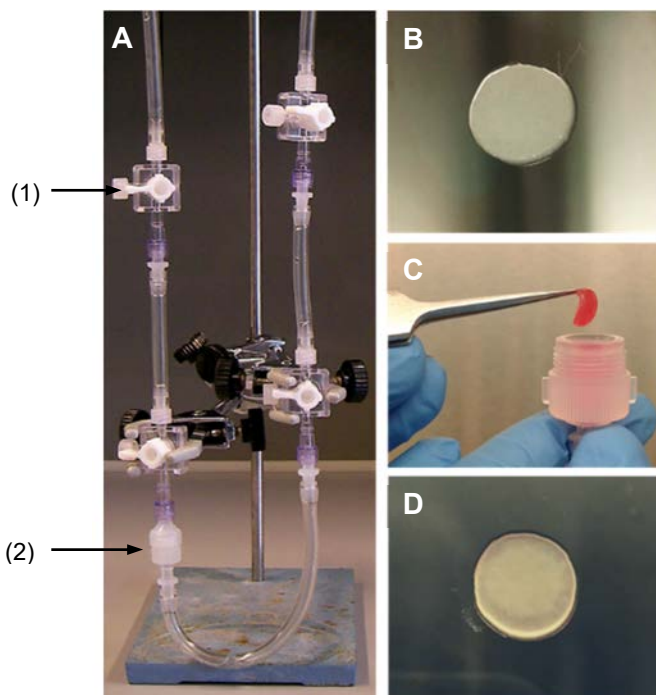


Figure 4.7. Perfusion seeding of cells inside Matriderm[™] scaffold using a perfusion loop. **A**, Image of the perfusion loop, composed of (1) three-way stopcocks and a (2) perfusion chamber. The rehydrated scaffold without cells (**B**) was installed inside the perfusion chamber between two silicone gaskets (**C**), and $3.5 \cdot 10^6$ cells were perfused through the scaffold. Gaskets provided mechanical support during perfusion, and routed the cell suspension through the central area of the scaffold. Cells were retained inside the scaffold when passing through it (**D**).

Perfusion loop assembly and initial seeding parameters were adapted from a previously published work²⁹⁷. The perfusion loop was assembled in sterile conditions, and filled with culture medium through three-way stopcocks. The hydrated scaffold without cells (**Figure 4.7B**) was installed inside the perfusion chamber and held in place by two gaskets (**Figure 4.7C**). Then, $3.5 \cdot 10^6$ neonatal rat heart cells concentrated in 1 ml of culture medium were injected inside the loop through the three-way stopcock located just over the perfusion chamber. To seed cells inside MatrigelTM, a forward-reverse flow of culture medium at 1 ml/min was applied during 2 h (**Figure 4.7D**). Finally, the tissue construct was incubated for 30 min in an incubator, transferred to the bioreactor and cultured under perfusion for 4 days. To analyze cell distribution, the cardiac construct was fixed, sectioned to obtain cross-sections and stained (for further details, see “3.3.2. Perfusion seeding” and “3.8. Histological analysis” sections).

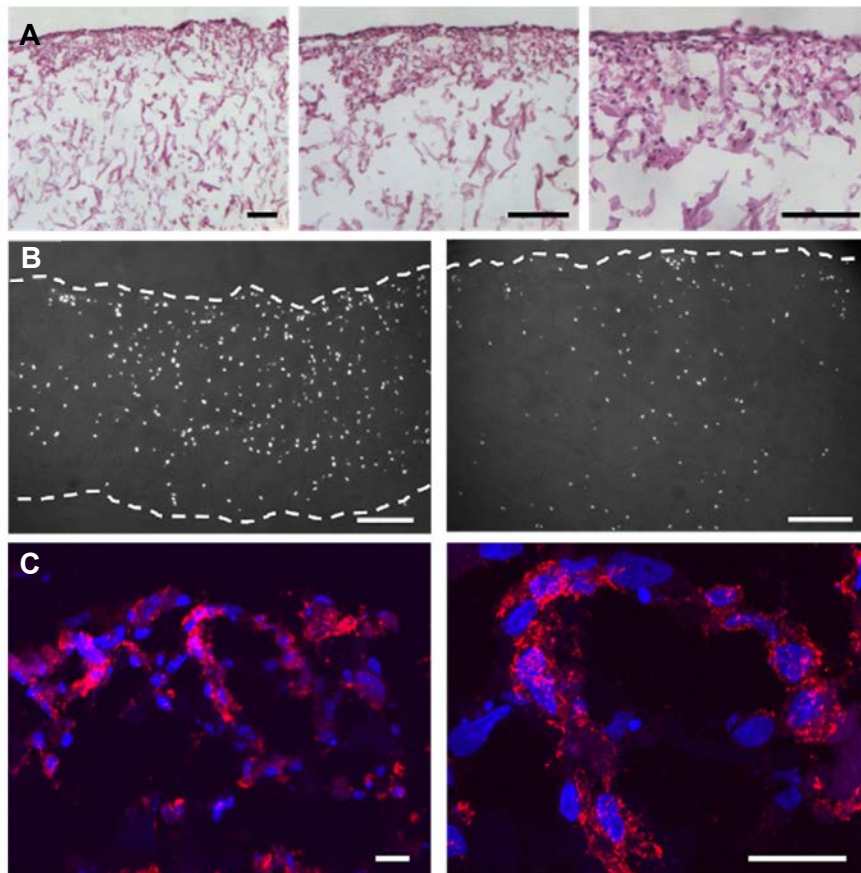


Figure 4.8. Distribution of neonatal rat cardiomyocytes in MatrigelTM scaffold when seeded in perfusion. **A**, Hematoxylin and eosin staining of tissue constructs cultured during 4 days in the bioreactor. Nuclei are stained blue, whereas cytoplasm and collagen scaffold have varying degrees of pink. Scale bars: 200 μ m. **B**, Staining of cell nuclei with DAPI in cross-sections of constructs cultured during 4 days in the bioreactor. White dashed lines indicate scaffold limits. Scale bars: 200 μ m. **C**, Immunostaining of constructs with an antibody against cardiac troponin T (red, specific of cardiomyocytes) and DAPI (blue, cell nuclei staining). Scale bars: 20 μ m.

Hematoxylin and eosin staining of the cross-section revealed that neonatal rat cardiac cells were capable of attaching inside Matrigel™ scaffold (**Figure 4.8A**), which was an improvement compared with the static seeding. However, cells were not distributed all along the scaffold, but located only at the top surface (~300 µm). As hematoxylin and eosin stained cells in a similar colour as scaffold fibres, we thought that results could be misleading. Therefore, the same construct was stained with 4',6-diamidino-2-phenylindole (DAPI) to allow a proper visualization of cell nuclei within the scaffold. This technique showed that, indeed, cells were seeded along all scaffold volume in a rather homogeneous way (**Figure 4.8B**), confirming that the absence of a cell delivery vehicle allowed deeper cell penetration. In addition, immunostaining analysis confirmed that cardiomyocytes were viable and adopted a more elongated shape after 4 days of cultivation than the statically seeded scaffolds (**Figure 4.8C**). Nevertheless, few cells were found in the cross-sections, so it was essential to optimize the process to successfully produce cardiac tissue constructs.

To elucidate the best parameters for an efficient seeding process, multiple perfusion conditions were assayed. For this, huge numbers of easily obtainable cells from an accessible source were absolutely needed. Therefore, human foreskin fibroblasts (HFF) were used instead of a primary culture on neonatal rat cardiomyocytes, as they were highly expandable and easier to obtain and maintain in culture. The initial perfusion seeding protocol (forward-reverse flow of culture medium at 1 ml/min for 2 h) was performed with HFF, and was used as the threshold to evaluate any meaningful improvement in cell seeding. This evaluation was based not only on qualitatively observations (cell density and distribution through Matrigel™ scaffold), but also quantitatively by calculating seeding efficiency (**Figure 4.9**). Efficiency was calculated considering the number of cells injected inside the perfusion loop ($3.5 \cdot 10^6$ cells) and the number of cells that remained inside the perfusion loop after the seeding process. The difference between the number of injected cells and the number of remaining cells inside the perfusion loop was, indeed, the number of cells retained inside the scaffold:

$$\text{Efficiency (\%)} = \frac{(\text{No. cells injected} - \text{No. cells inside the loop after seeding})}{\text{No. cells injected}} \times 100 \quad \text{Eq. 4.4}$$

The initial seeding protocol was modified in terms of flow rate, duration of the seeding and direction of the flow. First, we maintained the forward-reverse flow of culture medium for 2 h across the scaffold, but at 10 times slower flow rate (0.1 ml/min). Second, we maintained the same flow rate of 1 ml/min and forward-reverse flow of culture medium, but instead of applying it during 2 h, only one cycle was performed. Third, we again maintained the flow rate at 1 ml/min but instead of one cycle of forward-reverse perfusion, we applied the flow only in one direction (one-way perfusion). Finally, one-way perfusion of culture medium was applied at a slower flow rate (0.5 ml/min).

For each mentioned seeding condition, cell density and distribution through the scaffold was analyzed by DAPI staining of cross-sections (**Figure 4.9A**). It could be observed that, at low flow rates, cells were inhomogeneously distributed and less retained inside the scaffold than at higher flow rates. However, the most relevant effect was linked to the direction of the flow and the duration of the seeding process: a unidirectional seeding increased dramatically the number of cells retained inside the scaffold. Moreover, this high cell density was accompanied by a rather uniform distribution of cells, being more optimal when high flow rates were applied. Finally, shorter seeding times meant an increase of the number of cells retained inside the scaffold, even if a forward-reverse flow was applied. These observations were corroborated by seeding efficiency calculations (**Figure 4.9C**), where direction of the flow and seeding duration had the same effect on cell retention.

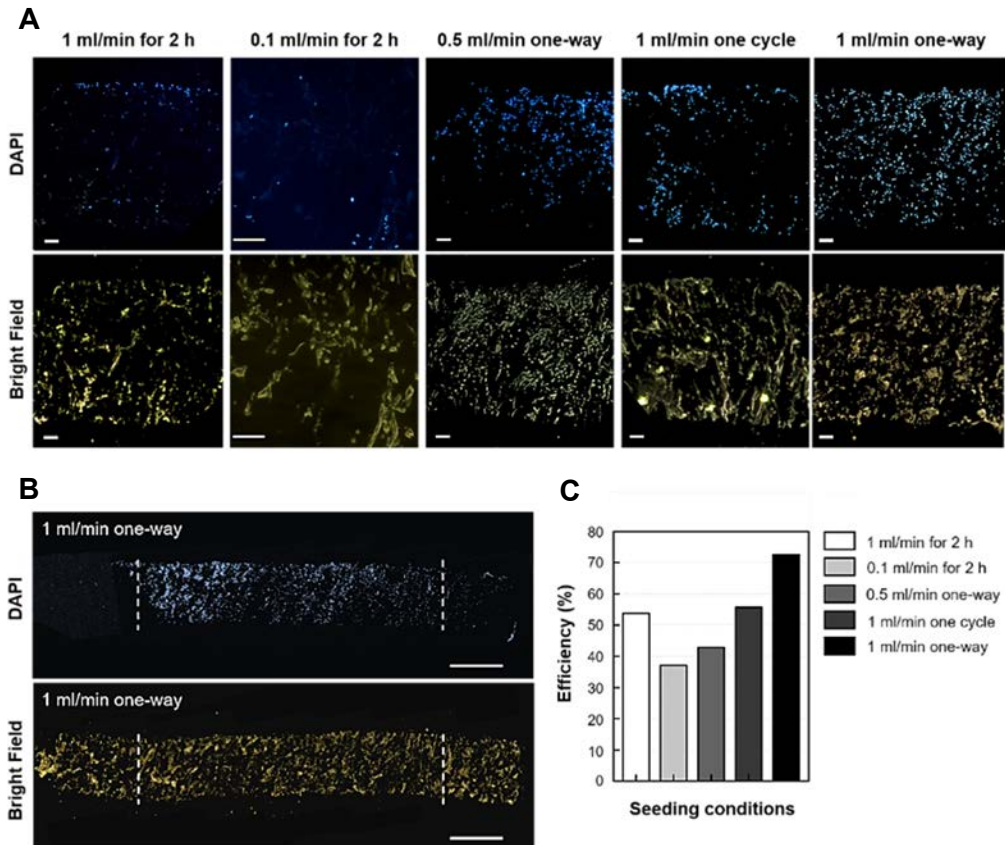


Figure 4.9. Optimization of cell seeding efficiency in Matrigel™ scaffold. **A**, Cross-sections of the scaffold after seeding human foreskin fibroblasts (HFF) using different perfusion parameters. DAPI (4',6-diamidino-2-phenylindole) staining revealed cell distribution through the scaffold for each condition. Scale bars: 100 μ m. **B**, Reconstruction of an entire cross-section of the most efficiently seeded scaffold. Dashed lines indicate gasket limits, where confinement of cells in the central part can be observed. Scale bar: 1 mm. **C**, Bar chart showing the efficiency for each cell seeding method.

On the whole, the most efficient method to seed cells inside Matrigel™ was obtained when applying one-way perfusion of culture medium at 1 ml/min (72.6% versus 53.7% for the formerly published protocol). Those perfusion seeding parameters allowed the retention of high cell numbers throughout the whole scaffold volume in a rather homogeneous way (**Figure 4.9B**). Therefore, we considered this seeding protocol suitable for a successful production of cardiac tissue constructs and we used it on the following experiments.

4.3. Design and fabrication of a parallelized perfusion bioreactor system

Cell culture results obtained with a single chamber perfusion bioreactor (**Figure 4.5A**) validated the applicability of the device to obtain cardiac tissue constructs, as cardiomyocytes attached and survived inside a 3D scaffold. However, having only one perfusion chamber restricted cardiac constructs production to one unit per assembled bioreactor. A parallel culture system was required to allow the culture of multiple cardiac tissue constructs under the same physicochemical conditions and from the same pool of cells, thus eliminating the variability associated to primary culture obtaining process. Having comparable tissue constructs simultaneously would allow studying with precision the influence of cell culture time or other external stimuli (e.g. electrical stimulation) on cardiac tissue constructs development.

4.3.1. Flow distribution in the parallelized perfusion bioreactor

To parallelize the perfusion bioreactor, both three-way stopcocks of the single chamber perfusion bioreactor were substituted by four port luer manifolds (**Figure 4.5A and 4.10A** respectively). Luer manifolds distributed the culture medium through four exits, so a perfusion chamber could be connected in each branch to have a parallel system. However, to ensure that in every branch of the bioreactor there was exactly the same flow rate, flow restrictors had to be installed, which were commercially available microfluidic channels (**Figure 4.10A**). The fluidic resistance exerted by the flow restrictor had to be much higher than the one exerted by the luer manifold to distribute the flow homogeneously through all branches. Thus, the resistance to the flow exerted by the luer manifold and the fluidic resistor had to be calculated. First, we had to elucidate the presence or absence of laminar flow by determining Reynolds number in both devices:

$$R_e = \frac{\rho v D}{\mu} \quad \text{Eq. 4.5}$$

Where R_e is the Reynolds number, ρ (kg/m³) is the density of the fluid (1030 kg/m³ for culture medium)⁴⁶⁶, v (m/s) is the mean velocity of the fluid, D (m) is the inner diameter of the tubing, and μ (N s/m²) is the dynamic viscosity of the fluid ($7 \cdot 10^{-4}$ N s/m²)

for culture medium at 37°C)³⁹⁸. To calculate the mean velocity of the fluid inside both the luer manifold and the flow restrictor, the following equation was applied:

$$v = \frac{Q}{A} \quad \text{Eq. 4.6}$$

Where v (m/s) is the mean velocity of the fluid, Q (m³/s) is the volumetric flow rate, and A (m²) is the cross-sectional area of the tubing. **Table 4.2** summarizes the results obtained for mean velocity of the fluid and Reynolds number calculations.

On the one hand, for a luer manifold of 4 mm inner diameter through which a volumetric flow rate of 0.4 ml/min ($6.67 \cdot 10^{-9}$ m³/s) was applied, the mean velocity of culture medium was $5.3 \cdot 10^{-4}$ m/s. On the other hand, for a fluidic resistor of 0.1 mm inner diameter through which a volumetric flow rate of 0.1 ml/min ($1.67 \cdot 10^{-9}$ m³/s) was applied, the mean velocity of culture medium was 0.07 m/s. With these values Reynolds number could be calculated, which was of 3.12 for the luer manifold and of 10.3 for the fluidic resistor. Such low Reynolds numbers (< 2000) indicated that laminar fluid flow was yielded in both devices, so the resistance could be calculated as follows:

$$R = \frac{8 \eta L}{\pi r^4} \quad \text{Eq. 4.7}$$

Where R (Pa s/m³) is the resistance to the laminar flow, η (N s/m²) is the viscosity of the fluid ($7.8 \cdot 10^{-4}$ N s/m² for DMEM culture medium⁴⁶²), L (m) is the tubing length and r (m) is the tubing radius. On the one hand, for a luer manifold of 10 cm length and 4 mm inner diameter, the resistance to the laminar flow was $1.24 \cdot 10^7$ Pa s/m³. On the other hand, for a fluidic resistor of 10.8 cm length and 0.1 mm inner diameter, the resistance to the laminar flow was $3.44 \cdot 10^{13}$ Pa s/m³. A summary of the calculations is provided in **Table 4.2**. Results indicated that the resistance exerted by the flow restrictor is six orders of magnitude higher than the one exerted by luer manifold. Therefore, installing a fluidic resistor with these dimensions in every branch of the bioreactor would ensure a homogeneous flow distribution.

Device	Diameter/ length	Flow rate (Q)	Mean velocity (v)	Reynolds number (R_e)	Resistance to laminar flow (R)
Luer manifold	4 mm / 10 cm	0.4 ml/min	$5.3 \cdot 10^{-4}$ m/s	3.12	$1.24 \cdot 10^7$ Pa s/m ³
Flow restrictor	0.1 mm / 10.8 cm	0.1 ml/min	0.07 m/s	10.3	$3.44 \cdot 10^{13}$ Pa s/m ³

Table 4.2. Fluidic characterization of the parallelized perfusion bioreactor. Mean velocity, Reynolds number and resistance to laminar flow were calculated to assure that the same flow rate was present in every branch of the bioreactor.

To verify that every branch of the bioreactor had the same flow rate, we measured the volume of culture medium flowing through each branch after 10 min of perfusion at 0.4 ml/min (**Figure 4.10B-C**). Results confirmed that a homogeneous distribution of culture medium was taking place, as equivalent flow rates at about 0.1 ml/min were coming through each bioreactor division. Consequently, we could conclude that a controlled flow perfusion bioreactor with a reliable parallelization system had been designed and properly assembled. Next, we went on validating the system as a cell culture platform by culturing cardiac tissue constructs in perfusion for several days.

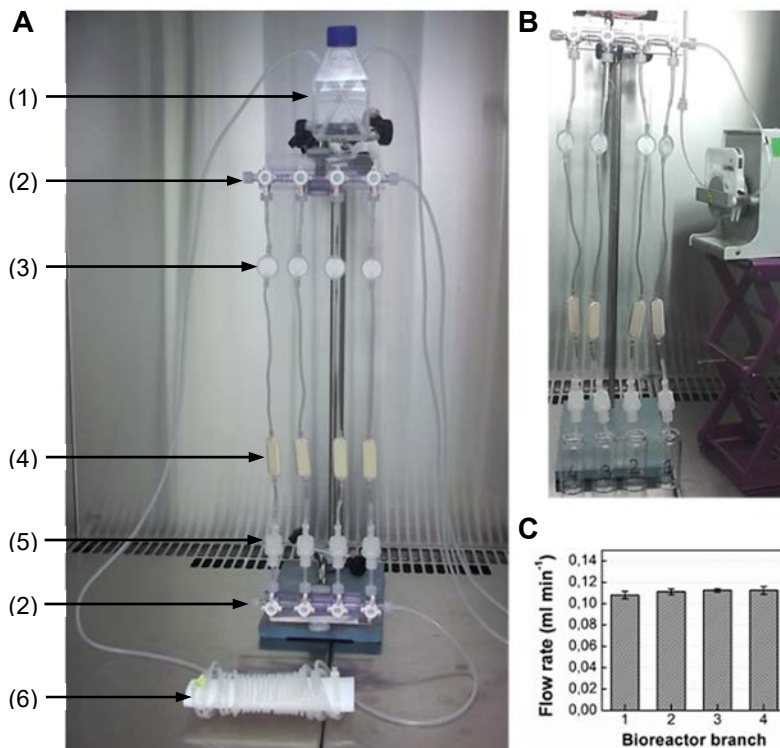


Figure 4.10. Parallelized perfusion bioreactor system. **A**, Image of the parallelized bioreactor, composed of a (1) medium reservoir, (2) four port luer manifolds, (3) de-bubble systems, (4) flow restrictors, (5) perfusion chambers and a (6) gas exchanger. **B**, Experimental setup to verify that the same flow rate was present in every branch of the bioreactor. The volume of culture medium passing through each branch after 10 min of perfusion was measured. **C**, Bar chart showing the measured flow rate in every branch of the bioreactor (n=3, mean \pm SD).

4.3.2. Preliminary cellular tests

4.3.2.1. Generation of rat cardiac tissue constructs

Once we had established an efficient seeding methodology and assembled and characterized a parallelized perfusion bioreactor system, we went on generating rat

cardiac tissue constructs. A primary culture of neonatal rat heart cells, which contained all the cell types composing the heart, was used in first instance to test the system because it was easier to handle than human induced pluripotent stem cells (hiPSC). Moreover, in the literature there is considerable knowledge and expertise on generating cardiac tissue constructs using neonatal rat cardiac cells^{281,297}, so they would be really useful to validate our approach. Likewise, rat cardiac tissue constructs would be a convenient tool to assess the organization and functionality of the constructs obtained with the perfusion bioreactor, and to compare the results with the state of the art.

For the generation of rat cardiac tissue constructs, $3.5 \cdot 10^6$ cells isolated from ventricles of 2-3-day-old rats were seeded inside Matrigel™ scaffold (see “3.3.2. *Perfusion seeding*” section for further details). To study tissue development over time, three scaffolds were produced, with seeding efficiencies of 77.7%, 62.3% and 71.4%. The first cardiac construct was fixed just after seeding to have an initial time point (zero-time point) as a reference. The other two cardiac constructs were installed inside the parallel perfusion bioreactor and cultured for 1 and 7 days respectively. Rat heart cells could attach and grow inside the 3D scaffold, forming a compact tissue after 7 days of culture that was evident even with the naked eye (**Figure 4.11**). As 2D controls, $0.5 \cdot 10^6$ cells from the same primary culture were seeded in a 12-well plate.

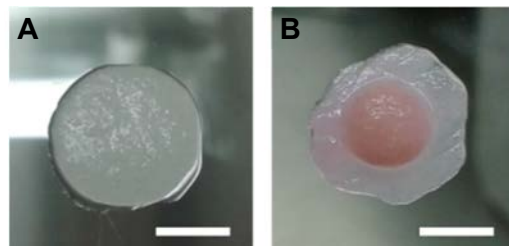


Figure 4.11. Image of Matrigel™ scaffold before and after culturing a primary culture of neonatal rat heart cells. A, Void scaffold upon rehydration process. **B,** Cardiac tissue construct generated after culturing neonatal rat heart cells inside the scaffold for 7 days in the parallelized perfusion bioreactor. A high cell density circle grew in the centre of the scaffold. Scale bars: 5 mm.

To evaluate the functionality of rat cardiac tissue constructs, the presence of spontaneous beating at seeding point and after 1 and 7 days of culture in perfusion was analyzed. For this, each construct was immersed in a Petri dish with culture medium at 37°C and observed under a microscope. Cardiac tissue constructs at seeding point and after 1 day of culture did not show any spontaneous contraction, neither at microscopic or macroscopic level. However, after 7 days of culture the cardiac construct contracted at microscopic level, meaning that further time in culture was necessary for restoration of cardiomyocytes contractile function (**Figure 4.12** and **Supplementary Videos 4.1 and 4.2**). Moreover, the contraction was performed not only by isolated groups of cells

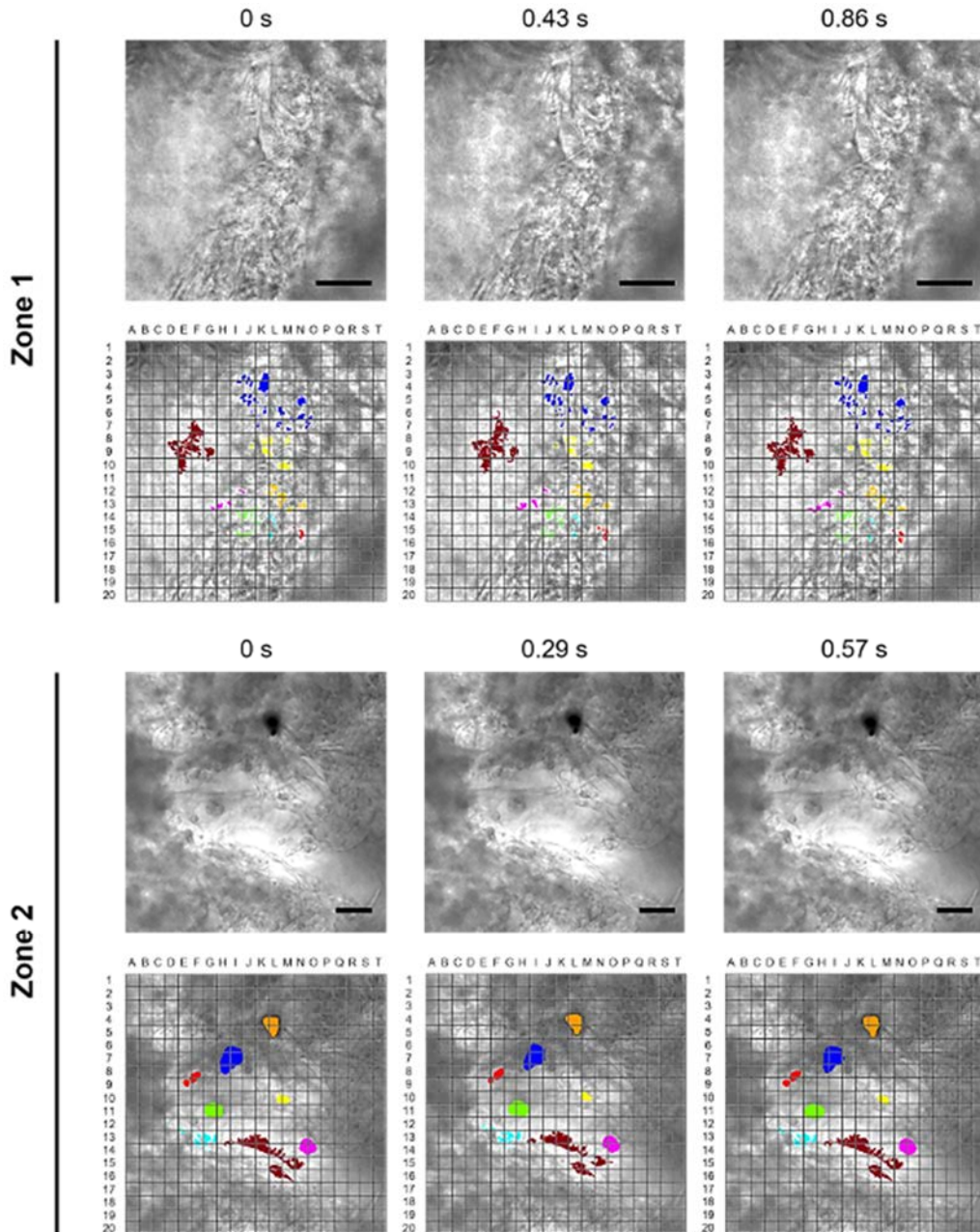


Figure 4.12. Beating analysis of a rat cardiac tissue constructs cultured for 7 days in the parallelized perfusion bioreactor. Cardiac construct beating was video recorded from its top view using an inverted microscope. Then, consecutive frames of the video were selected and well delimited zones were coloured. Changes in shape and position of coloured zones were tracked by superimposing a numbered grid to the images. Scale bars: 50 μm .

scattered along the scaffold, but by the whole construct. This is evidenced in **Figure 4.12**, where well delimited features in consecutive frames of the video were coloured and their movement tracked by means of a numbered grid. Coloured zones modified

their shape and position over time, and their displacement was similar for all of them. Therefore, cardiac tissue construct beating was performed by groups of cells (change in shape of coloured zones) in a coordinated way, resulting in a construct beating at the macroscale (equivalent displacement at the same time of the coloured zones).

After functional analysis, cardiac tissue constructs were fixed, sectioned and stained as described in “3.8.2.2. *Cardiac tissue constructs (in toto)*” section. As cardiac cell markers, antibodies against cardiac troponin I (cTnI) and α -sarcomeric actin (α -sa) were used. As universal cell markers, an antibody against α -tubulin (α -tub) to stain the cytoskeleton and 4',6-diamidino-2-phenylindole (DAPI) to stain cell nuclei were used. Immunofluorescence images revealed that constructs expressed cardiac markers at all timepoints studied, thus confirming that cardiomyocytes could attach and survive in the 3D scaffold when cultured in the perfusion bioreactor (**Figure 4.13**). Regarding cell morphology, cardiomyocytes at seeding point were round and did not show any defined sarcomeric organization or evidence of cell-cell interactions (**Figure 4.13**). After one day in culture, cardiomyocytes adopted a more elongated morphology and their cytoskeleton organized into nascent and small sarcomeres (**Figure 4.13**). Still, the most relevant differences were found in cardiomyocytes cultured during 7 days in the bioreactor. High cell densities zones were found in the construct, with both cardiomyocytes and non-cardiomyocytes interacting among them and involved in the performance of the previously observed contractions (**Figure 4.13**). Moreover, cardiac cells displayed more elongated morphologies than in previous timepoints, with abundant and well-defined sarcomeric structures. Therefore, a favorable evolution of the cardiac construct towards a more mature construct was taking place, agreeing with previous works where constructs cultured under perfusion for about 10 days showed an optimal tissue architecture^{398,467}. In standard 2D well plates, cardiomyocytes coming from the same primary culture showed well-developed sarcomeres and cell-cell interactions (**Figure 4.13**). However, their functional performance was different from the cardiac tissue construct. Cardiomyocytes in 2D well plates exerted sustained and synchronous contractions, but were organized in few layers of cells with individual beating colonies (**Supplementary Video 4.3**), whereas cardiomyocytes in the cardiac tissue construct assembled in more macroscopic structures.

Taken together, those preliminary results corroborated the suitability of the developed bioreactor to support neonatal rat cardiac cells culture in a 3D scaffold, as well as to generate contractile cardiac tissue constructs. Thus, the next step was to culture human induced pluripotent stem cells (hiPSC) in the parallelized perfusion bioreactor system to obtain human cardiac tissue constructs.

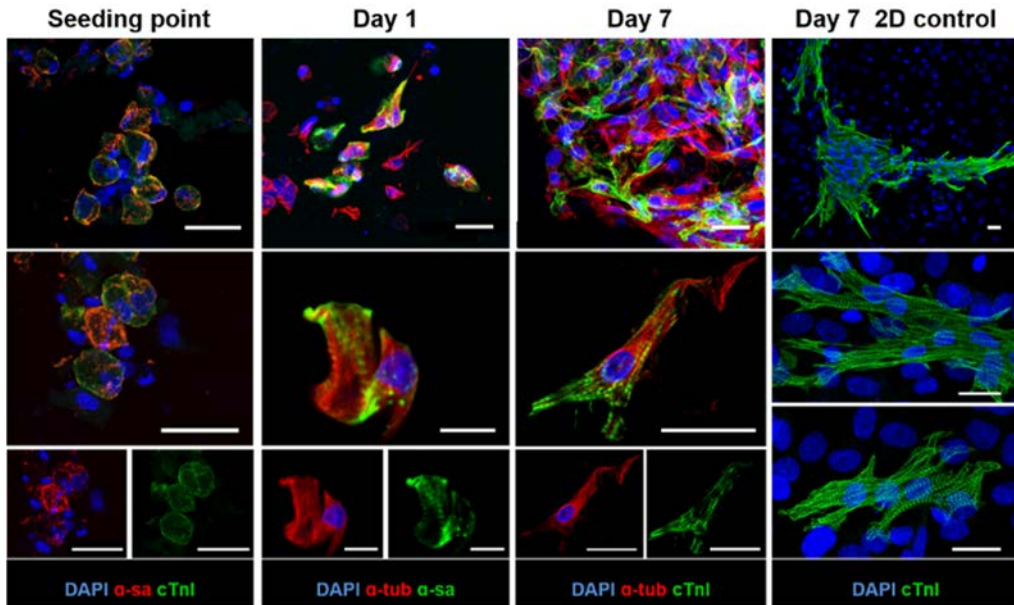


Figure 4.13. Immunostaining of rat cardiac tissue constructs cultured in the parallelized perfusion bioreactor. Cardiac constructs at seeding point and after 1 or 7 days of culture in the bioreactor were analysed, as well as the same pool of cells cultured in standard 2D well plates. Changes in sarcomeric organization and cell shape were noticeable over time in culture. DAPI: 4',6-diamidino-2-phenylindole; α -sa: α -sarcomeric actin; cTnI: cardiac troponin I; α -tub: α -tubulin. Scale bar: 25 μ m.

4.3.2.2. Generation of human cardiac tissue constructs

Generation of keratinocyte-derived induced pluripotent stem (KiPS) transgenic cell lines and their differentiation to the cardiac lineage was studied and optimized by Dr. Claudia Di Guglielmo during her PhD thesis. In this section, only the part of her work performed in collaboration is being reproduced. For further details, readers are encouraged to refer to Dr. Di Guglielmo's PhD thesis.

After validating the parallelized perfusion bioreactor approach with neonatal rat heart cells, we tried to generate human cardiac tissue constructs from human induced pluripotent stem cells (hiPSC). For that, it was important to consider that *in vitro* differentiation protocols gave rise to a mixture of different cell types in culture, and in a non-synchronized way. Moreover, monitoring the effectiveness of cardiac differentiation was crucial because high amounts of cardiac cells were needed to generate tissue-like cardiac tissue constructs. For that purposes, two reporter cell lines were produced, one expressing green fluorescent protein (GFP) when hiPSC were differentiated to early mesoderm (Brachyury (Bra) cell line) and another one expressing GFP when hiPSC were differentiated to cardiomyocytes (α -myosin heavy chain (α MHC) cell line)⁴³¹.

The first hypothesis we wanted to address was whether early mesoderm committed cells were able to reach terminal cardiac differentiation when cultured in the perfusion bioreactor. For this, cardiac differentiation was started on hiPSC-Brachyury transgenic cells in monolayer culture with modulators of canonical Wnt signaling⁴³³. On day 2 of differentiation, flow cytometry analysis revealed that 87.4% of cells were committed to mesoderm (**Figure 4.14A**), which was also confirmed by Brachyury and GFP additional expression analysis (**Figure 4.14B-C**). Those early mesoderm-committed cells were mixed with human foreskin fibroblasts (HFF) in a 1:1 proportion to obtain a co-culture, as the presence of non-cardiomyocytes helped the maturation of hiPSC-derived cardiomyocytes in comparison with a pure cardiomyocyte population²⁴⁶. Five MatrigelTM scaffolds were seeded with the co-culture, with seeding efficiencies of 98%, 97.25%, 96%, 86% and 98%. The first cardiac construct was fixed just after seeding (day 2 of differentiation) to have an initial timepoint as a reference to study cardiac differentiation over time. The other cardiac constructs were cultured in the parallelized perfusion bioreactor for 6, 13, 17 and 20 days, respectively, with culture medium composition being the same at each timepoint as the standard differentiation protocol in well plates. As 2D controls, $0.5 \cdot 10^6$ cells from the co-culture were seeded in a 12-well plate, and early mesoderm-committed hiPSC without HFF were also maintained in 12-well plates (standard differentiation protocol).

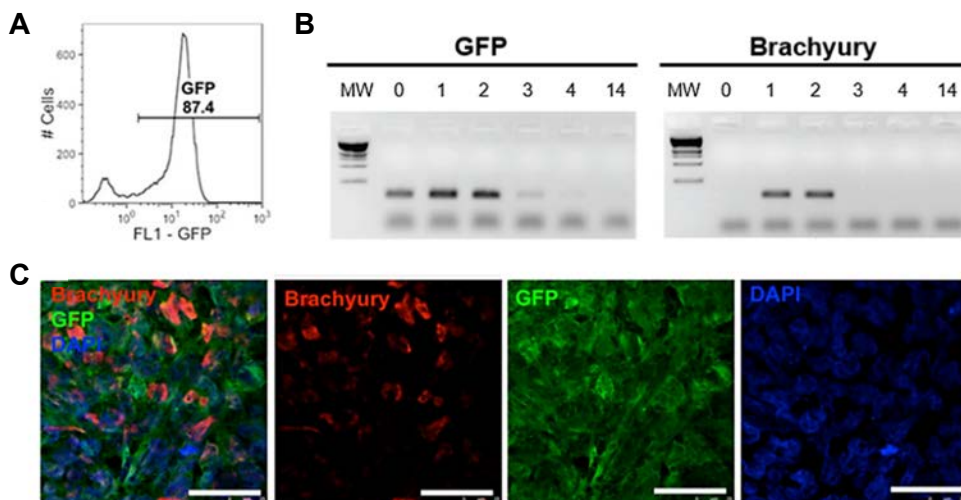


Figure 4.14. Analysis of mesoderm commitment of hiPSC-Brachyury transgenic cell line on day 2 of differentiation. **A**, Flow cytometry analysis of GFP expression on day 2 of differentiation. **B**, Semi-quantitative RT-PCR analysis of GFP and Brachyury confirm their expression (black lines) on day 2 of differentiation. MW: molecular weight; Numbers 0 to 14: days of differentiation. **C**, Immunostaining of GFP and Brachyury expressed by hiPSC on day 2 of differentiation. Colocalization of both proteins could be observed. GFP: green fluorescent protein; DAPI: 4',6-diamidino-2-phenylindole. Scale bars: 50 μ m. *Figure adapted from Di Guglielmo, C⁴³¹.*

Contractility of the generated cardiac tissue construct was assessed after each culture time by observing the presence of spontaneous beating. Unfortunately, spontaneous beating could not be identified in any of the tissue constructs, whereas in 2D controls beating areas were clearly detected from day 13 on. Therefore, cardiac constructs were fixed, sectioned and stained as described “3.8.2.2. Cardiac tissue constructs (*in toto*)” to analyze the efficiency of the differentiation process, as well as the morphology of the cells and to which extent they could colonize the scaffold. Initially, cell nuclei were stained in cross-sections of cardiac tissue constructs to study the presence of cells and their distribution at each timepoint. Interestingly, all cardiac tissue constructs contained a high number of cells that increased over time in culture (**Figure 4.15**), confirming not only cell survival but also proliferation inside the scaffold.

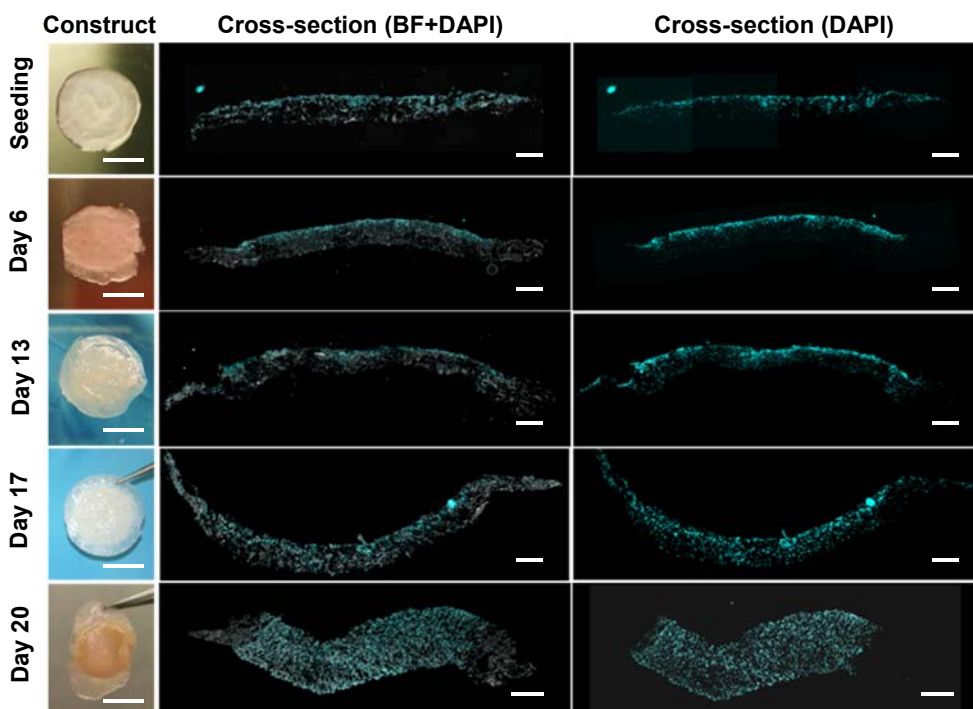


Figure 4.15. Human cardiac tissue constructs generation from a co-culture of early mesoderm-committed hiPSC and human foreskin fibroblasts (HFF). Cardiac constructs were cultured inside the parallelized perfusion bioreactor for different times to assess construct development. Images of the obtained cardiac constructs are shown, as well as reconstructions of entire cross-sections stained with DAPI. Constructs scale bar: 5 mm. Cross-sections scale bar: 1 mm. BF: bright field; DAPI: 4',6-diamidino-2-phenylindole. *Adapted from Di Guglielmo, C⁴³¹.*

To analyze the differentiation process and discriminate hiPSC-derived cardiomyocytes from HFF, we used antibodies against GFP (specific of hiPSC), α -tubulin (α -tub, cytoskeleton marker), cardiac troponin I (cTNI, cardiac specific marker) and α -sarcomeric actin (α -sa, cardiac specific marker). Immunostaining analysis showed that early mesoderm-committed cells were present in the cardiac construct at

seeding point, mixed with non-GFP expressing cells and displaying round shapes characteristic of not well-adhered cells (**Figure 4.16**). However, early mesoderm-committed cells were not able to differentiate to cardiomyocytes in co-culture, as expression of cardiac specific markers was absent both in cardiac tissue constructs and their corresponding 2D controls (**Figure 4.16**). The fact that cardiac markers were clearly displayed in hiPSC differentiated with the standard protocol suggested that the Brachyury-cell line had cardiogenic potential (**Figure 4.16**). Therefore, co-culturing early mesoderm-committed cells with HFF did not promote cardiac differentiation in any of the conditions studied. This was relatively unexpected, as cardiac constructs generated with a pure culture of GFP expressing cells gave similar results (data not shown), and it had been reported that non-cardiomyocytes helped the maturation of human embryonic stem cell (hESC)-derived cardiomyocytes during differentiation³²⁸.

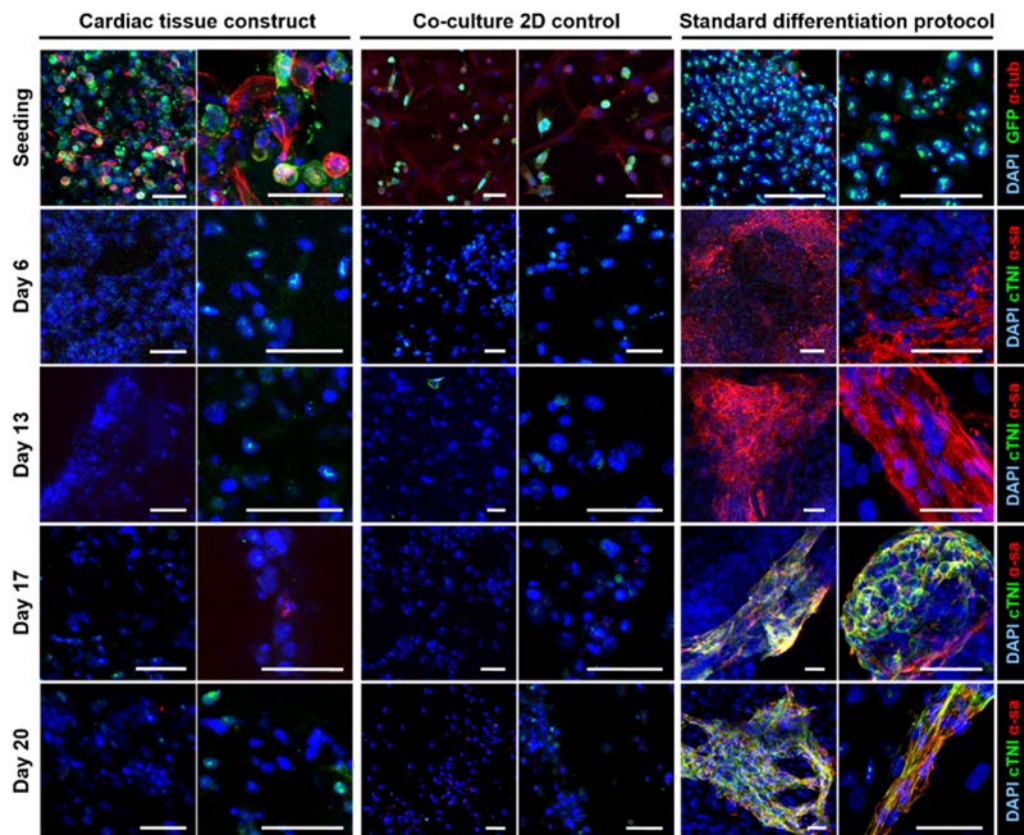


Figure 4.16. Immunostaining of human cardiac constructs cultured in the perfusion bioreactor and their corresponding 2D controls. A co-culture of early mesoderm-committed hiPSC and human foreskin fibroblasts (HFF) was seeded in 3D scaffolds to obtain *cardiac tissue constructs*. As controls, the same co-culture (*co-culture 2D control*) and early mesoderm-committed hiPSC without HFF (*standard differentiation protocol*) were maintained in well plates. Scale bars: 50 μ m. DAPI: 4',6-diamidino-2-phenylindole; GFP: green fluorescent protein; α -tub: α -tubulin; cTNI: cardiac troponin I; α -sa: α -sarcomeric actin. *Figure adapted from Di Guglielmo, C*⁴³¹.

Results obtained with Brachyury cell line lead us to hypothesize that the bioreactor could have a role in improving the maturation of cardiomyocytes derived from hiPSC. Nowadays, it is possible to produce cardiomyocytes from human pluripotent stem cells (hPSC), but they exhibit morphological and functional properties more similar to cardiomyocytes of the developing heart than of the adult⁴⁰. Therefore, providing hiPSC-derived cardiomyocytes with a more physiological environment by means of a 3D environment could favor their maturation towards a more adult-like phenotype. To address this issue, we took advantage of the α -myosin heavy chain (α MHC) transgenic cell line that express GFP when hiPSC are differentiated to cardiomyocytes. Cardiac differentiation was started on hiPSC- α MHC transgenic cells in monolayer culture using modulators of canonical Wnt signalling⁴³³. On day 20 of differentiation, flow cytometry analysis revealed that 44% of cells were differentiated to cardiomyocytes (**Figure 4.17A**), which was also confirmed by α MHC, GFP and cardiac troponin I (cTNI) expression analysis (**Figure 4.17B-C**). On day 30 of differentiation, hiPSC-derived cardiomyocytes were isolated by picking beating areas and were mixed with human foreskin fibroblasts (HFF) in a 3:1 proportion. Then, two MatrigelTM scaffolds were seeded with the co-culture, with seeding efficiencies of 85% and 92.6%. The first cardiac construct was fixed after 1 day of culture in the parallelized perfusion bioreactor, and the second one after 4 days of culture. As a 2D control, $2.5 \cdot 10^5$ cells from the same co-culture were seeded and maintained in a 6-well plate for equivalent times.

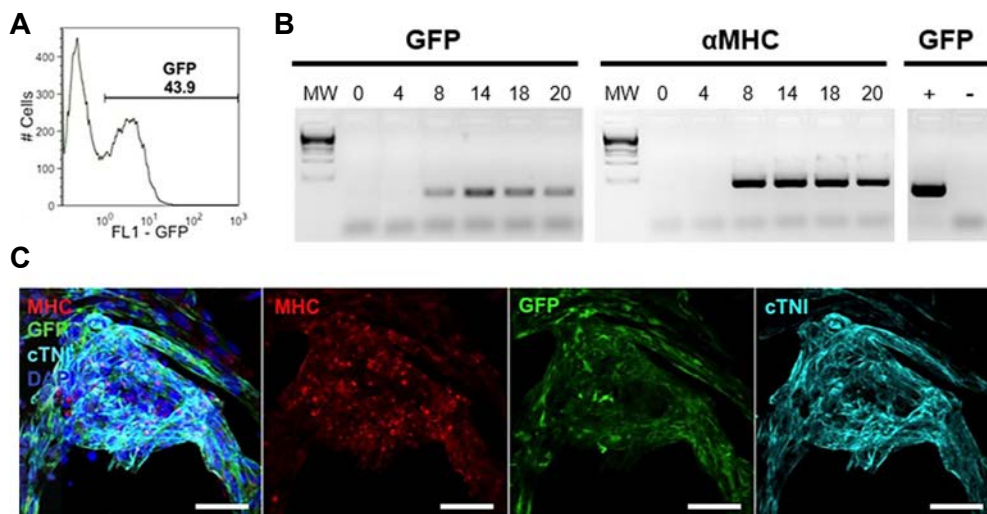


Figure 4.17. Cardiac differentiation analysis of hiPSC- α MHC transgenic cell line on day 20 of differentiation. **A**, Flow cytometry analysis of GFP expression on day 20 of differentiation. **B**, Semi-quantitative RT-PCR analysis of GFP and α MHC expression. α MHC expression was evaluated in GFP positive (+) and negative (-) cells. MW: molecular weight; Numbers 0 to 20: days of differentiation. **C**, Immunostaining of MHC, GFP and cTNI proteins expressed by hiPSC on day 20 of differentiation. Colocalization of the proteins could be observed. MHC: α -myosin heavy chain; GFP: green fluorescent protein; cTNI: cardiac troponin I; DAPI: 4',6-diamidino-2-phenylindole. Scale bars: 50 μ m. *Figure adapted from Di Guglielmo, C⁴³¹.*

To assess the functional activity of the generated cardiac tissue constructs, spontaneous beating was checked after each culture time. Unfortunately, spontaneous beating could not be identified in any of the tissue constructs, whereas in 2D controls beating areas were detected. Cardiac tissue constructs were fixed, sectioned and immunostained as described in “3.8.2.2. *Cardiac tissue constructs (in toto)*” section to analyze cell population morphology, distribution and presence or absence of cardiomyocytes. Antibodies against α -tubulin (alpha tubulin, cytoskeleton marker), cardiac troponin I (cTNI, cardiac specific marker), α -sarcomeric actin (ASA, cardiac specific marker) and α -sarcomeric actinin (AAS, cardiac specific marker) were used. Results showed that some hiPSC-derived cardiomyocytes were present in the cardiac construct after 1 day of culture in the bioreactor, mixed with non-cardiac cells and expressing cTNI and ASA cardiac markers (**Figure 4.18**). In addition, and more importantly, the same population of cells was maintained after 4 days of culture in perfusion, forming clusters of aggregated cells that expressed cTNI, ASA and AAS cardiac markers (**Figure 4.18**). Those observations were in agreement with the results obtained for co-culture 2D controls, where aggregates of cardiomyocytes interacted with non-cardiac cells and exhibited contractile activity (**Figure 4.18**). On the whole, those results suggested that a co-culture of hiPSC-derived cardiomyocytes and HFF was capable to attach and survive in a 3D scaffold under perfusion of culture medium for periods of time up to 4 days. Therefore, increasing both the number of cardiomyocytes seeded in the scaffold and the time in culture would be a strategy to follow for the development of tissue-like human cardiac tissue constructs. Moreover, results confirmed the need of having differentiated cardiomyocytes from hiPSC before seeding them in the scaffold, thus suggesting a pivotal role of the bioreactor in the maturation of hiPSC-derived cardiomyocytes.

Altogether, those preliminary results set the bases for the development of human cardiac tissue constructs with an improved maturity respect to standard differentiation protocols, but further optimization of culture parameters was absolutely needed. Apart from improving cell number and time of culture, we wanted to provide cells with a well-known regulatory signal that favours cardiomyocytes maturation and contractility within cardiac tissue constructs: electrical stimulation^{318,319}. Electrical stimulation has demonstrated to induce the establishment of synchronous contractions in cardiac tissue constructs, as well as to promote cardiomyocytes alignment and ultrastructural organization^{281,371}. Therefore, to obtain thick human cardiac constructs that resembled the human myocardium we wanted to include electrical stimulation to the parallelized perfusion bioreactor, a combination of signals that had hardly been explored^{288,407,408}.

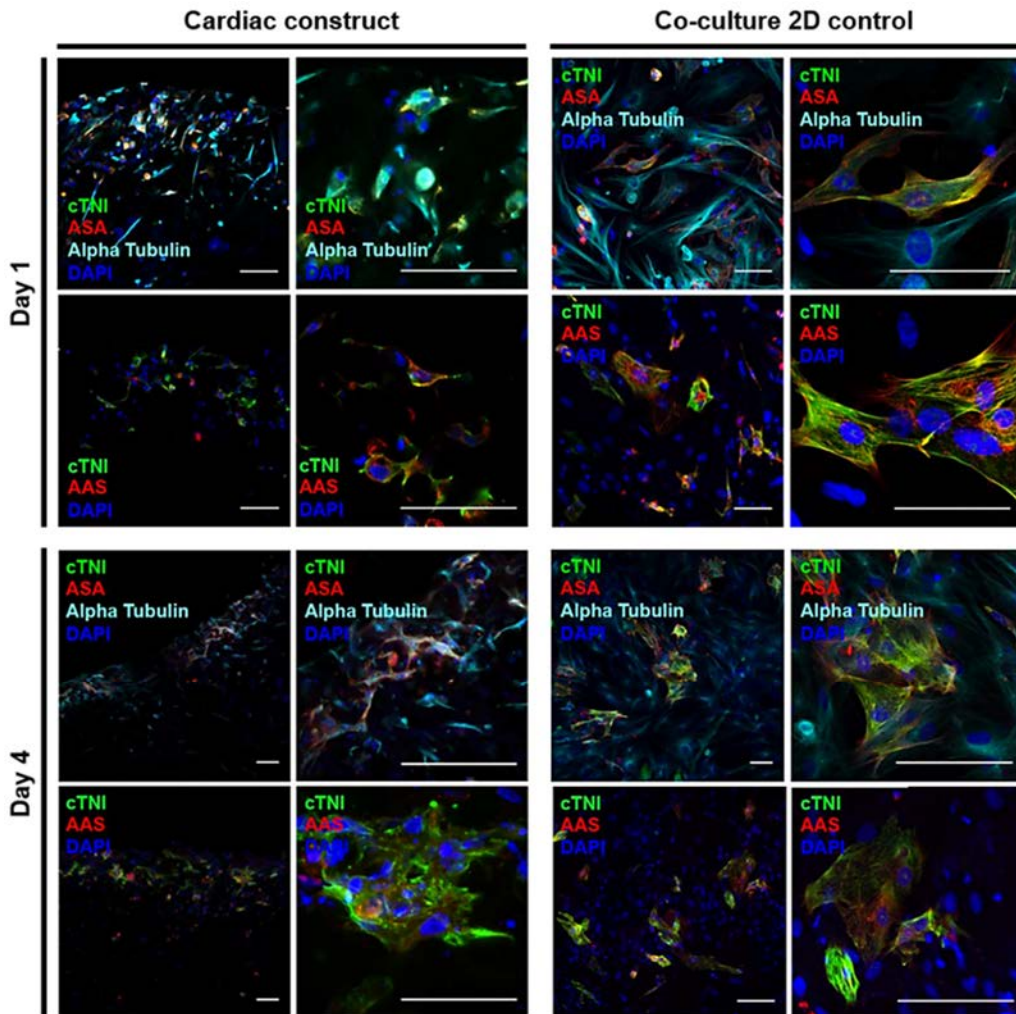


Figure 4.18. Immunostaining analysis of human cardiac constructs cultured in the perfusion bioreactor and their corresponding 2D controls. A co-culture of hiPSC-derived cardiomyocytes and human foreskin fibroblasts (HFF) was seeded in 3D scaffolds to obtain *cardiac constructs*. As a control, the same co-culture (*co-culture 2D control*) was maintained in well plates for equivalent culture times. Scale bars: 75 μm . cTNI: cardiac troponin I; ASA: α -sarcomeric actin; DAPI: 4',6-diamidino-2-phenylindole; AAS: α -sarcomeric actinin. *Figure adapted from Di Guglielmo, C⁴³¹.*

4.4. Design and fabrication of a custom-made perfusion chamber with electrical stimulation

Preliminary cellular tests suggested that perfusion alone was not enough to obtain tissue-like cardiac constructs, so we decided to electrically stimulate cardiomyocytes to improve their functionality, structural organization and coupling within the construct^{318,319}. We designed and fabricated a prototype of the perfusion chamber

including electrical stimulation because chambers combining both stimuli were not available in the market. We aimed at fabricating a chamber with dimensions equivalent to the perfusion chamber without electrodes, and capable to deliver a homogeneous electric field with an appropriate magnitude for cardiac cells stimulation. Taking this into account, three prototypes of the perfusion chamber were developed, and the suitability of each geometry was assessed in terms of electric field delivery, watertightness, material compatibility with sterilization procedures and cell survival.

4.4.1. First prototype: poly(methyl methacrylate) (PMMA) and polydimethylsiloxane (PDMS)

The first approach to fabricate a chamber including perfusion and electrical stimulation was based on structuring poly(methyl methacrylate) (PMMA) plastic and using polydimethylsiloxane (PDMS) as sealant, since our research group had extensive expertise in working with those materials^{468,469}. PMMA thick sheets were structured to have a central hole of 11 mm in diameter (where the cardiac tissue construct would be installed), two transversal channels of 2 mm in diameter (to allow electrodes entry to the center of the chamber), and four holes at PMMA corners (to mechanically bound PMMA sheets using screws and washers) (**Figure 4.19A**). To watertight the chamber, PDMS prepolymer was spun to obtain a thin sheet of silicone, which was placed between two structured PMMA sheets (**Figure 4.19B**). However, watertightness was impeded by transversal channels, as the thin film could not adapt to their shape. Therefore, we fabricated a mold to obtain a PDMS gasket that allowed electrodes entry to the chamber and fitted properly between PMMA sheets. The mold consisted in a Petri dish pierced with a 2 mm wire and containing a structured PMMA sheet at the bottom (**Figure 4.19C**). Then, the Petri dish was filled with PDMS prepolymer and, after curing, it was removed from the mold and cut to obtain a PDMS replica of the structured PMMA with a central channel (**Figure 4.19D**). Finally, PDMS replica were assembled with two structured PMMA sheets and bound with screws and washers to form the perfusion chamber (**Figure 4.19E-F**). The prototype demonstrated to be watertight when connected to a closed-circuit with perfusion of water at 0.1 ml/min during 2 days, thus being suitable for working under flow conditions.

Before using the new perfusion chamber with electrical stimulation, it was important to elucidate if the dimensions of the prototype were appropriate for our purposes. Specifically, we had to determine if the diameter of the electrodes and their position with respect to the cell construct were convenient to deliver a homogeneous electric field to the cultured cells. Besides, we had to establish if the proposed materials (PDMS, PMMA, and graphite electrodes recommended in the literature³⁸⁷) and culture medium electrical properties were appropriate for electrical stimulation of cardiac tissue constructs.

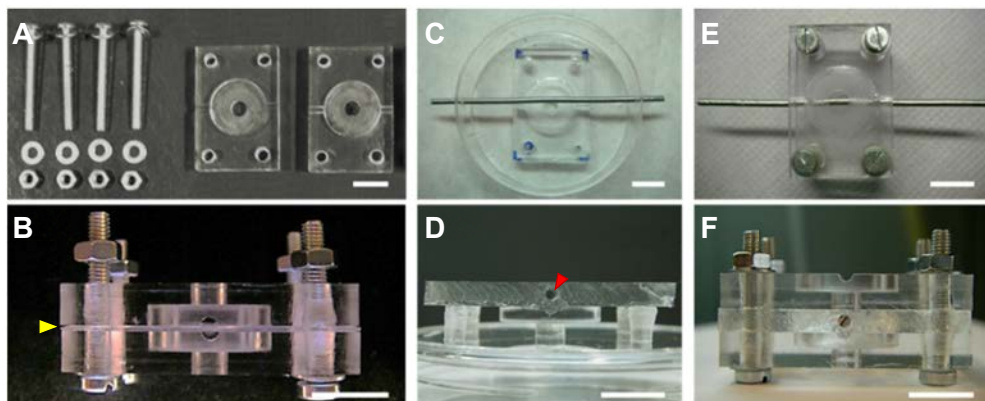


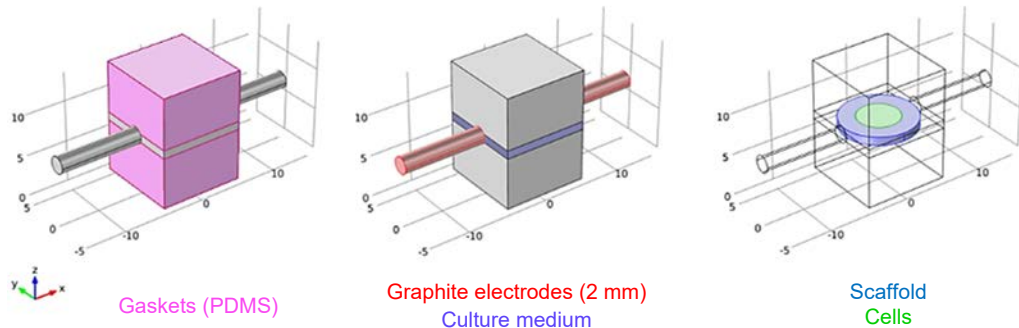
Figure 4.19. Fabrication and assembly of the first prototype of the perfusion chamber with electrical stimulation. **A**, Structured PMMA plastic sheets obtained after milling, together with screws and washers to mechanically bound both sheets. **B**, Side view of two structured PMMA sheets assembled to form the perfusion chamber. A thin layer of PDMS was used as a sealing element (yellow arrowhead). **C**, Mould used to obtain a PDMS replica of the structured PMMA with a 2 mm channel across the entire chamber. **D**, Side view of the PDMS replica of the structured PMMA, obtained from the mould in **C**. PDMS replica was used as a sealing element, and the 2 mm channel acted as an entry point for electrodes (red arrowhead). **E**, Top view of the perfusion chamber with a PDMS sealant that allowed electrodes entry. **F**, Side view of the perfusion chamber with a PDMS sealant that allowed electrodes entry. Scale bars: 1 cm.

To that end, we formulated an electric field model where chamber inner dimensions were reproduced, as well as materials composing each element (**Figure 4.20A**). Notably, to represent chamber interior, a prism was drawn instead of a cylinder to faithfully reproduce the interaction between electrodes and culture medium. Initially, we checked that the electric signal was properly transmitted throughout the chamber by plotting the electric potential in the geometry. Results showed that transmission of the electric signal was achieved when applying a differential voltage of 5 V between the electrodes, with potential drop occurring through the culture medium (**Figure 4.20B**).

Next, we modelled the electric field generated in the chamber to study electric field distribution (**Figure 4.21A**). With this, not only the magnitude of the stimulation sensed by cells was addressed, but also the homogeneity of the signal (**Figure 4.21B-D**). Results showed that cells within cardiac tissue construct would be stimulated with electric fields ranging from 290 to 460 V/m depending on their position within the construct. Specifically, cells located at the centre and top or bottom surfaces of the scaffold would receive a stimulation ranging from 330 to 460 V/m (green and red lines in **Figure 4.21B** transverse plot), whereas cells located at the centre and middle depth of the scaffold would receive a stimulation from 330 to 410 V/m (blue line in **Figure 4.21B** transverse plot). Regarding cells located at the seeding limits, the ones near to stimulation electrodes would receive electric field values ranging from 290 to 410 V/m (red and green lines in **Figure 4.21C** sagittal plot), whereas the ones far from the

stimulation electrodes would receive electric field values around 290 V/m (red and green lines in **Figure 4.21D** coronal plot). Finally, cells located at the centre of the scaffold would receive an electric stimulation ranging from 290 to 330 V/m when perpendicular to the electrodes (blue line in **Figure 4.21C** sagittal plot) or from 330 to 410 V/m when parallel to the electrodes (blue line in **Figure 4.21D** coronal plot). Taken together, those results suggested that the magnitude of the electric field in each location was within the recommended values for cardiac cells stimulation (from 200 to 600 V/m^{319,329,387,408}). However, the model revealed that electric field distribution was not uniform enough for all the cells within the construct, as differences as high as 170 V/m were encountered. Those differences could mean inhomogeneous cell conditioning and could lead to undesired differences in cell performance^{407,470}. Therefore, a redesign of the chamber was needed to create a more homogeneous environment for cell culture.

A Modelled geometry



B Electric potential (V)

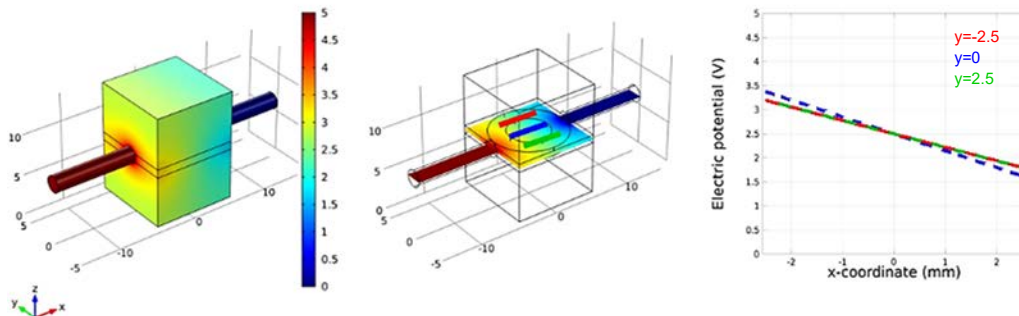


Figure 4.20. Electrode configuration and 3D modelling of the electric potential in the first prototype of the custom-made perfusion chamber. A, System configuration, where silicone gaskets, graphite electrodes of 2 mm in diameter, culture medium and cardiac construct position are represented. **B,** Electric potential through the geometry when applying a differential voltage of 5 V, including a cross-sectional plane of the result at cells location (green circle in A). The plot shows electric potential values along red, blue and green lines in cross-sectional plane, which is the place where cells are seeded in the scaffold.

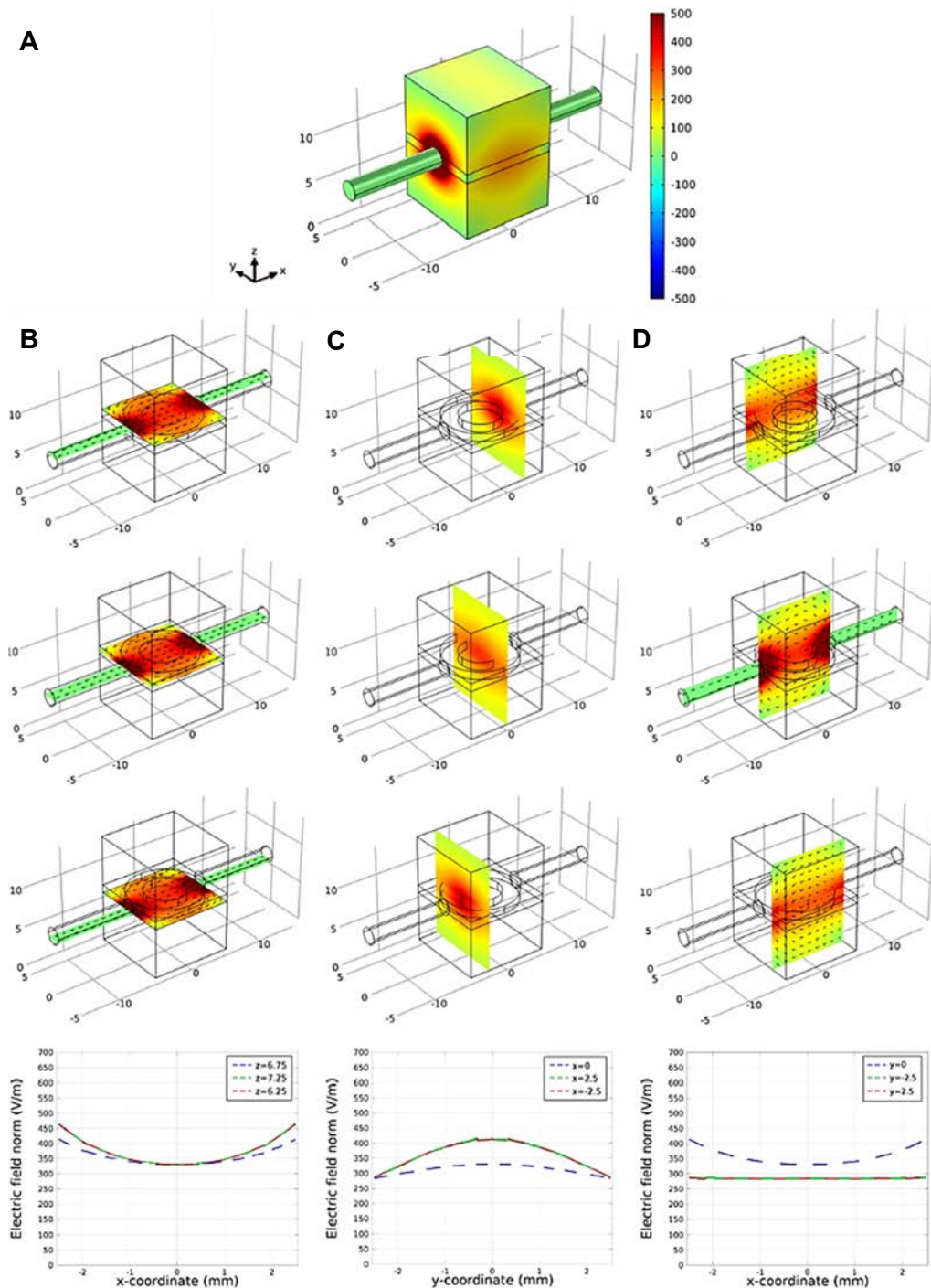
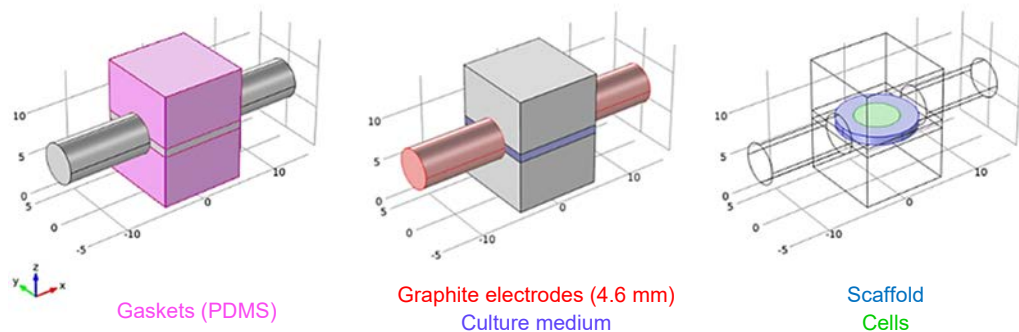


Figure 4.21. Plot of the simulation of the electric field in the first prototype of the custom-made perfusion chamber. **A**, Simulated electric field through the 3D geometry when applying a differential voltage of 5 V between the electrodes. Transverse (**B**), sagittal (**C**) and coronal (**D**) planes of the result are shown, and their position is determined by cell location. Black arrowheads indicate the direction of the electric field. Plots show electric field values only where cells are located (red, blue and green lines corresponding to the three planes of each reference plane).

To improve the homogeneity of the electric field distribution in our setup, we could either increase the distance between the electrodes or increase their effective area⁴⁵. However, we wanted to maintain the inner dimensions of the perfusion chamber with electrical stimulation close to the one without electrodes. Therefore, we decided to increase electrode effective area until the diameter of the electrode was equivalent to the length occupied by cells, which was of 5 mm. This turned our electrical stimulation system into a parallel plate electrode configuration, which is one of the simplest electrode design that generates a uniform electric field^{387,319}. To confirm that uniformity, we solved the 3D model for the same geometry but including graphite electrodes of 4.6 mm in diameter (**Figure 4.22A**). Signal transmission throughout the prototype and the cardiac tissue construct was corroborated, with potential drop occurring in the culture medium and potential values being slightly higher at the same positions than with previous electrodes (**Figure 4.22B**).

A Modelled geometry



B Electric potential (V)

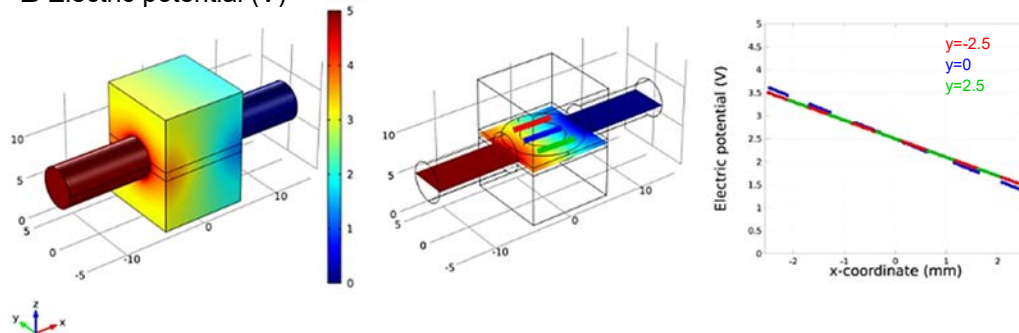


Figure 4.22. Electrode configuration and 3D modelling of the electric potential in the first prototype of the perfusion chamber with wide electrodes. A, System configuration, where silicone gaskets, graphite electrodes of 4.6 mm in diameter, culture medium and cardiac construct position are represented. **B**, Electric potential through the geometry when applying a differential voltage of 5 V, including a cross-sectional plane of the result at cells location (green circle in A). The plot shows electric potential values along red, blue and green lines in cross-sectional plane, which is the place where cells are seeded in the scaffold.

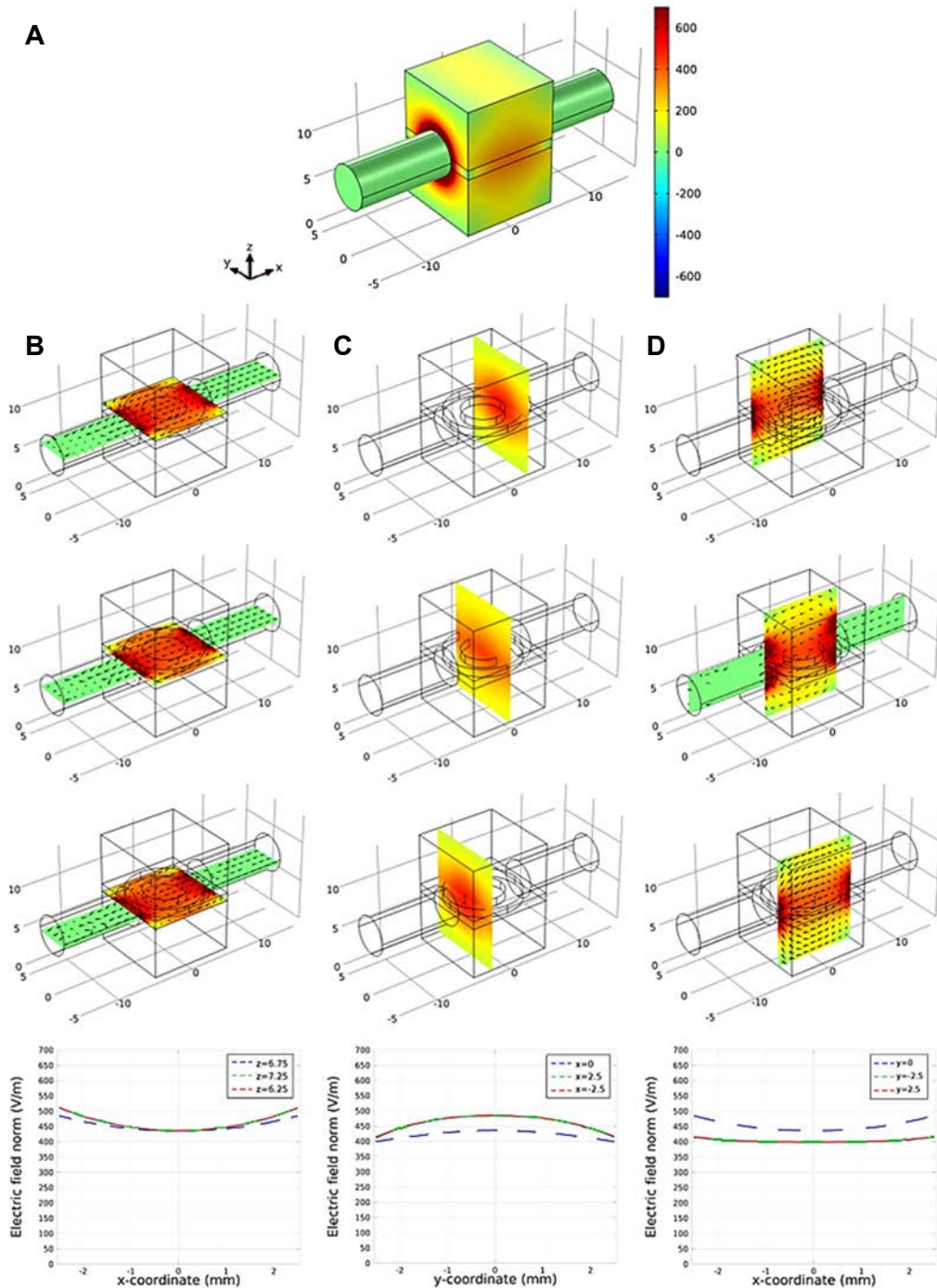


Figure 4.23. Electric field model in the first prototype of perfusion chamber with wide electrodes. A, Predicted electric field through the 3D geometry when applying a differential voltage of 5 V between the electrodes. Transverse (B), sagittal (C) and coronal (D) planes of the result are shown, and their position is determined by cells location. Black arrowheads indicate the direction of the electric field. Plots show electric field values only where cells are located (red, blue and green lines corresponding to the three planes of each reference plane).

Regarding the distribution of the electric field, the simulation predicted stimulation values of the electric field ranging from 400 to 500 V/m depending the position within the scaffold. Specifically, cells located at the centre and top or bottom surfaces of the scaffold would receive a stimulation ranging from 435 to 500 V/m (green and red lines in **Figure 4.23B** transverse plot), whereas cells located at the centre and middle depth of the scaffold would receive a stimulation from 435 to 485 V/m (blue line in **Figure 4.23B** transverse plot). Concerning cells located at the seeding limits, the ones near to stimulation electrodes would receive electric field values ranging from 415 to 485 V/m (red and green lines in **Figure 4.23C** sagittal plot), whereas the ones far from the stimulation electrodes would receive electric field values ranging from 400 to 415 V/m (red and green lines in **Figure 4.23D** coronal plot). Finally, cells located at the centre of the scaffold would receive an electric stimulation ranging from 400 to 435 V/m when perpendicular to the electrodes (blue line in **Figure 4.23C** sagittal plot) or from 435 to 485 V/m when parallel to electrodes (blue line in **Figure 4.23D** coronal plot). On the whole, the magnitude of the stimulation was optimal for cardiomyocytes culture^{387,408}. Moreover, cells would be exposed to a more uniform electric field distribution by using larger electrodes, as the maximum difference predicted was of 100 V/m. This difference was considered negligible because previous works could obtain tissue constructs with improved calcium handling when having that variability in electric field values³¹⁹. Thus, the designed configuration was considered suitable for the stimulation of cardiac tissue constructs.

To assemble the new perfusion chamber with electrodes of 4.6 mm in diameter, the thickness of the PDMS replica had to be increased. For that, a brass cylinder that fit the central hole of the chamber was fabricated (**Figure 4.24A**). The cylinder was 11 mm in diameter, 14 mm in height and it had a transversal hole in the centre of 4.6 mm in diameter, where electrodes were inserted. Then, the cylinder together with the electrodes was assembled with two structured PMMA sheets containing screws and washers, and everything was put in a plastic container. The plastic container was filled with PDMS prepolymer, and after curing it was removed from the mold (**Figure 4.24B**) and cut to obtain a PDMS replica of the structured PMMA with 4.6 mm central channel (**Figure 4.24C**). As the new PDMS replica increased whole chamber height, two additional PDMS gaskets of 11 mm in diameter and 6.5 mm in height had to be fabricated to place the scaffold in the center of stimulation electrodes (**Figure 4.24D**). Finally, all components were assembled to form the perfusion chamber with electrical stimulation (**Figure 4.24E-F**), and the prototype was connected to a closed-circuit filled with culture medium to test its watertightness and feasibility as a cell culture system (**Figure 4.24G**).

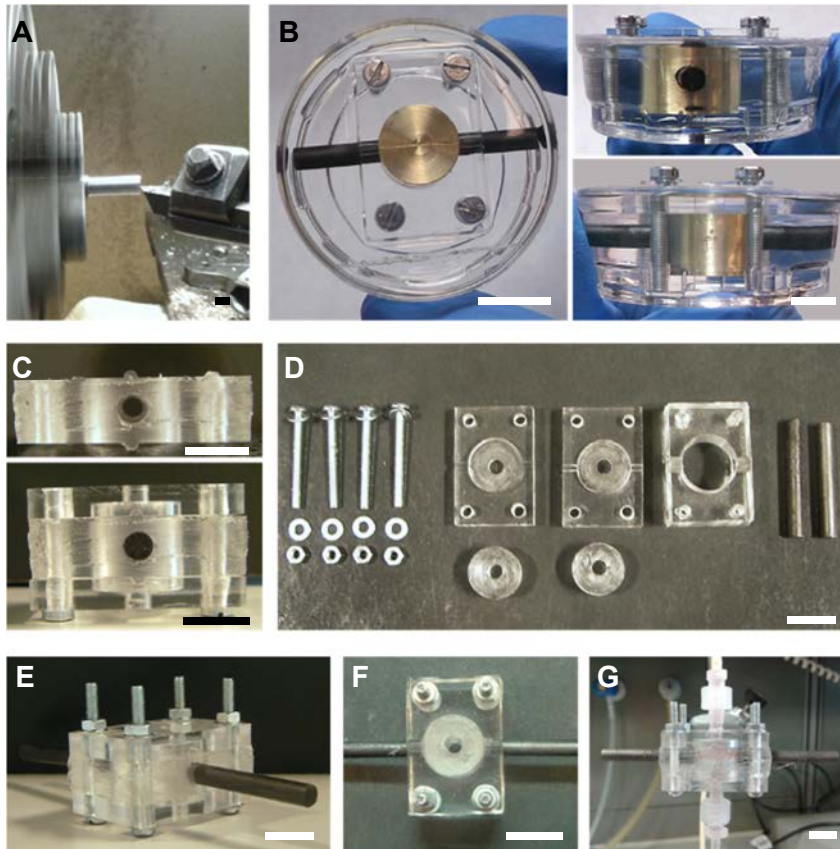


Figure 4.24. Fabrication and assembly of the perfusion chamber with electrical stimulation with electrodes of 4.6 mm in diameter. **A**, Turned brass using a lathe to obtain a cylinder that fitted inside the perfusion chamber. It included a central hole through which graphite electrodes could be inserted. **B**, Top and side views of the mould used to obtain a PDMS replica of the structured PMMA with a 4.6 mm channel across the entire chamber. **C**, Side view of the PDMS replica obtained from the mould in **B**, which acted as a sealing element. The 4.6 mm channel was the entry point for electrodes. **D**, Structured PMMA sheets, PDMS replica and PDMS gaskets together with screws and washers to form the entire chamber (3D view in **E**, top view in **F**). **G**, Side view of the perfusion chamber connected to a closed-circuit and filled with culture medium. Scale bars: 1 cm.

Initially, we measured electric potential values in the perfusion chamber to verify that the expected stimulation was properly delivered. To gather information about the center of the chamber, two gold electrodes were inserted through PDMS replica, perpendicular to graphite electrodes (**Figure 4.25A**). Then, rectangular pulses at 3 Hz of frequency, 2 ms of duration and 5 V of amplitude were applied between the graphite electrodes. Electric potentials between stimulation electrodes and between one stimulation electrode and the center of the chamber (gold electrodes) were measured. The intended waveform was faithfully applied and 2.2 V (**Figure 4.25B**) were measured in the center of the chamber, meaning an electric field of 400 V/m and thus coinciding with the predicted values by the model.

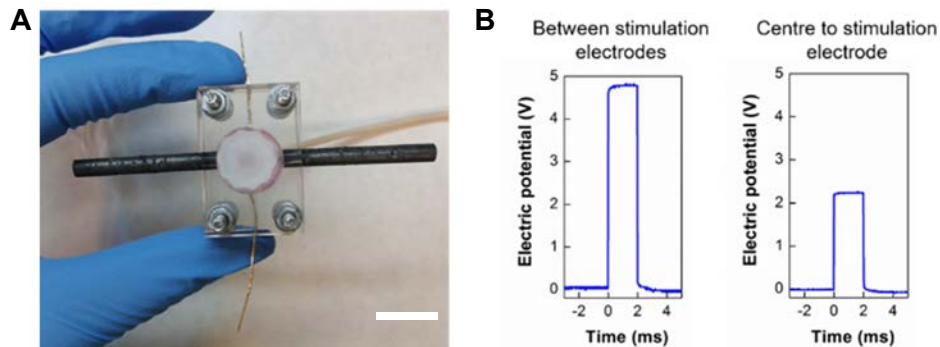


Figure 4.25. Electric potential measurements in the first prototype of the perfusion chamber with electrical stimulation. **A**, System configuration, where two gold electrodes of 0.5 mm in diameter were inserted through PDMS replica, perpendicular to stimulation electrodes (graphite electrodes). **B**, Voltage measurements in the first prototype of the perfusion chamber with electrical stimulation. Measured values coincide with the ones predicted by the model. Scale bar: 1cm.

After confirming prototype's ability to deliver the desired electric field, we tested its feasibility as a cell culture system. For that, we seeded $3.5 \cdot 10^6$ human foreskin fibroblasts (HFF) inside Matrigel™ scaffold, and cultured the tissue construct inside the chamber for 7 days in perfusion (see “3.3.2. Perfusion seeding” and “3.4.1. Single chamber perfusion bioreactor” sections for further details). Unfortunately, cells were not able to grow and colonize the scaffold because internal PDMS gaskets were not clamping the scaffold properly, so tissue construct was found detached and folded in a corner of the chamber. Moreover, leakage through graphite electrodes was found, mainly because of their high porosity and the pressure exerted by culture medium perfusion. In addition, clamping of croc clips from the function generator to graphite electrodes was inadequate because of large diameter of the electrodes. Regarding materials suitability, screws and washers oxidized due to incubator humidity, and PMMA sheets scratched due to ethanol sterilization and screws mechanical strain. Finally, the connection of the chamber to the fluidic circuit consisted in a luer connector glued with cyanoacrylate at the exit of the chamber, and it was not robust enough. This connection was very fragile, leaked after 4 days of culture and was very difficult to waterproof again. All those observations demonstrated that the first prototype of the perfusion chamber with electrical stimulation was not solid and well-developed enough to maintain a cell culture. However, both the geometry and electric field values were suitable for our purposes, so we went on fabricating the chamber in a most robust way by developing a second prototype.

4.4.2. Second prototype: 3D printing of acrylonitrile butadiene styrene (ABS)

The second prototype of the perfusion chamber with electrical stimulation was designed to overcome the problems of the first prototype in terms of cell culture capabilities. For this, the first issue to be addressed was watertightness of graphite electrodes and improvement of their clamping surface by croc clips. Waterproofing of carbon rod electrodes was performed using a heat-shrink tubing, and clamping surface improvement by drilling two holes in each electrode and threading a solid tinned annealed copper wire. Finally, the connection was insulated using an epoxy resin that contacted with heat-shrink tubing, thus obtaining watertight electrodes (**Figure 4.26A**). The second issue to be addressed was the robustness of the chamber in terms of leakage, assembly and cardiac construct clamping during the time needed for the experiments. For this, we designed a prototype with a cap and a base that would form the chamber when threaded together, thus simplifying the four screws and washers of the first prototype to only one thread (**Figure 4.26C**). Moreover, three holes would be accurately bored in the chamber and luer connectors adjusted for a reliable connection, which would be reinforced by cyanoacrylate gluing (**Figure 4.26C**). Finally, an effective clamping of the cardiac construct was designed, which consisted in placing the tissue construct between two gaskets that exerted pressure on it when closing the chamber (**Figure 4.26B**). To fabricate a prototype that met all those requirements in a trustworthy manner, 3D printing of each part was considered the most suitable process. The material chosen was acrylonitrile butadiene styrene (ABS), as it is a plastic material convenient for 3D printing processes, biocompatible and sterilisable by UV light (**Figure 4.26D**). Finally, the fabricated chamber was sterilised, assembled in sterile conditions and connected to a closed circuit filled with culture medium to test it as a cell culture system (**Figure 4.26E**). To faithfully reproduce culture conditions, one disk of hydrated Matrigel™ scaffold was placed inside the chamber, perfusion of culture medium at 0.1 ml/min was applied and the whole system was placed inside an incubator at 37°C and 5% CO₂. Unfortunately, leakage of culture medium through the wall of the chamber appeared after 1 day of culture, meaning that the layer-by-layer 3D printing process had not enough resolution or solidity to withstand culture medium pressure. Moreover, bacterial contamination was clearly identified at day 4 of culture, meaning that the sterilization method was not effective in our 3D chamber.

To overcome leakage and bacterial contamination problems, two strategies were adopted: first, each part of the chamber was infiltrated with cyanoacrylate to block the pores generated during fabrication. Second, ethylene oxide (EtO) was used as sterilization process because it is extensively used to sterilize medical and pharmaceutical products, and also because ABS plastic does not withstand ethanol or autoclave treatments. After both procedures, the chamber was assembled in sterile

conditions, connected to a closed-loop with perfusion of culture medium at 0.1 ml/min and put inside an incubator. Successful results were obtained after 7 days of culture with electrical stimulation, because neither leakage nor contamination was found in the system, suggesting that the chamber was suitable for cell culture combining perfusion and electrical stimulation.

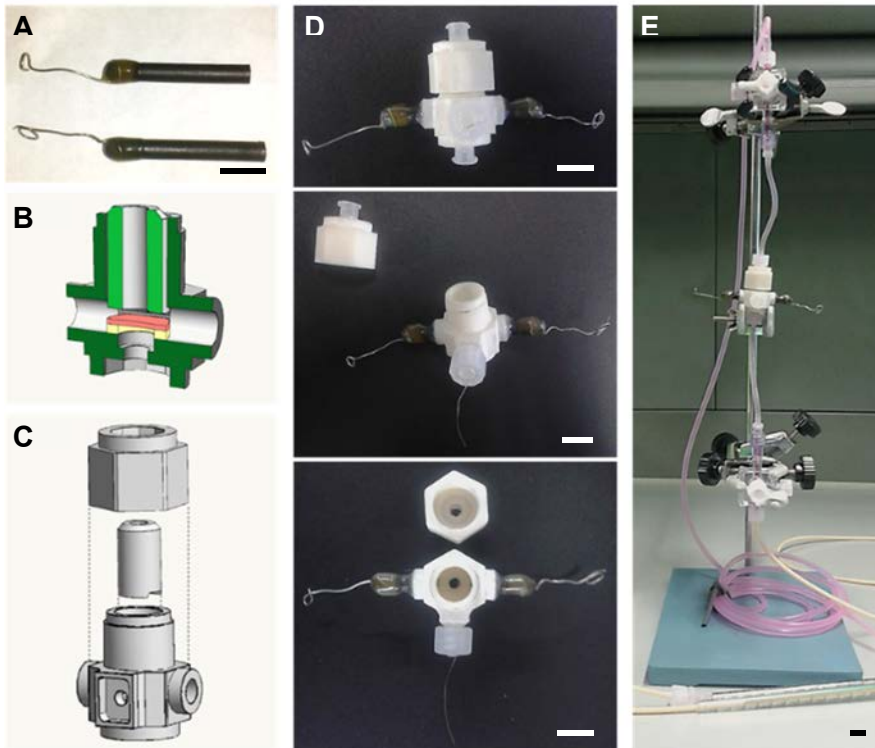


Figure 4.26. Fabrication and assembly of the second prototype of the perfusion chamber with electrical stimulation. **A**, Watertight carbon rod electrodes with solid tinned annealed copper wire threaded through them. **B**, Illustration of the second prototype cross-section, where an acrylonitrile butadiene styrene (ABS) gasket (blue), the tissue construct (pink) and a silicone gasket (yellow) are shown. **C**, Illustration of perfusion chamber with electrical stimulation assembly. Carbon rod electrodes were inserted through lateral holes, while gold electrode was inserted through the frontal hole. **D**, Frontal, perspective and top images of the second prototype of the perfusion chamber with electrical stimulation. **E**, Connection of the chamber to a closed-circuit filled with culture medium. Scale bar: 1 cm.

Before generating any tissue construct, we measured electric potential values in the perfusion chamber to verify that the expected stimulation was properly delivered. As the internal geometry was preserved between the first and the second prototype, similar potential values should be present inside the chamber. Therefore, rectangular pulses at 3 Hz of frequency, 2 ms of duration and increasing amplitudes from 1 V to 10 V were applied between graphite electrodes. Electric potentials between stimulation electrodes (**Figure 4.27A**) and between one stimulation electrode and the center of the chamber

(gold electrode) (**Figure 4.27B**) were measured. Results showed that the waveform was faithfully applied in all voltages studied, both between stimulation electrodes and center to stimulation electrode. Moreover, when applying a differential voltage of 5 V between graphite electrodes, in the center of the chamber there was a potential of 2.1 V, which meant an electric field of 420 V/m. That measured value was in agreement with the one predicted by the model (**Figure 4.23C**), thus indicating that the fabricated chamber was appropriate to electrically stimulate cardiac tissue constructs with the simulated electric field values.

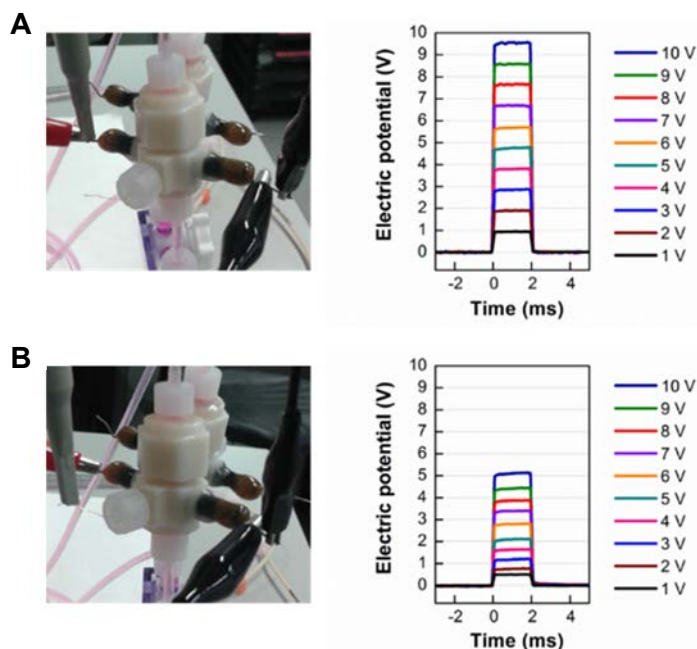


Figure 4.27. Electric potential measurements in the second prototype of the perfusion chamber with electrical stimulation. A, Voltage measurements between stimulation electrodes using an oscilloscope. Plot shows potential values when applying increasing differential voltages from 1 V to 10 V. **B,** Voltage measurements between one stimulation electrode and the centre of the chamber (gold electrode) using an oscilloscope. Plot shows potential values when applying increasing differential voltages from 1 V to 10 V.

Once we corroborated that electrical stimulus was properly delivered through the chamber and problems related to leakage and sterility were solved, we tested its feasibility as a cell culture system. For that, $3.5 \cdot 10^6$ neonatal rat heart cells were seeded inside Matrigel™ scaffold (see “3.3.2. *Perfusion seeding*” section for further details). Two constructs were produced, with seeding efficiencies of 71.7% and 72.9% respectively. The first tissue construct was cultured inside the chamber with perfusion of culture medium but without applying any electrical impulse (control), whereas the other construct was cultured with perfusion of culture medium and electrical stimulation. Regrettably, no cells were found inside the scaffolds after 7 days of culture, probably

because there were ethylene oxide remains inside the chamber that prevent cell survival and growth. Even so, we repeated the experiment without sterilizing the chamber again, as in principle it remained sterile and EtO gas could have been completely removed after the first trial. Unfortunately, bacterial contamination reappeared at day 4 of culture, meaning that it was necessary to sterilize the prototype after each experiment. On the whole, those results suggested that it was necessary to fabricate a chamber using a material resistant to ethanol and autoclave sterilization. In addition, chamber components (e.g. stimulation electrodes, gaskets, etc.) should be renewable to avoid cell culture contamination, so we went on fabricating the third prototype of the perfusion chamber with electrical stimulation.

4.4.3. Third prototype: precision machining of polypropylene (PP)

Cell culture experiments performed with the second prototype of the chamber highlighted the importance of using an autoclavable and ethanol-resistant material for chamber fabrication. Therefore, the third prototype of the perfusion chamber with electrical stimulation was made of polypropylene (PP) plastic, as it has very good resistance to alcohol, its melting temperature is around 170°C and it is biocompatible. Similarly to the second prototype, the PP chamber was composed of a cap and a base that formed the chamber when threaded together (**Figure 4.28A**), but it was fabricated by precision machining instead of by 3D printing. This technique allowed us to avoid layer-by-layer fabrication and posterior infiltration, thus obtaining solid parts without leakage problems. Regarding chamber connection to the bioreactor circuit, three holes were also bored in the chamber, and luer connectors adjusted and glued using cyanoacrylate. Likewise the second prototype, cardiac tissue construct clamping was performed by placing the tissue construct between two gaskets that exerted pressure on it when closing the chamber. The upper gasket was fabricated by precision machining of PP, while the silicone gasket was fabricated by polydimethylsiloxane (PDMS) molding (**Figure 3.9**). However, we improved the design of the prototype by adding two PP adapters screwed to chamber base that allowed the renewal of carbon rod electrodes after each experiment (**Figure 4.28A**).

Once fabricated, the PP chamber was autoclaved, assembled in sterile conditions and connected to a bioreactor filled with culture medium to test its suitability as cell culture system (**Figure 4.28B**). The chamber did not show any leakage or contamination problems after 7 days of culture with perfusion, thus suggesting that the chamber was suitable for cardiac constructs culture. To verify that cells could survive, grow and were capable to generate tissue constructs inside the prototype, $3.5 \cdot 10^6$ human foreskin fibroblasts (HFF) were seeded inside one Matrigel™ scaffold with a seeding efficiency of 69.5% (see “3.3.2. *Perfusion seeding*” section for further details). Then, the tissue construct was cultured in the prototype with perfusion of culture

medium and electrical stimulation during 7 days. Results confirmed that the chamber was suitable for tissue construct production, as HFF attached and grew inside the 3D scaffold so much that it was evident with the naked eye (**Figure 4.28C**). Finally, the construct was fixed, sectioned and cell nuclei were stained as described in “3.8.2.2. *Cardiac tissue constructs (in toto)*” section, which corroborated the presence of HFF throughout the scaffold (**Figure 4.28D-E**).

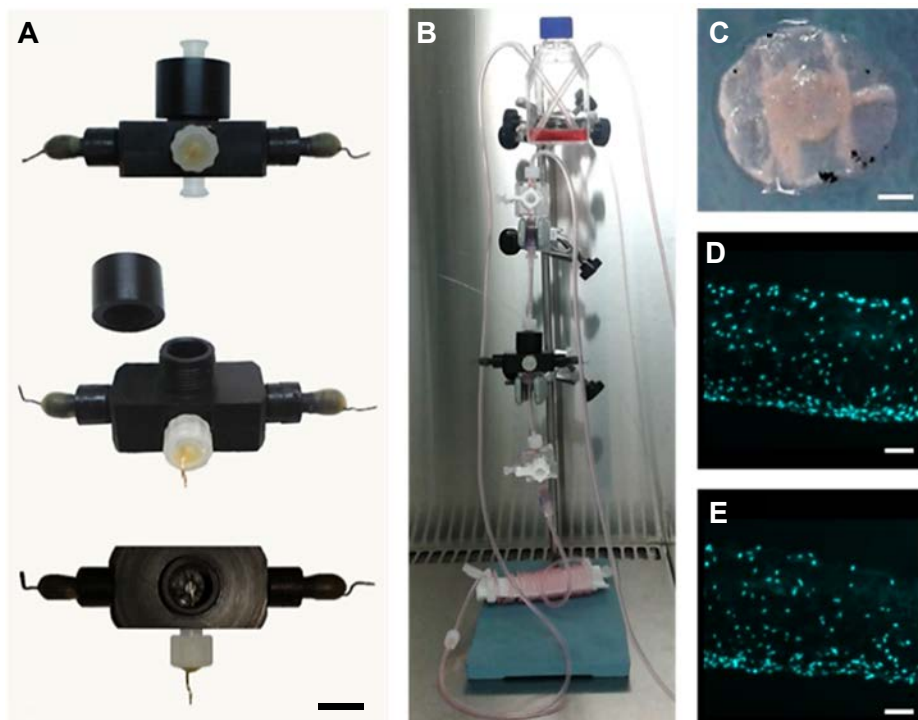


Figure 4.28. Fabrication, assembly and cell culture in the third prototype of the perfusion chamber with electrical stimulation. **A**, Frontal, perspective and top images of the prototype. Inside the chamber, the tissue construct is placed between two gaskets. Scale bar: 1 cm. **B**, Connection of the chamber to the bioreactor filled with culture medium. **C**, Tissue construct generated after culturing human foreskin fibroblasts (HFF) for 7 days under perfusion and electrical stimulation. High cell density zones grew in scaffold, coinciding with the internal geometry of the chamber. Scale bar: 2 mm. **D-E**, Cross-sections and DAPI (4',6-diamidino-2-phenylindole) nuclei staining of two different zones of the tissue construct obtained in C. Scale bars: 100 μ m.

We measured electric potential values in the perfusion chamber to verify that the expected stimulation was properly delivered. To that end, trains of rectangular pulses at 3 Hz of frequency, 2 ms of duration and 5 V of amplitude were applied between graphite electrodes, and electric potentials were measured at different positions. Results showed that the waveform was faithfully applied at the desired frequency, both between stimulation electrodes and center to one stimulation electrode (**Figure 4.29A**). To have an estimation about the current flowing through the chamber during electrical

stimulation, we built a circuit by placing either a 50 Ω or 200 Ω resistor in series with the bioreactor (**Figure 4.29B**). Then, the amount of current in the chamber was calculated by measuring the potential drop across the resistor and applying Ohm's law³¹⁸:

$$I = \frac{V}{R} \quad \text{Eq. 4.8}$$

Where I is the current, V is the measured voltage and R is the resistance exerted by the resistor. In our electrical stimulation setup, the calculated current value was of 2.45±0.07 mA.

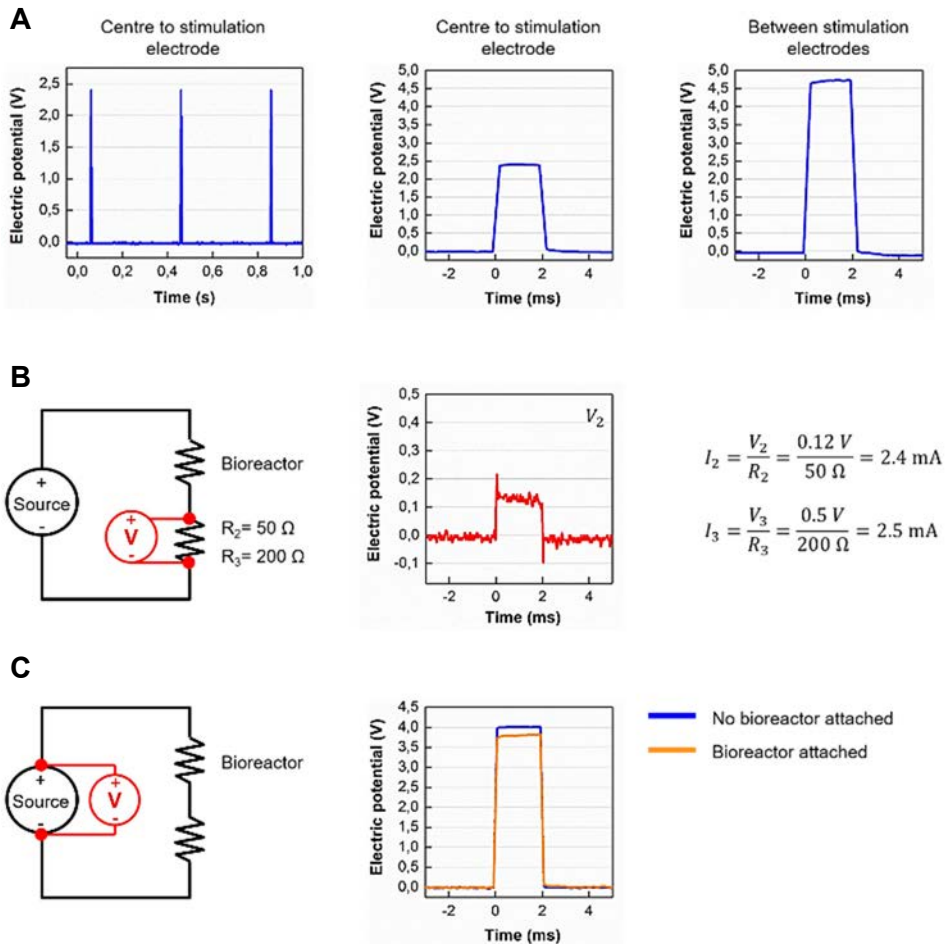
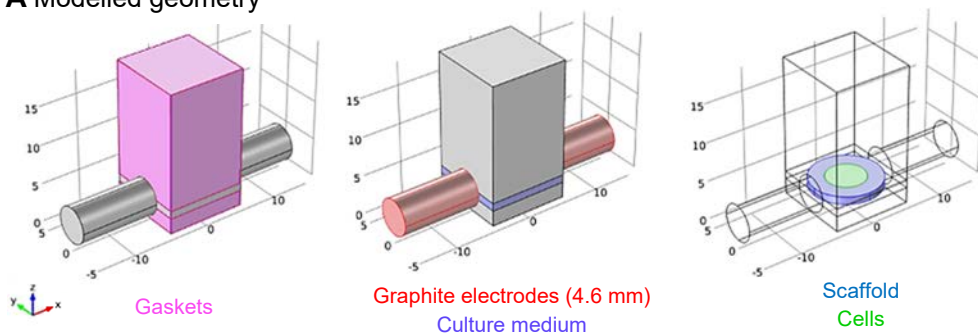


Figure 4.29. Characterization of the electrical stimulation system. **A**, Voltage measurements in the third prototype of the perfusion chamber with electrical stimulation. Plots show potential values when applying rectangular pulses at 3 Hz of frequency, 2 ms of duration and 5 V of amplitude between graphite electrodes. **B**, Equivalent circuit setup to verify electrical stimulation. Estimated current values in the bioreactor were elucidated by measuring the voltage across a resistor (R_1 and R_2) connected in series with the bioreactor, and back-calculating the current using Ohm's law. **C**, Equivalent circuit setup to verify that the current limit of the function generator is not surpassed by attaching the bioreactor. Voltage measurements of the source before and after the bioreactor was attached were performed.

To further characterize our electrical stimulation system, we checked that the current limit of the function generator was not surpassed when attaching the bioreactor. For that, voltages generated by the source before and after bioreactor installation were measured (**Figure 4.29C**). Results confirmed that the current limit was not surpassed, as waveforms were faithfully applied and differences between them were not significant.

Finally, electrical impedance of the system was measured using a multimeter. Electrical impedance is the total opposition that a circuit presents to electric current when a voltage is applied, and was important to elucidate it because could influence any posterior electric signal recording. An electrical impedance of 3 M Ω was found when measuring from the center of the chamber (gold electrode) to one graphite electrode, whereas the impedance was of 0.3 M Ω when measuring between graphite electrodes. The impedance between graphite electrodes was lower because electric current paths could be established within the culture medium, whereas the gold electrode was surrounded by the scaffold and the current was forced to go through it.

A Modelled geometry



B Electric potential (V)

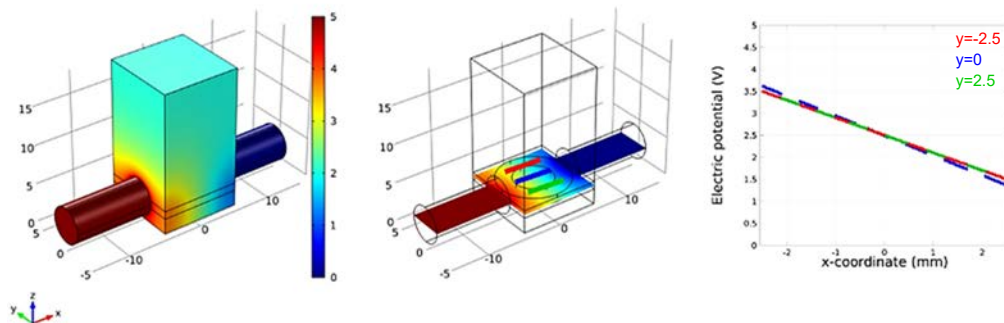


Figure 4.30. Electrode configuration and 3D modelling of the electric potential in the third prototype of the perfusion chamber with wide electrodes. **A**, System configuration, where gaskets, graphite electrodes of 4.6 mm in diameter, culture medium and cardiac construct positions are represented. **B**, Electric potential through the geometry when applying a differential voltage of 5 V, including a cross-sectional plane of the result at cells location (green circle in A). The plot shows electric potential values along red, blue and green lines in cross-sectional plane, which is the place where cells are seeded in the scaffold.

To verify that measured electric potential and current values were in accordance with a 3D model of the prototype, we formulated electric potential, electric field and current density models taking into account chamber interior dimensions and materials composing each element (**Figure 4.30A**). Signal transmission throughout the prototype and the cardiac construct was corroborated, with potential drop occurring in the culture medium and values being similar to previous prototypes (**Figure 4.30B**). Regarding electric field and current density distribution, cells composing the cardiac construct were stimulated with electric fields ranging from 400 to 485 V/m and current densities ranging from 575 to 700 A/m² depending on their position (**Figure 4.31A** and **4.32A**). Specifically, cells would receive a stimulation ranging from 435 to 485 V/m and 625 to 700 A/m² independently of their position in scaffold depth (blue, green and red lines in **Figure 4.31B** and **4.32B** transverse plots). Concerning cells located at the seeding limits, the ones near to stimulation electrodes would receive electric field values ranging from 415 to 485 V/m and current densities from 600 to 700 A/m² (red and green lines in **Figure 4.31C** and **4.32C** sagittal plots). Conversely, cells far from the stimulation electrodes would receive electric field values ranging from 400 to 415 V/m and current densities ranging from 575 to 700 A/m² (red and green lines in **Figure 4.31D** and **4.32D** coronal plots). Finally, cells located at the centre of the scaffold would receive an electrical stimulation ranging from 400 to 435 V/m and current densities ranging from 575 to 630 A/m² when perpendicular to the electrodes (blue line in **Figure 4.31C** and **4.32C** sagittal plots). When parallel to the electrodes, cells at the centre of the scaffold would receive an electrical stimulation from 435 to 485 V/m and current densities from 630 to 700 A/m² (blue line in **Figure 4.31D** and **4.32D** coronal plots).

On the whole, results confirmed that the model could predict the electrical stimulation delivered to the construct, as oscilloscope measurements in the centre of the chamber also indicated electric field values around 460 V/m (**Figure 4.29A**). Similarly, the measured current values flowing through the bioreactor (2.45 mA, **Figure 4.29B**) were properly predicted by the 3D model. We calculated the current density from that measurements by using the approximation that assumes the current simply proportional to the electric field:

$$J = \sigma E \quad \text{Eq. 4.9}$$

Where J (A/m²) is the current density, σ (S/m) is the conductivity of the medium (1.44 ± 0.03 S/m for DMEM culture medium) and E (V/m) the electric field. Current densities around 660 A/m² were calculated from current values measured in the prototype, coinciding with predicted values and corroborating the ability of the model to predict the stimulation delivered to cardiac tissue constructs.

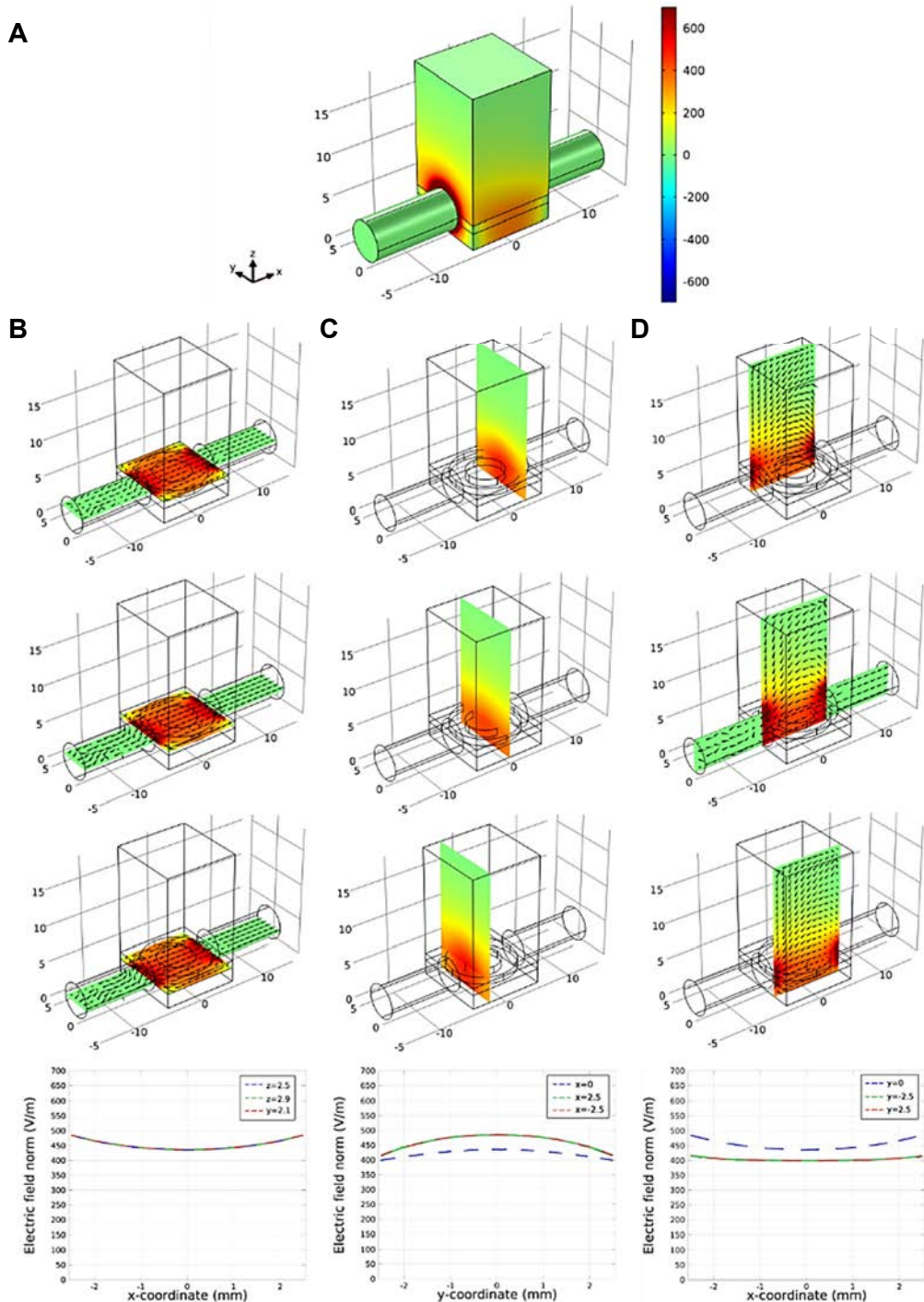


Figure 4.31. Electric field model in the third prototype of the chamber with electrical stimulation. A, Predicted electric field through the 3D geometry when applying a differential voltage of 5 V between the electrodes. Transverse (B), sagittal (C) and coronal (D) planes of the result are shown, and their position is determined by cells location. Black arrowheads indicate the direction of the electric field. Plots show electric field values only where cells are located (red, blue and green lines corresponding to the three planes of each reference plane).

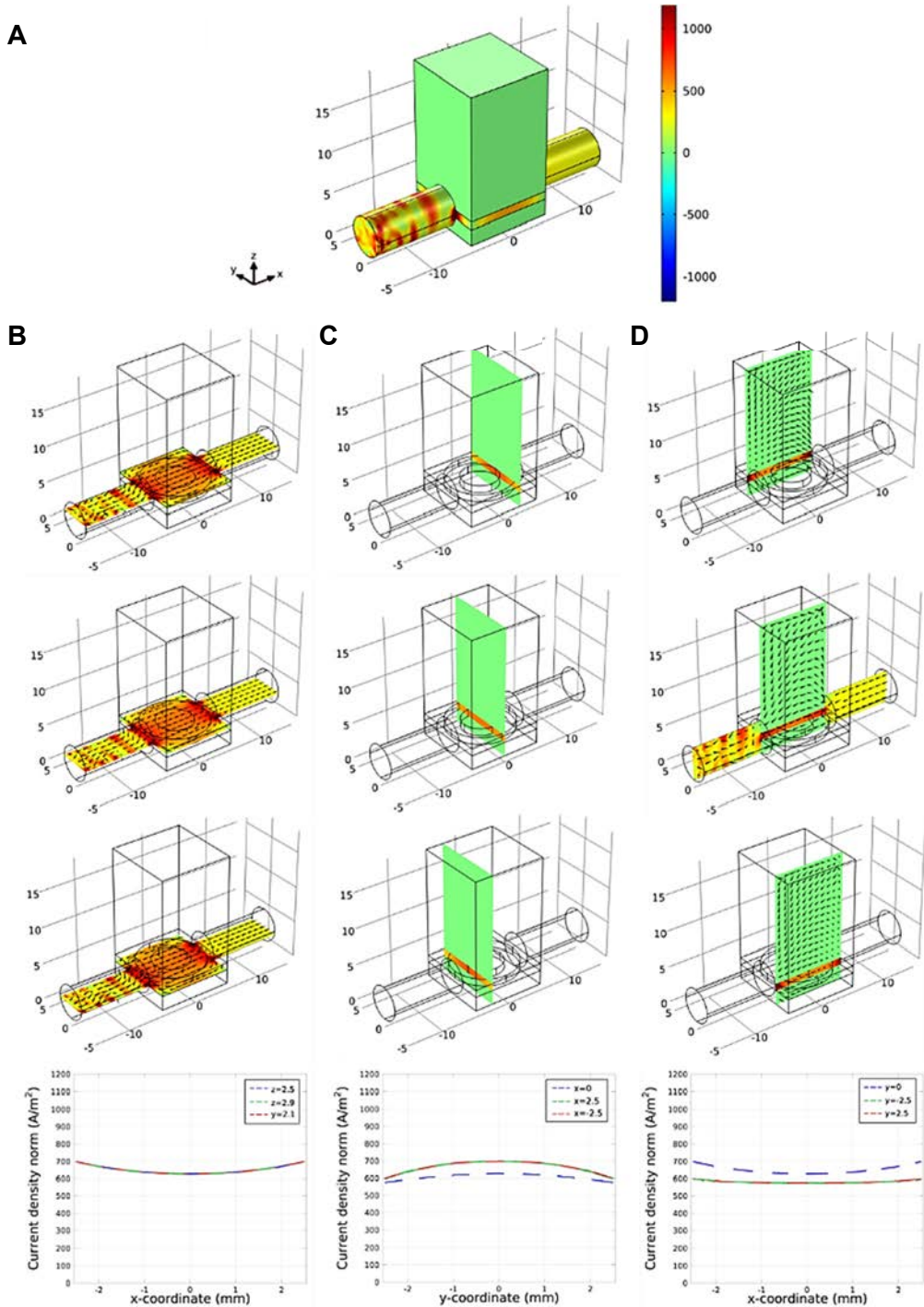


Figure 4.32. Current density model in the third prototype of the chamber with electrical stimulation. A, Predicted current density through the 3D geometry when applying a differential voltage of 5 V between the electrodes. Transverse (**B**), sagittal (**C**) and coronal (**D**) planes of the result are shown, and their position is determined by cells location. Black arrowheads indicate current direction. Plots show current density values only where cells are located (red, blue and green lines corresponding to the three planes of each reference plane).

Taken together, results indicated that the third prototype of the perfusion chamber including electrical stimulation could generate an electric field with a magnitude and uniformity suitable for cardiomyocytes culture. Moreover, the prototype did not show leakage or contamination problems, and human foreskin fibroblasts attached and grew inside the 3D scaffold when cultured under perfusion and electrical stimulation during 7 days. Therefore, the prototype was validated as a cell culture platform, and the next step was culturing cardiomyocytes in our advanced 3D culture system to attempt the generation of cardiac tissue constructs.

4.5. Generation of rat cardiac tissue constructs through perfusion and electrical stimulation

Previous results aimed at establishing which materials, devices and cell culture parameters were appropriate to develop tissue-like cardiac tissue constructs. To summarize, Matrigel™ collagen-elastin scaffold was selected because of its convenient composition, porosity and stiffness. Regarding cell seeding methodology, one-way perfusion of the cell suspension through the scaffold at 1 ml/min was identified as the most efficient and effective process. As a cell culture system, the design and fabrication of a parallelized perfusion bioreactor ensured the production of multiple tissue constructs under comparable conditions. Finally, a perfusion chamber including electrical stimulation was fabricated and validated as a cell culture system. **Figure 4.33** provides the reader with a summary of the strategy to attempt the generation of rat cardiac tissue constructs, which was used for all the experiments in the following sections.

First trials to produce cardiac tissue constructs with our advanced 3D culture system were performed with neonatal rat heart cells because they are easier to handle than human induced pluripotent stem cells (hiPSC), and they have been extensively used in the literature. Therefore, they would be useful to validate our system, establish a methodology to analyse the maturation level of the cardiac constructs obtained and set the bases for human cardiac tissue constructs development.

To generate cardiac tissue constructs from rat heart cells, primary cultures obtained from ventricles of 2-3-day-old neonatal rats were seeded inside Matrigel™ scaffold. Then, tissue constructs were installed inside the bioreactor and cultured under perfusion for 3 days. At day 4 of culture, electrical stimulation regimen was started in stimulated constructs, while control ones were cultured only under perfusion. Trains of rectangular pulses at 5 V of amplitude, 3 Hz of frequency and 2 ms of duration were continuously applied, in agreement with the literature^{281,387}. Control and electrically stimulated constructs were cultured during 7 days. At several timepoints, their functional

activity and structural organization was assessed to study the influence of the electrical stimulation on their development (for further details, see “3.4.2. *Parallelized perfusion bioreactor*” section).

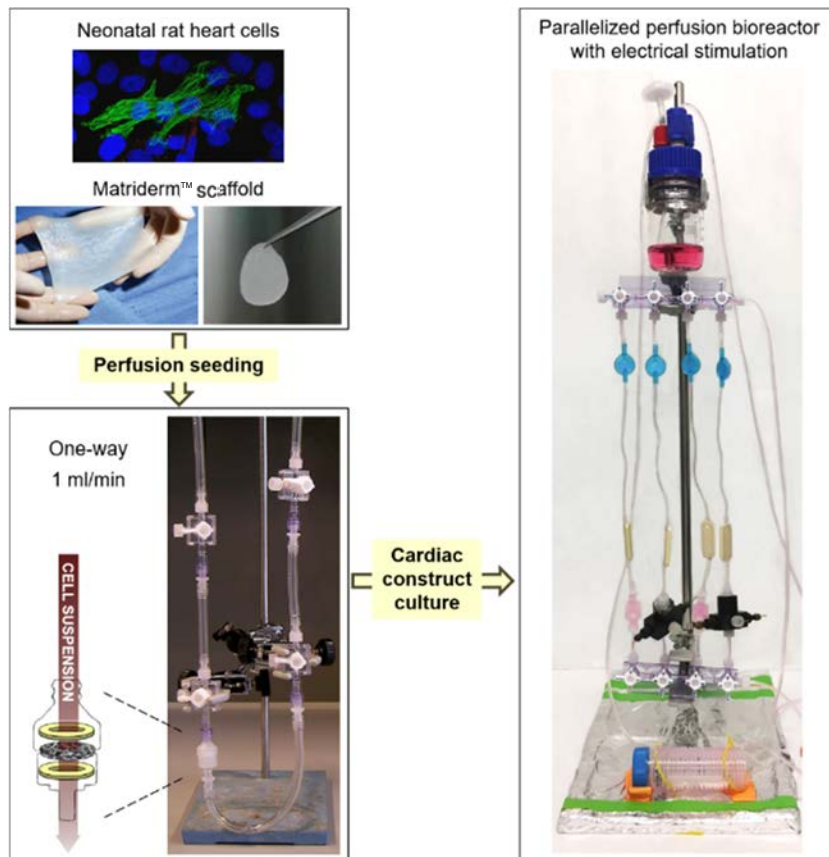


Figure 4.33. Scheme of the strategy employed to attempt the generation of rat cardiac tissue constructs. Neonatal rat heart cells were seeded inside the scaffold by perfusing the cell suspension through it. Then, constructs were installed in the perfusion bioreactor and cultured either with or without electrical stimulation.

4.5.1. Electrical stimulation improves the contractility of cardiac tissue constructs

After being cultured inside the bioreactor, the functional activity of the cardiac tissue constructs was analysed. Because previous results demonstrated that cardiac constructs were capable to contract at the macroscale (**Figure 4.12**), we fabricated a video recording setup to collect data about their contractile behaviour. The setup was formerly published as a bioreactor for the culture of cardiac constructs³¹⁸, and consisted in a Petri dish with two graphite electrodes glued at its bottom (**Figure 3.11** and **Figure 4.34A**). The constructs were placed in between the electrodes, and their response

to electrical stimuli was addressed. We first characterized the system to verify that the expected stimulation was properly delivered. For that, we filled the Petri dish with Tyrode's salt solution and measured the electric potential at the center of the dish (where the construct would be placed) and on the ground and source electrodes (**Figure 4.34B-D**). Results showed that the intended waveform was faithfully applied through the whole setup, and 2 V in the center of the Petri dish were measured when applying a differential potential of 5 V between the electrodes.

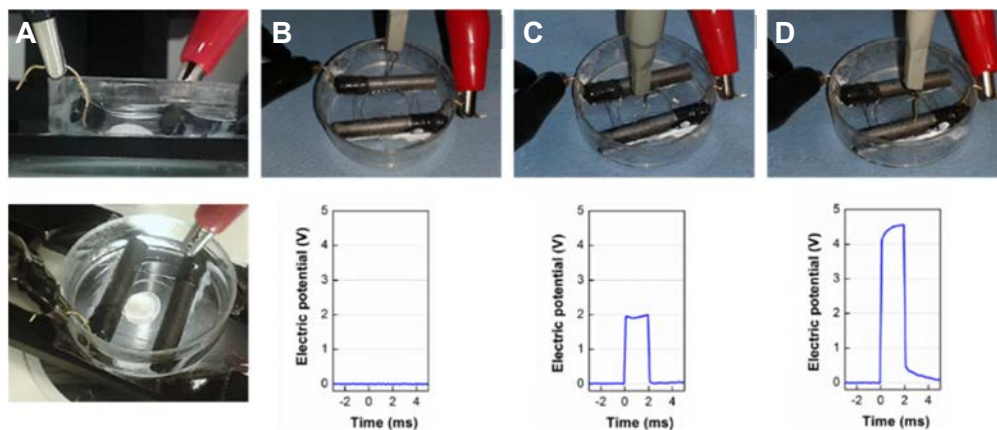


Figure 4.34. Video recording setup to study contractile behaviour of cardiac tissue constructs. **A**, Image showing the Petri dish with two graphite electrodes glued at the bottom, in between of which the cardiac construct is placed. For functional assessment, the system is filled with Tyrode's salt solution and different electrical stimuli are applied. Electric potentials are measured on the ground (**B**) and source (**D**) electrodes, as well as in the centre of the Petri dish (**C**) for appropriate characterization of the electrical stimulation system.

To study the effects of time in culture on rat cardiac tissue constructs contractile function, constructs were analyzed just after seeding and after 2 or 7 days of culture. Cardiac tissue constructs at seeding point and after 2 days of culture did not show any spontaneous contraction, neither at microscopic nor at macroscopic levels. However, after 7 days of culture cardiac constructs beat at macroscopic level, with contractions performed by the whole tissue construct in a coordinated way (**Supplementary Video 4.4**). Therefore, more than 2 days in culture was necessary to restore cardiomyocytes contractile function when seeded in a 3D scaffold.

To elucidate the role of electrical stimulation in the contractility of rat cardiac tissue constructs, they were cultured during 7 days in perfusion and subjected to either electrical stimulation or not (for further details, see “3.5.3. *Electrical stimulation regime for cardiac constructs culture*” section). Electrical stimulation had a direct impact on cell distribution within the construct, as cells concentrated in the region delimited by stimulating electrodes, being appreciable even with the naked eye (**Supplementary Video 4.4** and **4.5**, and **Figure 4.35A**). Their functional activity was assessed by

determining the excitation threshold (ET), the maximum capture rate (MCR) and the fractional area change (FAC) of their contractions (**Figure 4.35**). ET is the minimum voltage at which the entire construct starts beating synchronously and continuously to an imposed pacing, and MCR is the maximum frequency of sustained synchronous contractions. Finally, FAC is useful to assess the amplitude of contraction, and is calculated as the fractional change of the construct surface area upon contraction. Although ET and MCR did not show significant differences between control and electrically stimulated constructs (3.25 ± 1.06 V Control vs 3.27 ± 0.75 V ES, and 2.3 ± 0.42 Hz Control vs. 2.67 ± 0.41 Hz ES, **Figure 4.35B-C**), an enhanced contractility with an evident preferential axis of contraction could be observed (**Supplementary Videos 4.4-4.6**). Indeed, the constructs exposed to continuous electrical stimulation exhibited significantly higher contraction amplitudes, with values four times greater than non-stimulated ones (**Figure 4.35D**). On the whole, results suggested that electrical pacing improved cardiomyocytes beating synchrony and coupling, thus approaching tissue cardiac constructs to a more adult-like phenotype. Those observations were consistent with the literature, as identical electrical stimulation parameters were applied in similar constructs and increased FACs were also observed^{281,387}.

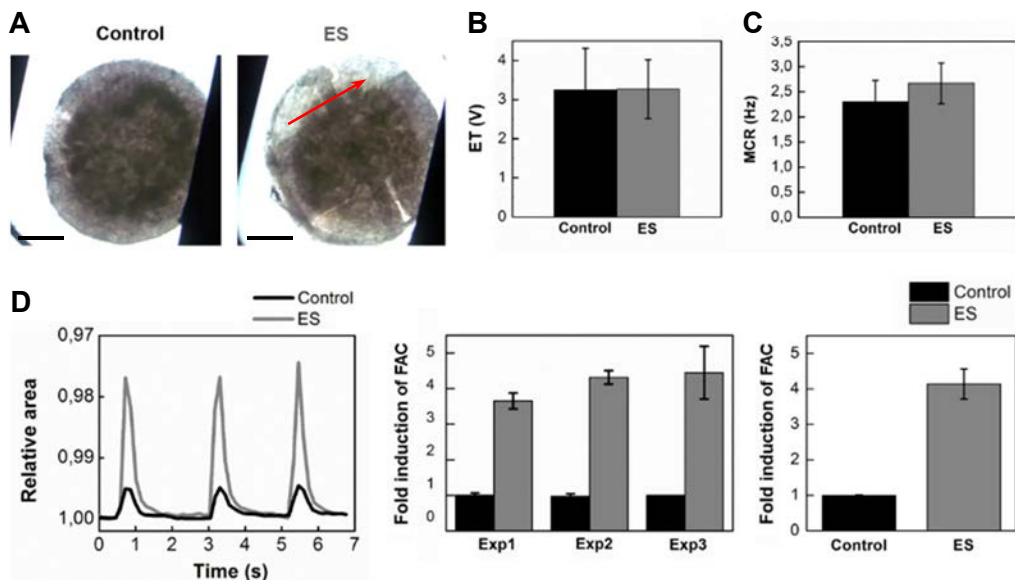


Figure 4.35. Analysis of the functional activity of rat cardiac tissue constructs after 7 days of culture. **A**, Top view images of constructs cultured without (Control) or with (ES) electrical stimulation. Red arrow indicates the direction of the electric field during culture. Scale bars: 2.5 mm. **B**, Excitation threshold (ET) of Control and ES constructs (n=3 per group). **C**, Maximum capture rate (MCR) of control and ES constructs (n=3 per group). **D**, Contraction amplitude analysis of control and ES constructs by means of Fractional Area Change (FAC). The area in pixels of each construct was obtained through a MATLAB program, and its oscillation was represented over time (relative to the maximum number of pixels recorded). Bar charts show the fold induction relative to the mean of the control (individual experiments (Exp1, Exp2 and Exp3) and total fold induction (n=3 per group, average \pm SD). ES: electrostimulated.

4.5.2. Time in culture and electrical stimulation potentiate the structural maturation of rat cardiac tissue constructs

The morphology, organization and distribution of heart cells within the tissue constructs was analyzed by immunofluorescence. Cardiac constructs were fixed, sectioned and stained as described in “3.8.2.2. Cardiac tissue constructs (*in toto*)”. As cardiac cell markers, antibodies against cardiac troponin I (cTNI) and α -sarcomeric actin (ASA) were used. As universal cell markers, an antibody against α -tubulin (α -tub) to stain the cytoskeleton and 4',6-diamidino-2-phenylindole (DAPI) to stain cell nuclei were used. Finally, connexin 43 (Cx43) antibody was used to stain gap junctions, and second harmonic generation (SHG) signal was recorded for collagen imaging. At seeding point, rat heart cells were round and individually scattered through the scaffold (**Figure 4.36**). Moreover, cardiomyocytes did not show any defined sarcomeric organization, and Cx43 was randomly distributed through their cytoplasm, suggesting that more time in culture was needed for the establishment of cell-cell interactions.

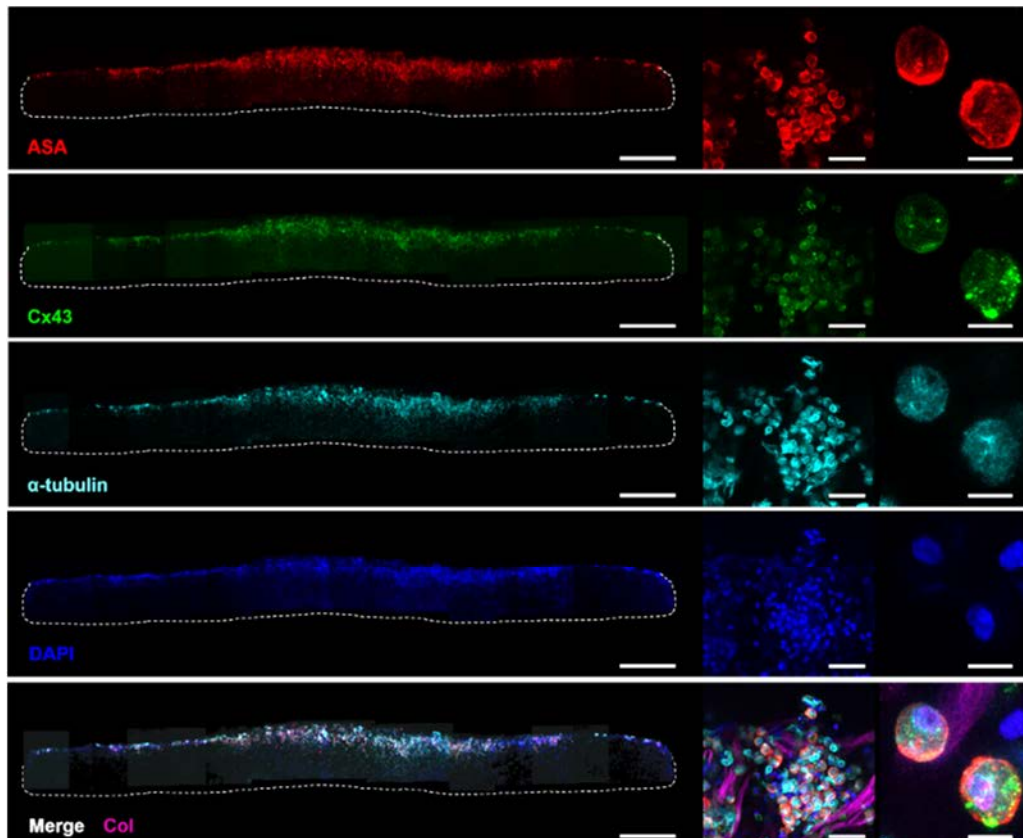


Figure 4.36. Immunostaining of engineered rat cardiac constructs at seeding point. Representative cross-sections and higher magnification images of cardiac constructs, where cardiomyocyte's morphology and distribution along the scaffold is shown. ASA: α -sarcomeric actin; Cx43: connexin 43; DAPI: 4',6-diamidino-2-phenylindole; Col: collagen. Scale bars: 1 mm (cross-sections), 50 μ m and 10 μ m (higher magnification images).

After 2 days in culture, rat heart cells clustered in groups and established more cell-matrix and cell-cell interactions, which led to a more elongated morphology (**Figure 4.37**). Although cardiomyocytes still had not recovered their particular rod shape and cytoskeletal organization, some isolated and small sarcomeres could be seen, suggesting a positive tendency towards structural restoration of cardiomyocytes. The positive effect of longer time periods in culture on cardiomyocyte structural organization was further analyzed by culturing cardiac constructs for 7 days. Immunofluorescence images revealed that rat heart cells organized in high cell density zones, with both cardiomyocytes and non-cardiomyocytes interacting among them (**Figure 4.38**). Specifically, cardiomyocytes displayed much more elongated morphologies than in previous timepoints, and presented well-defined sarcomeric structures. Besides, the improvement in cardiomyocyte structural organization coincided with the appearance of macroscopic contractions (**Supplementary Video 4.4**), thus confirming a favorable evolution of the cardiac construct towards a more mature stage over time in culture.

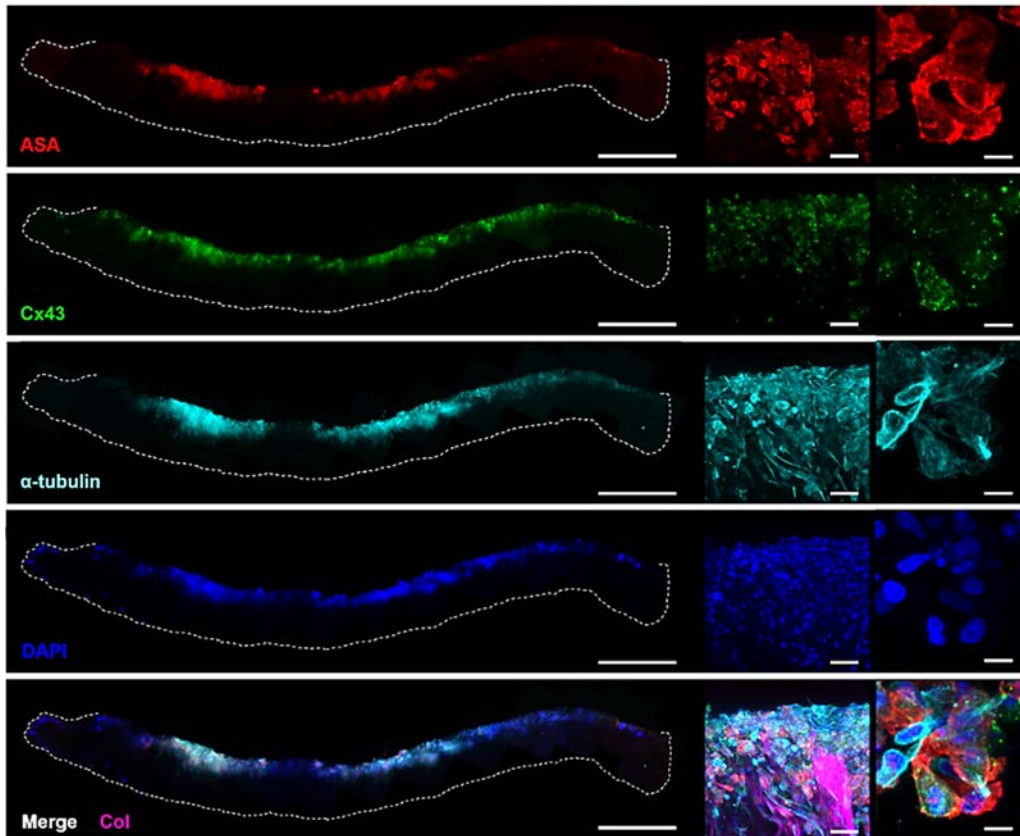


Figure 4.37. Immunostaining of engineered rat cardiac constructs after 2 days of culture in the bioreactor. Representative cross-sections and higher magnification images of cardiac constructs, where cardiomyocyte's morphology and distribution along the scaffold is shown. ASA: α -sarcomeric actin; Cx43: connexin 43; DAPI: 4',6-diamidino-2-phenylindole; Col: collagen. Scale bars: 1 mm (cross-sections), 50 μ m and 10 μ m (higher magnification images).

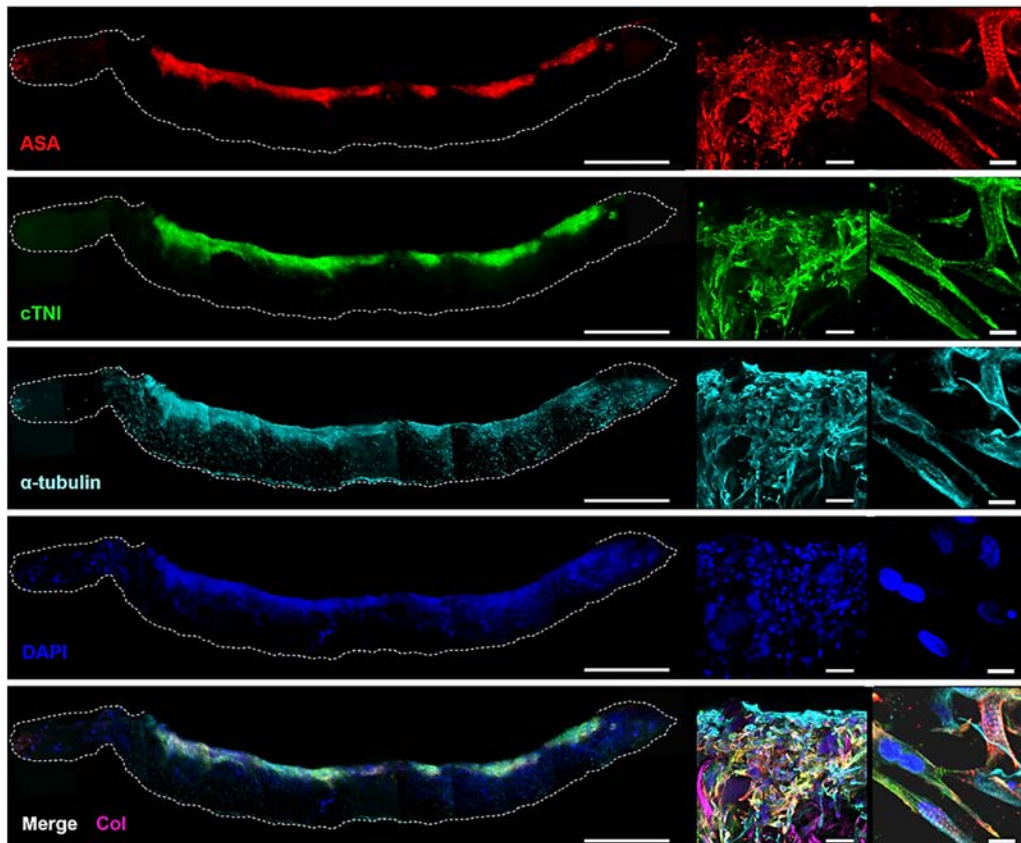


Figure 4.38. Immunostaining of engineered rat cardiac constructs after 7 days of culture without electrical stimulation. Representative cross-sections and higher magnification images of cardiac constructs, where cardiomyocyte's sarcomeric organization, alignment and distribution along the scaffold is shown. ASA: α -sarcomeric actin; cTNI: cardiac troponin I; DAPI: 4',6-diamidino-2-phenylindole; Col: collagen. Scale bars: 1 mm (cross-sections), 50 μ m and 10 μ m (higher magnification images).

Regarding the effects of electrical stimulation during culture, immunofluorescence images showed that both electrostimulated and control cardiac tissue constructs displayed positive expression of cardiac markers (**Figure 4.38** and **4.39**). However, cardiomyocytes that had undergone electrical stimulation showed a compact and extended distribution along the entire construct cross-section (**Figure 4.39**), whereas the non-stimulated ones formed intermittent groups with high cell densities (**Figure 4.38**). Interestingly, cardiomyocytes in electrostimulated tissues presented a highly elongated shape, with abundant and well-defined sarcomeres that aligned in the direction of the electric field (**Figure 4.39**). Although non-stimulated cardiac tissue constructs also contained highly elongated cardiomyocytes with evident and definite sarcomeric structures, they were scarcer and did not show any preferential direction of alignment (**Figure 4.38**). On the whole, those results suggested that pulsatile electric field stimulation had a direct impact on cell distribution and organization within the

construct, as it induced cardiomyocyte alignment parallel to the electric field. It is plausible that differences in cell arrangement have an impact on the contractile behavior of cardiac tissue constructs, as electrically stimulated ones elicit wide contractions in the direction of the electric field (**Supplementary Videos 4.4-4.6**). Those observations were consistent with the literature, as it was reported that the combined use of perfusion and electrical stimulation could induce cell alignment and coupling, and increase the amplitude of synchronous construct contractions^{281,407}.

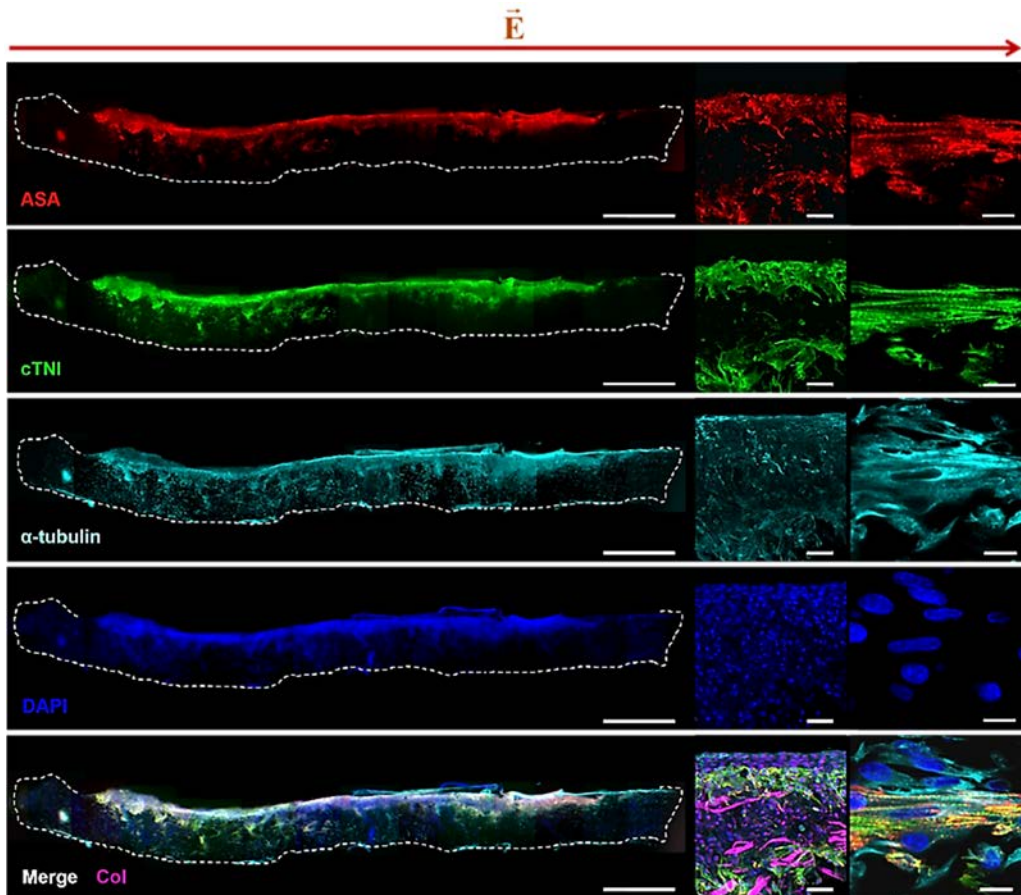


Figure 4.39. Immunostaining of engineered rat cardiac constructs after 7 days of culture under electrical stimulation. Representative cross-sections and higher magnification images of cardiac constructs, where cardiomyocyte's sarcomeric organization, alignment and distribution along the scaffold is shown. E: electric field; ASA: α -sarcomeric actin; cTNI: cardiac troponin I; DAPI: 4',6-diamidino-2-phenylindole; Col: collagen. Scale bars: 1 mm (cross-sections), 50 μ m and 10 μ m (higher magnification images).

Finally, we compared the phenotype of rat heart cells in our cardiac constructs with the one acquired by the same cell type when cultured in standard 2D cultures and in its native cardiac environment (adult rat heart). Cardiomyocytes cultured for 7 days in standard cell culture dishes assembled in beating colonies, and they were not aligned

in any particular direction (**Figure 4.40**). Although cardiomyocytes showed well-developed sarcomeres and cell-cell interactions in those conditions, their cytoskeleton extended in multiple directions, thus adopting irregular shapes that influenced their contractile behavior (**Supplementary Video 4.3**). In flat opposition to this, cardiomyocytes in the adult rat heart were large in size, and had an elongated anisotropic shapes precisely oriented to form highly aligned myofibers (**Figure 4.40**). Regarding cytoskeletal organization, myofibrils had excellent alignment of multiple, well-developed and abundant sarcomeres of uniform width. In this context, our findings suggested that cardiac constructs cultured under pulsatile electric fields approached to adult myocardium phenotype more than non-stimulated ones and standard 2D cultures, although it still differed importantly from the adult heart tissue (**Figure 4.40**).

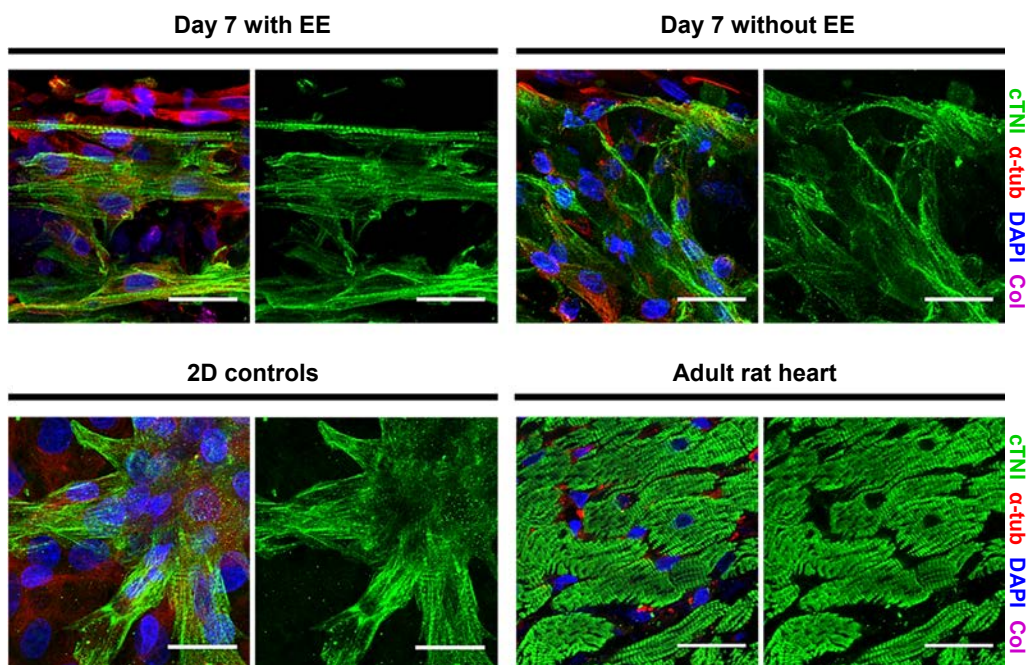


Figure 4.40. Rat heart cells morphology and arrangement in different environments. Cross-section images of cardiac constructs cultured for 7 days under perfusion and either with (left, top images) or without (right, top images) electrical stimulation are shown. To compare their structural organization with standard 2D cultures and native cardiac environment, immunofluorescence images of 2D controls (left, bottom images) and adult rat heart tissue (right, bottom images) are also provided. cTNI: cardiac troponin I; α -tub: α -tubulin; DAPI: 4',6-diamidino-2-phenylindole; Col: collagen. Scale bars: 25 μ m.

To further characterize cell organization and maturity, cardiac tissue constructs cultured for 7 days in the bioreactor were examined at ultrastructural level by transmission electron microscopy (TEM). During ultrathin sections screening, we found organized sarcomeres much more frequently in the electrically stimulated constructs

than in the control ones (data not shown). Images also revealed that constructs cultured under electrical stimulation had cardiomyocytes with a more aligned and well-defined sarcomeric banding than control ones (**Figure 4.41A**). Moreover, cells in electrostimulated constructs displayed advanced specialized intercellular unions, such as intercalated discs, desmosomes and gap junctions, whereas in control constructs they were less developed (**Figure 4.41A** and **inset**). We also compared the phenotype of cardiomyocytes in our tissue constructs with the one acquired in standard 2D cultures and in its native environment. Cardiomyocytes in 2D cultures also showed marked Z-discs (transverse matrix of proteins that limits the sarcomere) and specialized cellular unions, but differed from cardiac constructs in sarcomere bundles organization, as they extended randomly in multiple directions (**Figure 4.41A**). Despite improvements in cytoskeleton alignment with respect to 2D cultures and non-stimulated cardiac constructs, electrically stimulated cardiomyocytes were still far from achieving the organization level of neonatal rat heart (**Figure 4.41A**). For example, in the heart, mitochondria align in between parallel and large sarcomere bundles and some cardiomyocytes display binucleation, features that were not detected in any of our cardiac constructs. However, cardiomyocytes in electrically stimulated constructs regained some aspects of the myocardium that were not observed in the other conditions, such as aligned and frequent sarcomeres found at regular intervals, and well developed specialized intercellular unions. Therefore, it represented a step forward towards the generation of tissue-like cardiac constructs.

To quantify the morphometric differences observed between the groups of study, the width of myofibrillar bundles was measured through determination of Z-disc height (white square brackets in **Figure 4.41A**). Cardiomyocytes that had undergone electrical stimulation displayed wider sarcomeres in comparison with non-stimulated samples and standard 2D cultures (ES: $0.54 \pm 0.32 \mu\text{m}$, Control: $0.29 \pm 0.16 \mu\text{m}$ and 2D: $0.42 \pm 0.18 \mu\text{m}$; $p < 0.001$), thus corroborating that electrical pacing promoted myofibrillar bundles formation (**Figure 4.41B**). Still, cardiomyocytes in neonatal rat heart ventricles showed a significant increase in sarcomere width compared with electrically stimulated constructs ($0.71 \pm 0.36 \mu\text{m}$; $p < 0.001$).

In summary, those results suggested that cardiomyocytes acquired a higher degree of maturation when cultured in a 3D environment and stimulated with pulsatile electric fields, which was in agreement with previously published works^{318,337}. Although reaching an organization level equivalent to the rat heart was not achieved, conditioning cardiac constructs with electrical stimulation approached the possibility to obtain valuable *in vitro* models of cardiac tissue.

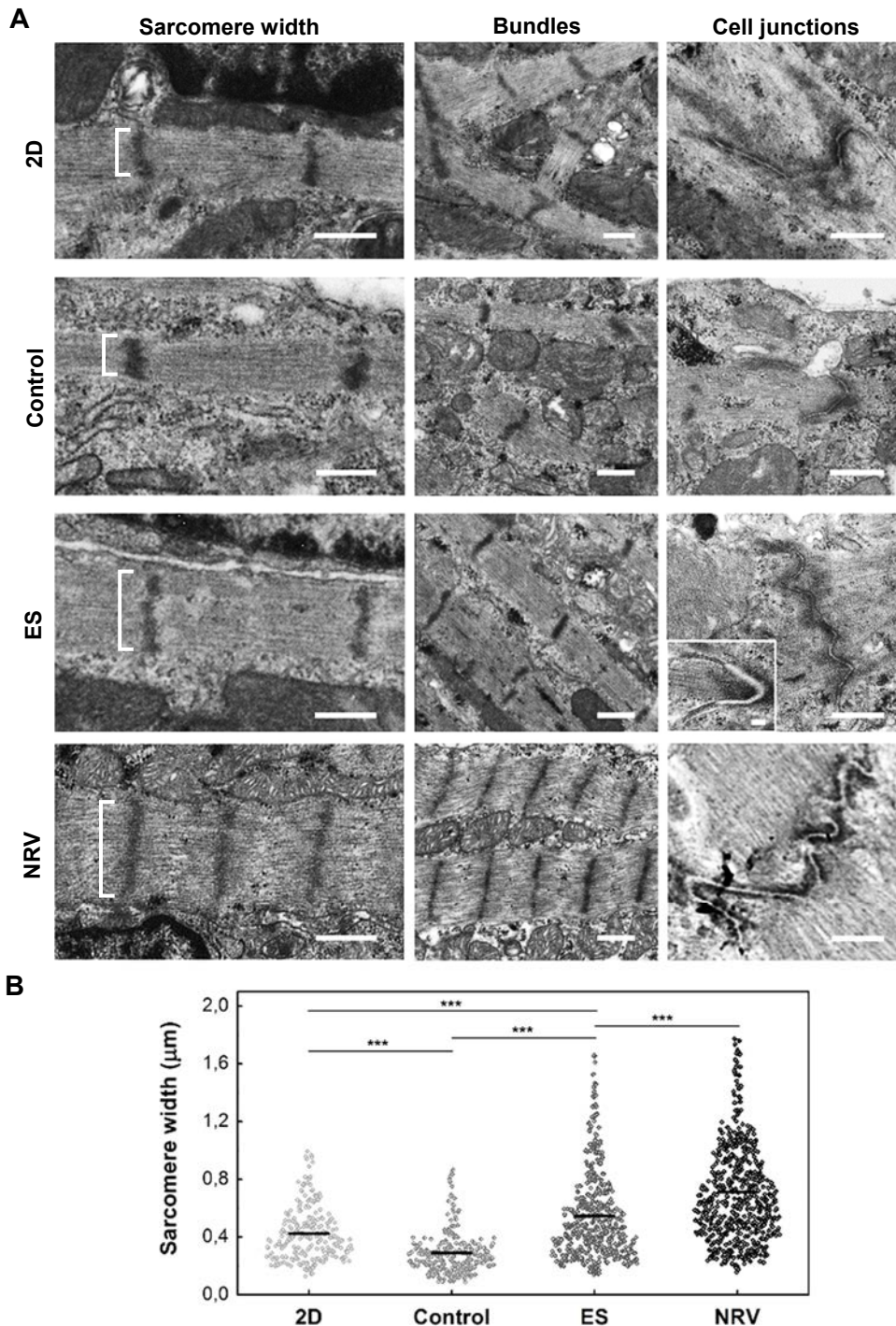


Figure 4.41. Ultrastructural organization of rat cardiomyocytes. **A**, Representative images of cardiomyocytes when cultured during 7 days in standard well plates (2D) and in 3D cardiac constructs without (Control) or with electrical stimulation (ES), as well as in its native environment (NRV, neonatal rat ventricle). Scale bars: 0.5 μm ; Inset: 0.1 μm . **B**, Morphometric analysis of sarcomere width, measured as indicated by white square brackets in **A** (** $p < 0.001$; $n \geq 2$ per group, Mann Whitney U test).

4.6. Generation of human cardiac tissue constructs through perfusion and electrical stimulation

4.6.1. Cardiac differentiation potential of human induced pluripotent stem cells (hiPSC)

The cardiac differentiation potential of several hiPSC clones was analyzed (*work performed in collaboration with Center of Regenerative Medicine in Barcelona (CMRB)*). For that, hiPSC were differentiated using a serum-free monolayer culture system with modulators of canonical Wnt signaling pathway, as previously described⁴³³. Morphology of hiPSC changed as expected over the days of differentiation (**Figure 4.42A**).

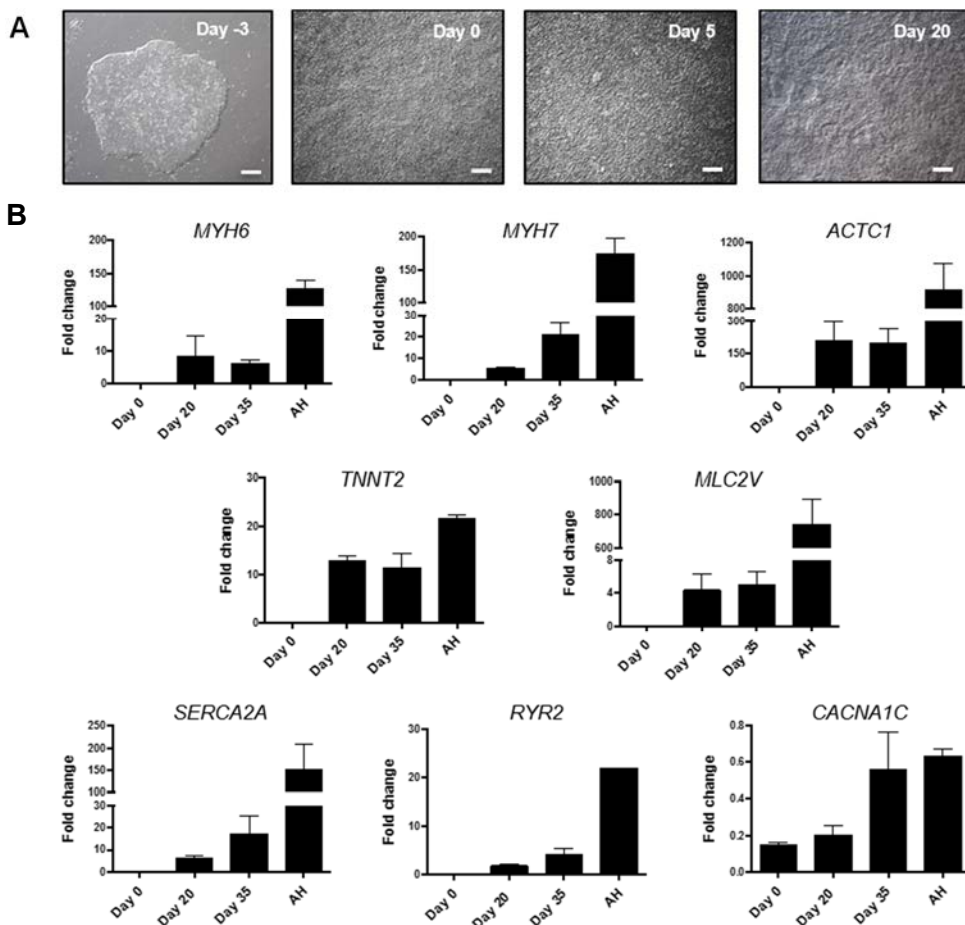


Figure 4.42. Cardiac differentiation potential of human induced pluripotent stem cells (hiPSC). **A**, Bright field images of human fibroblasts-derived iPS (FiPS) cells at day -3, 0, 5 and 20 of differentiation. Scale bars: 200 μ m. **B**, Expression of cardiac markers in hiPSC-CM at day 0, 20 and 35 of differentiation (mean \pm SD; n=2). *MYH6*: α -myosin heavy chain; *MYH7*: β -myosin heavy chain; *ACTC1*: cardiac muscle alpha actin; *TNNT2*: cardiac troponin T; *MLC2V*: myosin light chain 2v; *SERCA2A*: Sarcoplasmic Reticulum Ca^{2+} -ATPase isoform 2a; *RYR2*: ryanodine receptor 2; *CACNA1C*: calcium voltage-gated channel subunit alpha1 C; AH: adult heart.

The human clone that displayed the best *in vitro* cardiogenic potential was selected, which generated contracting monolayers at day 20 of differentiation (**Supplementary Video 4.7**). Cardiac specific genes α -myosin heavy chain (*MYH6*), β -myosin heavy chain (*MYH7*), cardiac muscle alpha actin (*ACTC1*), myosin light chain 2v (*MLC2V*), cardiac troponin T (*TNNT2*) and calcium channel markers ryanodine receptor 2 (*RYR2*), Sarcoplasmic Reticulum Ca^{2+} -ATPase isoform 2a (*SERCA2A*) and calcium voltage-gated channel subunit alpha1 C (*CACNA1C*) were positively expressed upon differentiation, although values still differed from the adult heart tissue (**Figure 4.42B**). Notably, contracting monolayers expressed high percentages of cardiac troponin I (cTNI) and myosin heavy chain (MHC) proteins (71.6 ± 5.3 % cTNI⁺/MHC⁺ cells) at day 20 of differentiation (**Figure 4.43A**). Immunofluorescence analysis showed

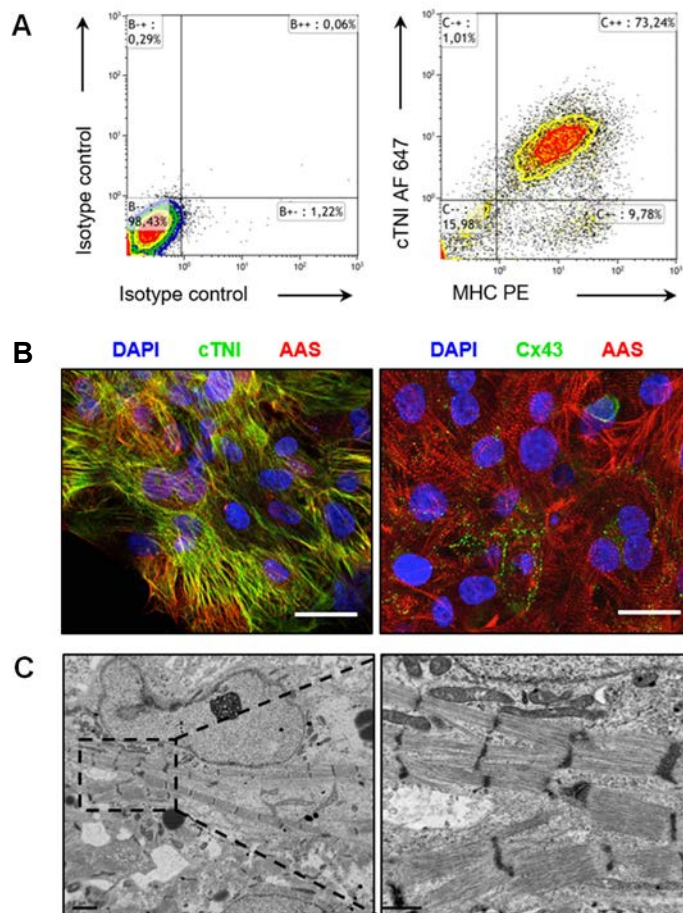


Figure 4.43. Human induced pluripotent stem cells-derived cardiomyocytes (hiPSC-CM) at day 20 of differentiation. **A**, Flow cytometry analysis of hiPSC-CM for cardiac troponin I (cTNI) and myosin heavy chain (MHC) expression (n=3). **B**, Immunofluorescence detection of cardiac proteins cTNI, α -actinin sarcomeric (AAS) and connexin 43 (Cx43). Nuclear staining was performed with 4',6-diamidino-2-phenylindole (DAPI). Scale bars: 25 μm . **C**, Representative images of hiPSC-CMs ultrastructural organization. Scale bars: 2 μm ; higher magnification: 1 μm .

that hiPSC-derived cardiomyocytes (hiPSC-CM) expressed the cytoskeletal cardiac proteins cardiac troponin I (cTNI) and α -actinin sarcomeric (AAS) organized in regular sarcomeric units, as well as the cardiac gap junction protein connexin-43 (Cx43) (**Figure 4.43B**). Cardiac differentiation was also confirmed at ultrastructural level, with cardiomyocytes showing a well-defined sarcomeric organization (**Figure 4.43C**).

4.6.2. Functional maturation of tissue-like human cardiac constructs is enhanced through electrical stimulation

At day 20 of differentiation, hiPSC-CM were selected and mixed with human foreskin fibroblasts (HFF) to obtain a co-culture. Then, the cell suspension was seeded inside Matriderm™ scaffold by applying perfusion in one direction at 1 ml/min, and tissue

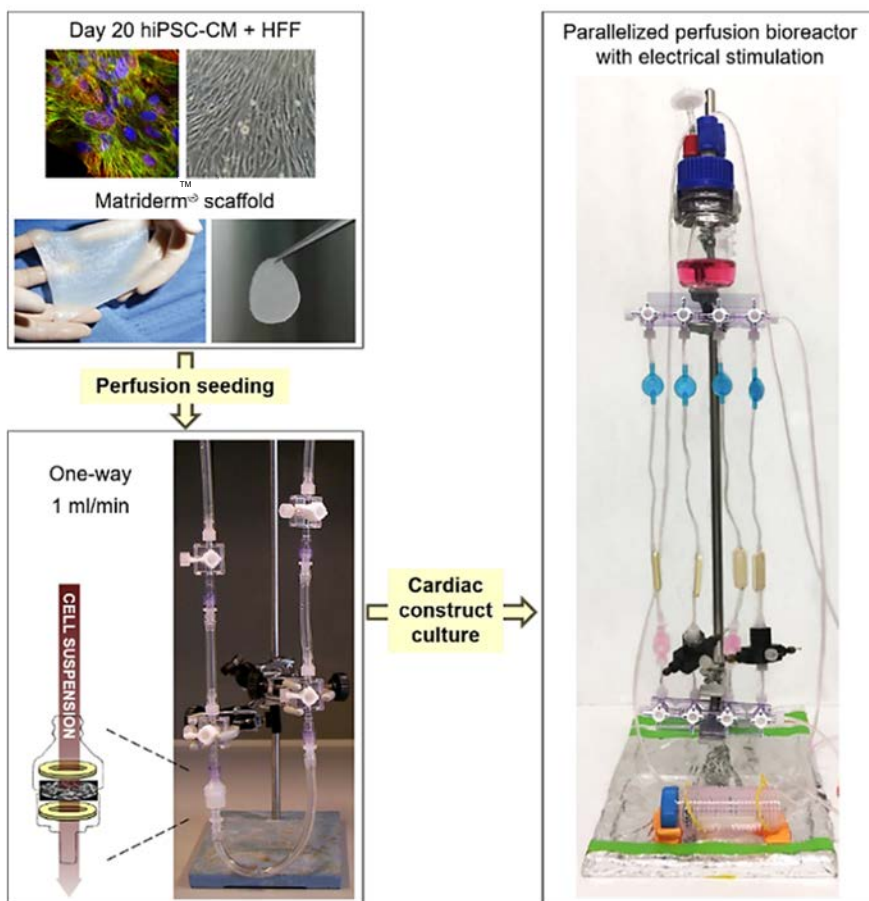


Figure 4.44. Scheme of the strategy to generate tissue-like human cardiac tissue constructs. Cardiomyocytes derived from human induced pluripotent stem cells (hiPSC-CM) were selected at day 20 of differentiation and mixed with human foreskin fibroblasts (HFF). Then, the cell suspension was seeded inside the scaffold by perfusion, cardiac constructs were installed in the bioreactor and they were cultured either with or without electrical stimulation.

constructs were cultured in the perfusion bioreactor either with or without electrical stimulation. **Figure 4.44** provides the reader with a summary of the strategy to generate human cardiac tissue constructs, which was used in all the following sections.

To study the functional activity of human cardiac tissue constructs at different timepoints and elucidate the effect of electrical stimulation on their contractile behaviour, tissue constructs were generated at seeding point and after 4, 7 and 14 days of culture. From day 4 on, some constructs were electrically stimulated (ES) and some not (Control). Cardiac tissue constructs at seeding point did not show any spontaneous contraction, neither at microscopic or macroscopic level. However, after 4 days of culture cardiac constructs beat at macroscopic level, with small contractions performed by the whole tissue construct (**Supplementary Video 4.8** and **Figure 4.45**). Therefore, contractile tissue constructs were obtained just before initiating electrical stimulation, and this coincided with hiPSC-CM functional restoration in 2D controls, as beating zones also appeared 4 days after seeding (data not shown). After 7 days of culture in the perfusion bioreactor without electrical stimulation (Control), an improved contractile behavior of cardiac constructs could be observed, mainly represented by an increase in the amplitude of contraction and coordination with respect to day 4 constructs (**Supplementary Video 4.9** and **Figure 4.45**). However, increasing culture time to 14 days did not mean evident changes in cardiac constructs amplitude of contraction or synchronization (day 14 Control in **Figure 4.45**), suggesting that perfusion and a 3D environment improved tissue constructs functionality mainly in the initial stages (**Supplementary Video 4.10**). Regarding the role of electrical stimulation in the contractility of human cardiac constructs, tissue constructs subjected to electrical stimulation were generated after 7 and 14 days of culture. The first observation was that electric field stimulation had a direct impact on cell distribution within the construct at both timepoints. Cells concentrated in the region delimited by stimulating electrodes, appearing as a darker rectangle-shaped region appreciable even with the naked eye (**Figure 4.45**). Moreover, electrical stimulation markedly improved cardiomyocytes beating synchrony and coupling compared with control samples, leading to cardiac tissue constructs with a more efficient signal propagation both at day 7 and day 14 (**Supplementary Videos 4.11** and **4.12**, and **Figure 4.45**).

To quantify these differences, the excitation threshold (ET), maximum capture rate (MCR) and fractional area change (FAC) were determined for each condition. ET is the minimum voltage at which the entire construct starts beating synchronously and continuously to an imposed external pacing, and MCR is the maximum frequency of sustained synchronous contractions. Finally, FAC is used to assess the amplitude of contraction, and is calculated as the fractional change of the construct surface area. The improved contractile function of the electrically stimulated constructs was evidenced by a significant increase in the contraction amplitude compared with the

control ones, suggesting a favorable maturation of the electromechanical coupling machinery (**Figure 4.46A**). Although ET and MCR did not show significant differences between the groups of study, a tendency towards lower ETs and higher MCRs in electrically stimulated constructs was observed (**Figure 4.46A**).

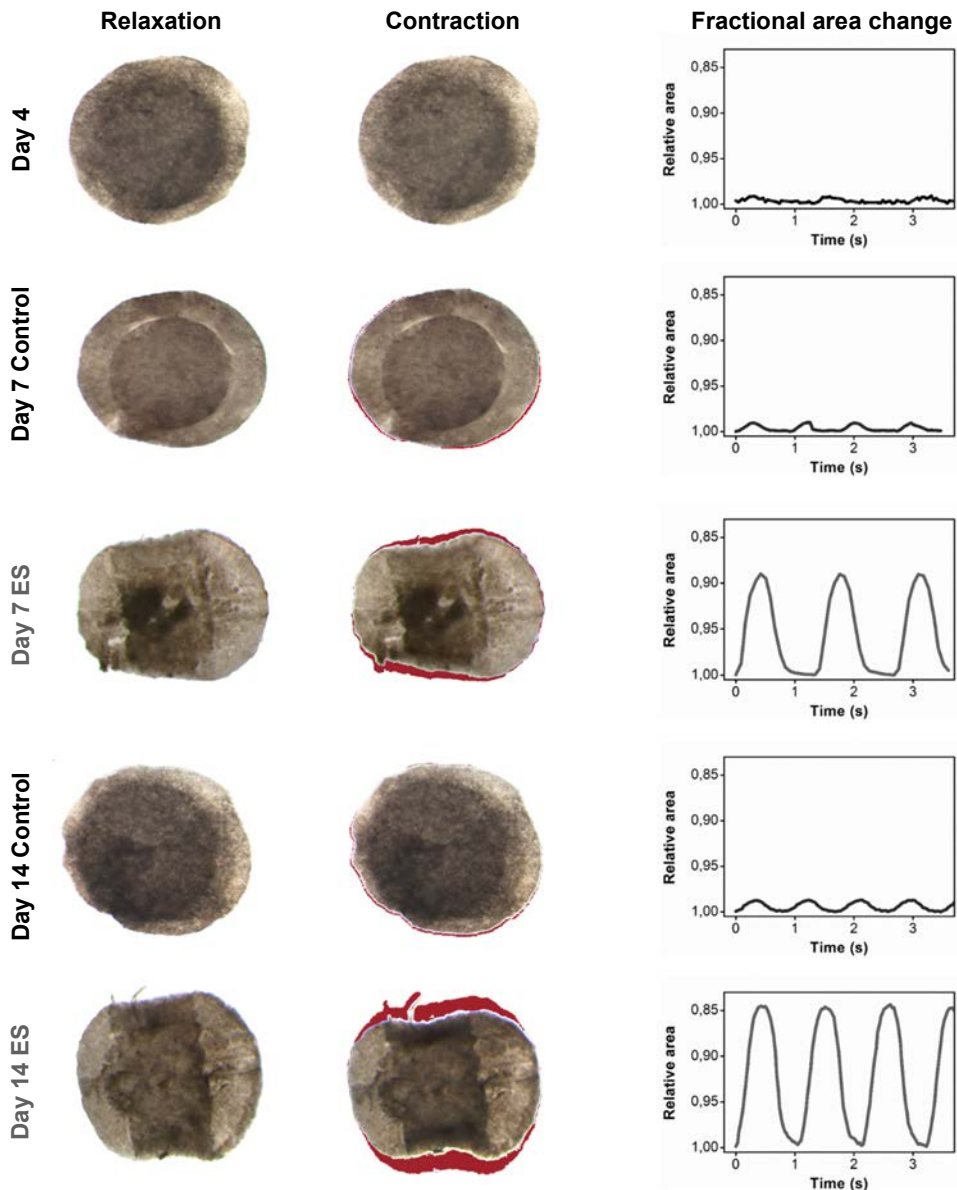


Figure 4.45. Amplitude of contraction of human cardiac tissue constructs. Spontaneous beating of non-stimulated (Control) and electrically stimulated (ES) constructs was video recorded after 4, 7 and 14 days in culture. Video frames of relaxed and contracted states are shown, with red shading representing relaxed area. The area in pixels of each construct was obtained through custom MATLAB program, and area changes in each beat were represented over time (fractional area change, FAC). Area is expressed relative to the maximum number of pixels of the construct (relaxed state).

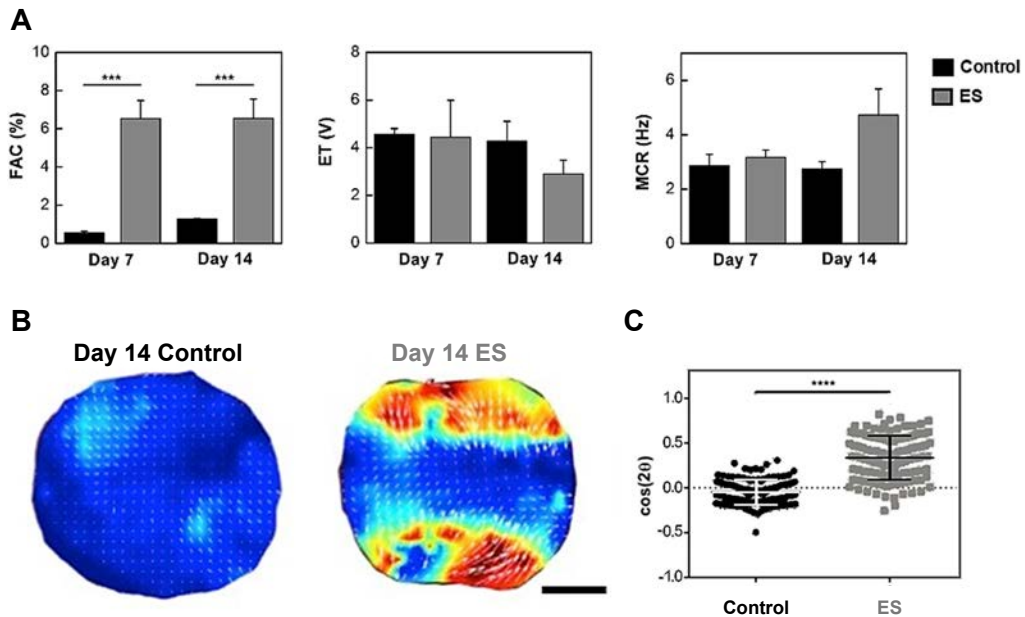


Figure 4.46. Functional assessment of hiPSC-derived engineered cardiac tissues. A, Fractional area change (FAC), excitation threshold (ET) and maximum capture rate (MCR) of non-stimulated (Control) and electrostimulated (ES) human cardiac tissue constructs after 7 and 14 days of culture. Data are expressed as average \pm standard error of the mean ($n \geq 2$ per group; $***p < 0.001$; Student's t-Test). **B,** Strain analysis of beating human cardiac constructs after 14 days of culture. Velocity maps of the contracted state are shown for Control and ES constructs. Red colours and long arrows represent high velocities, while blue colours and short arrows represent low velocities. Scale bars = 2.5 mm. **C,** Analysis of the alignment between the direction of the electric field and the direction of the beating of human cardiac constructs. The order parameter $\langle \cos 2\theta \rangle$ was used, with values close to 0 meaning random distribution and values close to 1 meaning parallel alignment ($***p < 0.001$; $n=2$ per group, test Mann-Whitney U test).

The effect of cell distribution within the construct on the contractility of tissue constructs was analyzed in further detail by Particle Image Velocimetry (PIV). Strain maps were generated for cardiac constructs cultured for 14 days in the bioreactor, and demonstrated that the strain per contraction was higher in the electrostimulated constructs compared with control ones, thus corroborating their enhanced contractile performance (**Figure 4.46B**). To gather information about the beating directionality of tissue constructs, the alignment between the velocity vector fields and the direction of the electric field was assessed by the order parameter $\langle \cos 2\theta \rangle$. Electrical stimulation oriented the beating of human cardiac constructs parallel to the direction of the electric field, whereas non-stimulated constructs resulted in a random distribution of the velocity vectors (**Figure 4.46C**). Therefore, cardiomyocytes cultured under a pulsatile electric field improved the directionality of human constructs contractions, having a close-to-human and statistically significant better performance than the control ones (**Figure 4.46C** and **Supplementary Videos 4.10** and **4.12**).

4.6.3. Perfusion together with electrical stimulation promote the structural maturation of tissue-like human cardiac constructs

The morphology, organization and distribution of the cardiomyocytes within human cardiac tissue constructs was analyzed by immunofluorescence. Constructs were fixed, sectioned and stained as described in “3.8.2.2. Cardiac tissue constructs (*in toto*)” section. Antibodies against cardiac troponin T (cTNT) and α -sarcomeric actin (ASA) were used as cardiac cell markers, a fluorescent conjugate of phalloidin (Ph) was used to stain cell cytoskeleton, and 4',6-diamidino-2-phenylindole (DAPI) was used to stain cell nuclei. Finally, second harmonic generation (SHG) signal was recorded for collagen imaging. At seeding point, human foreskin fibroblasts (HFF) were already starting to attach and spread inside Matrigel™ scaffold, whereas hiPSC-CM were round and individually scattered through the scaffold (**Figure 4.47A**). Moreover, hiPSC-CM did not show any defined sarcomeric organization. After 4 days in culture, hiPSC-CM clustered and adopted an elongated morphology, thus establishing cell-matrix and cell-cell interactions (**Figure 4.47B**). Although cardiomyocytes still had not fully recovered their particular rod shape and cytoskeletal organization, some isolated and small sarcomeres could be seen, suggesting a positive tendency towards cardiac cells structural restoration. These observations were in concordance with the results about the recovery of the beating function, which was found after 4 days of culture inside the bioreactor. The positive effect of longer cell culture times on cardiomyocytes structural organization was studied by culturing cardiac constructs for 7 and 14 days (**Figure 4.47C** and **4.47E**). Immunofluorescence images revealed that hiPSC-CM organized in high cell density zones, with both cardiomyocytes and non-cardiomyocytes interacting among them. Specifically, cardiomyocytes displayed more elongated morphologies than in previous timepoints, and well-defined sarcomeric structures were clearly visible, being more evident and well-developed over time in culture.

Immunofluorescence analysis was also performed on electrically stimulated constructs cultured for 7 and 14 days. Images showed that electrostimulated and control tissue constructs displayed positive expression of cardiac markers at both timepoints (**Figure 4.47C-F**). However, cardiomyocytes that had undergone electrical stimulation presented a highly elongated shape, with abundant and well-defined sarcomeres that aligned in the direction of the electric field (**Figure 4.47D** and **4.46F**). Although control cardiac tissue constructs also contained elongated cardiomyocytes with defined sarcomeric structures, they did not show any preferential direction of alignment (**Figure 4.47C** and **4.47E**). That difference was much more visible after 14 days of culture, as highly organized myofibrillar bundles aligned in the direction of the electric field reached an unprecedented level of order (**Figure 4.47F**), which translated to maximum contraction amplitudes (**Figure 4.46A**). Electrically stimulated cardiomyocytes also showed a compact and extended distribution along the entire construct thickness and

cross-section, whereas in the control samples they colonized the upper part of the scaffold and were less spread (**Figure 4.48**). On the whole, these results suggest that pulsatile electric field stimulation has a direct impact on cell distribution and organization within the human tissue construct, as it improved cardiomyocyte structure and alignment. Moreover, these differences in cell arrangement determine the contractile behavior of cardiac tissue constructs, as electrically stimulated ones produced significantly wider contractions and parallel to the electric field than control ones.

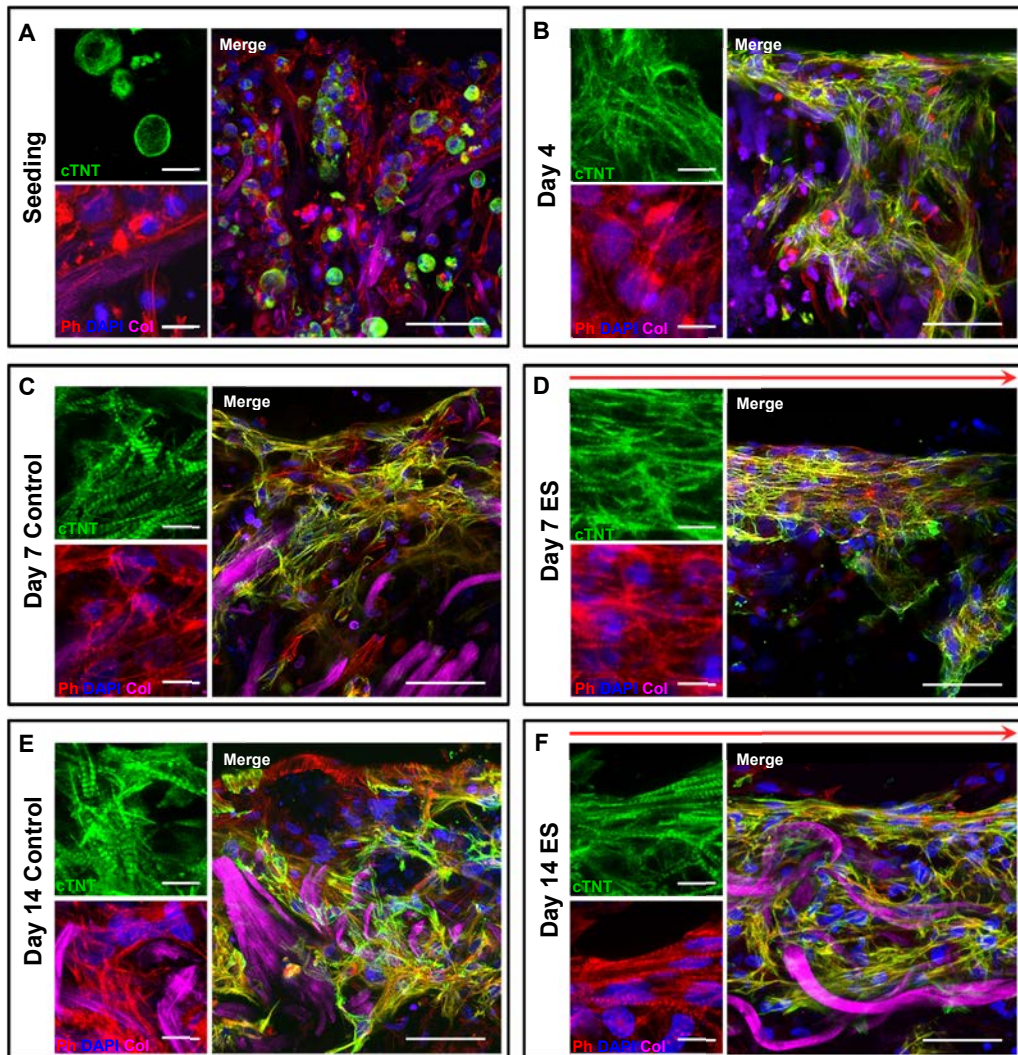


Figure 4.47. Immunostaining of engineered human cardiac constructs. Representative images of cardiac constructs at seeding point (**A**) and after 4 days of culture (**B**) are shown, as well as after 7 days of culture without (**C**, Control) or with (**D**, ES) electrical stimulation and after 14 days of culture without (**E**, Control) or with (**F**, ES) electrical stimulation. Top part of the images correspond to tissue construct upper limit, whereas bottom part corresponds to scaffold interior. Electrically stimulated cardiac constructs were sectioned to obtain cross-sections oriented in the direction of the electric field (red arrows). cTNT: cardiac troponin T; Ph: Phalloidin; DAPI: 4',6'-diamidino-2-phenylindole; Col: collagen. Scale bars: 50 μm ; High magnifications: 10 μm .

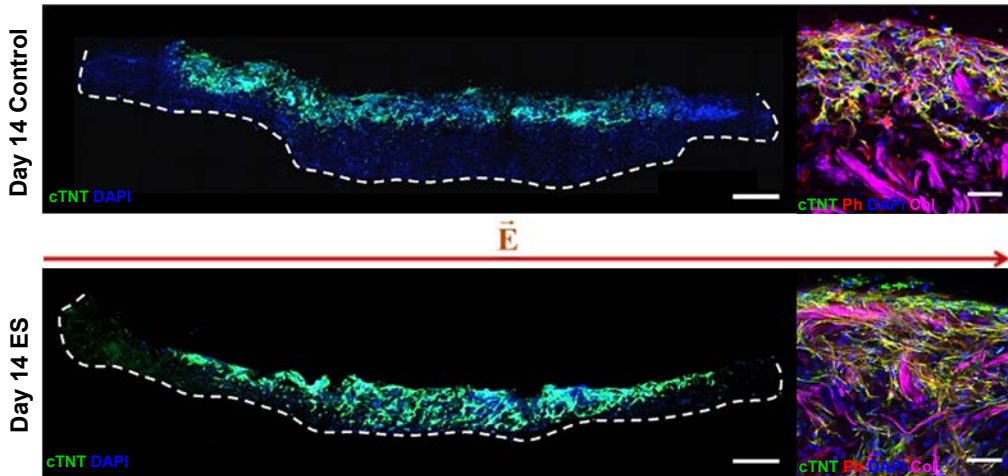


Figure 4.48. Immunostaining of human cardiac tissue constructs after 14 days of culture. Representative cross-sections and higher magnification images of constructs, where cardiomyocyte organization, alignment and distribution is shown. Electrically stimulated constructs were sectioned to obtain cross-sections oriented in the direction of the electric field (red arrow). E: electric field; cTNT: cardiac troponin T; DAPI: 4',6-diamidino-2-phenylindole; Ph: Phalloidin; Col: collagen. Scale bars: 500 μm (cross-sections) and 50 μm (higher magnifications).

To further analyze cardiomyocytes maturity, cardiac constructs cultured for 7 and 14 days were examined at their ultrastructural level by transmission electron microscopy (TEM). An enhanced organization level was found in constructs that had undergone electrical stimulation, as during screening of ultrathin sections we found structured sarcomeres more frequently than in control ones (data not shown). Images revealed that, although cardiomyocytes had a well-defined sarcomeric banding at both timepoints and conditions studied, sarcomeres were wider and more developed in electrostimulated tissue constructs than in control ones (**Figure 4.49A**). Moreover, cardiomyocytes in electrically stimulated constructs displayed advanced specialized intercellular junctions such as intercalated discs, desmosomes and gap junctions, whereas in control ones they were less developed (**Figure 4.49A** and **inset**). Those differences in the complexity of cell junctions was more evident after 14 days of culture, meaning that cardiomyocytes acquired optimal cell adhesion complexes for an appropriate electromechanical coupling⁴⁷. To quantify the morphometric differences observed between the groups, the width of myofibrillar bundles was measured through determination of Z-disc height (white square brackets in **Figure 4.49A**). Cardiomyocytes that had undergone electrical stimulation displayed a significant increase in sarcomere width in comparison with control constructs both at 7 and 14 days of culture, indicating that electrical stimulation promoted myofibrillar bundles formation (**Figure 4.49B**).

On the whole, results suggest that hiPSC-CM acquire a higher degree of maturation when stimulated with pulsatile electric fields. Although the effects of electrical stimulation on human cardiomyocytes has been reported on microtissues and

microphysiological systems^{319,337,333}, here we show for the first time its effect on macroscopic and thick human cardiac tissue constructs. Electrical stimulation has improved the structural organization, alignment and coupling of cardiomyocytes in our tissue constructs, leading to the formation of 3D tissue-like human cardiac constructs.

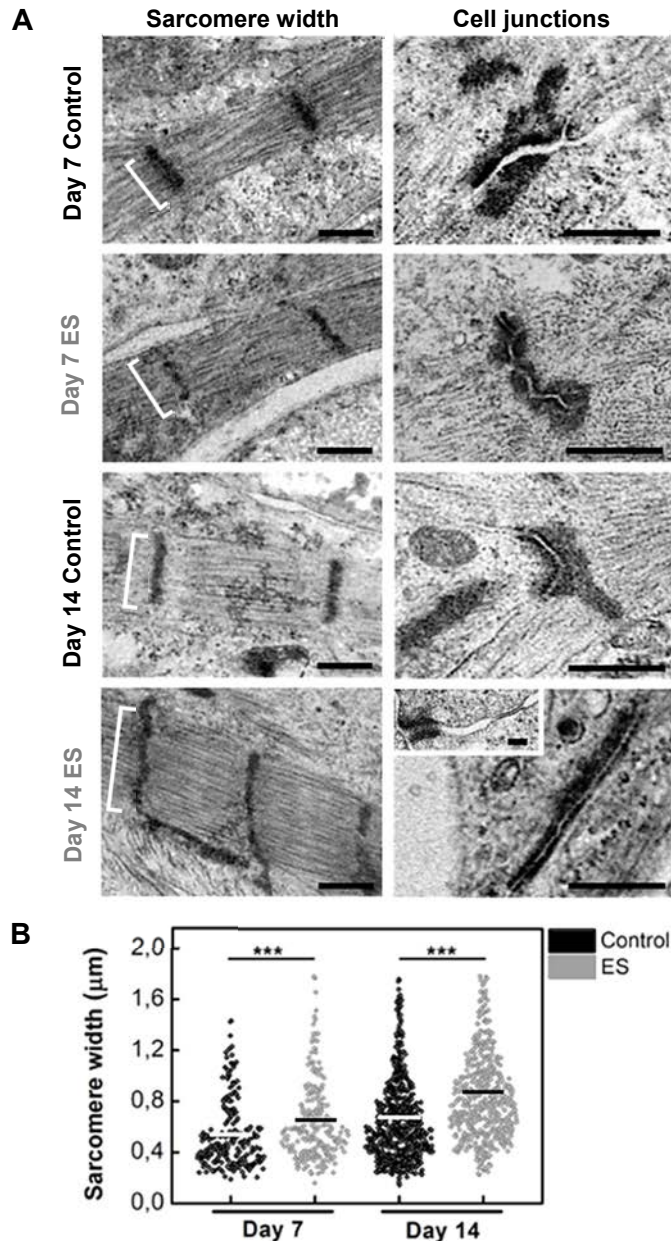


Figure 4.49. Ultrastructural organization of hiPSC-CM after 7 and 14 days in culture. A, Representative images of ultrastructural organization of cardiomyocytes in 3D cardiac constructs when cultured without (Control) or with electrical stimulation (ES). Scale bars: 0.5 μm ; high magnification inset: 0.1 μm . **B,** Morphometric analysis showing sarcomere width, measured as indicated by white square brackets in **A** (***) $p < 0.001$; $n \geq 1$ per group, Mann-Whitney U test).

4.6.4. Human cardiac tissue constructs display an increased expression of cardiac specific genes

To study the maturation of cardiomyocytes, the expression of cardiac genes in control and electrostimulated constructs was compared with the same culture seeded on multi-well plates (2D controls), as well as with fetal and adult human hearts. Collectively, results suggested that expression levels of cardiac specific genes increased considerably with time of culture, as well as when culturing cells in the bioreactor (**Figure 4.50**). Although non-statistical significant differences between control and electrostimulated constructs were detected, there was a tendency towards an upregulation of cardiac genes in electrically stimulated constructs at day 14 of culture. For example, expression of β -myosin heavy chain (β -MHC, encoded by *MYH7* gene) has been reported to increase in late gestational ages and in adult ventricle with respect to early fetal stages⁷⁸. A tendency towards an increased abundance of *MYH7* was also observed in electrically stimulated constructs at day 14 of culture, thus suggesting an improvement of cardiomyocytes level of maturation (**Figure 4.50**). Cytoskeletal cardiac genes *TNNT2* and *ACTC1* were also upregulated in electrically stimulated constructs at day 14 of culture with respect to non-stimulated (3D Ctrl) ones and 2D controls (**Figure 4.50**). Regarding the expression of ionic channels, the ventricular gap junction connexin 43 (encoded by *GJA1*) displayed an increased expression in electrically stimulated constructs at day 14 of culture with respect to non-stimulated (3D Ctrl) ones and 2D controls. Similarly, a tendency towards an upregulation of calcium channel genes was observed in electrostimulated constructs in comparison with control ones and standard 2D well plates, specially *SERCA2A* (**Figure 4.50**).

On the whole, gene expression analysis suggested that culturing human induced pluripotent stem cells-derived cardiomyocytes (hiPSC-CM) for 14 days in our advanced 3D culture system improved their maturation with respect to standard 2D cultures. Although expression values still differed importantly from the adult heart tissue, results showed a tendency towards an enhanced expression of cardiac-related genes when cardiac tissue constructs were electrically stimulated.

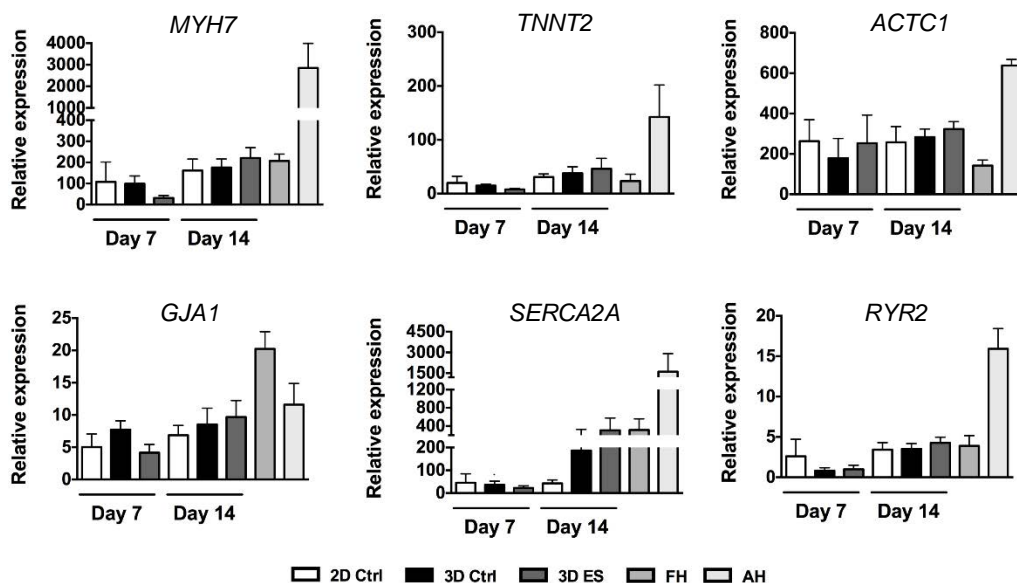


Figure 4.50. Endogenous gene expression of cardiac specific markers measured by qRT-PCR. Expression of cytoskeletal cardiac genes (*MYH7*: β -myosin heavy chain; *TNNT2*: cardiac troponin T; *ACTC1*: cardiac muscle alpha actin), a gap junction gene (*GJA1*: gap junction protein alpha 1) and calcium channel genes (*SERCA2A*: Sarcoplasmic Reticulum Ca^{2+} -ATPase isoform 2a; *RYR2*: ryanodine receptor 2) was analysed. Expression levels in human cardiac constructs cultured without (3D Ctrl) or with (3D ES) electrical stimulation were compared with the same cell population cultured in standard well plates (2D Ctrl), as well as with fetal human heart (FH) and adult human heart (AH).

4.7. Electrically stimulated human cardiac tissue constructs elicit ECG-like signals and predict drug-induced cardiotoxicity

Cardiac toxicity is an issue of immense significance for patients, pharmaceutical industry and regulatory organizations, as an estimated ~45% of all withdrawals and ~30% of restrictions to drug application are due to unexpected negative cardiovascular events²³³. Such safety issues are undetected due to the limitations of current preclinical testing platforms, which strongly rely on *in vitro* cell lines and non-human animal models¹⁷². Consequently, new generation *in vitro* models able to provide information about relevant human outcomes need to be developed, and human cardiac tissue constructs produced in this thesis could be a promising tool.

Aforementioned results demonstrated that the developed bioreactor was a technological setup able to generate *in vitro* models of human cardiac tissue. Cardiac tissue constructs displayed morphological characteristics of the human myocardium in

terms of cell alignment, elongation and cytoskeletal organization (**Figure 4.47** and **4.49**), had a spontaneous beating oriented in the direction of the electric field, and were able to follow external imposed pacing (**Figure 4.46**). Therefore, our final goal was to study if tissue constructs could respond as expected to certain cardioactive drugs. This would permit validating our human cardiac constructs as a truly close-to-human *in vitro* model for drug toxicity testing.

To gather information about the electrophysiology of the human cardiac constructs and their response to cardioactive drugs, a recording system of their electrical activity was developed. Bioelectrical signal recording can give information about the electric propagation within the construct, as well as to which extent cells are coupled and synchronized in a tissue-like manner⁴⁷¹. Usually, electrophysiological data from cardiac tissue constructs is obtained through action potential measurements on a representative cell population at the time of seeding²⁷⁷ or on isolated cardiomyocytes after tissue formation^{50,319}. Alternatively, some parameters can be obtained through voltage-sensing optical techniques, but it is still a challenge to develop an electrophysiological recording system that provides information from intact engineered heart tissues¹⁷². For this, we developed a system to online monitor the electrical activity of intact constructs by recording extracellular field potentials (EFPs), which is the charge redistribution in the surrounding medium of cardiomyocytes after action potential firing.

4.7.1. Bioelectrical signal generated by human cardiac tissue constructs resembles a surface electrocardiogram

To record the electrophysiological activity of human cardiac tissue constructs at day 14 of culture, we took advantage of the culture chambers designed and fabricated in-house (**Figure 4.28**). Chambers were constituted by three electrodes: two graphite electrodes to deliver electrical stimuli to the cultured constructs, and one gold electrode that we used to characterize and control the electrical stimulation system. For bioelectrical signal recording, electrodes were used for a three electrode measurement system (*work performed in collaboration with Biomedical signal processing and interpretation group, Institute for Bioengineering of Catalonia (IBEC)*). The gold electrode acted as an internal reference, and the electrical activity of cardiac constructs was acquired using the graphite electrodes (**Figure 4.51A**) (see “3.11. Recording and processing of bioelectrical signals generated by cardiac tissue constructs” section for further details). As a unique feature, signal recording of the beating of cardiac constructs could be performed while culturing them inside the bioreactor (**Figure 4.51B**). This would allow the online monitoring of the electrical activity of tissue constructs over time in culture, as well as studying the differences between electrically stimulated and control constructs at the same timepoint.

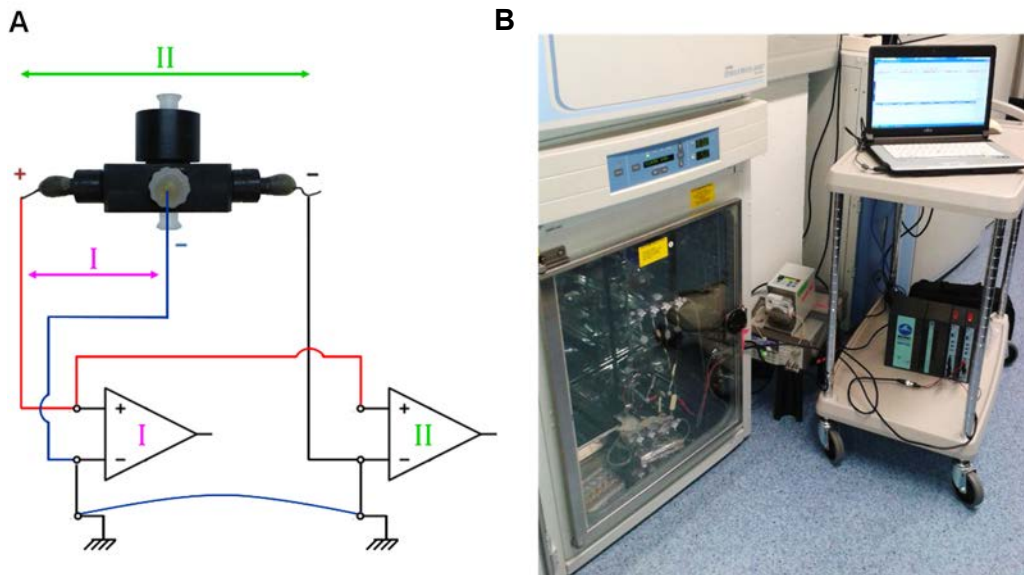


Figure 4.51. Scheme of the setup to record electrophysiological activity of human cardiac tissue constructs. **A**, Electric circuit representation of the signal acquisition system. Three electrodes were used for the recording: a source electrode (graphite, red line), a reference electrode (graphite, black electrode) and an internal reference electrode (gold, blue line). Channel I (purple) record was used as internal reference, while bioelectrical signal was acquired through channel II (green). Both signals were amplified, processed with the BIOPAC MP150 system and displayed in a laptop computer for online monitoring of tissue constructs electrical activity. **B**, Image of the setup to monitor electrical activity of human cardiac constructs. The parallelized perfusion bioreactor was installed inside the incubator to maintain appropriate culture conditions, and the BIOPAC system was connected to it through croc clips. Laptop computer displayed the bioelectrical signal generated by cardiac constructs in real time.

Human cardiac tissue constructs produced a bioelectrical signal that was a combination of the action potentials generated by hiPSC-CM composing the construct. Importantly, the recorded bioelectrical signal at day 14 of culture was similar to a regular surface electrocardiogram (ECG), including QRS complex and repolarizing T wave (**Figure 4.52**). Depending on the degree of synchronization and coupling of cardiomyocytes, the amplitude and width of QRS complex was affected. Accordingly, signals from control cardiac tissue constructs showed lower and wider QRS complexes than electrical stimulated ones (ES), which were narrower and steeper (**Figure 4.52A**). This indicated that hiPSC-CM in electrostimulated constructs were better coupled than control ones, thus displaying higher conduction velocities and improved propagation of the electrical impulse. In addition, the spontaneous beating rate of electrically stimulated constructs was significantly more stable than control ones (**Figure 4.52B**), suggesting that electrical pacing influenced the autonomous beating rate of cardiomyocytes. Regarding the pattern of the QRS, electrostimulated cardiac constructs displayed a time-invariant QRS shape (**Figure 4.52C**), which was stationary during baseline and

represented by one single shape in the 99% of all beats (**Figure 4.52D**). Conversely, four QRS patterns at baseline were obtained for control cardiac tissue constructs (**Figure 4.52C**), representing 38, 20, 20 and 19% of all beats, respectively, with a total value of 93% (**Figure 4.52D**). All these features suggested that electrostimulated cardiac constructs were the best option to study the effect of cardioactive drugs, as changes in heart rate and QRS shape would permit to estimate the effect of drugs in a realistic tissue-like human cardiac model.

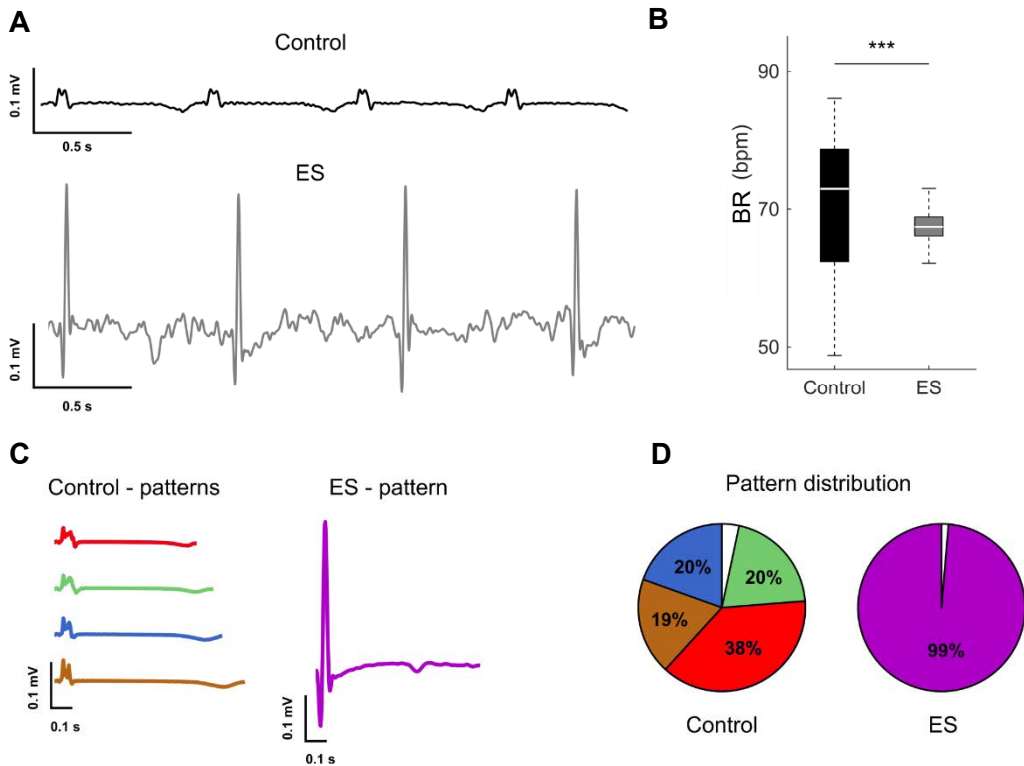


Figure 4.52. Bioelectrical signals generated by human cardiac tissue constructs during spontaneous beating. **A**, Representative bioelectrical signals of non-stimulated (Control) and electrically stimulated (ES) constructs during spontaneous beating. Signals resemble a regular surface electrocardiogram (ECG) for humans. **B**, Distribution of beating rate (BR), expressed as beats per minute (bpm) over 10 min of spontaneous beating recording (Control: 691 beats; ES: 611 beats). $***p < 0.001$; Mann-Whitney U test. **C**, Bioelectric patterns recorded for Control and ES constructs. Four patterns were found in Control recordings, whereas a single pattern was found in ES recordings. **D**, Percentage that patterns found in **C** represent of the total beats. Beat clustering was performed through cross-correlation between a representative beat and the rest of the beats. Beats were included within a cluster when the cross-correlation of corresponding QRS complex exceeded a threshold of 0.85.

4.7.2. Electrically stimulated human cardiac tissue constructs can predict drug-induced cardiotoxicity

To validate our human cardiac tissue constructs as an *in vitro* model for drug toxicity testing, we incubated the constructs at day 14 of culture with three different cardioactive drugs: isoproterenol (β -adrenergic agonist), carbachol (cholinergic agonist) and sotalol (human ether-a-go-go-related gene (hERG) potassium channel blocker and adrenergic antagonist). Sotalol is an antiarrhythmic drug currently used only in life-threatening arrhythmias, as it decreases heart rate and blocks the hERG potassium channel, responsible for action potential repolarization. However, this blockade causes a QT interval prolongation on a surface electrocardiogram (ECG), which is associated to fatal ventricular tachycardia such as Torsade de Pointes (TdP)⁴⁷². For that reason, sotalol is considered a standard QT prolonging drug with a high proarrhythmic risk because both effects have been clinically observed, but *in vitro* electrophysiological studies are unable to properly reproduce them^{244,473}. Therefore, treating our human cardiac constructs with this compound would allow us to know if they can be used as *in vitro* tissue models to detect drug-induced cardiotoxicity.

The effects of isoproterenol, carbachol and sotalol treatments on human cardiac constructs functionality was assessed using two different approaches: video recording and subsequent fractional area change (FAC) analysis, and bioelectric signal recording. The first approach is based on detecting affections in the contractile pattern of the constructs, whereas the second gives information about affections in the electrophysiology of the constructs.

To analyze drug effects on the contractile pattern of human cardiac tissue constructs at day 14 of culture, constructs were placed inside the video-recording setup (**Figure 4.34**) and drugs were added and washed out sequentially (for further details, see “3.7.3. Drug response analysis” section). For each drug treatment, cardiac tissue constructs were video recorded, their area in pixels was obtained through custom MATLAB program, and its oscillation was represented over time to study changes in the beat rate. Interestingly, constructs that had undergone electrical stimulation increased notably their beating frequency when incubated with isoproterenol, and decreased their beat rate when incubated with carbachol (**Figure 4.53A-B** and **Supplementary Videos 4.13** and **4.14**). Therefore, the expected positive and negative chronotropic effects were confirmed for each drug, indicating functional adrenergic and cholinergic signaling systems that affected global construct behavior. Regarding control cardiac tissue constructs, positive chronotropic effect after isoproterenol treatment and negative chronotropic effect after carbachol treatment could be observed, but the implications at whole construct level differed importantly from the electrically stimulated ones (**Figure 4.53A-B**). The increase in the beating rate caused a lack of coordination among cardiomyocytes composing the construct, leading to a loss of the synchronized beating

exhibited before applying the drug (**Figure 4.53A** and **Supplementary Video 4.15**). This indicated that control cardiac constructs had an inefficient cell-cell electrical coupling, which had been also suggested in the recording of spontaneous electrical activity due to the appearance of several ECG patterns and varying beating frequencies (**Figure 4.52**). Remarkably, a synchronized beating at the macroscale was recovered after carbachol treatment because of the decrease in the beating frequency (**Figure 4.53B** and **Supplementary Video 4.16**). Thus, results indicated that electrical stimulation was crucial for a functional excitation-contraction coupling, as stimulated constructs displayed improved electrical properties in comparison with control ones.

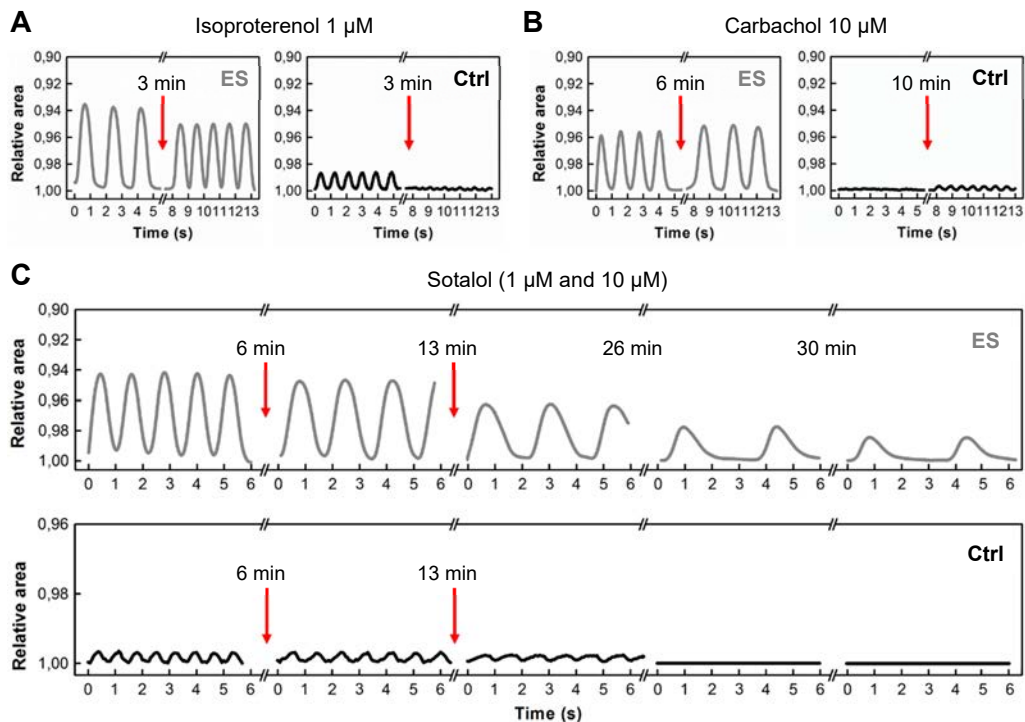


Figure 4.53. Chronotropic responses to pharmacological interventions of human cardiac constructs after 14 days of culture. Changes in the beat rate were analysed through custom MATLAB program. The area in pixels of each construct was obtained, and its oscillation was represented over time (relative to the highest number of pixels recorded). Red arrows indicate initiation of drug treatment and the incubation time at which the effect was observed. **A**, Positive chronotropic effect induced by the β -adrenergic agonist isoproterenol. **B**, Negative chronotropic effect induced by the muscarinic agonist carbachol. **C**, Negative chronotropic effect induced by the β -adrenergic antagonist sotalolol. Two concentrations were tested (first 1 μM and then 10 μM). Delayed repolarization due to QT interval prolongation was also analyzed. ES: electrically stimulated construct; Ctrl: control, non-stimulated construct.

To test the ability of our human cardiac construct to detect drug-induced cardiotoxicity, we incubated tissue constructs with two concentrations of sotalolol. Interestingly, cardiac constructs that had undergone electrical stimulation started to

display a reduction in beating frequency after 6 min of incubation with 1 μM sotalol (**Figure 4.53C**), which accounted for the adrenergic antagonist effect. However, and more importantly, a delayed repolarization started to be detected after 13 min of 10 μM sotalol incubation, which was reflected by a slower relaxation compared with previous timepoints (**Figure 4.53C**). After 30 min of incubation, a dramatic prolongation of the time of relaxation could be observed (**Figure 4.53C** and **Supplementary Video 4.17**). Regarding control cardiac constructs, a negative chronotropic effect could be detected over time of incubation with sotalol, but prolongation of the time of relaxation could not be addressed because the construct stopped beating (**Figure 4.53C** and **Supplementary Video 4.18**). Altogether, findings suggested that only electrically stimulated human cardiac constructs could be a promising tool for detecting drug-induced cardiotoxicity. However, video-optical recordings restricted the analysis of drug effects to affections of macroscopic contractile pattern. Therefore, to gather information about alterations in electrical propagation within the construct and to corroborate if the delayed repolarization was due to a QT interval prolongation, an electrophysiological recording of human cardiac constructs was needed.

To study the effects of pharmacological interventions on the electrophysiology of human cardiac constructs, a port for drug injection was installed within the perfusion bioreactor circuit (**Figure 3.13**). Then, isoproterenol, carbachol and sotalol were injected to the circuit and washed out following the same regimen than in video-optical recordings (for further details, see “3.7.3. Drug response analysis” section). Upon treatment with isoproterenol, electrostimulated cardiac constructs at day 14 of culture showed a statistically significant increment of the beating rate (**Figure 4.54A**). Accordingly, a statistically significant decrease of the beating rate upon treatment with carbachol was also observed (**Figure 4.54B**). Both findings were in accordance with the chronotropic effects of these drugs *in vivo*, as well as with results obtained from video-optical recordings (**Figure 4.53A-B**). Finally, drug-induced cardiotoxicity was assessed by treating cardiac tissue constructs with sotalol. In electrostimulated constructs, there was a regular decrease in beating frequency, which could be explained by sotalol action as adrenergic antagonist (**Figure 4.54C**). Although a similar effect was noted for control constructs, results were much more variable, and random increases and decreases in beating rate were found (**Figure 4.54D**). Importantly, electrophysiological recordings of electrostimulated cardiac constructs displayed typical features of arrhythmias, such as QRS skipping, prolongation of QT and RR intervals and regular blockades (**Figure 4.54C**). These features appeared progressively, and were more frequent over time of incubation, suggesting an increasing risk of arrhythmia. To our knowledge, this is the first time that cardiotoxic drug effects can be evidenced in thick 3D human cardiac tissue constructs acting as a whole. Importantly, the electrophysiological recording of control constructs did not show features of arrhythmias upon treatment with sotalol, probably owing to the worse electrical conduction within the construct (**Figure 4.54D**).

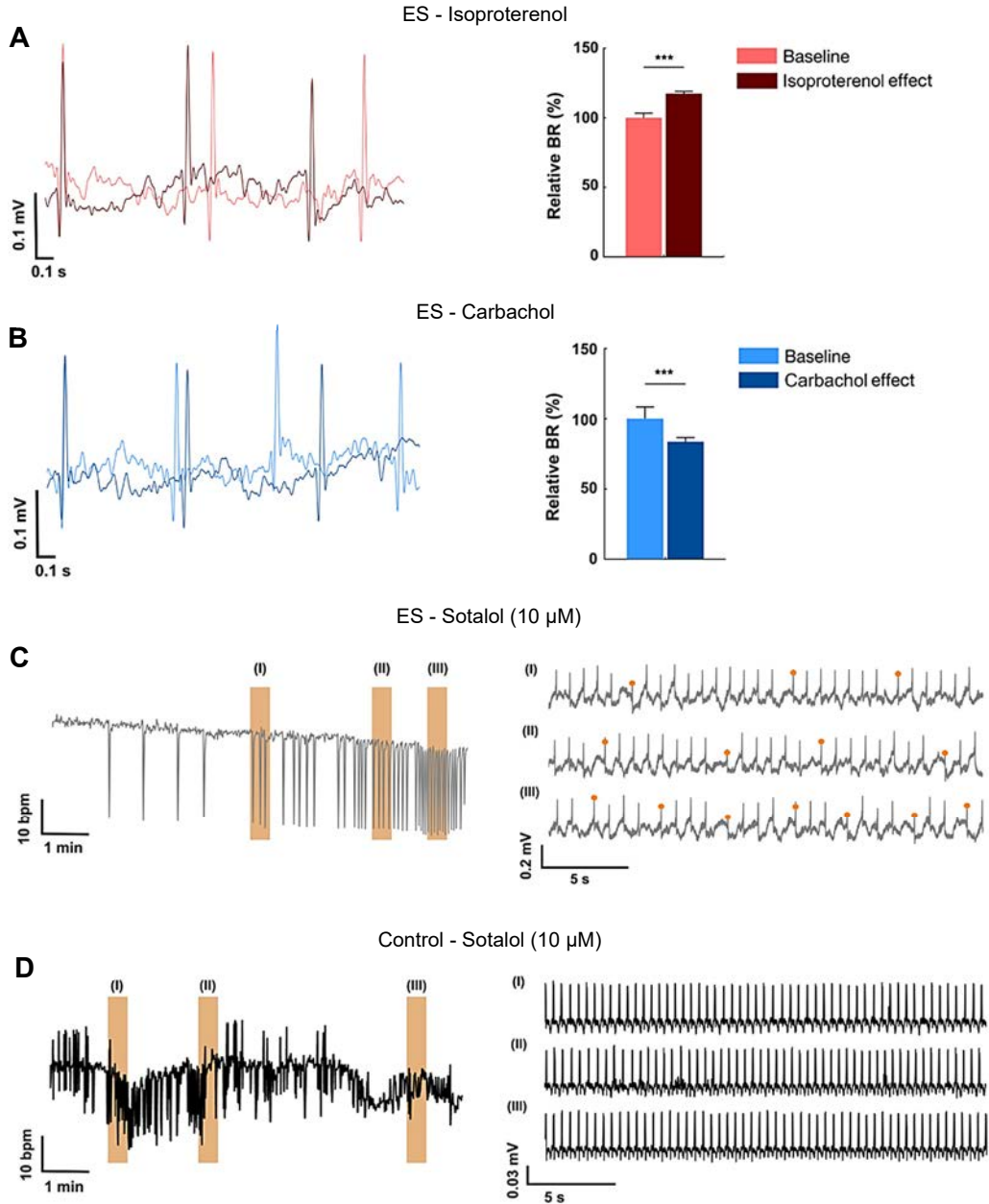


Figure 4.54. Effects of cardioactive drugs on the electrophysiology of human cardiac tissue constructs at day 14 of culture. Representative traces of ECG-like signals recorded for electrically stimulated (ES) constructs at baseline (first minute), and after isoproterenol (**A**) and carbachol (**B**) treatments (10 min incubation). Bar charts show the effect of isoproterenol and carbachol on beating rate (BR), relative to baseline. *** $p < 0.001$, Mann-Whitney U test. **C-D**, Instantaneous BR expressed as beats per minute (bpm) and representative traces of ECG-like signals for ES (**C**) and Control (**D**) constructs after treatment with 10 μ M sotalol. I, II, and III (brown shading) indicate the time lapse from which the traces of ECG-like signals have been obtained.

Taken together, results suggested that electrically stimulated human cardiac tissue constructs could be a promising tool for studying drug-induced cardiotoxicity. The regular and stable ECG-like signals allowed an objective and quantitative evaluation of drug effects on the electrophysiological activity of constructs. Moreover, and for the first time, typical features of arrhythmias could be detected upon treatment with sotalol in thick 3D human cardiac constructs. Therefore, our platform could be a valuable *in vitro* model of human cardiac tissue for preclinical cardiac toxicity studies.

5. DISCUSSION

Ischemic heart disease is one of the major causes of human death worldwide owing to the heart's minimal ability to repair following injury³. Other than heart transplantation, there are currently no effective or long-lasting therapies for end-stage heart failure^{168,171}. Therefore, it is crucial to develop not only alternative therapies that potentiate heart regeneration or repair, but also new tools to study human cardiac physiology and pathophysiology *in vitro*. In this context, cardiac tissue engineering is a promising strategy, as it aims at generating human cardiac tissue analogues that would open up new possibilities in the fields of drug discovery and toxicity testing, cardiac disease modelling, and regenerative medicine¹⁷².

The main aim of this thesis was to design and build a controlled flow perfusion bioreactor with appropriate biochemical and biophysical stimuli to obtain tissue-like human cardiac constructs. To date, the vast majority of studies that develop 3D cardiac tissue analogues using suitable biomimetic environments has been performed with rat^{282,297}, mouse²⁶⁰ and chick²⁶² cardiomyocytes. However, due to recent progress in the field of human stem cells, cardiac tissue engineering is moving away from animal-based approaches, facing the challenge of the production of human cardiac tissue constructs. Although major advances have been achieved^{50,277,319,410,418}, the generation of mature and thick 3D cardiac tissue constructs from human cells is still a challenge, which has been addressed in the present study.

The first challenge for engineering human cardiac tissue constructs is to secure an appropriate cardiomyocyte source in large quantities¹⁶⁴. Human pluripotent stem cells (hPSC), which comprise human embryonic stem cells (hESC)²⁶³ and human induced pluripotent stem cells (hiPSC)²⁶⁴, arguably possess the greatest potential for cardiac tissue engineering. They have an unlimited proliferation capacity while still retaining their pluripotency, and show robust cardiac differentiation potential. Moreover, they can differentiate into other cardiac cell types²⁰², and they have demonstrated to directly contribute to cardiac tissue in animal models of myocardial infarction^{210,211,213,214}. However, the clinical use of hESC is hampered by their immunogenicity, as well as by ethical and legal issues derived from their human embryonic origin^{474,475}. In turn, hiPSC circumvent the problems associated with hESC because they are derived from adult differentiated cells, and therefore constitute a promising cell source for cardiac tissue engineering. Moreover, hiPSC constitute a unique platform to obtain patient-specific cardiomyocytes for disease modelling²⁴⁸. In this study, two hiPSC lines (KiPS3F.7 and FiPS Ctrl1-mR5F-6) were successfully differentiated into functional cardiomyocytes using a serum-free monolayer culture system with modulators of canonical Wnt signaling pathway⁴³³. It has been reported that the differentiation potential of cell lines can differ from each other, or even between passages of the same line^{431,476}. This can account for the different percentages of cardiomyocytes obtained with our cell lines (44% for KiPS3F.7 *versus* 72% for FiPS Ctrl1-mR5F-6). As large numbers of

cardiomyocytes are needed to produce 3D cardiac tissue constructs, FiPS Ctrl1-mR5F-6 turned out to be the most suitable cell line, which demonstrated early, efficient and robust *in vitro* cardiogenesis. Nevertheless, preliminary experiments performed with KiPS3F.7 cell line were decisive to set the basis for human cardiac constructs development. We tested various differentiation protocols, and their rate of cardiac differentiation was assessed and optimized by generating a set of transgenic cell lines (work performed by Dr. Di Guglielmo⁴³¹ during her PhD thesis). Importantly, Brachyury (Bra) and α -myosin heavy chain (MHC) reporter cell lines helped us elucidating which differentiation stage and which cell population was appropriate for cardiac constructs generation. Although the supporting effect of human cardiac fibroblasts (HFF) in the formation and maturation of human cardiac constructs is well documented^{104,277,278}, co-culturing them with early mesoderm-committed cells did not promote cardiac differentiation or tissue formation in our study. Conversely, a co-culture of HFF and hiPSC-derived cardiomyocytes (hiPSC-CM) was capable to attach and survive in a 3D scaffold under perfusion of culture medium, suggesting that cells in more advanced differentiation stages were appropriate for human cardiac tissue constructs formation. In the literature, the vast majority of the studies pre-differentiate hiPSC into cardiomyocytes before generating tissue constructs^{319,410,418}, and biomimetic cell culture platforms improve their maturity level. Therefore, they support the hypothesis that our culture system could have a decisive role in improving maturation rather than differentiation of hiPSC-CM. However, some studies indicate that cues such as electrical stimulation, shear stress or substrate patterning influence hPSC differentiation into the cardiac lineage^{274,275,477}. Thus, optimizing culture conditions for hiPSC differentiation in our 3D culture system (e.g. adding electrical stimulation and lowering shear stresses at about 0.1 dyn/cm²⁴⁷⁷) could be an interesting goal for future investigations.

The use of hiPSC-CM in the study of human cardiac physiology and pathophysiology, as well as in regenerative medicine approaches is mainly limited by their immature phenotype. In comparison with human adult cardiomyocytes, hiPSC-CM display an immature, fetal-like phenotype. For example, they show underdeveloped and disorganized sarcomeres, heterogeneous shapes and smaller sizes, immature electrophysiological properties (e.g. higher resting membrane potentials, slow upstroke velocities and small action potentials), smaller forces of contraction and express typical fetal cardiac genes^{40,49,52}. In an attempt to induce hPSC-CM maturation, strategies that mimic native cardiac environment have been developed in the context of cardiac tissue engineering. The use of advanced 3D culture systems is believed to provide cells with important regulatory signals and cell-cell and cell-matrix interactions that are absent in standard 2D cultures. Therefore, the generation of 3D human cardiac tissue analogues would allow improving cardiomyocyte maturation, as well as obtaining information of the organization and function of cardiomyocytes at tissue level.

In this study, we have developed an advanced 3D culture system and followed the classical approach to tissue engineering, which involves seeding cardiac cells in biocompatible 3D scaffolds, and then culture the construct in a biomimetic signaling system, usually a bioreactor. Choosing an appropriate scaffold is decisive, as it provides cells with microenvironmental cues, mechanical support and architectural guidance. Such a scaffold should recapitulate important characteristics of the native cardiac extracellular matrix (ECM), including molecular composition, fibrillary structure and mechanical properties^{18,20}. As natural biomaterials have an excellent molecular composition for cell attachment, survival, and differentiation²⁹⁹, and motivated by the ability of collagen-based sponges to generate thick contractile tissue constructs^{281,297,318}, we selected Matriderm™ as a 3D scaffold. Matriderm™ is a commercial 3D collagen-based sponge currently used in clinics to support dermal regeneration, so it can be easily obtained from a reliable and reproducible source^{448,449}. According to manufacturer's datasheet, it is composed of native structurally intact collagen (types I, III and V) and elastin fibrils, which are basic components of cardiac ECM. Collagen typically gives the tissue its mechanical strength and stiffness, while elastin can provide elasticity and the ability to store elastic-strain energy³¹⁶. Specifically, collagen type I is the primary load-bearing protein in the heart, which transfers the force generated by cardiomyocytes, helps maintaining cardiomyocyte alignment, and provides passive tension during diastole^{66,478}. According to manufacturer's datasheet, the absence of chemical cross-linking of the collagen results in a matrix which is especially biocompatible, and has demonstrated low antigenicity. When implanted, Matriderm™ becomes fully degraded within 4 weeks in animal models, and within 6 weeks in humans. This can be considered an adequate lifespan for the scaffold to promote tissue repair, as cardiac tissue constructs implanted in rat infarcted hearts can engraft and improve cardiac function after ~1 month upon implantation^{278,282}. In addition, Matriderm™ promotes cell growth, supports the production of collagen matrix by fibroblasts, and is rapidly vascularized in human dermal regeneration processes⁴⁴⁹. Through Second Harmonic Generation (SHG) and two-photon excited fluorescence (TPEF) techniques, we could characterize that Matriderm™ was a complex matrix with thick collagen bundles (up to ~35 μm) and thinner elastin fibers (up to ~10 μm) in a net-like structure, interacting in an intricate manner and randomly distributed. Apart from biocompatibility and biodegradability, scaffold stiffness is an important parameter to take into consideration, as it affects the maturation, organization and functional behavior of cardiomyocytes^{296,294}. Mechanical analysis of excised cardiac tissue showed that the heart stiffens throughout development³⁷¹. For example, atomic force microscopy measurements revealed that embryonic/fetal murine heart tissue has a stiffness of 12 ± 4 kPa, while in neonates it is of 39 ± 7 kPa²⁹¹. This is in accordance with values obtained by means of uniaxial tension (embryonic/fetal: ~10 kPa; neonatal: ~20 kPa⁴⁷⁹) and micropipette aspiration (neonatal rat: 4.0 – 11.4 kPa; adult rat: 11.9 - 46.2 kPa³⁷⁵) measurements. Changes in tissue stiffness are accompanied by changes in

cardiomyocyte growth and function, and these phenomena are also observed when seeding cardiomyocytes in substrates with different stiffnesses. For example, neonatal rat ventricular myocytes cultured on a glass substrate (Young's Modulus ~50 GPa, about six orders of magnitude stiffer than rat myocardium) show decreased length to width ratios and increased stress fiber content compared to the ones seeded on substrates with Young's Modulus of 10 kPa⁴⁸⁰. In this study, Matriderm™ in hydrated conditions displayed a bulk stiffness of 0.19 ± 0.05 kPa when measuring at room temperature, and 0.06 ± 0.01 when measuring at 37°C. Those values are in agreement with the elastic modulus obtained for hydrated porous collagen-based scaffolds under uniaxial compression, as they are also around 0.2 kPa⁴⁵⁸. Soft bulk materials (~2 kPa) allow the generation of tissue constructs with greater contraction amplitudes and enhanced matrix deposition than stiffer ones²⁹⁶. However, literature shows conflicting reports because many works suggest that artificial substrates with stiffer bulk stiffness (10-50 kPa) enhance cardiomyocytes maturation⁴⁰, so it is an issue under debate. In any case, it is reasonably argued that biomaterials for *in vitro* applications of cardiac constructs can have very low stiffnesses, as long as cardiac cells can remodel it into a final product that is mechanically similar to the native myocardium²⁹⁰.

Apart from an appropriate scaffold, to obtain 3D cardiac tissue constructs that resemble myocardial tissue it is crucial to ensure an effective mass transport between cells and culture medium. Static cultures rely on diffusional transport mechanisms, which are efficient only within a superficial cell layer (~100-200 μm ⁴⁵⁹) and fail to support 3D tissues. Therefore, to improve oxygen and nutrients supply to cells cultured deep within the scaffold (>200 μm in depth), we have designed and built a perfusion bioreactor inspired in the pioneering work by Radisic and colleagues²⁹⁷. As an improvement to the mentioned work, we parallelized the perfusion bioreactor to allow the culture of multiple replicas of tissue constructs under the same physicochemical conditions and from the same pool of cells. This is important to obtain comparable tissue constructs, as it reduces the variability associated to rat cardiomyocytes isolation⁴⁸¹ or passages and differentiation potential of hiPSC⁴³¹ between different experiments. Perfusion of culture medium has demonstrated to potentiate cell survival within cardiac tissue constructs with high cell densities and optimal architecture^{398,467}. An important issue to take into account when culturing cells under perfusion is the shear stress to which they will be subjected³⁹⁸. It has been reported that physiological shear stress values improve cardiac cell-cell interaction and myofibrillar organization, whereas higher values (over 2.4 dyn/cm^2) have deleterious effects on cell survival⁴⁰⁴. In our 3D culture system, we estimated the minimum flow rate that should be applied for our 1 mm thick rat and human cardiac tissue constructs by taking into account their oxygen consumption rates (neonatal rat cardiomyocytes: 0.29 $\text{pmol}/\text{h}\cdot\text{cell}$; hiPSC-CM: 0.71 $\text{pmol}/\text{h}\cdot\text{cell}$ ²⁹), and the porosity and pore diameter of Matriderm™ scaffold (94%^{447,448} and 17 μm , respectively). For rat cardiac constructs, a flow rate of 0.1 ml/min

should be applied, whereas for hiPSC-CM it should be of 0.2 ml/min. Those flow rates evoke a shear stress of 0.66 dyn/cm² for rat cardiac constructs, while for human cardiac constructs it is of 1.32 dyn/cm². When culturing rat cardiac cells under shear stresses ranging from 0.05 to 1.5 dyn/cm², compact and contractile cardiac constructs with high expression of cardiac proteins (e.g. connexin 43) can be obtained³⁵⁰. Therefore, the calculated shear stresses were considered suitable for cardiomyocytes culture. Their adequacy was confirmed in preliminary cellular tests, as thick and contractile tissue constructs containing elongated cardiomyocytes and expressing cardiac markers could be obtained.

Cell seeding into our 3D scaffold was the first step towards the generation of thick cardiac constructs. Initial cell density has great influence on viability, mechanical integrity and functionality of the engineered cardiac tissue, and cells should be uniformly distributed for homogeneous tissue development^{403,459,463,464}. In this study, we evaluated the efficiency and cell distribution of two seeding methodologies: static seeding using Matrigel® as cell delivery vehicle and perfusion seeding using a perfusion loop. Although cell retention using static seeding was possible, cardiac cells were unable to attach and penetrate into the scaffold, as they remained embedded into the hydrogel even after 4 days of culture under perfusion. In addition, cardiomyocytes displayed round morphologies instead of elongated, indicating that static seeding was not suitable for our purposes. However, some studies reported the generation of thick and compact tissue constructs through its use^{281,297,324}. An explanation to this could be the different pore size of the scaffolds, as Matrigel™ pores range from 5 to 90 µm whereas in the mentioned studies they range from 20 to 200 µm, with Matrigel™ mean pore size being about three times smaller (17 µm versus 51 µm⁴⁸²). Therefore, we assayed the suitability of perfusion seeding, as it has been reported to be superior regarding cell seeding efficiency and homogeneity in 3D porous scaffolds^{398,403}. By applying one-way perfusion of culture medium at 1 ml/min, high cell numbers could be retained throughout the whole scaffold in a rather homogeneous way, confirming that the absence of a carrier hydrogel facilitated deeper cell penetration and attachment to the scaffold. This could be partially attributed to the size of Matrigel™ pores respect to cardiomyocytes size in suspension (17 µm and 10 µm⁴⁶⁵, respectively), and by the fact that pores were interconnected following a tortuous pathway, permitting cell retention inside the scaffold when passing through it.

Environmental cues are key determinants of cardiomyocyte phenotype and function, and regulate their capacity to form functional tissue units¹⁸. Therefore, to obtain 3D cardiac tissue constructs that resemble myocardial tissue, not only an appropriate scaffold and an effective mass transport are necessary, but also providing cells with relevant physical stimuli. For this, bioreactors are widely used as experimental platforms for investigating *in vitro* tissue formation and maturation^{396,397}. Taking this into

consideration, to obtain thick human cardiac constructs we have assembled and characterized a parallelized perfusion bioreactor including electrical stimulation, as perfusion and electrical pacing is a combination of signals that has hardly been explored^{288,407,408}.

Electrical stimulation was built into the culture system since it is a well-known regulatory signal that favors cardiomyocytes maturation and contractility within cardiac tissue constructs^{318,319}. To date, electrical stimulation has demonstrated to induce the establishment of synchronous contractions within cardiac tissue constructs, as it affects rate, duration and number of action potentials within cardiomyocytes³⁷¹. Accordingly, cardiomyocyte alignment and ultrastructural organization has also been reported to increase when 3D cardiac tissue constructs undergo electrical stimulation²⁸¹. In the absence of commercial systems to include the delivery of electrical impulses to the bioreactor, we designed and fabricated three prototypes of the perfusion chamber incorporating two graphite electrodes. We used carbon rod electrodes because they show high resistance to corrosion, are biocompatible and were found to have the best charge transfer characteristics for cardiac tissue engineering when compared with stainless steel, titanium and titanium nitride electrodes^{387,388}. One important issue to determine before fabricating the chamber was the diameter of the electrodes and their position with respect to the construct to deliver a homogeneous electric field. By formulating an electric field model, we determined that graphite electrodes of 4.6 mm in diameter separated 1 cm from each other generated a nearly homogeneous electric field and current density within our construct (maximum difference of 85 V/m and 125 A/m²). This difference was considered negligible, as previous works could obtain tissue constructs with improved calcium handling when having electric fields with comparable values dispersion³¹⁹. Moreover, the magnitude of the electric field (400 to 485 V/m) was within the recommended values for cardiac cells stimulation^{281,333,387,408}, so the designed configuration was considered suitable for the stimulation of cardiac tissue constructs. Concerning the fabrication of the perfusion chamber including electrical stimulation, precision machining of polypropylene (PP) plastic turned out to be the most suitable in terms of watertightness and cell culture capabilities. Precision machining allowed us obtaining solid parts without leakage problems, and PP demonstrated to be autoclavable, ethanol resistant and highly biocompatible. Moreover, the design allowed a proper delivery of rectangular pulses at 3 Hz of frequency, 2 ms of duration and 5 V of amplitude throughout the geometry, with measured voltage values in agreement with the ones predicted by the electric field model. Finally, cells could survive and were capable of generating tissue constructs inside the prototype, thus corroborating its suitability as a cell culture platform to electrically stimulate cardiac tissue constructs.

Through the use of our advanced 3D culture system, we have been able to generate functional an appreciably mature cardiac tissue constructs from neonatal rat

heart cells and human induced pluripotent stem cells-derived cardiomyocytes (hiPSC-CM). Specifically, our results indicate that perfusion of culture medium combined with electrical stimulation allows obtaining thick, tissue-like human cardiac tissue constructs. Although recent works indicate a marked trend in the field of cardiac tissue engineering towards miniaturization (e.g. generation of hPSC-derived cardiac microtissues and microphysiological systems), the production of 3D tissue-like human cardiac tissue constructs is still recognized as a challenge. Therefore, the work developed in this thesis has demonstrated to be useful to meet that purpose, as thick 3D human cardiac tissue constructs with tissue-like functionality have been successfully generated.

Electrical stimulation improved the structural organization, alignment and coupling of cardiomyocytes in our cardiac tissue constructs. Moreover, electrical stimulation promoted the formation of synchronous contractile constructs at the macroscale with an improved electrophysiological function. This is in line with previous studies, where electrical stimulation alone or in combination with mechanical loading also resulted in improved maturation of hPSC-CM in microtissues or cell aggregates^{319,329,333,337,412}. However, this has not been reported for thick 3D human cardiac tissue constructs. Moreover, we observed that the beneficial effects of electrical stimulation became much more evident over time in culture, agreeing with previous studies in 2D cultures and cell sheets where long-term culture improved hPSC-CM maturation at ultrastructural and electrophysiological levels^{63,65,334}. In the following paragraphs, we will discuss in detail specific outcomes of our cardiac tissue constructs.

When electrically stimulating cardiomyocytes in 3D structures, it is important to determine the stimulation regime that will be delivered. Generally, monophasic or biphasic square-wave pulses with amplitudes ranging from 2 to 6 V/cm and durations from 1 to 2 ms are applied. It has been reported that monophasic pulses avoid the possible undesirable effect of biphasic pulses in inhibiting action potentials³⁹³, while biphasic pulses have a reversal phase to avoid adverse electrochemical processes due to stimulating pulses³⁸⁴. However, the vast majority of adverse chemical reactions are prevented when applying relatively short pulses (2 ms) with relatively long time between pulses (frequencies \sim 1 Hz), thus suggesting monophasic pulses as the best option. Moreover, 1-2 ms is a sufficiently long pulse to excite cells³¹⁸. Regarding the optimal frequency for cardiac tissue constructs stimulation, there is still no clear consensus. For rat cardiac tissue constructs it is well accepted that mimicking rat heart rate is preferably, and although many studies use 1 Hz of frequency^{281,407}, 3 Hz has been proposed as the most suitable³⁸⁷. For human cardiomyocytes, some studies use a physiological pulse rate of 1 Hz to mimic human adult heart rate, but higher stimulus frequencies seem to improve structural and functional maturation of human 3D cardiac tissue constructs^{319,337}. Nevertheless, a recent study indicates that 3D aggregates of hPSC-CM adapt their autonomous beating rate to the frequency at which they are

stimulated³³³. In this context, we have selected a stimulation regime comprising monophasic square-wave pulses of 4.6 V/cm in amplitude and 2 ms of duration. For neonatal rat cardiomyocytes we selected 3 Hz of frequency, whereas for hiPSC-CM we selected 1 Hz of frequency. These parameters have demonstrated to be suitable for simulating each culture, as they have promoted the generation of functional and organized cardiac tissue constructs with an increased maturation level compared with non-stimulated ones.

In vivo, cardiomyocytes orientate their intracellular contractile apparatus and align with neighboring cells to facilitate fast electrical conduction and efficient muscle contraction³⁶⁸. When isolated from the heart tissue, cardiomyocytes lose many of their surface channels and receptors, disassemble their myofibrillar structure and acquire round shape³³⁶. It has been demonstrated that cardiomyocytes can recover some features of native myocardium if forced to adopt an anisotropic morphology *in vitro*, thus improving their maturation⁴⁸³. When cardiomyocytes are anisotropically aligned, there is an increase of conduction velocity in the longitudinal direction due to the formation of appropriate intercalated discs, and sarcomere alignment is also potentiated^{40,362}. To reestablish cardiomyocytes shape and structure *in vitro*, regulatory signals such as substrate patterning, mechanical stimulation or electrical stimulation can be applied. Although topographical cues are stronger regulators of cellular orientation than electric field stimulation, cell elongation and alignment in the direction of the electric field has also been reported^{281,484}. In constructs produced from neonatal rat cardiac cells, electrical stimulation induced cell alignment and coupling²⁸¹, and electrically stimulated human microtissues exhibited a better muscular network of aligned cardiomyocytes than non-stimulated ones³³⁷. Our results not only are in accordance with those observations, but also achieve to demonstrate the effects of electrical stimulation on thick 3D human cardiac tissue constructs. Rat and human cardiac tissue constructs that had undergone electrical stimulation displayed cardiomyocytes aligned in the direction of the electric field. Interestingly, this alignment was preserved along the entire length of the construct (~1 cm), and was particularly evident in the most superficial layers. Although some features of native myocardium were not fully reproduced in our human cardiac tissue constructs (e.g. internal organization, cellular arrangement and hypertrophy degree), cardiomyocytes contained highly organized and oriented myofibers when electrostimulated. Moreover, electrical pacing influenced cell distribution at the macroscale, as cells concentrated in the region of the scaffold delimited by the stimulating electrodes.

Apart from elongation and alignment, electrical conditioning of cardiac tissue constructs promotes other morphological and functional improvements on cardiomyocytes. Electrical stimulation promotes cardiomyocyte ultrastructural organization, hypertrophy, excitability, and electrical coupling³⁷⁸. Specifically, at

ultrastructural level, stimulated neonatal rat cardiomyocytes show centrally positioned and elongated nucleus, abundant mitochondria between myofibrils and long, well aligned registers of sarcomeres containing visible M-lines, Z-discs and H, I and A bands. Moreover, morphometric analysis reveal that stimulated constructs have a sarcomere volume fraction comparable to neonatal rat ventricles, and display frequent intercalated discs positioned between aligned Z-discs and well-developed gap junctions²⁸¹. Similarly, electrical conditioning of human cardiac tissue constructs promotes various morphological improvements. However, electrical stimulation is usually experimentally associated to mechanical loading, so their individual contributions cannot be fully established. It has been reported that electrical stimulation increases cardiomyocyte area, the number of H zones and I bands per Z-disc and the number of Z-discs. In addition, the number of mitochondria and desmosomes are increased, as well as the proximity of mitochondria to the contractile apparatus and the development of nascent intercalated discs³¹⁹. In our study, myofibrils with organized and well-developed sarcomeres were more frequently found in the electrically stimulated constructs compared with controls. Moreover, electrostimulated constructs displayed advanced specialized intercellular unions such as intercalated discs, desmosomes and gap junctions, whereas in control constructs they were less developed. Interestingly, both rat and human cardiomyocytes that had undergone electrical stimulation displayed a significant increase in sarcomere width in comparison with non-stimulated constructs, meaning that myofibrillar bundles formation was promoted⁶². Besides, sarcomere width is associated with uniform and synchronous contractions, as they maintain the alignment of parallel filaments and hold adjacent sarcomeres in register during twitch contraction⁴⁸⁵. However, comparing exact values of sarcomeric widths between different studies is difficult due to the absence of standardized measuring techniques. Although the lack of structures such as H-bands, M-lines and T-tubules indicate an absence of terminal differentiation, our results suggest that electrical stimulation improves the ultrastructural organization of cardiomyocytes in thick 3D human cardiac tissue constructs.

Constructs that undergo electrical stimulation progressively develop conductive and contractile properties of cardiac tissue. Electrical stimulation improves the electrical properties of tissue constructs with respect to control ones, as it decreases excitation threshold (ET)^{319,322}, increases maximum capture rate (MCR)^{281,319,329}, and increases electrophysiological parameters such as conduction velocity (11.5-18.5 cm/s), I_{Kr} current and I_{K1} density³¹⁹. In addition, electrical stimulation improves Ca^{2+} handling properties of the constructs, as it increases Ca^{2+} transient amplitude and release rate, decreases time to peak amplitude and time to baseline, and increases the sensitivity to pharmacological agents such as caffeine and thapsigargin³¹⁹. Regarding contractile behavior, electrical stimulation induces synchronous macroscopic contractions and increases contraction amplitudes. Specifically, electrical pacing significantly increased

the fractional area change (FAC) of neonatal rat cardiac tissue constructs, with 4-fold higher amplitudes respect to non-stimulated ones²⁸¹. The results obtained with our advanced 3D bioreactor system are in line with these observations, as electrical stimulation improved both rat and human cardiac tissue constructs beating synchrony and coupling at the macroscale. Although our control and electrically stimulated constructs did not show statistically significant differences in ET and MCR parameters, a trend towards lower ETs and higher MCRs could be observed for electrically stimulated ones. Importantly, electrostimulated neonatal rat cardiac tissue constructs displayed 4-fold higher contraction amplitudes than control ones, and in human cardiac tissue constructs the difference increased up to 6- to 12-fold. Strikingly, during spontaneous beating, we could register maximum FACs of 14% in human electrically stimulated constructs after 14 days of culture. Those results illustrate, for the first time to our knowledge, the dramatic effect of electrical stimulation on macroscopic contraction amplitudes of human cardiac tissue constructs. We attribute these effects to the effective alignment and coupling of cardiomyocytes in the direction of the electric field, as human cardiac constructs that had undergone electrical stimulation beat in an oriented manner and exerted higher strain per contraction than control ones. In future experiments, it would be interesting to evaluate parameters related to Ca²⁺ handling (e.g. incubation with calcium sensitive dyes such as fluo-4 AM), action potential propagation through the construct (e.g. incubation with voltage sensitive dyes such as Di-4-ANEPPS), and construct contractile force. However, technical issues (e.g. microscope focal distance or having a setup to fix the sample and monitor construct outcomes) would have to be addressed.

Whole-genome expression analyses have revealed strong effects of electrical stimulation on global gene expression, both in rat and human cardiomyocytes^{333,337}. Specifically, downregulation of the fetal cardiac gene program and upregulation of cardiac structural (e.g. *MYH7* and *TNNT2*) and ion channel genes (e.g. *KCNJ2*, *KCNH2* and *GJA5*) has been reported, although not always with significant differences^{319,333,337}. In our study, although overall expression values differed importantly from adult heart tissue, the expression of cardiac specific genes increased considerably with time of culture, and more importantly when culturing cells in our advanced 3D culture system compared with time-matched 2D cultures. No statistical significant differences between control and electrostimulated constructs were detected, but there was a trend towards an enhanced expression of some maturity-related cardiac genes (e.g. *MYH7*, *TNNT2*, *GJA1* and *SERCA2A*) in electrically stimulated human cardiac constructs. The lack of significance could be partially explained by the fact that hPSC-CM are often a mixture of atrial and ventricular cardiomyocytes, which can affect the expression levels of proteins such as MHC and MLC^{63,79}.

To evaluate the functionality of human cardiac tissue constructs, the analysis of ion currents and electric conduction is decisive. As such, electrophysiological markers are among the most useful to evaluate proarrhythmia when hPSC-CM are treated with pharmacological agents²⁴⁴, and allow the characterization of hPSC-CM maturity level⁴¹⁹. To date, action potentials in cardiac tissue constructs are mainly recorded on a representative cell population at the time of seeding²⁷⁷ or on isolated cardiomyocytes after tissue formation^{50,319} through intracellular recordings (e.g. patch clamp) or microelectrode arrays (MEA). To evaluate the functionality of intact engineered cardiac tissues, current methodologies mostly include video-optical recordings of constructs beating, so parameters such as response to electrical pacing or drug treatments are restricted to affections in contractile pattern⁵⁰. This implies a lack of direct measurements of electrophysiological parameters such as action potential amplitude, duration, Ca²⁺ handling properties or cardiomyocyte coupling within tissue constructs. In this study, we report for the first time to our knowledge an electrophysiological recording system that provides information about the electrical activity of intact thick 3D cardiac tissue constructs in real time. Specifically, the combination of action potentials generated by hiPSC-CM composing cardiac constructs produce ECG-like signals, which could be monitored online. Although both electrically stimulated and control tissue constructs displayed waveforms including QRS complex and T wave, control ones showed lower and wider QRS complexes compared with stimulated ones. This indicated that electrical stimulation improved electrophysiological properties of cardiac constructs, such as conduction velocity, Ca²⁺ handling, and hiPSC-CM coupling and synchrony, being in accordance with previous single-cell recordings from dissociated constructs³¹⁹. Importantly, in electrostimulated constructs the ECG-like signal maintained a time-invariant shape and a significantly more stable beating rate than non-stimulated cardiac constructs. Therefore, electrically stimulated cardiac constructs appear as the best option to obtain cardiac tissue analogues, which could be used to repair the damaged myocardium or as human *in vitro* models for drug testing and disease modelling.

To verify the usefulness of electrically stimulated cardiac constructs as an *in vitro* model of human myocardium, the effect of cardioactive drugs was tested. To that end, a drug injection port was installed within the bioreactor, and isoproterenol (β -adrenergic agonist), carbachol (cholinergic agonist) and sotalol (hERG potassium channel blocker) were delivered to the constructs. Measuring changes in beating rate and QRS shape in real time allowed estimating the effect of the drugs in a tissue-like human cardiac model. Constructs that had undergone electrical stimulation significantly increased their beating rate when incubated with isoproterenol, and decreased it when incubated with carbachol, thus indicating functional adrenergic and cholinergic systems that affected global construct behavior. To test the ability of human cardiac constructs to detect drug-induced cardiotoxicity, we used the standard QT prolonging drug sotalol, as it has high proarrhythmic risk²⁴⁴. Cardiac toxicity is an issue of immense significance for patients,

pharmaceutical industry and regulatory organizations, as an estimated ~45% of all withdrawals and ~30% of restrictions to drug use are due to unexpected negative cardiovascular events²³³. Interestingly, when our electrically stimulated constructs were treated with sotalol, a regular and progressive decrease in heart rate was observed, which could be explained by sotalol action as adrenergic antagonist. Although a similar effect was noted for our control cardiac constructs, the results were much more variable (e.g. random increases and decreases in beating rate), probably owing to the worse electrical conduction of action potentials within the construct. More importantly, the electrophysiological recording of electrically stimulated cardiac constructs displayed typical features of arrhythmias, such as QRS skipping, prolongation of RR intervals, and regular blockades. Moreover, these features tended to increase over time of incubation with the drug, suggesting the possibility to detect drug-induced arrhythmias in stimulated cardiac tissue constructs. To the best of our knowledge, this is the first time that cardiotoxic drug effects can be evidenced in thick 3D cardiac tissue constructs acting as a whole. Thus, our electrostimulated human cardiac constructs are a promising tool for cardiac toxicity studies that can help bridging the gap between *in vivo* and *in vitro* studies. There are some drug candidates that give *in vivo* QT results that are inconsistent with the findings in *in vitro* electrophysiological studies¹²⁷. One example of this inconsistency is sotalol, which prolongs QT *in vivo* much more than the expected from its 50% inhibitory concentration (IC₅₀) for hERG channel current *in vitro*⁴⁷³. The main reasons for this discrepancy may be that *in vitro* safety screens are based on hERG channel assays in non-cardiac cell lines, and drug-induced QT prolongation can be mediated by ion channels other than hERG. In addition, some compounds can affect multiple ion channels, so hERG assays alone are limited and non-representative to predict drug effects⁴²⁷. Although platforms such as hESC-CM clusters, microphysiological systems and microtissues have been capable to detect cardiotoxicity to some extent, they present problems such as variability in cell response or complete arrest of constructs contraction when treated with drugs^{12,317,415,427,486}. Therefore, our platform is an advantageous *in vitro* evaluation system, as it is constituted by human cardiomyocytes that express multiple ion channels and function as a syncytium in a regular and stable manner. Although the true predictive value of this method for toxicology studies needs to be assessed with larger series of proarrhythmic and safe drugs, the system developed in this study holds great promise as a tool for cardiac toxicity studies. The fact that our stimulated human cardiac tissue construct demonstrated a dramatic response to a drug that showed discrepancies between *in vivo* and *in vitro* studies, strengthens the capabilities of our platform in predicting cardiotoxicity. Moreover, ECG-like signals allow the evaluation of drugs by using classical electrophysiological measurements in clinics, such as heart rate variability, RR interval or QRS complex shape, so our platform could be highly valuable in assessing the effect of arrhythmic drugs in an objective and quantitative manner.

Taken together, our results indicate that the advanced 3D culture system developed in this study allows generating and monitoring human cardiac tissue constructs with tissue-like functionality. Medium perfusion in combination with electrical stimulation and collagen-based porous scaffold improves the structural and functional maturation of cardiomyocytes. Importantly, in this advanced 3D culture system, cardiomyocytes couple to form macroscopic constructs that contract synchronously and display improved electrophysiological functions. Finally, the capability of stimulated human cardiac tissue constructs to respond to cardiotoxic drugs makes it a promising tool in drug discovery and toxicity testing. Despite the important contribution of this work to cardiac tissue engineering field, reaching a fully adult phenotype of cardiomyocytes remains a challenging task, and maturation continues to be an area of active research. The lack of standardized methodologies to stimulate cardiomyocytes and assess their maturation level, together with the lack of consensus to what constitutes a mature cardiomyocyte complicate comparisons between studies and are hindrances to advancement. Therefore, it is necessary to establish standard operating procedures, assays and maturation readouts to achieve consistency, efficiency, reproducibility and high-throughput. Although the body of data regarding human cardiac tissue constructs production is not immense, discoveries and achievements over the past years and current worldwide efforts signal continued progress. A shift from the bench to the clinic may be on the horizon, but success will depend on how effectively and how efficiently engineering and biology can be integrated to create surrogates and/or *in vitro* models of human cardiac tissue.

6. CONCLUSIONS

- 1.** The parallelized perfusion bioreactor system developed in this thesis can successfully generate thick 3D cardiac tissue constructs. Perfusion ensures an effective mass transport between cells and culture medium, and parallelization allows culturing multiple replicas of the constructs. The design, fabrication and characterization of the perfusion chamber including electrical stimulation allows the production of functional and structurally organized cardiac constructs from rat and human cardiac cells. Moreover, the prototype is appropriate to monitor the electrical activity of cardiac constructs in real time.
- 2.** Perfusion of culture medium combined with electrical stimulation leads to the generation of more mature cardiac tissue constructs than perfusion alone. Electrical stimulation improves the structural organization, alignment and coupling of cardiomyocytes, and promotes the formation of synchronous contractile constructs at the macroscale. Moreover, the beneficial effects of electrical stimulation on the maturity of human cardiac constructs becomes more evident over time in culture.
- 3.** In this study, we report for the first time to our knowledge an electrophysiological recording system that provides information about the electrical activity of intact 3D cardiac tissue constructs in real time. Specifically, the combination of action potentials generated by human induced pluripotent stem cell-derived cardiomyocytes composing cardiac constructs produce ECG-like signals, which can be monitored online.
- 4.** Electrically stimulated human cardiac constructs display a time-invariant QRS shape, higher and narrower QRS complexes and significantly more stable beating rate than in control ones, suggesting improved electrophysiological functions. Moreover, constructs that had undergone electrical stimulation display typical features of arrhythmias upon treatment with sotalol. To the best of our knowledge, this is the first time that cardiotoxic drug effects can be evidenced in thick 3D human cardiac tissue constructs acting as a whole.
- 5.** Taken together, results demonstrate that the advanced 3D culture system developed in this study allows generating and monitoring human cardiac tissue constructs with tissue-like functionality. Medium perfusion in combination with electrical stimulation and collagen-based porous scaffold promotes the structural and functional maturation of cardiomyocytes. Finally, the capability of stimulated human cardiac tissue constructs to respond to cardiotoxic drugs makes it a promising tool for drug discovery and toxicity testing.

7. REFERENCES

1. Eisenberg LM, Markwald RR. Cellular recruitment and the development of the myocardium. *Dev. Biol.* 274, 225–232 (2004).
2. Buckingham M, Meilhac S, Zaffran S. Building the mammalian heart from two sources of myocardial cells. *Nat. Rev. Genet.* 6, 826–835 (2005).
3. Vunjak-Novakovic G, Lui KO, Tandon N, Chien KR. Bioengineering heart muscle: a paradigm for regenerative medicine. *Annu. Rev. Biomed. Eng.* 13, 245–67 (2011).
4. Weinhaus A, Roberts K. *Anatomy of the Human Heart*. in *Handbook of Cardiac Anatomy, Physiology, and Devices* (ed. Iuzzo, P.) 71–96 (Springer, 2009).
5. Vunjak-Novakovic G, Tandon N, Godier A, Maidhof R, Marsano A, Martens TP, Radisic M. Challenges in cardiac tissue engineering. *Tissue Eng. Part B. Rev.* 16, 169–87 (2010).
6. Buckberg GD. Basic science review: The helix and the heart. *J. Thorac. Cardiovasc. Surg.* 124, 863–883 (2002).
7. Akhyari P, Kamiya H, Haverich A, Karck M, Lichtenberg A. Myocardial tissue engineering: the extracellular matrix. *Eur J Cardiothorac Surg* 34, 229–241 (2008).
8. Torrent-Guasp F, Buckberg GD, Clemente C, Cox JL, Coghlan HC, Morteza G. The Structure and Function of the Helical Heart and Its Buttress Wrapping. I. The Normal Macroscopic Structure of the Heart. *Semin Thorac Cardiovasc Surg* 13, 301–319 (2001).
9. Paulsen F, Waschke J. *Sobotta Atlas of Human Anatomy*. (Elsevier, 2011).
10. Vliegen HW, van der Laarse A, Cornelisse CJ, Eulderink F. Myocardial changes in pressure overload-induced left ventricular hypertrophy. *Eur. Heart J.* 12, 488–94 (1991).
11. Camelliti P, Borg TK, Kohl P. Structural and functional characterisation of cardiac fibroblasts. *Cardiovasc. Res.* 65, 40–51 (2005).
12. Amano Y, Nishiguchi A, Matsusaki M, Iseoka H, Miyagawa S, Sawa Y, Seo M, Yamaguchi T, Akashi M. Development of vascularized iPSC derived 3D-cardiomyocyte tissues by filtration Layer-by-Layer technique and their application for pharmaceutical assays. *Acta Biomater.* 33, 110–121 (2016).
13. Adler C, Ringlage W, Böhm N. DNS-Gehalt und Zellzahl in Herz und Leber von Kindern. *Pathol Res Pr.* 172, 25–41 (1981).
14. Bers D. *Excitation-Contraction Coupling and Contractile Force*. (Springer Netherlands, 2001).
15. Xin M, Olson EN, Bassel-Duby R. Mending broken hearts: cardiac development as a basis for adult heart regeneration and repair. *Nat Rev Mol Cell Biol* 14, 529–541 (2013).
16. Laske T, Shrivastav M, Iuzzo P. *The cardiac conduction system*. in *Handbook of Cardiac Anatomy, Physiology, and Devices* (ed. Iuzzo, P.) 159–175 (Springer, 2009).
17. Fozzard H. Excitation-contraction coupling in the heart. *Adv. Exp. Med. Biol.* 308, 135–42 (1991).
18. Lanza R, Langer R, Vacanti JP. *Principles of Tissue Engineering*. (Elsevier Academic Press, 2014).
19. Rienks M, Papageorgiou AP, Frangogiannis NG, Heymans S. Myocardial extracellular matrix: An ever-changing and diverse entity. *Circ. Res.* 114, 872–888 (2014).
20. Christalla P, Hudson JE, Zimmermann W-H. The cardiogenic niche as a fundamental building block of engineered myocardium. *Cells. Tissues. Organs* 195, 82–93 (2012).
21. Weber KT. Cardiac interstitium in health and disease: The fibrillar collagen network. *J. Am. Coll. Cardiol.* 13, 1637–1652 (1989).
22. Giudicessi JR, Ackerman MJ. Potassium-channel mutations and cardiac arrhythmias - diagnosis and therapy. *Nat Rev Cardiol* 9, 319–332 (2012).
23. Nerbonne JM, Kass RS. Molecular physiology of cardiac repolarization. *Physiol Rev* 85, 1205–1253 (2005).

REFERENCES

24. Fabiato A. Calcium-induced release of calcium from the cardiac sarcoplasmic reticulum. *Am. J. Physiol.* 245, C1–C14. (1983).
25. Ferrini B, Fossa AA. The impact of drug-induced QT interval prolongation on drug discovery and development. *Nat. Rev. Drug Discov.* 2, 439–447 (2003).
26. Severs NJ. The cardiac muscle cell. *Bioessays* 22, 188–99 (2000).
27. Iyer RK, Chiu LLY, Reis L a, Radisic M. Engineered cardiac tissues. *Curr. Opin. Biotechnol.* 22, 706–14 (2011).
28. Carrier RL, Rupnick M, Langer R, Schoen FJ, Freed LE, Vunjak-Novakovic G. Effects of oxygen on engineered cardiac muscle. *Biotechnol. Bioeng.* 78, 617–25 (2002).
29. Sekine K, Kagawa Y, Maeyama E, Ota H, Haraguchi Y, Matsuura K, Shimizu T. Oxygen consumption of human heart cells in monolayer culture. *Biochem. Biophys. Res. Commun.* 452, 834–839 (2014).
30. Ho SY. Anatomy and myoarchitecture of the left ventricular wall in normal and in disease. *Eur. J. Echocardiogr.* 10, 3–7 (2009).
31. Bird SD, Doevendans PA, Van Rooijen MA, Brutel De La Riviere A, Hassink RJ, Passier R, Mummery CL. The human adult cardiomyocyte phenotype. *Cardiovasc. Res.* 58, 423–434 (2003).
32. Gerdes A, Kellerman S, Moore J, Muffly K, Clark L, Reaves P, Malec K, McKeown P, Schocken D. Structural remodeling of cardiac myocytes in patients with ischemic cardiomyopathy. *Circulation* 86, 426–430 (1992).
33. Barnett V. *Cellular myocytes.* in *Handbook of Cardiac Anatomy, Physiology, and Devices* (ed. Iuzzo, P.) 147–158 (Springer, 2009).
34. Peters NS, Green CR, Poole-Wilson P a., Severs NJ. Reduced content of connexin43 gap junctions in ventricular myocardium from hypertrophied and ischemic human hearts. *Circulation* 88, 864–875 (1993).
35. Mescher AL. *Junqueira's Basic Histology: Text and Atlas.* (The McGraw-Hill Companies, Inc, 2013).
36. Hirschy A, Schatzmann F, Ehler E, Perriard J-C. Establishment of cardiac cytoarchitecture in the developing mouse heart. *Dev. Biol.* 289, 430–41 (2006).
37. Forbes M, Sperelakis N. Intercalated discs of mammalian heart: a review of structure and function. *Tissue Cell* 17, 605–48 (1985).
38. Noorman M, van der Heyden MAG, va Veen TAB, Cox MGPJ, Hauer RNW, de Bakker JMT, va Rijen HVM. Cardiac cell–cell junctions in health and disease: Electrical versus mechanical coupling. *J. Mol. Cell. Cardiol.* 47, 23–31 (2009).
39. Gartner L, Hiatt J. *Color textbook of histology.* (Elsevier, 2001).
40. Yang X, Pabon L, Murry CE. Engineering adolescence: maturation of human pluripotent stem cell-derived cardiomyocytes. *Circ. Res.* 114, 511–23 (2014).
41. Hwang PM, Sykes BD. Targeting the sarcomere to correct muscle function. *Nat Rev Drug Discov* 14, 313–28 (2015).
42. Huxley H, Hanson J. Changes in the cross-striations of muscle during contraction and stretch and their structural interpretation. *Nature* 173, 973–976 (1954).
43. Parry D, Squire J. Structural role of tropomyosin in muscle regulation: analysis of the X-ray diffraction patterns from relaxed and contracting muscles. *J. Mol. Biol.* 75, 33–35 (1973).
44. Li MX, Spyrapoulos L, Sykes BD. Binding of cardiac troponin-I 147-163 induces a structural opening in human cardiac troponin-C. *Biochemistry* 38, 8289–8298 (1999).
45. Bassani J, Bassani RA, Bers DM. Relaxation in rabbit and rat cardiac cells: species-dependent differences in cellular mechanisms. *J. Physiol.* 476, 279–293 (1994).
46. Bedada FB, Chan SSK, Metzger SK, Zhang L, Zhang J, Garry DJ, Kamp TJ, Kyba M, Metzger JM.

- Acquisition of a quantitative, stoichiometrically conserved ratio-metric marker of maturation status in stem cell-derived cardiac myocytes. *Stem Cell Reports* 3, 594–605 (2014).
47. Feric NT, Radisic M. Maturing human pluripotent stem cell-derived cardiomyocytes in human engineered cardiac tissues. *Adv. Drug Deliv. Rev.* 96, 110–134 (2016).
 48. Li RK, Mickle DAG, Weisel RD, Carson S, Omar SA, Tumiati LC, Wilson GJ, Williams WG. Human pediatric and adult ventricular cardiomyocytes in culture: Assessment of phenotypic changes with passaging. *Cardiovasc. Res.* 32, 362–373 (1996).
 49. Ribeiro MC, Tertoolen LG, Guadix JA, Bellin M, Kosmidis G, D'Aniello C, Monshouwer-Kloots J, Goumans MJ, Wang Y li, Feinberg AW, Mummery CL, Passier R. Functional maturation of human pluripotent stem cell derived cardiomyocytes in vitro - Correlation between contraction force and electrophysiology. *Biomaterials* 51, 138–150 (2015).
 50. Schaaf S, Shibamiya A, Mewe M, Eder A, Stöhr A, Hirt MN, Rau T, Zimmermann WH, Conradi L, Eschenhagen T, Hansen A. Human engineered heart tissue as a versatile tool in basic research and preclinical toxicology. *PLoS One* 6, (2011).
 51. Chung C, Bien H, Entcheva E. The Role of Cardiac Tissue Alignment in Modulating Electrical Function. *J. Cardiovasc. Electrophysiol.* 18, 1323–1329 (2007).
 52. Veerman CC, Kosmidis G, Mummery CL, Casini S, Verkerk AO, Bellin M. Immaturity of Human Stem-Cell-Derived Cardiomyocytes in Culture: Fatal Flaw or Soluble Problem? *Stem Cells Dev.* 24, 1035–1052 (2015).
 53. Pasumarthi KBS, Field LJ. Cardiomyocyte cell cycle regulation. *Circ. Res.* 90, 1044–1054 (2002).
 54. Laflamme MA, Murry CE. Heart regeneration. *Nature* 473, 326–335 (2011).
 55. Maillet M, van Berlo JH, Molkenin JD. Molecular basis of physiological heart growth: fundamental concepts and new players. *Nat Rev Mol Cell Biol* 14, 38–48 (2013).
 56. Dorn GW, Robbins J, Sugden PH. Phenotyping hypertrophy: Eschew obfuscation. *Circ. Res.* 92, 1171–1175 (2003).
 57. Chaudhry HW, Dashoush NH, Tang H, Zhang L, Wan X, Wu EX, Wolgemuth DJ. Cyclin A2 mediates cardiomyocyte mitosis in the postmitotic myocardium. *J. Biol. Chem.* 279, 35858–35866 (2004).
 58. Ahuja P, Sdek P, MacLellan WR. Cardiac Myocyte Cell Cycle Control in Development, Disease, and Regeneration. *Physiol Rev* 87, 521–544 (2007).
 59. Bergmann O, Bhardwaj R, Bernard S, Zdunek S, Barnabé-Heider F, Walsh S, Zupicich J, Alkass K, Buchholz B, Druid H, Jovigne S, Frisén J. Evidence for Cardiomyocyte Renewal in Humans. *Science* 324, 98–102 (2009).
 60. Beltrami A, Barlucchi L, Torella D, Baker M, Limana F, Chimenti S, Al. E. Adult cardiac stem cells are multipotent and support myocardial regeneration. *Cell* 114, 763–776 (2003).
 61. Gregorio C, Antin P. To the heart of myofibril assembly. *Trends Cell Biol* 10, 355–362. (2000).
 62. Lu TY, Lin B, Kim J, Sullivan M, Tobita K, Salama G, Yang L. Repopulation of decellularized mouse heart with human induced pluripotent stem cell-derived cardiovascular progenitor cells. *Nat. Commun.* 4, 2307 (2013).
 63. Lundy SD, Zhu W-Z, Regnier M, Laflamme MA. Structural and functional maturation of cardiomyocytes derived from human pluripotent stem cells. *Stem Cells Dev.* 22, 1991–2002 (2013).
 64. *Rubin's Pathology: Clinicopathologic Foundations of Medicine.* (Wolters Kluwer Health/Lippincott Williams & Wilkins, 2012).
 65. Snir M, Kehat A, Gepstein I, Coleman R, Itskovitz- Eldor J, Livne E, Gepstein L. Assessment of the ultrastructural and proliferative properties of human embryonic stem cell-derived cardiomyocytes. *Am J Physiol Heart Circ Physiol.* 285, H2355–H2363 (2003).
 66. Vunjak Novakovic G, Eschenhagen T, Mummery C. Myocardial tissue engineering: In vitro models. *Cold Spring Harb. Perspect. Med.* 4, a014076 (2014).

REFERENCES

67. Mummery C. Differentiation of Human Embryonic Stem Cells to Cardiomyocytes: Role of Coculture With Visceral Endoderm-Like Cells. *Circulation* 107, 2733–2740 (2003).
68. Vreeker A, Van Stuijvenberg L, Hund TJ, Mohler PJ, Nikkels PGJ, Van Veen TAB. Assembly of the cardiac intercalated disk during preand postnatal development of the human heart. *PLoS One* 9, (2014).
69. Jansen JA, van Veen TA, Bakker JM de, Rijen HV van. Cardiac connexins and impulse propagation. *J.Mol. Cell. Cardiol.* 48, 76–82 (2010).
70. Zwi L, Caspi O, Arbel G, Huber I, Gepstein A, Park I-H, Gepstein L. Cardiomyocyte differentiation of human induced pluripotent stem cells. *Circulation* 120, 1513–23 (2009).
71. Angst BD, Khan LU, Severs NJ, Whitely K, Rothery S, Thompson RP, Magee AI, Gourdie RG. Dissociated spatial patterning of gap junctions and cell adhesion junctions during postnatal differentiation of ventricular myocardium. *Circ Res* 80, 88–94. (1997).
72. Linke W, Hamdani N. Gigantic business: titin properties and function through thick and thin. *Circ Res* 114, 1052–1068 (2014).
73. Lahmers S, Wu Y, Call DR, Labeit S, Granzier H. Developmental Control of Titin Isoform Expression and Passive Stiffness in Fetal and Neonatal Myocardium. *Circ. Res.* 94, 505–513 (2004).
74. LeWinter M, Granzier H. Cardiac titin: a multifunctional giant. *Circulation* 121, 2137–2145 (2010).
75. Opitz CA, Leake MC, Makarenko I, Benes V, Linke WA. Developmentally Regulated Switching of Titin Size Alters Myofibrillar Stiffness in the Perinatal Heart. *Circ. Res.* 94, 967–975 (2004).
76. Krüger M, Linke W. Titin-based mechanical signalling in normal and failing myocardium. *J Mol Cell Cardiol* 46, 490–498 (2009).
77. Xu XQ, Soo SY, Sun W, Zweigerdt R. Global expression profile of highly enriched cardiomyocytes derived from human embryonic stem cells. *Stem Cells* 27, 2163–74 (2009).
78. Reiser PJ, Portman M a, Ning XH, Schomisch Moravec C. Human cardiac myosin heavy chain isoforms in fetal and failing adult atria and ventricles. *Am. J. Physiol. Heart Circ. Physiol.* 280, H1814–H1820 (2001).
79. Ivashchenko CY, Pipes GC, Lozinskaya IM, Lin Z, Xu X, Needle S, Grygielko E, Hu E, Toomey J, Lepore J, Willette RN. Human induced pluripotent stem cell derived cardiomyocytes exhibit temporal changes in phenotype. *Am J Physiol Heart Circ Physiol.* 6, H913–H922 (2013).
80. Mahdavit V, Lompre A, Chambers A, Nadal-Ginard B. Expression of the Cardiac Ventricular alpha and beta Myosin Heavy Chain Genes Is Developmentally and Hormonally Regulated. *J. Biol. Chem.* 259, 6437–6446 (1984).
81. Chuva de Sousa Lopes S, Hassink R, Feijen A, van Rooijen M, Doevendans P, Tertoolen L, Brutel de la Riviere A, Mummery C. Patterning the heart, a template for human cardiomyocyte development. *Dev. Dyn.* 235, 1994–2002 (2006).
82. Hailstones D, Barton P, Chan-Thomas P, Sasse S, Sutherland C, Hardeman E, Gunning P. Differential regulation of the atrial isoforms of the myosin light chains during striated muscle development. *J Biol Chem* 267, 23295–23300. (1992).
83. Macera M, Szabo P, Wadgaonkar R, Siddiqui M, Verma R. Localization of the gene coding for ventricular myosin regulatory light chain (MYL2) to human chromosome 12q23-q24.3. *Genomics* 13, 829–831. (1992).
84. Thompson BR, Houang EM, Sham YY, Metzger JM. Molecular determinants of cardiac myocyte performance as conferred by isoform-specific tni residues. *Biophys. J.* 106, 2105–2114 (2014).
85. Hunkeler N, Kullman J, Murphy A. Troponin I isoform expression in human heart. *Circ Res* 69, 1409–1414. (1991).
86. Amin A, Tan H, Wilde A. Cardiac ion channels in health and disease. *Hear. Rhythm* 7, 117–126 (2010).
87. J M, Guo L, Fiene S, Anson B, Thomson J, Kamp T, Kolaja K, Swanson B, January C. High purity human-induced pluripotent stem cell-derived cardiomyocytes: electrophysiological properties of action

- potentials and ionic currents. *Am J Physiol Heart Circ Physiol.* 301, H2006–H2017 (2011).
88. Sartiani L, Bettiol E, Stillitano F, Mugelli A, Cerbai E, Jaconi ME. Developmental changes in cardiomyocytes differentiated from human embryonic stem cells: a molecular and electrophysiological approach. *Stem Cells* 25, 1136–1144 (2007).
 89. Koncz I, Szel T, Bitay M, Cerbai E, Jaeger K, Fulop F, Jost N, Virag L, Orvos P, Talosi L, Kristof A, Baczko I, Papp JG, Varro A. Electrophysiological effects of ivabradine in dog and human cardiac preparations: potential antiarrhythmic actions. *Eur. J. Pharmacol.* 668, 419–426 (2011).
 90. Beuckelmann D, Nábauer M, Erdmann E. Intracellular calcium handling in isolated ventricular myocytes from patients with terminal heart failure. *Circulation* 85, 1046–1055 (1992).
 91. Li S, Chen G, Li R. Calcium signalling of human pluripotent stem cell-derived cardiomyocytes. *J Physiol* 591, 5279–5290 (2013).
 92. Bers DM. Cardiac excitation-contraction coupling. *Nature* 415, 198–205 (2002).
 93. Nakanishi T, Seguchi M, Takao A. Development of the myocardial contractile system. *Experientia* 44, 936–944 (1988).
 94. Itzhaki I, Rapoport S, Huber I, Mizrahi I, Zwi-Dantsis L, Arbel G, Schiller J, Gepstein L. Calcium handling in human induced pluripotent stem cell derived cardiomyocytes. *PLoS One* 6, e18037 (2011).
 95. Binah O, Dolnikov K, Sadan O, Shilkrot M, Zeevi-Levin N, Amit M, Danon A, Itskovitz-Eldor J. Functional and developmental properties of human embryonic stem cells-derived cardiomyocytes. *J. Electrocardiol.* 40, S192-6 (2007).
 96. Lee YK, Ng KM, Lai WH, Chan YC, Lau YM, Lian Q, Tse HF, Siu CW. Calcium homeostasis in human induced pluripotent stem cell-derived cardiomyocytes. *Stem Cell Rev.* 7, 976–986 (2011).
 97. Ferrantini C, Crocini C, Coppini R, Vanzi F, Tesi C, Cerbai E, Poggesi C, Pavone F, Sacconi L. The transverse-axial tubular system of cardiomyocytes. *Cell Mol Life Sci* 70, 4695–4710 (2013).
 98. Synnergren J, Ameén C, Jansson A, Sartipy P. Global transcriptional profiling reveals similarities and differences between human stem cell-derived cardiomyocyte clusters and heart tissue. *Physiol Genomics* 44, 245–258 (2012).
 99. Hasenfuss G, Mulieri L, Blanchard E, Holubarsch C, Leavitt B, Littleman F, Alpert N. Energetics of isometric force development in control and volume-overload human myocardium. Comparison with animal species. *Circ Res* 68, 836–46 (1991).
 100. Wiegerinck RF, Cojoc A, Zeidenweber CM, Ding G, Shen M, Joyner RW, Fernandez JD, Kanter KR, Kirshbom PM, Kogon BE, Wagner MB. Force frequency relationship of the human ventricle increases during early postnatal development. *Pediatr. Res.* 65, 414–419 (2009).
 101. Germanguz I, Sedan O, Zeevi-Levin N, Shtrichman R, Barak E, Ziskind A, Eliyahu S, Meiry G, Amit M, Itskovitz-Eldor J, Binah O. Molecular characterization and functional properties of cardiomyocytes derived from human inducible pluripotent stem cells. *J. Cell. Mol. Med.* 15, 38–51 (2011).
 102. Ursem NT, Struijk PC, Hop WC, Clark EB, Keller BB, Wladimiroff JW. Heart rate and flow velocity variability as determined from umbilical Doppler velocimetry at 10–20 weeks of gestation. *Clin. Sci.* 95, 539–545 (1998).
 103. Lee EJ, Peng J, Radke M, Gotthardt M, Granzier HL. Calcium sensitivity and the Frank–Starling mechanism of the heart are increased in titin N2B region-deficient mice. *J. Mol. Cell. Cardiol.* 49, 449–458. (2010).
 104. Tulloch NL, Muskheli V, Razumova M V, Korte FS, Regnier M, Hauch KD, Pabon L, Reinecke H, Murry CE. Growth of engineered human myocardium with mechanical loading and vascular coculture. *Circ. Res.* 109, 47–59 (2011).
 105. Turnbull IC, Karakikes I, Serrao GW, Backeris P, Lee J-J, Xie C, Senyei G, Gordon RE, Li RA, Akar FG, Hajjar RJ, Hultot J-S, Costa KD. Advancing functional engineered cardiac tissues toward a preclinical model of human myocardium. *FASEB J.* 28, 644–654 (2014).
 106. Xu C, Police S, Rao N, Carpenter MK. Characterization and Enrichment of Cardiomyocytes Derived

REFERENCES

- From Human Embryonic Stem Cells. *Circ. Res.* 91, 501 LP-508 (2002).
107. Weiss S, Oz S, Benmocha A, Dascal N. Regulation of Cardiac L-Type Ca²⁺ Channel CaV1.2 Via the β -Adrenergic-cAMP-Protein Kinase A Pathway. *Circ. Res.* 113, 617–631 (2013).
 108. Dolnikov K, Shilkrot M, Zeevi-Levin N, Gerech-Nir S, Amit M, Danon A, Itskovitz-Eldor J, Binah O. Functional Properties of Human Embryonic Stem Cell-Derived Cardiomyocytes: Intracellular Ca²⁺ Handling and the Role of Sarcoplasmic Reticulum in the Contraction. *Stem Cells* 24, 236–245 (2006).
 109. Eschenhagen T, Eder A, Vollert I, Hansen A. Physiological aspects of cardiac tissue engineering. *Am. J. Physiol. Heart Circ. Physiol.* 303, H133–43 (2012).
 110. Pillekamp F, Hausteil M, Khalil M, Emmelheinz M, Nazzal R, Adelman R, Nguemo F, Rubenchyk O, Pfannkuche K, Matzkies M, Reppel M, Bloch W, Brockmeier K, Hescheler J. Contractile Properties of Early Human Embryonic Stem Cell-Derived Cardiomyocytes: Beta-Adrenergic Stimulation Induces Positive Chronotropy and Lusitropy but Not Inotropy. *Stem Cells Dev.* 21, 2111–2121 (2012).
 111. Liu J, Sun N, Bruce MA, Wu JC, Butte MJ. Atomic Force Mechanobiology of Pluripotent Stem Cell-Derived Cardiomyocytes. *PLoS One* 7, 1–7 (2012).
 112. Yokoo N, Baba S, Kaichi S, Niwa A, Mima T, Doi H, Yamanaka S, Nakahata T, Heike T. The effects of cardioactive drugs on cardiomyocytes derived from human induced pluripotent stem cells. *Biochem. Biophys. Res. Commun.* 387, 482–488 (2009).
 113. Eder A, Vollert I, Hansen A, Eschenhagen T. Human engineered heart tissue as a model system for drug testing. *Adv. Drug Deliv. Rev.* 96, 214–224 (2016).
 114. Mummery C, Ward-van Oostwaard D, Doevendans P, Spijker R, van den Brink S, Hassink R, van der Heyden M, Opthof T, Pera M, de la Riviere AB, Passier R, Tertoolen L. Differentiation of Human Embryonic Stem Cells to Cardiomyocytes. *Circulation* 107, 2733 LP-2740 (2003).
 115. Gwathmey JK, Hajjar RJ. Relation between steady-state force and intracellular [Ca²⁺] in intact human myocardium. Index of myofibrillar responsiveness to Ca²⁺. *Circulation* 82, 1266 LP-1278 (1990).
 116. Böhm M, La Rosée K, Schwinger RHG, Erdmann E. Evidence for reduction of norepinephrine uptake sites in the failing human heart. *J. Am. Coll. Cardiol.* 25, 146–153 (1995).
 117. Coltart DJ, Spilker BA. Development of human foetal inotropic responses to catecholamines. *Experientia* 28, 525–526 (1972).
 118. Toraason M, Richards DE, Mathias PI. Ca²⁺ mobilization in fetal-human cardiac myocytes is stimulated by isoproterenol and inhibited by ryanodine. *Vitr. Cell. Dev. Biol. Anim.* 34, 19–21 (1998).
 119. Resch BA, Papp JG. Effect of adrenaline, noradrenaline, isoproterenol and tyramine on the isolated surviving human fetal heart. *Zentralbl. Gynakol.* 104, 1451–1461 (1982).
 120. Brito-Martins M, Harding SE, Ali NN. β 1- and β 2-adrenoceptor responses in cardiomyocytes derived from human embryonic stem cells: comparison with failing and non-failing adult human heart. *Br. J. Pharmacol.* 153, 751–759 (2008).
 121. Von Scheidt W, Bohm M, Stablein A, Autenrieth G, Erdmann E. Antiadrenergic effect of M-cholinoceptor stimulation on human ventricular contractility in vivo. *Am. J. Physiol. Heart Circ. Physiol.* 263, H1927 LP-H1931 (1992).
 122. Koglin J, Böhm M, von Scheidt W, Stäblein A, Erdmann E. Antiadrenergic effect of carbachol but not of adenosine on contractility in the intact human ventricle in vivo. *J. Am. Coll. Cardiol.* 23, 678–683 (1994).
 123. Coltart DJ, Spilker BA, Meldrum SJ. An electrophysiological study of human foetal cardiac muscle. *Experientia* 27, 797–799 (1971).
 124. Harris K, Aylott M, Cui Y, Louttit JB, McMahon NC, Sridhar A. Comparison of electrophysiological data from human-induced pluripotent stem cell-derived cardiomyocytes to functional preclinical safety assays. *Toxicol. Sci.* 134, 412–426 (2013).
 125. Kuryshev YA, Brown AM, Duzic E, Kirsch GE. Evaluating State Dependence and Subtype Selectivity of Calcium Channel Modulators in Automated Electrophysiology Assays. *Assay Drug Dev. Technol.* 12, 110–119 (2014).

126. Schwinger RHG, Böhm M, Erdmann E. Different negative inotropic activity of Ca²⁺-antagonists in human myocardial tissue. *Klin. Wochenschr.* 68, 797–805 (1990).
127. Yamazaki K, Hihara T, Kato H, Fukushima T, Fukushima K. Beat-to-Beat Variability in Field Potential Duration in Human Embryonic Stem Cell-Derived Cardiomyocyte Clusters for Assessment of Arrhythmogenic Risk, and a Case Study of Its Application. *Pharmacol. Pharm.* 2014, 117–128 (2014).
128. Mehta A, Chung Y, Sequiera GL, Wong P, Liew R, Shim W. Pharmacoelectrophysiology of Viral-Free Induced Pluripotent Stem Cell-Derived Human Cardiomyocytes. *Toxicol. Sci.* 131, 458 (2012).
129. Kang J, Chen X-L, Ji J, Lei Q, Rampe D. Ca²⁺ Channel Activators Reveal Differential L-Type Ca²⁺ Channel Pharmacology between Native and Stem Cell-Derived Cardiomyocytes. *J. Pharmacol. Exp. Ther.* 341, 510 LP-517 (2012).
130. Chin TK, Graham KS, Calendine C, He YH. Neuroregulation of Calcium Channel Function in Human Fetal Cardiac Myocyte Clusters. *Pediatr Res* 45, 21A–21A (1999).
131. Bkaily G, El-Bizri N, Bui M, Sukarieh R, Jacques D, Fu MLX. Modulation of intracellular Ca²⁺ via L-type calcium channels in heart cells by the autoantibody directed against the second extracellular loop of the α 1-adrenoceptors. *Can. J. Physiol. Pharmacol.* 81, 234–246 (2003).
132. Sheng X, Reppel M, Nguemo F, Mohammad FI, Kuzmenkin A, Hescheler J, Pfannkuche K. Human Pluripotent Stem Cell-Derived Cardiomyocytes: Response to TTX and Lidocain Reveals Strong Cell to Cell Variability. *PLoS One* 7, e45963 (2012).
133. Gibson JK, Yue Y, Bronson J, Palmer C, Numann R. Human stem cell-derived cardiomyocytes detect drug-mediated changes in action potentials and ion currents. *J. Pharmacol. Toxicol. Methods* 70, 255–267 (2014).
134. Godfraind T, Eglème C, Finet M, Jaumin P. The Actions of Nifedipine and Nisoldipine on the Contractile Activity of Human Coronary Arteries and Human Cardiac Tissue in Vitro. *Pharmacol. Toxicol.* 61, 79–84 (1987).
135. Splawski I, Timothy KW, Sharpe LM, Decher N, Kumar P, Bloise R, Napolitano C, Schwartz PJ, Joseph RM, Condouris K, Tager-Flusberg H, Priori SG, Sanguinetti MC, Keating MT. CaV1.2 Calcium Channel Dysfunction Causes a Multisystem Disorder Including Arrhythmia and Autism. *Cell* 119, 19–31 (2004).
136. Chen L, El-Sherif N, Boutjdir M. Unitary Current Analysis of L-type Ca²⁺ Channels in Human Fetal Ventricular Myocytes. *J. Cardiovasc. Electrophysiol.* 10, 692–700 (1999).
137. Baruscotti M, Bucchi A, DiFrancesco D. Physiology and pharmacology of the cardiac pacemaker ('funny') current. *Pharmacol. Ther.* 107, 59–79 (2005).
138. Bárándi L, Virág L, Jost N, Horváth Z, Koncz I, Papp R, Harmati G, Horváth B, Szentandrassy N, Bányász T, Magyar J, Zaza A, Varró A, Nánási PP. Reverse rate-dependent changes are determined by baseline action potential duration in mammalian and human ventricular preparations. *Basic Res. Cardiol.* 105, 315–323 (2010).
139. Catterall WA, Goldin AL, Waxman SG. International Union of Pharmacology. XLVII. Nomenclature and Structure-Function Relationships of Voltage-Gated Sodium Channels. *Pharmacol. Rev.* 57, 397 LP-409 (2005).
140. Jacques D, Bkaily G, Jasmin G, Ménard D, Proschek L. *Early fetal like slow Na⁺ current in heart cells of cardiomyopathic hamster.* in *The Cellular Basis of Cardiovascular Function in Health and Disease* (eds. Singal, P. K., Panagia, V. & Pierce, G. N.) 249–256 (Springer US, 1997).
141. Walker D. Functional Development of the Autonomic Innervation of the Human Fetal Heart. *Neonatology* 25, 31–43 (1974).
142. Khana MG. *Caffeine and the heart.* in *Encyclopedia of Heart Diseases* (ed. Khana, M. G.) 189–191 (Elsevier Academic Press, 2006).
143. Liu J, Fu JD, Siu CW, Li RA. Functional Sarcoplasmic Reticulum for Calcium Handling of Human Embryonic Stem Cell-Derived Cardiomyocytes: Insights for Driven Maturation. *Stem Cells* 25, 3038–3044 (2007).
144. Li G-R, Feng J, Yue L, Carrier M, Nattel S. Evidence for Two Components of Delayed Rectifier K⁺

REFERENCES

- Current in Human Ventricular Myocytes. *Circ. Res.* 78, 689–696 (1996).
145. Danielsson C, Brask J, Sköld A-C, Genead R, Andersson A, Andersson U, Stockling K, Pehrson R, Grinnemo K-H, Salari S, Hellmold H, Danielsson B, Sylvén C, Elinder F. Exploration of human, rat, and rabbit embryonic cardiomyocytes suggests K-channel block as a common teratogenic mechanism. *Cardiovasc. Res.* 97, 23–32 (2012).
 146. Nalos L, Varkevisser R, Jonsson MKB, Houtman MJC, Beekman JD, van der Nagel R, Thomsen MB, Duker G, Sartipy P, de Boer TP, Peschar M, Rook MB, van Veen TAB, van der Heyden MAG, Vos MA. Comparison of the IKr blockers moxifloxacin, dofetilide and E-4031 in five screening models of proarrhythmia reveals lack of specificity of isolated cardiomyocytes. *Br. J. Pharmacol.* 165, 467–478 (2012).
 147. Jones DK, Liu F, Vaidyanathan R, Eckhardt LL, Trudeau MC, Robertson GA. hERG 1b is critical for human cardiac repolarization. *Proc. Natl. Acad. Sci.* 111, 18073–18077 (2014).
 148. Rampe D, Wible B, Brown AM, Dage RC. Effects of terfenadine and its metabolites on a delayed rectifier K⁺ channel cloned from human heart. *Mol. Pharmacol.* 44, 1240 LP-1245 (1993).
 149. Lu HR, Hermans AN, Gallacher DJ. Does terfenadine-induced ventricular tachycardia/fibrillation directly relate to its QT prolongation and Torsades de Pointes? *Br. J. Pharmacol.* 166, 1490–1502 (2012).
 150. Crumb WJ, Wible B, Arnold DJ, Payne JP, Brown AM. Blockade of multiple human cardiac potassium currents by the antihistamine terfenadine: possible mechanism for terfenadine-associated cardiotoxicity. *Mol. Pharmacol.* 47, 181 LP-190 (1995).
 151. Hove-Madsen L, Llach A, Molina CE, Prat-Vidal C, Farré J, Roura S, Cinca J. The proarrhythmic antihistaminic drug terfenadine increases spontaneous calcium release in human atrial myocytes. *Eur. J. Pharmacol.* 553, 215–221 (2006).
 152. Guo L, Abrams RMC, Babiarz JE, Cohen JD, Kameoka S, Sanders MJ, Chiao E, Kolaja KL. Estimating the Risk of Drug-Induced Proarrhythmia Using Human Induced Pluripotent Stem Cell-Derived Cardiomyocytes. *Toxicol. Sci.* 123, 281 (2011).
 153. Poindexter BJ, Smith JR, Buja LM, Bick RJ. Calcium signaling mechanisms in dedifferentiated cardiac myocytes: comparison with neonatal and adult cardiomyocytes. *Cell Calcium* 30, 373–382 (2001).
 154. Davia K, Davies CH, Harding SE. Effects of inhibition of sarcoplasmic reticulum calcium uptake on contraction in myocytes isolated from failing human ventricle. *Cardiovasc. Res.* 33, 88–97 (1997).
 155. Kane KA. Comparative electrophysiological effects of Org 6001, a new orally active antidysrhythmic agent, and lignocaine on human ventricular muscle. *Br. J. Pharmacol.* 68, 25–31 (1980).
 156. Bennett PB, Valenzuela C, Chen L-Q, Kallen RG. On the Molecular Nature of the Lidocaine Receptor of Cardiac Na⁺ Channels. *Circ. Res.* 77, 584–592 (1995).
 157. Zhu W-Z, Santana LF, Laflamme MA. Local Control of Excitation-Contraction Coupling in Human Embryonic Stem Cell-Derived Cardiomyocytes. *PLoS One* 4, e5407 (2009).
 158. Mendis S, Puska P, Norrving B. *Global Atlas on cardiovascular disease prevention and control.* World Health Organization (2011).
 159. World Health Organization. Global Status Report On Noncommunicable Diseases 2014. (2014).
 160. World Health Organization. *Global Health Estimates: Deaths by Cause, Age, Sex and Country, 2000-2012.* (2014).
 161. Baig M, Mahon N, McKenna W, Caforio A, Bonow R, Francis G, Gheorghiade M. The pathophysiology of advanced heart failure. *Heart Lung* 28, 87–101 (1999).
 162. Thygesen K, Alpert J, Jaffe A, Simoons M, Chaitman B, White H. Third universal definition of myocardial infarction. *Nat Rev Cardiol* 9, 620–633 (2012).
 163. Jennings R, Murry C, Steenbergen CJ, Reimer K. Development of cell injury in sustained acute ischemia. *Circulation* 82, 112-12 (1990).
 164. Mann L. *Heart Failure: A companion to Braunwald's Heart Disease.* (Elsevier Inc, 2011).

165. Sutton M, Sharpe N. Left ventricular remodeling after myocardial infarction: pathophysiology and therapy. *Circulation* 101, 2981–2988 (2000).
166. Jiang F, Yang J, Zhang Y, Dong M, Wang S, Zhang Q, Liu FF, Zhang K, Zhang C. Angiotensin-converting enzyme 2 and angiotensin 1-7: novel therapeutic targets. *Nat. Rev. Cardiol.* 11, 413–26 (2014).
167. Chen Q-Z, Harding SE, Ali NN, Lyon AR, Boccaccini AR. Biomaterials in cardiac tissue engineering: Ten years of research survey. *Mater. Sci. Eng. R Reports* 59, 1–37 (2008).
168. Jawad H, Lyon AR, Harding SE, Ali NN, Boccaccini AR. Myocardial tissue engineering. *Br. Med. Bull.* 87, 31–47 (2008).
169. Rosamond W, Flegal K, Furie K, Go A, Greenlund K, Haase N, Hailpern SM, Ho M, Howard V, Kissela B, Kittner S, Lloyd-Jones D, McDermott M, Meigs J, Moy C, Nichol G, O'Donnell C, Roger V, Sorlie P, et al. Heart disease and stroke statistics-2008 Update: A report from the American heart association statistics committee and stroke statistics subcommittee. *Circulation* 117, (2008).
170. Hawkins NM, Petrie MC, MacDonald MR, Hogg KJ, McMurray JJ V. Selecting patients for cardiac resynchronization therapy: Electrical or mechanical dyssynchrony? *Eur. Heart J.* 27, 1270–1281 (2006).
171. Packer M. The impossible task of developing a new treatment for heart failure. *J. Card. Fail.* 8, 193–196 (2002).
172. Tzatzalos E, Abilez OJ, Shukla P, Wu JC. Engineered heart tissues and induced pluripotent stem cells: Macro- and microstructures for disease modeling, drug screening, and translational studies. *Adv. Drug Deliv. Rev.* 96, 234–244 (2016).
173. Griffith LG, Swartz M a. Capturing complex 3D tissue physiology in vitro. *Nat. Rev. Mol. Cell Biol.* 7, 211–24 (2006).
174. Wollert KC, Drexler H. Cell therapy for the treatment of coronary heart disease: a critical appraisal. *Nat. Rev. Cardiol.* 7, 204–15 (2010).
175. Taylor D a, Atkins BZ, Hungspreugs P, Jones TR, Reedy MC, Hutcheson K a, Glower DD, Kraus WE. Regenerating functional myocardium: improved performance after skeletal myoblast transplantation. *Nat. Med.* 4, 929–933 (1998).
176. Soonpaa M, Koh G, Klug M, Field L. Formation of nascent intercalated disks between grafted fetal cardiomyocytes and host myocardium. *Science* 264, 98–101 (1994).
177. Robey TE, Saiget MK, Reinecke H, Murry CE. Systems approaches to preventing transplanted cell death in cardiac repair. *J. Mol. Cell. Cardiol.* 45, 567–581 (2008).
178. Chien KR, Domian IJ, Parker KK. Cardiogenesis and the complex biology of regenerative cardiovascular medicine. *Science* 322, 1494–1497 (2008).
179. Li RK, Jia ZQ, Weisel RD, Mickle DA, Zhang J, Mohabeer M, Rao V, Ivanov J. Cardiomyocyte transplantation improves heart function. *Ann Thorac Surg* 62, 654-60–1 (1996).
180. Dowell JD, Rubart M, Pasumarthi KB, Soonpaa MH, Field LJ. Myocyte and myogenic stem cell transplantation in the heart. *Cardiovasc. Res.* 58, 336–350 (2003).
181. Wollert KC, Bethmann K, Drexler H. *Cell-Based Therapies and Tissue Engineering in Heart Failure*. in *Heart Failure* 742–752 (Elsevier Inc., 2011).
182. Segers VFM, Lee RT. Stem-cell therapy for cardiac disease. *Nature* 451, 937–42 (2008).
183. Menasche P. Skeletal myoblasts as a therapeutic agent. *Prog. Cardiovasc. Dis.* 50, 7–17 (2007).
184. Laflamme MA, Murry CE. Regenerating the heart. *Nat. Biotechnol.* 23, 845–56 (2005).
185. Mozid AM, Arnous S, Sammut EC, Mathur A. Stem cell therapy for heart diseases. *Br Med Bull* 98, 143–159 (2011).
186. van den Bos EJ, Thompson RB, Wagner A, Mahrholdt H, Morimoto Y, Thomson LE, Wang LH, Duncker DJ, Judd RM, Taylor D. Functional assessment of myoblast transplantation for cardiac repair with

REFERENCES

- magnetic resonance imaging. *Eur J Hear. Fail* 7, 435–443 (2005).
187. McConnell PI, del Rio CL, Jacoby DB, Pavlicova M, Kwiatkowski P, Zawadzka A, Dinsmore JH, Astra L, Wisel S, Michler RE. Correlation of autologous skeletal myoblast survival with changes in left ventricular remodeling in dilated ischemic heart failure. *J Thorac Cardiovasc Surg* 130, 1001 (2005).
 188. Perez-Illzarbe M, Agbulut O, Pelacho B, Ciorba C, San Jose-Eneriz E, Desnos M, Hagege AA, Aranda P, Andreu EJ, Menasche P, Prosper F. Characterization of the paracrine effects of human skeletal myoblasts transplanted in infarcted myocardium. *Eur J Hear. Fail* 10, 1065–1072 (2008).
 189. Menasché P, Alfieri O, Janssens S, McKenna W, Reichenspurner H, Trinquart L, Vilquin J-T, Marolleau J-P, Seymour B, Larghero J, Lake S, Chatellier G, Solomon S, Desnos M, Hagege AA. The Myoblast Autologous Grafting in Ischemic Cardiomyopathy (MAGIC) Trial. *Circulation* 117, 1189 LP-1200 (2008).
 190. Pelacho B, Mazo M, Montori S, Simón-Yarza AM, Gavira JJ, Blanco-Prieto MJ, Prósper F. *Cardiac regeneration with stem cells*. in *Regenerative Medicine and Cell Therapy* (eds. Baharvand, H. & Aghdami, N.) (Humana Press, 2013).
 191. Mazo M, Gavira JJ, Abizanda G, Moreno C, Ecay M, Soriano M, Aranda P, Collantes M, Alegria E, Merino J, Penuelas I, Garcia-Verdugo JM, Pelacho B, Prosper F. Transplantation of mesenchymal stem cells exerts a greater long-term effect than bone marrow mononuclear cells in a chronic myocardial infarction model in rat. *Cell Transpl.* 19, 313–328 (2010).
 192. Menasché P, Vanneaux V. Stem cells for the treatment of heart failure. *Curr. Res. Transl. Med.* 64, 97–106 (2016).
 193. Faiella W, Atoui R. Therapeutic use of stem cells for cardiovascular disease. *Clin. Transl. Med.* 5, 34 (2016).
 194. Bayes-Genis A, Soler-Botija C, Farré J, Sepúlveda P, Raya A, Roura S, Prat-Vidal C, Gálvez-Montón C, Montero J, Büscher D, Izpisua Belmonte J. Human progenitor cells derived from cardiac adipose tissue ameliorate myocardial infarction in rodents. *J Mol Cell Cardiol.* 49, 771–80 (2010).
 195. Wang L, Deng J, Tian W, Xiang B, Yang T, Li G, Wang J, Gruwel M, Kashour T, Rendell J, Glogowski M, Tomanek B, Freed D, Deslauriers R, Arora RC, Tian G. Adipose-derived stem cells are an effective cell candidate for treatment of heart failure: an MR imaging study of rat hearts. *Am J Physiol Heart Circ Physiol.* 297, H1020-31 (2009).
 196. Leri A, Kajstura J, Anversa P. Role of cardiac stem cells in cardiac pathophysiology: a paradigm shift in human myocardial biology. *Circ Res.* 109, 941–961 (2011).
 197. Dawn B, Stein A, Urbanek K, Rota M, Whang B, Rastaldo R, Al. E. Cardiac stem cells delivered intravascularly traverse the vessel barrier, regenerate infarcted myocardium, and improve cardiac function. *Proc Natl Acad Sci* 102, 3766–3771 (2005).
 198. Oh H, Bradfute S, Gallardo T, Nakamura T, Gausson V, Mishina Y, Al. E. Cardiac progenitor cells from adult myocardium: homing, differentiation, and fusion after infarction. *Proc Natl Acad Sci USA* 100, 12313–12318 (2003).
 199. Bu L, Jiang X, Martin-Puig S, Caron L, Zhu S, Shao Y, Al. E. Human ISL1 heart progenitors generate diverse multipotent cardiovascular cell lineages. *Nature* 460, 113–117 (2009).
 200. Lee S, White A, Matsushita S, Malliaras K, Steenbergen C, Zhang Y, Al. E. Intramyocardial injection of autologous cardiospheres or cardiosphere-derived cells preserves function and minimizes adverse ventricular remodeling in pigs with heart failure post-myocardial infarction. *J Am Coll Cardiol* 57, 455–465. (2011).
 201. Radisic M, Sefton M V. *Cardiac Tissue*. in *Principles of Regenerative Medicine* 877–909 (Elsevier Inc., 2011).
 202. Fox IJ, Daley GQ, Goldman SA, Huard J, Kamp TJ, Trucco M. Use of differentiated pluripotent stem cells in replacement therapy for treating disease. *Science* 345, 1247391 (2014).
 203. Laflamme M, Chen K, Naumova A, Muskheli V, Fugate J, Dupras S, Al. E. Cardiomyocytes derived from human embryonic stem cells in pro-survival factors enhance function of infarcted rat hearts. *Nat Biotechnol* 25, 1015–1024 (2007).

204. Takahashi K, Yamanaka S. Induction of pluripotent stem cells from mouse embryonic and adult fibroblast cultures by defined factors. *Cell* 126, 663–676 (2006).
205. Mummery CL, Zhang J, Ng ES, Elliott DA, Elefanty AG, Kamp TJ. Differentiation of Human Embryonic Stem Cells and Induced Pluripotent Stem Cells to Cardiomyocytes. *Circ. Res.* 111, 344 LP-358 (2012).
206. Dubois NC, Craft AM, Sharma P, Elliott DA, Stanley EG, Elefanty AG, Gramolini A, Keller G. SIRPA is a specific cell-surface marker for isolating cardiomyocytes derived from human pluripotent stem cells. *Nat Biotech* 29, 1011–1018 (2011).
207. Tohyama S, Hattori F, Sano M, Hishiki T, Nagahata Y, Matsuura T, Hashimoto H, Suzuki T, Yamashita H, Satoh Y, Egashira T, Seki T, Muraoka N, Yamakawa H, Ohgino Y, Tanaka T, Yoichi M, Yuasa S, Murata M, *et al.* Distinct Metabolic Flow Enables Large-Scale Purification of Mouse and Human Pluripotent Stem Cell-Derived Cardiomyocytes. *Cell Stem Cell* 12, 127–137 (2013).
208. Masumoto H, Yamashita JK. Exploiting human iPS cell-derived cardiovascular cell populations toward cardiac regenerative therapy. *Stem Cell Transl. Investig.* 1–5 (2016).
209. Blin G, Nury D, Stefanovic S, Neri T, Guillevic O, Brinon B, Al. E. A purified population of multipotent cardiovascular progenitors derived from primate pluripotent stem cells engrafts in postmyocardial infarcted nonhuman primates. *J Clin Invest* 120, 1125–39. (2010).
210. Chong JJH, Yang X, Don CW, Minami E, Liu Y-W, Weyers JJ, Mahoney WM, Van Biber B, Cook SM, Palpant NJ, Gantz J a, Fugate J a, Muskheili V, Gough GM, Vogel KW, Astley C a, Hotchkiss CE, Baldessari A, Pabon L, *et al.* Human embryonic-stem-cell-derived cardiomyocytes regenerate non-human primate hearts. *Nature* 510, 273–7 (2014).
211. Shiba Y, Fernandes S, Zhu W-Z, Filice D, Muskheili V, Kim J, Palpant NJ, Gantz J, Moyes KW, Reinecke H, Van Biber B, Dardas T, Mignone JL, Izawa A, Hanna R, Viswanathan M, Gold JD, Kotlikoff MI, Sarvazyan N, *et al.* Human ES-cell-derived cardiomyocytes electrically couple and suppress arrhythmias in injured hearts. *Nature* 489, 322–5 (2012).
212. Moon S-H, Kang S-W, Park S-J, Bae D, Kim SJ, Lee H-A, Kim KS, Hong K-S, Kim JS, Do JT, Byun KH, Chung H-M. The use of aggregates of purified cardiomyocytes derived from human {ESCs} for functional engraftment after myocardial infarction. *Biomaterials* 34, 4013–4026 (2013).
213. Carpenter L, Carr C, Yang CT, Stuckey DJ, Clarke K, Watt SM. Efficient Differentiation of Human Induced Pluripotent Stem Cells Generates Cardiac Cells That Provide Protection Following Myocardial Infarction in the Rat. *Stem Cells Dev.* 21, 977–986 (2012).
214. Templin C, Zweigerdt R, Schwanke K, Olmer R, Ghadri J-R, Emmert MY, Müller E, Küest SM, Cohrs S, Schibli R, Kronen P, Hilbe M, Reinisch A, Strunk D, Haverich A, Hoerstrup S, Lüscher TF, Kaufmann PA, Landmesser U, *et al.* Transplantation and Tracking of Human-Induced Pluripotent Stem Cells in a Pig Model of Myocardial Infarction. *Circulation* 126, 430 LP-439 (2012).
215. Puymirat E, Geha R, Tomescot A, Bellamy V, Larghero J, Trinquart L, Bruneval P, Desnos M, Hagège A, Pucéat M, Menasché P. Can Mesenchymal Stem Cells Induce Tolerance to Cotransplanted Human Embryonic Stem Cells? *Mol. Ther.* 17, 176–182 (2009).
216. Karantalis V, DiFede DL, Gerstenblith G, Pham S, Symes J, Zambrano JP, Fishman J, Pattany P, McNiece I, Conte J, Schulman S, Wu K, Shah A, Breton E, Davis-Sproul J, Schwarz R, Feigenbaum G, Mushtaq M, Suncion VY, *et al.* Autologous mesenchymal stem cells produce concordant improvements in regional function, tissue perfusion, and fibrotic burden when administered to patients undergoing coronary artery bypass grafting: The Prospective Randomized Study of Mesenchymal Stem Ce. *Circ. Res.* 114, 1302–10 (2014).
217. Heldman A, DiFede D, Fishman J, Zambrano J, Trachtenberg B, Karantalis V, Mushtaq M, Williams A, Suncion V, McNiece I, Ghersin E, Soto V, Lopera G, Miki R, Willens H, Hendel R, R M, Willens H, Hendel R, *et al.* Transendocardial mesenchymal stem cells and mononuclear bone marrow cells for ischemic cardiomyopathy: The tac-hft randomized trial. *JAMA* 311, 62–73 (2014).
218. Mushtaq M, DiFede DL, Golpanian S, Khan A, Gomes SA, Mendizabal A, Heldman AW, Hare JM. Rationale and Design of the Percutaneous Stem Cell Injection Delivery Effects on Neomyogenesis in Dilated Cardiomyopathy (The POSEIDON-DCM Study). *J. Cardiovasc. Transl. Res.* 7, 769–780 (2014).
219. Mathiasen AB, Qayyum AA, Jørgensen E, Helqvist S, Fischer-Nielsen A, Kofoed KF, Haack-Sørensen M, Ekblond A, Kastrup J. Bone marrow-derived mesenchymal stromal cell treatment in patients with

REFERENCES

- severe ischaemic heart failure: a randomized placebo-controlled trial (MSC-HF trial). *Eur. Heart J.* 36, 1744 (2015).
220. Lezaic L, Socan A, Poglajen G, Peitl PK, Sever M, Cukjati M, Cernelc P, Wu JC, Haddad F, Vrtovec B. Intracoronary Transplantation of CD34⁺ Cells Is Associated With Improved Myocardial Perfusion in Patients With Nonischemic Dilated Cardiomyopathy. *J. Card. Fail.* 21, 145–152 (2017).
221. Chugh AR, Beache GM, Loughran JH, Mewton N, Elmore JB, Kajstura J, Pappas P, Tatooles A, Stoddard MF, Lima JAC, Slaughter MS, Anversa P, Bolli R. Administration of Cardiac Stem Cells in Patients With Ischemic Cardiomyopathy: The SCIPIO Trial. *Circulation* 126, S54 LP-S64 (2012).
222. Patel AN, Henry TD, Quyyumi AA, Schaer GL, Anderson RD, Toma C, East C, Remmers AE, Goodrich J, Desai AS, Recker D, DeMaria A. Ixmyelocel-T for patients with ischaemic heart failure: a prospective randomised double-blind trial. *Lancet* 387, 2412–2421 (2016).
223. Malliaras K, Makkar RR, Smith RR, Cheng K, Wu E, Bonow RO, Marbán L, Mendizabal A, Cingolani E, Johnston P V, Gerstenblith G, Schuleri KH, Lardo AC, Marbán E. Intracoronary Cardiosphere-Derived Cells After Myocardial Infarction: Evidence of Therapeutic Regeneration in the Final 1-Year Results of the {CADUCEUS} Trial (CARDiosphere-Derived aUtologous stem {CELLS} to reverse ventricUlar dySfunction). *J. Am. Coll. Cardiol.* 63, 110–122 (2014).
224. Wollert KC, Meyer GP, Lotz J, Ringes Lichtenberg S, Lippolt P, Breidenbach C, Fichtner S, Korte T, Hornig B, Messinger D, Arseniev L, Hertenstein B, Ganser A, Drexler H. Intracoronary autologous bone-marrow cell transfer after myocardial infarction: the BOOST randomised controlled clinical trial. *Lancet* 364, 141–148 (2004).
225. Assmus B, Rolf A, Erbs S, Elsässer A, Haberbosch W, Hambrecht R, Tillmanns H, Yu J, Corti R, Mathey DG, Hamm CW, Süselbeck T, Tonn T, Dimmeler S, Dill T, Zeiher AM, Schächinger V. Clinical Outcome 2 Years After Intracoronary Administration of Bone Marrow-Derived Progenitor Cells in Acute Myocardial Infarction. *Circ. Hear. Fail.* 3, 89–96 (2010).
226. Perin EC, Sanz-Ruiz R, Sánchez PL, Lasso J, Pérez-Cano R, Alonso-Farto JC, Pérez-David E, Fernández-Santos ME, Serruys PW, Duckers HJ, Kastrup J, Chamuleau S, Zheng Y, Silva G V, Willerson JT, Fernández-Avilés F. Adipose-derived regenerative cells in patients with ischemic cardiomyopathy: The PRECISE Trial. *Am. Heart J.* 168, 88–95.e2 (2014).
227. Sanganalmath SK, Bolli R. Cell therapy for heart failure: A comprehensive overview of experimental and clinical studies, current challenges, and future directions. *Circ. Res.* 113, 810–834 (2013).
228. He J-Q, Ma Y, Lee Y, Thomson JA, Kamp TJ. Human Embryonic Stem Cells Develop Into Multiple Types of Cardiac Myocytes. *Circ. Res.* 93, 32 LP-39 (2003).
229. Scott CW, Peters MF, Dragan YP. Human induced pluripotent stem cells and their use in drug discovery for toxicity testing. *Toxicol. Lett.* 219, 49–58 (2013).
230. Herper M. The cost of creating a new drug now \$5 billion, pushing big pharma to change. *Forbes* (2013).
231. Report. Top R&D drug failures — toxicity and serious adverse events in late stage drug development are the major causes of drug failure. *Global Business Intelligence Research* (2011).
232. Ferri N, Siegl P, Corsini A, Herrmann J, Lerman A, Benghozi R. Drug attrition during pre-clinical and clinical development: Understanding and managing drug-induced cardiotoxicity. *Pharmacol. Ther.* 138, 470–484 (2013).
233. Lavery HG, Benson C, Cartwright EJ, Cross MJ, Garland C, Hammond T, Holloway C, McMahon N, Milligan J, Park BK, Pirmohamed M, Pollard C, Radford J, Roome N, Sager P, Singh S, Suter T, Suter W, Trafford A, *et al.* How can we improve our understanding of cardiovascular safety liabilities to develop safer medicines? *Br. J. Pharmacol.* 163, 675–693 (2011).
234. Shah RR. Can pharmacogenetics help rescue drugs withdrawn from the market? *Pharmacogenomics* 7, 889–908 (2006).
235. Ewer MS, Ewer SM. Cardiotoxicity of anticancer treatments: what the cardiologist needs to know. *Nat. Rev. Cardiol.* 7, 564–575 (2010).
236. Zhao Y, Korolj A, Feric N, Radisic M. Human pluripotent stem cell-derived cardiomyocyte based models for cardiotoxicity and drug discovery. *Expert Opin. Drug Saf.* 15, 1455–1458 (2016).

237. Liang P, Lan F, Lee AS, Gong T, Sanchez-Freire V, Wang Y, Diecke S, Sallam K, Knowles JW, Wang PJ, Nguyen PK, Bers DM, Robbins RC, Wu JC. Drug screening using a library of human induced pluripotent stem cell-derived cardiomyocytes reveals disease-specific patterns of cardiotoxicity. *Circulation* 127, 1677–1691 (2013).
238. Tandon N, Marolt D, Cimetta E, Vunjak-Novakovic G. Bioreactor engineering of stem cell environments. *Biotechnol. Adv.* 31, 1020–31 (2013).
239. Lloyd KCK. A knockout mouse resource for the biomedical research community. *Ann. N. Y. Acad. Sci.* 1245, 24–26 (2011).
240. Shultz LD, Brehm MA, Bavari S, Greiner DL. Humanized mice as a preclinical tool for infectious disease and biomedical research. *Ann. N. Y. Acad. Sci.* 1245, 50–54 (2011).
241. Mathur A, Ma Z, Loskill P, Jeeawoody S, Healy KE. In vitro cardiac tissue models: Current status and future prospects. *Adv. Drug Deliv. Rev.* 96, 203–213 (2016).
242. Kaese S, Verheule S. Cardiac electrophysiology in mice: a matter of size. *Front. Physiol.* 3, 345 (2012).
243. Qureshi ZP, Seoane-Vazquez E, Rodriguez-Monguio R, Stevenson KB, Szeinbach SL. Market withdrawal of new molecular entities approved in the United States from 1980 to 2009. *Pharmacoepidemiol. Drug Saf.* 20, 772–777 (2011).
244. Gintant G, Sager PT, Stockbridge N. Evolution of strategies to improve preclinical cardiac safety testing. *Nat. Rev. Drug Discov.* 1–15 (2016).
245. Sager PT, Gintant G, Turner JR, Pettit S, Stockbridge N. Rechanneling the cardiac proarrhythmia safety paradigm: A meeting report from the Cardiac Safety Research Consortium. *Am. Heart J.* 167, 292–300 (2014).
246. Kurokawa YK, George SC. Tissue engineering the cardiac microenvironment: Multicellular microphysiological systems for drug screening. *Adv. Drug Deliv. Rev.* 96, 225–233 (2016).
247. Hirt MN, Hansen A, Eschenhagen T. Cardiac tissue engineering: state of the art. *Circ. Res.* 114, 354–67 (2014).
248. Martins AM, Vunjak-Novakovic G, Reis RL. The current status of iPS cells in cardiac research and their potential for tissue engineering and regenerative medicine. *Stem Cell Rev.* 10, 177–90 (2014).
249. Carvajal-Vergara X, Sevilla A, D'Souza SL, Ang YS, Schaniel C, Lee DF, Yang L, Kaplan AD, Adler ED, Rozov R, Ge Y, Cohen N, Edelmann LJ, Chang B, Waghray A, Su J, Pardo S, Lichtenbelt KD, Tartaglia M, *et al.* Patient-specific induced pluripotent stem-cell-derived models of LEOPARD syndrome. *Nature* 465, 808–812 (2010).
250. Mercola M, Colas A, Willems E. Induced pluripotent stem cells in cardiovascular drug discovery. *Circ. Res.* 112, 534–548 (2013).
251. Itzhaki I, Maizels L, Huber I, Zwi-Dantsis L, Caspi O, Winterstern A, Feldman O, Gepstein A, Arbel G, Hammerman H, Boulos M, Gepstein L. Modelling the long QT syndrome with induced pluripotent stem cells. *Nature* 471, 225–229 (2011).
252. Alessandra M, Milena B, Andrea W, Billy JC, T. LJ, Lorenz B-F, Tatjana D, Alexander G, Christian H, Franz H, Melchior S, Daniel S, Albert S, Karl-Ludwig L. Patient-Specific Induced Pluripotent Stem-Cell Models for Long-QT Syndrome. *N. Engl. J. Med.* 363, 1397–1409 (2010).
253. Davis RP, Casini S, van den Berg CW, Hoekstra M, Remme CA, Dambrot C, Salvatori D, Oostwaard DW, Wilde AAM, Bezzina CR, Verkerk AO, Freund C, Mummery CL. Cardiomyocytes Derived From Pluripotent Stem Cells Recapitulate Electrophysiological Characteristics of an Overlap Syndrome of Cardiac Sodium Channel Disease. *Circulation* 125, 3079 LP-3091 (2012).
254. Yazawa M, Hsueh B, Jia X, Pasca AM, Bernstein JA, Hallmayer J, Dolmetsch RE. Using induced pluripotent stem cells to investigate cardiac phenotypes in Timothy syndrome. *Nature* 471, 230–234 (2011).
255. Fatima A, Xu G, Shao K, Papadopoulos S, Lehmann M, Arnáiz-Cot JJ, Rosa AO, Nguemo F, Matzkies M, Dittmann S, Stone SL, Linke M, Zechner U, Beyer V, Hennies HC, Rosenkranz S, Klauke B, Parwani AS, Haverkamp W, *et al.* In vitro Modeling of Ryanodine Receptor 2 Dysfunction Using Human Induced

REFERENCES

- Pluripotent Stem Cells. *Cell. Physiol. Biochem.* 28, 579–592 (2011).
256. Sun N, Yazawa M, Liu J, Han L, Sanchez-Freire V, Abilez OJ, Navarrete EG, Hu S, Wang L, Lee A, Pavlovic A, Lin S, Chen R, Hajjar RJ, Snyder MP, Dolmetsch RE, Butte MJ, Ashley EA, Longaker MT, *et al.* Patient-Specific Induced Pluripotent Stem Cells as a Model for Familial Dilated Cardiomyopathy. *Sci. Transl. Med.* 4, 130ra47 LP-130ra47 (2012).
257. Lan F, Lee AS, Liang P, Sanchez-Freire V, Nguyen PK, Wang L, Han L, Yen M, Wang Y, Sun N, Abilez OJ, Hu S, Ebert AD, Navarrete EG, Simmons CS, Wheeler M, Pruitt B, Lewis R, Yamaguchi Y, *et al.* Abnormal Calcium Handling Properties Underlie Familial Hypertrophic Cardiomyopathy Pathology in Patient-Specific Induced Pluripotent Stem Cells. *Cell Stem Cell* 12, 101–113 (2013).
258. Shafiee A, Atala A. Tissue Engineering: Toward a New Era of Medicine. *Annu. Rev. Med.* 68, 29–40 (2017).
259. Ye L, Zimmermann W-H, Garry DJ, Zhang J. Patching the Heart. *Circ. Res.* 113, 922 LP-932 (2013).
260. de Lange WJ, Hegge LF, Grimes AC, Tong CW, Brost TM, Moss RL, Ralphe JC. Neonatal Mouse-Derived Engineered Cardiac Tissue Novelty and Significance. *Circ. Res.* 109, 8–19 (2011).
261. Stoehr A, Neuber C, Baldauf C, Vollert I, Friedrich FW, Flenner F, Carrier L, Eder A, Schaaf S, Hirt MN, Aksehirioglu B, Tong CW, Moretti A, Eschenhagen T, Hansen A. Automated analysis of contractile force and Ca²⁺ transients in engineered heart tissue. *Am. J. Physiol. Hear. Circ. Physiol.* 306, H1353 LP-H1363 (2014).
262. Eschenhagen T, Fink C, Remmers U, Scholz H, Wattchow J, Weil J, Zimmermann W, Dohmen HH, Schäfer H, Bishopric N, Wakatsuki T, Elson EL. Three-dimensional reconstitution of embryonic cardiomyocytes in a collagen matrix: a new heart muscle model system. *FASEB J.* 11, 683–694 (1997).
263. Thomson JA, Itskovitz-Eldor J, Shapiro SS, Waknitz MA, Swiergiel JJ, Marshall VS, Jones JM. Embryonic Stem Cell Lines Derived from Human Blastocysts. *Science* 282, 1145–1147 (1998).
264. Takahashi K, Tanabe K, Ohnuki M, Narita M, Ichisaka T, Tomoda K, Yamanaka S. Induction of Pluripotent Stem Cells from Adult Human Fibroblasts by Defined Factors. *Cell* 131, 861–872 (2007).
265. Yu J, Vodyanik M, Smuga-Otto K, Antosiewicz-Bourget J, Frane J, Tian S, Nie J, Jonsdottir G, Ruotti V, Stewart R, Slukvin I, Thomson J. Induced Pluripotent Stem Cell Lines Derived from Human Somatic Cells. *Science* 21, 1917–1920 (2007).
266. Aasen T, Raya A, Barrero MJ, Garreta E, Consiglio A, Gonzalez F, Vassena R, Bilić J, Pekarik V, Tiscornia G, Edel M, Boué S, Izpisua Belmonte JC. Efficient and rapid generation of induced pluripotent stem cells from human keratinocytes. *Nat. Biotechnol.* 26, 1276–84 (2008).
267. Zhao T, Zhang Z-N, Rong Z, Xu Y. Immunogenicity of induced pluripotent stem cells. *Nature* 474, 212–215 (2011).
268. Young MA, Larson DE, Sun C-W, George DR, Ding L, Miller CA, Lin L, Pawlik KM, Chen K, Fan X, Schmidt H, Kalicki-Veizer J, Cook LL, Swift GW, Demeter RT, Wendl MC, Sands MS, Mardis ER, Wilson RK, *et al.* Background Mutations in Parental Cells Account for Most of the Genetic Heterogeneity of Induced Pluripotent Stem Cells. *Cell Stem Cell* 10, 570–582 (2017).
269. Robinton DA, Daley GQ. The promise of induced pluripotent stem cells in research and therapy. *Nature* 481, 295–305 (2012).
270. Yang L, Soonpaa MH, Adler ED, Roepke TK, Kattman SJ, Kennedy M, Henckaerts E, Bonham K, Abbott GW, Linden RM, Field LJ, Keller GM. Human cardiovascular progenitor cells develop from a KDR+ embryonic-stem-cell-derived population. *Nature* 453, 524–8 (2008).
271. Lian X, Hsiao C, Wilson G, Zhu K, Hazeltine LB, Azarin SM, Raval KK, Zhang J, Kamp TJ, Palecek SP. Robust cardiomyocyte differentiation from human pluripotent stem cells via temporal modulation of canonical Wnt signaling. *Proc. Natl. Acad. Sci.* 109, E1848–E1857 (2012).
272. Kraehenbuehl TP, Langer R, Ferreira LS. Three-dimensional biomaterials for the study of human pluripotent stem cells. *Nat. Methods* 8, 731–6 (2011).
273. Vunjak-Novakovic G, Scadden DT. Biomimetic platforms for human stem cell research. *Cell Stem Cell* 8, 252–61 (2011).

274. Serena E, Figallo E, Tandon N, Cannizzaro C, Gerecht S, Elvassore N, Vunjak-Novakovic G. Electrical stimulation of human embryonic stem cells: cardiac differentiation and the generation of reactive oxygen species. *Exp. Cell Res.* 315, 3611–3619 (2009).
275. Castano AG, Hortigüela V, Lagunas A, Cortina C, Montserrat N, Samitier J, Martínez E. Protein patterning on hydrogels by direct microcontact printing: application to cardiac differentiation. *Rsc Adv.* 4, 29120–29123 (2014).
276. Porter KE, Turner NA. Cardiac fibroblasts: At the heart of myocardial remodeling. *Pharmacol. Ther.* 123, 255–278 (2009).
277. Zhang D, Shadrin IY, Lam J, Xian HQ, Snodgrass HR, Bursac N. Tissue-engineered cardiac patch for advanced functional maturation of human ESC-derived cardiomyocytes. *Biomaterials* 34, 5813–5820 (2013).
278. Tiburcy M, Hudson JE, Balfanz P, Schlick SF, Meyer T, Chang Liao M-L, Levent E, Raad F, Zeidler S, Wingender E, Riegler J, Wang M, Gold JD, Kehat I, Wettwer E, Ravens U, Dierickx P, van Laake L, Goumans M-J, *et al.* Defined Engineered Human Myocardium with Advanced Maturation for Applications in Heart Failure Modelling and Repair. *Circulation* (2017).
279. Naito H, Melnychenko I, Didié M, Schneiderbanger K, Schubert P, Rosenkranz S, Eschenhagen T, Zimmermann WH. Optimizing engineered heart tissue for therapeutic applications as surrogate heart muscle. *Circulation* 114, 72–79 (2006).
280. Kensah G, Roa Lara A, Dahlmann J, Zweigerdt R, Schwanke K, Hegermann J, Skvorc D, Gawol A, Azizian A, Wagner S, Maier LS, Krause A, Dräger G, Ochs M, Haverich A, Gruh I, Martin U. Murine and human pluripotent stem cell-derived cardiac bodies form contractile myocardial tissue in vitro. *Eur. Heart J.* 34, 1134–1146 (2013).
281. Radisic M, Park H, Shing H, Consi T, Schoen FJ, Langer R, Freed LE, Vunjak-Novakovic G. Functional assembly of engineered myocardium by electrical stimulation of cardiac myocytes cultured on scaffolds. *Proc. Natl. Acad. Sci. U. S. A.* 101, 18129–18134 (2004).
282. Zimmermann WH, Melnychenko I, Wasmeier G, Didié M, Naito H, Nixdorff U, Hess A, Budinsky L, Brune K, Michaelis B, Dhein S, Schwoerer A, Ehmke H, Eschenhagen T. Engineered heart tissue grafts improve systolic and diastolic function in infarcted rat hearts. *Nat. Med.* 12, 452–458 (2006).
283. Rask F, Dallabrida SM, Ismail NS, Amoozgar Z, Yeo Y, Rupnick MA, Radisic M. Photocrosslinkable chitosan modified with angiopoietin-1 peptide, QHREDGS, promotes survival of neonatal rat heart cells. *J. Biomed. Mater. Res. Part A* 95A, 105–117 (2010).
284. Engelmayr GC, Cheng M, Bettinger CJ, Borenstein JT, Langer R, Freed LE. Accordion-like honeycombs for tissue engineering of cardiac anisotropy. *Nat. Mater.* 7, 1003–1010 (2008).
285. Zong X, Bien H, Chung C-Y, Yin L, Fang D, Hsiao BS, Chu B, Entcheva E. Electrospun fine-textured scaffolds for heart tissue constructs. *Biomaterials* 26, 5330–5338 (2005).
286. Yeong WY, Sudarmadji N, Yu HY, Chua CK, Leong KF, Venkatraman SS, Boey YCF, Tan LP. Porous polycaprolactone scaffold for cardiac tissue engineering fabricated by selective laser sintering. *Acta Biomater.* 6, 2028–34 (2010).
287. Ifkovits JL, Wu K, Mauck RL, Burdick JA. The influence of fibrous elastomer structure and porosity on matrix organization. *PLoS One* 5, (2010).
288. Ott HC, Matthiesen TS, Goh S-K, Black LD, Kren SM, Netoff TI, Taylor D a. Perfusion-decellularized matrix: using nature's platform to engineer a bioartificial heart. *Nat. Med.* 14, 213–21 (2008).
289. Garreta E, de Oñate L, Fernández-Santos ME, Oria R, Tarantino C, Climent AM, Marco A, Samitier M, Martínez E, Valls-Margarit M, Matesanz R, Taylor DA, Fernández-Avilés F, Izpisua Belmonte JC, Montserrat N. Myocardial commitment from human pluripotent stem cells: Rapid production of human heart grafts. *Biomaterials* 98, 64–78 (2016).
290. Reis L, Chiu LLY, Feric N, Fu L, Radisic M. Biomaterials in myocardial tissue engineering. *J. Tissue Eng. Regen. Med.* 10, 11–28 (2016).
291. Jacot JG, Martin JC, Hunt DL. Mechanobiology of Cardiomyocyte Development. *J Biomech* 43, 93–8 (2010).

REFERENCES

292. Prakash Y, Cody M, Housmans P, Hannon J, Sieck G. Comparison of cross-bridge cycling kinetics in neonatal vs. adult rat ventricular muscle. *J Muscle Res Cell Motil* 20, 717–723 (1999).
293. Huyer LD, Montgomery M, Zhao Y, Xiao Y, Conant G, Korolj A, Radisic M. Biomaterial based cardiac tissue engineering and its applications. *Biomed. Mater.* 10, 34004 (2015).
294. Wang PY, Tsai WB, Voelcker NH. Screening of rat mesenchymal stem cell behaviour on polydimethylsiloxane stiffness gradients. *Acta Biomater.* 8, 519–30 (2012).
295. Jacot JG, McCulloch AD, Omens JH. Substrate stiffness affects the functional maturation of neonatal rat ventricular myocytes. *Biophys. J.* 95, 3479–87 (2008).
296. Marsano A, Maidhof R, Wan LQ, Wang Y, Gao J, Tandon N, Vunjak-Novakovic G. Scaffold stiffness affects the contractile function of three-dimensional engineered cardiac constructs. *Biotechnol. Prog.* 26, 1382–1390 (2010).
297. Radisic M, Marsano A, Maidhof R, Wang Y, Vunjak-Novakovic G. Cardiac tissue engineering using perfusion bioreactor systems. *Nat. Protoc.* 3, 719–38 (2008).
298. Patel M, Fisher JP. Biomaterial Scaffolds in Pediatric Tissue Engineering. *Pediatr Res* 63, 497–501 (2008).
299. Prabhakaran MP, Venugopal J, Kai D, Ramakrishna S. Biomimetic material strategies for cardiac tissue engineering. *Mater. Sci. Eng. C* 31, 503–513 (2011).
300. Huber A, Badylak SF. *Biological scaffolds for regenerative medicine*. in *Principles of Regenerative Medicine* (eds. Atala, A., Lanza, R., Thomson, J. A. & Nerem, R.) 623–635 (Elsevier Academic Press, 2011).
301. Odedra D, Chiu L, Reis L, Al. E. *Cardiac tissue engineering*. in *Biomaterials for Tissue Engineering Applications: A Review of Past and Future Trends* (eds. Burdick, J. & Mauck, R.) 421–456 (Springer, 2011).
302. Dawson J, Schussler O, Al-Madhoun A, Menard C, Ruel M, Skerjanc IS. Collagen scaffolds with or without the addition of RGD peptides support cardiomyogenesis after aggregation of mouse embryonic stem cells. *In Vitro Cell Dev Biol Anim.* 47, 653–664 (2011).
303. Guo Z, Iku S, Zheng X, Sammons RL, Kuboki Y. Three-Dimensional Geometry of Honeycomb Collagen Promotes Higher Beating Rate of Myocardial Cells in Culture. *Artif. Organs* 36, 816–819 (2012).
304. Schussler O, Coirault C, Louis-Tisserand M, Al-Chare W, Oliviero P, Menard C, Michelot RJ, Bochet P, Salomon DR, Chachques JC, Carpentier A, Lecarpentier Y. Use of arginine-glycine-aspartic acid adhesion peptides coupled with a new collagen scaffold to engineer a myocardium-like tissue graft. *Nat Clin Pr. Cardiovasc Med* 6, 240–249 (2009).
305. Shachar M, Benishti N, Cohen S. Effects of mechanical stimulation induced by compression and medium perfusion on cardiac tissue engineering. *Biotechnol. Prog.* 28, 1551–1559 (2012).
306. Rosellini E, Cristallini C, Barbani N, Vozzi G, Giusti P. Preparation and characterization of alginate/gelatin blend films for cardiac tissue engineering. *J. Biomed. Mater. Res. Part A* 91A, 447–453 (2009).
307. Dvir T, Timko BP, Brigham MD, Naik SR, Karajanagi SS, Levy O, Jin H, Parker KK, Langer R, Kohane DS. Nanowired three-dimensional cardiac patches. *Nat Nano* 6, 720–725 (2011).
308. Lu W, Lü S, Wang H, Li D, Duan C, Liu Z, Hao T, He W, Xu B, Fu Q, Song Y, Xie X, Wang C. Functional Improvement of Infarcted Heart by Co-Injection of Embryonic Stem Cells with Temperature-Responsive Chitosan Hydrogel. *Tissue Eng. Part A* 15, 1437–1447 (2008).
309. Martins AM, Eng G, Caridade SG, Mano JF, Reis RL, Vunjak-Novakovic G. Electrically conductive chitosan/carbon scaffolds for cardiac tissue engineering. *Biomacromolecules* 15, 635–43 (2014).
310. Reis LA, Chiu LLY, Liang Y, Hyunh K, Momen A, Radisic M. A peptide-modified chitosan–collagen hydrogel for cardiac cell culture and delivery. *Acta Biomater.* 8, 1022–1036 (2012).
311. Morritt AN, Bortolotto SK, Dilley RJ, Han X, Kompa AR, McCombe D, Wright CE, Itescu S, Angus JA, Morrison WA. Cardiac Tissue Engineering in an In Vivo Vascularized Chamber. *Circulation* 115, 353

- LP-360 (2007).
312. Christman KL, Vardanian AJ, Fang Q, Sievers RE, Fok HH, Lee RJ. Injectable Fibrin Scaffold Improves Cell Transplant Survival, Reduces Infarct Expansion, and Induces Neovasculature Formation in Ischemic Myocardium. *J. Am. Coll. Cardiol.* 44, 654–660 (2004).
 313. Black L 3rd, Meyers J, Weinbaum J, Shvelidze Y, Tranquillo R. Cell-Induced Alignment Augments Twitch Force in Fibrin Gel–Based Engineered Myocardium via Gap Junction Modification. *Tissue Eng. Part A* 15, 3099–3108 (2009).
 314. Lisi A, Briganti E, Ledda M, Losi P, Grimaldi S, Marchese R, Soldani G. A Combined Synthetic-Fibrin Scaffold Supports Growth and Cardiomyogenic Commitment of Human Placental Derived Stem Cells. *PLoS One* 7, e34284 (2012).
 315. Liao B, Christoforou N, Leong KW, Bursac N. Pluripotent stem cell-derived cardiac tissue patch with advanced structure and function. *Biomaterials* 32, 9180–7 (2011).
 316. Grover CN, Cameron RE, Best SM. Investigating the morphological, mechanical and degradation properties of scaffolds comprising collagen, gelatin and elastin for use in soft tissue engineering. *J. Mech. Behav. Biomed. Mater.* 10, 62–74 (2012).
 317. Hansen A, Eder A, Bönstrup M, Flato M, Mewe M, Schaaf S, Aksehirioglu B, Schwörer A, Uebeler J, Eschenhagen T. Development of a drug screening platform based on engineered heart tissue. *Circ. Res.* 107, 35–44 (2010).
 318. Tandon N, Cannizzaro C, Chao P-HG, Maidhof R, Marsano A, Au HTH, Radisic M, Vunjak-Novakovic G. Electrical stimulation systems for cardiac tissue engineering. *Nat. Protoc.* 4, 155–73 (2009).
 319. Nunes SS, Miklas JW, Liu J, Aschar-Sobbi R, Xiao Y, Zhang B, Jiang J, Massé S, Gagliardi M, Hsieh A, Thavandiran N, Laflamme MA, Nanthakumar K, Gross GJ, Backx PH, Keller G, Radisic M. Biowire: a platform for maturation of human pluripotent stem cell-derived cardiomyocytes. *Nat. Methods* 10, 781–7 (2013).
 320. Gálvez-Montón C, Fernandez-Figueras MT, Martí M, Soler-Botija C, Roura S, Perea-Gil I, Prat-Vidal C, Llucà-Valldeperas A, Raya Á, Bayes-Genis A. Neoinnervation and neovascularization of acellular pericardial-derived scaffolds in myocardial infarcts. *Stem Cell Res. Ther.* 6, 108 (2015).
 321. Rockwood DN, Akins Jr. RE, Parrag IC, Woodhouse KA, Rabolt JF. Culture on electrospun polyurethane scaffolds decreases atrial natriuretic peptide expression by cardiomyocytes in vitro. *Biomaterials* 29, 4783–4791 (2008).
 322. Park H, Larson BL, Kolewe ME, Vunjak-Novakovic G, Freed LE. Biomimetic scaffold combined with electrical stimulation and growth factor promotes tissue engineered cardiac development. *Exp. Cell Res.* 321, 297–306 (2014).
 323. Ishii O, Shin M, Sueda T, Vacanti JP. In vitro tissue engineering of a cardiac graft using a degradable scaffold with an extracellular matrix-like topography. *J. Thorac. Cardiovasc. Surg.* 130, 1358–63 (2005).
 324. Park H, Radisic M, Lim JO, Chang BH, Vunjak-Novakovic G. A novel composite scaffold for cardiac tissue engineering. *In Vitro Cell. Dev. Biol. Anim.* 41, 188–96 (2005).
 325. Fleischer S, Shapira A, Feiner R, Dvir T. Modular assembly of thick multifunctional cardiac patches. *Proc. Natl. Acad. Sci.* 114, 1898–1903 (2017).
 326. Peters N, Severs N, Rothery S, Lincoln C, Yacoub M, Green C. Spatiotemporal relation between gap junctions and fascia adherens junctions during postnatal development of human ventricular myocardium. *Circulation* 90, 713–725 (1994).
 327. Parsa H, Ronaldson K, Vunjak-Novakovic G. Bioengineering methods for myocardial regeneration. *Adv. Drug Deliv. Rev.* 96, 195–202 (2016).
 328. Kim C, Majdi M, Xia P, Wei K a, Talantova M, Spiering S, Nelson B, Mercola M, Chen H-SV. Non-cardiomyocytes influence the electrophysiological maturation of human embryonic stem cell-derived cardiomyocytes during differentiation. *Stem Cells Dev.* 19, 783–795 (2010).
 329. Thavandiran N, Dubois N, Mikryukov A, Massé S, Beca B, Simmons C a, Deshpande VS, McGarry JP, Chen CS, Nanthakumar K, Keller GM, Radisic M, Zandstra PW. Design and formulation of functional

REFERENCES

- pluripotent stem cell-derived cardiac microtissues. *Proc. Natl. Acad. Sci.* 110, E4698-707 (2013).
330. Chavakis E, Koyanagi M, Dimmeler S. Enhancing the outcome of cell therapy for cardiac repair: Progress from bench to bedside and back. *Circulation* 121, 325–335 (2010).
331. Kuo PL, Lee H, Bray MA, Geisse NA, Huang YT, Adams WJ, Sheehy SP, Parker KK. Myocyte shape regulates lateral registry of sarcomeres and contractility. *Am. J. Pathol.* 181, 2030–2037 (2012).
332. Mihic A, Li J, Miyagi Y, Gagliardi M, Li S-H, Zu J, Weisel RD, Keller G, Li R-K. The effect of cyclic stretch on maturation and 3D tissue formation of human embryonic stem cell-derived cardiomyocytes. *Biomaterials* 35, 2798–2808 (2014).
333. Eng G, Lee BW, Protas L, Gagliardi M, Brown K, Kass RS, Keller G, Robinson RB, Vunjak-Novakovic G. Autonomous beating rate adaptation in human stem cell-derived cardiomyocytes. *Nat. Commun.* 7, 1–10 (2016).
334. Kadota S, Minami I, Morone N, Heuser JE, Agladze K, Nakatsuji N. Development of a reentrant arrhythmia model in human pluripotent stem cell-derived cardiac cell sheets. *Eur. Heart J.* 34, 1147–1156 (2013).
335. Hazeltine L, Simmons C, Salick M, Lian X, Badur M, Han W, Al. E. Effects of substrate mechanics on contractility of cardiomyocytes generated from human pluripotent stem cells. *Int J Cell Biol* 2012, (2012).
336. Zimmermann W, Schneiderbanger K, Schubert P, Didié M, Münzel F, Heubach JF, Kostin S, Neuhuber WL, Eschenhagen T. Tissue Engineering of a Differentiated Cardiac Muscle Construct. *Circ. Res.* 90, 223 LP-230 (2002).
337. Hirt MN, Boeddinghaus J, Mitchell A, Schaaf S, Börnchen C, Müller C, Schulz H, Hubner N, Stenzig J, Stoehr A, Neuber C, Eder A, Luther PK, Hansen A, Eschenhagen T. Functional improvement and maturation of rat and human engineered heart tissue by chronic electrical stimulation. *J. Mol. Cell. Cardiol.* 74, 151–161 (2014).
338. Masuda S, Shimizu T. Three-dimensional cardiac tissue fabrication based on cell sheet technology. *Adv. Drug Deliv. Rev.* 96, 103–109 (2016).
339. Kang H-W, Lee SJ, Ko IK, Kengla C, Yoo JJ, Atala A. A 3D bioprinting system to produce human-scale tissue constructs with structural integrity. *Nat. Biotechnol.* 34, 312–319 (2016).
340. Tiburcy M, Didié M, Boy O, Christalla P, Döker S, Naito H, Karikkineth BC, El-Armouche A, Grimm M, Nose M, Eschenhagen T, Ziesenis A, Katschinski DM, Hamdani N, Linke W a, Yin X, Mayr M, Zimmermann W-H. Terminal differentiation, advanced organotypic maturation, and modeling of hypertrophic growth in engineered heart tissue. *Circ. Res.* 109, 1105–14 (2011).
341. Herron TJ, Da Rocha AM, Campbell KF, Ponce-Balbuena D, Willis BC, Guerrero-Serna G, Liu Q, Klos M, Musa H, Zarzoso M, Bizy A, Furness J, Anumonwo J, Mironov S, Jalife J. Extracellular matrix-mediated maturation of human pluripotent stem cell-derived cardiac monolayer structure and electrophysiological function. *Circ. Arrhythmia Electrophysiol.* 9, (2016).
342. Deng X-F, Rokosh DG, Simpson PC. Autonomous and Growth Factor–Induced Hypertrophy in Cultured Neonatal Mouse Cardiac Myocytes. *Circ. Res.* 87, 781 LP-788 (2000).
343. Frey N, Katus H a., Olson EN, Hill J a. Hypertrophy of the Heart: A New Therapeutic Target? *Circulation* 109, 1580–1589 (2004).
344. Klein I, Ojamaa K. Thyroid Hormone and the Cardiovascular System. *N. Engl. J. Med.* 344, 501–509 (2001).
345. Krüger M, Sachse C, Zimmermann WH, Eschenhagen T, Klede S, Linke WA. Thyroid Hormone Regulates Developmental Titin Isoform Transitions via the Phosphatidylinositol-3-Kinase/ AKT Pathway. *Circ. Res.* 102, 439 LP-447 (2008).
346. Lee Y-K, Ng K-M, Chan Y-C, Lai W-H, Au K-W, Ho C-YJ, Wong L-Y, Lau C-P, Tse H-F, Siu C-W. Triiodothyronine Promotes Cardiac Differentiation and Maturation of Embryonic Stem Cells via the Classical Genomic Pathway. *Mol. Endocrinol.* 24, 1728–1736 (2010).
347. Yang X, Rodriguez M, Pabon L, Fischer K a, Reinecke H, Regnier M, Sniadecki NJ, Ruohola-Baker H, Murry CE. Tri-iodo-L-thyronine promotes the maturation of human cardiomyocytes-derived from induced

- pluripotent stem cells. *J. Mol. Cell. Cardiol.* 72, 296–304 (2014).
348. Ito H, Hiroe M, Hirata Y, Tsujino M, Adachi S, Shichiri M, Koike A, Nogami A, Marumo F. Insulin-like growth factor-I induces hypertrophy with enhanced expression of muscle specific genes in cultured rat cardiomyocytes. *Circulation* 87, 1715–1721 (1993).
349. Montessuit C, Palma T, Viglino C, Pellioux C, Lerch R. Effects of insulin-like growth factor-I on the maturation of metabolism in neonatal rat cardiomyocytes. *Pflügers Arch.* 452, 380–386 (2006).
350. Cheng M, Moretti M, Engelmayer GC, Freed LE. Insulin-like Growth Factor-I and Slow, Bi-directional Perfusion Enhance the Formation of Tissue-Engineered Cardiac Grafts. *Tissue Eng. Part A* 15, (2009).
351. Porrello ER, Widdop RE, Delbridge LMD. Early origins of cardiac hypertrophy: Does cardiomyocyte attrition programme for pathological 'catch-up' growth of the heart? *Clin. Exp. Pharmacol. Physiol.* 35, 1358–1364 (2008).
352. McDevitt TC, Laflamme MA, Murry CE. Proliferation of cardiomyocytes derived from human embryonic stem cells is mediated via the IGF/PI 3-kinase/Akt signaling pathway. *J. Mol. Cell. Cardiol.* 39, 865–873 (2005).
353. Takahashi T, Lord B, Schulze P, Fryer R, Sarang S, Gullans S, Lee R. Ascorbic acid enhances differentiation of embryonic stem cells into cardiac myocytes. *Circulation* 107, 1912–1916 (2003).
354. Cao N, Liu Z, Chen Z, Wang J, Chen T, Zhao X, Ma Y, Qin L, Kang J, Wei B, Wang L, Jin Y, Yang H-T. Ascorbic acid enhances the cardiac differentiation of induced pluripotent stem cells through promoting the proliferation of cardiac progenitor cells. *Cell Res.* 22, 219–36 (2012).
355. Zhu W-Z, Xie Y, Moyes KW, Gold JD, Askari B, Laflamme MA. Neuregulin/ErbB Signaling Regulates Cardiac Subtype Specification in Differentiating Human Embryonic Stem Cells. *Circ. Res.* 107, 776–86 (2010).
356. Iglesias-García O, Baumgartner S, Macrí-Pellizzeri L, Rodríguez-Madoz JR, Abizanda G, Guruceaga E, Albiasu E, Corbacho D, Benavides-Vallve C, Soriano-Navarro M, González-Granero S, Gavira JJ, Krausgrill B, Rodríguez-Mañero M, García-Verdugo JM, Ortiz-de-Solorzano C, Halbach M, Hescheler J, Pelacho B, *et al.* Neuregulin-1 β induces mature ventricular cardiac differentiation from induced pluripotent stem cells contributing to cardiac tissue repair. *Stem Cells Dev.* 24, 484–96 (2015).
357. Fu J-D, Rushing SN, Lieu DK, Chan CW, Kong C-W, Geng L, Wilson KD, Chiamvimonvat N, Boheler KR, Wu JC, Keller G, Hajjar RJ, Li RA. Distinct Roles of MicroRNA-1 and -499 in Ventricular Specification and Functional Maturation of Human Embryonic Stem Cell-Derived Cardiomyocytes. *PLoS One* 6, e27417 (2011).
358. van Rooij E, Sutherland LB, Qi X, Richardson JA, Hill J, Olson EN. Control of Stress-Dependent Cardiac Growth and Gene Expression by a MicroRNA. *Science* 316, 575 LP-579 (2007).
359. Callis TE, Pandya K, Seok HY, Tang R-H, Tatsuguchi M, Huang Z-P, Chen J-F, Deng Z, Gunn B, Shumate J, Willis MS, Selzman CH, Wang D-Z. MicroRNA-208a is a regulator of cardiac hypertrophy and conduction in mice. *J. Clin. Invest.* 119, 2772–2786 (2009).
360. Salick MR, Napiwocki BN, Sha J, Knight GT, Chindhy SA, Kamp TJ, Ashton RS, Crone WC. Micropattern width dependent sarcomere development in human ESC-derived cardiomyocytes. *Biomaterials* 35, 4454–4464 (2014).
361. Kai D, Prabhakaran MP, Jin G, Ramakrishna S. Guided orientation of cardiomyocytes on electrospun aligned nanofibers for cardiac tissue engineering. *J. Biomed. Mater. Res. Part B Appl. Biomater.* 98B, 379–386 (2011).
362. Bursac N, Parker KK, Iravanian S, Tung L. Cardiomyocyte Cultures With Controlled Macroscopic Anisotropy. *Circ. Res.* 91, e45 LP-e54 (2002).
363. McDevitt T, Angello J, Whitney M, Reinecke H, Hauschka S, Murry C, Stayton P. In vitro generation of differentiated cardiac myofibers on micropatterned laminin surfaces. *J Biomed Mater Res* 60, 472–479 (2002).
364. Feinberg AW, Alford PW, Jin H, Ripplinger CM, Werdich AA, Sheehy SP, Grosberg A, Parker KK. Controlling the contractile strength of engineered cardiac muscle by hierarchal tissue architecture. *Biomaterials* 33, 5732–5741 (2012).

REFERENCES

365. Parrag IC, Zandstra PW, Woodhouse KA. Fiber alignment and coculture with fibroblasts improves the differentiated phenotype of murine embryonic stem cell-derived cardiomyocytes for cardiac tissue engineering. *Biotechnol. Bioeng.* 109, 813–822 (2012).
366. Kim D-H, Lipke EA, Kim P, Cheong R, Thompson S, Delannoy M, Suh K-Y, Tung L, Levchenko A. Nanoscale cues regulate the structure and function of macroscopic cardiac tissue constructs. *Proc. Natl. Acad. Sci.* 107, 565–570 (2010).
367. Wang P-Y, Yu J, Lin J-H, Tsai W-B. Modulation of alignment, elongation and contraction of cardiomyocytes through a combination of nanotopography and rigidity of substrates. *Acta Biomater.* 7, 3285–3293 (2011).
368. Grosberg A, Alford PW, McCain ML, Parker KK. Ensembles of engineered cardiac tissues for physiological and pharmacological study: heart on a chip. *Lab Chip* 11, 4165–73 (2011).
369. Chen A, Lieu DK, Freschauf L, Lew V, Sharma H, Wang J, Nguyen D, Karakikes I, Hajjar RJ, Gopinathan A, Botvinick E, Fowlkes CC, Li RA, Khine M. Shrink-Film Configurable Multiscale Wrinkles for Functional Alignment of Human Embryonic Stem Cells and their Cardiac Derivatives. *Adv. Mater.* 23, 5785–5791 (2011).
370. Chen A, Lee E, Tu R, Santiago K, Grosberg A, Fowlkes C, Khine M. Integrated platform for functional monitoring of biomimetic heart sheets derived from human pluripotent stem cells. *Biomaterials* 35, 675–683 (2014).
371. Stoppel WL, Kaplan DL, Black LD. Electrical and mechanical stimulation of cardiac cells and tissue constructs. *Adv. Drug Deliv. Rev.* 96, 135–155 (2016).
372. Zimmermann WH. Biomechanical regulation of in vitro cardiogenesis for tissue-engineered heart repair. *Stem Cell Res. Ther.* 4, 137 (2013).
373. Liaw NY, Zimmermann WH. Mechanical stimulation in the engineering of heart muscle. *Adv. Drug Deliv. Rev.* 96, 156–160 (2016).
374. Tse JR, Engler AJ. *Preparation of Hydrogel Substrates with Tunable Mechanical Properties.* in *Current Protocols in Cell Biology* (John Wiley & Sons, Inc., 2001).
375. Bhana B, Iyer RK, Chen WLK, Zhao R, Sider KL, Likhitpanichkul M, Simmons CA, Radisic M. Influence of substrate stiffness on the phenotype of heart cells. *Biotechnol. Bioeng.* 105, 1148–1160 (2010).
376. Blaauw E, van Nieuwenhoven FA, Willemsen P, Delhaas T, Prinzen FW, Snoeckx LH, van Bilsen M, van der Vusse GJ. Stretch-induced hypertrophy of isolated adult rabbit cardiomyocytes. *Am. J. Physiol. Hear. Circ. Physiol.* 299, H780 LP-H787 (2010).
377. Salameh A, Karl S, Djilali H, Dhein S, Janousek J, Daehnert I. Opposing and synergistic effects of cyclic mechanical stretch and α - or β -adrenergic stimulation on the cardiac gap junction protein Cx43. *Pharmacol. Res.* 62, 506–513 (2010).
378. Rangarajan S, Madden L, Bursac N. Use of flow, electrical, and mechanical stimulation to promote engineering of striated muscles. *Ann. Biomed. Eng.* 42, 1391–1405 (2014).
379. Brown MA, Iyer RK, Radisic M. Pulsatile perfusion bioreactor for cardiac tissue engineering. *Biotechnol. Prog.* 24, 907–920 (2008).
380. Streckfuss-Bömeke K, Wolf F, Azizian A, Stauske M, Tiburcy M, Wagner S, Hübscher D, Dressel R, Chen S, Jende J, Wulf G, Lorenz V, Schön MP, Maier LS, Zimmermann WH, Hasenfuss G, Guan K. Comparative study of human-induced pluripotent stem cells derived from bone marrow cells, hair keratinocytes, and skin fibroblasts. *Eur. Heart J.* 34, 2618 (2013).
381. Nuccitelli R. Endogenous ionic currents and DC electric fields in multicellular animal tissues. *Bioelectromagnetics Suppl* 1, 147–157 (1992).
382. Balint R, Cartmell SH. Electrical Stimulation: A Novel Tool for Tissue Engineering. *Tissue Eng. Part B. Rev.* 19, 48–57 (2013).
383. Hronik-Tupaj M, Kaplan DL. A review of the responses of two- and three-dimensional engineered tissues to electric fields. *Tissue Eng. Part B. Rev.* 18, 167–80 (2012).

-
384. Merrill DR, Bikson M, Jefferys JGR. Electrical stimulation of excitable tissue: Design of efficacious and safe protocols. *J. Neurosci. Methods* 141, 171–198 (2005).
385. Ercan B, Webster TJ. The effect of biphasic electrical stimulation on osteoblast function at anodized nanotubular titanium surfaces. *Biomaterials* 31, 3684–3693 (2010).
386. Ranjan R, Thakor N V. Electrical stimulation of cardiac myocytes. *Ann. Biomed. Eng.* 23, 812–821 (1995).
387. Tandon N, Marsano A, Maidhof R, Wan L, Park H, Vunjak-Novakovic G. Optimization of electrical stimulation parameters for cardiac tissue engineering. *J. Tissue Eng. Regen. Med.* 5, 115–125 (2011).
388. Tandon N, Cannizzaro C, Figallo E, Voldman J, Vunjak-novakovic G. Characterization of Electrical Stimulation Electrodes for Cardiac Tissue Engineering. *EMBS Annu. Int. Conf.* 845–848 (2006).
389. Hronik-Tupaj M, Rice WL, Cronin-Golomb M, Kaplan DL, Georgakoudi I. Osteoblastic differentiation and stress response of human mesenchymal stem cells exposed to alternating current electric fields. *Biomed. Eng. Online* 10, 9 (2011).
390. Meng S, Rouabhia M, Zhang Z. *Electrical Stimulation in Tissue Regeneration*. in *Applied Biomedical Engineering* (eds. Gargiulo, G. & McEwan, A.) 37–62 (InTech, 2011).
391. Baumgartner S, Halbach M, Krausgrill B, Maass M, Srinivasan SP, Sahito RGA, Peinkofer G, Nguemo F, Müller-Ehmsen J, Hescheler J. Electrophysiological and Morphological Maturation of Murine Fetal Cardiomyocytes During Electrical Stimulation In Vitro. *J. Cardiovasc. Pharmacol. Ther.* 20, 104–112 (2014).
392. Kujala K, Ahola A, Pekkanen-Mattila M, Ikonen L, Kerkelä E, Hyttinen J, Aalto-Setälä K. Electrical Field Stimulation with a Novel Platform: Effect on Cardiomyocyte Gene Expression but not on Orientation. *Int. J. Biomed. Sci.* 8, 109–120 (2012).
393. Plonsey R, Barr R. *Electrical stimulation of excitable tissue*. in *Bioelectricity: A Quantitative Approach* 190–193 (Springer Science, 2007).
394. Lieu DK, Fu J-D, Chiamvimonvat N, Tung KC, McNerney GP, Huser T, Keller G, Kong C-W, Li RA. Mechanism-Based Facilitated Maturation of Human Pluripotent Stem Cell-Derived Cardiomyocytes. *Circ. Arrhythmia Electrophysiol.* 6, 191 LP-201 (2013).
395. Doss MX, Di Diego JM, Goodrow RJ, Wu Y, Cordeiro JM, Nesterenko V V, Barajas-Martínez H, Hu D, Urrutia J, Desai M, Treat JA, Sachinidis A, Antzelevitch C. Maximum Diastolic Potential of Human Induced Pluripotent Stem Cell-Derived Cardiomyocytes Depends Critically on IKr. *PLoS One* 7, e40288 (2012).
396. Bilodeau K, Mantovani D. Bioreactors for Tissue Engineering: Focus on Mechanical Constraints. A Comparative Review. *Tissue Eng.* 12, 2367–2383 (2006).
397. Massai D, Cerino G, Gallo D, Pennella F, Deriu M a, Rodriguez A, Montevicchi FM, Bignardi C, Audenino A, Morbiducci U. Bioreactors as engineering support to treat cardiac muscle and vascular disease. *J. Healthc. Eng.* 4, 329–70 (2013).
398. Carrier RL, Rupnick M, Langer R, Schoen FJ, Freed LE, Vunjak-Novakovic G. Perfusion improves tissue architecture of engineered cardiac muscle. *Tissue Eng.* 8, 175–88 (2002).
399. Martin I, Wendt D, Heberer M. The role of bioreactors in tissue engineering. *Trends Biotechnol.* 22, 80–86 (2004).
400. Carrier RL, Papadaki M, Rupnick M, Schoen FJ, Bursac N, Langer R, Freed LE, Vunjak-Novakovic G. Cardiac tissue engineering: cell seeding, cultivation parameters, and tissue construct characterization. *Biotechnol. Bioeng.* 64, 580–9 (1999).
401. Bursac N, Papadaki M, White J a, Eisenberg SR, Vunjak-Novakovic G, Freed LE. Cultivation in rotating bioreactors promotes maintenance of cardiac myocyte electrophysiology and molecular properties. *Tissue Eng.* 9, 1243–1253 (2003).
402. Jasmund I, Bader A. *Bioreactor Developments for Tissue Engineering Applications by the Example of the Bioartificial Liver*. in *Tools and Applications of Biochemical Engineering Science* (eds. Schügerl, K. et al.) 99–109 (Springer Berlin Heidelberg, 2002).

REFERENCES

403. Maidhof R, Marsano A, Lee EJ, Vunjak-Novakovic G. Perfusion seeding of channeled elastomeric scaffolds with myocytes and endothelial cells for cardiac tissue engineering. *Biotechnol. Prog.* 26, 565–72 (2010).
404. Dvir T, Levy O, Shachar M, Granot Y, Cohen S. Activation of the ERK1/2 cascade via pulsatile interstitial fluid flow promotes cardiac tissue assembly. *Tissue Eng.* 13, 2185–93 (2007).
405. Coulombe KLK, Bajpai VK, Andreadis ST, Murry CE. Heart regeneration with engineered myocardial tissue. *Annu. Rev. Biomed. Eng.* 16, 1–28 (2014).
406. Feng Z, Matsumoto T, Nomura Y, Nakamura T. An electro-tensile bioreactor for 3-D culturing of cardiomyocytes. A bioreactor system that simulates the myocardium's electrical and mechanical response in vivo. *IEEE Eng. Med. Biol. Mag.* 24, 73–79 (2005).
407. Barash Y, Dvir T, Tandeitnik P, Ruvinov E, Guterman H, Cohen S. Electric field stimulation integrated into perfusion bioreactor for cardiac tissue engineering. *Tissue Eng. Part C. Methods* 16, 1417–1426 (2010).
408. Maidhof R, Tandon N, Lee EJ, Luo J, Duan Y, Yeager K, Konofagou E, Vunjak-Novakovic G. Biomimetic perfusion and electrical stimulation applied in concert improved the assembly of engineered cardiac tissue. *J. Tissue Eng. Regen. Med.* 6, (2011).
409. Kensah G, Gruh I, Viering J, Schumann H, Dahlmann J, Meyer H, Skvorc D, Bär A, Akhyari P, Heisterkamp A, Haverich A, Martin U. A novel miniaturized multimodal bioreactor for continuous in situ assessment of bioartificial cardiac tissue during stimulation and maturation. *Tissue Eng. Part C. Methods* 17, 463–473 (2011).
410. Hinson JT, Chopra A, Nafissi N, Polacheck WJ, Benson CC, Swist S, Gorham J, Yang L, Schafer S, Sheng CC, Haghghi A, Homsy J, Hubner N, Church G, Cook SA, Linke WA, Chen CS, Seidman JG, Seidman CE. Titin mutations in iPS cells define sarcomere insufficiency as a cause of dilated cardiomyopathy. *Science* 349, 982–6 (2015).
411. Soong PL, Tiburcy M, Zimmermann W-H. Cardiac differentiation of human embryonic stem cells and their assembly into engineered heart muscle. *Curr. Protoc. Cell Biol.* Chapter 23, Unit23.8 (2012).
412. Ruan J, Tulloch NL, Razumova M V, Saiget M, Muskheli V, Pabon L, Reinecke H. Mechanical Stress Conditioning and Electrical Stimulation Promote Contractility and Force Maturation of Induced Pluripotent Stem Cell-Derived Human Cardiac Tissue. *Circulation* 206–221 (2016).
413. Huebsch N, Loskill P, Deveshwar N, Spencer CI, Judge LM, Mandegar MA, B. Fox C, Mohamed TMA, Ma Z, Mathur A, Sheehan AM, Truong A, Saxton M, Yoo J, Srivastava D, Desai TA, So P-L, Healy KE, Conklin BR. Miniaturized iPS-Cell-Derived Cardiac Muscles for Physiologically Relevant Drug Response Analyses. *Sci. Rep.* 6, 24726 (2016).
414. Xiao Y, Zhang B, Liu H, Miklas JW, Gagliardi M, Pahnke A, Thavandiran N, Sun Y, Simmons C, Keller G, Radisic M. Microfabricated perfusable cardiac biowire: a platform that mimics native cardiac bundle. *Lab Chip* 14, 869–82 (2014).
415. Mathur A, Loskill P, Shao K, Huebsch N, Hong S, Marcus SG, Marks N, Mandegar M, Conklin BR, Lee LP, Healy KE. Human iPSC-based Cardiac Microphysiological System For Drug Screening Applications. *Sci. Rep.* 5, 8883 (2015).
416. Wang G, McCain ML, Yang L, He A, Pasqualini FS, Agarwal A, Yuan H, Jiang D, Zhang D, Zangi L, Geva J, Roberts AE, Ma Q, Ding J, Chen J, Wang D-Z, Li K, Wang J, Wanders RJ a, *et al.* Modeling the mitochondrial cardiomyopathy of Barth syndrome with induced pluripotent stem cell and heart-on-chip technologies. *Nat. Med.* 20, 616–23 (2014).
417. Masumoto H, Ikuno T, Takeda M, Fukushima H, Marui A, Katayama S, Shimizu T, Ikeda T, Okano T, Sakata R, Yamashita JK. Human iPS cell-engineered cardiac tissue sheets with cardiomyocytes and vascular cells for cardiac regeneration. *Sci. Rep.* 4, 1–7 (2014).
418. Ma Z, Koo S, Finnegan MA, Loskill P, Huebsch N, Marks NC, Conklin BR, Grigoropoulos CP, Healy KE. Three-dimensional filamentous human diseased cardiac tissue model. *Biomaterials* 35, 1367–1377 (2014).
419. Bedada FB, Wheelwright M, Metzger JM. Maturation status of sarcomere structure and function in human iPSC-derived cardiac myocytes. *Biochim. Biophys. Acta. Mol. Cell Res.* 1863, 1829–1838

- (2016).
420. Pradhapan P, Kuusela J, Viik J, Aalto-Setälä K, Hyttinen J. Cardiomyocyte MEA data analysis (CardioMDA)--a novel field potential data analysis software for pluripotent stem cell derived cardiomyocytes. *PLoS One* 8, e73637 (2013).
 421. Nguemo F, Šarić T, Pfannkuche K, Watzele M, Reppel M, Hescheler J. In vitro Model for Assessing Arrhythmogenic Properties of Drugs Based on High-resolution Impedance Measurements. *Cell. Physiol. Biochem.* 29, 819–832 (2012).
 422. Yan P, Acker CD, Zhou W-L, Lee P, Bollensdorff C, Negrean A, Lotti J, Sacconi L, Antic SD, Kohl P, Mansvelder HD, Pavone FS, Loew LM. Palette of fluorinated voltage-sensitive hemicyanine dyes. *Proc. Natl. Acad. Sci.* 109, 20443–20448 (2012).
 423. Stoelzle-Feix S. State-of-the-art automated patch clamp: heat activation, action potentials, and high throughput in ion channel screening. *Methods Mol. Biol.* 1183, 65–80 (2014).
 424. Asai Y, Tada M, Nakatsuji TGO and N. Combination of Functional Cardiomyocytes Derived from Human Stem Cells and a Highly-Efficient Microelectrode Array System: An Ideal Hybrid Model Assay for Drug Development. *Current Stem Cell Research & Therapy* 5, 227–232 (2010).
 425. Stett A, Egert U, Guenther E, Hofmann F, Meyer T, Nisch W, Haemmerle H. Biological application of microelectrode arrays in drug discovery and basic research. *Anal. Bioanal. Chem.* 377, 486–495 (2003).
 426. Trantidou T, Terracciano CM, Kontziampasis D, Humphrey EJ, Prodromakis T. Biorealistic cardiac cell culture platforms with integrated monitoring of extracellular action potentials. *Sci. Rep.* 5, 11067 (2015).
 427. Yamazaki K, Hihara T, Taniguchi T, Kohmura N, Yoshinaga T, Ito M, Sawada K. A novel method of selecting human embryonic stem cell-derived cardiomyocyte clusters for assessment of potential to influence QT interval. *Toxicol. Vitro.* 26, 335–342 (2012).
 428. Nakamura Y, Matsuo J, Miyamoto N, Ojima A, Ando K, Kanda Y, Sawada K, Sugiyama A, Sekino Y. Assessment of Testing Methods for Drug-Induced Repolarization Delay and Arrhythmias in an iPS Cell-Derived Cardiomyocyte Sheet: Multi-site Validation Study. *J. Pharmacol. Sci.* 501, 494–501 (2014).
 429. Sirenko O, Crittenden C, Callamaras N, Hesley J, Chen Y-W, Funes C, Rusyn I, Anson B, Cromwell EF. Multiparameter In Vitro Assessment of Compound Effects on Cardiomyocyte Physiology Using iPSC Cells. *J. Biomol. Screen.* 18, 39–53 (2012).
 430. Feiner R, Engel L, Fleischer S, Malki M, Gal I, Shapira A, Shacham-Diamand Y, Dvir T. Engineered hybrid cardiac patches with multifunctional electronics for online monitoring and regulation of tissue function. *Nat. Mater.* 1–8 (2016).
 431. Di Guglielmo C. Biotechnological approaches to cardiac differentiation of human induced pluripotent stem cells. (Universitat de Barcelona, 2016).
 432. Kita-Matsuo H, Barcova M, Prigozhina N, Salomonis N, Wei K, Jacot JG, Nelson B, Spiering S, Haverslag R, Kim C, Talantova M, Bajpai R, Calzolari D, Tershikh A, McCulloch AD, Price JH, Conklin BR, Chen HSV, Mercola M. Lentiviral vectors and protocols for creation of stable hESC lines for fluorescent tracking and drug resistance selection of cardiomyocytes. *PLoS One* 4, (2009).
 433. Lian X, Zhang J, Azarin SM, Zhu K, Hazeltine LB, Bao X, Hsiao C, Kamp TJ, Palecek SP. Directed cardiomyocyte differentiation from human pluripotent stem cells by modulating Wnt/ β -catenin signaling under fully defined conditions. *Nat. Protoc.* 8, 162–75 (2013).
 434. Schneider CA, Rasband WS, Eliceiri KW. NIH Image to ImageJ: 25 years of image analysis. *Nat. Methods* 9, 671–675 (2012).
 435. Jiang X, Zhong J, Liu Y, Yu H, Zhuo S, Chen J. Two-photon fluorescence and second-harmonic generation imaging of collagen in human tissue based on multiphoton microscopy. *Scanning* 33, 53–56 (2011).
 436. Zoumi A, Lu X, Kassab GS, Tromberg BJ. Imaging coronary artery microstructure using second-harmonic and two-photon fluorescence microscopy. *Biophys. J.* 87, 2778–2786 (2004).
 437. Richards-Kortum R, Sevick-Muraca E. Quantitative optical spectroscopy for tissue diagnosis. *Annu. Rev. Phys. Chem.* 47, 555–606 (1996).

REFERENCES

438. Haus HA. *Electromagnetic Fields and Energy*. Englewood Cliffs, NJ Prentice-Hall (1989).
439. Westerweel J. Fundamentals of digital particle image velocimetry. *Meas. Sci. Technol.* 8, 1379–1392 (1997).
440. Sveen JK. *An introduction to MatPIV v. 1.6.1*. in *Mechanics and Applied Mathematics 2*, (Department of Mathematics, Univeristy of Oslo, 2004).
441. Martí M, Mulero L, Pardo C, Morera C, Carrió M, Laricchia-Robbio L, Esteban CR, Izpisua Belmonte JC. Characterization of pluripotent stem cells. *Nat. Protoc.* 8, 223–53 (2013).
442. Livak KJ, Schmittgen TD. Analysis of relative gene expression data using real-time quantitative PCR and. *Methods* 25, 402–408 (2001).
443. Wu Z, Huang E N. Ensemble Empirical Mode Decomposition. 1, 385–388 (2011).
444. Heart rate variability. Standards of measurement, physiological interpretation, and clinical use. *Eur. Heart J.* 17, 354–81 (1996).
445. Cimetta E, Godier-Furnémont A, Vunjak-Novakovic G. Bioengineering heart tissue for in vitro testing. *Curr. Opin. Biotechnol.* 24, 926–32 (2013).
446. Shivashankar G. *Nuclear Mechanics and Genome Regulation*. (2010).
447. van Zuijlen P, van Trier A, Vloemans J, Groenevelt F, Kreis R, Middelkoop E. Graft Survival and Effectiveness of Dermal Substitution in Burns and Reconstructive Surgery in a One-Stage Grafting Model. 615–623 (1999).
448. Wollina U. One-stage Reconstruction of Soft Tissue Defects with the Sandwich Technique: Collagen-elastin Dermal Template and Skin Grafts. *J. Cutan. Aesthet. Surg.* 4, 176–82 (2011).
449. Shukla AK, Dey N, Nandi P, Ranjan M. Acellular Dermis as a Dermal Matrix of Tissue Engineered Skin Substitute for Burns Treatment. *Ann Public Heal. Res* 2, 1023 (2015).
450. Middelkoop E, de Vries H, Ruuls L, Everts V, Wildevuur C, Westerhof W. Adherence, proliferation and collagen turnover by human fibroblasts seeded into different types of collagen sponges. *Cell Tissue Res* 280, 447–53 (1995).
451. De Vries HJC, Middelkoop E, Mekkes JR, Dutrieux RP, Wildevuur CHR, Westerhof W. Dermal regeneration in native non-cross-linked collagen sponges with different extracellular matrix molecules. *Wound Repair Regen.* 2, 37–47 (1994).
452. De Vries HJC, Mekkes JR, Middelkoop E, Hinrichs WLJ, Wildevuur CRH, Westerhof W. Dermal substitutes for full-thickness wounds in a one-stage grafting model. *Wound Repair Regen.* 1, 244–252 (1993).
453. Enomoto DNH, Mekkes JR, Bossuyt PMM, Hoekzema R, Bos JD. Quantification of cutaneous sclerosis with a skin elasticity meter in patients with generalized scleroderma. *J. Am. Acad. Dermatol.* 35, 381–387 (1996).
454. Janzekovic Z. A new concept in the early excision and immediate grafting of burns. *J Trauma* 10, 1103–8 (1970).
455. De Vries HJC, Zeegelaar JE, Middelkoop E, Gijsbers G, Van Marle J, Wildevuur CHR, Westerhof W. Reduced wound contraction and scar formation in punch biopsy wounds. Native collagen dermal substitutes. A clinical study. *Br. J. Dermatol.* 132, 690–697 (1995).
456. Artel A, Mehdizadeh H, Chiu Y-C, Brey EM, Cinar A. An agent-based model for the investigation of neovascularization within porous scaffolds. *Tissue Eng. Part A* 17, 2133–2141 (2011).
457. Gao J, Crapo PM, Wang Y. Macroporous elastomeric scaffolds with extensive micropores for soft tissue engineering. *Tissue Eng.* 12, 917–25 (2006).
458. Harley BA, Leung JH, Silva ECCM, Gibson LJ. Mechanical characterization of collagen-glycosaminoglycan scaffolds. *Acta Biomater.* 3, 463–474 (2007).
459. Radisic M, Euloth M, Yang L, Langer R, Freed LE, Vunjak-Novakovic G. High-density seeding of

- myocyte cells for cardiac tissue engineering. *Biotechnol. Bioeng.* 82, 403–14 (2003).
460. Kretzmer G, Schugerl K. Response of mammalian cells to shear stress. *Appl. Microbiol. Biotechnol* 34, 613–616 (1991).
461. Stathopoulos N, Hellums J. Shear stress effects on human embryonic kidney cells in vitro. *Biotechnol. Bioeng.* 27, 1021–1026 (1985).
462. Bacabac R, Smit T, Cowin S, Van Loon J, Nieuwstadt F, Heethaar R, Klein-Nulend J. Dynamic shear stress in parallel-plate flow chambers. *J. Biomech.* 38, 159–167 (2005).
463. Dar A, Shachar M, Leor J, Cohen S. Optimization of cardiac cell seeding and distribution in 3D porous alginate scaffolds. *Biotechnol. Bioeng.* 80, 305–12 (2002).
464. Grayson WL, Bhumiratana S, Cannizzaro C, Chao P-HG, Lennon DP, Caplan AI, Vunjak-Novakovic G. Effects of initial seeding density and fluid perfusion rate on formation of tissue-engineered bone. *Tissue Eng. Part A* 14, 1809–20 (2008).
465. Murthy SK, Sethu P, Vunjak-Novakovic G, Toner M, Radisic M. Size-based microfluidic enrichment of neonatal rat cardiac cell populations. *Biomed. Microdevices* 8, 231–237 (2006).
466. Freed LE, Vunjak-Novakovic G. *Tissue engineering of cartilage.* in *Biomedical Engineering Handbook* 1788–1807 (CRC Press, 1995).
467. Dvir T, Benishti N, Shachar M, Cohen S. A novel perfusion bioreactor providing a homogenous milieu for tissue regeneration. *Tissue Eng.* 12, 2843–2852 (2006).
468. Comelles J, Hortigüela V, Samitier J, Martínez E. Versatile gradients of covalently bound proteins on microstructured substrates. *Langmuir* 28, 13688–13697 (2012).
469. Comelles J, Estévez M, Martínez E, Samitier J. The role of surface energy of technical polymers in serum protein adsorption and MG-63 cells adhesion. *Nanomedicine* 6, 44–51 (2010).
470. Dura B, Kovacs GT a, Giovangrandi L. Spatiotemporally controlled cardiac conduction block using high-frequency electrical stimulation. *PLoS One* 7, e36217 (2012).
471. Wang L, Liu L, Li X, Magome N, Agladze K, Chen Y. Multi-electrode monitoring of guided excitation in patterned cardiomyocytes. *Microelectron. Eng.* 111, 267–271 (2013).
472. Pfeiffer ER, Vega R, McDonough PM, Price JH, Whittaker R. Specific prediction of clinical QT prolongation by kinetic image cytometry in human stem cell derived cardiomyocytes. *J. Pharmacol. Toxicol. Methods* 81, 263–273 (2016).
473. Katagi J, Nakamura Y, Cao X, Ohara H, Honda A, Izumi-Nakaseko H, Ando K, Sugiyama A. Why Can dl-Sotalol Prolong the QT Interval In Vivo Despite Its Weak Inhibitory Effect on hERG K⁺ Channels In Vitro? Electrophysiological and Pharmacokinetic Analysis with the Halothane-Anesthetized Guinea Pig Model. *Cardiovasc. Toxicol.* 16, 138–146 (2016).
474. Šarić T, Frenzel LP, Hescheler J. Immunological barriers to embryonic stem cell-derived therapies. *Cells Tissues Organs* 188, 78–90 (2008).
475. Passier R, van Laake LW, Mummery CL. Stem-cell-based therapy and lessons from the heart. *Nature* 453, 322–9 (2008).
476. Yu P, Pan G, Yu J, Thomson JA. FGF2 sustains NANOG and switches the outcome of BMP4-induced human embryonic stem cell differentiation. *Cell Stem Cell* 8, 326–334 (2011).
477. Ting S, Chen A, Reuveny S, Oh S. An intermittent rocking platform for integrated expansion and differentiation of human pluripotent stem cells to cardiomyocytes in suspended microcarrier cultures. *Stem Cell Res.* 13, 202–213 (2014).
478. Fomovsky GM, Thomopoulos S, Holmes JW. Contribution of extracellular matrix to the mechanical properties of the heart. *J. Mol. Cell. Cardiol.* 48, 490–496 (2010).
479. Gershlak JR, Resnikoff JIN, Sullivan KE, Williams C, Wang RM, Black LD. Mesenchymal stem cells ability to generate traction stress in response to substrate stiffness is modulated by the changing extracellular matrix composition of the heart during development. *Biochem. Biophys. Res. Commun.*

REFERENCES

- 439, 161–166 (2013).
480. Chopra A, Tabdanov E, Patel H, Janmey P a., Kresh JY. Cardiac myocyte remodeling mediated by N-cadherin-dependent mechanosensing. *Am. J. Physiol. Heart Circ. Physiol.* 300, H1252-66 (2011).
481. Louch WE, Sheehan KA, Wolska BM. Methods in cardiomyocyte isolation, culture, and gene transfer. *J. Mol. Cell. Cardiol.* 51, 288–298 (2011).
482. Valls-Margarit M. Master project dissertation. Cardiac tissue engineering: Bioengineering heart muscle. (Universitat Pompeu Fabra, 2012).
483. Kuo P-L, Lee H, Bray M-A, Geisse NA, Huang Y-T, Adams WJ, Sheehy SP, Parker KK. Myocyte Shape Regulates Lateral Registry of Sarcomeres and Contractility. *Am. J. Pathol.* 181, 2030–2037 (2012).
484. Au HTH, Cheng I, Chowdhury MF, Radisic M. Interactive effects of surface topography and pulsatile electrical field stimulation on orientation and elongation of fibroblasts and cardiomyocytes. *Biomaterials* 28, 4277–4293 (2007).
485. Rodriguez AG, Han SJ, Regnier M, Sniadecki NJ. Substrate stiffness increases twitch power of neonatal cardiomyocytes in correlation with changes in myofibril structure and intracellular calcium. *Biophys. J.* 101, 2455–2464 (2011).
486. Beauchamp P, Moritz W, Kelm JM, Ullrich ND, Agarkova I, Anson B, Suter TM, Zuppinger C. Development and characterization of a scaffold-free 3D spheroid model of iPSC-derived human cardiomyocytes. *Tissue Eng. Part C Methods* 21, 852–861 (2015).

8. RESUM EN CATALÀ

La cardiopatia isquèmica és una de les principals causes de mort a nivell mundial. Segons l'Organització Mundial de la Salut, l'any 2012 la cardiopatia isquèmica va ser responsable de 7.4 milions de morts. Malauradament, s'espera que la mortalitat deguda a malalties cardiovasculars augmenti de 17.5 milions el 2012 a 22.2 milions el 2030. Una de les raons principals que expliquen aquests fets és que, després d'una lesió, el cor humà té una capacitat de reparació i/o regeneració molt limitada. Exceptuant el trasplantament de cor, les teràpies actuals són insuficients per restablir la funció del cor en estadis avançats d'insuficiència cardíaca. Així doncs, no només cal desenvolupar teràpies alternatives que fomentin la regeneració i/o reparació del cor, sinó també noves eines per estudiar la fisiologia i fisiopatologia cardíaca *in vitro*. Una de les estratègies més prometedores per assolir aquests objectius és l'enginyeria tissular cardíaca, ja que té com a finalitat generar constructes de teixit cardíac que mimetitzin el teixit real. Aquests constructes podrien utilitzar-se com a models *in vitro* del miocardi humà i també com a empelts de teixit cardíac per reparar el cor malmès. Per tant, disposar de constructes cardíacs 3D que recreïn el miocardi humà podria revolucionar el procés de descobriment de fàrmacs, l'estudi de malalties cardíques i el camp de la medicina regenerativa.

Per tal de generar constructes de teixit cardíac humà, les cèl·lules mare de pluripotència induïda humanes (hiPSC) representen una opció molt prometedora, ja que poden donar lloc a grans quantitats de cardiomiòcits funcionals. No obstant això, els cardiomiòcits obtinguts mostren un fenotip immadur i semblant a l'estadi fetal quan són cultivats en sistemes 2D estàndards, de manera que el seu ús es veu limitat. Per tal de promoure la maduració dels cardiomiòcits derivats de hiPSC (hiPSC-CM) és necessari reproduir l'entorn cardíac real. Entre les diverses opcions existents, l'estratègia clàssica es basa en l'ús de tres elements principals: les cèl·lules cardíques, que doten al teixit artificial de la capacitat d'exercir la seva funció; una estructura 3D constituïda per biomaterials i que actua com a bastida per al desenvolupament del teixit; i un sistema de senyalització que reproduïx els estímuls de l'entorn cardíac natiu, normalment un bioreactor, gràcies al qual els constructes cardíacs es formen i maduren. Tot i que s'han aconseguit avenços científics importants, generar constructes grans i semblants al miocardi humà adult a partir de hiPSC-CM segueix sent un repte per a la comunitat científica. En aquest context, la hipòtesi d'estudi és que, mitjançant la combinació de hiPSC-CM amb un material de bastida 3D i estímuls biofísics similars a l'entorn cardíac, es podrien generar constructes de teixit cardíac semblants al miocardi humà tant a nivell estructural com funcional.

Per tal d'abordar la hipòtesi plantejada, en aquest treball s'ha caracteritzat una bastida 3D constituïda principalment per col·lagen i elastina, i s'ha definit un mètode eficient per sembrar cèl·lules cardíques dins l'estructura. Bàsicament, aquest mètode consisteix en perfondre les cèl·lules cardíques a través de la bastida a 1 ml/min i en

un sol sentit, de manera que les cèl·lules queden retingudes en l'estructura 3D. A més a més, s'ha desenvolupat un bioreactor de perfusió de sistema en paral·lel que assegura un transport de massa efectiu entre les cèl·lules i el medi de cultiu. Aquest aspecte és de gran rellevància quan es volen obtenir constructes cardíacs amb un gruix de més de 200 µm, ja que només per difusió la quantitat d'oxigen i nutrients que arriba a les cèl·lules situades a l'interior del teixit és insuficient per a la seva supervivència. També s'ha dissenyat i fabricat una càmera de perfusió que inclou elèctrodes per estimular elèctricament les cèl·lules durant el seu cultiu, així com també per monitorar la funció del teixit artificial. Amb aquest sistema s'han pogut generar constructes de teixit cardíac 3D a partir de cèl·lules cardíques de rata neonatal, els quals han demostrat tenir activitat contràctil i assolir un nivell de maduresa superior quan se'ls ha estimulat elèctricament. Convé ressaltar que el desenvolupament d'aquest avançat sistema de cultiu ha permès generar constructes de teixit cardíac humà 3D amb una funcionalitat semblant a la del teixit real. A més a més, el sistema també ha permès monitorar l'electrofisiologia del teixit artificial en temps real.

Els resultats obtinguts indiquen que la perfusió de medi de cultiu, juntament amb l'estimulació elèctrica i una bastida de col·lagen porosa, promouen la maduració estructural i funcional dels hiPSC-CM. En conjunt, l'estimulació elèctrica millora l'organització estructural, l'alineació i l'acoblament dels cardiomiòcits que componen el teixit artificial respecte els que no han estat estimulats. Així mateix, l'estimulació elèctrica promou la formació de teixits artificials que es contreen de manera síncrona a nivell macroscòpic i que presenten funcions electrofisiològiques òptimes. És important mencionar que en aquest treball s'ha desenvolupat un sistema de registre que permet, per primera vegada, obtenir informació sobre l'activitat electrofisiològica dels constructes cardíacs intactes. Concretament, la combinació de potencials d'acció generats pels hiPSC-CM que componen els constructes cardíacs produeixen senyals semblants a un ECG, una característica única segons els nostre coneixement. Finalment, s'ha pogut demostrar que els constructes de teixit cardíac humà sotmesos a l'estimulació elèctrica són útils per detectar la cardiotoxicitat associada a fàrmacs, ja que després del tractament amb sotalol l'interval QT es prolonga i el complex QRS mostra una forma alterada.

En conclusió, els resultats obtinguts en aquesta tesi demostren que el sistema de cultiu desenvolupat és capaç de generar constructes de teixit cardíac humà, macroscòpics i amb una funcionalitat semblant al teixit real. Els efectes de l'estimulació elèctrica en els cardiomiòcits s'han estudiat a múltiples nivells: molecular (presència, distribució i expressió de proteïnes cardíques), ultraestructural (amplitud del sarcòmer i organització i presència d'unions cel·lulars especialitzades), cel·lular (morfologia i alineació), i funcional (amplitud, direccionalitat i esforç de les contraccions, i registre electrofisiològic). En conjunt, els resultats suggereixen una millora de la maduració dels

constructes cardíacs quan es sotmeten a estímuls elèctrics similars als de l'entorn natiu. Igualment, el sistema de registre en temps real que s'ha dissenyat permet obtenir informació essencial sobre la funcionalitat de constructes cardíacs intactes. Així doncs, l'estratègia d'enginyeria tissular cardíaca desenvolupada en aquest treball obre un gran ventall de possibilitats en la recerca cardiovascular.

9. APPENDICES

9.1. Prototype drawings

Total or partial reproduction is forbidden without permission.

Con la junta plana suministrada por Maria Valls montada en 'A', ajustar piezas 7000001-E-0410-003-000, 7000001-E-0410-004-000 y 7000001-E-0410-005-000 para que se cumpla la cota indicada en negro y el conjunto sea estanco.

Con la junta torica suministrada por Maria Valls montada en 'B', ajustar piezas 7000001-E-0410-002-000 y 7000001-E-0410-004-000 para el conjunto sea estanco.

CORTE A-A

Posición	-
Cantidad	1
Material	Polipropileno Natural Blanco
Tolerancia general	DN 750
*Medidas importantes a verificar	
Peso en Kg	-

Modif.	Fecha/Date	Nombre/Name	Descripción/Description
Disenado/Designed	18/07/2016	DVM	ESCALA / SCALE
Dibujado/Drawn	18/07/2016	DVM	ESCALA / SCALE
Revisado/Checked	-	-	LOCALIDAD / CITY
Cliente / Customer:	-	-	PAIS / COUNTRY:

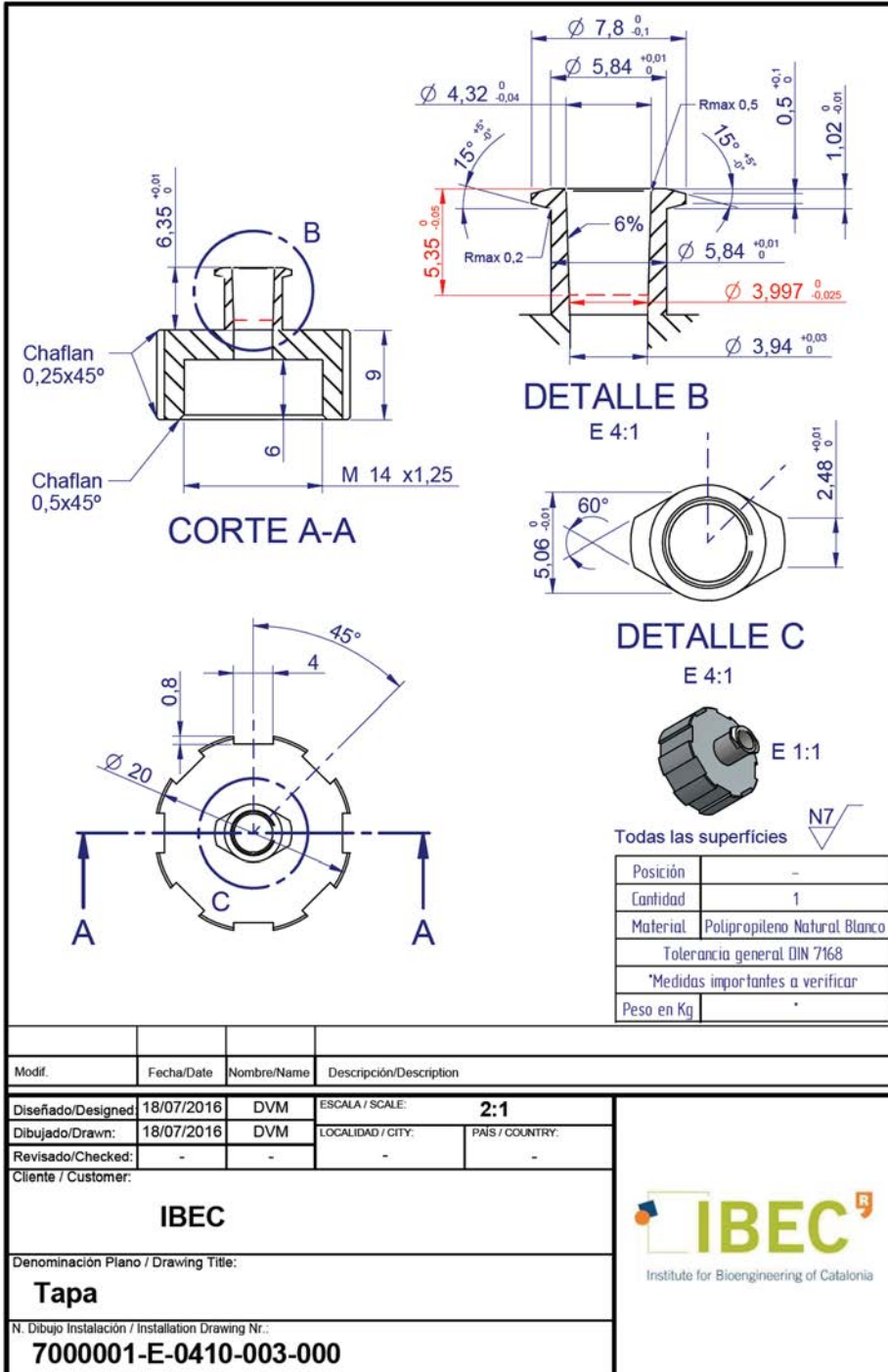
IBEC

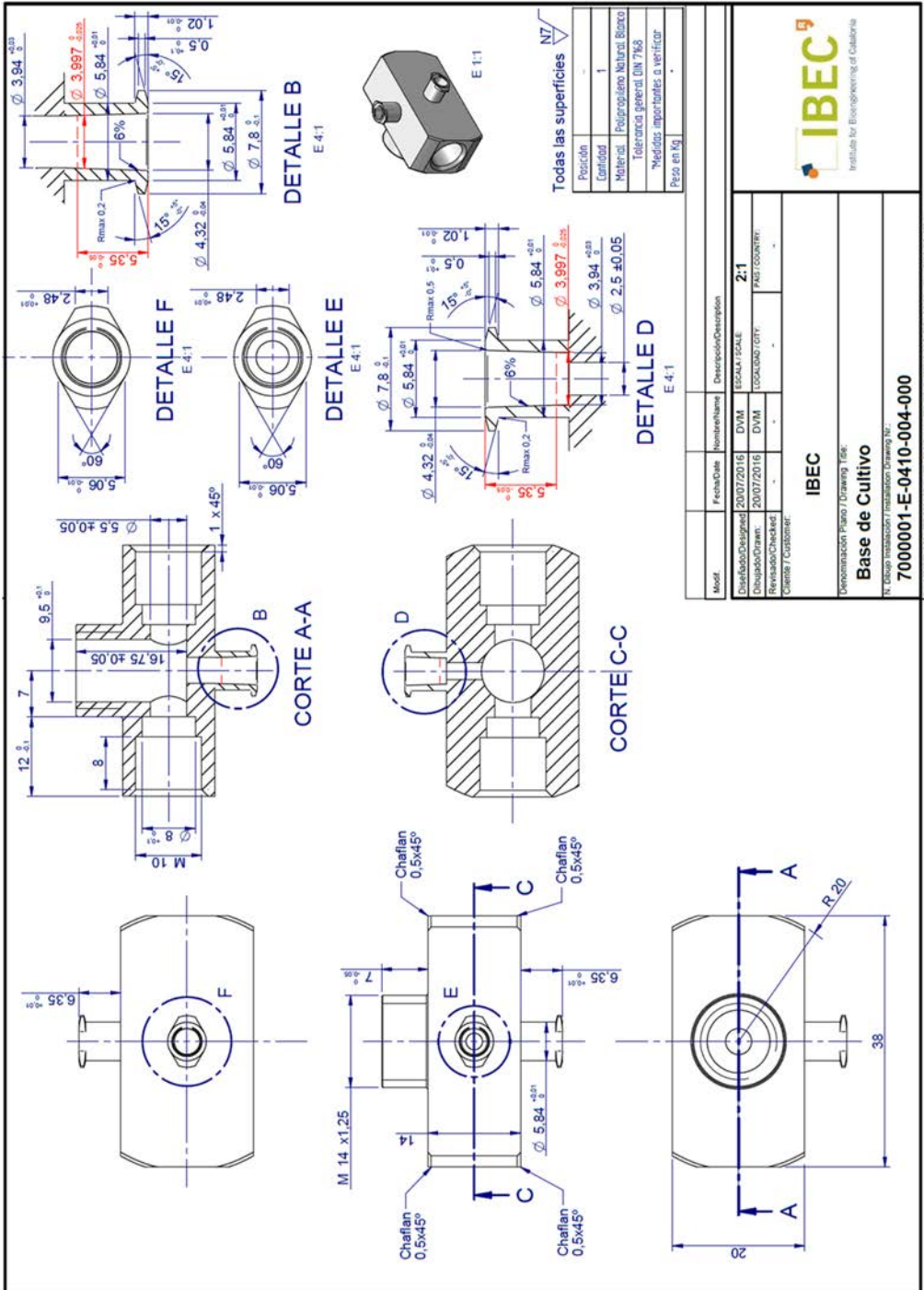
Instituto for Bioengineering of Catalonia

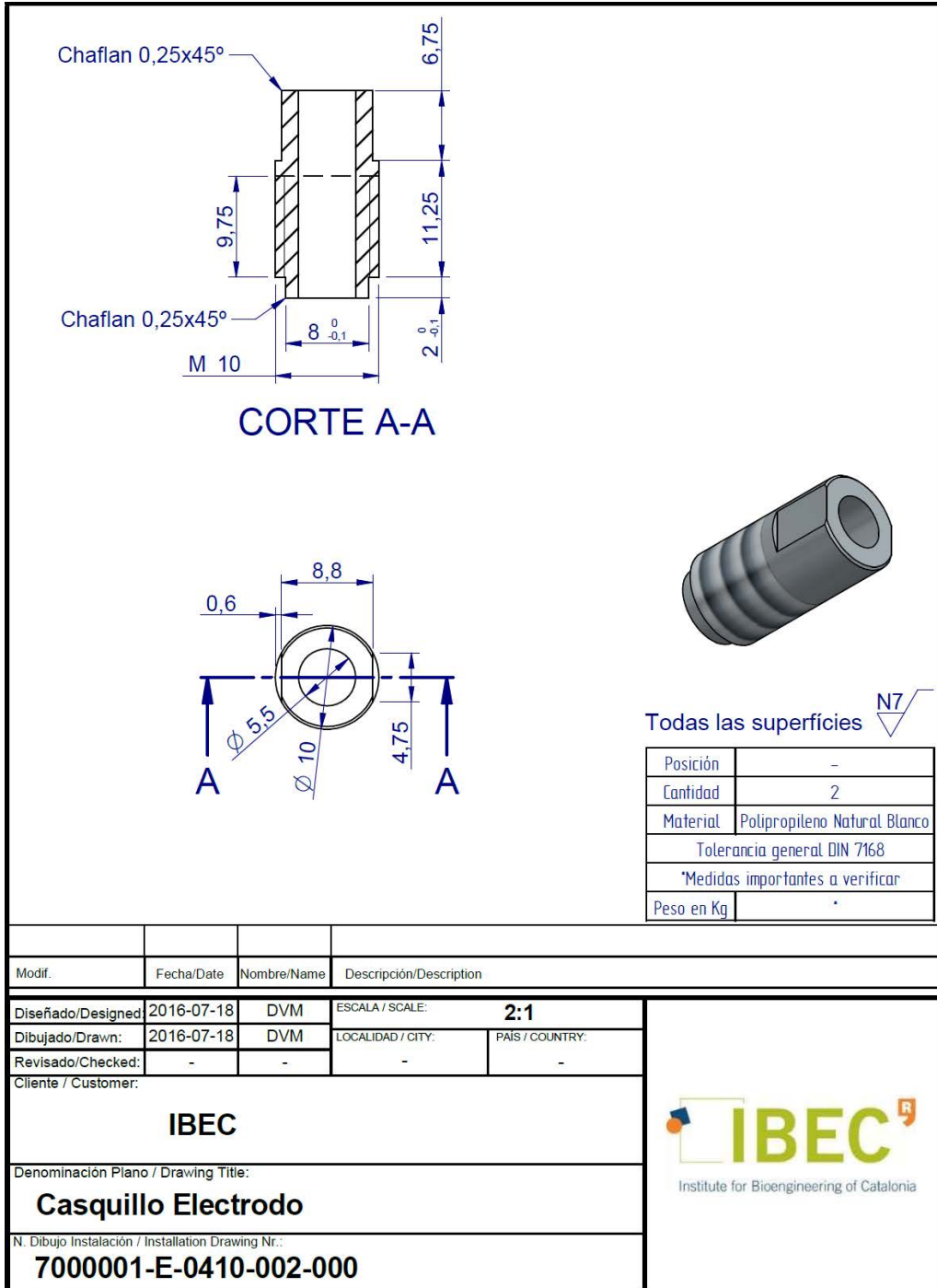
Denominación Plano / Drawing Title:
Conjunto Camara de Cultivo
 7000001-E-0410-001-000

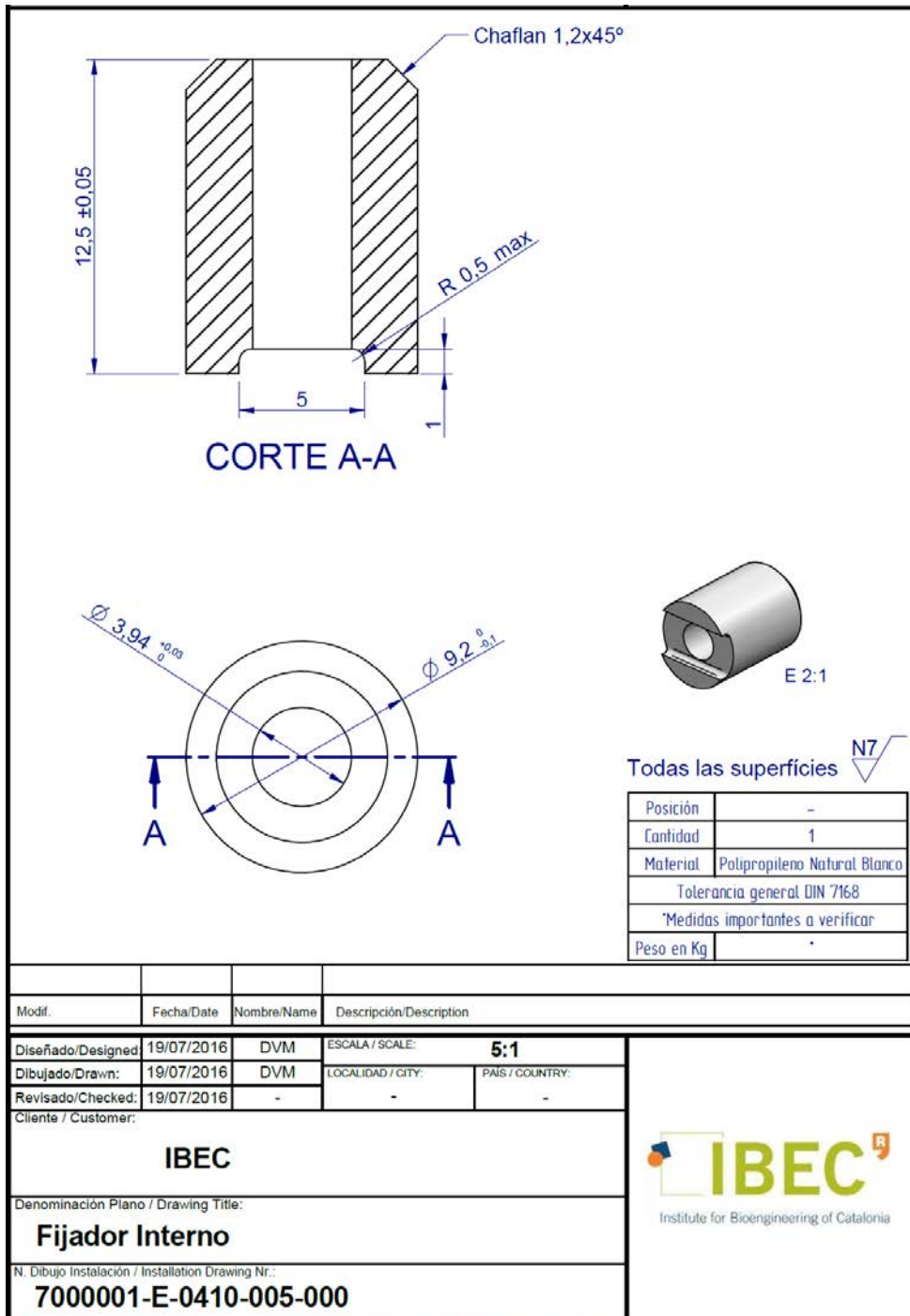
N.º Diseño / Revision / Impression Drawing No.:

Declaración de Intenciones de Reproducción: Este documento es propiedad de IBEC. Toda reproducción, total o parcial, sin la autorización expresa de IBEC quedará sujeta a sanciones. IBEC se reserva todos los derechos de explotación de este documento. No se permite la explotación económica ni la transformación de esta obra. Queda permitida la impresión en su totalidad.









PLANO PROPIEDAD DE INSTITUT DE BIOINGENYERIA DE CATALUNYA PROHIBIDA SU REPRODUCCION TOTAL O PARCIAL SIN AUTORIZACION PREVIA.
DRAWING PROPERTY OF INSTITUTE FOR BIOENGINEERING OF CATALONIA TOTAL OR PARTIAL REPRODUCTION IS FORBIDDEN WITHOUT PERMISSION.

9.2. Journal articles related to the thesis

Journal article in preparation (not published).

Advanced 3D culture system for the generation and monitoring of human cardiac patches with tissue-like functionality

Maria Valls-Margarit^{1*}, Olalla Iglesias-García^{2*}, Claudia Di Guglielmo^{2,3}, Leonardo Sarlabous^{3,4,8}, Roberto Paoli⁵, Jordi Comelles¹, Dolores Blanco^{3,4,8}, Oscar Castillo-Fernández⁶, Josep Samitier^{3,5,7}, Raimon Jané^{3,4,8}, Elena Martínez^{1,3,7#}, Ángel Raya^{2,3,9#}

¹*Biomimetic systems for cell engineering, Institute for Bioengineering of Catalonia (IBEC), Barcelona, Spain.*

²*Center of Regenerative Medicine in Barcelona (CMRB), Barcelona, Spain.*

³*Center for Networked Biomedical Research on Bioengineering, Biomaterials and Nanomedicine (CIBER-BBN).*

⁴*Biomedical signal processing and interpretation, Institute for Bioengineering of Catalonia (IBEC), Barcelona, Spain.*

⁵*Nanobioengineering, Institute for Bioengineering of Catalonia (IBEC), Barcelona, Spain.*

⁶*Institute of Microelectronics of Barcelona, IMB-CNM (CSIC), Campus UAB, Bellaterra, Spain.*

⁷*Department of Engineering: Electronics, University of Barcelona (UB), Barcelona, Spain.*

⁸*Department of Automatic Control, Universitat Politècnica de Catalunya - BarcelonaTech (UPC), Barcelona, Spain.*

⁹*Institució Catalana de Recerca i Estudis Avançats (ICREA).*

** These authors contributed equally to this work.*

Share senior co-authorship.

ABSTRACT

Engineering thick and 3D human cardiac tissue remains a challenge due to the complex structure of the native myocardium. Mimicking native cardiac environment through the use of advanced 3D culture systems brings additional complexity with respect to currently available engineered cardiac microtissue models. We fabricated a novel parallelized perfusion bioreactor that supports the development of 3D tissue constructs, reproduces the electrophysiological complexity of the native myocardium by providing electrical stimulation, and allows monitoring tissue function over time. Electrical stimulation promoted the generation of multiple cardiac tissue constructs containing contractile and aligned cardiomyocytes with well-developed ultrastructural organization. Stimulated constructs displayed improved synchronization and electrical signal propagation, and produced ECG-like signals. Electrostimulated human-derived cardiac tissue constructs may serve as *in vitro* models to predict proarrhythmic drug effects including heart rate alterations and QT interval prolongation. Overall, this technology may allow for the production of macroscopic human cardiac muscle with improved electrophysiological functions and potential use in regenerative medicine.

Key words: cardiac tissue engineering; human induced pluripotent stem cells; 3D cardiac patch; perfusion bioreactor; electrical stimulation; tissue functionality; heart physiology; ECG-like signals; proarrhythmic drugs.

INTRODUCTION

Nowadays, cardiac tissue engineering field is translating the acquired knowledge with animal-based tissue constructs into the production of human engineered cardiac tissues (hECTs), which should be able to provide physiologically relevant information. To date, much efforts have been put in developing human heart microtissues that better recapitulate the complexity and electro-mechanical function of native myocardium compared to standard 2D *in vitro* culture systems¹⁻⁴.

Several approaches have been explored to generate cardiac tissues analogues, including scaffold-free 3D cardiac spheroids that could spontaneously and synchronously contract^{5,6}. However, although this organoid-based cellular platform was found to be applicable for use in toxicology and drug development, it was not able to reproduce the physiological architecture and function of human myocardium. Therefore, more complex devices that combined multiple relevant regulatory signals in 3D environments had to be developed. In this regard, cardiac patches were generated, which used porous collagen-based scaffolds that provided an ideal support for cell adhesion and distribution^{7,8}. Such constructs needed a controlled microenvironment with appropriate oxygen and nutrients supply to the cultured cells⁹⁻¹¹. To that end, Radisic and colleagues developed a perfusion bioreactor system that allowed the generation of thick cardiac tissue constructs full of viable cells with aerobic metabolism¹⁰. However, to increase the functionality of hECTs, additional exogenous stimulus are needed, such as the electrical signals that haven shown to improve 3D cardiac tissue constructs electrophysiological properties, cellular and ultrastructural organization and expression of cardiac specific proteins¹²⁻¹⁴. Altogether, these systems could be used as high-throughput screening platforms, thus becoming essential tools in preclinical toxicology and drug screening process¹⁵⁻¹⁷. However, advanced models with tissue-like functionality have yet to be achieved.

Here, we present advanced 3D culture system that combines biophysical cues including medium perfusion and pulsatile electric field stimulation to generate cardiac tissues from hiPSCs. The obtained cardiac tissue constructs recapitulate some important features of adult cardiac tissue. Electrical stimulation promotes the generation of constructs with unprecedented conductive and contractile properties after 14 days of culture. Importantly, the custom-made perfusion chamber with electrical stimulation allows the online monitoring of the electrophysiological signal generated by contractile cardiac tissues, which resembles an electrocardiogram (ECG) signal. Finally, electrically stimulated cardiac tissue constructs exhibit heart rate alterations and QT interval prolongation when treated with a cardiotoxic drug, which makes our system ideal for studying long term effects of new drug treatments on cardiac activity. This technology constitutes a novel *in vitro* cardiac tissue model that opens up new possibilities for studying complex biological questions of human heart physiology both *in vitro* and *in vivo*.

MATERIALS AND METHODS

Parallelized perfusion bioreactor system

Parallelized perfusion bioreactor (**Fig. 1a**) was composed of a medium reservoir (Sartorius Stedim Biotech) connected through gas-permeable platinum-cured silicone tubing (1.6 mm inner diameter, Thermo Fisher Scientific) to a PharMed[®] BPT 3-Stop pump tubing (0.89 mm ID, Cole Parmer). The pump tubing was connected to a multichannel peristaltic pump (REGLO Digital, 2 channels, Ismatec) that propelled the culture medium to a four-port luer manifold (Thermo Fisher Scientific). In each port of the luer manifold, the infusion line of the elastomeric infusion system DOSI-FUSER[®] was connected, composed of an air and particle filter (1.2 μm particle filter and 0.02 μm vent filter) and a flow restrictor (1·10⁻² cm inner diameter and 10.8 cm length) (L25915-250D2, Leventon). The flow restrictor allowed an equal distribution of the culture medium throughout the four branches of the bioreactor, and the filter acted as a high fidelity de-bubbling system to avoid entrapment of bubbles inside perfusion chambers. An in-line luer injection port (Inycom) was assembled before the perfusion chambers to allow direct drug injections. Finally, the four branches were assembled with another luer manifold attached to a gas exchanger, composed of 3 m of gas-permeable platinum-cured silicone tubing (1.6 mm inner diameter, Thermo Fisher Scientific) coiled around a holder. To close the circuit, the gas exchanger was connected to the medium reservoir. All connections between the components were performed using male and female luer lock connectors (for 1.6 mm tube inner diameter, Value Plastics). Two different perfusion chambers were used to either electrically stimulate cardiac patches or not. The perfusion chamber without electrodes was a Swinnex filter holder (13 mm, Merck Millipore), while the perfusion chamber that enabled electrical stimulation was designed and fabricated in-house (**Supplementary information**). Notably, both chambers had equivalent inner dimensions to obtain comparable tissue constructs. In both chambers the cardiac patch was held in place by two gaskets, and a continuous perfusion of culture medium at 0.1 ml/min per chamber was applied (0.4 ml/min total system flow). For electrically stimulated cardiac patches, trains of monophasic square-wave pulses of 2 ms of duration and 5 V of amplitude (peak to peak) were continuously applied from day 4 of culture until the end of the experiment. For rat cardiac patches, the frequency of the pulses was of 3 Hz, while for human cardiac patches was of 1 Hz. Control cardiac patches were cultured under the same conditions but without electrical stimulation. All the components were sterilized by either autoclaving or 70% ethanol with subsequent MilliQ water rinse. The whole system was placed inside an incubator with temperature and CO₂ control (37°C and 5% CO₂).

Electric field modelling

COMSOL Multiphysics[®] software was used to predict the electric field and the current density that stimulates cells in our custom-made perfusion chamber. The electric current module was used, which considers the conductivity and permittivity of each material to solve a current conservation problem for a given electric potential. Electric fields throughout our geometry were calculated by assuming steady state, as previously described^{18,14,13}). To run the simulation, the exact geometry of our perfusion chamber

was designed except for its internal part, where a prism was drawn to faithfully reproduce the interaction between electrodes and culture medium (**Figure 1b**). The model was solved for a mesh with an average element size of 0.0473 mm² by applying a differential potential of 5 V between the stimulating electrodes (graphite rods, 3/16" in diameter, Monocomp Instrumentación). The conductivity value of the cell culture medium used for the simulation was 1.44 ± 0.03 S/m, measured with a conductivity meter (Crison) using DMEM 4.5 g/l glucose (Life Technologies).

Structural and mechanical analysis of the scaffold

A commercially available collagen and elastin-based sponge (Matrigel[®], MedSkin Solutions Dr. Suwelack AG) was used as 3D scaffold. Scaffold morphology and mean pore size was analysed in dry conditions by scanning electron microscopy (SEM) (Nova NanoSEM[™] 230, FEI) using the low vacuum mode (1 mbar water pressure) without any conductive coating. Second Harmonic Generation (SHG) and two-photon excited fluorescence (TPEF, autofluorescence) using an inverted confocal microscope (Leica SP5, Leica Microsystems) was used to elucidate scaffold morphology in hydrated conditions^{19,20}. The stiffness of the hydrated scaffold (disks of 1 cm in diameter) was measured in compression using a Q800 Dynamic Mechanical Analyzer (TA instruments). A ramp strain of -0.5%/min rate to a maximum strain of -5% and a preload force of 0.01 N were applied. Young Modulus (E) of the scaffold was determined from the slope of the stress-strain curves at room temperature and at 37 °C.

Human iPSC culture and cardiac differentiation

Human induced pluripotent stem cells (hiPSC) (FiPS Ctrl1-mR5F-6; cell line registered in the National Stem Cell Bank, Institute of Health Carlos III, Spanish Ministry) were cultured on Matrigel[®] (10 cm diameter, Corning) coated dishes with mTeSR1 medium (Stem Cell Technologies). Cells were differentiated into cardiomyocytes in monolayer culture with modulators of canonical Wnt signaling as described in the **Supplementary information**. Briefly, monolayer cultures on Matrigel[®] in a serum-free medium were treated with 10 μM GSK3 inhibitor (CHIR99021, Stemgent) for 24 h (day 0 to day 1). On day 3 of differentiation, cells were treated with 5 μM Wnt inhibitor IWP4 (Stemgent) for 2 days. Contracting cardiomyocytes were obtained between 8 and 12 days of differentiation. Beating clusters were disaggregated (at day 20 and at day 35) by incubation with 0.25% trypsin-EDTA (Gibco) for 5-8 min at 37 °C, both for their characterization and for cardiac constructs generation.

Cardiac constructs generation

Engineered cardiac tissue constructs were generated using a porous collagen and elastin-based scaffold of 1 mm thickness (Matrigel[®]). The commercial scaffold was cut in disks of 1 cm in diameter and hydrated in phosphate buffered saline (PBS) (Thermo Fisher Scientific) for 24 hours before use. For rat cardiac patches generation, 3.5 × 10⁶ cells isolated from rat heart ventricles were resuspended in 1 ml of supplemented DMEM (see **Supplementary information** for further details). For human

cardiac patches generation, $3.5 \cdot 10^6$ human iPSC-derived cardiomyocytes selected at day 20 of differentiation and $0.5 \cdot 10^6$ human foreskin fibroblasts (HFF) were resuspended in 1 ml of RPMI (Invitrogen) supplemented with B27 (Life Technologies) medium. Each cell suspension was seeded into the scaffold using an adapted version of a previously described perfusion loop system¹¹. Briefly, the cell suspension was loaded inside the loop and a flow rate of 1 ml/min was applied in one direction, forcing the cell suspension to pass through the scaffold. As the scaffold was held in place by two silicone gaskets, only the central part of it was seeded with cells. After seeding, tissue constructs were placed in 60 mm ultra-low attachment dishes (Corning) and incubated at 37°C in 5% CO₂ and humidified atmosphere to allow cell attachment. Rat cardiac patches were incubated for 1.5 hours, while human cardiac patches were incubated for 3.5 hours. Then, tissue constructs were transferred into the bioreactor perfusion chambers and cultured under perfusion during 3 days. At day 4 of culture, electric field stimulation regimen was applied on “electrostimulated” tissue constructs, while “control” ones were cultured only under perfusion. All tissue constructs were cultured either for 7 or 14 days before assessing their functional and structural organization level. As 2D controls of cardiac patches, $0.5 \cdot 10^6$ cells isolated from rat heart ventricles or day 20-differentiated cardiomyocytes together with 10% HFF were seeded on 0.1% gelatin-coated 12-well plates with or without 12 mm coverslips (Thermo Scientific) for further analysis.

Immunostaining analysis

Scaffolds were fixed overnight with 4% paraformaldehyde (PFA, Sigma) at 4°C and included in 8% agarose (Conda) for 5 min at 4°C. Blocks were cut in 200 µm sections using a vibratome (0.075 mm/s advance rate, 81 Hz vibration and 1 mm amplitude) (Leica VT1000S). After three washes in 1X TBS (30 min each), sections were incubated in blocking solution I (1X TBS, 0.5% Triton-X100 (Sigma) and 6% donkey serum (Chemicon)) for 2 h at room temperature, and incubated with primary antibodies diluted in blocking solution II (1X TBS, 0.1% Triton-X100 and 6% donkey serum) for 72 h at 4°C in agitation. After four washes in 1X TBS (30 min each), sections were incubated with secondary antibodies diluted in blocking solution II for 2 h in the dark and overnight at 4°C. Finally, sections were washed thrice with 1X TBS for 30 min each and incubated with DAPI (Invitrogen) for 1 h at room temperature. Rat neonatal and differentiated cardiomyocytes seeded on gelatin-coated coverslips were fixed with 4% PFA for 15 min at room temperature and used as 2D controls respectively. Images were taken using a SP5 confocal microscope (Leica Microsystems). Primary and secondary antibodies are listed in **Supplementary Table S1**.

Functional analysis of cardiac patches

Contractile function of cardiac patches was assessed in response to electric field stimulation or spontaneous beating as previously described^{13,12}. Briefly, two holes were drilled at one edge of two carbon rod electrodes, and a gold wire of 0.5 mm in diameter was thread through them. Insulation of the connection was performed using heat-shrink tubing, and both electrodes were glued using cyanoacrylate at the bottom of a 35 mm

MatTek glass bottom dish (MatTek In Vitro Life Science Laboratories), 1 cm apart from the edge of each electrode. The space between the electrodes was filled with Tyrode's salts solution (Sigma-Aldrich Química), and cardiac patches were imaged and video recorded using a Stereo Microscope Leica MZ10F (Leica Microsystems) with a DFC4025C Digital Microscope Camera (Leica Microsystems). Temperature was maintained at 37°C using a microscope-stage automatic thermocontrol system for transmitted light bases (Leica MATS Type TL, Leica Microsystems), and electrical pulses were applied using a function generator (Agilent Technologies). To measure the amplitude of contraction of each cardiac patch, spontaneous beating of the constructs was recorded for at least 10 s. Then, the Fractional Area Change (FAC) of 10 beats was calculated using a published custom MATLAB program (The MathWorks) and as formerly described¹³. Particle Image Velocimetry (PIV) was used to measure the velocity fields in beating cardiac tissue constructs. Briefly, spontaneous beating of cardiac patches was video recorded using a Stereo Microscope Leica MZ10F (Leica Microsystems) with a DFC4025C Digital Microscope Camera (Leica Microsystems). Then, movies were analyzed using the MatPIV software package for MATLAB (The MathWorks)²¹. Each frame was cross-correlated with the preceding one using a 77 μm x 77 μm interrogation window, obtaining local displacements fields (velocity field). The alignment between velocity vectors fields and the direction of the electric field was assessed by the order parameter $\langle \cos 2\theta \rangle$. If vectors were aligned in the direction of electric field, $\langle \cos 2\theta \rangle$ value was 1, whereas if vectors were perpendicular to the electric field, its value was -1. Random distribution was represented by a $\langle \cos 2\theta \rangle$ close to 0.

Quantitative real-time polymerase chain reaction

Total RNA was isolated from differentiated cells and cardiac constructs using Trizol RNA Isolation Reagent (Life Technologies), and 1 μg was used to synthesize cDNA using Transcriptor first-strand cDNA synthesis kit (Roche) according to the manufacturer's protocol. The quantitative real-time polymerase chain reaction (qRT-PCR) was carried out using the 7300 Real-Time PCR System (Applied Biosystems). Human *GAPDH* was used as a housekeeping gene. RNA from human fetal and adult heart (Clontech) was used as positive control. Specific primers are listed in **Supplementary Table S2**.

Transmission electron microscopy

Cardiac constructs were fixed with 2.5% glutaraldehyde (Electron Microscopy Sciences) for 2 h at 4°C. After washing with 0.1 M cacodylate buffer (pH = 7.2) (Sigma-Aldrich), cardiac constructs were gradually dehydrated with ethanol and embedded in epoxy resin (Ted Pella). Semithin sections (0.25 μm) were cut with a diamond knife using an ultramicrotome (Leica UC6), and stained lightly with 1% toluidine blue (Panreac). Later ultra-thin sections (0.08 μm) were cut with a diamond knife, contrasted with uranyl acetate (Electron Microscopy Sciences) and lead citrate (Electron Microscopy Sciences) and examined under a JEOL 1011 transmission electronic microscope (JEOL).

Drug treatment

Isoproterenol, carbachol and sotalol were purchased from Sigma-Aldrich. All chemicals were dissolved in distilled water to make stock solutions, and serial dilutions were made in RPMI (Invitrogen) culture medium. To test changes in the β -adrenergic response, 1 μ M isoproterenol was injected to the bioreactor circuit through the luer injection port (Inycom). For cholinergic stimulation, 10 μ M carbachol was injected, and sotalol was added at low (1 μ M) and high (10 μ M) concentrations to evaluate the blockade of hERG current. Spontaneous activity of cardiac constructs was recorded as baseline period. Cardiac constructs were treated with pharmacological agents during 10 min for immediate analysis, followed by 5 min washout for isoproterenol and carbachol, and 15 min for sotalol.

Recording and processing of bioelectric signals generated by cardiac patches

Extracellular field potentials (EFP), generated by the charge redistribution in cardiomyocytes surrounding medium, were acquired through three electrodes using an advanced transducer amplifier. The gold electrode acted as internal reference, and electrical activity of cardiac patches was acquired using both graphite electrodes. The obtained ECG-like signal is generated by synchronized action potentials of cardiomyocytes. Its shape is similar to regular surface ECG signals for humans, including QRS complex and T wave (**Fig. 3a and 3c**). The biomedical instrumentation for recording the bioelectrical signals was the Biopac MP100 system (Santa Barbara, CA, USA, 16 Bits AD conversion; DAC100C, gain 50, maximum bandwidth DC-5KHz, input impedance 2 M Ω , CMRR = 90 dB min). EFPs recordings were monitored and stored in a computer using the AcqKnowledge software v.4.1, and were analyzed with MATLAB (v. R2014b, Natick, MA, USA). EFPs signals were recorded at a sampling frequency of 12.5 KHz, and were filtered and decimated at a sampling rate of 500 Hz.

Bioelectric signals were bandpass filtered (zero-phase fourth-order Butterworth filter with cut-off frequency of 0.2 and 40 Hz, respectively) to use the main bandwidth of the classical electrocardiographic studies. Previously, the 50 Hz line interference and harmonics were cancelled by a comb-notch filter. To a better identification of different patterns in the ECG-like signals, Ensemble Empirical Mode Decomposition²² (Noise level: 1dB; Iterations: 200) was used to cancel the multicomponent noise.

Instantaneous heart rate expressed as beats per minute (bpm) was calculated over extracellular field potentials generated in both control and ES patches at baseline and after drug application. Relative HR to baseline was calculated to evaluate the behavior of cardioactive drug effects. The square root of the mean squared differences of successive intervals (RMSSD)²³, one of the most commonly used measures to evaluate the HR variability in clinical settings, was also calculated.

Statistical analysis

In the case of normal distributions, differences between groups were compared using Student's t-test analysis. Non-parametric analysis were performed using Mann-Whitney

U test and in case of 3 and more groups 1-way unrepeatd measures ANOVA with appropriate *post-hoc* testing was performed. The performed tests are specified in the respective figure legends. Statistical analyses were performed using GraphPad Prism 6 or Origin 8.5 software (OriginLab, Northampton, MA). Differences were considered statistically when $p < 0.05$.

RESULTS

Development of a parallelized bioreactor comprising perfusion and electrical stimulation

To generate tissue-like cardiac patches a parallelized perfusion bioreactor with electrical stimulation was designed (**Fig. 1a**). Parallelization of the culture system allowed the production of multiple cardiac tissue constructs in the same physiological conditions. Fluidic restrictors were installed into the parallelized system to ensure the same flow rate in every branch of the bioreactor. The fluidic resistance exerted by the fluidic resistor had to be much higher than the one exerted by the luer manifold to distribute the flow homogeneously through all branches. Thus, the resistance to laminar flow exerted by both components was calculated:

$$(1) \quad R = \frac{8 \eta x L}{\pi r^4}$$

Where R ($\text{Pa}\cdot\text{s}/\text{m}^3$) is the resistance, η ($\text{N}\cdot\text{s}/\text{m}^2$) is the viscosity of the fluid, L (m) is length of the tubing and r (m) its radius. Eventually, a fluidic resistor of $3 \cdot 10^{13} \text{ Pa}\cdot\text{s}/\text{m}^3$ was chosen for a luer manifold exerting $1 \cdot 10^7 \text{ Pa}\cdot\text{s}/\text{m}^3$.

To get an optimal interstitial flow in the perfusion bioreactor, we calculated the shear stress to which cells would be exposed as previously described¹¹. Initially, the minimum flow rate needed for cardiac patches culture had to be determined, and it depended on the overall mass balance of oxygen. A flow rate of 0.1 ml/min was required for rat cardiac patches culture, whereas a flow rate of 0.2 ml/min was required for human cardiac tissues. Then, shear stress was estimated by taking into account culture medium viscosity ($0.0078 \text{ dyn}\cdot\text{s}/\text{cm}^2$)²⁴, scaffold volume (19.6 mm^3), void fraction (0.94), mean pore radius ($8.5 \mu\text{m}$, **Supplementary Fig. 1**), and the calculated flow rates. Perfusion of culture medium at 0.1 ml/min evoked a hydrodynamic shear around $0.7 \text{ dyn}/\text{cm}^2$, while perfusion at 0.2 ml/min yielded a shear stress around $1.3 \text{ dyn}/\text{cm}^2$.

To include electrical stimulation to the parallelized perfusion bioreactor, we determined the appropriate electrodes configuration by formulating an electric field model (**Fig. 1b**). We simulated the electric field and current density generated by two graphite electrodes separated 1 cm apart and in contact with culture medium. Solving the model gave an electric field around $400 \text{ V}/\text{m}$ and a current density around $600 \text{ A}/\text{m}^2$ in the center of the chamber when a differential voltage of 5 V was applied. Similar values were obtained in the whole region of the cardiac patch containing cells (from $x = -2.5$ to $x = 2.5$), being suitable for cardiomyocytes stimulation.

Geometry, material and configuration requirements determined from the model were

considered to fabricate the custom-made perfusion chamber with electrical stimulation. Upon fabrication, electric field values in the perfusion chamber were measured to verify that the expected stimulation was properly delivered (**Fig. 1c**). Rectangular pulses at 3 Hz of frequency, 2 ms of duration and increasing differential voltages from 1 to 5 V were applied to the chamber. Electric potentials between stimulating electrodes and between one stimulation electrode and the center of the chamber (gold electrode) were measured. The intended waveform was faithfully applied in all voltages studied. Besides, when applying 5 V between graphite electrodes, 2 V were measured in the center of the chamber, meaning an electric field of 400 V/m and thus coinciding with the predicted values by the model.

Perfusion together with electrical stimulation promote structural maturation of tissue-like human cardiac patches

First, to test the suitability of the advanced 3D culture system to generate tissue-like cardiac patches a primary culture of neonatal rat cardiomyocytes was used. The generation of functional and appreciably mature cardiac tissue constructs from neonatal rat cardiomyocytes validated the suitability of our *in vitro* system (**Supplementary Fig. 2**). Therefore, similar culture conditions were used to create human cardiac patches from hiPSC-derived cardiomyocytes (hiPSC-CMs). Cells displayed robust *in vitro* cardiac differentiation potential (**Supplementary Fig. 3a**), obtaining contracting monolayers expressing high percentages of cardiac troponin I (cTnI) and myosin heavy chain (MHC) proteins (71.6 ± 5.3 % cTnI⁺/MHC⁺ cells) after 20 days of differentiation (**Supplementary Fig. 3b**). Cardiomyocytes derived from hiPSCs were selected at day 20 of differentiation and seeded into Matrigel[®] scaffold for human cardiac constructs generation. Tissue constructs were cultured for 14 days under perfusion (Control group) or under perfusion together with electrical stimulation (Electrical stimulation group, ES). Immunostaining analysis revealed the presence of cardiomyocytes distributed along the scaffold that strongly expressed cardiac contractile proteins, including cardiac troponin T (cTnT) and α -sarcomeric actin (ASA) (**Fig. 2a**). Human cardiac patches exhibited similar characteristics than rat cardiac patches in terms of cardiomyocytes distribution, morphology and alignment. Electrically stimulated constructs exhibited improved cardiomyocyte organization and myofibrillar alignment when compared to non-stimulated tissues (**Fig. 2a**). Gene expression profile of control and electrostimulated patches was also examined, and compared with the same culture seeded on typical multi-well plates (2D controls). Expression of cardiac specific genes increased considerably with time of culture, and more importantly when culturing cells in our advanced 3D culture system (**Fig. 2b**). Although non-statistical significant differences between control and electrostimulated patches were detected, there was a clear tendency towards an enhanced expression of maturity-related cardiac genes Myh7, cTnT and Gja1 and Serca2a channel marker in the electrically stimulated patches (**Fig. 2b**). At ultrastructural level, cardiomyocytes in the electrically stimulated patches displayed a significant increase in the sarcomere width in comparison with the non-stimulated constructs both after 7 and 14 days in culture (Day 7: 0.54 ± 0.27 μ m (Control), 0.66 ± 0.34 μ m (ES); Day 14: 0.68 ± 0.36 μ m (Control), 0.88 ± 0.39 μ m (ES); $p < 0.001$) (**Fig. 2c,d**), indicating a higher degree of maturation. Moreover, after 14 days

in culture, more developed intercalated discs were detected in the electrostimulated patches (**Fig. 2c**).

Functional maturation of tissue-like human cardiac patches is enhanced through electrical stimulation

To examine the effect of electrical stimulation on the contractile behavior of human cardiac patches, we analyzed their spontaneous beating after 7 and 14 days in culture. Biomimetic electrical pacing markedly improved cardiomyocytes beating synchronicity and coupling, leading to the generation of cardiac tissue constructs with a more efficient signal propagation both at day 7 and day 14 (**Supporting movies 4-9**). Electric field stimulation had a direct impact on cell distribution within the patch, as cells concentrated in the region delimited by stimulating electrodes, being appreciable even with the naked eye (**Fig. 3a**). This cell arrangement and beating synchronicity was translated in a significant increase in the contraction amplitude of electrically stimulated constructs compared with the control ones (Day 7: 0.54 ± 0.09 % (Control), 6.54 ± 0.93 % (ES); Day 14: 1.27 ± 0.03 % (Control), 7.87 ± 1.31 % (ES) $p < 0.001$), suggesting a favorable maturation of the electromechanical coupling machinery (**Fig. 3b**). This effect on tissue constructs contractility was analyzed in further detail by Particle Image Velocimetry (PIV). The generated strain maps demonstrated that the strain per contraction was higher in the electrostimulated constructs when compared to non-stimulated ones, thus corroborating their enhanced contractile performance (**Fig. 3c**). To gather information about the directionality of tissue constructs beating, the alignment between velocity vectors fields and the direction of the electric field was assessed by the order parameter $\langle \cos 2\theta \rangle$ (**Fig. 3d**). Electrical stimulation oriented human cardiac patches beating parallel to the direction of the electric field, whereas non-stimulated constructs elicited random velocity vectors distribution. Therefore, cardiomyocytes cultured under a pulsatile electric field significantly improved the directionality of human patches contractions ($p < 0.001$), thus having a much more close-to-human functional performance than control ones.

Electrically stimulated human cardiac patches elicit ECG-like signals and predict drug-induced cardiotoxicity

The combination of action potentials generated by the hiPSC-CM from human cardiac patches produce ECG-like signals from the human cardiac patches (**Fig. 3a**). Its shape was similar to regular surface ECG signals for humans, including QRS complex and T wave. Depending on the degree of synchronization for cell action potentials, the amplitude and width of QRS complex was affected. Accordingly, signals from control cardiac patches showed a lower and wider QRS complex than in the case of electrical stimulated patches (ES). But, in both cases, the T wave was well identified, as a sign of cell repolarization. The electrical stimulation on cardiac patch strongly affected to the quality of bioelectrical pathways and produced three remarkable signal characteristics:

- a) Narrow and steepest QRS complex (**Fig 3a**) with a time-invariant shape.

- b) More stable heart rate, due to a better electrical propagation of action potentials (**Fig. 3b**). The distribution of instantaneous heart rate expressed as beats per minute (bpm), over 10 minutes of spontaneous beating, achieved statistically significant differences between the heart rate in control (691 beats) and ES (611 beats), $p < 0.001$, Mann-Whitney U test.
- c) The pattern of QRS is stationary during baseline (**Fig 3c,d**), where one single pattern represented the 99% of all cardiac patch beats. Conversely, four QRS patterns at baseline were obtained in control recordings. These patterns represent 38, 20, 20 and 19%, respectively, with a total value of 93%.

Beat clustering was performed through cross-correlation between a representative beat and the rest of beats. Beats were included within a cluster when the cross-correlation of corresponding QRS complex exceeds a threshold of 0.85.

Therefore, the electrostimulated cardiac patches appears as the best option to study the effect of cardiac drugs to human derived cardiac tissues. Measuring the changes in heart rate and QRS shape would permit to estimate the effect of drugs in a realistic tissue-like human cardiac model. In addition, the study of sudden instantaneous changes in the heart rate, related to premature beats activation, and the effect on QT interval prolongations could predict the cardiotoxic effects of antiarrhythmic or proarrhythmic drugs.

In this work, it was studied the effect of Isoproterenol in the cardiac patch. As expected, the RR interval increased, and produced a statistically significant increment of heart rate (**Fig. 4a**). On the other hand, it was analyzed the effect of Carbachol (**Fig 4b**). In this case, it was obtained a slower cardiac activity with a significant lower heart rate. Both findings are according with expected effects of these drugs. The third experiment was developed with Sotalolol, to assess the cardiotoxicity effects in the cardiac patch. In case of electrically stimulated patch, it was demonstrated that the heart rate decrease regularly (**Fig. 4e**). But, in addition, it appeared a relevant effect with the activation of premature beats in a progressive way. That implies an isolated larger RR interval associated with beats of different QRS shape (**Fig 4f**). The trend to increase this effect, suggests a modification of cardiac patch rhythm and increasing of risk of malignant arrhythmia. Similar effect, with RR decreasing and premature beats, was observed in the control patch (**Fig. 4c,d**). But, in this case, the worst electrical conduction of action potentials produced a higher variability of the experiment, with higher heart rate.

One of the main advantages of the proposed human cardiac patches is the availability to provide ECG-like signals to monitor in real-time the activity of the cardiac path and its response to drugs. This cardiac patch offers an excellent platform to assess the effect of arrhythmic drugs, in an objective and quantitative way, related to mechanical and bioelectrical behavior of cardiac cells. As an example, classical measurements of Heart Rate Variability (HRV) can be also calculated from the ECG-like signals, acquired during the experiments. In this way, the RMSSD index was 78 ms and 29 ms for control and ES, respectively. The RMSSD for ES before and after Isoproterenol application were 29 ms and 11.6 ms, respectively. The RMSSD for ES before and after Carbachol application were 65.5 ms and 31.5 ms, respectively.

DISCUSSION

Despite recent advances on *in vitro* generation of human heart tissue analogues, they are limited by the existing tissue engineering technologies, which are not able to recapitulate the complex organization and function of the human myocardium. In this study we present an innovative platform technology for the *in vitro* production of contractile human cardiac tissue constructs consisting of a bioreactor with perfusion and electric field stimulation dual capabilities, therefore supporting tissue-like functionality. Notably, *in vitro* culture of hiPSC-derived cardiomyocytes for over 14 days under electrical stimulation induced cell alignment and structural maturation, increased contractility, and resulted in an improvement in beat conductivity and synchronization with respect to controls. Importantly, this system enabled monitoring of tissue function in real time, providing for the first time our knowledge a platform for the evaluation of the electrophysiological properties of 3D millimeter sized-tissues.

In essence, the development of close-to-human *in vitro* cardiac models requires thicker cardiac constructs, which are dependent on medium perfusion to ensure an adequate delivery of nutrients, metabolites, and oxygen throughout the tissue¹¹. In addition, electrical stimulation resembling native heart pacing can be used to obtain functional cardiac tissue constructs modelling natural human heart physiology. Herein we have developed a parallelized bioreactor system including electrodes to electrically stimulate cells during culture in perfusion. Cardiac constructs were stimulated at a frequency of 1 Hz to mimic native adult heart rate, as it was previously shown that 3D aggregates of cardiomyocytes adapted their autonomous beating rate to the frequency at which they were stimulated²⁵. After 14 days in culture, the stimulated tissue constructs displayed a remarkable level of structural organization. Cells in stimulated constructs were aligned and elongated, whereas unstimulated cells showed a random orientation within the construct. At the gene level, electrical stimulation upregulated cardiac-specific *MHY7* and *TNNT2*, and the Ca²⁺ channel *SERCA2A*. Electrical stimulation also yielded improved myofilament structure, as evidenced by wider sarcomeres and well-developed intercellular unions that correlated with better electrical properties in the engineered human cardiac tissues. Moreover, the application of electrical stimulation during culture markedly enhanced the contractile behaviour of the constructs. After 14 days in culture, improved electromechanical coupling in stimulated cardiomyocytes resulted in contractions with an amplitude 6-fold higher than that in unstimulated constructs. These results are in line with other studies where electrical stimulation, alone or in combination with mechanical loading, promoted electrophysiological maturation of cardiomyocytes^{26,27}. However, while our culture system supported a high degree of cardiomyocyte maturation, terminal differentiation was not reached.

Multimodal stimulation bioreactors have been previously applied for *in vitro* culture of murine cardiomyocyte 3D tissue structures^{18,28,29}. However, this research has been rarely transferred to the human cardiac tissue engineering model, where there has been a trend towards the generation of cardiac microtissues and microphysiological systems. Microtissues have been fabricated with natural-based hydrogels, which are casted in band or ring shapes and are fixed at both ends mainly through a two-post configuration^{3,4,8,30–36}. Other configurations have included casting cell/hydrogel mixture in hexagonal posts³⁷ or around a wire-like template (e.g. a surgical suture or a tubing)

to obtain biowires^{1,38}. Some of these approaches included other regulatory signals apart from static stretching, such as electrical pacing^{1,3,33,38} or cyclic stretching^{8,35}. Similarly, highly miniaturized microphysiological systems have been developed as “heart-on-chip” technologies allowing for increased throughput and controlled microenvironments for drug screening¹⁷ and human cardiac disease studies³⁹. However, these approaches are still far from the initial goal of cardiac tissue engineering, which is the generation of thick 3D human cardiac tissue constructs not only for *in vitro* studies, but also with appropriate dimensions and easy to handle for regenerative medicine purposes. This idea of generating 3D tissue-like human cardiac constructs has only been attempted in a few recent studies where hPSC-CM are seeded in 0.5-1 mm thick scaffolds^{35,40}. However, they do not stimulate the generated tissue with combined electromechanical signals neither make use of perfusion bioreactors to maintain the viability of the construct, so their functionality and structure is still far from resembling the adult myocardium.

To date, action potentials in cardiac tissue constructs are recorded on a representative cell population at the time of seeding³⁷, or on isolated cardiomyocytes after tissue formation through intracellular recordings^{4,26}. Therefore, it is necessary to develop an electrophysiological recording system that provides information from intact 3D engineered heart tissues. Notably, herein we present a novel recording system that enables real-time monitoring of the electrophysiological activity in thick 3D human cardiac constructs. The recording of ECG-like signals allowed us to assess the effect of proarrhythmic drugs on the electrical behavior of the electrostimulated cardiac tissues. Moreover, this response was not identifiable in unstimulated controls, further supporting a role for electric stimulation in optimal maturation of the cultured cardiomyocytes.

In summary, we have developed a new technology that 1) allowed the generation of multiple millimeter-sized human cardiac tissue constructs 2) induced cardiomyocyte maturation and organization in 3D cardiac constructs that displayed tissue-like functionality, and 3) enabled the evaluation of the electrophysiological properties of intact thick 3D human cardiac constructs, representing an important advance towards the generation of human cardiac tissue analogues.

Acknowledgments

Authors would like to thank S. Jiménez, L. Mulero and C. Pardo for excellent technical assistance with molecular and histological analysis. We thank J. Martín from Leventon S.A.U. (WerfenLife Company) for kindly donating parts from the elastomeric infusion system DOSI-FUSER®.

REFERENCES

1. Nunes SS, Miklas JW, Liu J, Aschar-Sobbi R, Xiao Y, Zhang B, Jiang J, Massé S, Gagliardi M, Hsieh A, Thavandiran N, Laflamme MA, Nanthakumar K, Gross GJ, Backx PH, Keller G, Radisic M. Biowire: a platform for maturation of human pluripotent stem cell-derived cardiomyocytes. *Nat. Methods* 10, 781–7 (2013).
2. Ma Z, Wang J, Loskill P, Huebsch N, Koo S, Svedlund FL, Marks NC, Hua EW, Grigoropoulos CP, Conklin BR, Healy KE. Self-organizing human cardiac microchambers mediated by geometric confinement. *Nat. Commun.* 6, 7413 (2015).
3. Thavandiran N, Dubois N, Mikryukov A, Massé S, Beca B, Simmons C a, Deshpande VS, McGarry JP, Chen CS, Nanthakumar K, Keller GM, Radisic M, Zandstra PW. Design and formulation of functional pluripotent stem cell-derived cardiac microtissues. *Proc. Natl. Acad. Sci.* 110, E4698-707 (2013).
4. Schaaf S, Shibamiya A, Mewe M, Eder A, Stöhr A, Hirt MN, Rau T, Zimmermann WH, Conradi L, Eschenhagen T, Hansen A. Human engineered heart tissue as a versatile tool in basic research and preclinical toxicology. *PLoS One* 6, (2011).
5. Fennema E, Rivron N, Rouwkema J, van Blitterswijk C, De Boer J. Spheroid culture as a tool for creating 3D complex tissues. *Trends Biotechnol.* 31, 108–115 (2013).
6. Beauchamp P, Moritz W, Kelm JM, Ullrich ND, Agarkova I, Anson B, Suter TM, Zuppinger C. Development and characterization of a scaffold-free 3D spheroid model of iPSC-derived human cardiomyocytes. *Tissue Eng. Part C Methods* 21, 852–861 (2015).
7. Liao B, Christoforou N, Leong KW, Bursac N. Pluripotent stem cell-derived cardiac tissue patch with advanced structure and function. *Biomaterials* 32, 9180–7 (2011).
8. Tulloch NL, Muskheli V, Razumova M V, Korte FS, Regnier M, Hauch KD, Pabon L, Reinecke H, Murry CE. Growth of engineered human myocardium with mechanical loading and vascular coculture. *Circ. Res.* 109, 47–59 (2011).
9. Carrier RL, Rupnick M, Langer R, Schoen FJ, Freed LE, Vunjak-Novakovic G. Perfusion improves tissue architecture of engineered cardiac muscle. *Tissue Eng.* 8, 175–188 (2002).
10. Radisic M, Yang L, Boublik J, Cohen RJ, Langer R, Freed LE, Vunjak-Novakovic G. Medium perfusion enables engineering of compact and contractile cardiac tissue. *Am. J. Physiol. Heart Circ. Physiol.* 286, H507–H516 (2004).
11. Radisic M, Marsano A, Maidhof R, Wang Y, Vunjak-Novakovic G. Cardiac tissue engineering using perfusion bioreactor systems. *Nat. Protoc.* 3, 719–38 (2008).
12. Radisic M, Park H, Shing H, Consi T, Schoen FJ, Langer R, Freed LE, Vunjak-Novakovic G. Functional assembly of engineered myocardium by electrical stimulation of cardiac myocytes cultured on scaffolds. *Proceedings of the National Academy of Sciences of the United States of America* 101, 18129–34 (2004).
13. Tandon N, Cannizzaro C, Chao P-HG, Maidhof R, Marsano A, Au HTH, Radisic M, Vunjak-Novakovic G. Electrical stimulation systems for cardiac tissue engineering. *Nat. Protoc.* 4, 155–73 (2009).
14. Tandon N, Marsano A, Maidhof R, Wan L, Park H, Vunjak-Novakovic G. Optimization of electrical stimulation parameters for cardiac tissue engineering. *J. Tissue Eng. Regen. Med.* 5, 115–125 (2011).
15. Hansen A, Eder A, Bönstrup M, Flato M, Mewe M, Schaaf S, Aksehirlioglu B, Schwörer A, Uebeler J, Eschenhagen T. Development of a drug screening platform based on engineered heart tissue. *Circ. Res.* 107, 35–44 (2010).
16. Amano Y, Nishiguchi A, Matsusaki M, Iseoka H, Miyagawa S, Sawa Y, Seo M, Yamaguchi T, Akashi M. Development of vascularized iPSC derived 3D-cardiomyocyte tissues by filtration Layer-by-Layer technique and their application for pharmaceutical assays. *Acta Biomater.* 33, 110–121 (2016).

17. Mathur A, Loskill P, Shao K, Huebsch N, Hong S, Marcus SG, Marks N, Mandegar M, Conklin BR, Lee LP, Healy KE. Human iPSC-based Cardiac Microphysiological System For Drug Screening Applications. *Sci. Rep.* 5, 8883 (2015).
18. Barash Y, Dvir T, Tandelitnik P, Ruvinov E, Guterman H, Cohen S. Electric field stimulation integrated into perfusion bioreactor for cardiac tissue engineering. *Tissue Eng. Part C. Methods* 16, 1417–1426 (2010).
19. Jiang X, Zhong J, Liu Y, Yu H, Zhuo S, Chen J. Two-photon fluorescence and second-harmonic generation imaging of collagen in human tissue based on multiphoton microscopy. *Scanning* 33, 53–56 (2011).
20. Richards-Kortum R, Sevick-Muraca E. Quantitative optical spectroscopy for tissue diagnosis. *Annu. Rev. Phys. Chem.* 47, 555–606 (1996).
21. Sveen JK. *An introduction to MatPIV v. 1.6.1.* in *Mechanics and Applied Mathematics 2*, (Department of Mathematics, Univeristy of Oslo, 2004).
22. Wu Z, Huang E N. Ensemble Empirical Mode Decomposition. 1, 385–388 (2011).
23. Heart rate variability. Standards of measurement, physiological interpretation, and clinical use. *Eur. Heart J.* 17, 354–81 (1996).
24. Bacabac R, Smit T, Cowin S, Van Loon J, Nieuwstadt F, Heethaar R, Klein-Nulend J. Dynamic shear stress in parallel-plate flow chambers. *J. Biomech.* 38, 159–167 (2005).
25. Eng G, Lee BW, Protas L, Gagliardi M, Brown K, Kass RS, Keller G, Robinson RB, Vunjak-Novakovic G. Autonomous beating rate adaptation in human stem cell-derived cardiomyocytes. *Nat. Commun.* 7, 1–10 (2016).
26. Nunes SS, Miklas JW, Liu J, Aschar-Sobbi R, Xiao Y, Zhang B, Jiang J, Massé S, Gagliardi M, Hsieh A, Thavandiran N, Laflamme MA, Nanthakumar K, Gross GJ, Backx PH, Keller G, Radisic M. Biowire: a platform for maturation of human pluripotent stem cell-derived cardiomyocytes. *Nat. Methods* 10, 781–7 (2013).
27. Godier-Furnémont AFG, Tiburcy M, Wagner E, Dewenter M, Lämmle S, El-Armouche A, Lehnart SE, Vunjak-Novakovic G, Zimmermann WH. Physiologic force-frequency response in engineered heart muscle by electromechanical stimulation. *Biomaterials* 60, 82–91 (2015).
28. Maidhof R, Tandon N, Lee EJ, Luo J, Duan Y, Yeager K, Konofagou E, Vunjak-Novakovic G. Biomimetic perfusion and electrical stimulation applied in concert improved the assembly of engineered cardiac tissue. *J. Tissue Eng. Regen. Med.* 6, (2011).
29. Kensah G, Gruh I, Viering J, Schumann H, Dahlmann J, Meyer H, Skvorc D, Bär A, Akhyari P, Heisterkamp A, Haverich A, Martin U. A novel miniaturized multimodal bioreactor for continuous in situ assessment of bioartificial cardiac tissue during stimulation and maturation. *Tissue Eng. Part C. Methods* 17, 463–473 (2011).
30. Hinson JT, Chopra A, Nafissi N, Polacheck WJ, Benson CC, Swist S, Gorham J, Yang L, Schafer S, Sheng CC, Haghghi A, Homsy J, Hubner N, Church G, Cook SA, Linke WA, Chen CS, Seidman JG, Seidman CE. Titin mutations in iPS cells define sarcomere insufficiency as a cause of dilated cardiomyopathy. *Science* 349, 982–6 (2015).
31. Kensah G, Roa Lara A, Dahlmann J, Zweigerdt R, Schwanke K, Hegermann J, Skvorc D, Gawol A, Azizian A, Wagner S, Maier LS, Krause A, Dräger G, Ochs M, Haverich A, Gruh I, Martin U. Murine and human pluripotent stem cell-derived cardiac bodies form contractile myocardial tissue in vitro. *Eur. Heart J.* 34, 1134–1146 (2013).
32. Soong PL, Tiburcy M, Zimmermann W-H. Cardiac differentiation of human embryonic stem cells and their assembly into engineered heart muscle. *Curr. Protoc. Cell Biol.* Chapter 23, Unit23.8 (2012).
33. Ruan J, Tulloch NL, Razumova M V, Saiget M, Muskheli V, Pabon L, Reinecke H. Mechanical Stress Conditioning and Electrical Stimulation Promote Contractility and Force Maturation of Induced Pluripotent Stem Cell-Derived Human Cardiac Tissue. *Circulation*

206–221 (2016).

34. Turnbull IC, Karakikes I, Serrao GW, Backeris P, Lee J-J, Xie C, Senyei G, Gordon RE, Li RA, Akar FG, Hajjar RJ, Hulot J-S, Costa KD. Advancing functional engineered cardiac tissues toward a preclinical model of human myocardium. *FASEB J.* 28, 644–654 (2014).
35. Tiburcy M, Hudson JE, Balfanz P, Schlick SF, Meyer T, Chang Liao M-L, Levent E, Raad F, Zeidler S, Wingender E, Riegler J, Wang M, Gold JD, Kehat I, Wettwer E, Ravens U, Dierickx P, van Laake L, Goumans M-J, *et al.* Defined Engineered Human Myocardium with Advanced Maturation for Applications in Heart Failure Modelling and Repair. *Circulation* (2017).
36. Huebsch N, Loskill P, Deveshwar N, Spencer CI, Judge LM, Mandegar MA, B. Fox C, Mohamed TMA, Ma Z, Mathur A, Sheehan AM, Truong A, Saxton M, Yoo J, Srivastava D, Desai TA, So P-L, Healy KE, Conklin BR. Miniaturized iPSC-Cell-Derived Cardiac Muscles for Physiologically Relevant Drug Response Analyses. *Sci. Rep.* 6, 24726 (2016).
37. Zhang D, Shadrin IY, Lam J, Xian HQ, Snodgrass HR, Bursac N. Tissue-engineered cardiac patch for advanced functional maturation of human ESC-derived cardiomyocytes. *Biomaterials* 34, 5813–5820 (2013).
38. Xiao Y, Zhang B, Liu H, Miklas JW, Gagliardi M, Pahnke A, Thavandiran N, Sun Y, Simmons C, Keller G, Radisic M. Microfabricated perfusable cardiac biowire: a platform that mimics native cardiac bundle. *Lab Chip* 14, 869–82 (2014).
39. Wang G, McCain ML, Yang L, He A, Pasqualini FS, Agarwal A, Yuan H, Jiang D, Zhang D, Zangi L, Geva J, Roberts AE, Ma Q, Ding J, Chen J, Wang D-Z, Li K, Wang J, Wanders RJa, *et al.* Modeling the mitochondrial cardiomyopathy of Barth syndrome with induced pluripotent stem cell and heart-on-chip technologies. *Nat. Med.* 20, 616–23 (2014).
40. Ma Z, Koo S, Finnegan MA, Loskill P, Huebsch N, Marks NC, Conklin BR, Grigoropoulos CP, Healy KE. Three-dimensional filamentous human diseased cardiac tissue model. *Biomaterials* 35, 1367–1377 (2014).
41. Lian X, Zhang J, Azarin SM, Zhu K, Hazeltine LB, Bao X, Hsiao C, Kamp TJ, Palecek SP. Directed cardiomyocyte differentiation from human pluripotent stem cells by modulating Wnt/ β -catenin signaling under fully defined conditions. *Nat. Protoc.* 8, 162–75 (2013).

FIGURE LEGENDS

Figure 1. Parallelized perfusion bioreactor for cardiac patches generation. (a) Bioreactor overall view: medium reservoir (1), luer manifold (2), de-bubbler (3), flow restrictor (4), perfusion chambers (5) and gas exchanger (6). The bioreactor supports the culture of up to four cardiac patches simultaneously. Two different perfusion chambers are used to either electrically stimulate cardiac patches while culturing or not. (b) 3D modelling of the electric field generated in our custom-made perfusion chamber when applying a differential voltage of 5 V. Electrode configuration (red and blue cylinders in the geometry, the blue being the ground) and predicted electric field and current density are displayed both in 3D and top views. Black arrowheads indicate the direction of the electric field. Plots show electric field and current density values at the positions where cells are seeded in the scaffold (central circle in the top view). (c) Images of the fabricated perfusion chamber with electrical stimulation. (d) Voltage measurements in the perfusion chamber with electrical stimulation. Measured electric field values coincide with the values predicted by the model.

Figure 2. Morphology and ultrastructural organization of human cardiac constructs. (a) Representative cross-sections of cardiac constructs after 14 days of culture without (Control) or with electrical stimulation (ES). hiPSC-derived cardiomyocytes positive for cardiac troponin (cTnT; green), Phalloidin (Ph; red) and α -sarcomeric actin (ASA; cyan) were detected in the scaffold. Nuclei were stained with 4', 6-diamidino-2-phenylindole (DAPI; blue). Cardiac patches were analysed by Second Harmonic Generation for the detection of collagen (Col; violet). Scale bars: 500 μ m, higher magnifications: 100 μ m, 20 μ m and 10 μ m, respectively. (b) Standard 2D culture of hiPSC-CM in monolayers. Cardiomyocytes were positive for cardiac troponin (cTnT; green) and Phalloidin (Ph; red). Nuclei were stained with 4', 6-diamidino-2-phenylindole (DAPI; blue). Scale bar: 50 μ m. (c) Ultrastructural analysis of hiPSC-derived cardiac tissue. Representative electron microscopy images of cardiac patches were shown after 7 and 14 days of culture. Scale bars: 1 μ m (bundles) and 0.5 μ m (sarcomere width and cell junctions). (d) Morphometric analysis showing sarcomere width. Cardiomyocytes in electrically stimulated patches showed wider sarcomeres than in control ones (** $p < 0.001$, $n = 2$ per group, Mann Whitney U test). Data are expressed as mean \pm standard deviation (SD).

Figure 3. Functional assessment of hiPSC-derived engineered cardiac tissue. (a) Top view images of the human cardiac tissue constructs after 7 and 14 days of culture, both with (ES) or without (Control) electrical stimulation. (b) Contraction amplitude analysis of control and electrostimulated human cardiac patches after 7 and 14 days of culture. The area in pixels of each construct was obtained through custom MATLAB program, and its oscillation was represented over time. Bar chart shows the percentage of Fractional Area Change (FAC) (average \pm SD) for each cardiac patch ($n = 2$ per group). Electrical stimulation increased the amplitude of contraction of the human engineered cardiac tissue at both timepoints (** $p < 0.001$; Mann Whitney U test). ES: Electrical stimulation. (c) Strain analysis of beating human cardiac patches after 14 days

of culture. Velocity maps are shown, with red colors and longer arrows representing higher velocities, and blue colors and shorter arrows lower velocities. Scale bars: 2.5 mm. **(d)** Analysis of the alignment between the direction of the electric field and the direction of human cardiac patches beating. The order parameter $\cos 2\theta$ was used, with values close to 0 meaning random distribution and values close to 1 meaning parallel alignment (** $p < 0.001$; $n = 2$ per group, Mann-Whitney U test).

Figure 4. Baseline extracellular bioelectrical potentials generated by human cardiac patches. **(a)** Representative bioelectric signals at baseline of control and electrically stimulated (ES) human patches. Bioelectric signals were bandpass filtered (zero-phase fourth-order Butterworth filter with cut-off frequency of 0.2 and 40 Hz, respectively). **(b)** Distribution of instantaneous heart rate expressed as beats per minute (bpm), over 10 minutes of spontaneous beating. ***Statistically significant differences between the heart rate in control (691 beats) and ES (611 beats), $p < 0.001$, Mann-Whitney U test. **(c,d)** Four bioelectric patterns at baseline were obtained by signal averaging in control recordings, while a single pattern was found in ES recordings. These patterns represent the 93% in control and 99% in ES of the total beats, respectively.

Figure 5. Cardioactive drug effects over electrostimulated human derived cardiac tissues mimic native tissue responses. **(a, b)** Representative traces of bioelectric signals of electrically stimulated (ES) human patches at baseline (first minute), and after Isoproterenol and Carbachol drugs were incubated (minute 10), respectively. Signals were filtered as explained before (see description in figure 3). Bar graphs show the effect of Isoproterenol and Carbachol drugs over the heart rate (HR). Relative HR to baseline increased significantly when incubated with isoproterenol while decreased significantly when incubated with Carbachol. ***Statistically significant differences between the relative heart rate for Isoproterenol ($p < 0.001$, Mann-Whitney U test) and Carbachol drugs ($p < 0.001$, Mann-Whitney U test). **(c, e)** Instantaneous HR expressed as beats per minute (bpm) was determined from the bioelectric signals of control and ES patches after Sotalol-high concentration was added, respectively. HR in both patches shows a decreasing trend when drug was incubated. **(d, f)** Representative traces of bioelectric signals after Sotalol-high concentration was incubated in control and ES human patches, respectively. Electrostimulated human derived cardiac tissues could predict proarrhythmic sotalol effects, including heart rate alterations and QT interval prolongation. I, II, and III (brown shading) indicate the time lapse from which the traces of ECG-like signals have been obtained.

Figure 1.

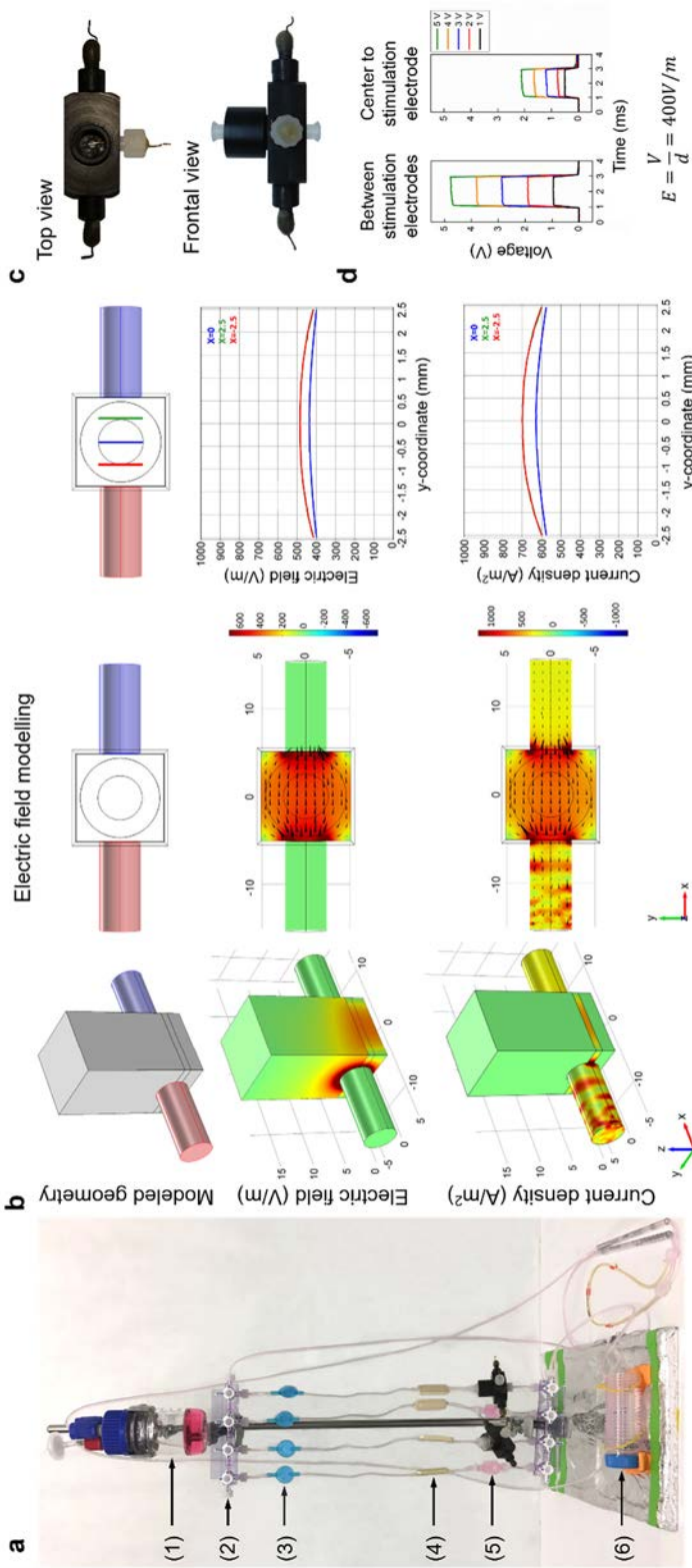


Figure 2.

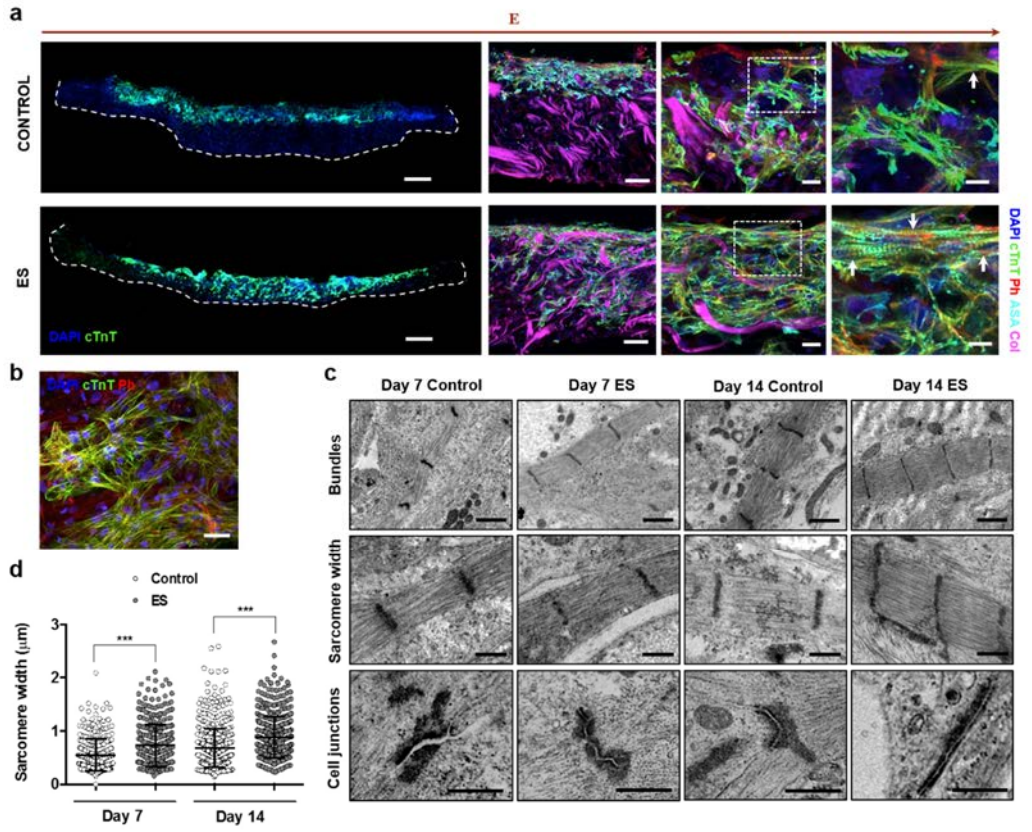


Figure 3.

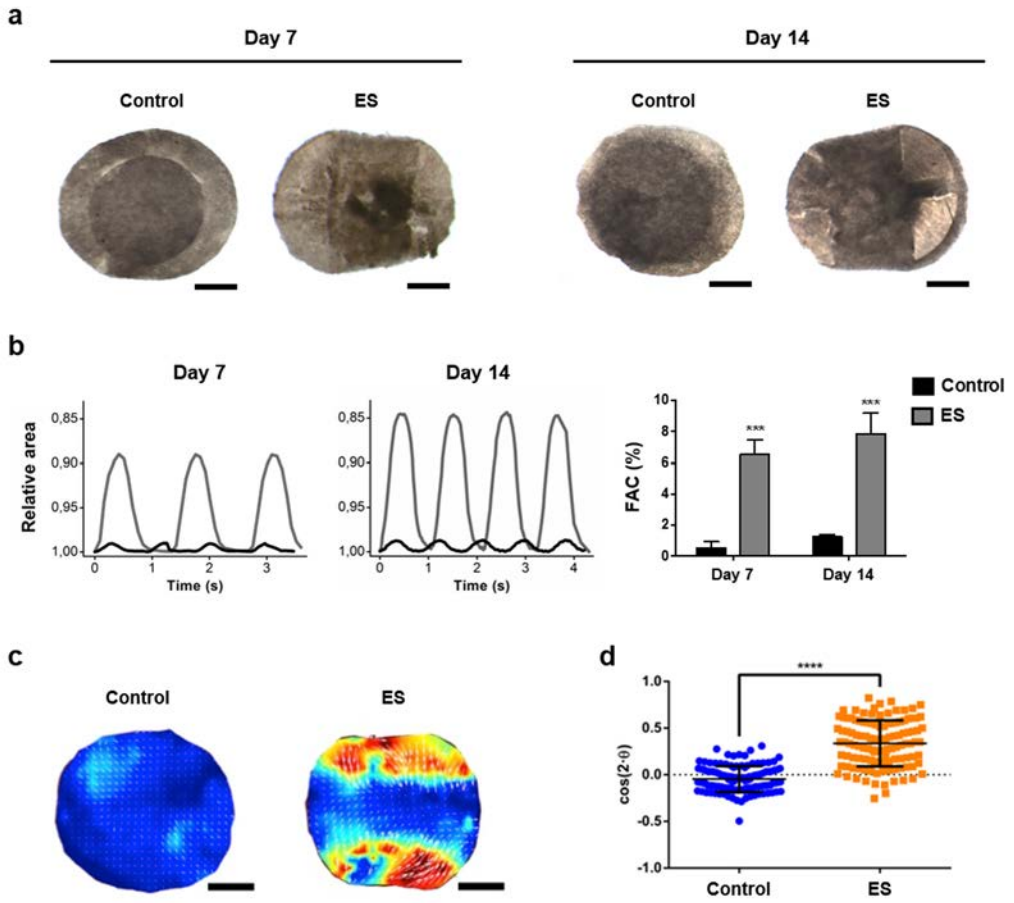


Figure 4.

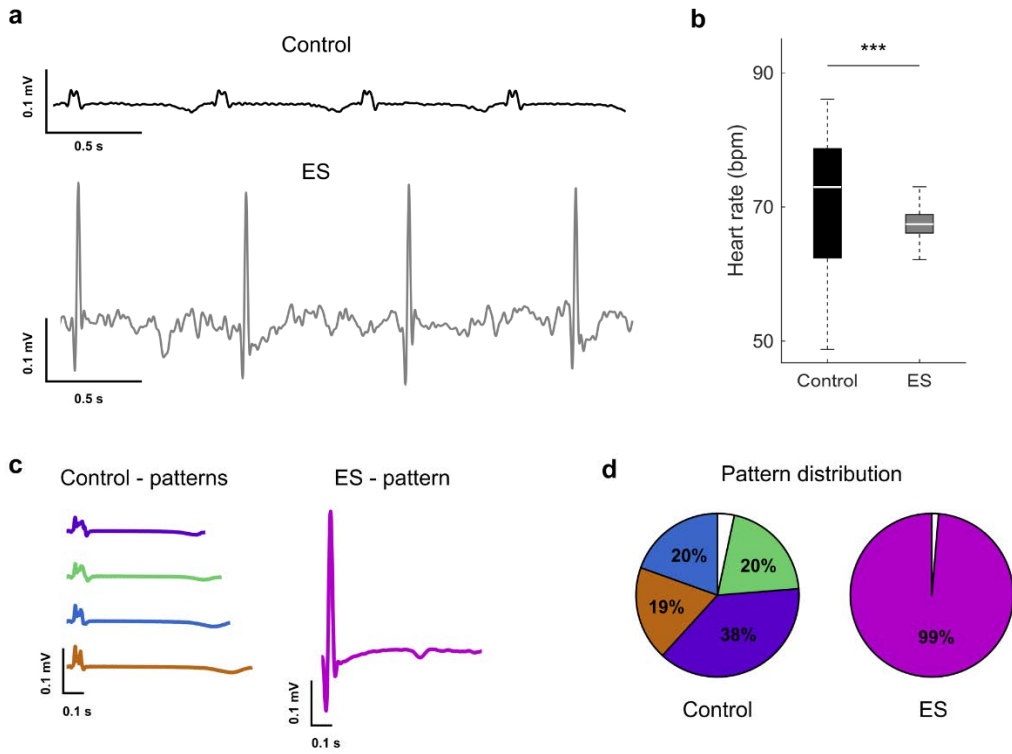
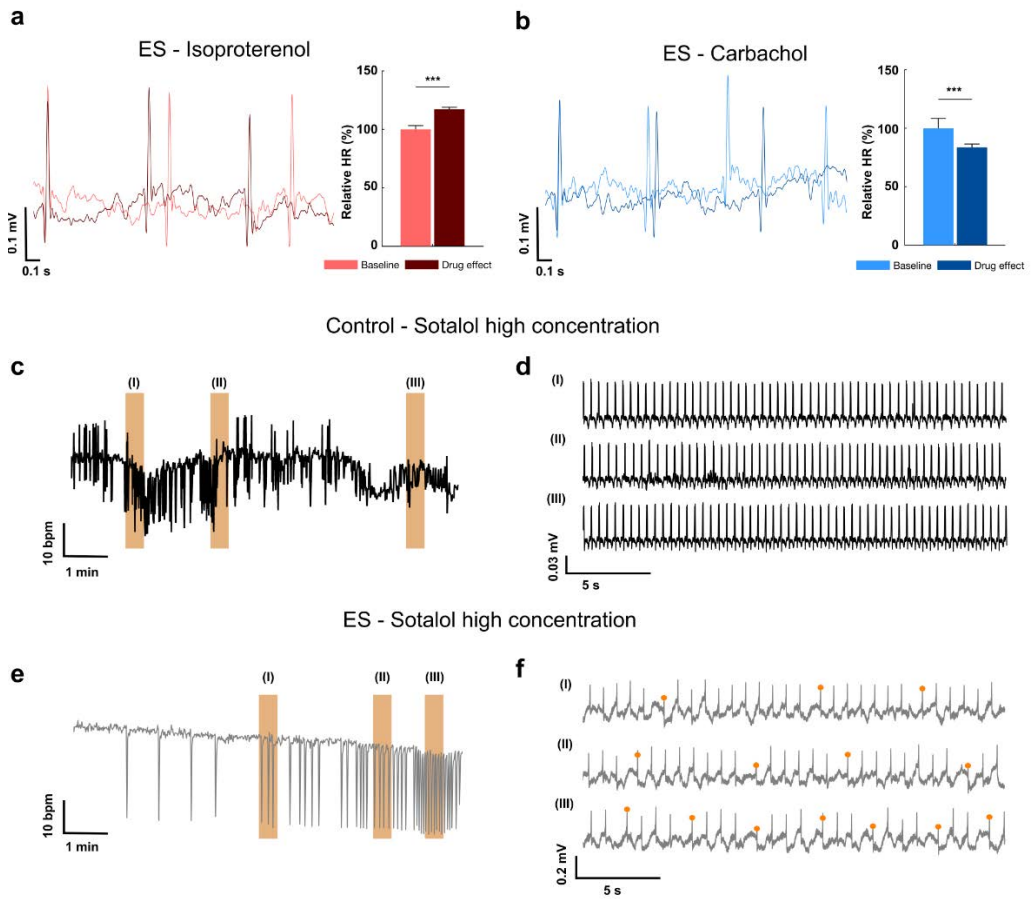


Figure 5.



SUPPLEMENTARY INFORMATION

Electrical stimulation improves structural organization and contractile function of rat-derived cardiac tissues

To test the suitability of the advanced 3D culture system to generate tissue-like cardiac patches, a primary culture of neonatal rat cardiomyocytes was used. Tissue constructs were cultured for 7 days under perfusion (Control group) or under perfusion plus electrical stimulation (Electrical stimulation group, ES), and cell morphology and distribution was analysed by immunofluorescence (**Supplementary Fig. 2a**). Both electrostimulated and non-stimulated patches showed positive expression of cardiac markers. However, electrostimulated cardiomyocytes showed a compact and extended distribution along the patch cross-section, whereas the non-stimulated ones formed intermittent groups with high cell densities. Interestingly, cells in electrostimulated tissues displayed abundant and well defined striations aligned in the direction of the electric field, whereas the control ones were scarcer and did not show a preferential direction of alignment (**Supplementary Fig. 2a**).

To further characterize cell organization and maturity, cardiac tissues were examined at ultrastructural level by transmission electron microscopy (TEM). Tissue constructs cultured under electrical stimulation showed cardiomyocytes with a well-developed and organized sarcomeric banding, including well-defined Z-bands and intercellular unions composed of desmosomes (**Supplementary Fig. 2b**). Moreover, cells in electrostimulated tissues displayed wider sarcomeres in comparison with non-stimulated samples and standard 2D cultures (ES: $0.54 \pm 0.32 \mu\text{m}$; Control: $0.29 \pm 0.16 \mu\text{m}$ and 2D: $0.42 \pm 0.18 \mu\text{m}$; $p < 0.001$), suggesting the formation of myofibrillar bundles (**Supplementary Fig. 2c**).

Functional activity of rat cardiac patches was also assessed after 7 days in culture by determining the fractional area change (FAC). Cardiac patches exposed to continuous electrical pacing exhibited contraction amplitude values four times higher than non-stimulated ones (**Supplementary Fig. 2d**). Moreover, an enhanced contractility with an evident preferential axis of contraction could be observed (**Supporting Movies 1-3**).

SUPPLEMENTARY METHODS

Fabrication and characterization of the perfusion chamber with electrical stimulation

Our custom-made perfusion chamber with electrical stimulation was fabricated by precision machining of polypropylene (PP) plastic, followed by gluing of luer connectors using cyanoacrylate. To achieve a completely watertight chamber, silicone O-rings (4.6 mm inner diameter, The O-Ring Store, LLC) and thread seal tape was used. The perfusion chamber had an inlet and an outlet to allow culture medium perfusion, two carbon rod electrodes of 3/16" in diameter (Monocomp Instrumentación) to electrically stimulate cells and one gold electrode of 0.5 mm in diameter (Advent Research Materials) as a measuring electrode (**Figure 1C**). Two holes were drilled at one edge of each rod electrode, and a solid tinned annealed copper wire (RS Pro) was thread

through the holes. Insulation of the connection was performed using Araldite® epoxy resin, and waterproofing of rod electrodes was achieved using heat-shrink tubing (Thermo Fisher Scientific). Electric potential values between stimulation electrodes and between one stimulation electrode and the center of the chamber (gold electrode) were characterized using a function generator (Agilent Technologies) and an oscilloscope (Agilent Technologies) (**Figure 1D**).

Isolation and culture of neonatal rat cardiomyocytes

Hearts from 2-3-day-old Sprague-Dawley rats were isolated following a protocol approved by Animal Experimentation Ethics Committee of the University of Barcelona (Barcelona, Spain). Briefly, ventricular tissue was excised, cut into two parts and washed with cold Calcium and Bicarbonate-Free Hank's Balanced Salt Solution with HEPES (CBFHH) buffer. Then, ventricles were cut sharply into small pieces (<1 mm³) and subjected to 20-25 cycles (3 min each, room temperature) of enzymatic digestion using ice-cold 2 mg/ml trypsin (BD Difco™) in CBFHH and ice-cold 4 µg/ml DNase I (Calbiochem, Merck Millipore) in CBFHH. Pooled supernatants were collected and centrifuged at 100 x g for 12 min, and the pellet was resuspended in cold DMEM containing 1 g/l glucose (Life Technologies) supplemented with 10% FBS, 100 µM nonessential amino acids (Life Technologies), 2 mM L-glutamine (Life Technologies), 50 U/ml penicillin and 50 µg/ml streptomycin (Life Technologies). Cell suspension was filtered through a 250 µm stainless steel test sieve (Filtración Vibración), seeded into Matrigel® scaffolds or in 12-well plates and cultured in DMEM containing 4.5 g/l glucose (Life Technologies) supplemented with 10% horse serum (Life Technologies), 2% Chick Embryo Extract (EGG Tech), 100 µM nonessential amino acids, 2 mM L-glutamine, 50 U/ml penicillin and 50 µg/ml streptomycin.

Human iPSC culture and cardiac differentiation

Human iPSC were cultured on 10 cm Matrigel (Corning) coated dishes with mTeSR1 medium (Stem Cell Technologies). Medium was changed every day, excluding the day right after passaging. Cells were split 1:6 – 1:10 by incubation with 0.5 mM EDTA (Invitrogen) for 2 min at 37°C and cell aggregates were plated on Matrigel coated dishes and maintained in culture for subsequent passages. Human iPSC were differentiated into cardiomyocytes in monolayer culture with modulators of canonical Wnt signaling as previously described⁴¹. Cells maintained on Matrigel in mTeSR1 medium were dissociated into single cells with Accutase (Labclinics) at 37°C for 8 min and seeded onto Matrigel-coated 12-well plate at a density of 1.5 million cells per well in mTeSR1 medium supplemented with 10 µM ROCK inhibitor (Sigma). Cells were cultured in mTeSR1 medium, changed daily during 3 days. When human iPSC achieved confluence, cells were treated with 10 µM GSK3 inhibitor (CHIR99021, Stemgent) in RPMI (Invitrogen) supplemented with B27 lacking insulin (Life Technologies), 1% glutamax (Gibco), 0.5% penicillin-streptomycin (Gibco), 1% non-essential amino acids (Lonza), and 0.1mM 2-mercaptoethanol (Gibco) (RPMI/B27-insulin medium) for 24 h (day 0 to day 1). After 24 h, the medium was changed to RPMI/B27-insulin and cultured for another 2 days. On day 3 of differentiation, cells were treated with 5 µM Wnt inhibitor IWP4 (Stemgent) in RPMI/B27-insulin medium and cultured without medium change for 2 days. Cells were maintained in RPMI supplemented with B27 (Life Technologies), 1%

L-glutamine, 0.5% penicillin-streptomycin, 1% non-essential amino acids, and 0.1 mM 2-mercaptoethanol (RPMI/B27 medium) starting from day 5, with medium change every 2 days. On day 12, contracting cardiomyocytes were obtained. Beating clusters were disaggregated (at day 20 and at day 35) by incubation with 0.25% trypsin-EDTA (Gibco) for 5-8 min at 37 °C, both for their characterization and *in vitro* studies.

Flow cytometry analysis

Characterization of human iPSC-CM was performed by flow cytometry analysis. Cells were dissociated on day 19 of differentiation using 0.25% trypsin-EDTA at 37 °C for 5 min and then fixed with 4% paraformaldehyde (Sigma) for 20 min at room temperature. After washing with 1X saponin (Sigma), cells were permeabilized using Cell Permeabilization Kit (Invitrogen) and blocked with 5% mouse serum during 15 min at room temperature. Then, cells were stained with the antibodies mouse PE-anti myosin heavy chain (MHC) (IgG2b, 1:400 BD Biosciences) and mouse Alexa Fluor 647 cardiac troponin I (cTnI) (IgG2b, 1:100, BD Biosciences). Mouse IgG2b PE (1:400 BD Biosciences) and mouse IgG2b Alexa Fluor 647 (1:100, BD Biosciences) antibodies were used as isotype controls. After 15 min incubation at room temperature in the dark and washing twice with 1X saponin, cells were analyzed with FACS MoFlo (Beckman Coulter) and data acquired and analysed with Kaluza software (Beckman Coulter).

Supplementary Table S1. List of the primary and secondary antibodies used for immunohistochemistry analysis.

Type	Antibody	Host	Dilution	Manufacturer
Primary	Actin α -sarcomeric (Monoclonal IgM)	Mouse	1:400	Sigma-Aldrich, A2172
Primary	α -actinin sarcomeric (Monoclonal IgG1)	Mouse	1:100	Sigma-Aldrich, A7811
Primary	α -tubulin (Monoclonal IgG1)	Mouse	1:500	Sigma-Aldrich, T6074
Primary	Connexin-43 (Polyclonal IgG)	Rabbit	1:250	Abcam, ab11370
Primary	Troponin I (Polyclonal IgG)	Rabbit	1:25	Santa Cruz, sc-15368
Primary	Troponin T (Monoclonal IgG1)	Mouse	1:100	Thermo Fisher, MS-295-P
-	Phalloidin Texas Red [®]	-	1:40	Life technologies, T7471
Secondary	Alexa Fluor [®] 488 Goat IgG	Donkey	1:200	Jackson, 705-545-147
Secondary	Alexa Fluor [®] 488 Mouse IgG	Goat	1:200	Jackson, 115-546-071
Secondary	Alexa Fluor [®] 488 Mouse IgG	Donkey	1:200	Jackson, 715-545-151
Secondary	Cy TM 3 Mouse IgG	Goat	1:200	Jackson, 115-165-071
Secondary	Cy TM 5 Mouse IgG	Goat	1:200	Jackson, 115-175-071
Secondary	Cy TM 2 Mouse IgM	Goat	1:200	Jackson, 115-225-075
Secondary	Cy TM 3 Mouse IgM	Donkey	1:200	Jackson, 715-165-140
Secondary	Cy TM 3 Mouse IgM	Goat	1:200	Jackson, 115-165-075
Secondary	DyLight TM 649 Mouse IgM	Goat	1:200	Jackson, 115-495-075
Secondary	Cy TM 5 Mouse IgM	Rabbit	1:200	Jackson, 315-175-049
Secondary	Alexa Fluor [®] 488 Rabbit IgG	Donkey	1:200	Jackson, 711-545-152
Secondary	Cy3 Rabbit IgG	Donkey	1:200	Jackson 711-165-152

Supplementary Table S2. Quantitative real-time polymerase chain reaction primers

Gene	Sense	Antisense
<i>MYH7</i>	GCATCATGGACCTGGAGAAT	ATCCTTGCGTTGAGAGCATT
<i>ACTC1</i>	GCTCTGGGCTGGTGAAGG	TTCTGACCCATACCCACCAT
<i>TNNT2</i>	TGCAGGAGAAGTTCAAGCAGCAGA	AGCGAGGAGCAGATCTTTGGTGAA
<i>GJA1</i>	CAATCACTTGGCGTGACTTC	CCTCCAGCAGTTGAGTAGGC
<i>SERCA2A</i>	TGAGACGCTCAAGTTTGTGG	TCATGCACAGGGTTGGTAGA
<i>GAPDH</i>	AGGGATCTCGCTCCTGGAA	AGGGATCTCGCTCCTGGAA

SUPPLEMENTARY FIGURES

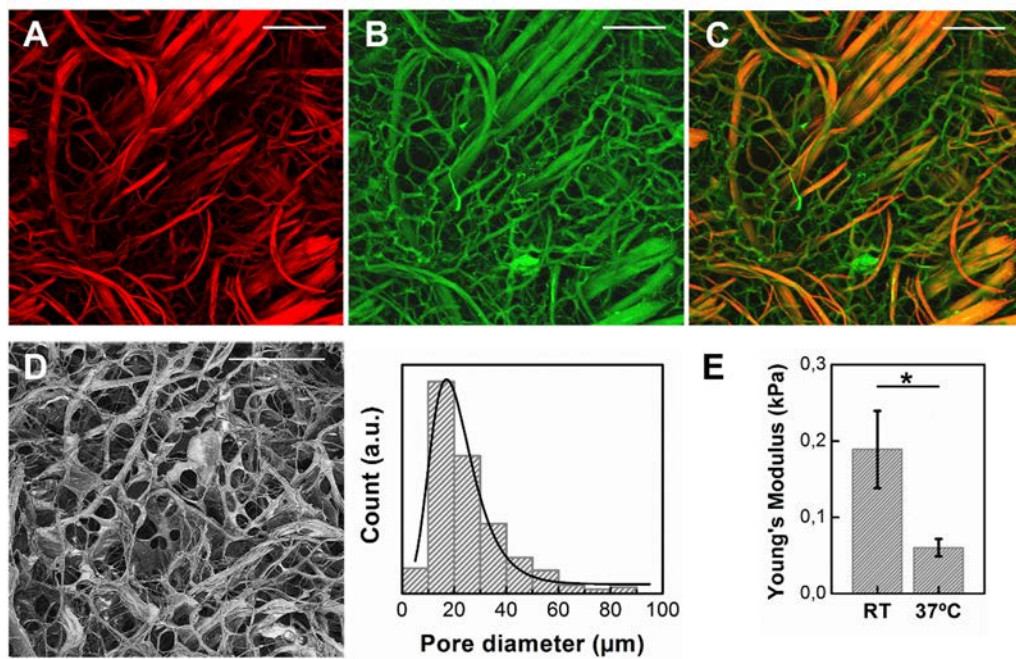
Supplementary Figure 1. Matrigel[®] collagen-elastin scaffold characterization. A-C, selective imaging of Matrigel[®] scaffold by second harmonic generation (SHG) and two-photon excited fluorescence (TPEF, autofluorescence). **A)** Matrigel[®] imaged by SHG. **B)** Matrigel[®] imaged by two-photon excited fluorescence (TPEF). **C)** Overlay image of A and B. **D)** Scanning electron micrograph of Matrigel[®] and porosity analysis. Feret's diameter has been calculated for scaffold pores, and values have been fitted in a single peak. The most frequent pore size is 17 μm . **E)** Matrigel[®] stiffness in compression at room temperature (RT) and at 37°C (average \pm SD; n=3 per group). Young's Modulus (E) has been determined from the slope of stress-strain curves ($*p < 0.05$; Student's t-test). Scale bars: 100 μm .

Supplementary Figure 2. Generation of functional and structurally organized rat cardiac patches after 7 days of culture in a perfusion bioreactor. A) Immunostaining of engineered rat cardiac patches. Representative cross-sections and higher magnification images, where cardiomyocytes' distribution along the scaffold and their sarcomeric organization and alignment is shown. E: electric field; DAPI: 4',6-diamidino-2-phenylindole; cTNI: cardiac troponin I; ASA: α -sarcomeric actin. Scale bars: 400 μm , higher magnifications: 100 and 50 μm . **B)** Representative images of cardiomyocyte ultrastructural organization (sarcomeric structure and cellular junctions) when cultured with or without electrical stimulation. Scale bar: 0.5 μm **C)** Morphometric analysis showing sarcomere width (measured as indicated by square brackets in B). ES: Electrical stimulation; NRV: neonatal rat ventricle ($***p < 0.001$; n \geq 2 per group, Mann Whitney U test). **D)** Contraction amplitude analysis of control and electrostimulated cardiac patches by means of Fractional Area Change (FAC). The area in pixels of each construct was obtained through custom MATLAB program (black dashed line), and its oscillation was represented over time (relative to the highest number of pixels recorded). Bar chart shows the fold induction relative to controls mean (n=3 per group). Scale bar: 0.25 μm . ES: Electrical stimulation.

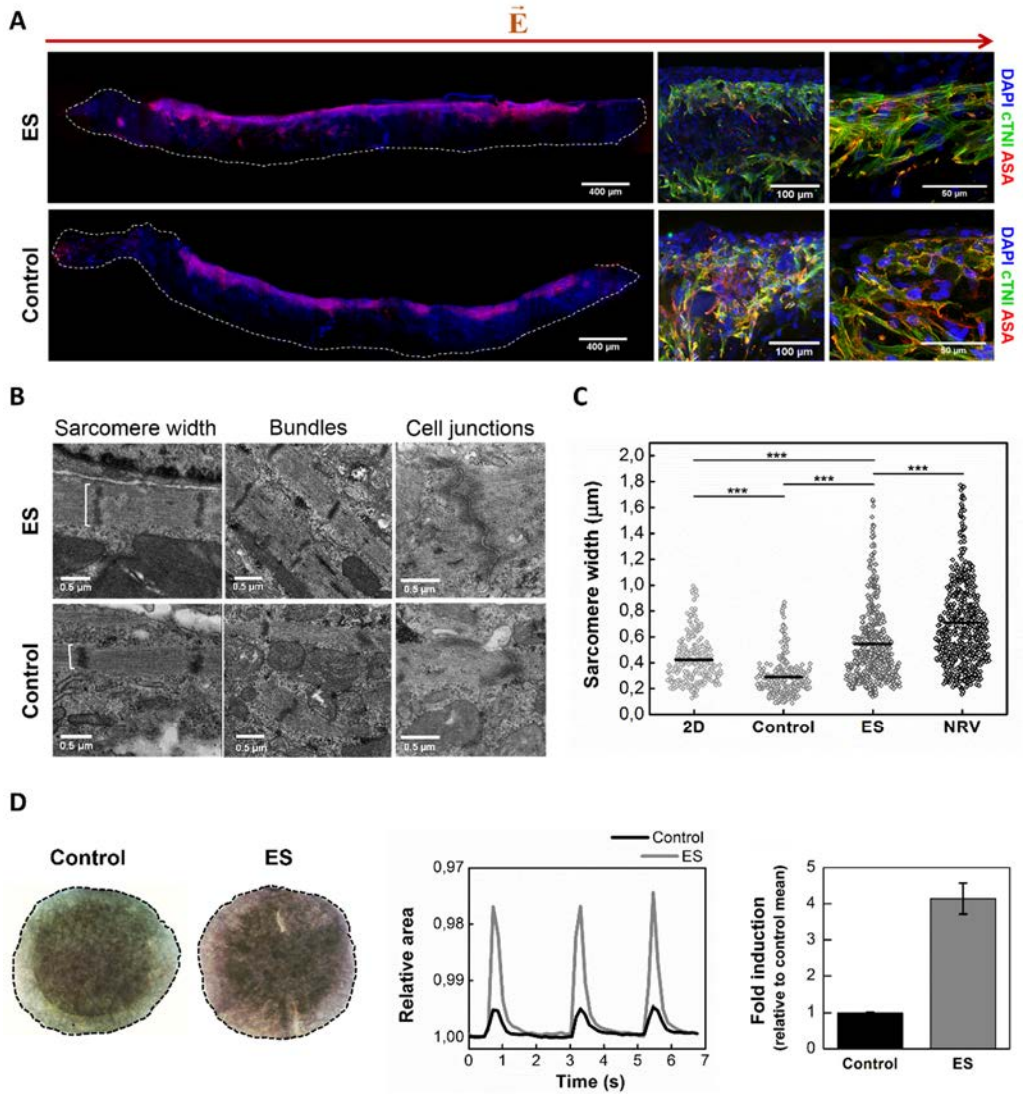
Supplementary Figure 3. Cardiac differentiation potential of hiPSCs. A) Schematics of the protocol for the differentiation of cardiomyocytes from hiPSCs with modulators of Wnt signalling pathway. Bright field images of the cell morphology at day -3, day -2, day 0, day 5 and day 20 of differentiation are shown. **B)** Flow cytometry analysis of cardiomyocytes differentiated from hiPSCs at day 20 of differentiation. Cells were analysed for cardiac troponin I (cTnI) and myosin heavy chain (MHC) expression. High purity of cardiomyocytes of over 70% was obtained (n=3). **C)** Immunofluorescence detection of cardiac proteins. Cardiomyocytes were selected at day 20 of differentiation and stained for cTnI (Cy2: green), α -actinin sarcomeric (AAS) (Cy3: red) and connexin-43 (Cx43) (Cy2: green). Nuclear staining was performed with DAPI. **D)** Expression of cardiac markers in differentiated hiPSCs. Cardiac gene expression was determined by quantitative PCR at day 0, day 20 and day 35 of differentiation. Up-regulation of cardiac specific genes and channel markers was detected in differentiated cells (n=2), although expression values still differed from adult heart (AH) tissue. Data are expressed as mean \pm SD. **E)** Representative images of hiPSC-CMs ultrastructural organization. Scale bars: 200 μ m (A), 25 μ m (C), 2 μ m (E); higher magnifications in E: 1 μ m.

Supplementary Figure 4. Endogenous gene expression of cardiac specific markers measured by qRT-PCR. Expression of cardiac markers in: 34-day-old cardiomyocyte monolayer standard culture (2D Ctrl); non-stimulated (Control) cardiac patches (3D Ctrl); electrostimulated cardiac patches (3D ES); fetal heart (FH) and adult heart (AH) (n=3-4/group). *MYH7*: β -myosin heavy chain; *TNNT2*: cardiac troponin T; *ACTC1*: cardiac muscle alpha actin; *GJ1A*: gap junction protein alpha 1; *SERCA2A*: Sarcoplasmic Reticulum Ca^{2+} -ATPase isoform 2a; *RYR2*: ryanodine receptor 2.

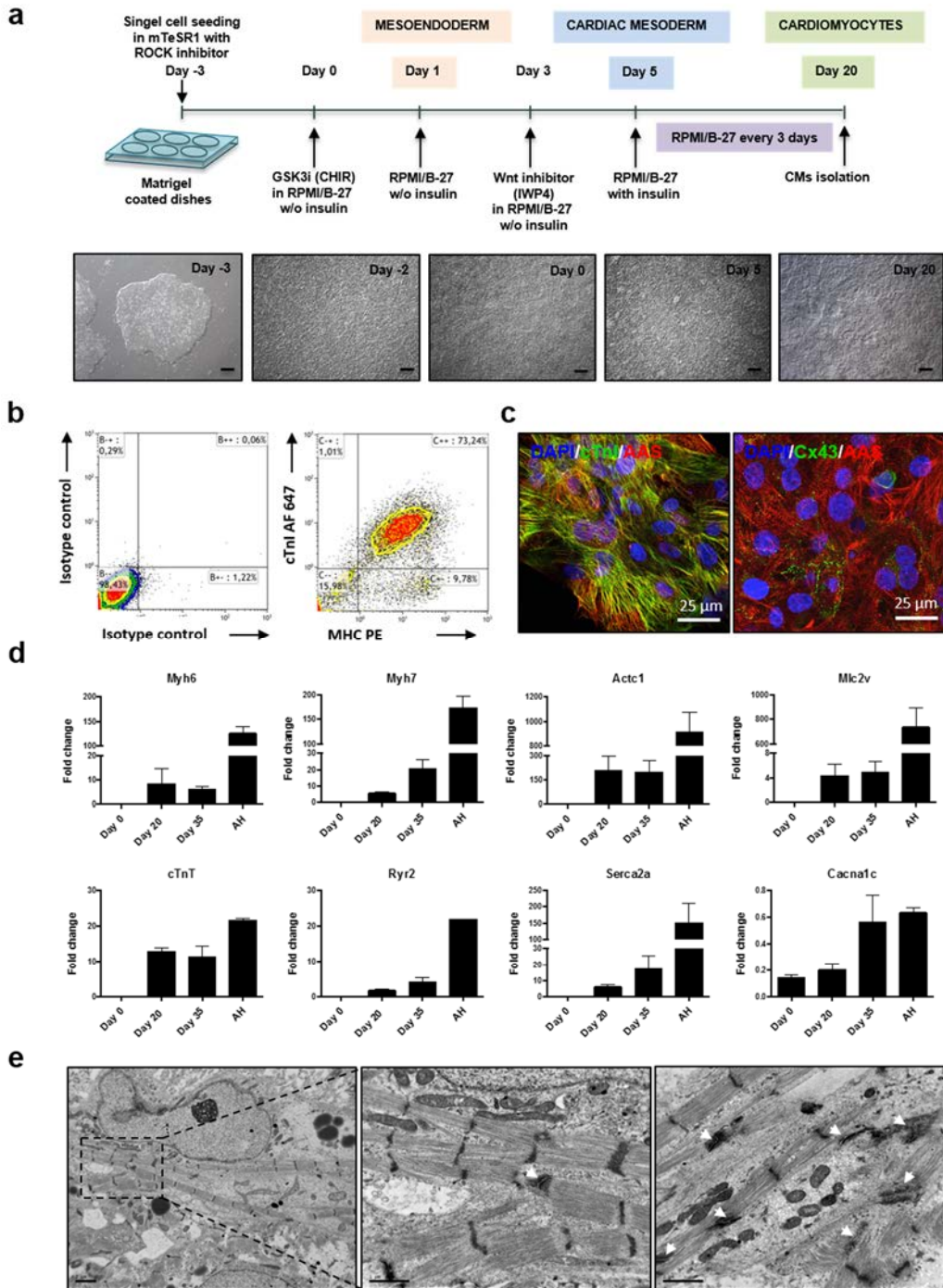
Supplementary Figure 1.



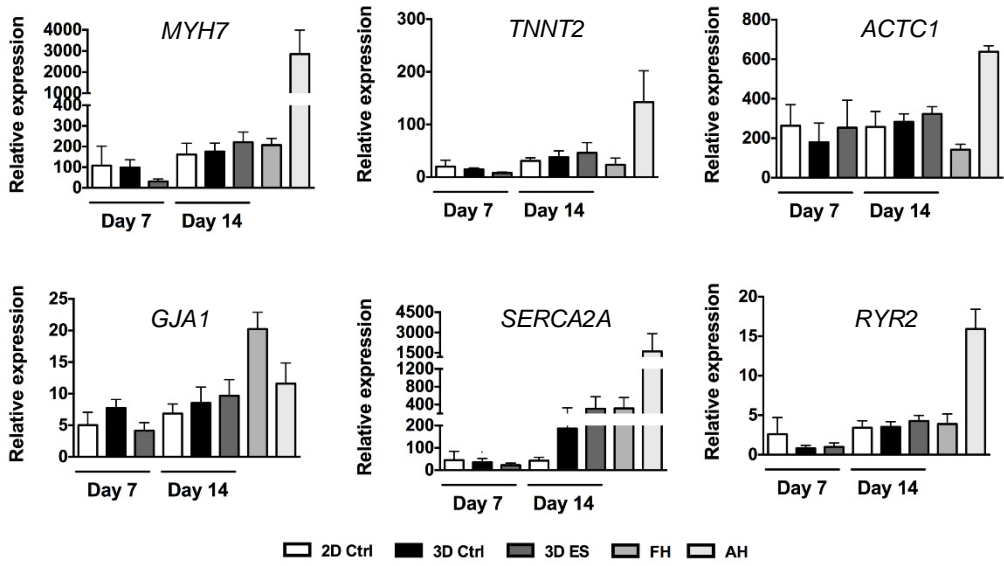
Supplementary Figure 2.



Supplementary Figure 3.



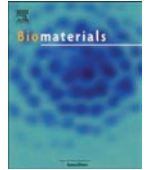
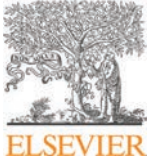
Supplementary Figure 4.



9.3. **Other journal articles**

Accepted journal article (document attached below):

Garreta E, de Oñate L, Fernández-Santos ME, Oria R, Tarantino C, Climent AM, Marco A, Samitier M, Martínez E, Valls-Margarit M, Matesanz R, Taylor DA, Fernández-Avilés F, Izpisua Belmonte JC, Montserrat N. Myocardial commitment from human pluripotent stem cells: Rapid production of human heart grafts. *Biomaterials* 98, 64–78 (2016).



Myocardial commitment from human pluripotent stem cells: Rapid production of human heart grafts



Elena Garreta ^{a,1}, Lorena de Oñate ^{a,b,1}, M. Eugenia Fernández-Santos ^{c,d}, Roger Oriá ^{e,f}, Carolina Tarantino ^a, Andreu M. Climent ^g, Andrés Marco ^a, Mireia Samitier ^a, Elena Martínez ^h, Maria Valls-Margarit ^h, Rafael Matesanz ⁱ, Doris A. Taylor ^{j,k,l}, Francisco Fernández-Avilés ^{c,d,***}, Juan Carlos Izpisua Belmonte ^{m,**}, Nuria Montserrat ^{a,*}

^a Pluripotent Stem Cells and Activation of Endogenous Tissue Programs for Organ Regeneration, Institute for Bioengineering of Catalonia (IBEC), Barcelona, Spain

^b Center of Regenerative Medicine in Barcelona (CMRB), Barcelona, Spain

^c Department of Cardiology, Hospital General Universitario Gregorio Marañón, Universidad Complutense de Madrid, Spain

^d Cell Production Unit, Department of Cardiology, Instituto de Investigación Sanitaria Hospital Gregorio Marañón (IISGM), Madrid, Spain

^e Institute for Bioengineering of Catalonia (IBEC), Barcelona, Spain

^f University of Barcelona, Barcelona, Spain

^g Bioartificial Organs Laboratory, Instituto de Investigación Sanitaria Hospital Gregorio Marañón (IISGM), Madrid, Spain

^h Biomimetic Systems for Cell Engineering, Institute for Bioengineering of Catalonia (IBEC), Barcelona, Spain

ⁱ National Transplant Organization (ONT), Spanish Ministry of Health and Consumption, Spain

^j Center for Cardiovascular Repair, University of Minnesota, Minneapolis, MN, USA

^k Department of Regenerative Medicine Research, Texas Heart Institute, Houston, TX, USA

^l Department of Integrative Biology and Physiology, University of Minnesota, Minneapolis, MN, USA

^m Gene Expression Laboratory, Salk Institute for Biological Studies, La Jolla, CA, USA

ARTICLE INFO

Article history:

Received 16 December 2015

Received in revised form

1 April 2016

Accepted 4 April 2016

Available online 26 April 2016

Keywords:

Gene targeting

Pluripotent stem cells

Extracellular matrix

Cardiac function

ABSTRACT

Genome editing on human pluripotent stem cells (hPSCs) together with the development of protocols for organ decellularization opens the door to the generation of autologous bioartificial hearts. Here we sought to generate for the first time a fluorescent reporter human embryonic stem cell (hESC) line by means of Transcription activator-like effector nucleases (TALENs) to efficiently produce cardiomyocyte-like cells (CLCs) from hPSCs and repopulate decellularized human heart ventricles for heart engineering. In our hands, targeting myosin heavy chain locus (MYH6) with mCherry fluorescent reporter by TALEN technology in hESCs did not alter major pluripotent-related features, and allowed for the definition of a robust protocol for CLCs production also from human induced pluripotent stem cells (hiPSCs) in 14 days. hPSCs-derived CLCs (hPSCs-CLCs) were next used to recellularize acellular cardiac scaffolds. Electrophysiological responses encountered when hPSCs-CLCs were cultured on ventricular decellularized extracellular matrix (vdECM) correlated with significant increases in the levels of expression of different ion channels determinant for calcium homeostasis and heart contractile function. Overall, the approach described here allows for the rapid generation of human cardiac grafts from hPSCs, in a total of 24 days, providing a suitable platform for cardiac engineering and disease modeling in the human setting.

© 2016 The Author(s). Published by Elsevier Ltd. This is an open access article under the CC BY-NC-ND license (<http://creativecommons.org/licenses/by-nc-nd/4.0/>).

* Corresponding author. Pluripotent stem cells and activation of endogenous tissue program for organ regeneration. Institute for Bioengineering of Catalonia (IBEC), C/ Baldiri Reixac 15-21, 08028-Barcelona, Spain.

** Corresponding author. Gene Expression Laboratory, Salk Institute for Biological Studies, 10010 North Torrey Pines Road, La Jolla, California 92037, USA

*** Corresponding author. Department of Cardiology, Hospital General Universitario Gregorio Marañón, University Complutense of Madrid, C/ Dr Esquerdo 46, 28007 Madrid, Spain.

E-mail addresses: faviles@secardiologia.es (F. Fernández-Avilés), belmonte@salk.edu (J.C. Izpisua Belmonte), nmontserrat@ibecbarcelona.eu (N. Montserrat).

¹ Both authors equally contributed to the development of the work presented here.

1. Introduction

The derivation of human embryonic stem cells (hESCs) [1] together with the finding that human somatic cells could be converted towards human induced pluripotent stem cells (hiPSCs) [2] opened new venues for the production of protocols aiming to generate patient cardiac-like cells (CLCs) with an impact in heart regenerative therapies [3]. Recently, organ decellularization is envisioned as an attractive strategy for the development of bio-functional organs for drug screening and personalized medicine [4–8]. In the last years, several works have proved the feasibility to use cardiac extracellular matrix (ECM) from murine, pig or rat origin for cardiac engineering using human ESCs (hESCs) [9–11]. Interestingly, CLCs derived from human iPSCs (hiPSCs–CLCs) have recently proved to repopulate human hearts [4]. Here we describe a rapid protocol for the generation of human cardiac grafts by co-culturing hESCs and hiPSCs (human pluripotent stem cells–hPSCs) on cardiac ECM from human origin avoiding the use of extensive culture in bioreactors. Moreover, our experimental setting allowed for the investigation of the effect of human ventricular decellularized ECM (vdECM) on electrophysiological responses related to cardiac function.

Protocols for derivation of cardiac like cells (CLCs) from hPSCs (hPSCs–CLCs) have traditionally relied on the time consuming production of embryoid bodies (EBs), achieving low yields of CLCs generation, thus hampering the reproducibility and scale up of such procedures [3,12,13]. Interestingly, in the last years several authors, including us, have demonstrated that is possible to induce cardiac differentiation from hPSCs grown as monolayers [14–17]. Although challenging, those protocols still did not provide exact information about the identity of the generated cells. In this regard, the generation of cardiac hPSCs reporter cell lines may lead to the definition of the developmental cues driving cardiac differentiation, and more importantly, to develop rapid methods for the enrichment of different cardiac cell types during the onset of differentiation. So far only two previous reports using Bacterial Artificial Chromosome (BACs) showed the possibility to target cardiac-related loci in hPSCs by homologous recombination [18,19]. In the same manner, transposon-based approaches have led to the generation of hESCs reporter cell lines for cardiac differentiation [20,21]. These studies showed that reporter hPSCs lines could lead to the identification of novel markers for hPSCs–CLCs generation and expansion *in vitro*. In the last years, genome editing technologies as CRISPR/Cas9 and TALEN platforms, have emerged as powerful tools for targeting in site-specific manner unique and multiple human loci, allowing to study gene function, disease modeling and drug discovery, among other applications. To our knowledge, neither CRISPR/Cas9 nor TALEN platforms have been explored for the generation of cardiac reporter hPSCs lines.

MYH6 is an important transcription factor essential for cardiac muscle contraction, and recently, mouse MYH6-GFP fibroblasts have been used for the study of cardiac conversion [22]. Based on those findings, and taking advantage of TALEN technology, we have targeted human MYH6 locus with mCherry fluorescent reporter preserving the regulatory sequences near the native ATG start codon for translation of MYH6 gene. In our hands, TALEN engineering and subsequent cell culture pressure did not hamper mCherry MYH6 reporter hESC line to exhibit classical pluripotent-related features, and more importantly, enabled us to define a robust protocol for the generation of CLCs from different hPSC lines. Next, we made use of our recently reported method of perfusion decellularization in human hearts for the generation of vdECMs constructs. After only 10 days, hPSCs–CLCs grown on human vdECMs exhibit a higher degree of physiological and molecular cardiac differentiation compared to hPSCs–CLCs counterparts

cultured in matrigel substrates. Overall, here we set up a rapid protocol for the development of human heart grafts for drug screening and disease modeling applications.

2. Methods

2.1. Donor heart harvest and heart decellularization

Between May 2010 and June 2013, we harvested 52 human hearts that were determined by the Spanish National Transplant Organization (ONT) as not suitable for transplantation. The ONT is part of the Spanish Ministry of Health and Consumption and is in charge of coordinating the donation, extraction, preservation, distribution, exchange, and transplantation of organs, tissues, and cells throughout the Spanish Health Care System. Approval for all studies was obtained from the relevant investigation and ethics committees of the Hospital General Universitario Gregorio Marañón on and from the ONT. The relatives of each donor provided an informational brochure stating that the heart would be used for this investigational purpose. After approval was obtained, and other organs suitable for transplantation were explanted, we used standard transplantation protocols to remove the heart. Briefly, a median sternotomy was performed to expose the mediastinum, the pericardium was opened, and the superior and inferior vena cava were dissected. The hearts were maintained in saline at 4 °C until decellularization was performed within few hours after harvesting.

We used our previously described perfusion decellularization protocol to remove the cells from the heart while retaining the ECM [5]. Briefly, hearts were perfused with 1% sodium dodecyl sulfate (SDS) in deionized water via antegrade flow through the ascending aorta; perfusion was stopped at day 4–8. Hearts were then rinsed extensively with approximately 20 L of phosphate-buffered saline (PBS). Thirteen hearts were not decellularized and served as cadaveric controls. Thick slices (400 µm) of decellularized heart ventricles were obtained using a vibratome, and further seeded with hPSCs–CLCs. Slices were kept at 4 °C in PBS in the presence of penicillin and streptomycin (Penicillin 10.000 U/ml:Streptomycin 10.000 µg/ml–Invitrogen#15140-122) until further use.

2.2. DNA quantification

To assess total DNA content in the ECM scaffolds, samples were digested as described previously [23]. After isolation, DNA content was quantified using the Picogreen DNA assay following manufacturer's instructions (Invitrogen).

2.3. Cell lines

Control fibroblasts (ATCC® SCRC-1041) were grown in DMEM supplemented with 10% fetal bovine serum, 2 mM L-glutamine, 0.1 mM 2-mercaptoethanol, nonessential amino acids and penicillin-streptomycin (Penicillin 10.000 U/ml:Streptomycin 10.000 µg/ml–Invitrogen#15140-122). hESC ES4 line from Banco Nacional de Lineas Celulares and hiPSCs (FiPS#1 line) were grown in mTeSR1 (05850, Stem Cell Technologies) in matrigel substrate (354277, Corning) following manufacturer recommendations.

2.4. Antibodies

The following antibodies were used: tumor rejection antigen 1 (TRA-1), TRA-1–81 (MAB4381, 1:100, Chemicon); OCT-3/4 (sc-5279, 1:25, Santa Cruz Biotechnology); NANOG (AF1997, 1:25, R&D Systems); Paired Box 6 (PAX6, PRB-278P, 1:100, Covance); Microtubule-Associated Protein 2 (MAP2, sc-32791, 1:25, Santa

Cruz Biotechnology) α 1-fetoprotein (AFP, A0008, 1:200, Dako); Forkhead Box Protein A2 (FOXA-2, AF2400, 1:50, R&D Systems); α -sarcomeric actinin (ASA, A7811, 1:100, Sigma); RFP (ab34771, 1:400, Abcam); Myosin Heavy Chain (MYH6, GTX20015, 1:100, GeneTex); GATA 4 binding 4 (GATA4, sc9053, 1:25, Santa Cruz Biotechnology); NKX2.5 (sc8697, 1:25, Santa Cruz Biotechnology); Troponin T (TNN, MS-295-P1ABX, 1:500, Thermo Scientific); Collagen Type IV (CIV22; ref: 760-2632; Dako); Actin Muscle Specific (HHF 35; ref: 760-260; Roche); Desmin (DE-R-11; ref 760-2513; Roche). Secondary antibodies used were all the Alexa Fluor Series from Jackson ImmunoResearch (all 1:200). For immunohistochemistry anti-Mouse HRP-DAB Cell & Tissue Staining Kit (R&D, CTS002). Images were taken using a Leica SP5 confocal microscope and Nikon-TE200.

2.5. Genome editing of human embryonic stem cells with TALENs

TALENs were designed and assembled as described [24,25]. Each TALEN consists of 34 amino acids, where the TALEN repeat variable diresidues (RVDs) in the 12th and 13th amino acid positions of each repeat specify the DNA base being targeted according to the code: NG = T, HD = C, NI = A, and NN = G or A. Tandem arrays of customized TALE repeats were assembled using hierarchical ligation and combining separate digest and ligation steps into single Golden Gate reactions [26,27]. First, each nucleotide-specific monomer sequence: NI, HD, NG, NN (from TALE Toolbox kit Addgene cat no: 100000019) was amplified with ligation adaptors that uniquely specify the monomer position within the future TALEN tandem repeats, thus generating a monomer library. Once TALEN targeting sites were identified using TAL effector Nucleotide Targeter program [28], for each 20 bp TALEN target desired (5' and 3'), the appropriate monomers were ligated into hexamers and amplified via PCR (specific primers were provided in TALE toolbox kit Addgene cat no: 100000019- Table S1). Then, by a second Golden Gate digestion-ligation with the appropriate TALE cloning backbone (pCMV_NLS (NI,HD, NG, NN)_FokI), the desired MYH6 sequence-specific TALEN were fully assembled. TALEN Backbone was a gift from Feng Zhang (Addgene plasmid # 31179) [24]. All TALENs used the +63 truncation point [25]. The complete sequence of all TALENs used in this work is provided in supplementary information (Fig. S1). After Sanger analysis for verification, HEK 293 cells were transfected with TALENs as described previously [25,29]. Four hundred thousand cells were transfected, and subsequently genomic DNA was extracted without selecting for transfected cells using DNeasy Blood & Tissue kit (Qiagen). TALEN activity was assayed via Surveyor nuclease assay (Transgenomic) using the following primers for the amplification of the expected targeting area: Surveyor MYH6 Forward 5'-cactcagcgcacaaccttagcactaccag-3' and Surveyor MYH6 Reverse 5'-ccaggggtgattctctggctgtgtgag-3'. Primers were used at a final concentration of 1 μ M each in 50 μ L reactions using TAKARA LA Taq pol Hot Start (Takara). PCR reactions were as follows: an initial denaturation step (94 °C, 1 min); next, 35 cycles of a denaturation step of 20 s at 94 °C, annealing and extension step of 5 min at 68 °C, and a final extension step of 10 min at 72 °C. After absolute quantification of PCR products, 800 ng were used to perform the DNA heteroduplex formation on a 96 well thermocycler with programmable temperature stepping functionality (Applied Biosystems) and following transgenomic Surveyor mutation detection kit (Life Technologies) indications.

2.6. MYH6 donor vector (d-vector) design and construction

MYH6 donor vector (MYH6 d-vector) was generated by In-Fusion[®] cloning method (Clontech) following manufacturer's indications. MYH6 genomic sequence was purchased in BACPAC

Resources Center (RP11-929J10; BPRC) and used as template for 1 Kb homology arms amplification by PCR. Then, HA_mCherry_Poly cassette was amplified from pCAG_HA_mCherry_Poly based vector from The Scripps Institute [30] by adding an extra Kozac sequence to enhance mCherry future expression. A first In-Fusion[®] reaction was done with 25 ng of pZero_FRT_Neo [31] double digested with *Bam*HI and *Nde*I restriction enzymes (New England Biolabs) and pZero_5'arm_HAMCherry_FRT_Neo was generated. Next MYH6 3' homology arm was cloned by a second In-Fusion[®] reaction on pZero_5'arm_HAMCherry_FRT_Neo vector digested with *Eco*RV and *Xho*I restriction enzymes (New England Biolabs) to generate a final donor vector: pZero_5'arm_HAMCherry_FRT_Neo_3'arm (Fig. S2). PCRs were performed with primers listed on Table S2. PCR conditions were: 3 min at 94 °C; 30 cycles of denaturation at 94 °C for 30 s, primer annealing at 60 °C for 30 s, extension at 68 °C for 1–2 min and final extension step of 5 min at 65 °C.

2.7. Targeting of hESCs using TALEN mediated homologous recombination

ES4 was cultured in 10 μ M Rho Kinase (ROCK)-inhibitor (Calbiochem; Y-27632) 1–3 h prior to electroporation. Cells were harvested using Accumax (Stem Cell Technologies cat no 07921) and 1×10^6 cells resuspended in 800 μ L phosphate buffered saline (PBS) and 15 μ g of each pair of TALEN constructs (30 μ g total) plus 30 μ g of donor vector were added into cell suspensions. Electroporation conditions were fixed at 500 μ F; 200 Ω ; 250 V in Gene Pulser Xcell[™]. 72 h after electroporation cells were selected by the acquisition of Neomycin resistance adding 50 μ g/ml of Neomycin (G418, GIBCO). Targeted clones were selected by two different PCR reactions with GXL polymerase (TAKARA). Primers for short and long PCR products are listed in Table S3.

2.8. Southern blot analysis on targeted ES4 clones

Genomic DNA from ES4 clones positive for targeting by PCR screening was isolated using All Prep DNA/RNA columns (Qiagen) following manufacturer's guidelines. Briefly, 5 μ g of genomic DNA was digested with 40 U of *Bcl*III restriction enzyme (New England Biolabs) overnight and separated by electrophoresis on a 1% agarose gel. Next, DNA was transferred to a neutral nylon membrane (Hybond-N, Amersham) and hybridized with DIG-dUTP labeled probes generated by PCR using the PCR DIG Probe Synthesis Kit (Roche Diagnostics). Probes were detected by an AP-conjugated DIG-Antibody (Roche Diagnostics) using CDP-Star (Sigma-Aldrich) as a substrate for chemiluminescence. Primers for probe synthesis are listed in Table S4. Genomic DNA from clone #3 was verified by Sanger (Fig. S3).

2.9. Reprogramming of human fibroblasts

Episomal plasmids published elsewhere [32] were used to generate hiPSCs lines in a period of only 20–22 days. Fibroblasts were cultured and maintained in fibroblasts media: DMEM (Invitrogen, cat.no. 11965-092), 10% FBS (Invitrogen, cat. no. 10270-106), 1 mM Glutamax (Gibco[®], Life Technologies cat.no.35050-038) and 50 U/ml, 50 μ g/ml of Penicillin/Streptomycin (Gibco[®], Life Technologies cat.no.15140-122) in a humidified 37 °C 5% CO₂ incubator. When cells reached 80% of confluence, 500,000 of cells trypsinized with 0.25% Trypsin/EDTA (Invitrogen, cat. no. 25200-056) and washed with PBS. Next, cells were resuspended in pre-warmed Human MSC Nucleofactor Solution at room temperature. Nucleofactor Solution was prepared following Human MSC Nucleofactor[®] Kit recommendations (VPE-1001, Amaxa). Then, plasmid mixture containing 1 μ g of each pCLXE episomal based plasmid were added

to the nucleofection solution [pCXLE-hSK (Addgene plasmid # 27078), pCXLE-hOCT3/4-shp53-F (Addgene plasmid #27077), pCXLE-hUL (Addgene plasmid #27080) were a gift from Shinya Yamanaka]. Nucleofection reaction was performed in a provided Amaxa certified cuvette using nucleofection program U-23 from the Nucleofector™ 2b Device (Amaxa cat.no. AAB-1001). Cells were immediately transferred into two wells of a six-well culture plate with pre-warmed fibroblast culture media and incubated for 4 additional days with daily media change. Finally, nucleofected cells were subcultured onto matrigel (354277, Corning) coated plates in the presence of mTeSR1 (05850, Stem Cell Technologies).

2.10. Induced pluripotent stem cells generation and subculture

On day 23 hiPSC colonies were picked manually and expanded in matrigel (354277, Corning) coated plates in the presence of mTeSR1 (05850, Stem Cell Technologies). From this stage on hiPSC colonies were amplified by trypsinization in matrigel (354277, Corning).

2.11. Immunocytochemistry and fluorescence microscopy

ES4 and ES4 TALEN mCherry_MHY6/wt #3 (ES4 mCherry_MHY6), FiPS#1 line, hPSCs-CLCs, ventricular decellularized ECMs (vdECMs) and recellularized vdECMs were fixed in 2% paraformaldehyde in PBS. After fixation, samples were blocked and permeabilized for 1 h at room temperature in the presence of 0.5% Triton X100 and 6% donkey serum. Subsequently, samples were incubated with the indicated primary antibodies overnight at 4 °C. Samples were then washed thrice with PBS and incubated for 2 h at room temperature with the respective secondary antibodies. Samples were washed thrice with PBS and counterstained with DAPI (Invitrogen) before analysis. Samples were imaged using a SP5 (Leica) microscope.

2.12. RT-PCR analysis

Total RNA was isolated using All Prep RNA columns (Qiagen) according to the manufacturer's recommendations. 2 µg of TURBO™ DNase (Ambion, AM2238) treated total RNA was used for cDNA synthesis using the SuperScript II Reverse Transcriptase kit for RT-PCR (Invitrogen). Real-time PCR was performed using the SYBR Green PCR Master Mix (Applied Biosystems) in an ABI Prism 7300 thermocycler (Applied Biosystems) and primers (Table S5).

2.13. In vitro differentiation of human pluripotent stem cell lines

ES4 mCherry_MHY6 line was differentiated *in vitro* towards the three germ layers of the embryo. Monolayers of hPSCs were disaggregated and subsequently induced to form Embryoid Bodies (EBs) by centrifugation of cells within round-bottomed low attachment 96-well plates at 950 g for 5 min as described elsewhere [33]. After 3–4 days EBs were transferred to 0.1% gelatin-coated glass chamber slides and cultured in differentiation medium (DMEM supplemented with 20% fetal bovine serum, 2 mM L-glutamine, 0.1 mM 2-mercaptoethanol, nonessential amino acids and penicillin-streptomycin) for 2–3 weeks to allow spontaneous endoderm formation. The medium was changed every other day. For mesoderm differentiation, EBs were maintained on gelatin-coated glass chamber slides in differentiation medium supplemented with 100 µM ascorbic acid (Sigma). For ectoderm differentiation, EBs were cultured on matrigel coated glass chamber slides in N2B27 medium (DMEM/F12 and neurobasal medium 1:1 supplemented with 1% N2 (Invitrogen), 0.5% B27 (Invitrogen), 2 mM L-glutamine and penicillin-streptomycin) supplemented

with 1 µM retinoic acid (Sigma) for 2–3 weeks. The medium was changed every other day.

2.14. In vitro generation of cardiomyocyte-like cells (CLCs) from human pluripotent stem cells (hPSCs)

Single cell suspension of hPSCs were seeded onto matrigel (BD Biosciences) pre-coated cell culture dishes at a density of 125,000 cells per cm² in mTeSR medium (StemCell Technologies). Cells were then maintained in mTeSR for 48 h. Differentiation was initiated by treatment with 12 µM CHIR99021 (Selleck) in RPMI (Invitrogen) supplemented with B27 minus insulin (Life Technologies), 2 mM L-glutamine, 0.1 mM 2-mercaptoethanol, nonessential amino acids and penicillin-streptomycin (RPMI/B27-insulin medium) for 24 h (day 0 to day 1). On day 1, inhibitor was then removed by intensive washing once with RPMI and medium was changed to RPMI/B27-insulin. On day 3, cells were treated with 5 µM Wnt inhibitor IWP4 (Stemgent) in RPMI/B27-insulin medium and cultured without medium change for 48 h. On day 5, cells were washed once with RPMI to eliminate the inhibitor and maintained in RPMI (Invitrogen) supplemented with B27 (Life Technologies), 2 mM L-glutamine, 0.1 mM 2-mercaptoethanol, nonessential amino acids and penicillin-streptomycin (RPMI/B27 medium). From day 5, cells were maintained in RPMI/B27 medium with medium change every 2 days. On day 14, beating monolayers were obtained.

2.15. Flow cytometry

Cells were disaggregated from cell culture plates by incubation with Accumax (Invitrogen) for 5 min at 37 °C. Cells were vortexed to disrupt the aggregates, and neutralized by adding DMEM medium containing 10% fetal bovine serum (FBS). Next cells were washed once in PBS without Ca/Mg²⁺ supplemented with 0.1 mM EDTA (fluorescence-activated cell sorter (FACS) buffer), and resuspended in 500 µL of FACS buffer for analysis. Approximately one million cells were used for each flow sample. Data were collected and analyzed on an Aria FUSION (Becton Dickinson) flow cytometer.

2.16. Second harmonic generation (SHG) and two-photon excited fluorescence (TPEF)

Heart ECM was imaged by a nonlinear technique of SHG and TPEF. This technique enables noninvasive visualization of collagen and elastin in intact unstained tissues [34–36]. Collagen is a non-centrosymmetric molecule that efficiently generates the second harmonic of incident light, while elastin is a significant source of ECM autofluorescence that can be imaged by TPEF. The SHG-TPEF setup consisted of a Leica inverted confocal laser scanning microscope SP-5 with META scanning module equipped with a mode-locked near-infrared MAITAI Wide Band (710 nm–990 nm) laser (Spectra Physics Millennia Pro 10sJ). The exciting laser beam was tuned to 900 nm and the SHG collagen signal was obtained using a 447–453 nm bandpass filter. The TPEF signal was collected in a second channel by tuning the exiting laser beam to 810 nm, using a 460–600 nm bandpass filter. DAPI stained nuclei in hPSCs-CLCs grown on vdECMs were detected in the same channel as elastin. Images were taken using a Leica HCX PL APO CS 40.0 × 1.25-NA oil-immersion objective.

2.17. Strain analysis

Measurements of contractile strain were performed by recording high resolution microscopical movies by using a (EMCCD; Evolve-128: 128 × 128, 24 × 24 µm-square pixels, 16 bit;

Photometrics, Tucson, AZ, USA) mounted in an OLYMPUS Stereo Microscope MVX10 (0.63 × objective). Specifically, 500 frames per second were acquired with a spatial resolution of 39 μm per pixel. Total area covered by the image was 5 × 5 mm. Custom software written in MATLAB was used to measure the deformation of culture due to cardiac cells contraction. Maximal strain capacity was measured as the ratio of elongation in the direction of maximal contraction.

2.18. Optical mapping

Simultaneous voltage and calcium imaging was developed by recording emission light of di-4-ANBDQPPQ (provided by Dr Leslie M. Loew from the Richard D. Berlin Center for Cell Analysis and Modeling, University of Connecticut Health Center, USA) and rhod-2(AM) (Ca²⁺ sensitive probe, TEFLabs, Inc, Austin, TX, USA) respectively. The optical mapping system (Essel Research, Toronto, Canada) consisted in a multiple light-emitting diodes as excitation light sources and a high-speed an electron-multiplying charge-coupled device (EMCCD) camera as recording system [37]. Specifically, in order to excite voltage dye di-4-ANBDQPPQ, cell cultures were illuminated with a filtered red LED light source: LED CBT-90-B (peak power output 53 W; peak wavelength 460 nm; Luminus Devices, Billerica, MA, USA) with a plano-convex lens (LA1951; focal length 0 25.4 mm; Thorlabs, New Jersey, USA) and a red excitation filter (D470/20X (Chroma Technology, Bellows Falls, VT, USA). In order to excite calcium dye rhod-2, cell cultures were illuminated with a filtered green LED light source: LED: CBT-90-G (peak power output 58 W; peak wavelength 524 nm; Luminus Devices, Billerica, USA), with a plano-convex lens (LA1951; focal length = 25.4 mm; Thorlabs, New Jersey, USA) and a green excitation filter (D540/25X; Chroma Technology, Bellows Falls, USA). Two such light sources were used to achieve homogeneous illumination. Fluorescence was recorded with EMCCD camera (Evolve-128; 128 × 128, 24 × 24 μm-square pixels, 16 bit; Photometrics, Tucson, AZ, USA), with a custom multiband-emission filter (ET585/50-800/200 M; Chroma Technology) placed in front of a high-speed camera lens (DO-2595; Navitar Inc., Rochester, USA). Custom software written in MATLAB was used to control the system and to perform optical mapping image processing.

2.19. Optical mapping dye loading

For calcium transient (CaT) imaging, hPSCs-CLCs were stained by immersion in 3 mL of a modified Krebs solution at 36.5 °C (containing, in mM: NaCl, 120; NaHCO₃ 25; CaCl₂ 1.8; KCl 5.4; MgCl₂ 1; glucose 5.5; H₂O₄PNa·H₂O 1.2) with rhod-2 AM dissolved in DMSO (1 mM stock solution; 3.3 μl per ml in culture medium) and Probenecid (TEFLabs, Inc, Austin, TX, USA) at 420 μM for 30 min under incubation conditions. After calcium dye incubation, culture medium was changed to fresh modified Krebs with di-4-ANBDQPPQ voltage dye [38] dissolved in pure ethanol (27.3 mM stock solution, 2 μl per ml in culture medium) and Pluronic F-127 (Life Technologies) was added to a final concentration of 0.2–0.5%. After voltage dye incubation during 5 min, culture medium was changed to fresh Krebs solution at 36.5 °C supplemented with 10 μM blebbistatin. All chemicals were obtained from Sigma-Aldrich (Dorset, UK) or Fisher Scientific Inc. (New Jersey, USA).

2.20. Spinning disk confocal microscopy

Images of beating hPSCs-CLCs monolayers and co-cultures on vdECMs were acquired using a CFI Plan Achromat UW 2× objective in a spinning disk confocal microscope (Andor). hPSCs-CLCs cultures were maintained at 37 °C in RPMI/B27 medium and imaged

every 50 and 100 μm for 20–30 s. Images were exported into ImageJ for processing.

2.21. Statistical analysis

Data are mean ± SD. mRNA expression by qPCR during the time course of cardiac differentiation was analyzed with one-way ANOVA and Bonferroni post-test. Different letters indicate significant difference between groups ($p < 0.05$). When analyzing statistical differences between two different experimental groups (matrigel and vdECMs culture systems) two-tailed student's *t*-test was used. Results were considered statistically significant if the *p*-value was less than *0.05, **0.01 and ***0.001. Statistical analysis were performed using Graph Pad 5.0 and SPSS (v.11).

3. Results

3.1. TALEN-mediated targeting of the MYH6 locus in human embryonic stem cells (hESCs) does not affect pluripotency-associated features

We made use of TALEN technology to target the MYH6 human locus in hESC, namely ES4 line (Fig. S4). Following design and assembly of the *in silico* designed TALEN pairs (Table S1) TALEN endonuclease-associated activity was tested in HEK293 cells prior to genome engineering of ES4 line by means of Surveyor nuclease assay (Fig. S5). We then evaluated the efficiency of the best TALEN pair for producing a knock in reporter allele by targeting the MYH6 human locus using drug selection. The DSB induced in ES4 line was subsequently repaired through homologous recombination (HR) with MYH6 donor vector (Fig. 1A). Thus after clone expansion and antibiotic selection we identified 24 putative mCherry_MYH6 targeted ES4 clones resistant for Neomycin that were subsequently analyzed by PCR screening, identifying a total of 18 out of 24 positively targeted ES4 clones when TALEN pair 1 was used (Fig. S6). Southern blot analysis was performed in 4 out of 18 putative MYH6 targeted clones, revealing that 3 of them contained a MYH6 targeted allele (Fig. S7).

We proceed to characterize one of those clones, namely ES4 TALEN mCherry_MHY6/wt #3 (ES4 mCherry_MYH6), for the expression of nuclear transcription factors as OCT4, NANOG and TRA-1-81 surface marker by immunofluorescence, confirming their pluripotent nature (Fig. 1B). We next explored if gene targeting hampered ES4 mCherry_MYH6 differentiation towards the three germ layers of the embryo and we found that ES4 mCherry_MYH6 line exhibited the capacity to generate cells from ectodermal, mesodermal and endodermal lineages (Fig. 1C). Remarkably, mCherry expression was limited to the cardiac mesodermal lineage and not found in the ectoderm and endoderm germ layers, indicating a proper response of our reporter cell line under differentiation (Fig. 1C). In addition, ES4 mCherry_MYH6 line exhibited the classical ES-associated morphology (Fig. 1D, top panel), and continued to express pluripotent-related markers, including Dppa4, Nanog, Oct4, Rex1, Sox2, Cripto, Dnmt3b, Sall2 and Utf1 (Fig. 1D, bottom panel).

3.2. Chemically defined media sustains cardiac differentiation from hPSCs

To demonstrate that ES4 mCherry_MYH6 line recapitulated MYH6 activity, we established a protocol for the generation of cardiac-like cells (CLCs) from hPSCs (hPSCs-CLCs) grown as monolayers based on a stage specific activation and suppression of the canonical Wnt signaling. Concisely, ES4 mCherry_MYH6 cells were exposed to GSK3B inhibitor (CHIR99021) from day 0 to day 1,

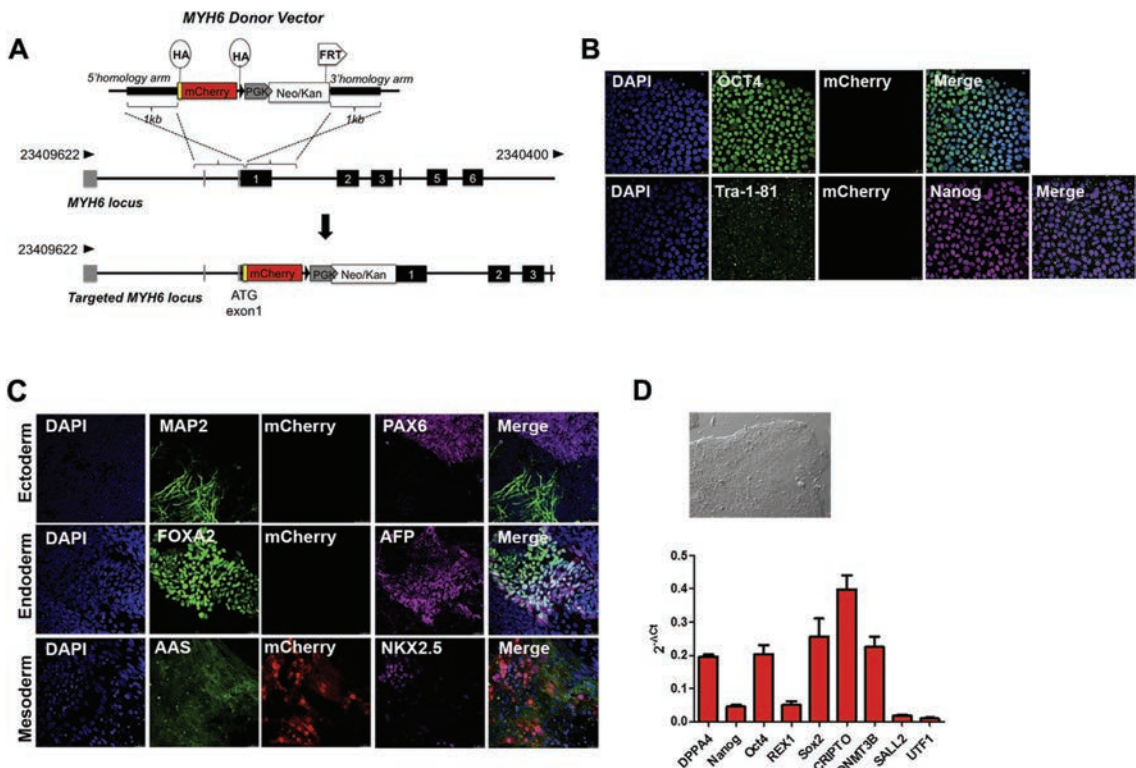


Fig. 1. TALEN engineering in hESCs. **A**, MYH6 donor vector includes a mCherry cassette HA-tagged (HA), a PKG promoter and a neomycin-kanamycin resistant cassette (Neo/Kan); both flanked by FRT sites. Dashed lines indicate the sites of HR in the MYH6 locus. HR results in *knock in* of the complete cassette into the ATG start site of MYH6 locus, generating a mCherry-tagged MYH6 allele. **B** Immunodetection for OCT4, NANOG and TRA-1-81 in ES4 mCherry_MYH6 line, (scale bars, 50 μm). Note mCherry signal was not detected. **C** *In vitro* differentiation of ES4 MYH6_mCherry line into ectoderm [Microtubule-Associated Protein 2 (MAP2) and Paired Box 6 (PAX 6)], endoderm [α -fetoprotein (AFP), Forkhead box protein A2 (FOXA2)], mesoderm [K2 Homeobox 5 (NKX2.5) and α -sarcomeric actinin (ASA)], (scale bars, 25 μm). **D** *Top panel*, representative contrast phase image of an undifferentiated ES4 mCherry_MYH6 clone that grows as a compact and tight adherent colony. *Bottom panel*, qPCR analysis for the evaluation of mRNA expression of pluripotency associated markers after TALEN engineering in ES4 line. Data were represented as mean \pm standard deviation.

followed by Wnt production-4 inhibitor (IWP4) from day 3 to day 5 of differentiation. From day 5, monolayers were kept in RPMI/B27 medium (Fig. 2A). We further explored the expression of mCherry fluorescent reporter during the time course of differentiation and observed that already at day 7 mCherry fluorescent protein was detected by optical microscopy (Fig. 2B left panel). In the same manner mRNA expression analysis by qPCR showed that mCherry mRNA expression mirrored endogenous MYH6 activity, indicating the potential use of our cellular system to properly dissect cardiac differentiation from hPSCs (Fig. 2B right panel). Moreover, flow cytometric analysis showed that mCherry protein expression was present as soon as day 5 during differentiation, and that 14 days after differentiation 90% of the cells expressed mCherry fluorescent protein (Fig. 2C).

We further assessed the profile of mRNA expression during the onset of cardiac differentiation in ES4 mCherry_MYH6 line, and found out that our protocol induced the expression of mRNAs related with early mesoderm and cardiac progenitors up to day 5 during differentiation (PDGFR α , ISL-1, c-KIT). The expression of mRNAs related to cardiac program from day 5 to later stages during differentiation (GATA4, NKX2.5, MYH6, MYL2, NPPA, TNNT2, MYL7) was also analyzed. As expected, the levels of expression for pluripotent-related mRNAs as OCT4, NANOG and SOX2 markedly decreased from day 5 during differentiation (Fig. 3A and Fig. S8). Full beating monolayers were obtained at day 14 of differentiation

(Video S1 and S2). Beating monolayers of ES4 mCherry_MYH6 derived CLCs (mCherry-CLCs) were also characterized by immunofluorescence for the expression of protein markers at day 14 of differentiation, showing that mCherry-CLCs expressed major proteins associated with cardiac structural function: Alpha Sarcomeric Actinin (ASA), Troponin T (TNN), Myosin Heavy Chain (MYH6); and nuclear transcription factors related to cardiac fate [K2 Homeobox 5 (NKX2.5)], together with Connexin 43 (CX43), a protein related to electrical coupling (Fig. 3B, C). In order to investigate the robustness of our protocol we further test our optimized culture conditions in both hESCs (ES4) and transgene-free and feeder-free hiPSCs derived from dermal fibroblasts (FiPS#1). Full beating monolayers were obtained from both ES4 and FiPS#1 lines after 14 days of differentiation (Video S3 and Video S4). In addition, both ES4 (Fig. S9) and FiPS#1 (Fig. S10) expressed cardiac related markers at the different selected time points as shown by qPCR. Similarly, both ES4 and FiPS#1 expressed major proteins associated with cardiac structural function after 14 days of differentiation, confirming that our culture conditions supported the generation of CLCs from different hPSC lines (Fig. S11 and Fig. S12, respectively). Altogether, our protocol sustained the derivation of hPSCs-CLCs monolayers in the presence of chemically defined media, providing a reproducible and efficient method for the generation of hPSCs-CLCs on matrigel coated plates.

Supplementary video related to this article can be found at

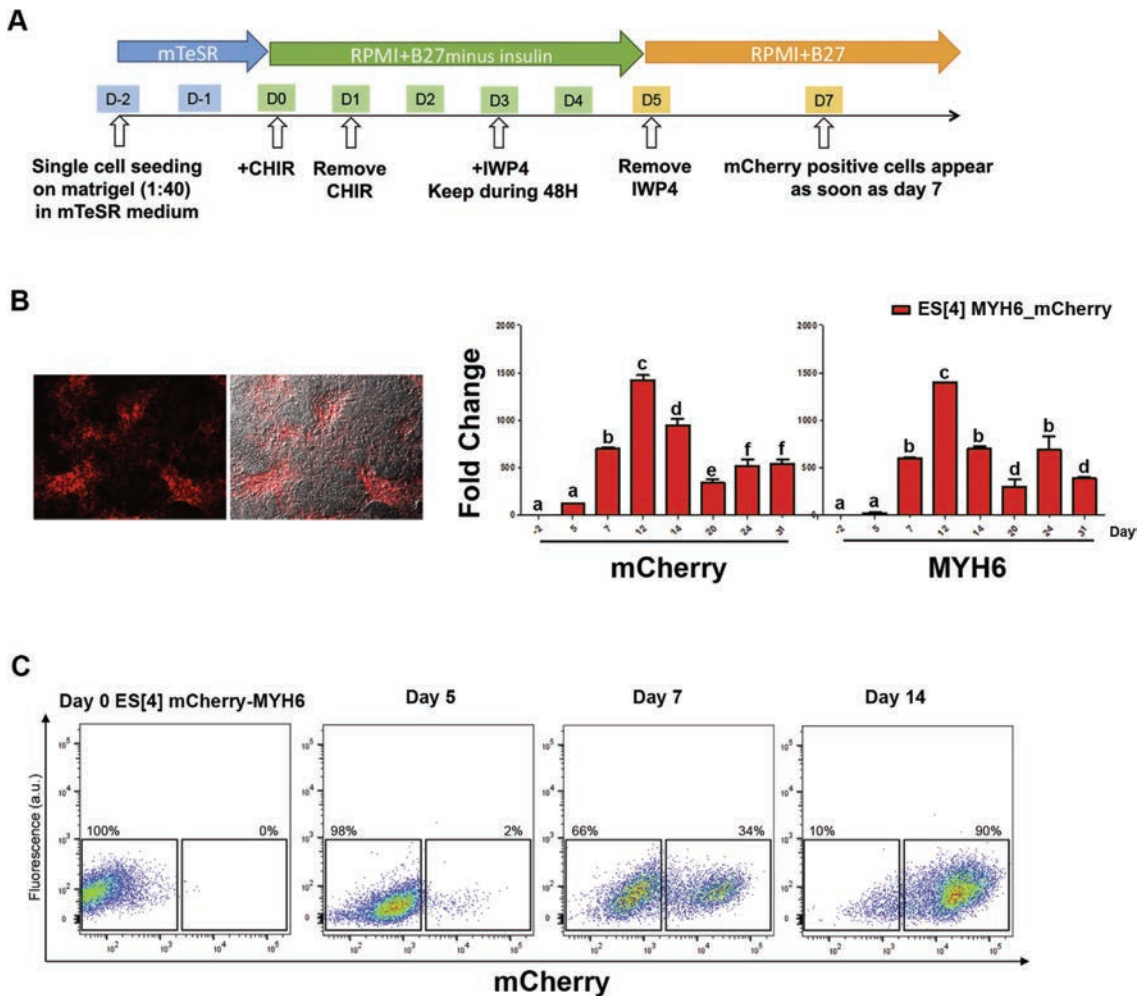


Fig. 2. mCherry targeting in MYH6 locus in ES4 line mirrors MYH6 activity during cardiac differentiation. **A** Time line of human ES4 mCherry_MYH6 cardiac differentiation. **B** *Left panel*, optical microscopy for mCherry detection in ES4 mCherry_MYH6 after 7 days of cardiac differentiation. *Right panel*, evaluation of mRNA expression of mCherry reporter and MYH6 gene by qPCR in ES4 mCherry_MYH6 line during the time course of cardiac differentiation at the indicated days. Data were represented as mean \pm standard deviation. Different letters indicate significant differences between groups ($p < 0.05$). **C** FACS analysis for mCherry fluorescent protein during the time course of cardiac differentiation in ES4 mCherry_MYH6 at the indicated days.

<http://dx.doi.org/10.1016/j.biomaterials.2016.04.003>.

3.3. In vitro recellularization of human ventricular decellularized matrices (vdECMs) with hPSCs-CLCs

Next, we applied our previously published protocol of perfusion decellularization to generate human vdECMs scaffolds that preserved three dimensional architecture and vascular integrity [5]. Following this protocol, we prepared 400 μ m thick vdECMs slices to seed hPSCs-CLCs at day 14 of differentiation in order to explore the effect of human cardiac vdECM on hPSCs-CLCs functional activity and differentiation. Prior to recellularization, immunohistochemistry against proteins from the cellular compartment including muscle specific actin and desmin, as well as basement membrane proteins of the ECM, such as collagen IV, revealed the absence of cellular content and retention of collagen IV in decellularized heart tissue scaffolds (Fig. S13A). In addition, residual DNA content in vdECMs was less than 3% (Fig. S13B), confirming a major removal of

nuclear material. Furthermore, immunofluorescence analysis for laminin, collagen IV and elastin confirmed the preservation of these ECM components in our vdECMs, similarly to those in the native heart (Fig. 4A). Indeed, the presence of a dense fibrillary collagen microstructure was observed on vdECMs by SHG-TPEF microscopy (Fig. 4B). DAPI staining was not visible in vdECMs, indicating again the loss of cellular material (Fig. 4A, B). Overall, our results suggested that our decellularization protocol sufficed for the production of cardiac scaffolds that accomplished the established criteria of decellularization [39].

Next, we set up a protocol for the generation of small heart constructs for cardiac engineering by culturing mCherry-CLCs on vdECMs under our chemically defined conditions for 10 additional days. Thick slices of vdECM supported the engraftment of mCherry-CLCs, which could adhere and cover the scaffold. In this manner, spontaneously beating slices were produced and maintained in culture for 10 days (Fig. 5A). mCherry-CLCs continued to express major proteins associated with cardiac structural function [Alpha

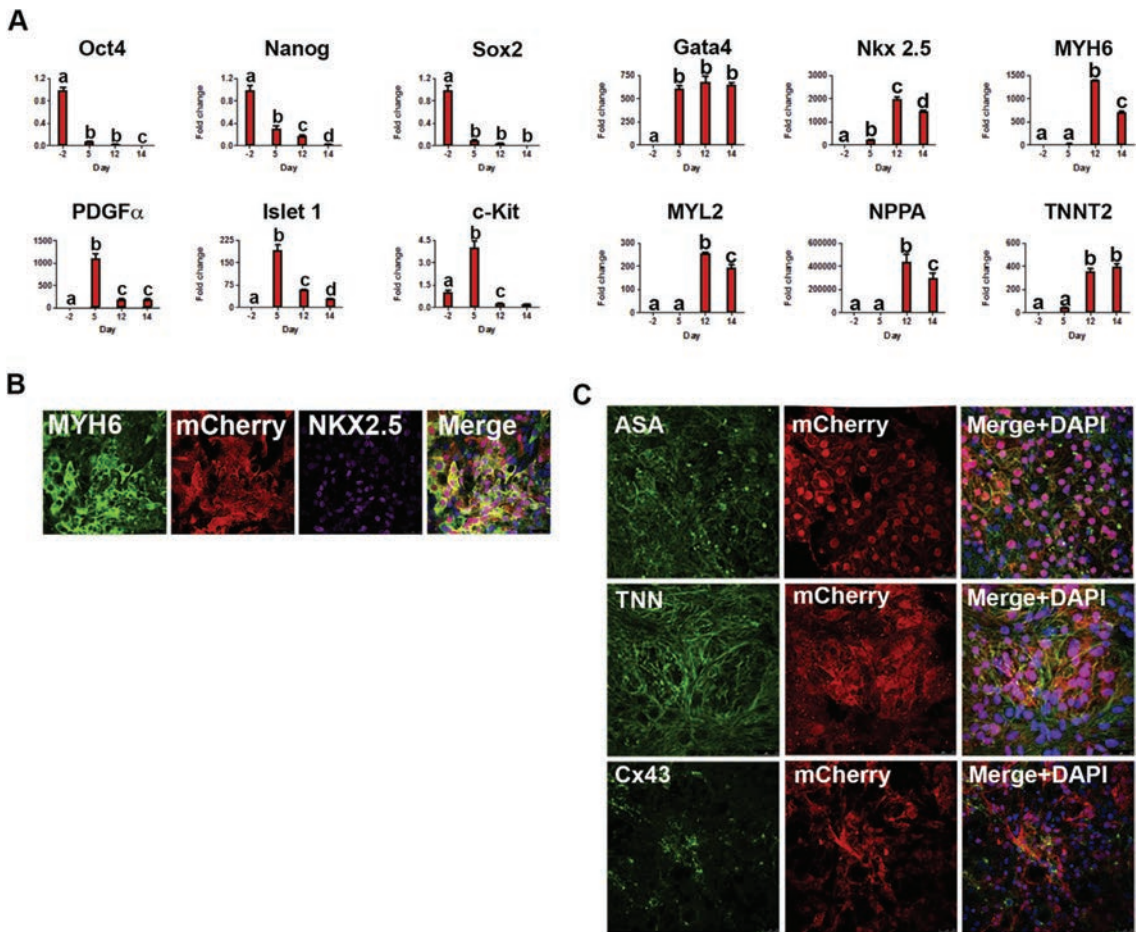


Fig. 3. Generation of CLCs from ES4 mCherry_MYH6 line. **A** mRNA analysis by qPCR analysis for different genes related to cardiac program and pluripotency network at the indicated days ($n = 3$). Data were represented as mean \pm standard deviation. Different letters indicate significant differences between groups ($p < 0.05$). **B** Immunofluorescence analysis for MYH6, NKX2.5, and mCherry in mCherry-CLCs at 14 days of differentiation (scale bars, 25 μm). **C** Immunofluorescence analysis for ASA, Troponin T (TNN), Connexin 43 (CX43) and mCherry in mCherry-CLCs at 14 days of differentiation (scale bars, 25 μm).

Sarcomeric Actinin (ASA), Troponin T (TNN), Myosin Heavy Chain (MYH6), nuclear transcription factors related to cardiac fate [K2 Homeobox 5 (NKX2.5)] and CX43 (Fig. 5B), indicating the maintenance of the cardiac phenotype after 10 days of culture with vdECMs. Interestingly, the generated cardiac grafts showed uniform contraction (Video S5 and Video S6), indicating the presence of cell-cell interconnections as well as cellular interactions with the vdECM. We subsequently transferred the same culture conditions to fabricate cardiac grafts from both ES4 derived CLCs (ES4-CLCs) and FiPS#1 derived CLCs (FiPS#1-CLCs). Cardiac grafts generated from both ES4-CLCs and FiPS#1-CLCs showed similar characteristics in terms of cardiac proteins expression (Fig. 6A and Fig. 6B, respectively) and uniform contraction (Video S7 and Video S8, respectively), confirming the robustness of our method. Moreover, to characterize the mechanical function of the spontaneously beating human cardiac grafts, we determined the contractile strain of hPSCs-CLCs seeded on vdECM by measuring the relative cardiac graft deformation in the direction of maximal tissue contraction. Human cardiac grafts exhibited a 3.78-fold increase in strain compared to hPSCs-CLCs cultured on matrigel ($15.53 \pm 3.33\%$ and $4.21 \pm 0.93\%$, respectively) (Fig. S14; Video S9 and Video S10). These

results are in agreement with previous findings when analyzing myocardial strain in the human heart [40].

Supplementary video related to this article can be found at <http://dx.doi.org/10.1016/j.biomaterials.2016.04.003>.

3.4. Human vdECMs promote a higher degree of differentiation in hPSCs-CLCs when compared to matrigel, as assessed by electrophysiological and molecular analysis

Next, we sought to evaluate if hPSCs-CLCs grown either on vdECMs or matrigel presented electrically and mechanically connected functional activity. Simultaneous recording of voltage and calcium demonstrated the coordinated activity of cardiac structures for all cases, indicating the functional gap junctions' interconnection between hPSCs-CLCs (Fig. 7A, B). Maturation degree was evaluated by comparing the main electrophysiological properties from optical mapping recordings at 1 Hz pacing rate [(i.e. wavefront propagation conduction velocity (CV), mean action potential duration at 90% repolarization (APD90), mean calcium transient duration at 90% return to baseline (CaT90), and Ca $^{2+}$ (Ca) Upstroke Time] (Fig. 7C–F). We observed a dramatic increase in the CV when

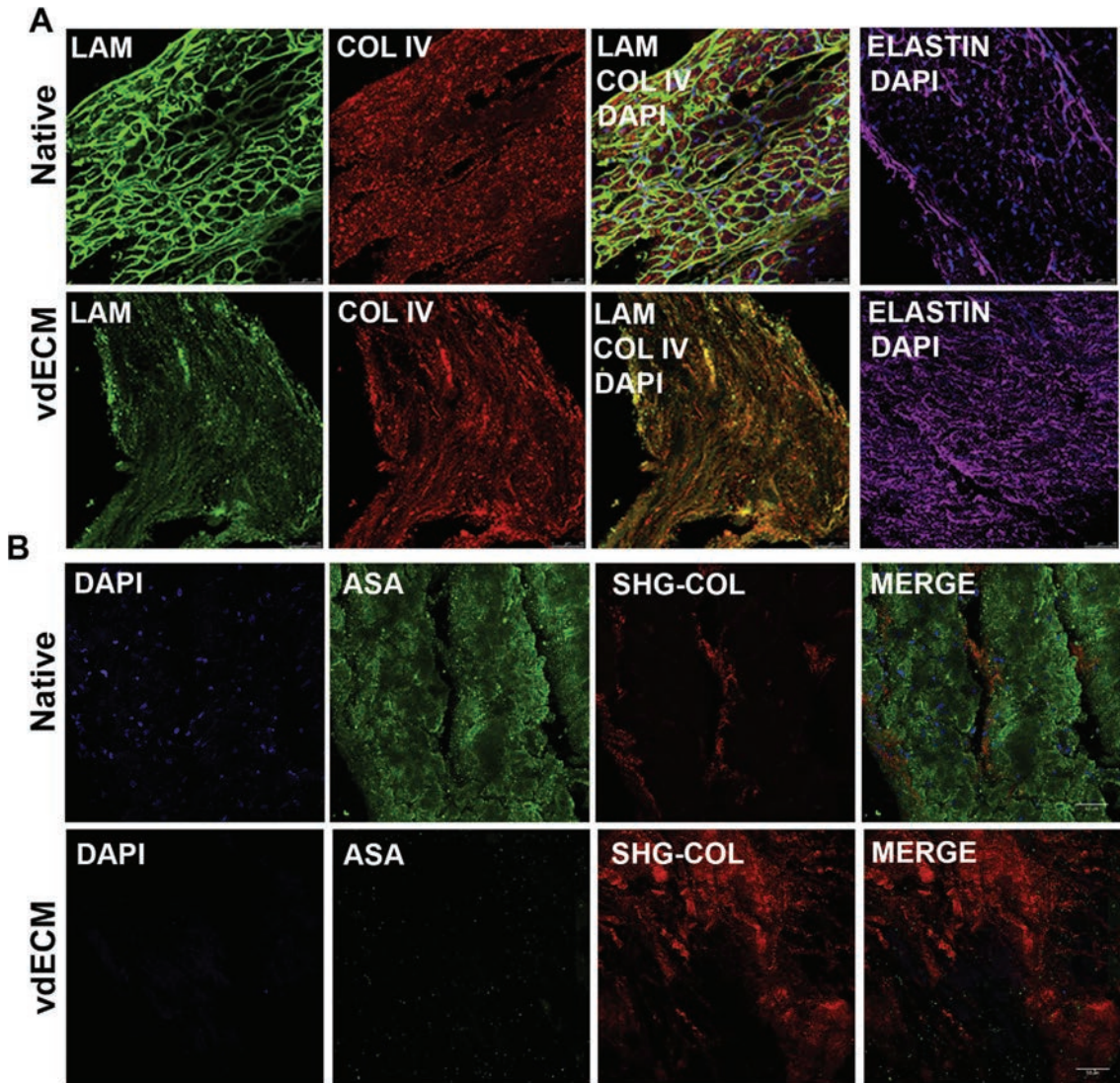


Fig. 4. Characterization of vdECMs composition. **A** Immunofluorescence analysis for LAMININ (LAM), COLLAGEN IV (COL IV), ELASTIN (ELASTIN) and DAPI staining in native human heart (Native) and vdECMs (scale bars, 50 μ m). **B** Native human heart and vdECMs were analyzed by Second harmonic generation (SHG) for the detection of Collagen (SHG-Col) and by immunofluorescence analysis for ASA and DAPI staining (scale bars, 50 μ m).

hESC-CLCs were cultured on top of vdECMs compared to matrigel (7.45 ± 0.94 cm/s versus 2.54 ± 0.75 cm/s) (Fig. 7C). Similar results were observed for FiPS#1-CLCs (8.30 ± 0.49 cm/s versus 2.03 ± 0.18 cm/s, respectively) (Fig. 7C). Increases in CV when hPSCs-CLCs were cultured on vdECMs were related to a higher degree of excitability of sodium current, as 10 μ M flecainide infusion resulted in a more significant reduction of the conduction velocity of hPSCs-CLCs (i.e. $63 \pm 9\%$ versus $44 \pm 11\%$ for hESC-CLCs and $71 \pm 13\%$ versus $41 \pm 5\%$ for FiPS#1-CLCs) (Fig. 7H).

To assess if increases in the CV were also associated with higher contraction capability due to differences in culture substrates, we evaluated the kinetics of calcium as an indicative parameter of hPSCs-CLCs maturation. hPSCs-CLCs cultured on vdECMs showed a reduction in the duration of CaT90 and calcium upstroke time compared to matrigel (Fig. 7E, F). Such variations were not

associated with significant differences in the duration of APD90 (Fig. 7D). Specifically, faster calcium transient increases in hESC-CLCs cultured on vdECMs were associated with a higher degree of maturation of late inward calcium current (I_{CaL}), since 4 μ M verapamil infusion resulted in a more significant reduction of the upstroke velocity of the calcium transient (Fig. 7G).

Moreover, we investigated if such findings could correlate with differences at the level of mRNA expression (Fig. 7I). Increases in the levels of expression of SCN5A mRNA when hPSCs-CLCs were cultured on vdECMs compared to matrigel condition were in agreement with increases in conduction velocities (Fig. 7C, H). Similar results were found for inward rectifier potassium current (KCNJ2). Interestingly, increases in KCNJ2 are associated with lower resting potential in cardiomyocytes, leading to higher conduction velocities [41], as observed in Fig. 7C. So far, acquisition of KCNJ2

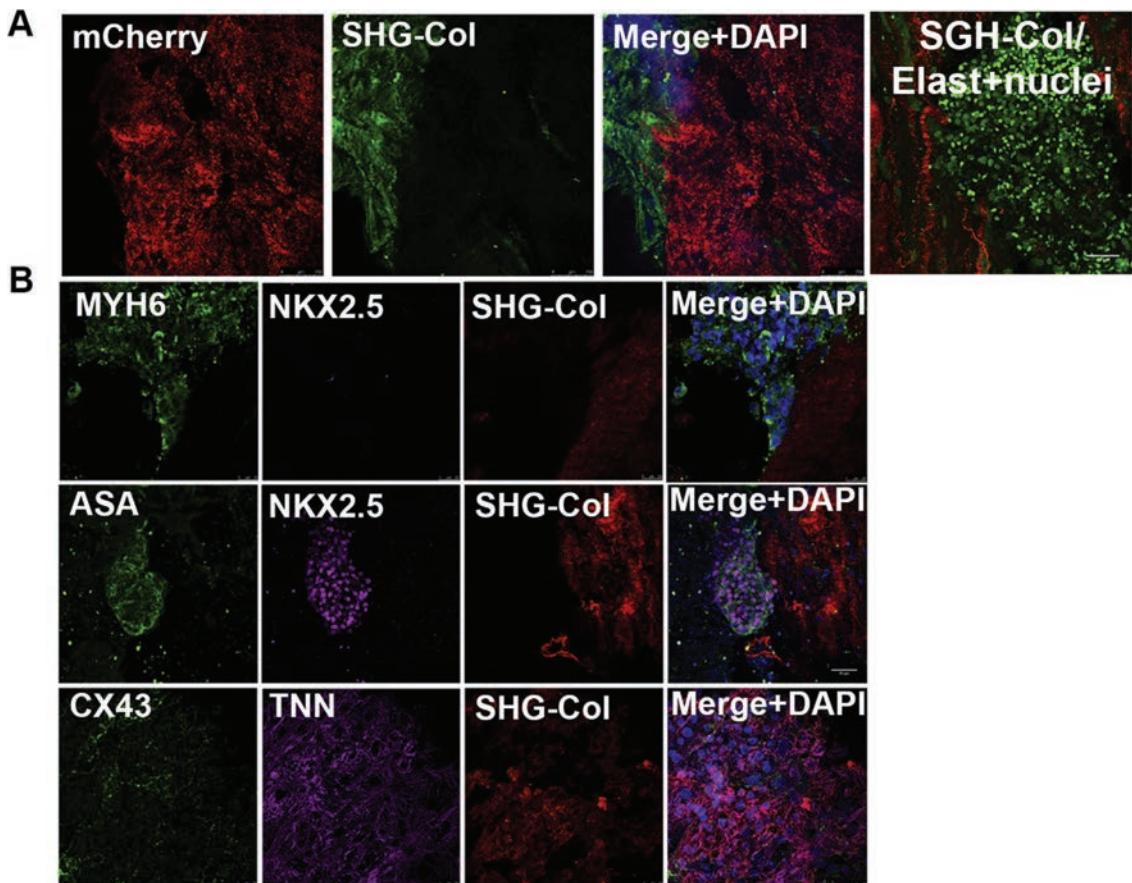


Fig. 5. Cardiac differentiation of ES4 mCherry_MHY6 derived CLCs on vdECMs. **A** Left panels, ES4 mCherry_MHY6 derived CLCs were cultured on top of vdECMs during 10 days and further analyzed for mCherry fluorescence together with the detection of collagen from the underlying vdECM by Second Harmonic Generation (SHG-Col) (scale bars, 250 μ m). Right panel, higher magnification image showing the fibrillary microstructure of collagen from the underlying vdECM and elastin/nuclei by SHG-TPEF (scale bar, 50 μ m). **B** Immunofluorescence analysis for: Top panels, MYH6, Nkx2.5 and detection of collagen by SHG (SHG-Col), (scale bars 25 μ m). Middle panels, ASA, NKX2.5 and SHG-Col (scale bars 50 μ m). Bottom panels, CX43, TNN and SHG-Col (scale bars 25 μ m).

mRNA expression has been predicted as a limiting step for CLCs production from hPSCs [41], indicating that under our defined conditions, vdECMs may play a role in the expression of this current. Similarly, increases in the levels of expression of KCNA4 mRNA in hPSCs-CLCs suggested that vdECM, rather than matrigel, may represent a more physiological microenvironment for the proper differentiation of hPSCs-CLCs.

In order to ascertain the effect of the different substrates on intracellular calcium homeostasis, mRNA expression levels of the CACNA1C subunit from the L-type calcium channel current, and sarco/endoplasmic reticulum Ca²⁺ ATPase (SERCA) pump were investigated. Interestingly, hPSCs-CLCs co-cultured on vdECMs compared to matrigel, exhibited higher levels of expression of CACNA1C and SERCA mRNAs [42], which correlated with increases in calcium upstroke (Fig. 7F, G). mRNA levels of the KCNH2 unit of the rapidly (I_{Kr}) activating delayed rectifier potassium channel and KCNQ1/2 [(two members of the potassium voltage-gated channel subfamily Q of the slowly (I_{Ks}) activating delayed rectifier potassium channels)] were differentially regulated when hPSCs-CLCs were cultured on matrigel or vdECMs conditions. These findings may explain the similar duration of action potentials observed (Fig. 7D). Altogether, our results suggest a pivotal role of vdECMs in

providing a suitable microenvironment for the *in vitro* generation of hPSC-derived cardiac grafts.

4. Discussion

In humans, the existence of scar tissue following myocardial infarction indicates that the ability to generate new cardiomyocytes after pathological conditions is completely absent. Given that heart disease is the most significant cause of morbidity and mortality worldwide, the possibility to replace fibroblastic-like scar has been one the major goals in the cardiac field in the last years. So far, different cell therapy approaches have been proposed: from the use of allogenic cell sources alone or in combination with biomimetic materials to the possibility to reprogram *in situ* cardiac fibroblasts. In an attempt to provide novel platforms for heart regeneration, heart engineering has been envisioned as a promising approach for the generation of donor grafts. Recently, the generation of acellular matrices from different organs by decellularization has emerged as an encouraging technology to produce tissue scaffolds that retain the main properties of the organ ECM [7,8]. Within the last years, different groups, including us, have faced major problems when developing efficient protocols for heart decellularization. In this

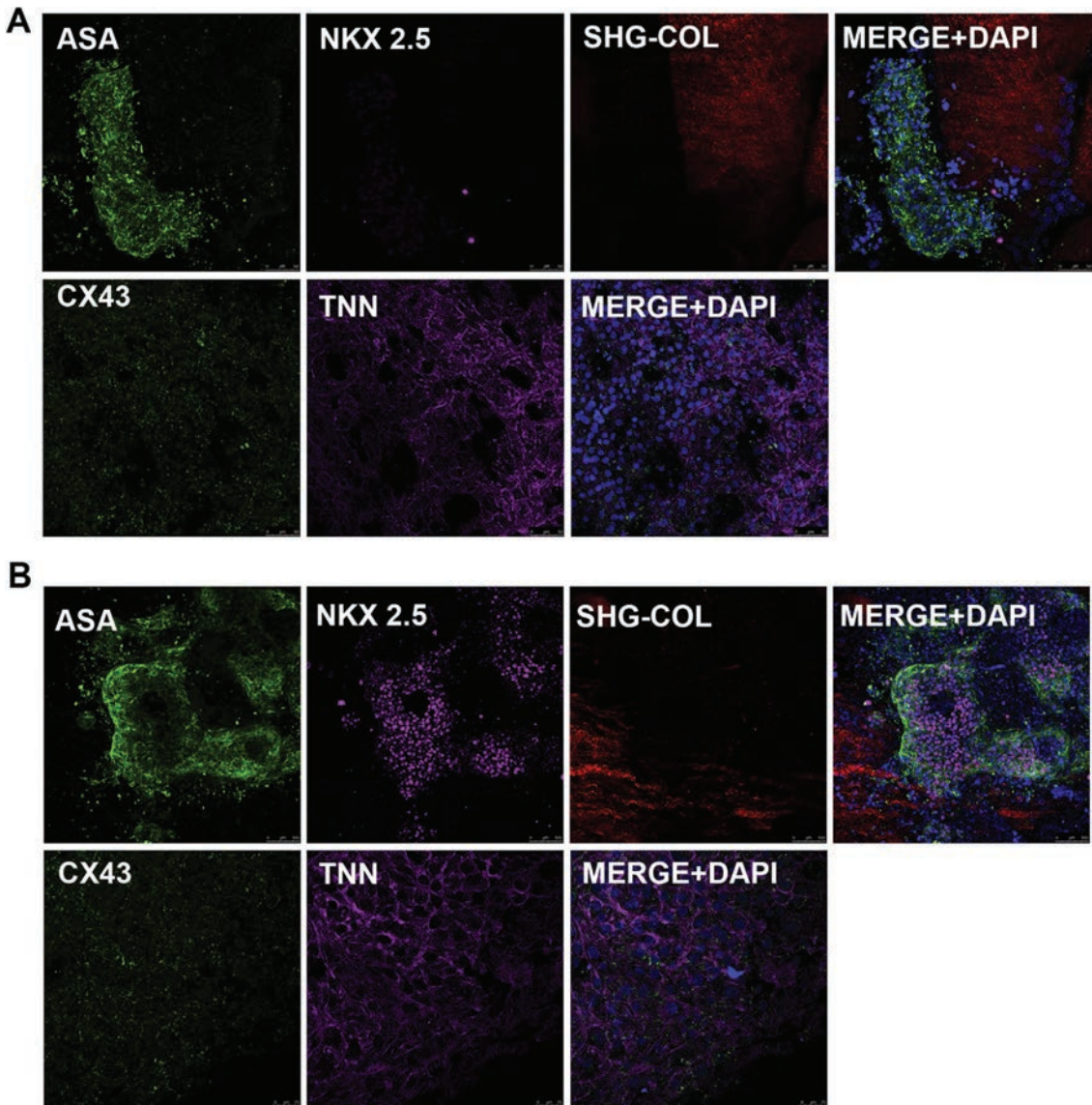


Fig. 6. Cardiac differentiation of hESC- and hiPSC- CLCs on vdECMs. **A** ES4-CLCs and **B** FiPS#1-CLCs were seeded on top of vdECMs during 10 days and further analyzed by immunofluorescence analysis for ASA and NKX2.5 (top panels in A and B), and CX43 and TNN (bottom panels in A and B) together with the detection of collagen by SHG (SHG-Col). Scale bars in A, 50 μ m. Scale bars in B, 100 μ m (top panels) and 25 μ m (bottom panels).

regard, we have recently described that is possible to apply perfusion decellularization in human hearts, leading to a structurally intact decellularized extracellular matrix (dECM) preserving ultra- and macro-structures together with mechanical properties [5].

Besides the definition of suitable strategies for organ engineering, the choice of cell type for cardiac recellularization limits further applications in clinics. Lately hPSCs, such as hESCs and hiPSCs, have been heralded as major cell sources for regenerative applications, including heart engineering. hPSCs exhibit the capability to differentiate under the appropriated stimuli to cells from the three germ layers of the embryo, both *in vitro* and *in vivo*. These capabilities offer great advantages when trying to develop autologous cells for

transplantation. However, protocols for cardiac differentiation of hPSCs are frequently based on the formation of EBs, hampering the reproducibility and scale up of such procedures in clinics [3,12,13]. Lately, we have demonstrated that is possible to induce cardiac differentiation from hPSCs grown as monolayers, making use of chemically defined media [16]. Although valuable, those protocols still cannot provide definitive information on the identity of the generated cells [14,16]. In this regard, the generation of cardiac hPSCs reporter cell lines can help to the identification and purification of different cardiac cell types during the onset of differentiation (i.e: cardiac mesoderm precursors, cardiac progenitor cells, mature cardiomyocytes, among others), and importantly, to develop efficient and robust protocols to generate the required

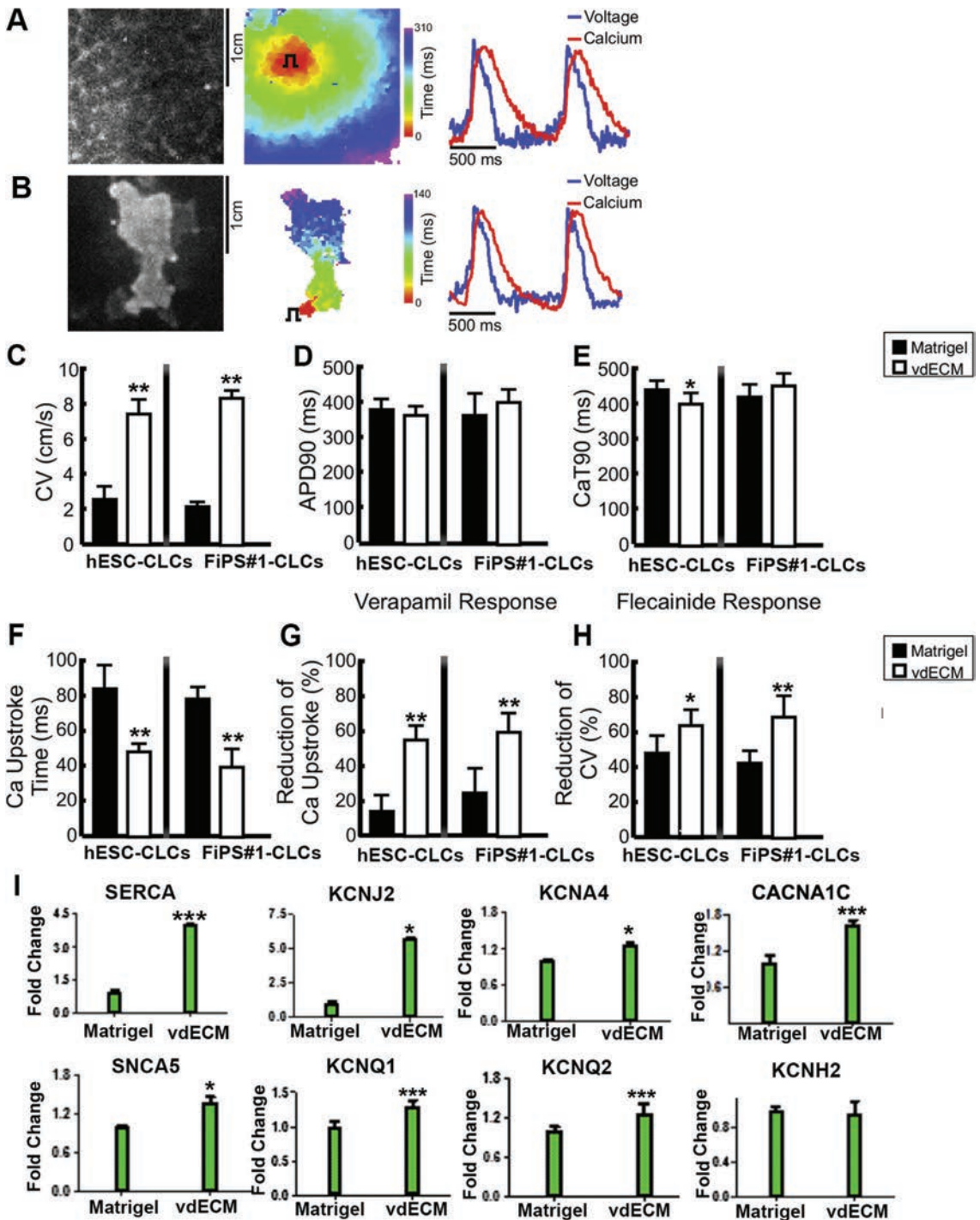


Fig. 7. Simultaneous optical mapping of transmembrane voltage and intracellular transient calcium of cardiac structures from hPSCs grown on vdECMs and matrigel. A, B Simultaneous optical mapping of transmembrane voltage and intracellular transient calcium of hPSCs-CLCs on matrigel (A) and vdECMs (B). Grayscale images of normalized fluorescence intensity map. Middle panel illustrate the propagation of transmembrane voltage. Right panels represent transmembrane voltage (blue) and calcium transient (red) traces of representative recorded pixels. C–F. Electrophysiological properties of hESC-CLCs and FiPS#1-CLCs grown on matrigel and vdECMs: C wavefront propagation conduction velocity, D action potential duration (APD90), E calcium transient duration (CaT90) and F Calcium (Ca) upstroke time measured on hESC-CLCs and FiPS#1-CLCs grown on matrigel and vdECMs. G Effect of verapamil on reduction of Ca upstroke time. H Effect of flecainide on reduction of conduction velocity. I mRNA analysis by qPCR for the indicated markers (n = 3) (*p < 0.05; **p < 0.01, ***p < 0.001).

amount of cardiac cells needed in the clinical setting.

Recent genome editing technologies including CRISPR/Cas9 and TALEN platforms have demonstrated to target unique and multiple human loci in site-specific manner. Interestingly, recent works have investigated the impact of genome editing platforms in the incidence of off-target mutations. In this regard it has been shown that off-target mutations attributable to the nucleases were rarely exhibited in CRISPR-Cas9 and TALEN targeted hPSCs clones [43]. We have also recently interrogated by whole-genome sequencing the mutational load in individual gene-corrected hiPSC clones at single-base resolution, showing that gene correction by helper-dependent adenoviral vector (HDAdV) or TALEN exhibited few off-target effects and a low level of sequence variation [44]. Importantly, others have described the generation of a high-fidelity Cas9 variant (named SpCas9-HF1) designed to reduce non-specific DNA interactions, showing no detectable genome-wide off-target effects [45].

Here we decided to take advantage of TALEN platform to target MYH6 locus with mCherry fluorescent reporter in order to generate a reporter cell line mirroring MYH6 endogenous activity during the onset of cardiac differentiation. In the present work, we have derived three different mCherry MYH6 reporter hESC lines that serve as an unprecedented scenario for the definition of a chemically defined protocol for cardiac differentiation of hPSCs. In our hands, gene targeting and subsequent cell culture pressure did not hamper ES4 mCherry_MYH6 line to exhibit typical pluripotent-related features, as described by others when targeting other human locus by means of this approach [24,29,46–48]. Following our cardiac differentiation protocol, CLCs expressing mCherry fluorescent protein were generated in only 7 days, mirroring MYH6 endogenous expression. Moreover, we could successfully apply the same cardiac differentiation strategy to hPSCs lines, demonstrating the suitability of our protocol for the generation of CLCs from monolayer cultures of different hPSCs lines. In our hands, TALEN engineering allowed not only to generate for the first time a hESCs cardiac reporter cell line by means of this genome editing platform, but also, to define a robust protocol of cardiac differentiation from hPSCs.

Important cell functions such as proliferation and differentiation can be modulated by the biochemical and biophysical properties of their microenvironment [49–51]. Mechanical cues from the ECM including rigidity, microstructure and 3D architecture have shown to exert changes in intracellular cell signaling cascades and subsequently drive cell fate [52–54]. Elegant studies have previously shown the benefits when using murine cardiac ECM in promoting cardiac differentiation from hPSCs [9,11]. Also, others have recently demonstrated that engineered heart slices from pig and rat represented a suitable platform for the culture of neonatal rat ventricular cardiomyocytes, behaving as an integrated and functional tissue-like constructs [10]. Understanding cellular interactions of CLCs with the ECM of human origin can have important implications in the development of functional tissue engineered grafts from hPSCs. Here, we show that hPSCs-CLCs co-cultured on human vECMs for 10 days displayed better electrophysiological responses compared to matrigel, which is mostly used to produce high yields of cardiomyocytes from hPSCs. Importantly, our findings were together in agreement with increases in the expression of different cardiac channels such as SNCA5, KCNJ2, KCNA4, CACNA1C, SERCA2, KCNQ1, and KCNQ2, pinpointing a pivotal role of human cardiac ECM as an inducer of cardiac-related electrophysiological features.

5. Conclusions

Decellularization of a whole heart can lead to hundreds of acellular slices ready to use as scaffolds for the approach described

here. The present protocol allows for the generation of cardiac grafts showing enhanced electrophysiological properties in a relatively short time period (24 days), avoiding time consuming co-culture techniques (i.e: bioreactor, perfusion system, among others), and anticipating that such procedure can be immediately applied in laboratories with special focus in heart bioengineering and cardiac disease modeling.

Disclosures

None.

Sources of funding

E.G was partially supported by La Fundació Privada La Marató de TV3, 121430/31/32 and Spanish Ministry of Economy and Competitiveness-MINECO (SAF2014-59778). LO was supported by grants from Spanish Ministry of Economy and Competitiveness-MINECO (BFU2009-13513 and SAF2014-59778) and by La Fundació Privada La Marató de TV3 (121430/31/32). M.E.F, A.C and F.F.A from Instituto de Salud Carlos III-ISCII (MINECO: PI10-00141 and PI10-02038), Red de Investigación Cardiovascular (RIC) and Red TerCel from ISCII (Ministry of Economy and Competitiveness, Spain) and CAM: S2010/BMD-2420. R.O was founded by Secretaria d'Universitats i Recerca del Departament d'Economia i Coneixement de la Generalitat de Catalunya. E.M and M.V by 2014 SGR 1442. J.C.I.B. was supported by grants from the G. Harold and Leila Y. Mathers Charitable Foundation, The Leona M. and Harry B. Helmsley Charitable Trust (2012-PG-MED002) and The Moxie Foundation. N.M was partially supported by StG-2014-640525_REGMAMKID, La Fundació Privada La Marató de TV3 (121430/31/32), MINECO (SAF2014-59778 and BFU2009-13513), the Spanish Ministry of Science and Innovation (PLE 2009-147) and 2014 SGR 1442.

Acknowledgments

Authors gratefully acknowledge the help of M. Schwarz, P. Schwarz, and Ana Fernández Baza for administrative help and logistic coordination. TALEN Backbone was a gift from Feng Zhang. We also thank all the medical, nursing staff, and personnel in the Hospital General Universitario Gregorio Marañón, the University of Minnesota, the Texas Heart Institute, and the ONT who made the study possible. Most of all, we thank all the relatives of each donor patient for donating specifically the hearts to be used for this investigational purpose; without their help and support science would never advance.

Appendix A. Supplementary data

Supplementary data related to this article can be found at <http://dx.doi.org/10.1016/j.biomaterials.2016.04.003>.

References

- [1] J.A. Thomson, Embryonic stem cell lines derived from human blastocysts, *Sci.* (80-) 282 (1998) 1145–1147, <http://dx.doi.org/10.1126/science.282.5391.1145>.
- [2] K. Takahashi, K. Tanabe, M. Ohnuki, M. Narita, T. Ichisaka, K. Tomoda, et al., Induction of pluripotent stem cells from adult human fibroblasts by defined factors, *Cell* 131 (2007) 861–872, <http://dx.doi.org/10.1016/j.cell.2007.11.019>.
- [3] C.L. Mummery, J. Zhang, E.S. Ng, D.A. Elliott, A.G. Elefanty, T.J. Kamp, Differentiation of human embryonic stem cells and induced pluripotent stem cells to cardiomyocytes: a methods overview, *Circ. Res.* 111 (2012) 344–358, <http://dx.doi.org/10.1161/CIRCRESAHA.110.227512>.
- [4] J.P. Guyette, J. Charest, R.W. Mills, B. Jank, P.T. Moser, S.E. Gilpin, J.R. Gershlag, T. Okando, T. Okamoto, G. Gonzalez, D.J. Milan, G.R. Gaudette, H.C. Ott, Bioengineering human myocardium on native extracellular matrix, *Circ. Res.* 118 (2016) 56–72.

- [5] P.L. Sánchez, M.E. Fernández-Santos, S. Costanza, A.M. Climent, I. Moscoso, M.A. Gonzalez-Nicolas, et al., Acellular human heart matrix: a critical step toward whole heart grafts, *Biomaterials* 61 (2015) 279–289, <http://dx.doi.org/10.1016/j.biomaterials.2015.04.056>.
- [6] H.C. Ott, T.S. Matthiesen, S.-K. Goh, L.D. Black, S.M. Kren, T.I. Netoff, et al., Perfusion-decellularized matrix: using nature's platform to engineer a bio-artificial heart, *Nat. Med.* 14 (2008) 213–221, <http://dx.doi.org/10.1038/nm1684>.
- [7] D. Rana, H. Zreiqat, N. Benkirane-Jessel, S. Ramakrishna, M. Ramalingam, Development of decellularized scaffolds for stem cell-driven tissue engineering, *J. Tissue Eng. Regen. Med.* (2015), <http://dx.doi.org/10.1002/term.2061>.
- [8] L.F. Tapias, H.C. Ott, Decellularized scaffolds as a platform for bioengineered organs, *Curr. Opin. Organ Transpl.* 19 (2014) 145–152, <http://dx.doi.org/10.1097/MOT.0000000000000051>.
- [9] S.L.J. Ng, K. Narayanan, S. Gao, A.C.A. Wan, Lineage restricted progenitors for the repopulation of decellularized heart, *Biomaterials* 32 (2011) 7571–7580, <http://dx.doi.org/10.1016/j.biomaterials.2011.06.065>.
- [10] A. Blazeski, G.M. Kostecki, L. Tung, Engineered heart slices for electrophysiological and contractile studies, *Biomaterials* 55 (2015) 119–128, <http://dx.doi.org/10.1016/j.biomaterials.2015.03.026>.
- [11] T.Y. Lu, B. Lin, J. Kim, M. Sullivan, K. Tobita, G. Salama, et al., Repopulation of decellularized mouse heart with human induced pluripotent stem cell-derived cardiovascular progenitor cells, *Nat. Commun.* 4 (2013) 2307, <http://dx.doi.org/10.1038/ncomms3307>.
- [12] N. Cao, Z. Liu, Z. Chen, J. Wang, T. Chen, X. Zhao, Y. Ma, L. Qin, J. Kang, B. Wei, L. Wang, Y. Jin, H.T. Yang, Ascorbic acid enhances the cardiac differentiation of induced pluripotent stem cells through promoting the proliferation of cardiac progenitor cells, *Cell Res.* 22 (2011) 219–236.
- [13] R.P. Davis, S. Casini, C.W. Van Den Berg, M. Hoekstra, C.A. Remme, C. Dambrot, et al., Cardiomyocytes derived from pluripotent stem cells recapitulate electrophysiological characteristics of an overlap syndrome of cardiac sodium channel disease, *Circulation* 125 (2012) 3079–3091, <http://dx.doi.org/10.1161/CIRCULATIONAHA.111.066092>.
- [14] X. Lian, C. Hsiao, G. Wilson, K. Zhu, L.B. Hazeltime, S.M. Azarin, et al., Robust cardiomyocyte differentiation from human pluripotent stem cells via temporal modulation of canonical Wnt signaling, *Proc. Natl. Acad. Sci. U. S. A.* 109 (2012) E1848–E1857, <http://dx.doi.org/10.1073/pnas.1200250109>.
- [15] X. Lian, J. Zhang, S.M. Azarin, K. Zhu, L.B. Hazeltime, X. Bao, et al., Directed cardiomyocyte differentiation from human pluripotent stem cells by modulating Wnt/ β -catenin signaling under fully defined conditions, *Nat. Protoc.* 8 (2013) 162–175, <http://dx.doi.org/10.1038/nprot.2012.150>.
- [16] Y. Gu, G.-H. Liu, N. Plongthongkum, C. Benner, F. Yi, J. Qu, et al., Global DNA methylation and transcriptional analyses of human ESC-derived cardiomyocytes, *Protein Cell* 5 (2014) 59–68, <http://dx.doi.org/10.1007/s12328-013-0016-x>.
- [17] J. Zhang, M. Klos, G.F. Wilson, A.M. Herman, X. Lian, K.K. Raval, et al., Extracellular matrix promotes highly efficient cardiac differentiation of human pluripotent stem cells: the matrix sandwich method, *Circ. Res.* 111 (2012) 1125–1136, <http://dx.doi.org/10.1161/CIRCRESAHA.112.273144>.
- [18] D.A. Elliott, S.R. Braam, K. Koutsis, E.S. Ng, R. Jenny, E.L. Lagerqvist, et al., NKX2-5-eGFP/w hESCs for isolation of human cardiac progenitors and cardiomyocytes, *Nat. Methods* 8 (2011) 1037–1040, <http://dx.doi.org/10.1038/nmeth.1740>.
- [19] S.C. Den Hartogh, C. Schreurs, J.J. Monshouwer-Kloots, R.P. Davis, D.A. Elliott, C.L. Mummery, et al., Dual reporter MESP1 mCherry/w-NKX2-5 eGFP/w hESCs enable studying early human cardiac differentiation, *Stem Cells* 33 (2015) 56–67, <http://dx.doi.org/10.1002/stem.1842>.
- [20] T.I. Orbán, A. Apáti, A. Németh, N. Varga, V. Krizsik, A. Schamberger, K. Szébenyi, Z. Erdei, G. Várady, E. Karászi, L. Homolya, K. Németh, E. Göcza, C. Miskey, L. Mátés, Z. Ivics, Z. Izsóvá, B. Sarkadi, Applying a “double-feature” promoter to identify cardiomyocytes differentiated from human embryonic stem cells following transposon-based gene delivery, *Stem Cells* 27 (2009) 1077–1087.
- [21] K. Szébenyi, A. Pentek, Z. Erdei, G. Várady, T.I. Orbán, B. Sarkadi, et al., Efficient generation of human embryonic stem cell-derived cardiac progenitors based on tissue-specific enhanced green fluorescence protein expression, *Tissue Eng. Part C Methods* 21 (2015) 35–45, <http://dx.doi.org/10.1089/ten.TEC.2013.0646>.
- [22] M. Ieda, J.D. Fu, P. Delgado-Olguin, V. Vedantham, Y. Hayashi, B.G. Bruneau, et al., Direct reprogramming of fibroblasts into functional cardiomyocytes by defined factors, *Cell* 142 (2010) 375–386, <http://dx.doi.org/10.1016/j.cell.2010.07.002>.
- [23] T.W. Gilbert, J.M. Freund, S.F. Badyal, Quantification of DNA in biologic scaffold materials, *J. Surg. Res.* 152 (2009) 135–139, <http://dx.doi.org/10.1016/j.jss.2008.02.013>.
- [24] N.E. Sanjana, L. Cong, Y. Zhou, M.M. Cunniff, G. Feng, F. Zhang, A transcription activator-like effector toolbox for genome engineering, *Nat. Protoc.* 7 (2012) 171–192, <http://dx.doi.org/10.1038/nprot.2011.431>.
- [25] J.C. Miller, S. Tan, G. Qiao, K.A. Barlow, J. Wang, D.F. Xia, et al., A TALE nuclease architecture for efficient genome editing, *Nat. Biotechnol.* 29 (2011) 143–148, <http://dx.doi.org/10.1038/nbt.1755>.
- [26] C. Engler, R. Gruetzner, R. Kandzia, S. Marillonnet, Golden gate shuffling: a one-pot DNA shuffling method based on type IIIs restriction enzymes, *PLoS One* 4 (2009) e5553, <http://dx.doi.org/10.1371/journal.pone.0005553>.
- [27] E. Weber, C. Engler, R. Gruetzner, S. Werner, S. Marillonnet, A modular cloning system for standardized assembly of multigene constructs, *PLoS One* 6 (2011) 38–43, <http://dx.doi.org/10.4161/bug.3.1.18223>.
- [28] E.L. Doyle, N.J. Booher, D.S. Standage, D.F. Voytas, V.P. Brendel, J.K. Vandyk, et al., TAL Effector-Nucleotide Targeter (TALEN-T) 2.0: tools for TAL effector design and target prediction, *Nucleic Acids Res.* 40 (2012) 117–122, <http://dx.doi.org/10.1093/nar/gks608>.
- [29] D. Hockemeyer, H. Wang, S. Kiani, C.S. Lai, Q. Gao, P. John, et al., Genetic engineering of human ES and iPS cells using TALE nucleases, *Nat. Biotechnol.* 29 (2012) 731–734, <http://dx.doi.org/10.1038/nbt.1927.Genetic>.
- [30] J. Courchet, T.L. Lewis, S. Lee, V. Courchet, D.Y. Liou, S. Aizawa, et al., XTerminal axon branching is regulated by the LKB1-NUAK1 kinase pathway via presynaptic mitochondrial capture, *Cell* 153 (2013) 1510–1525, <http://dx.doi.org/10.1016/j.cell.2013.05.021>.
- [31] G.-H. Liu, K. Suzuki, M. Li, J. Qu, N. Montserrat, C. Tarantino, et al., Modelling Fanconi anemia pathogenesis and therapeutics using integration-free patient-derived iPSCs, *Nat. Commun.* 5 (2014) 4330, <http://dx.doi.org/10.1038/ncomms5330>.
- [32] K. Okita, Y. Matsumura, Y. Sato, A. Okada, A. Morizane, S. Okamoto, et al., A more efficient method to generate integration-free human iPS cells, *Nat. Methods* 8 (2011) 409–412, <http://dx.doi.org/10.1038/nmeth.1591>.
- [33] T. Aasen, A. Raya, M.J. Barrero, E. Garreta, A. Consiglio, F. Gonzalez, et al., Efficient and rapid generation of induced pluripotent stem cells from human keratinocytes, *Nat. Biotechnol.* 26 (2008) 1276–1284, <http://dx.doi.org/10.1038/nbt.1503>.
- [34] M.A. Wallenburg, J. Wu, R.-K. Li, I.A. Vitkin, Two-photon microscopy of healthy, infarcted and stem-cell treated regenerating heart, *J. Biophot.* 4 (2011) 297–304, <http://dx.doi.org/10.1002/jbio.201000059>.
- [35] N. Merna, C. Robertson, A. La, S.C. George, Optical imaging predicts mechanical properties during decellularization of cardiac tissue, *Tissue Eng. Part C Methods* 19 (2013) 802–809, <http://dx.doi.org/10.1089/ten.TEC.2012.0720>.
- [36] E. Melo, E. Garreta, T. Luque, J. Cortiella, J. Nichols, D. Navajas, et al., Effects of the decellularization method on the local stiffness of acellular lungs, *Tissue Eng. Part C Methods* 20 (2014) 412–422, <http://dx.doi.org/10.1089/ten.TEC.2013.0325>.
- [37] P. Lee, M. Klos, C. Bollensdorff, L. Hou, P. Ewart, T.J. Kamp, et al., Simultaneous voltage and calcium mapping of genetically purified human induced pluripotent stem cell-derived cardiac myocyte monolayers, *Circ. Res.* 110 (2012) 1556–1563, <http://dx.doi.org/10.1161/CIRCRESAHA.111.262535>.
- [38] P. Lee, F. Taghavi, P. Yan, P. Ewart, E.A. Ashley, L.M. Loew, et al., In situ optical mapping of voltage and calcium in the heart, *PLoS One* 7 (2012) e42562, <http://dx.doi.org/10.1371/journal.pone.0042562>.
- [39] P.M. Crapo, T.W. Gilbert, S.F. Badyal, An overview of tissue and whole organ decellularization processes, *Biomaterials* 32 (2011) 3233–3243, <http://dx.doi.org/10.1016/j.biomaterials.2011.01.057>.
- [40] J. Garot, D.A. Bluemke, N.F. Osman, C.E. Rochitte, E.R. McVeigh, E.A. Zerhouni, et al., Fast determination of regional myocardial strain fields from tagged cardiac images using harmonic phase MRI, *Circulation* 101 (2000) 981–988, <http://dx.doi.org/10.1161/01.CIR.101.9.981>.
- [41] M. Hoekstra, C.L. Mummery, A.A.M. Wilde, C.R. Bezzina, A.O. Verkerk, Induced pluripotent stem cell derived cardiomyocytes as models for cardiac arrhythmias, *Front. Physiol.* 3 AUG (2012) 1–14, <http://dx.doi.org/10.3389/fphys.2012.00346>.
- [42] D.M. Bers, Calcium fluxes involved in control of cardiac myocyte contraction, *Circ. Res.* 87 (2000) 275–281.
- [43] A. Veres, B.S. Gosis, Q. Ding, R. Collins, A. Ragavendran, H. Brand, S. Erdin, A. Cowan, M.E. Talkowski, K. Musunuru, Low incidence of off-target mutations in individual CRISPR-Cas9 and TALEN targeted human stem cell clones detected by whole-genome sequencing, *Cell Stem Cell* 15 (2014) 27–30.
- [44] K. Suzuki, C. Yu, J. Qu, M. Li, X. Yao, T. Yuan, et al., Targeted gene correction minimally impacts whole-genome mutational load in human-disease-specific induced pluripotent stem cell clones, *Cell Stem Cell* 15 (2014) 31–36, <http://dx.doi.org/10.1016/j.stem.2014.06.016>.
- [45] B.P. Kleinstiver, V. Pattanayak, M.S. Prew, S.Q. Tsai, N.T. Nguyen, Z. Zheng, et al., High-fidelity CRISPR–Cas9 nucleases with no detectable genome-wide off-target effects, *Nature* (2016), <http://dx.doi.org/10.1038/nature16526>.
- [46] N.A. Krentz, C. Nian, F. Lynn, TALEN/CRISPR-mediated eGFP knock-in add-on at the OCT4 locus does not impact differentiation of human embryonic stem cells towards endoderm, *PLoS One* 9 (2014) e114275.
- [47] H. Pan, W. Zhang, W. Zhang, G.-H. Liu, Find and replace: editing human genome in pluripotent stem cells, *Protein Cell* 2 (2011) 950–956, <http://dx.doi.org/10.1007/s12328-011-1132-0>.
- [48] D.A. Ovchinnikov, D.M. Titmarsh, P.R.J. Fortuna, A. Hidalgo, S. Alharbi, D.J. Whitworth, et al., Transgenic human ES and iPS reporter cell lines for identification and selection of pluripotent stem cells in vitro, *Stem Cell Res.* 13 (2014) 251–261, <http://dx.doi.org/10.1016/j.scr.2014.05.006>.
- [49] D.E. Discher, D.J. Mooney, P.W. Zandstra, Growth factors, matrices, and forces combine and control stem cells, *Science* 324 (2009) 1673–1677, <http://dx.doi.org/10.1126/science.1171643>.
- [50] P.C.D.P. Dingal, D.E. Discher, Combining insoluble and soluble factors to steer stem cell fate, *Nat. Mater.* 13 (2014) 532–537, <http://dx.doi.org/10.1038/nmat3997>.
- [51] N. Huebsch, P.R. Arany, A.S. Mao, D. Shvartsman, O.A. Ali, S.A. Bencherif, et al., Harnessing traction-mediated manipulation of the cell/matrix interface to control stem-cell fate, *Nat. Mater.* 9 (2010) 518–526, <http://dx.doi.org/>

- [10.1038/nmat2732](https://doi.org/10.1038/nmat2732).
- [52] J.H. Wen, L.G. Vincent, A. Fuhrmann, Y.S. Choi, K.C. Hribar, H. Taylor-Weiner, et al., Interplay of matrix stiffness and protein tethering in stem cell differentiation, *Nat. Mater. Adv.* (2014) 1–21, <http://dx.doi.org/10.1038/nmat4051>.
- [53] B.M. Baker, C.S. Chen, Deconstructing the third dimension - how 3D culture microenvironments alter cellular cues, *J. Cell Sci.* 125 (2012) 3015–3024, <http://dx.doi.org/10.1242/jcs.079509>.
- [54] O.F. Zouani, C. Chanseau, B. Brouillaud, R. Bareille, F. Deliane, M.-P. Foulc, et al., Altered nanofeature size dictates stem cell differentiation, *J. Cell Sci.* 125 (2012) 1217–1224, <http://dx.doi.org/10.1242/jcs.093229>.